Quality Prediction and Control of Continuously Cast Slabs

by

Ferdinando Roux Camisani-Calzolari

Submitted in partial fulfillment of the requirements for the degree
PhD (Electronic Engineering)
in the
Faculty of Engineering, Built Environment and Information Technology
UNIVERSITY OF PRETORIA

February 2003

Summary

Surface defects in the continuous casting process require treatment by grinding. This extra phase in the process causes lower throughput of final product and extra energy costs. The elimination of slab treatment after casting implies that slabs can be directly rolled or hot charged, resulting in higher throughput and lower energy costs. To increase the number of slabs that can be directly rolled or hot charged, defects have to be predicted before a slab has completed the casting process. This eliminates post-casting surface inspection, and allows the steel-making company to schedule slabs so that defect-free slabs can be direct rolled or hot charged. Slabs with defects are still sent for treatment. The control of continuous casting parameters can lead to the eradication of defects so that all slabs are defect-free, thus eliminating the grinding process altogether. Transversal and longitudinal cracking, casting powder entrapment and other inclusions, bleeders, deep and uneven oscillation marks, stopmarks and depressions are the defects which are considered for prediction and control and are the output variables of the predictor. Only the variables in the mould are considered as inputs to the predictor, and as manipulated variables to control the occurrence of defects. 1060, 1280, 1335 and 1575mm wide slabs are considered, and the prediction techniques are applied on a real stainless-steel producing plant in South Africa.

A literature overview on the causes of defects, goodness-of-fit tests, correlation, auto-regression with exogenous input and a linear quadratic tracker at steady-state is presented. Goodness-of-fit tests are used to determine which mould variables have an effect on the occurrence of defects, and correlation is used to find linear dependence among mould variables. A structure of two models is proposed. The first model describes the effect of mould level, water inlet temperature and casting speed (MV—manipulated variables) on 38 thermocouple temperatures (IV—intermediate variable). Casting speed is a manipulated variable while mould level and water inlet temperature are measured disturbances. This model is known as the MV to IV model, and is used to control the occurrence of defects. The second model describes the effect of the thermocouple temperatures on the defects at different positions and locations on the slabs (OV—output variables). This model is known as the IV to OV model and is the predictor of defects. The models are determined using time-series methods in the form of auto regression with exogenous input using data of approximately 500 slabs cast over a period of 6 months. The models are validated using new data at the same plant from 44 slabs gathered three years later, with good results. As an example, published results give a sensitivity and specificity of 61.5% and 75% respectively for longitudinal cracks on validation data, while the presented method gives 63.6% and 93.5% respectively. The IV to OV model is used in an inversion to determine the optimal thermocouple temperatures for each slab width. The MV to IV model is then used to design a controller to maintain the thermocouple temperature set-points. Three controllers were designed and compared in simulation. The system is inherently uncontrollable, because one manipulated variable exists to control 38 outputs. The linear quadratic tracker at steady-state gave the best results with an overall tracking improvement over the uncontrolled case of 30%, 40% and 1% for the 1060, 1280 and 1575mm wide slabs respectively; with single output control second with 23%, 39% and -2% improvement respectively and the worst case controller came in last with 13%, 31% and -6 % improvement respectively. An increase of the number of thermocouples embedded in the mould walls, as well as proper installation of the thermocouples can improve the predictor. An increase in the number of manipulated variables by using individually controlled water pockets in the mould can improve the control of defects.

Keywords

continuous casting, model, defect, predict, control, direct rolling, hot charging, goodness-of-fit, correlation, time-series, ARX, LQR, bump-less transfer (Afrikaans)

Opsomming

Oppervlakdefekte wat vorm in die stringgietmasjien benodig behandeling d.m.v slyping. Hierdie ekstra fase in die proses veroorsaak laer deurset van finale produk en ekstra energiekostes. Die uitskakeling van platblok behandeling na gieting beteken dat platblokke direk gewals of warm gelaai kan word, wat 'n hoër deurset en verlaagde energiekoste tot gevolg kan hê. Om die hoeveelheid platblokke wat direk gewals of warm gelaai kan word te verhoog, moet die defekte voorspel word voordat die platblok klaar gegiet is. Die voorspeller verwyder na-gieting inspeksies en laat die staalmaker toe om platblokke te skeduleer sodat defeklose platblokke direk gewals of warm gelaai kan word. Platblokke met defekte word steeds gestuur vir behandeling. Die beheer van stringgietmasjienparameters kan lei tot die uitskakeling van defekte sodat alle platblokke defekloos is en sodoende die slypingsfase algeheel uitskakel. Transversale en longitudinale krake, gietpoeier vasvanging en ander inklusies, bloeiers, diep on ongelyke ossillasiemerke, stopmerke en depressies is die defekte wat oorweeg is vir voorspelling en beheer en is die uitsetveranderlikes van die voorspeller. Slegs die veranderlikes in die gietvorm word oorweeg as insette tot die voorspeller; en as gemanipuleerde veranderlikes om die voorkoms van defekte te beheer. 1060, 1280, 1335 en 1575mm wye platblokke word beskou, en die voorspellingstegnieke word op die aanleg van 'n vlekvryestaal produseerder in Suid-Afrika getoets.

'n Literatuuroorsig aangaande die oorsake van defekte, passings-akkuraatheid toetse, korrelasie, outoregressie met eksogene inset en 'n lineêre kwadratiese volger by gestadige toestande word weergegee. Passings-akkuraatheid toetse word gebruik om te bepaal watter gietvormveranderlikes 'n effek op die defekvoorkoms het, en korrelasie word gebruik om lineêre afhanklikheid tussen gietvormveranderlikes te vind. 'n Struktuur met twee modelle word voorgestel. Die eerste model beskryf die effek van gietvlak, water inlaattemperatuur en gietspoed (MV—gemanipuleerde veranderlikes) op 38 termokoppeltemperature (IV—intermediêr). Gietspoed is 'n gemanipuleerde veranderlike terwyl gietvlak en waterinlaattemperatuur is gemete versteurings. Hierdie model staan bekend as die MV na IV model, en word gebruik om die voorkoms van defekte te beheer. Die tweede model beskryf die effek van termokoppeltemperature op die defekte by verskillende posisies en liggings (OV—uiset veranderlikes). Hierdie model staan bekend as die IV na OV model en is die voorspeller van defekte. Die modelle word bepaal deur van tyd-reeks metodes gebruik te maak in die vorm van outo-regressie met eksogene inset en data van ongeveer 500 platblokke wat oor 'n tydperk van 6 maande gegiet was. Die modelle word bekragtig deur nuwe data van 44 platblokke wat drie jaar later ingesamel is, met goeie resultate. As voorbeelde gee gepubliseerde resultate 'n sensitiwiteit en spesifisiteit van 61.5% en 75% respektiewelik vir longitudinale krake op bekragtigingsdata, terwyl die voorgestelde tegniek 63.6% en 93.5% respektiewelik gee. Die IV na OV model word gebruik in 'n inversie om die optimale termokoppeltemperature vir elke platblokwydte te gee. Die MV na IV model word dan gebruik om 'n beheerder te ontwerp om die termokoppeltemperature se stelpunte te handhaaf. Drie beheerders word ontwerp en d.m.v. simulasie vergelyk. Die stelsel is inherent onbeheerbaar want slegs een gemanipuleerde veranderlike is beskikbaar om 38 uitsette te beheer. Die lineêre kwadratiese volger by gestadige toestande het die beste resultaat gelewer met 'n algemene volgfout verbetering teenoor die onbeheerde geval van 30%, 40% en 1% vir die 1060mm, 1280mm en 1575mm wye platblokke respektiewelik. Die enkeluitsetbeheerder was tweede met 23%, 39% en -2% verbetrings respektiewelik en die slegste geval beheerder was laaste met 13%, 31% en -6% verbeterings respektiewelik. 'n Verhoging in die hoeveelheid termokopples wat in die gietvorm se wand ingeplant word, asook die korrekte installering van die termokoppels kan tot gevolg hê dat die voorspeller verbeter. 'n Verhoging in die hoeveelheid gemanipuleerde veranderlikes d.m.v. waterholtes in die gietvorm wat individueel beheer kan word kan die beheer van defekte verbeter.

Sleutelwoorde

stringgiet masjien, model, defek, voorspel, beheer, direk wals, warm laai, passings-akkuraatheid, korrelasie, tyd-reeks, ORX, LKR, stamplose-oordrag

Acknowledgements

The author wishes to thank the following persons and institutions for their contribution to this thesis.

- Prof. Ian K. Craig, the promoter of this thesis, whose guidance and knowledge of various aspects on control systems engineering proved very valuable.
- Prof. P. Chris Pistorius, the fellow promoter of this thesis, whose guidance and knowledge on metallurgical aspects also proved useful.
- Mr. J. Ackermann of Columbus Stainless Steel who provided some of the data and allowed the author to gather data at the plant.
- Mr. R.J. Grimbeek of STATOMET at the University of Pretoria, for the sample-size calculation of §3.1.2.3 on page 62.
- The National Research Foundation (NRF) of South Africa for sponsorship during the research.
- The Mellon Foundation for sponsorship during the research.
- My parents, for their support.
- My wife Petra, whose loving support was greatly appreciated.

Contents

Chapter 1

Introduction

THE continuous casting of steel slabs is an established technology to solidify molten steel into its solid form. Surface defects form during the continuous casting process. As a consequence of these defects, an intermediate stage between casting and hot-rolling is needed to remove these defects. The intermediate grinding stage causes large delays before slabs can be rolled, implying throughput losses for the steel-making company. These delays also mean that energy costs are increased, because grinding can not take place at the elevated temperatures of a cast slab; and hot-rolling must occur at an elevated temperature. The slab must therefore be cooled, grinded and reheated. These defects also make technologies such as direct rolling and hot charging infeasible, since the defects have a detrimental effect on post-casting operations.

The problem addressed in this thesis is to determine a model to relate mould variables to surface defects. This model can be used as a predictor to determine when defects will occur, thus making scheduling for direct rolling or hot charging of some slabs possible. Only defected slabs are then sent for treatment. The model can also be used to design controllers to eradicate or reduce the defects so that higher throughput is obtained.

1.1 Background

During the past fourty years, continuous casting has become the predominant method to solidify molten steel into semi-finished shapes [1]. The advent of continuous casting has overshadowed the traditional method of ingot casting [2]. Continuous casting allows the

uninterrupted constant casting of steel from its molten state to its solidified state, whereas ingot casting requires a cooling period before final solidification takes place so that the ingot mould can be used again [1].

The continuous solidification of steel means that more steel is cast per unit time compared to ingot casting, thus increasing the throughput of the cast product and ultimately the final product.

In continuous casting, metallurgically prepared molten steel is poured from the ladle into a tundish which ensures that steel is always available for casting into a mould. When all steel from the ladle is cast, the ladle is changed, but casting continues because some steel remains in the tundish. The open-ended mould is the primary extractor of heat. During solidification in the mould, a solidified shell of steel forms which is strong enough to withstand the ferro-static pressure of the liquid steel within. The strand moves out of the mould at the casting speed and enters the secondary cooling zone where further solidification takes place by spraying water onto the surface of the strand. On exit from the secondary cooling zone, the strand cools off naturally in air until fully solidified and is then cut. The cut slabs are then sent for further processing such as grinding, rolling *etc.*

During the casting operation, internal and external defects form which are detrimental to the post-casting processes. The external (surface) defects form in the mould (see Chapter 2), with possible aggravation in the secondary cooling zone.

The purpose of this thesis is to explore methods to predict and control surface defects in continuous casting.

1.2 Motivation

To increase the throughput of rolled product and to decrease the cost due to energy consumption, steel companies are required to optimise their continuous casting processes in such a way that hot charging or direct rolling becomes possible [3, 4].

In hot charging, the cast product is sent for rolling before the slab cools off below $650°C$ [3]; thus reducing the time required for reheating of the slab [5] and minimising the cost of energy required [6]. In direct rolling, the casting process and slab scheduling are optimised to such an extent that the slabs are directly sent for rolling, thus eliminating the energy and time required for the reheating furnace. Direct rolling is however impossible if the extent of

surface defects is so severe that post-casting treatment of the slab is required. The treatment usually implies grinding or spot treatment of the slab surface. The treatment cannot be done at the elevated temperatures which are required for hot rolling ($1150°C$ [3]) and thus the throughput of the product is reduced due to the time required to 1) cool, 2) treat, 3) reheat the cast slab. The cost of energy consumed in the reheating furnace also implies unnecessary financial losses.

If hot charging (rather than direct rolling) is practised, surface treatment does not appear to imply as great a loss, since some reheating is required whether surface treatment is applied or not. However, the time taken to treat the surface implies a reduction in throughput.

Grinding is always performed at some steel-making companies, because of the fear of defects slipping by the inspection line. Some steel-making companies report hot charging of 30% of their slabs without any conditioning [7] while other companies report direct rolling and hot charging of up to 80% of their cast slabs [8, 9] and blooms [2] without any conditioning. Some companies even implement direct rolling when the caster is far from the hot-rolling mill [10]. In general, hot charging is more successful in billets than in slabs [6, 11].

Many researchers have attempted to improve the surface quality of the cast product by Computer Aided Quality Control (CAQC) methods [12–16]. In these methods, some form of non-human surface defect measurement is employed and used to "train" a database linking mould and secondary cooling zone conditions to the different defects. The database can then be used in conjunction with continuous casting process measurements to

1. predict the quality of the cast product,
2. determine whether the slab can be hot charged or direct rolled,
3. update the database in cases where new defects or steel types occur, and
4. apply control to eradicate the occurrence of defects.

The defect detection databases are usually in-house, and literature on the matter is very limited (see *e.g.* Hatanaka, Tanaka, and Kominami [17], Hunter, Normanton, Scoones, Spaccarotella, Milone, Vicino, Lamant, Morand, and Do Thong [18] and Creese *et al.* [15]); with most discussions covering only a fraction of the procedures (see *e.g.* Matsuzuka, Fujita, Yabuta, and Itoh [19]).

The motivation for this work is that if defects can be eradicated through the *control* of mould parameters, direct rolling will be made possible by removing the grinding stage. If, at least,

defects can be *predicted* with high accuracy, more slabs can be sent for hot charging directly after casting. Those slabs which do have defects will be sent for grinding, making the scheduling task easier.

A further motivation is that an industrial partner was found in South Africa which was very willing to aid in this study by providing data and allowing the researcher to test most of the techniques in practice.

1.3 Aims

To be able to predict when defects are going to occur, a model must be found which relates mould parameters to the defects. The aim of this work is therefore to determine such a model. A further aim is to use the model to design controllers which manipulate casting parameters such that defects can be eliminated or reduced considerably.

The specific defects that will be considered are transversal and longitudinal cracks, inclusions, oscillation marks, stopmarks, bleeders and depressions, as these are the foremost defects that occur. These defects are the *outputs* of the model.

The *inputs* of the model are the casting parameters. Since it has been found that the above defects originate in the mould, only mould parameters will be considered as inputs. Pre- and post-mould processes are assumed to compound any defects which may occur, and thus act as disturbances.

Since first-principle models presented in the literature are usually 1) vague in terms of effectiveness or accuracy, 2) do not clearly show that they work, 3) have no relation to mould parameters so that prediction can not be performed, 4) and are complicated; a system identification approach to modelling will be used. Artificial intelligence (AI) techniques such as artificial neural networks (ANN) have previously been used to predict defects [18], and will thus not be considered in this work as a modelling tool, except to compare published results and results of this work. The aim of this work is then to use system identification on practical data as the modelling technique.

1.4 Approach

The approach followed in this work is to find a model describing the effect of mould variables (inputs) on the formation of defects (outputs) using data from an industrial continuous caster in South Africa. The mould variables are obtained from the level 2 system of the continuous caster, and the defects are obtained by plant personnel inspecting the slabs off-line. The defect data are read into a computer for analysis and model training. A reduction of the number of mould variables (inputs) is carried out using statistical hypothesis testing and correlation analysis. From this data, it also becomes clear that the mould/defect data can be split into two models, one describing the effect of casting speed, mould level and inlet temperature on thermocouple temperatures and another describing the effect of thermocouple temperatures on defects. The outcome of the model split is that the continuous measurement of thermocouples makes it possible to apply feedback control. The thermocouple temperature set-points are then determined such that no defects will occur due to mould temperature; and the casting speed as manipulated variable is used to maintain these thermocouple temperatures in a feedback fashion. The models are derived and validated using ARX (auto regressive with exogenous input) methods together with plant data. Three controllers are designed and compared to show the improvement for thermocouple temperature set-point tracking. These controllers are not tested on the plant, but in simulation.

1.5 Contribution

Several contributions are made in this work. Firstly, the thesis shows that it is feasible to split the model for defect prediction into two models, one that relates the manipulated variable (casting speed) to intermediate variables (thermocouple temperatures) and another to relate the intermediate variables to outputs (defects). The advantage of the split is that feedback control can be used by measuring thermocouple temperatures, instead of defects which are difficult to measure and have a long time delay before they can be measured. The model split also implies that the thermocouples are the only variables to be measured to predict the defects; and thus act as a soft sensor of defects.

The second contribution is that both models can be trained (and verified) from real plant data using ARX methods, as is demonstrated in this work. The model is also motivated from defect literature.

Thirdly, the model relating the thermocouple temperatures and defects is used to determine the optimal set-points for the thermocouple temperatures such that few or no defects occur due to mould temperature variation.

Fourthly, it is shown how controllers can be designed to improve the set-point tracking of thermocouple temperatures using casting speed as a manipulated variable. Three different controllers are designed and compared in this work.

The literature contributions of this thesis can be found in one published [20] and three submitted journal articles [21–23]. Further literature contributions can be found in six conference proceedings [24–29] and one submitted conference article [30].

1.6 Outline

Chapter 2 describes the background needed for this thesis and includes an overview of the process and the predominant defects that are present in continuous casting. A description of the Kolmogorov-Smirnov and Anderson-Darling goodness-of-fit tests and correlation analysis is also given. ARX as the system identification technique to model the system is described. Lastly, a single-input, multiple-output (SIMO) controller in the form of a steady-state linear quadratic tracker will be described.

Chapter 3 deals with modelling aspects. The different variables that are found in the mould are explained. The defect data and the data gathering from cast slabs by humans are also explained. The extraction of data from the level 2 system of the plant, based on auxiliary data and time-position reconciliation, is described. A statistical analysis, using the goodness-of-fit tests and correlation to reduce the number of variables and to show that the model can be split into two models, is also given. The use of ARX as a modelling tool to find models for the manipulated to intermediate variable model and intermediate to output variable model is then perused. The models are shown to be accurate using training and validation sets. The intermediate to output variables are thresholded to ensure that a defect occurs only when the output variable passes a certain value. The intermediate to output variable model is used to determine set-points for the thermocouple temperatures (intermediate variables) such that no defects occur due to mould temperature.

Chapter 4 shows the application of control to reduce variation in thermocouple temperature within the mould, thus reducing the occurrence of defects. Three controllers are compared.

The first is SIMO and called a linear quadratic tracker at steady-state (LQTSS). The second is a single-input, single-output (SISO) controller which uses one thermocouple output to reduce the variation in temperature and is called a single output controller (SOC). The third is called a worst-case controller (WCC) and uses the worst performing temperature error together with bump-less transfer to control the variation in temperature.

Chapter 5 gives an assessment of the study and recommendations for future work.

Chapter 2

Background

AN understanding of the continuous casting process is necessary so that the methods used in later chapters can be fully comprehended. This chapter aims to inform the reader of the literature regarding the subject matter and the techniques that are used in this thesis.

A brief description of the continuous casting process which highlights the main functional units is given in §2.1. In §2.2.1, a review is given of the literature regarding the causes or influencing factors of defects in the process. The review is rather detailed, because a thorough understanding of the defects and their causes gives greater insight into the design of a defect predictor. This section also describes several models for defect propagation and prediction found in literature.

§2.2.2 describes specific statistical hypothesis tests that are used in chapter 3. These hypothesis tests are known as goodness-of-fit tests and determine whether data come from a given theoretical distribution. The hypothesis tests will be used to reduce the number of variables that are present for a defect prediction model.

Correlation analysis is described in §2.2.3. The correlation can be used to detect one-to-one relationships of variables so that the number of variables can be reduced in a prediction model. If one-to-one relationships do exist, the model size is reduced to avoid repetition of information.

The Box-Jenkins [31] type modelling strategy known as ARX (Auto Regression with eXogenous input) is described in §2.2.4. This form of system identification is popular for the determination of empirical linear system models used for control system design. The tech-

nique will be applied to the current control / modelling problem. A brief overview of the system identification technique will be given.

A controller for a SIMO type system that can track set-points will be described in §2.2.5. The controller forms part of an optimal set of controllers based on the solution of the Riccati equation. The controller is designed for steady-state operation. The design of this controller is simple, and guarantees system stability. The design procedure will be covered briefly. This controller is one of three controllers that will be compared to improve the response of the system. The other controllers are simple to understand and will not be explained in this chapter.

2.1 Continuous casting process

The description of the continuous casting process is done for a *bow-type* continuous caster (see Fig. 2.1) since it is the most predominant caster found in practice. Each critical component of the caster is described [1].

2.1.1 Ladle

Molten steel arrives at the continuous casting machine in a container known as the ladle. In steel casters, the ladle contains between 70-300 tons of molten steel at between 1500 and 1600 °C [1]. The ladle is then placed on one end of a rotating platform known as the turntable. The turntable can accommodate at least two ladles simultaneously. When all the steel from one ladle is cast, the turntable swings around and casting proceeds from the second ladle. This method of ladle switching ensures that steel is usually available for casting. The turntable method is the most widely used mechanism to switch ladles. Some casters use a slide mechanism by which the ladle is slid into position before casting commences. However, this method causes a long delay between switching because one ladle has to be extracted before another ladle can be slid into position. At the bottom of the ladle there is usually a slide-gate mechanism that controls the rate of flow of molten steel into another container known as the tundish.

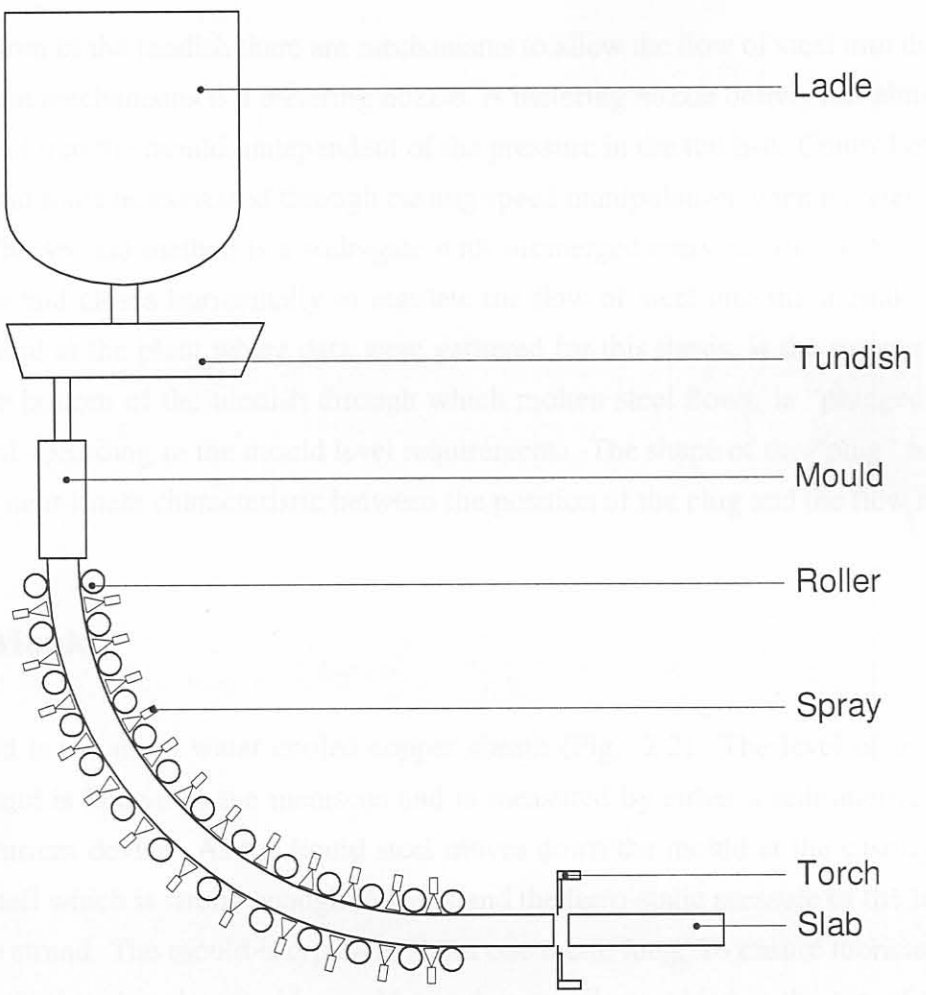

Figure 2.1 Side view of a bow-type continuous caster

2.1.2 Tundish

The tundish acts as a reservoir of molten steel. The reason that liquid metal is not poured directly into the mould from the ladle is three-fold. Firstly, if a ladle is not available for casting, continuity is not assured. Secondly, the tundish is designed to accommodate complex mechanisms to control the flow of steel into the mould. Thirdly, the tundish can be designed to provide liquid steel to several moulds as is the case with multi-strand casters.

At the bottom of the tundish there are mechanisms to allow the flow of steel into the mould[a]. One of these mechanisms is a metering nozzle. A metering nozzle delivers an almost steady flow of steel into the mould, independent of the pressure in the tundish. Control of the level in the mould must be exercised through casting speed manipulation when a metering nozzle is used. The second method is a slide-gate with submerged entry nozzle (SEN). The slide-gate opens and closes horizontally to regulate the flow of steel into the mould. The third method, used at the plant where data were gathered for this thesis, is the stopper rod. The hole at the bottom of the tundish through which molten steel flows, is "plugged up" by a stopper rod according to the mould level requirements. The shape of the "plug" is designed to allow a near-linear characteristic between the position of the plug and the flow rate.

2.1.3 Mould

The mould is usually a water cooled copper sheath (Fig. 2.2). The level of molten steel in the mould is known as the meniscus and is measured by either a radiometric device or an eddy current device. As the liquid steel moves down the mould at the casting speed, it forms a shell which is strong enough to withstand the ferro-static pressure of the liquid steel within the strand. The mould is typically about one metre long. To ensure lubrication of the solidified shell within the mould, mould powders or oil are added at the top of the mould [33]. These additives form a thin crystalline layer as well as a liquid layer between the steel and the copper plate (sheath) to reduce friction. The fluxes also provide insulation from the atmosphere at the top of the mould to prevent oxidation. Sometimes the mould flux is insufficiently distributed along the mould, or the mould is too hot so that the strand surface fuses with the mould surface. This is known as a sticker break-out and results in tearing of the strand shell so that liquid steel pours out from beneath the mould. Break-outs are extremely costly because of losses due to scrapping of steel and destruction of equipment by the liquid metal which results in down-time. Special thermocouples are sometimes inserted

[a] see *e.g.* Hill and Wilson [32] for a discussion on the importance of the design of the mould inflow

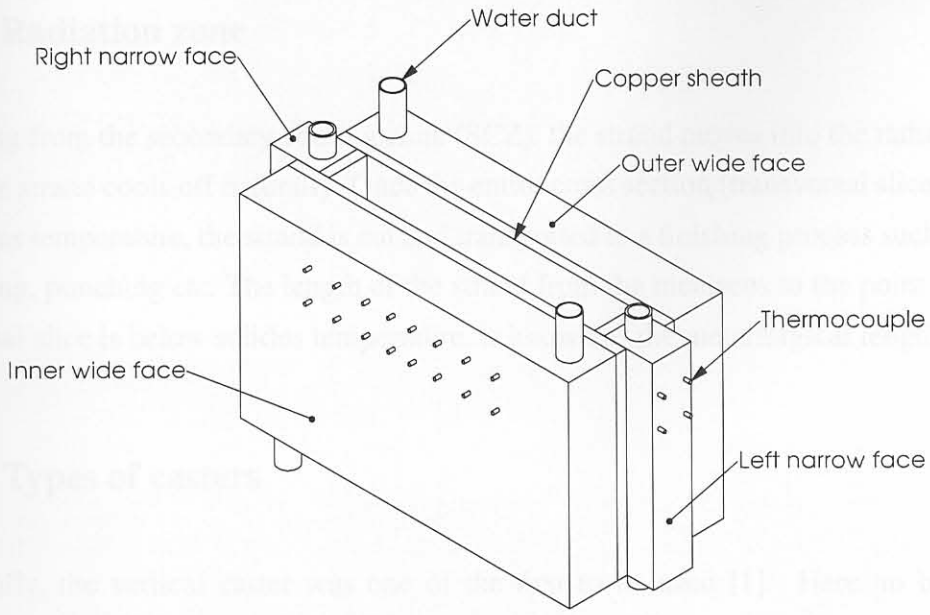

Figure 2.2 Isometric view of a continuous caster mould.

in the mould to measure temperature gradients from the top to the bottom of the mould. Should the temperature gradient be too large, a break-out may occur. The thermocouples act as a break-out-detector, warning the operator of possible break-outs. The mould oscillates to aid in the extraction of the solidified strand (see *e.g.* Burgess, Guzman, and Singh [34]). The mould width is adjustable by moving the narrow sides in or out. Typical widths for slab casters are 1000mm, 1280mm and 1575mm.

2.1.4 Secondary cooling zone

On exit from the mould, the strand enters the secondary cooling zone which ranges in length from 6 to 20 metres. Directly below the mould there is usually a device known as the spray ring which provides water flow to the strand to aid in cooling, and to ensure a smooth heat-transfer gradient between the mould and secondary cooling zone. In the secondary cooling zone, rollers support the strand and aid in bending and straightening in the case of bow type casters. Water sprays extract the heat from the strand. These sprays are grouped in three to six spray zones. Water flow in each spray zone is independently controlled by valves.

2.1.5 Radiation zone

On exiting from the secondary cooling zone (SCZ), the strand moves into the radiation zone where the strand cools off naturally. Once the entire cross section (transversal slice) is below the solidus temperature, the strand is cut and transported to a finishing process such as grinding, rolling, punching *etc.* The length of the strand from the meniscus to the point where the transversal slice is below solidus temperature, is known as the metallurgical length.

2.1.6 Types of casters

Historically, the vertical caster was one of the first to be used [1]. Here no bending or straightening is required but the machine needs considerable physical space and there are serious shape problems due to gravity adversely affecting the flow of steel. The bow caster was the next in the casting evolution and is the most widely used casting method today. One of the newest types of casters is the horizontal continuous casting process whereby casting is performed horizontally. The only real disadvantage of bow casting compared to the other two mentioned is that the bow caster requires the bending and subsequent straightening of the strand which might lead to some surface imperfections.

2.1.7 New caster technologies

The major parameter by which the success of any casting process is measured, is its throughput over all unit processes. The throughput is the amount of steel cast as a function of time. A thinner strand cools down quicker, but less steel is cast. This trade-off actually swings totally towards faster cooling times because the relationship between cooling time (t) and section thickness (l) is not linear ($t \propto l^2$) [35]. Since the strand is now thinner, rolling throughput is increased.

Current development in continuous casting includes thin-slab casting and strip casting (see *e.g.* Brückner [36]). Thin-slab casting is a fairly established technology and this type of caster has found its place in many steel companies. Strip casting is a method by which rollers are used to cool the molten metal while simultaneously forcing a thin shape; and is currently being implemented at some steel-making companies.

2.2 Literature overview

This section describes the most relevant literature which was found regarding the scope of this thesis.

2.2.1 Defects

There are several defects that occur when continuous casting is applied. Any defects in a solidifying strand are primarily caused by the mould [37]. The secondary cooling zone can only compound the defect, not eradicate it.

The primary control problem in continuous casting is the level of steel in the mould. The level of steel in the mould should not vary much, but remain as constant as possible. The *mould level control problem* is the main problem that is addressed by control system researchers in the field of continuous casting[b]. Mould level oscillations tend to cause depressed regions filled with solidified mould powders, resulting in surface defects. Until now, researchers have not been able to agree on the causes of mould level oscillation though many theories exist [49].

Some of the metallurgical and mechanical problems that arise in continuous casting are summarized by Brimacombe and Samarasekera [50, pp. 182–185]:

1. The *cleanliness* of the steel can be affected *e.g.* there can be
   - oxidation of steel with oxygen from air or refractories,
   - pickup of exogenous inclusions [51, 52] from ladle and tundish refractories and mould powders,
   - bad control of fluid flow in the tundish so that inclusions do not float out,
   - bad mould powder and startup/shutdown procedures, causing break-outs.
2. *Cracks* occurring in, or on the steel such as [53, 54]

[b] see *e.g.* De Keyser [38], De Keyser [39], Inkinen, Lautala, and Saarelainen [40], Kong and De Keyser [41], Graebe, Goodwin, and Elsley [42], Jenkins, Thomas, Chen, and Mahapatra [43], Nilles and Marique [44], Mellberg [45], Hesketh, Clements, and Williams [46], Hattori, Nagata, Inaba, Ishitobi, Yamamoto, Okada, and Zeze [47] and Andrzejewski, Köhler, and Pluschkell [48]

- surface cracks which are a serious quality problem because the cracks oxidize and give rise to oxide-rich seams in the rolled product or, to an even greater extent, cause the strand to be scrapped due to extremely deep longitudinal cracks [55], and
- internal cracks which can also be a problem particularly if during rolling, they do not close, leaving voids in the steel product.
- As the strand moves from one cooling zone to the next, changes in heat extraction cause 1) shifts in thermal gradients through the solidifying shell and 2) stress generation resulting from differential expansion or contraction [56, 57].

3. *Macro-segregation.* There are higher concentrations of certain elements in certain regions of the strand, causing cracks during rolling [58].
4. Cross sectional or *transverse shape.* Deviations from the specified shape due to non-homogeneous cooling in the mould requires excessive reworking.

Though many types of defects occur in continuous casting, the defects discussed here are limited to those specified by personnel at the steel-making plant as well as the available data. The first limitation is that only surface defects are considered. Internal defects fall outside the scope of this thesis; and, after all, the surface defects are the reason for the grinding process. Secondly, only variables present in the mould are used as the parameters under investigation. This means that defects which arise in *e.g.* the secondary cooling zone are not considered. Because of the aforementioned limitation, the compounding effect which the secondary cooling zone has on some defects that start in the mould could possibly not show in the mould variables. The same type of reasoning can be followed for the tundish; except that the tundish precedes the mould in the process and therefore *does* have an influence on mould variables (*e.g.* mould level). Therefore, one can assume that a surface defect that occurs due to some varying parameter in the tundish should be visible in the mould parameters.

The defects which do occur during casting operation at the industrial partner are discussed in the following sections, with specific emphases on their descriptions and causes.

2.2.1.1 Transversal cracking (defect 1a)

The occurrence of transverse cracks seems to be a problem which occurs frequently around the world, considering the amount of literature found on the subject. Transverse cracking in

general occurs due to fast or uneven cooling, sticking in the mould, and bending or straightening at low temperatures [59][c]. Transversal cracks fall under the general heading of *cracks* as described above (point 2, §2.2.1).

The occurrence of this defect coincides with the occurrence of oscillation marks[d] (§2.2.1.6) and transversal depressions (§2.2.1.8) [69]. The defect is generally not easily noticeable until after the slab has been "dressed" or rolled to plate [70].

The occurrence of transversal cracks is subdivided into transversal corner cracking and transversal facial cracking. These two occurring cracks are discussed in the next sections.

Transversal corner cracks These cracks occur on the radiused or chamfered part of the section, normal to the axis of the product [59]. Fig. 2.3 shows the occurrence of a transversal corner crack in the case of a 9 inch bloom. Transversal corner cracks occur for the following

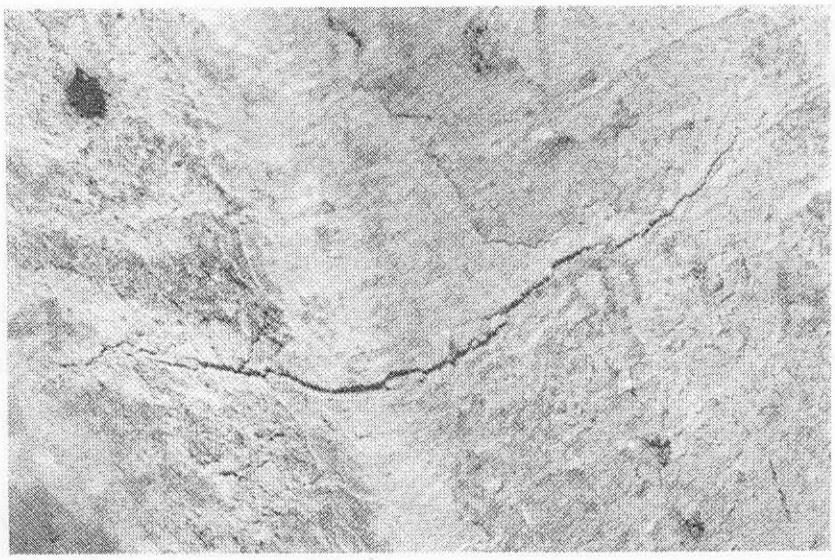

Newton *et al.* [59, p. 5]

Figure 2.3 Transversal corner crack.

reasons.

1. Bending or straightening at temperatures that are too low [59].

[c]see also Mintz, Yue, and Jones [60], Billany, Normanton, Mills, and Grieveson [61], Yasumoto, Maehara, Nagamichi, and Tomono [62], Diener, Drastik, Redenz, and Wagner [63] and Harste and Tacke [64]

[d]see Mintz *et al.* [60], Szekeres [65], Takeuchi and Brimacombe [66], Wolf [67] and Muller [68]

2. Sticking of the product in the mould due to increases in friction of the mould-strand interface [59]. Friction increases occur for several reasons as described by Emling [71], *e.g.* unsuitable mould taper, oscillation, powder and temperature; and casting speed variations.

Composition can be a factor which increases the occurrence of the defect *e.g.* manganese levels higher than 1% with 0.03% vanadium has been found to increase the occurrence of the defect [70] for carbon steels. Brimacombe and Sorimachi [53] further state that aluminium or niobium together with more than 1% manganese increases the chances of occurrence of the defect in carbon steels[e].

The effect generally originates in the mould, but can also originate just below the mould during tension on the strand in a region of low ductility as described by Brimacombe and Sorimachi [53] as well as Saito, Kimura, Ueta, Kimura, Takemoto, and Mine [76].

Uneven water temperature or flow or improper use of mould powders or uneven cooling in the mould which leads to rhomboicity in billets and blooms can also form longitudinal corner cracks [69].

Transversal facial cracks These cracks are defined by Newton *et al.* [59, p. 6] as "a crack not on the radiused or chamfered part of the section, normal to the axis of the product". A drawing of the defect is given in Fig. 2.4. The main causes that are associated with this crack is given below [59].

1. Too severe cooling in the mould or sprays (in the case of large sections such as slabs).
2. Sticking in the mould due to friction.

Leclerc and Pollak [77] state that transversal depressions originate in the mould and may occur due to the oscillation cycle and the entrapment of mould powder at the corner of the slab. The cracks occur at the bottom of the oscillation marks [53, 76, 77] due to a frictional irregularity which is caused by the weakening effect of entrapped mould powder below the oscillation mark upon flattening. To eradicate this problem, the negative strip ratio[f] should

[e] See the articles by Mintz [72], Burden, Funnell, Whitaker, and Young [73], Unger, Biesterfeld, Berentzen, and Thielmann [74] and Razumov, Zabil'skii, Umanets, Lebedev, and Obukhov [75], where reference is made to the detailed influence of N, V, Ti, Cu, Sn, S and P on hot ductility and the occurrence of transversal cracks.

[f] Ratio based on the difference between the average downward velocity of the mould during one oscillation cycle and the casting speed when the mould velocity exceeds the casting speed [65].

not exceed 0.7, and the corners of the mould must not get too cold [77].

Discussion The information on the above mentioned cracks is not sufficient to make a distinction between the two subgroups of cracks (*i.e.* corner and facial cracks), especially since the causes are so similar.

Based on the literature, the mould can cause transversal cracking on the slab surface if the following should happen.

1. Severe cooling in the mould.
2. High friction in the mould.
3. Improper oscillation technique.
4. Carbon steel compositions where 1% manganese is involved.

The mould parameters which would be expected to show the effect of the above mentioned abnormalities are

1. Thermocouple temperatures and longitudinal/transversal temperature gradients, average heat flux, water inlet temperature and flow.

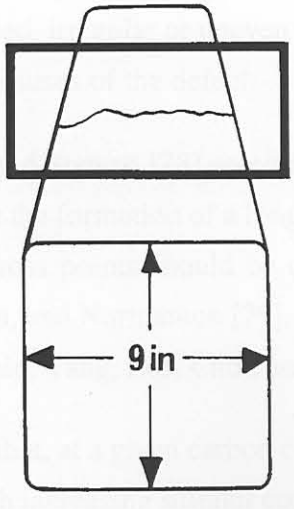

Newton *et al.* [59, p. 6]

Figure 2.4 Transversal facial crack on a 9 inch bloom.

2. Mould powder addition method and composition[g], varying casting speed and thermocouple temperature break-out system.

3. Oscillation frequency, stroke, drive current and negative strip.

4. The type of steel being cast, on-line composition analysis of the steel[g].

2.2.1.2 Longitudinal cracking (defect 1b)

The occurrence of longitudinal cracks is definitely also widespread across the world, since there is so much literature available on the subject.

Longitudinal cracks are generally caused by improper mould design and condition, high teeming temperature, fast or uneven cooling of the product in both the mould and secondary cooling zone, withdrawal speed and steel composition.

Leclerc and Pollak [77, p. 127] state that "A crack will occur when the strains exceed the resistance of the primary grains to rupture. Shrinkage strains are at a maximum along the axis of the slab and increase with size. Longitudinal full face cracks therefore affect large slabs more and are mainly situated on the axis. Any frictional irregularity between ingot mould and slab dangerously increases local strains, so that the condition of the surface and section of the mould are very important."

The occurrence of the defect is generally more prevalent for wide slabs [53]. The article also states that varying casting speed, irregular or uneven water cooling in the mould, mould oscillation and mould powder are causes of the defect.

Hunter, Madill, Scoones, Hewitt, and Stewart [78] assert that a change of $10 - 15°C$ on thermocouple readings would indicate the formation of a longitudinal crack, so that longitudinal temperature gradients and zero cross points should be considered. Also see Humphreys, Madill, Ludlow, Stewart, Thornton, and Normanton [79], Nakajima, Hiraki, Kawamoto, and Kanazawa [80] and Kang, Lee, Shin, Yang, Lee, Choi, and Lee [81].

Kim, Yeo, Oh, and Lee [82] state that, at a given carbon content, the possibility of longitudinal surface cracking increases with increasing sulphur content[h].

[g] not measure on-line

[h] Moiseev, Esaulov, Nikolaev, Emel'yanov, and Gubin [83] state that a sulphur content of less than 0.02% reduces the risk of longitudinal cracking.

Longitudinal corner cracks Longitudinal corner cracks are defined by Newton *et al.* [59, p. 2] as a crack on the radiused or chamfered part of the section running in the direction of the axis of the product. An example of the defect is given in Fig. 2.5. Mould wear or

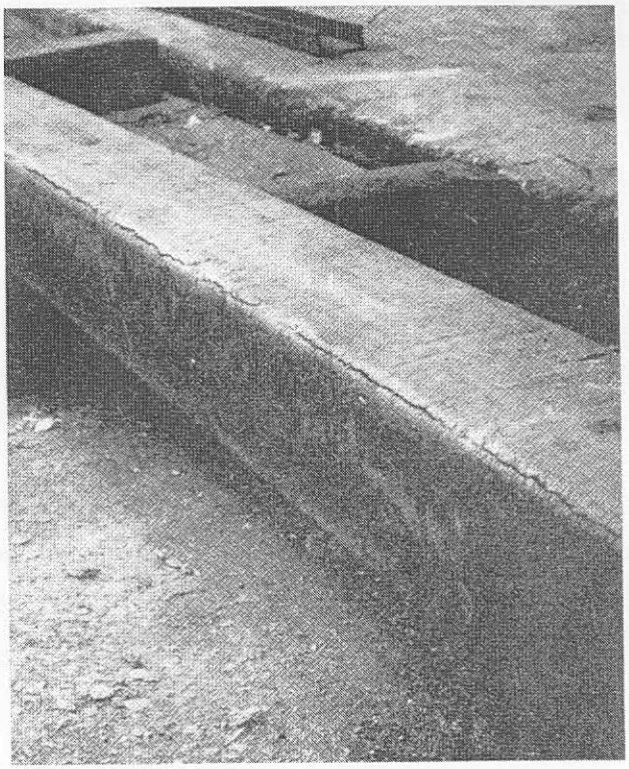

Newton *et al.* [59, p. 2]

Figure 2.5 Longitudinal corner crack.

distortion can cause longitudinal corner cracks, as can uneven mould cooling [59].

Fig. 2.6 taken from Schrewe [1] shows the formation of corner cracks due to shell withdrawal from the heat extracting mould wall for different cross sections. The author states that the gap formed due to the retraction is filled with gas and air. These gases affect the heat transfer efficiency, which means that the heat transfer is uneven which is in turn responsible for uneven solidification. The non-contacting area of the strand undergoes re-heating. This process continues until the strand is strong enough to support the forces of the ferro-static pressure. These expansions and retractions could force the formation of longitudinal corner cracks. The effect of mould taper reversal owed to distortion or wear can also cause these cracks [84]. High tundish temperature & high casting speed are also causes for the formation of the defect. Also, 0.17–0.25% carbon with sulphur$>0.035\%$ or phosphorus $>0.035\%$ are common denominators for the occurrence of the defect [84] in carbon steels.

Saito *et al.* [76] determined that mould level control also has a predominant effect on the

formation of the cracks (see also the paper by Humphreys *et al.* [79]). Large mould level variations can cause depressions which in turn can lead to the formation of longitudinal corner cracks. They further state that mould level variations below 3mm will be adequate to ensure that the defect will not appear due to fluctuations at the meniscus.

Longitudinal facial cracks These cracks are described by Newton *et al.* [59, p. 3] as "a crack not on the radiused or chamfered part of the section, running in the direction of the axis of the product".

Gray *et al.* [70] report that carbon levels in the region of 0.12% ensure that an increase in the occurrence of the defect will result. Specifically, values outside the range of between 0.05% and 0.2% seem to yield very few defects.

Fig. 2.7 shows the relation between casting speed and the occurrence of the defect. This graph indicates that both high or low casting speeds can cause the defect, and that it is solely dependent on the used casting powder's viscosity [70]. Gray *et al.* [70] also state that the origin of the defect is in the mould and that excessive cooling in the mould could result in the defect.

Cracks are generally more prevalent for 2% manganese in aluminium-manganese alloys, 0.3% silicon in aluminium-silicon alloy and 15% zinc in aluminium-zinc alloys [85].

Heard and McLean [84] state that carbon levels higher than 0.12% with an increase in sulphur and a decrease in the Mn/S ratio could cause facial cracks. Similar comments are made by Malinochka, Moiseeva, Esaulova, Esaulov, and Shmelev [86]. High or varying casting

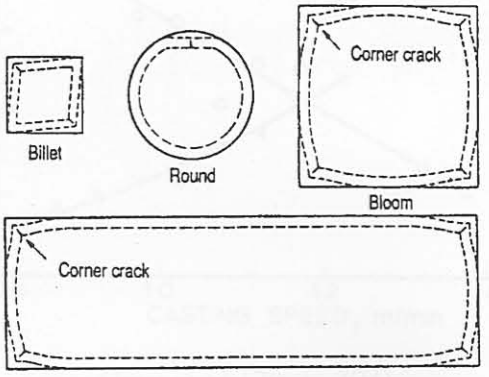

Schrewe [1, p. 106]

Figure 2.6 Gap formation and change in cross section resulting from shrinkage in the mould.

speed also has an influence on the occurrence of the defect. Furthermore, high pouring temperatures, improper mould cooling, taper loss, irregular mould oscillation, mould powder (see *e.g.* Kawamoto, Tsukaguchi, Nishida, Kanazawa, and Hiraki [87]) and a worn mould are also responsible for the defect. The defect seems to be prevalent in large cross sections such as wide slabs.

The occurrence of mid-facial cracks is a consequence of a ductile-brittle transition temperature in the mould possibly with the added effect of mould powder inclusion within the crack [55]. There is non-uniformity in cooling within the mould known as hot-spots which are caused by either uneven mould flux distribution or air gaps and therefore originate at the meniscus. Brimacombe *et al.* [55, p. 225] further state that "Under the influence of the thermally generated tensile strains, the crack will open initially close to the solidification front in the high-temperature region of low ductility within the hot spot. If the region is several millimeters beneath the slab surface, the surface, being cooler, will be below the ductile-brittle transition temperature and, therefore, will behave in a ductile manner. In this condition the surface in the vicinity of the hot spot will 'neck', while the interior of the shell in the non-ductile region is separating to form a crack...". This implies that the thermocouple temperature may show an increase due to the hot spot which might indicate the formation of the defect.

Fig. 2.8 from Irving and Perkins [88] shows the percentage of good slabs (*i.e.* slabs without any defects present) occurring versus % carbon, Mn/S ratio and % sulphur for carbon steels.

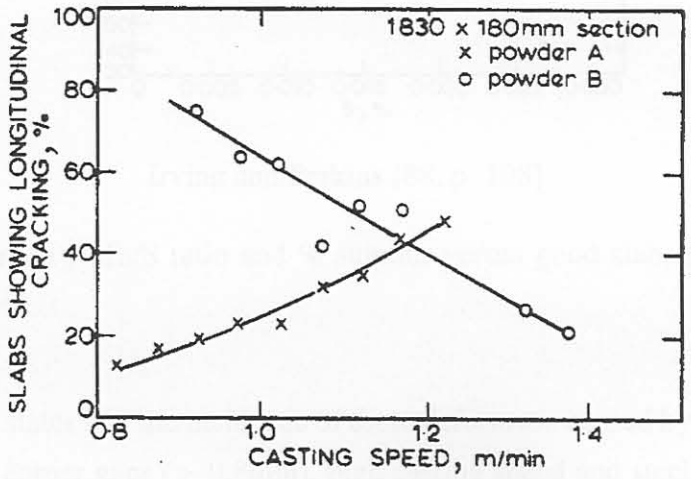

Gray *et al.* [70, p. 304]

Figure 2.7 Longitudinal facial cracking as a function of casting speed for different casting powders.

This figure shows that steels with a carbon content of 0.12% are most prone to the defect. The same can be said for low Mn/S ratios and high sulphur content. The incidence under these circumstances is higher for low casting speeds (large cross sections) than for fast casting speeds (small cross sections). Table 2 in Irving and Perkins [88] also indicates that faster casting speeds—even with large cross sections—seem to show a decrease in the appearance of the defects. The quality of the cast slab is sensitive to the type of mould powder used, especially in cases where mould oil is the flux agent [69]. The paper by Brimacombe and

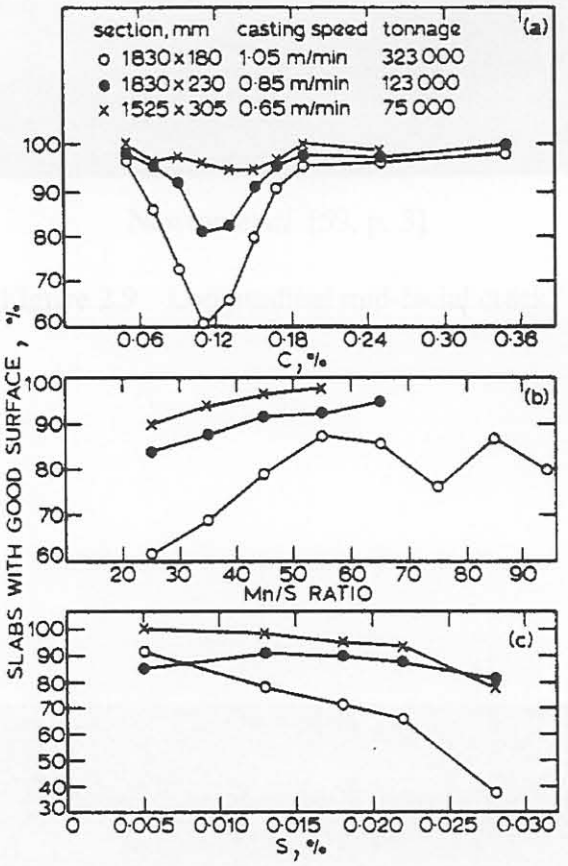

Irving and Perkins [88, p. 108]

Figure 2.8 % carbon , Mn/S ratio and % sulphur versus good slabs (longitudinal facial cracks) in carbon steels.

Samarasekera [50] states that the incidence of these defects are caused by mould taper reversal in billets, high corner gaps (> 0.8mm), high casting speed and steel containing 0.17 to 0.25% carbon, sulphur levels lower than 0.035% and a phosphorus composition higher than 0.035% in carbon steels.

There are two categories, mid-facial (Fig. 2.9) and "near to the corner" (Fig. 2.10) longitudinal facial cracks.

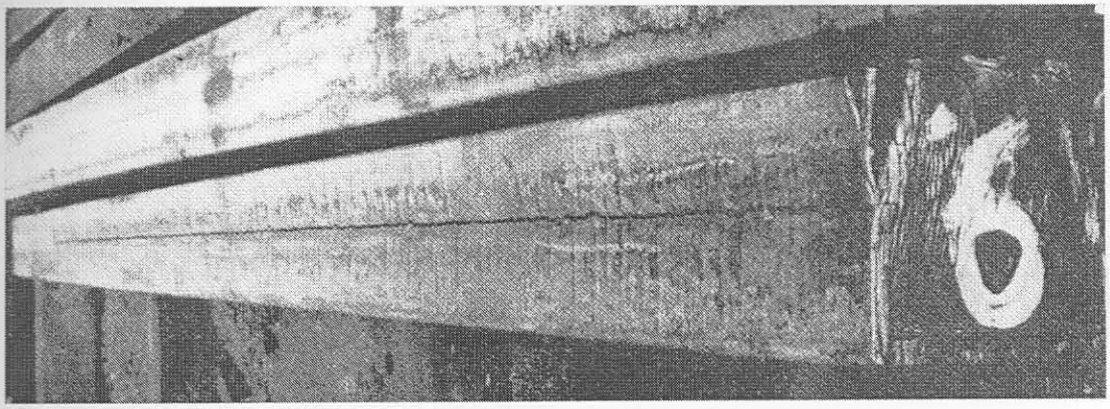

Newton *et al.* [59, p. 3]

Figure 2.9 Longitudinal mid-facial crack.

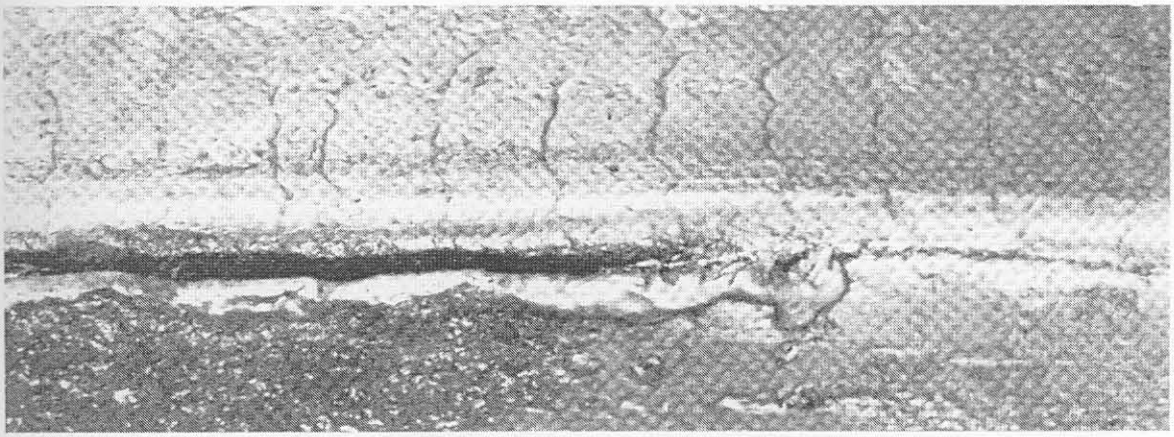

Newton *et al.* [59, p. 4]

Figure 2.10 Longitudinal "Near to the Corner" facial crack.

Discussion The formation of longitudinal cracks in the case of the industrial partner seems to be minimal since the defect occurs on very few slabs.

For the purpose of this thesis, it will be wise then only to consider the formation of longitudinal facial cracks as a whole as described in literature. Based on literature, it seems that facial cracking is more prevalent than corner cracking. The occurrence of facial cracking is due to the following mould conditions:

1. Improper mould design and condition.
2. High teeming (pouring) temperature.
3. Fast or uneven cooling in the mould.
4. Withdrawal speed.
5. Steel composition.
6. Frictional irregularity, *i.e.* wrong taper.
7. Cross sectional size.
8. Mould oscillation.
9. Mould level.

The occurrence of mould level control (point 9) was the only parameter which did not feature in the literature as a probable cause for the occurrence of longitudinal facial cracks, but was investigated anyway. The mould parameters which could indicate the above mentioned abnormal operating conditions are (by point number)

1. Off-line copper mould inspection.
2. Thermocouple measurements.
3. Thermocouple measurements as well as computed longitudinal and transversal gradients. Mould temperature pattern. Average heat flux. Water inlet temperature and flow.
4. Casting speed fluctuations/ abnormalities.
5. Metallurgical evaluation of steel off-line.

6. Evaluation of casting powder.
7. Stroke length, oscillation frequency and negative strip.
8. Mould level and mould level control.

Naturally, the off-line inspected parameters will be obtained too late to be used in a forecasting system.

2.2.1.3 Inclusions (defects 2a & 2b)

The incidence of surface inclusions falls under the category *cleanliness* as described in §2.2.1 on page 14. From the available literature, it seems that inclusions are difficult to detect online because the formation of these defects using abnormal mould parameter perturbations is not discussed.

Newton *et al.* [59] describe inclusions under *entrapped scum* and *carburization*, while the personnel at the industrial partner specifically define their inclusions as *casting powder entrapment* (defect 2a) and *other inclusions* (defect 2b). The term *entrapped scum* is meant to reflect products of de-oxidation or of refractory erosion that are trapped at the meniscus, forming patches at the strand surface, or of slag particles that are entrapped. *Carburization* specifically indicates the localised pickup of carbon from improper lubricating oils or powders (see Fig. 2.11 and also McPherson and McIntosh [89]). This specifically happens

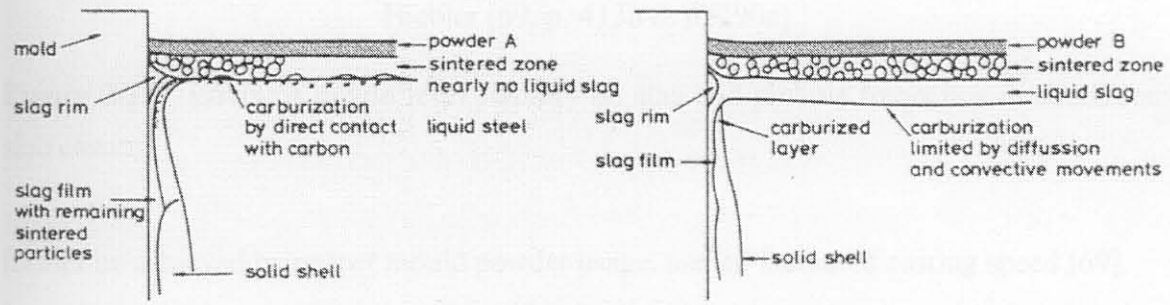

Hiebler [69, p. 405b & p. 284a]

Figure 2.11 Carburization for the case of insufficient (powder A) and sufficient (powder B) liquid slag layer thickness in continuous slab casting of SUS 321 grade.

in low-carbon stainless steels. The defect can commonly only be detected by micro examination or examination of the pickled rolled product. *Casting powder entrapment* is the

inclusion which results specifically from improper powder addition or improper powder type and bad mould level control and can also cause other defects (see §2.2.1.1). *Other inclusions* is understood to describe all other possible inclusions, be it from improper slag outflow in the tundish, refractory de-oxidation or de-oxidation of any non-metallic inclusion in the steel [90].

Due to the low incidence of articles describing the defects under *casting powder entrapment* or *other inclusions*, the available literature found on inclusions in general will be described under one heading.

Hiebler [69] state that a highly stable mould level is the most vital prerequisite in minimising slag inclusion and pinhole occurrence (Fig. 2.12). Also, the minimisation of the defect can

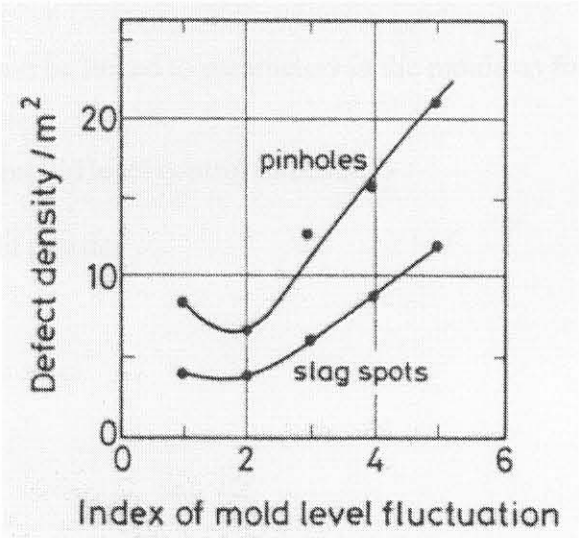

Hiebler [69, p. 413b & p. 290a]

Figure 2.12 Effect of mould level stability on slag and pinhole frequency in continuous slab casting.

further be achieved by proper mould powder usage, and an increased casting speed [69].

The casting powder which is used is in itself responsible for the absorption of other inclusions [91]. This implies that the effect of improper mould powder usage is two-fold. Firstly, the mould powder itself becomes an inclusion and secondly, the mould powder will not absorb other impurities, meaning that inclusions will result. The correct mould powder and mould powder usage are therefore essential as an initial step in the prevention of inclusions[i].

[i] see also Mills, Grieveson, Olusanya, and Bagha [92], Mills [93] and Soares, Fonseca, Neuman, Menezes, Lavinas, and Dweck [94] for detailed discussions on mould powder usage.

The article by Nuri *et al.* [52] states that it is difficult to determine the amount of inclusions by conventional methods such as printing paper analysis[j] when the slab surface roughness increases considerably. This implies that inclusions can be even more difficult to detect when an on-line system such as an optical slab surface inspection system or inspections by humans are used.

From the above discussion, it is clear that inclusions are caused by the following:

1. Bad mould level control.
2. Improper mould powder or mould powder usage.
3. Improper nominal casting speed or casting speed variations.

The above can once again be linked to parameters in the mould as follows:

1. Mould level and mould level control indicator.
2. Analysis of mould powder[k].
3. Casting speed.

2.2.1.4 Sticking

The occurrence of *sticking* or *stickers* was not investigated by the author because the test slabs which were available did not have the defect on any of them (0% occurrence). This is due to the fact that the slabs which did have the defect were probably scrapped. The defect will however be discussed because of its close relation to bleeder defects.

Stickers are generally caused by a hot spot forming at the surface of the strand, which, together with improper mould powder usage, cause the strand to *weld* itself to the copper mould surface. In severe cases, the shell ruptures below the mould causing the molten steel to flow out of the hole in the thinned strand shell. This destructive phenomenon is known as a *break-out*[l]. In less critical situations, the slab skin may repair itself by re-solidification at the mould wall with no sticking so that a *bleeder* occurs (see §2.2.1.5).

[j] A thin layer of *e.g.* gold or sulphur is deposited onto paper. The paper is then adhered to the slab surface where protruding inclusions make imprints on the deposit. The paper is then examined under a scanning electron microscope to investigate the defects.

[k] this is generally not feasible on-line

[l] see *e.g.* Savage and Pritchard [95]

The occurrence of an impending break-out is easily detected by thermocouples arranged as rows down the mould. An increase in thermocouple readings close to the meniscus coupled with an increase in thermocouples further from the meniscus after a period of time is usually an indication of the impending break-out and corrective action such as casting speed reduction can be made [17, 71, 96, 97].

Due to the unavailability of test slabs with the relevant defect, the literature—which is ample—will not be discussed within this thesis.

2.2.1.5 Bleeding (defect 4)

A *bleed* is defined by Newton *et al.* [59, p. 9] as "Exudation of molten metal through a rupture in the skin".

Hiebler [69, p. 285a] states that "Liquid steel may penetrate until re-solidification takes place at the mould wall, *i.e.* , 'bleeding', 'false wall', or 'double skin', and, if steel flow is not stopped, result in a break-out...". The bleeder is thus a "recovered" or re-solidified sticker [98]. Examples of the defect are given in Fig. 2.13 and Fig. 2.14. Kumar, Walker,

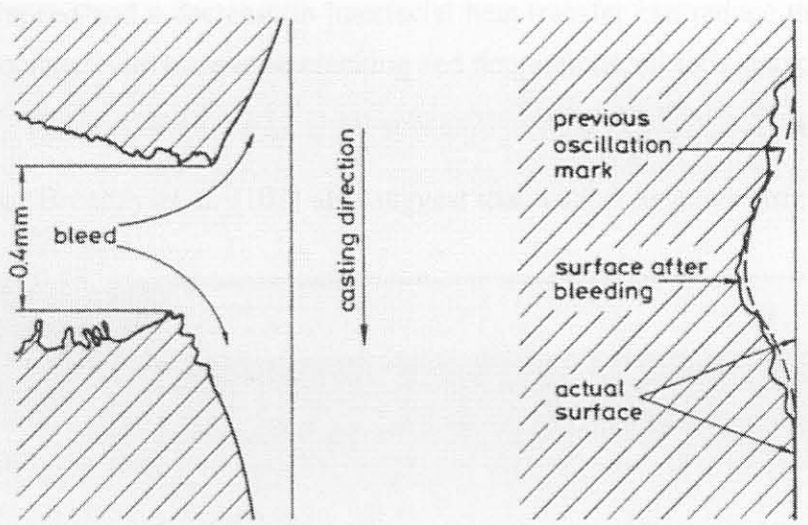

Hiebler [69, p. 406b&p. 285a]

Figure 2.13 Schematic depicting occurrence of *bleeding* in continuous casting

Samarasekera, and Brimacombe [99] determined that uneven oscillation marks are associated with the occurrence of bleeds, especially in the case of billets. The defect occurs close to the meniscus, and due to the relation of the defect to uneven oscillation marks, the defect

is also associated with depressions. The authors further say that the occurrence of the defect can be detected by periodic decreases (known as *valleys*) in the thermocouple readings.

2.2.1.6 Oscillation marks (defects 5a & 5b)

Oscillation marks are caused by the oscillating action of the mould. The defect is a *shape* problem as defined under point 4 in §2.2.1. An example of an oscillation mark is given in Fig. 2.15, and the formation mechanism is shown by Bobadilla, Jolivet, Lamant, and Larrecq [100] in Fig. 2.16. The defect is usually "... separated by a distance related to the amount the product has ascended in one cycle of the reciprocation" in the longitudinal direction [59, p. 14]. The heavy/deep oscillation mark can lead to *skin drag*, characterised by *longitudinal displacement* of part or parts of the reciprocation marks. This is assumed to indicate an uneven oscillation mark.

The defect is almost always present to some degree on the surface of the strand. The oscillation marks are sometimes due to cyclic rupturing and re-welding of the strand surface [69]. A long "time of heal" is required to ensure that the defect is a minimum. This can be achieved by short strokes and high cycle frequency (short negative strip time). Also, high superheat and/or casting speed and a decrease in interfacial heat transfer can reduce the defect. The defects are associated with transverse cracking and depressions, surface cracks and pinholes [101].

Schrewe [1] and Brendzy *et al.* [101] also suggest that a short negative strip time together

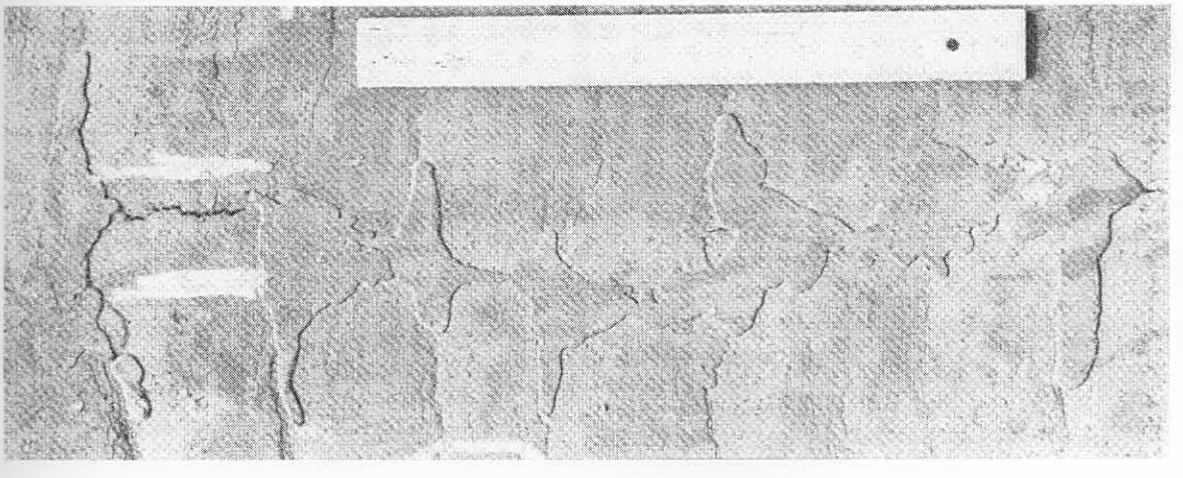

Newton *et al.* [59, p. 9]

Figure 2.14 Occurrence of a bleed in a continuously cast slab.

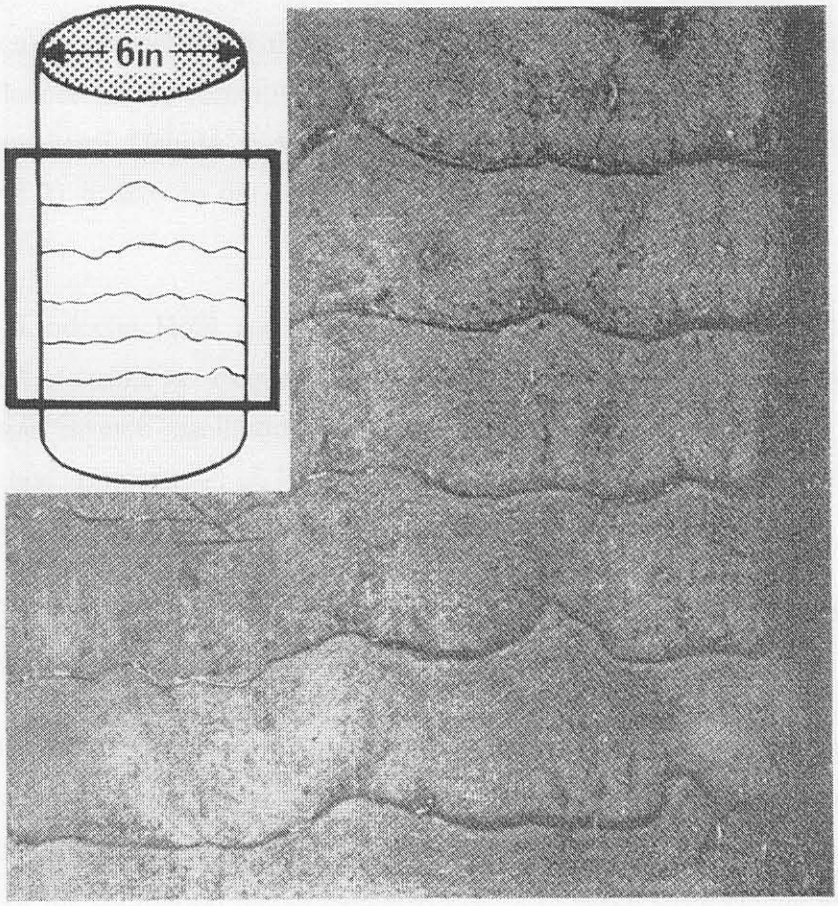

Newton *et al.* [59, p. 14]

Figure 2.15 Oscillation marks on a round.

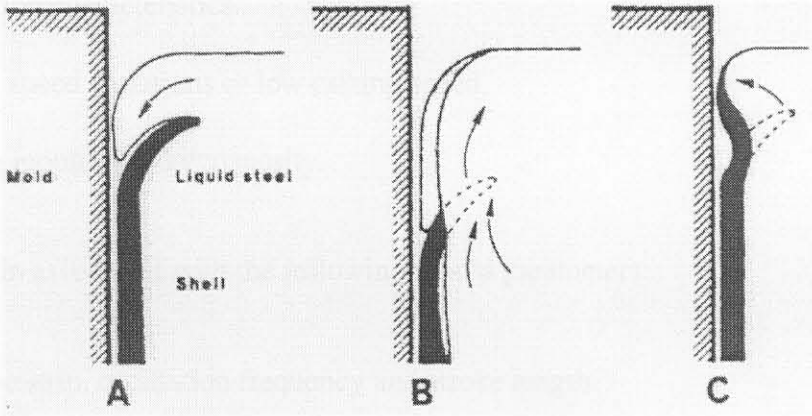

Bobadilla *et al.* [100, p. 277]

Figure 2.16 Three main mechanisms for the formation of oscillation marks in billets: A. overflow; B. overflow + remelting; C. meniscus bent back.

with carbon content control in the steel decreases the occurrence of the defect. The *stiffness* of the meniscus is controlled by the composition of the steel and can therefore also have a positive influence on the formation of oscillation marks. In contrast, Suzuki, Mizukami, Kitagawa, Kawakami, Uchida, and Komatsu [102] state that the 1) shape of the oscillation frequency, and 2) stroke, do not seem to have a remarkable effect on the severity of the oscillation marks.

The article by Lindorfer, Hödl, and Mörwald [103] shows that the conventional mould oscillation method[m] of stroke *vs.* frequency as a function of casting speed requires more mould powder than the "inverse" oscillation method[n]. The industrial partner currently uses the conventional method. Lindorfer *et al.* [103] also state that in their study, they could not find any relation between negative strip time and oscillation mark depth.

Szekeres [65] also states that the oscillation mark is a region where transverse cracking could occur (see also §2.2.1.1).

The effects of casting speed and negative strip time on oscillation mark depth for different carbon levels can be found in the articles by [91, 104]. High casting speed decreases the severity of the defect. A short negative strip time seems to have the same type of effect on the depth of the oscillation marks (see also Fig. 2.17 taken from Hague and Parlington [105]). The oscillation marks can be divided into deep oscillation marks (defect 5a) and uneven oscillation marks (defect 5b), but no literature was found to describe each defect separately. The main causes of the defects are

1. Oscillation characteristics.
2. Casting speed variations or low casting speed.
3. Varying mould powder viscosity.

These are again associated with the following mould parameters:

1. Negative strip, oscillation frequency and stroke length.
2. Casting speed.
3. In-mould flux viscosity.

[m] stroke remains constant and frequency increases with increasing casting speed
[n] stroke increases as frequency decreases with increasing casting speed

2.2.1.7 Stopmarks (defect 6)

The stopmarks defect was not found in the literature, but occurs when there is an abrupt slow-down in the casting procedure. A stopmark is defined as "a band-like pattern around the full perimeter of an extruded section and perpendicular to its length. A stop mark occurs whenever the extrusion process is suspended" [106].

Though no literature was found on the subject, stopmarks will be investigated, as they occur on slabs cast by the industrial partner.

2.2.1.8 Depressions (defect 8)

Depressions are one of the most frequently occurring surface defects at the industrial partner.

Depressions fall under point 4 in §2.2.1. They are divided into transversal and longitudinal depressions. Longitudinal depressions are linked to longitudinal cracks and are narrow sunken areas along the length of the strand. Transversal depressions are caused due to a lack of contact to the mould wall and show up as a sunken area along the transversal section of the

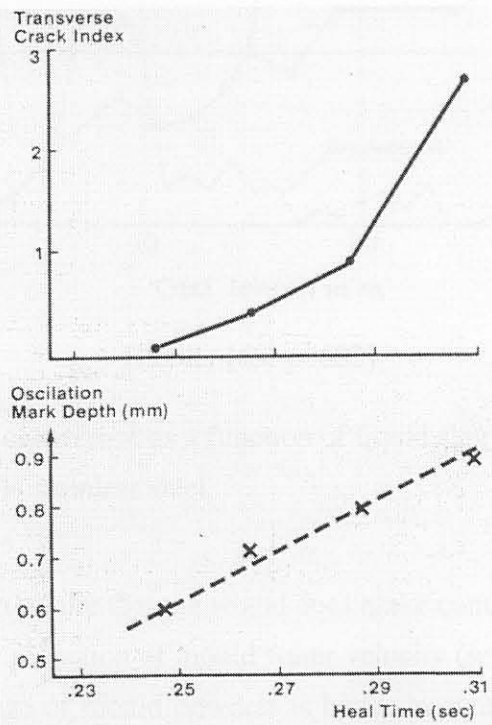

Hague and Parlington [105, p. 37]

Figure 2.17 Effect of heal time on oscillation mark depth.

strand. This lack of contact is generally due to improper mould powder usage or too rapid cooling. The defect can lead to transversal facial cracking (§2.2.1.1), bleeding (§2.2.1.5) or break-outs (§2.2.1.4) [59].

Chandra, Brimacombe, and Samarasekera [107] state that mould taper reversal and mould distortion as well as carbon content of the steel could influence the occurrence of the defect.

The first slab cast also has the most depressions [104, 108, 109] while slabs that follow are less prone to the defect.

Transversal depressions Hiebler [69] state that transversal depressions result from a non-uniformity (unevenness) in the shell growth, and that the effect of carbon is quintessential in the formation thereof. The effect of mould powder used shows from Fig. 2.18 that depression formation decreases as the molten slag layer increases. This once again shows that proper usage of mould powders is very important for the prevention of several defects. A remedy

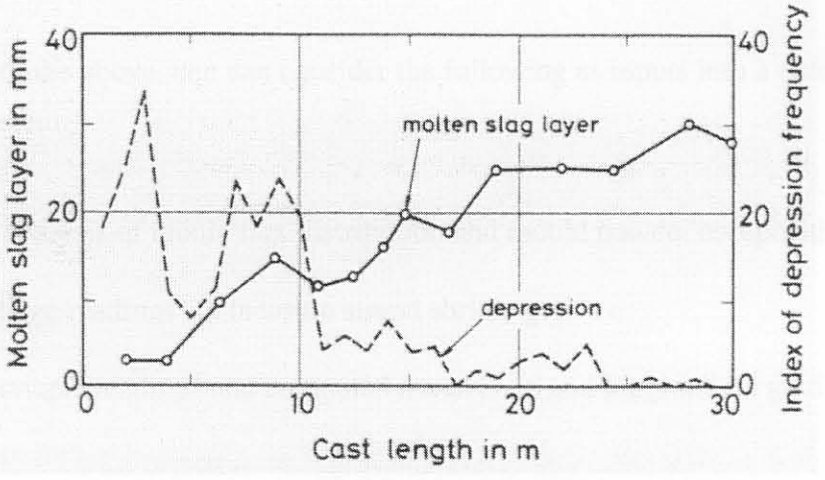

Hiebler [69, p. 603]

Figure 2.18 Depression occurrence as a function of liquid slag layer thickness in continuous slab casting of SUS 304 stainless steel.

is the use of *soft cooling* to ensure that the strand does make contact with the mould surface. This could be done by the reduction of mould water velocity (see *e.g.* Wolf [110] and Wolf [111]), but the proper usage of mould powders is better in controlling mould-slab surface contact [69].

Longitudinal depressions Longitudinal depressions are very closely associated to longitudinal cracking, and hence their causes are similar. See §2.2.1.2. Longitudinal off-corner depressions occur due to improper usage of mould powder and too rapid cooling together with improper mould taper at the corner of the slab so that the strand shrinks away from the mould [91].

Discussion The occurrence of the defect will not be treated under the two sub-depression headings. The formation of the defects are generally due to:

1. Mould powder.
2. Mould taper and distortion.
3. Too rapid cooling in the mould or secondary cooling zone.
4. Mould-shell contact.

Associated with the above, one can consider the following as inputs into a defect prediction and control system:

1. On-line analysis of mould flux distribution and mould powder composition.
2. Strain gauge readings[o] to measure strand shrinkage.
3. Thermocouple readings and computed *transversal* and longitudinal gradients.

2.2.1.9 Defect summary

Table 2.1 shows a summary of the general causes for defects based on the literature in the previous sections. It is interesting to note that most authors do not explicitly link mould level to defects, with only longitudinal cracking and inclusions being explicitly mentioned. Contrary to this, researchers address the mould level control problem as the most important single factor that contributes to surface defects (see §2.2.1). However, every considered defect is linked by the literature to some variable in the mould. The mould is therefore quintessential in the formation of defects.

[o]not use at the industrial partner

Table 2.1 Summary of causes for defect occurrence based on the literature review. An "•" indicates that the variable in question has an influence on the defect. Bold variables can be measured on-line.

	Transversal cracking (1a)	Longitudinal cracking (1b)	Inclusions (2a & 2b)	Bleeders (4)	Oscillation marks (5a & 5b)	Stopmarks (6)	Depressions (8)
Mould level		•	•				
Mould powder	•	•	•		•		•
Mould friction	•						
Mould taper	•	•					•
Mould oscillation	•	•	•		•		
Casting speed	•	•	•		•	•	
Temperature	•	•		•	•		•
Composition	•	•			•		•
Tundish			•				
Superheat					•		
Bending	•						

Another important point to note from the literature is that strand temperature plays a role in all the defects except inclusions and stopmarks. This suggests that temperature is a very valuable variable to use in any type of defect predictor.

Mould powder and mould friction are very closely related and are difficult to measure on-line, as is the taper of the mould [112].

Composition is a factor which does not change dynamically during casting. However, the composition of some steels is a factor that is influential in the formation of certain defects.

Measurement of inclusion outflow in the tundish is also difficult to quantify on-line and superheat is generally not measured at regular intervals (see *e.g.* Ozgu [112]).

2.2.1.10 Defect models

Some literature exists on the modelling of defects. Chipalo, Gilchrist, and Smith [113] and Gilchrist and Smith [114] show results of a finite element technique to model the *propagation* of cracks. The actual model is not presented and no relation to casting variables are given.

Kametani [115] gives a method to determine the frequency distributions of longitudinal crack length and frequency. Again there is no relation to casting variables. Hunter *et al.* [78] speak of a prediction algorithm based on a exponential smoothing technique which uses a non-weighted average of previous temperature values to predict temperature in the mould, and according to the difference between the actual and predicted temperatures decide whether a longitudinal crack will occur or not. The model is not presented and accuracies of up to 80% for longitudinal cracks longer than 400mm have been achieved. Hunter *et al.* [18] use artificial neural networks to predict longitudinal depressions and cracks. For stainless steel, they predict 61.5% of the longitudinal cracks accurately.

De Santis and Ferretti [116] mathematically describe the path that an inclusion takes from the tundish through the SEN into the liquid pool. The use of the model to predict *surface* inclusions is not described. Bouris and Bergeles [117] describe a model to *track* an inclusion which travels to the slag-steel interface, thus being able to remain there to be trapped at the surface to form a surface inclusion. The application of the model to predict when inclusions will occur at the surface, based on plant parameters, is not made. Sawada, Takeuchi, Tanaka, Okazawa, and Shigematsu [118] also describe a model to track inclusions inside the mould from the SEN output, but do not explain how the model can be used to predict surface inclusions based on process parameters, Yamada, Fukumoto, Tanaka, Matsumiya, and Wajima

[119] describe the size distribution and amount of particles inside the liquid pool, but do not give the actual model nor its relationship to casting parameters. McDavid and Thomas [120] give a model to determine the behaviour of the slag/flux at the meniscus, sometimes causing a concentration of flux near the surface which may cause quality problems. Bailey, Chow, Cross, Fryer, and Pericleous [121] give detailed models and model simulations for inclusions and porosity in ingot-type moulds. This has however not been extended to continuous casting.

Henriksen, Jensen, and Mortensen [122] describe a simulation package for bleeder modelling, but do not show the model in the paper.

King, Lacey, Please, Willmott, and Zoryk [123] present a model to describe the formation of oscillation marks but state that only initial results of the model are available. Sha, Diedrichs, and Schwerdtfeger [124] present a model to describe the behaviour at the liquid/liquid interface of steel and slag during oscillation motion. This theory can possibly be used to derive a model for oscillation mark formation.

Thomas, Moitra, and Zhu [125] and Thomas, Moitra, and McDavid [126] describe the use of a coupled finite element model to model the thermo-mechanical behaviour of a thin slice as it moves through the caster. This model is then applied to longitudinal depression investigations. The model is however not given.

Thomas, Lui, and Ho [127] give a model for transversal depressions, and describe their effect of heat transfer in the mould. The authors state that "These results should be useful in the difficult task of interpreting transient mold thermocouple signals for on-line quality monitoring".

Gugliermina, Codur, and Cardouat [128] discuss models to predict defects but do not state what type of models are used, nor give results of the accuracy of the models. The same can be said of the paper by Irving [129].

Short, Barber, Normanton, Patrick, and York [130] discuss models to predict surface temperature in the mould, but do not present the model and do not indicate whether the outflow from the SEN is included in the model.

Some other types of models may aid in an eventual first principles model for defects. Royzman [131] gives a model describing friction in the mould. O'Malley [132] gives a description of transient temperature behaviour in the mould. Matsumiya, Ohashi, and Abe [133] give a model of thermal stress that result from the bending and unbending of the strand. Li and Ruan

[134] give a model of thermal stresses and temperature during aluminium casting. Lamant, Larrecq, Birat, Hensgen, Weber, and Dhuyvetter [135] give a model of slab bulging. Harste, Deisinger, Steinert, and Tacke [136] give a thermal and mechanical model of the entire casting process. Das and Sarkar [137] give a control volume approach to thermal modelling in continuous casting. Breslin, Hetherington, and Walker [138] speak of models for high temperature materials, air gap formation, ferro-static loading, flux heat transfer and mould taper, but do not actually give the models. Lastly, Camisani-Calzolari [35] gives a thermal model and optimisation procedure for the secondary cooling zone.

The preceding explanation of literature described the causes of defects in the continuous casting process. Table 2.1 gives a summary of the causes of the defects. First principle models of defect propagation and prediction have been found in literature, but do not give the mathematical models in the papers or are not suitable for predicting defects based on process variables. The derivation of a first principle model falls outside the scope of this work.

2.2.2 Goodness-of-fit tests

In certain situations such as encountered in this thesis, it is necessary to perform a statistical hypothesis test that determines whether an independent random variable, X_1 belongs to the same distribution as another random variable, X_2. Such tests are known as goodness-of-fit tests [139].

Goodness-of-fit tests determine whether a sample of values (which make up an empirical distribution) come from a given theoretical distribution. With enough data, the distribution of *e.g.* X_2 can be thought of as the "theoretical distribution". X_1 can then be seen as the "empirical distribution". The hypothesis test then determines whether the empirical distribution (distribution of X_1) comes from the theoretical distribution (distribution of X_2). X_1 can be the mean value of a parameter in the mould on slabs where defects occur, and X_2 can be the mean value of the same parameter on slabs where defects do not occur. In such a case, if the distributions of X_1 and X_2 are similar, then that parameter may not have any effect on the formation of the defects.

One of the oldest of these tests is the χ^2-test [140], but more recent tests such as the Kolmogorov-Smirnov and Anderson-Darling tests are more accurate in the outcome of the hypothesis decision [140], and will be used in the remainder.

2.2.2.1 Background

Assume that X is a statistically independent random variable with a probability density function given by $f(x)$, and its cumulative density function is given by

$$F(x) = \int_{-\infty}^{x} f(x)dx. \tag{2.1}$$

The cumulative density function can be directly approximated from the observation values of the sample. Assume that x_i denotes the i-th observation of the random variable X, and that there are n observations. The probability density function can then be *approximated* by a train of Dirac-delta ($\delta(x - x_i)$) functions each with strength $1/n$. The approximation to the probability density function is then

$$f(x) \approx \frac{1}{n}\sum_{i=1}^{n}\delta(x - x_i), \tag{2.2}$$

when there are n observations. To approximate the cumulative density function from the above train of Dirac-delta functions from the probability density function, one can go ahead as follows

$$\begin{aligned} F(x) &= \int_{-\infty}^{x} f(x)dx, && (2.3)\\ &\approx \frac{1}{n}\int_{-\infty}^{x}\left(\sum_{i=1}^{n}\delta(x - x_i)\right)dx, && (2.4)\\ &= \frac{1}{n}\sum_{i=1}^{n}\left(\int_{-\infty}^{x}\delta(x - x_i)dx\right), && (2.5)\\ &= \frac{1}{n}\sum_{i=1}^{n}u(x - x_i). && (2.6) \end{aligned}$$

$u(x - x_i)$ is the unit step function defined by

$$u(x - x_0) = \begin{cases} 1 & x \geq x_0 \\ 0 & x < 0 \end{cases}. \tag{2.7}$$

This idea is illustrated in Fig. 2.19.

2.2.2.2 Kolmogorov-Smirnov test

The first of the goodness-of-fit tests used in this thesis is known as the Kolmogorov-Smirnov test.

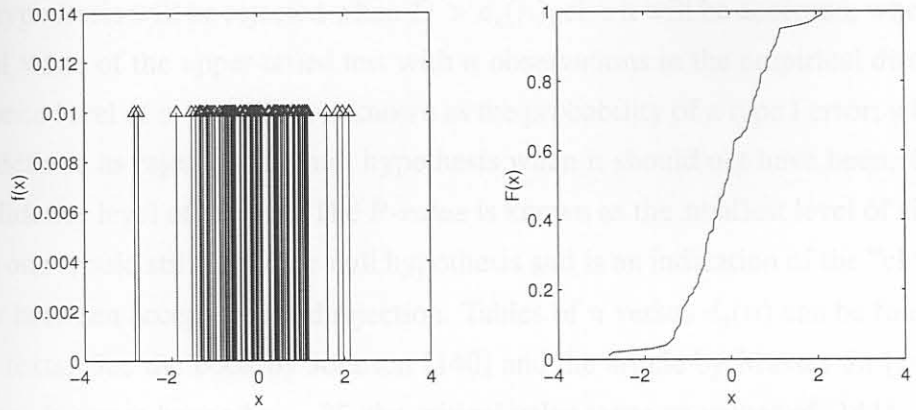

Figure 2.19 Illustration of the effect of using the pulse train probability density function $f(x)$ to determine the cumulative density function $F(x)$ of the random variable X.

Assume that the theoretical cumulative density function is given by $F(x)$ and that the empirically determined distribution is given by $F_n(x)$.

Note that the theoretical distribution is always based on a continuous distribution. The theoretical distribution is usually not continuous, but if there are many observations, the discrete distribution can approximate the continuous distribution approximately *i.e.* the discrete distribution becomes an accurate estimator of the continuous distribution.

The Kolmogorov-Smirnov statistic is given by Massey Jr. [141] as

$$D = max\left|F_n(x) - F(x)\right|, \quad \forall x; \tag{2.8}$$

that is, it is the maximum difference (evaluated at all points of x) of the theoretical and empirical distributions. The null hypothesis (H_0) states that the empirical observations belong to the theoretical distribution. The alternative hypothesis (H_1) states that the two distributions do not belong to the same distribution, *i.e.* they are different.

Rejection of the null hypothesis is a *strong conclusion* and acceptance of the null hypothesis is usually a *weak conclusion*. In the case of a weak conclusion, it is advisable to check the probability of making a type II error (β). A type II error is defined as accepting a null hypothesis when the null hypothesis should not have been accepted and is related to the

power of the test through $\mathcal{P} = 1 - \beta$. The Kolmogorov-Smirnov test has weak power (*i.e.* β is large) [140].

The null hypothesis will be rejected when $D > d_c(n)$, else it will be accepted, where $d_c(n)$ is the critical value of the upper-tailed test with n observations in the empirical distribution at a significance level of $\alpha = 0.05$. α is known as the probability of a type I error; where a type I error is defined as rejecting the null hypothesis when it should not have been. $\mathcal{C} = 1 - \alpha$ is the confidence level of the test. The *P-value* is known as the smallest level of significance for which one would still reject the null hypothesis and is an indication of the "closeness" of the border between acceptance and rejection. Tables of n versus $d_c(n)$ can be found in most statistical texts. See the book by Johnson [140] and the article by Massey Jr. [141]. When observations increase beyond $n = 35$, the critical value takes on values of [141]

$$d_c(n) = \frac{1.36}{\sqrt{n}}, \quad \forall n > 35. \tag{2.9}$$

Also, with $\mathcal{P} = 0.95$ and $\mathcal{C} = 0.95$, the maximum detectable difference of the cumulative distributions is given by $\Delta = 2.2/\sqrt{n}$ [141].

2.2.2.3 Anderson-Darling test

As noted in §2.2.2.2, the Kolmogorov-Smirnov test has weak power. It does not have a great ability to detect situations when there is a significant difference between the empirical and theoretical distributions. Furthermore, this deficit is usually found in the tails of a Normal or near-Normal probability distribution. Another test emerged to counter this problem, and though well documented, is not as well known. The test is known as the Anderson-Darling test for goodness-of-fit [140, 142].

The test statistic is a normalized version of the Kolmogorov-Smirnov test and is given by

$$A^2 = \int_{-\infty}^{\infty} \frac{F_n(x) - F(x)}{F(x)(1 - F(x))} dx. \tag{2.10}$$

The computation of the statistic seems complex, but it can be shown that [140]

$$A^2 = -\frac{\sum_{i=1}^{n}(2i-1)[\ln \mathrm{u}_i + \ln(1 - \mathrm{u}_{n+1-i})]}{n} - n, \tag{2.11}$$

where $\mathrm{u}_i = F(x_{(i)})$ is the value of the theoretical cumulative distribution at the i-th largest empirical observation.

The null hypothesis is the same as with the Kolmogorov-Smirnov test. The null hypothesis will be rejected when the statistic is larger than a critical value in the upper-tailed test. This

value is reported by Johnson [140] as $a_c^2 = 2.492$ with $\mathcal{C} = 0.95$ for normal or near-normal distributions. This means that the null hypothesis will be rejected when $A^2 > 2.492$ to strongly conclude that the empirical distribution is not from the theoretical distribution.

Generally, fewer than 10 observations from the empirical distribution can give unreliable results and more than 40 samples are rarely used in the test [139]. The P-value and power of the test is generally distribution specific, and will thus not be considered here.

The statistical tests to determine whether an empirical distribution forms part of a theoretical distribution was described. Probably, the most accurate tests of this type of goodness-of-fit tests are the Kolmogorov-Smirnov and Anderson-Darling tests. The Kolmogorov-Smirnov test has higher accuracy than the Anderson-Darling test at low sample sizes but is weak in the tails of the distribution. The Anderson-Darling test has high accuracy compared to the Kolmogorov-Smirnov test over the whole distribution but is only truly valid for sample sizes between 10 and 40. For these reasons, both tests can be used when goodness-of-fit tests are required and results can be interpreted accordingly. Another example where statistics are used can be found in the paper by Peters, Link, and Heckenthaler [143] who use statistical methods in the form of multivariate analysis of variance (ANOVA) to find plant-wide dependencies of quality on process variables, but who do not give any results.

2.2.3 Correlation

The term correlation refers to that inference where one tries to determine whether a strong linear relation exists between two random variables. When there is weak correlation, the two random variables, X and Y are not necessarily independent from each other, but may have a strong non-linear relation [144].

This technique can be used to determine whether there are strong linear relations between different inputs. For example, Ikäheimonen, Leiviskä, Russka, and Matkala [145] show how correlation can be used to find the relation between nozzle clogging in the mould and process parameters.

The basic correlation analysis is performed using the correlation coefficient (normalized covariance), and is given by [140]

$$\rho_{XY} = \frac{S_{xy}}{\sqrt{S_{xx}S_{yy}}}, \tag{2.12}$$

where

$$S_{xx} = \sum_{i=1}^{n} (x_i - \bar{x})^2 , \tag{2.13}$$

$$S_{yy} = \sum_{i=1}^{n} (y_i - \bar{y})^2 , \tag{2.14}$$

$$S_{xy} = \sum_{i=1}^{n} (x_i - \bar{x})(y_i - \bar{y}) . \tag{2.15}$$

$\bar{x}$ is the mean value of the random variable X, and x_i is a sample from X. The same can be said about Y. When $|\rho_{XY}| = 1$, there is a perfect linear relationship between X and Y. When $0.75 < |\rho_{XY}| < 1$, there is a strong linear relationship between X and Y *etc.*

2.2.4 Auto regression with exogenous input

This section briefly describes the auto regression with exogenous input (ARX) algorithm and how the model information matrices are calculated (see *e.g.* Ljung [146] for an in depth discussion on this subject.). Firstly, let an $\mathbb{R}^{m\times 1}$ input vector be defined as follows:

$$\mathbf{u}[nT] = \begin{bmatrix} u_1[nT] \\ u_2[nT] \\ \vdots \\ u_m[nT] \end{bmatrix} , \tag{2.16}$$

where $u_i[nT]$ is the i-th input sampled every $t = nT$ seconds at a specific discrete-time described by $n = 0, 1, 2, \ldots, N-1$. Further, define an $\mathbb{R}^{p\times 1}$ output vector as follows:

$$\mathbf{y}[nT] = \begin{bmatrix} y_1[nT] \\ y_2[nT] \\ \vdots \\ y_p[nT] \end{bmatrix} , \tag{2.17}$$

where $y_j[nT]$ is the j-th output at every $t = nT$ seconds at a specific discrete-time described by $n = 0, 1, 2, \ldots, N-1$. The ARX model can then be written as

$$\begin{aligned} \mathbf{A}_0\mathbf{y}[nT] \;+\; & \mathbf{A}_1\mathbf{y}[(n-1)T] + \mathbf{A}_2\mathbf{y}[(n-2)T] + \cdots + \mathbf{A}_{n_a}\mathbf{y}[(n-n_a)T] = \\ \mathbf{B}_0\mathbf{u}[nT] \;+\; & \mathbf{B}_1\mathbf{u}[(n-1)T] + \mathbf{B}_2\mathbf{u}[(n-2)T] + \cdots + \mathbf{B}_{n_b-1}\mathbf{u}[(n-n_b+1)T]. \end{aligned} \tag{2.18}$$

In this realization $\mathbf{A}_0$ is an identity matrix because it is assumed that no outputs influence other outputs at the current discrete-time step. The matrices, $\mathbf{A}_v \in \mathbb{R}^{p\times p}$ are related to the

time-shifted outputs and are defined by

$$\mathbf{A}_v = \begin{bmatrix} a_{1,1}^{(v)} & a_{1,2}^{(v)} & \cdots & a_{1,p}^{(v)} \\ a_{2,1}^{(v)} & a_{2,2}^{(v)} & \cdots & a_{2,p}^{(v)} \\ \vdots & \vdots & \ddots & \vdots \\ a_{p,1}^{(v)} & a_{p,2}^{(v)} & \cdots & a_{p,p}^{(v)} \end{bmatrix} \quad \forall \quad v = 0, 1, 2, \ldots, n_a. \tag{2.19}$$

The $a_{:,:}^{v}$ are constants which ultimately define the output part of the model. Usually, these matrices are diagonal which implies that there is no feedback *i.e.* no outputs influence other outputs directly.

Similarly, the matrices, $\mathbf{B}_w \in \mathbb{R}^{p \times m}$ are related to the time-shifted inputs and are defined by

$$\mathbf{B}_w = \begin{bmatrix} b_{1,1}^{(w)} & b_{1,2}^{(w)} & \cdots & b_{1,m}^{(w)} \\ b_{2,1}^{(w)} & b_{2,2}^{(w)} & \cdots & b_{2,m}^{(w)} \\ \vdots & \vdots & \ddots & \vdots \\ b_{p,1}^{(w)} & b_{p,2}^{(w)} & \cdots & b_{p,m}^{(w)} \end{bmatrix} \quad \forall \quad w = 0, 1, 2, \ldots, n_b - 1. \tag{2.20}$$

The $b_{:,:}^{w}$ are constants which ultimately define the input part of the model.

One can now define the $\mathbb{R}^{pn_a + mn_b \times p}$ system matrix as

$$\Theta = \begin{bmatrix} \mathbf{A}_1 & \cdots & \mathbf{A}_{n_a} & \mathbf{B}_0 & \mathbf{B}_1 & \cdots & \mathbf{B}_{n_b-1} \end{bmatrix}^\top, \tag{2.21}$$

and the data vector of $\mathbb{R}^{pn_a + mn_b \times 1}$ as

$$\psi[nT] = \begin{bmatrix} -\mathbf{y}[(n-1)T] \\ -\mathbf{y}[(n-2)T] \\ \vdots \\ -\mathbf{y}[(n-n_a)T] \\ \mathbf{u}[nT] \\ \mathbf{u}[(n-1)T] \\ \mathbf{u}[(n-2)T] \\ \vdots \\ \mathbf{u}[(n-n_b+1)T] \end{bmatrix}. \tag{2.22}$$

The system in Eq. 2.18 can then be written as

$$\mathbf{y}[nT] = \Theta^\top \psi[nT]. \tag{2.23}$$

However, the system in Eq. 2.23 will give a predictor based on only one time sample. The result is that the predictor will only be able to detect a situation which is exactly similar to the

training set of data. To compensate for this, one needs several samples to define an adequate model. This can be achieved by lumping the different time instance data together and thus forming a predictor which is averaged about all the data. This, in effect, eliminates the time dimension of the system. Thus, define an output $\mathbb{R}^{p\times N}$ matrix as follows:

$$\mathbf{Y}[nT] = \begin{bmatrix} \mathbf{y}[nT] & \mathbf{y}[(n+1)T] & \mathbf{y}[(n+2)T] & \cdots & \mathbf{y}[(n+N-1)T] \end{bmatrix}, \tag{2.24}$$

and a $\mathbb{R}^{pn_a+mn_b\times N}$ data matrix as follows:

$$\mathbf{\Psi}[nT] = \begin{bmatrix} \boldsymbol{\psi}[nT] & \boldsymbol{\psi}[(n+1)T] & \boldsymbol{\psi}[(n+2)T] & \cdots & \boldsymbol{\psi}[(n+N-1)T] \end{bmatrix}. \tag{2.25}$$

The system can now be written as

$$\mathbf{Y}[nT] = \mathbf{\Theta}^\top \mathbf{\Psi}[nT]. \tag{2.26}$$

An estimate of the outputs will be given by

$$\hat{\mathbf{Y}}[nT, \hat{\mathbf{\Theta}}] = \hat{\mathbf{\Theta}}^\top \mathbf{\Psi}[nT], \tag{2.27}$$

where $\hat{\mathbf{Y}}[nT, \hat{\mathbf{\Theta}}]$ is the estimated values of the outputs, based on some specific $\mathbf{\Theta}$, and $\mathbf{\Psi}[nT]$ are past values of the outputs and inputs.

To determine an estimate of the predictor ($\hat{\mathbf{\Theta}}$), a least squares approach can be used. Define the error between the true and predicted outputs as follows

$$\mathbf{\Xi}[nT, \hat{\mathbf{\Theta}}] = \mathbf{Y}[nT] - \hat{\mathbf{Y}}[nT, \hat{\mathbf{\Theta}}], \tag{2.28}$$

for a particular set of time samples. Define the least square error of $\mathbf{\Xi}$ as

$$V(\hat{\mathbf{\Theta}}) = \frac{1}{2}\|\mathbf{\Xi}[nT, \hat{\mathbf{\Theta}}]\|_F^2 = \frac{1}{2}\mathrm{tr}\left(\mathbf{\Xi}[nT, \hat{\mathbf{\Theta}}]^\top \mathbf{\Xi}[nT, \hat{\mathbf{\Theta}}]\right) \tag{2.29}$$

$$= \frac{1}{2}\mathrm{tr}\left(\left[\mathbf{Y}[nT] - \hat{\mathbf{Y}}[nT, \hat{\mathbf{\Theta}}]\right]^\top \left[\mathbf{Y}[nT] - \hat{\mathbf{Y}}[nT, \hat{\mathbf{\Theta}}]\right]\right) \tag{2.30}$$

$$= \frac{1}{2}\mathrm{tr}\left(\left[\mathbf{Y}[nT] - \hat{\mathbf{\Theta}}^\top \mathbf{\Psi}[nT]\right]^\top \left[\mathbf{Y}[nT] - \hat{\mathbf{\Theta}}^\top \mathbf{\Psi}[nT]\right]\right), \tag{2.31}$$

and $\|\boldsymbol{X}\|_F^2$ is the Frobenius norm of $\mathbf{X}$. To determine the minimum least square error, the above expression is differentiated to $\hat{\mathbf{\Theta}}$ and set equal to zero to give the least squares predictor, based on plant input/output data.

$$\left.\frac{\partial V(\hat{\mathbf{\Theta}})}{\partial \hat{\mathbf{\Theta}}}\right|_{\mathbf{\Theta}\to\hat{\mathbf{\Theta}}} = \mathbf{\Psi}[nT]\mathbf{\Psi}[nT]^\top \hat{\mathbf{\Theta}} - \mathbf{\Psi}[nT]\mathbf{Y}[nT]^\top = \mathbf{0}. \tag{2.32}$$

This gives the least square output error predictor

$$\hat{\mathbf{\Theta}} = \left[\mathbf{\Psi}[nT]\mathbf{\Psi}[nT]^\top\right]^{-1} \mathbf{\Psi}[nT]\mathbf{Y}[nT]^\top. \tag{2.33}$$

The least square predictor is then implemented by

$$\hat{\mathbf{y}}_{LS}[nT] = \hat{\Theta}^{\top} \psi^*[nT], \tag{2.34}$$

where $\psi^*[nT]$ is the input consisting of the past predicted outputs and the past and present inputs, since no step-ahead prediction is used:

$$\psi^*[nT] = \begin{bmatrix} -\hat{\mathbf{y}}_{LS}[(n-1)T] \\ -\hat{\mathbf{y}}_{LS}[(n-2)T] \\ \cdots \\ -\hat{\mathbf{y}}_{LS}[(n-n_a)T] \\ \mathbf{u}[nT] \\ \mathbf{u}[(n-1)T] \\ \mathbf{u}[(n-2)T] \\ \cdots \\ \mathbf{u}[(n-n_b+1)T] \end{bmatrix}. \tag{2.35}$$

The preceding discussion has been given to make the terminology clear. To solve the ARX models, the MATLAB system identification toolbox [147] was used.

2.2.5 Linear quadratic tracker at steady-state (LQTSS)

The linear quadratic regulator (LQR) is an optimal state feedback controller used to regulate the state of a system to compensate for disturbances in the system state. The LQR drives the state of a system to zero by manipulation of the inputs.

It is often not the intension to drive the state of the system to zero, but rather to allow the system output to track a reference input [148]. This can be achieved by a linear quadratic tracker (LQT). The LQT is essentially an LQR with a feed-forward path added to the control scheme [148].

The LQT is generated by optimizing a performance index subject to the constraints that the system dynamics impose. A control law, based on the current state of the system as well as future knowledge of the desired reference trajectory is implemented in a feed-forward-feedback scheme. These ideas will be discussed here.

2.2.5.1 State-space model

A multi-input, multi-output (MIMO), linear, time-invariant (LTI) system can be described in state-space by

$$\dot{\mathbf{x}}(t) = \mathbf{A}\mathbf{x}(t) + \mathbf{B}\mathbf{u}(t), \quad \mathbf{x}(t_0) = \mathbf{x}_0 \tag{2.36}$$

$$\mathbf{y}(t) = \mathbf{C}\mathbf{x}(t) + \mathbf{D}\mathbf{u}(t), \tag{2.37}$$

where $\mathbf{x} \in \mathbb{R}^{N_x \times 1}$ is a vector of the N_x states of the system, $\mathbf{y} \in \mathbb{R}^{N_y \times 1}$ is a vector of the N_y outputs of the system and $\mathbf{u} \in \mathbb{R}^{N_u \times 1}$ is a vector of the N_u inputs of the system. $\mathbf{A} \in \mathbb{R}^{N_x \times N_x}$ is the system matrix, $\mathbf{B} \in \mathbb{R}^{N_x \times N_u}$ is the input matrix, $\mathbf{C} \in \mathbb{R}^{N_y \times N_x}$ is the output matrix and $\mathbf{D} \in \mathbb{R}^{N_y \times N_u}$ is the feed-forward matrix [149]. $\mathbf{x}_0$ is the initial condition of the state at time t_0. Assume in this study that the state-space representation can be generated without the use of the feed-forward matrix (*i.e.* $\mathbf{D} = \mathbf{0}$).

2.2.5.2 Linear quadratic tracker

The LQT optimises the performance index

$$J(t_0) = \frac{1}{2}\mathbf{e}^\top(T)\mathbf{P}\mathbf{e}(T) + \frac{1}{2}\int_{t_0}^{T} \mathbf{e}^\top(t)\mathbf{Q}\mathbf{e}(t) + \mathbf{u}(t)\mathbf{R}\mathbf{u}^\top(t)dt, \tag{2.38}$$

where

$$\mathbf{e}(t) = \mathbf{r}(t) - \mathbf{z}(t), \tag{2.39}$$

is the tracking error between the desired performance output, $\mathbf{r} \in \mathbb{R}^{N_s \times 1}$ and the performance output of the system $\mathbf{z} \in \mathbb{R}^{N_s \times 1}$ [148]. N_s is the resulting dimension specified by the designer[p]. The performance output is defined by

$$\mathbf{z}(t) = \mathbf{H}\mathbf{x}(t), \tag{2.40}$$

where $\mathbf{H} \in \mathbb{R}^{N_s \times N_x}$ is a diagonal weighting matrix which can be chosen to be equal to the output matrix of the system ($\mathbf{C}$) to induce tracking on the output. $\mathbf{P} \geq \mathbf{0} \in \mathbb{R}^{N_s \times N_s}$ is the final tracking error weight. Similarly, $\mathbf{Q} \geq \mathbf{0} \in \mathbb{R}^{N_s \times N_s}$ is the tracking error weighting and $\mathbf{R} > \mathbf{0} \in \mathbb{R}^{N_u \times N_u}$ is the control weighting.

The optimal LQT can then be calculated from the solution of ($\mathbf{S} \in \mathbb{R}^{N_x \times N_x}$) in the following Riccati equation:

$$-\dot{\mathbf{S}}(t) = \mathbf{A}^\top\mathbf{S}(t) + \mathbf{S}(t)\mathbf{A} - \mathbf{S}(t)\mathbf{B}\mathbf{R}^{-1}\mathbf{B}^\top\mathbf{S}(t) + \mathbf{H}^\top\mathbf{Q}\mathbf{H} \quad \forall \quad t \leq T, \tag{2.41}$$

[p]Usually $N_s = N_y$

and $\mathbf{S}(T) = \mathbf{H}^\top \mathbf{P}\mathbf{H}$. The solution of $\mathbf{S}(t)$ in Eq. 2.41 is then used to give the optimal feedback gain:

$$\mathbf{K}(t) = \mathbf{R}^{-1}\mathbf{B}^\top \mathbf{S}(t), \tag{2.42}$$

where $\mathbf{K}(t) \in \mathbb{R}^{N_u \times N_x}$. The optimal feedback gain is used together with a feed-forward control to give the input

$$\mathbf{u}(t) = -\mathbf{K}(t)\mathbf{x}(t) + \mathbf{v}(t), \tag{2.43}$$

where $\mathbf{v}(t) \in \mathbb{R}^{N_u \times 1}$ is the feed-forward control defined by

$$\mathbf{v}(t) = \mathbf{R}^{-1}\mathbf{B}^\top \mathbf{w}(t), \tag{2.44}$$

where $\mathbf{w}(t) \in \mathbb{R}^{N_x \times 1}$ is input dependent and solved backward in time by the following differential equation:

$$-\dot{\mathbf{w}}(t) = (\mathbf{A} - \mathbf{B}\mathbf{K})^\top \mathbf{w}(t) + \mathbf{H}^\top \mathbf{Q}\mathbf{r}(t) \quad \forall \quad t \leq T, \tag{2.45}$$

and $\mathbf{w}(T) = \mathbf{H}^\top \mathbf{P}\mathbf{r}(T)$. Eqs. 2.44 & 2.45 can be merged to give the feed-forward control transfer function between $\mathbf{R}(s)$ and $\mathbf{V}(s)$ as

$$\mathbf{V}(s) = \mathbf{F}(s)\mathbf{R}(s) = \mathbf{R}^{-1}\mathbf{B}^\top \left[-s\mathbf{I} - (\mathbf{A} - \mathbf{B}\mathbf{K})^\top\right]^{-1} \mathbf{H}^\top \mathbf{Q}\mathbf{R}(s). \tag{2.46}$$

The LQT implementation is depicted in Fig. 2.20.

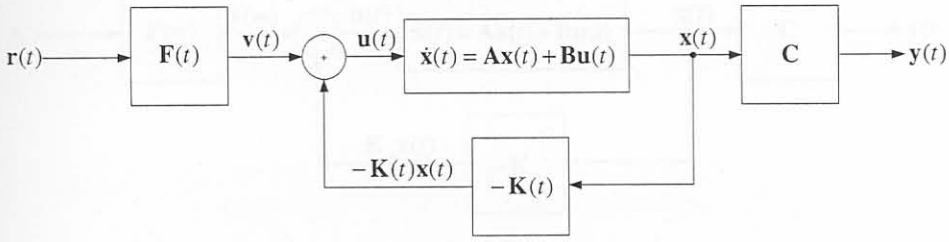

Figure 2.20 Linear quadratic tracker. Note that $\mathbf{F}(t) = \mathcal{L}^{-1}\{\mathbf{F}(s)\}$

2.2.5.3 Steady-state application

For some applications, certain conditions arise which makes the above solution to the LQT simpler. These conditions are:

1. The tracker must follow a constant input: $\mathbf{r}(t) = \mathbf{r}_0$.
2. The tracker is optimal at steady-state ($t \to \infty$).

Under the conditions above, Eq. 2.45 reduces to

$$\mathbf{w}(\infty) = \left[-(\mathbf{A} - \mathbf{B}\mathbf{K}_\infty)^\top\right]^{-1} \mathbf{H}^\top \mathbf{Q}\mathbf{r}_0, \tag{2.47}$$

where $\mathbf{w}(\infty)$ is constant and $\mathbf{K}_\infty$ is the optimal infinite horizon gain given by

$$\mathbf{K}_\infty = \mathbf{R}^{-1}\mathbf{B}^\top \mathbf{S}_\infty, \tag{2.48}$$

which optimises the infinite horizon performance index

$$J(t_0) = \frac{1}{2}\int_0^\infty \mathbf{e}^\top(t)\mathbf{Q}\mathbf{e}(t) + \mathbf{u}(t)\mathbf{R}\mathbf{u}^\top(t)dt, \tag{2.49}$$

$\mathbf{S}_\infty$ is the limiting solution to the time-varying Riccati equation and can be found by solving the algebraic Riccati equation (ARE)

$$0 = \mathbf{A}^\top \mathbf{S}_\infty + \mathbf{S}_\infty \mathbf{A} - \mathbf{S}_\infty \mathbf{B}\mathbf{R}^{-1}\mathbf{B}^\top \mathbf{S}_\infty + \mathbf{H}^\top \mathbf{Q}\mathbf{H}. \tag{2.50}$$

As a consequence of the above, Eq. 2.46 reduces to a time equivalent[q] of

$$\mathbf{v}(\infty) = \mathbf{R}^{-1}\mathbf{B}^\top \left[-(\mathbf{A} - \mathbf{B}\mathbf{K}_\infty)^\top\right]^{-1} \mathbf{H}^\top \mathbf{Q}\mathbf{r}_0 = \mathbf{F}(\infty)\mathbf{r}_0, \tag{2.51}$$

where $\mathbf{v}(\infty)$ is then a constant. Finally, the control law is implemented by

$$\mathbf{u}(t) = -\mathbf{K}_\infty \mathbf{x}(t) + \mathbf{v}(\infty), \tag{2.52}$$

The steady-state LQT (LQTSS) implementation is depicted in Fig. 2.21.

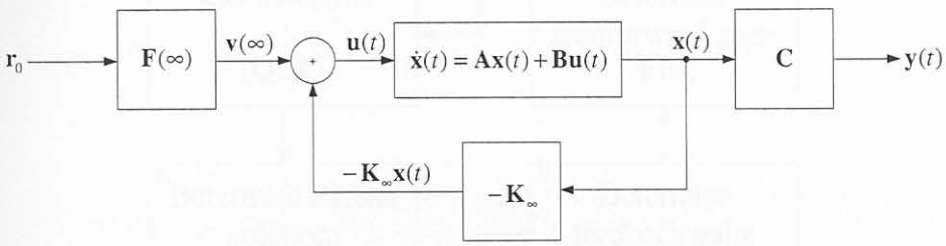

Figure 2.21 Linear quadratic tracker at steady-state.

2.2.5.4 Transfer function of the LQTSS

Using the result in §2.2.5.3 and replacing Eq. 2.51 in Eq. 2.52 and this result in Eq. 2.36 and Eq. 2.37 and simplifying, the following closed-loop state-space system results.

$$\dot{\mathbf{x}}(t) = (\mathbf{A} - \mathbf{B}\mathbf{K}_\infty)\mathbf{x}(t) + \mathbf{B}\mathbf{F}(\infty)\mathbf{r}(t), \quad \mathbf{x}(t_0) = \mathbf{x}_0 \tag{2.53}$$

$$\mathbf{y}(t) = (\mathbf{C} - \mathbf{D}\mathbf{K}_\infty)\mathbf{x}(t) + \mathbf{D}\mathbf{F}(\infty)\mathbf{r}(t), \tag{2.54}$$

[q]note that in the time domain, $\mathbf{F}(t)$ when t tends to infinity is denoted by $\mathbf{F}(\infty)$ and this same *constant* is denoted by $\mathbf{F}(0)$ in the s-plane, *i.e.* $\mathbf{F}(s \to 0) = \mathbf{F}(t \to \infty)$.

where $\mathbf{r}(t)$ is the desired trajectory of the output $\mathbf{y}(t)$. Assuming that the initial conditions are zero, the transfer function of the system above is given by

$$\mathbf{Y}(s) = \left\{[\mathbf{C} - \mathbf{D}\mathbf{K}_\infty][s\mathbf{I} - (\mathbf{A} - \mathbf{B}\mathbf{K}_\infty)]^{-1}\mathbf{B}\mathbf{F}(0) + \mathbf{D}\mathbf{F}(0)\right\}\mathbf{R}(s). \tag{2.55}$$

2.2.5.5 Design procedure

The design procedure for the steady-state LQT is shown in Fig. 2.22. The first step in the

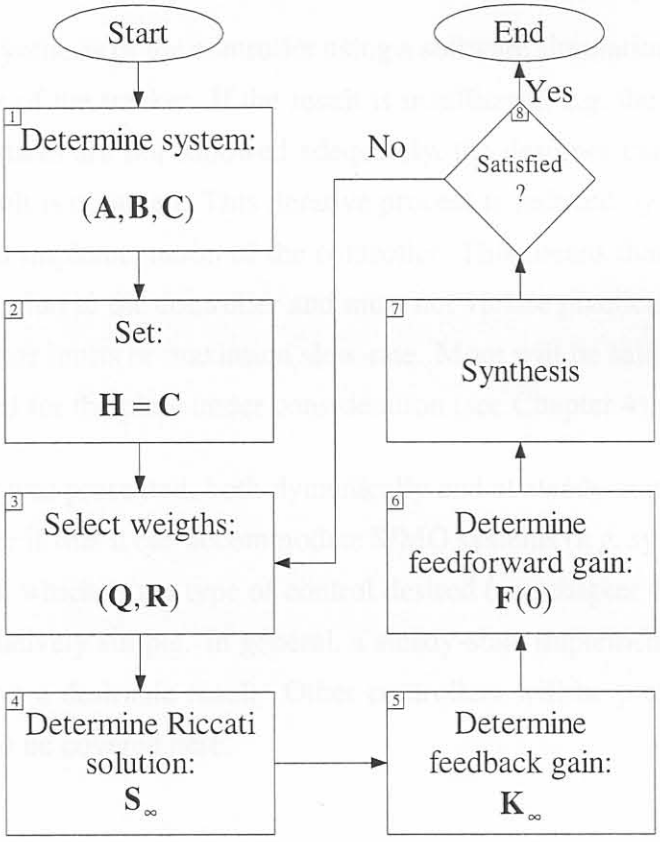

Figure 2.22 Design procedure for the LQTSS.

design procedure is to find an adequate state-space representation of the plant for which the LQTSS has to be designed. This step (step 1 in the figure) is critical to find an LQTSS that will minimise the performance index of Eq. 2.49.

Once the plant is known, step two is performed so that the tracker follows the outputs and not the state. This step is carried out by setting the weighting matrix $\mathbf{H}$ equal to the output matrix $\mathbf{C}$. For a linear first order system without any coupling between outputs, the mentioned procedure will be valid since the output and the state can be equal. Therefore only the

outputs need to be measured (same as measuring the states) and step 2 is then essentially left out of the implementation.

Step 3 requires the selection of the input and tracking error weighting matrices, $\mathbf{R}$ and $\mathbf{Q}$, respectively (see chapter 4 which discusses the selection procedure used in this work). Once the system is known and the weighting matrices have been selected, the next step is to determine the solution to the ARE. The result of step 4 is a solution of $\mathbf{S}_\infty$. With the solution of the ARE known, the feedback gain, $\mathbf{K}_\infty$ can be computed (step 5) and then the feed-forward gain $\mathbf{F}(0)$ may be computed next (step 6).

Step 7 involves the synthesis of the controller using a software simulation and then determining the effectiveness of the tracker. If the result is insufficient, *e.g.* the actuator constraints are violated or the states are not followed adequately, the designer can repeat steps 3 to 7 until the desired result is obtained. This iterative process is induced by step 8 and is necessary for the practical implementation of the controller. This means that the algorithm must find an adequate solution to the controller and must not violate practical constraints such as *e.g.* maximum actuator limits or maximum slew-rate. More will be said about this when the controller is designed for the plant under consideration (see Chapter 4).

The LQT controller was presented, both dynamically and at steady-state. The advantage of this type of controller is that it can accommodate SIMO systems (*e.g.* systems with one input and several outputs), which is the type of control desired (see chapter 4). The design of the controller is also relatively simple. In general, a steady-state implementation of the LQT is adequate [148] to get a desirable result. Other controllers will be presented later, and are simple enough not to be covered here.

2.3 Conclusion

A brief overview of the continuous casting process was given. A literature overview regarding the defects that are present during continuous casting was presented. Statistical hypothesis tests to determine whether an empirical distribution is part of some theoretical distribution were also presented. Correlation methods to determine linear dependence were given. Auto regression with exogenous input as a system identification procedure was perused and a special type of controller known as the linear quadratic tracker at steady-state was explained.

Chapter 3

Modelling

THIS chapter describes the use of system identification techniques to derive a relationship between variables in the mould and surface defects. In essence, this relationship is a model with mould variables as inputs and defects as outputs. The model can be used to predict when defects will occur, hence it is called a predictor.

First principles methods would be an ideal way to derive a model to predict defects (see §2.2.1.10). A first principles model requires metallurgical modelling at a micro-structure level; a process that is not fully understood in the continuous casting process today. It involves variables such as dendritical arm growth, chemical composition, strain and stress, to name only a few. Except for this vast number of variables which have to be formulated into a mathematical model, the training and testing of such a model require vast amounts of data from several different types of sensors which do not exist.

The use of artificial neural networks (ANN) [17, 18] or expert systems [15] to predict defects has been implemented in practice, though very little information on such systems is available in the literature, with most designs being proprietary. The neural network modelling approach does not easily allow physical meaning of variables to be worked into the model *i.e.* first-principle information that could have been used is lost. Such black box type models are also undesired since control system analysis techniques do not truly exist for neural networks. This implies that controller design using ANN is largely limited to empirical tuning methods. The usefulness of the neural network or expert system does not go beyond it being a predictor of defects.

System identification (*i.e.* empirical modelling) techniques have to be used, because a first principles model is beyond the scope of this study, and AI methods have either been used or

are undesirable. This method of modelling is also a black box approach, but the selection of the structure of the model can be facilitated by an understanding of first-principle models as described in Chapter 2. The system identification technique used in this chapter is in essence a Box-Jenkins type approach known as auto-regression with exogenous input. It operates as a linear discrete filter, with past values of inputs and outputs weighed to give current outputs. The weights (regressors) mentioned are determined using regression with plant input and output data, and are tested on plant input and output data sets which are the same or differ from the original training set. The modelling technique is simple, effective and manageable given the large model structures and sets of data to work with, and can be used for analysis and design using standard control system techniques.

This chapter starts with a description of the mould variables (inputs) and defect (outputs) data. The data are then perused using statistical hypothesis testing and correlation analysis to determine if some variables can be excluded from the model. An interesting result that will be covered is that the model can be split into two sub-models, making feedback control possible. The models are then derived using system identification techniques. Finally, some concluding remarks are made.

3.1 Data

This section describes the mould variable data and defect data. The data were gathered at a South African stainless steel producer over a period of six months from May to September, 1999. A validation set of data were gathered in June, 2002. The data can be categorised by the inputs[a] which are the mould variables such as casting speed, thermocouple temperatures *etc.* and the outputs which are defect data such as transversal cracks, inclusions, depressions *etc.* These data are required to derive a model to predict the occurrence of defects based on variation of parameters in the mould. The concept is illustrated in Fig. 3.1. The following sections describe the mould variable data, defect data and processing of the data.

3.1.1 Mould variable data

There are numerous variables[b] that are measured within the mould. The data are usually gathered on the level 1 system of the company, and stored on the level 2 system. Altogether

[a]Note that disturbances also act on the system and these will also be described in the following sections.

[b]see *e.g.* Fisher and Mesic [150] for a description of the database structures at a continuous casting plant.

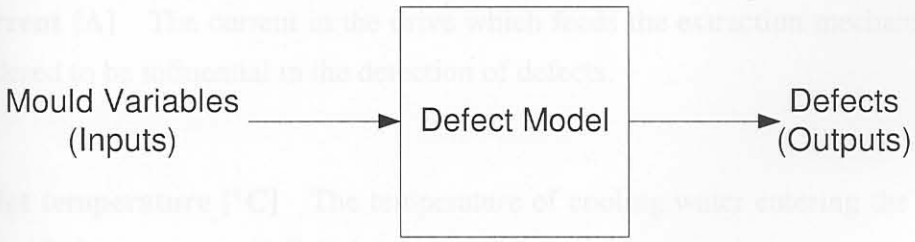

Figure 3.1 Block diagram of the total transfer from mould variables (inputs) to defects (outputs).

800 slabs were inspected for defects over the 6 month time period, but data for only about 500 slabs were available due to errors in the data gathering system which were caused by down-time or maintenance of the system. This is a small percentage of actual cast product, because slab inspection of every slab that was cast was not possible due to man-power constraints. About 3.3GB of mould variable data were collected.

3.1.1.1 Mould variables

The following variables characterise the operation of the mould. They pertain to the inputs in Fig. 3.1. Data for each of these variables were obtained from the level 2 system of the plant. These data are sampled at two second intervals.

Casting speed [mm/min] The casting speed is the speed at which the strand moves through the caster. It can be classified as a manipulated variable.

Mould level [mm] This indicates the fluctuations of the mould level at the meniscus and is measured by an Eddy-current sensor. The general consensus is that mould level should not fluctuate greatly, and should remain constant at a predefined value. At the industrial partner, mould level is controlled using the slide gate of the tundish as an actuator. The mould level can be classified as a measured disturbance.

Mould level controller activation [binary 0 or 1] The mould level controller activation is a binary switch which indicates whether the automatic mould level controller is switched on or whether mould level is manually controlled. The effect of the switch's position is seen in the variation of the mould level.

Drive current [A] The current in the drive which feeds the extraction mechanism and is not considered to be influential in the detection of defects.

Water inlet temperature [°C] The temperature of cooling water entering the mould. It can be classified as a measured disturbance.

Negative strip [mm] The length by which the mould moves faster downward relative to the strand during the oscillation of the mould. This value remains constant for all casts.

Oscillation frequency [Hz] The frequency at which the mould oscillates. The oscillation is sinusoidal. It is considered to be a manipulated variable.

Water flow rate [l/min] The flow-rate at which cooling water flows into each of the four mould faces. It should remain at the maximum possible value. It is therefore uncontrollable and is considered to be a measured disturbance.

Thermocouple temperatures [°C] These temperatures are measured through thermocouples situated in two rows with 8 on each wide face at both the top and bottom rows and 2 on each narrow face for both the top and bottom rows. Fig. 3.2 shows the location and naming conventions for the thermocouples. No classification can be awarded to this variable since it does not fall within the category of a manipulated variable or a disturbance.

Heat fluxes $[kW/m^2]$ The heat flux in each of the four faces of the mould. This variable also remains unclassified since it is not a manipulated variable or a disturbance.

Delta T [°C] A variable which describes the overall temperature distribution of the mould in each of the four faces. This variable also remains unclassified since it is not a manipulated variable or a disturbance.

Longitudinal temperature differences [°C] The temperature difference between the top row of thermocouples and the bottom row of thermocouples. These variables have tradi-

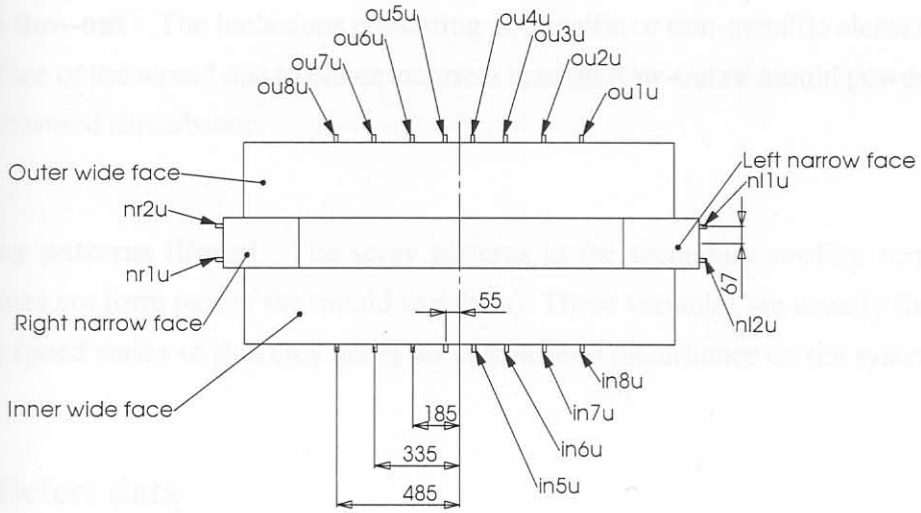

Figure 3.2 Top view of the mould depicting location and naming conventions of the thermocouples. Note that in this view, the thermocouples shown are the top row of thermocouples. The bottom row of thermocouples have names "ou8*l*", "nr1*l*", *etc.*

tionally been used in the detection of break-outs. No classification can be awarded to this variable since it does not fall within the category of a manipulated variable or a disturbance.

Steel flow-rate [l/min] The amount of molten steel flowing into the mould from the tundish. This variable is not measured and is considered to be an unmeasured disturbance. The position of the stopper rod (or slider gate) in the submerged entry nozzle is not measured and therefore the steel flow-rate can not be inferred.

Superheat [°C] The temperature of the in-flowing steel above the liquidus temperature. This variable is not measured and is considered to be an unmeasured disturbance.

Mould powder The mould powder is added at the top of the mould to aid in the lubrication of the strand so that it does not stick to the copper faces. This variable is unmeasured and is therefore considered to be an unmeasured disturbance.

Roller bulging [mm] As the strand moves through the secondary cooling zone, the rollers compress the delicate strand so that liquid metal within moves upward to affect the mould level. The effect is in essence difficult to detect and is considered to be a unmeasured disturbance.

Inclusion flow-out The inclusions consisting of metallic or non-metallic elements trapped at the surface of the strand due to either incorrect tundish flow-out or mould powder addition is an unmeasured disturbance.

SCZ spray patterns [l/min] The spray patterns in the secondary cooling zone (*i.e.* this variable does not form part of the mould variables). These variables are usually fixed or vary as casting speed varies so that they act as an unmeasured disturbance on the system.

3.1.2 Defect data

3.1.2.1 Defect measurement

The cost of an automatic electronic defect measurement system is extremely high, and hence they are very rarely found in practice[c]. Therefore, another method to gather defect data from cast slabs had to be found. For this a Human Measurement System (HMS) was used (see Hague and Parlington [105] for a similar idea). Three grinding plant operators with many years of experience on defects were instructed to investigate the slabs for defects during their (separate) shifts. (The operators inspect the slabs and mark defects which have to be grinded as part of the grinding process.) The idea is simple. Human operators use a schematic representation of the slabs to indicate positions where specific defects occur. They also award—based on their experience—a value of the severity of the defect (see *e.g.* Brockhoff, Hücking, Wagener, and Reichelt [154] for an index describing the severity of some defects). These values are termed as follows.

- None *i.e.* no defect occurred.
- Very slight *i.e.* the defect is very slight in the opinion of the operator.
- Slight.
- Medium *i.e.* the defect is considered to be a standard severity of the occurring defect.
- Bad.
- Very bad.

[c] see *e.g.* Mayos, Turon, Alexandre, Salon, Depeyris, and Rios [151], Knox [152] and Foster [153]

The date, slab number, grade (type), width and length are also indicated on the slab. Each slab inspection report has four slab faces depicted on it. They are for slabs that are inspected before grinding and after grinding (about 3mm off) and for the top and the bottom of the slab. A typical slab inspection report as designed by the author is shown in Fig. 3.3. At the bottom of the slab inspection report is a description of the different defects which the operator must consider together with a numbering scheme to identify each defect's severity on the specific slab face.

The example shows that an inclusion occurred 3 metres from the top of the slab on the left portion of the slab with medium (m) severity. After grinding, the defect was still present, but now only had a severity of "very slight". A longitudinal crack also formed on the bottom part of the slab at the centre location. The defect severity was bad (b). After grinding the defect was removed. For the purposes of this study, only defects on the wide faces were considered, since internal defects constitute a lesser problem and is directly proportional to the composition of the steel.

Each slab on the slab inspection report is divided (in length) into one metre intervals. This means that the average distance within which the operator would be able to indicate a defect would be 1/2 metres because the operator can indicate a defect on the separating line or on the space between two separating lines (see Fig. 3.3). Each slab is further divided into three segments along the transversal axis, *i.e.* a left side, right side and the center. This further restricts the area within which the operator can indicate the defect—these concepts are illustrated in Fig. 3.4. The figure also illustrates the naming conventions for the location of the defects. The casting direction is into the page and the top side is associated with the front or short wide face of the mould and the bottom side is associated with the back or long wide face.

Once all the slab inspection reports had been gathered, the data had to be converted into electronic format for manipulation on a personal computer.

3.1.2.2 Defuzzyfication

The slab inspection report data are read into a file for computer use. Since the slab was divided into 1/2 m segments, the defect files are said to be sampled at 1/2 metre intervals. The fuzzy levels of severity of each defect are then quantised into discrete numerical values, and this was done as follows.

SLAB INSPECTION REPORT DATE: 22/06/1999

SLAB No.: 3 1 7 4 0 9 3 TYPE: 3 0 4 3 1

WIDTH: 1 2 8 5 LENGTH: 1 1 1 0 4 INSP: John

TOP BEFORE GROUND■

	L	C	R
1			
2			
3	2b (m)		
4			
5			
6			
7			
8			
9			
10			
11			
12			

TOP AFTER GROUND■

	L	C	R
1			
2			
3	2b (vs)		
4			
5			
6			
7			
8			
9			
10			
11			
12			

□BOTTOM BEFORE GROUND

	L	C	R
1			
2			
3			
4		1b (b)	
5			
6			
7			
8			
9			
10			
11			
12			

□BOTTOM AFTER GROUND

	L	C	R
1			
2			
3			
4			
5			
6			
7			
8			
9			
10			
11			
12			

1a: transversal cracks, 1b: longitudinal cracks, 2a: casting powder entrapment, 2b other inclusions, 3: sticker, 4: bleeder, 5a: deep oscillation marks, 5b: uneven oscillation marks, 6: stopmarks, 7: footprints, 8: depressions.
vs: very slight, s: slight, m: medium, b: bad, vb: very bad

Figure 3.3 Slab inspection report (SIR).

- None: 0.
- Very slight: 1.
- Slight: 2.
- Medium: 3.
- Bad: 4.
- Very bad: 5.

There are several problems associated with this method of defect measurement. Firstly, there may be noise on the measurements because the value systems of the different operators can be different *i.e.* a very slight defect may be considered to be a slight defect by one operator and a medium defect by another. Secondly, the data are not necessarily ordinal, *i.e.* the distance between 1 and 2 is not necessarily the same as the distance between 2 and 3. This is a consequence of the value system of the different instruments (humans) in the HMS. The third problem is that the defect may not be seen by the operator and the fourth problem is that the defects are only measured several hours after they actually occurred, because the slab must cool down substantially before grinding can take place and before the operator

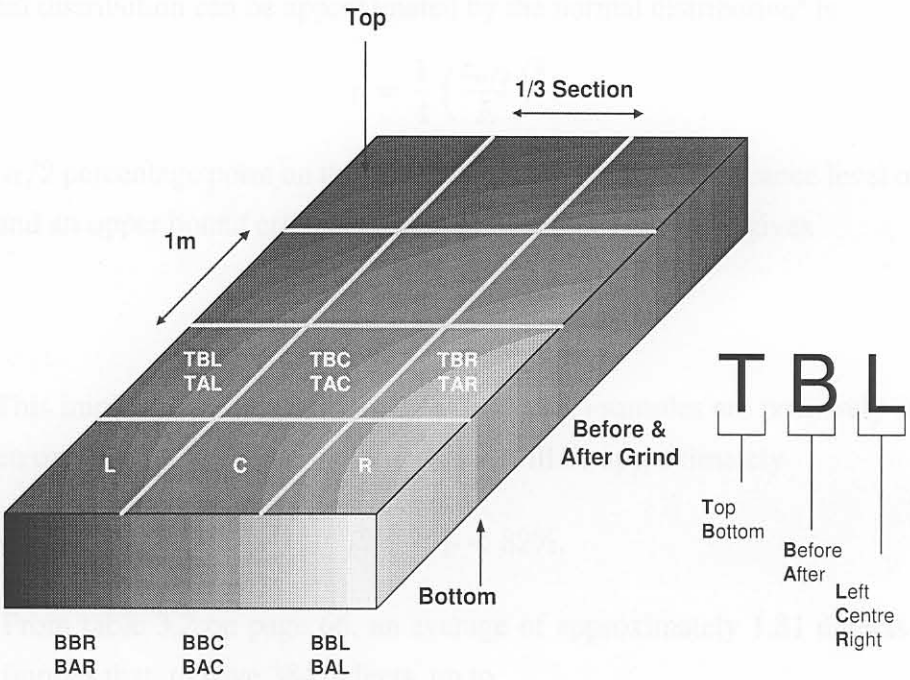

Figure 3.4 Sub-division of the slabs into top and bottom; left, right and center; and before and after grinding. The casting direction is into the page.

can inspect the slab (*i.e.* casuing a large delay). Lastly, not all slabs can be inspected. This delay and the non-inspection of many slabs make a feedback control scheme very difficult to implement.

3.1.2.3 Accuracy of the HMS

To quantify the accuracy of the HMS, several methods exist, but experiment design procedures will show that the quantification of the HMS constitutes a separate study.

One sample accuracy The first method that can be followed is to determine how accurate one person of the HMS is. This can be done statistically. Assume that n defects occur over some trial period in which one person of the HMS is instructed to investigate the slabs. This person may detect x number of the n defects. A point estimator of the population proportion (p) of positively[d] identifying a defect is then given by $\hat{p} = \frac{x}{n}$. n and p are parameters of a binomial distribution. The question is to determine how many defects have to be investigated before a "good" inference can be made on the population proportion, p. This question is simply answered in most statistical texts (see Montgomery *et al.* [144]). For a specified error E, an upper bound (conservative estimate) on the required sample size for estimating p when the binomial distribution can be approximated by the normal distribution[e] is

$$n = \frac{1}{4}\left(\frac{z_{\alpha/2}}{E}\right)^2. \tag{3.1}$$

$z_{\alpha/2}$ is the $\alpha/2$ percentage point on the normal distribution at a significance level of α. Using $\alpha = 0.05$ and an upper bound error of $E = 0.05$, the above equation gives

$$n = \frac{1}{4}\left(\frac{1.96}{0.05}\right)^2 = 384, \tag{3.2}$$

samples. This implies that if *e.g.* 296 of 384 ($p = 0.77$) samples are positively seen by the person, then one is 95% confident that the person will be approximately

$$72\% < p < 82\%, \tag{3.3}$$

accurate. From table 3.2 on page 66, an average of approximately 1.81 defects occur per slab. This implies that, to have 384 defects, up to

$$\frac{384}{1.81} \approx 213, \tag{3.4}$$

[d] assume that the same procedure can be followed for when the person sees a defect which is not truly there.
[e] $np > 5$ and $n(1-p) > 5$

slabs have to be inspected (conservative) to be 95% confident that an error of less than 5% in the accuracy estimate of the person is made.

During the validation data gathering experiment, estimates of p were determined (n=116 and x=113) to be in the region of 92 to 99% over all operators involved. These values are high because an undetected defect causes problems in post casting treatment, and operators are experienced in detecting surface defects and well aware of the importance of detecting a surface defect before grinding.

Repeatability Define one person in the HMS as one defect measurement instrument. Repeatability [155] has two possible meanings in this work. The first is the repeatability of one instrument within the HMS to measure defects consistently. This is defined as the repeatability "within" an instrument. The second is the repeatability among instruments in the HMS to measure defects consistently. This is defined as the repeatability "among" instruments.

To determine the repeatability within an instrument requires that an experiment be designed whereby an instrument measures the same set of defects a number (v) of times (see previous paragraph). Because the instrument may have memory, the defects should be randomized before each experiment run, and the instrument should not know that the defects that are being measured are the same defects as for all the experiment runs. The accuracy of that instrument in each of the v experiment runs can give an indication of the repeatability within the instrument to measure defects.

The repeatability among instruments can be measured by allowing w different instruments to measure the same defects. The accuracy of the various w instruments can then be used to determine a measure of repeatability among instruments.

To quantify the repeatability of the HMS within certain bounds is not a trivial task, since many instruments have to perform many runs on many defects ($n \times v \times w$ defects). Rather, hypothesis testing can be used in the form of a (two-way) analysis of variance (ANOVA) [156] to determine whether there is a significant difference between the runs of the experiment and whether there is a significant difference among the instruments. The following example will illustrate the concept. Assume that $w = 3$ instruments are used to measure the same randomized set of $n = 384$ defects $v = 4$ times. A table describing (example) data is given in table 3.1. The entries represent the fraction of correctly identifying defects, *e.g.* for the first instrument on the first run, a mean proportion of 81% of the defects were identified, *i.e.* 311 of the 384 defects were seen by the human (instrument). The result of the ANOVA

Table 3.1 ANOVA table for the experiment example.

	Run 1	Run 2	Run 3	Run 4
Instrument 1	.81	.83	.80	.85
Instrument 2	.90	.92	.91	.92
Instrument 3	.85	.86	.86	.86

calculation ($\alpha = 0.05$) is that, among columns (repeatability within an instrument), the F-statistic has a value of 2.98 which is less than the critical value of 4.76 implying that the instrument is repeatable. The F-statistic among rows *i.e.* among instruments is 67.4 which is higher than the critical value of 5.14 implying that the instruments vary amongst each other *i.e.* are not repeatable among each other.

The result of the example is that humans are consistent in their measurements but among the humans there is inconsistency.

The main question that has to be asked is: how many instruments (w) must perform how many runs (v) of the experiment so that the result of the test is significant. This can be calculated using the power (*e.g.* $\beta = 0.3$) of the ANOVA test together with a preliminary estimate of the overall variance of the instruments [157, 158]. Unfortunately, this was not possible, since only *one* human was available per shift to perform the inspections (one data point allows no variation and can not be used in a statistical test). The re-inspection of the slabs (runs) was also not possible since this would result in financial losses for the company, because the inspected slabs would have to be taken out of production until all inspections were done.

An initial estimate for v and w was performed for this thesis based on the assumption that $\alpha = 0.5$ and $n = 384$, by R.J. Grimbeek of STATOMET, University of Pretoria. It was assumed that a power of 70% was adequate and it was assumed that variation among the rows (instruments) and columns (runs) varied as

$$p = \bar{p} - (i-1)\epsilon^{i-1}, \tag{3.5}$$

where $\bar{p}$ is an initial estimate of the best performing candidate out of i runs or instruments. ϵ is an initial guess on the variability among or within instruments. It was assumed that $\bar{p} = 0.95$ *i.e.* the best performing instrument had a detection rate of 95% on one of the runs. The variability was chosen as $\epsilon = 0.1$. For three candidates on one run the detection rates (p) would then be 0.95, 0.93 and 0.85. Using these assumptions in the ANOVA with the desired power, delivered $v = 2$ and $w = 3$. This implies that three instruments (people) would have

to inspect 384 defects twice, so that a power level of 70% can be reached. Only one person was available per shift to perform the inspections, so that an initial estimate of the variance in the system could not be calculated, and hence sample sizes could not be determined. The HMS accuracy can thus not be quantified at this stage.

The ANOVA test only gives an outcome based on whether a present defect was detected or not, and further complexities such as the severity of the defects and probabilities of detecting a defect when there is not one can also be worked into the test, resulting in larger sample sizes. These matters can be considered for future research.

For now, it is assumed that the humans are accurate in detecting a defect, due to training, knowledge and experience in the detection of defects. Any errors that occur on their part forms an uncertainty in the model, which can only be disregarded once the model validation procedure has proven that the modelling techniques work.

Precision For any particular defect, the precision [155] is one, *i.e.* a severity level in increments of one are allowable. The precision for the instrument is also difficult to quantify, since the values are measured by humans and are therefore not truly ordinal, and for the same reasons stated in the previous paragraph.

Resolution The resolution is defined [155] as the smallest change in the input (defect severity) which would cause a change in the instrument's output (severity level indicated by human). The resolution is also difficult to measure accurately due to the lack of instruments and defects as stated under the paragraph with the heading "repeatability".

3.1.2.4 Practical defect occurrence

Defects occurred at the rates depicted in Table 3.2 during the training period, and can be seen as a generalisation of the occurrence of defects at the plant. The number of defects is also known as the index of the defect and is simply a count of the specific defect. The average defects per slab is an indication of the frequency of the defect. The number of defected slabs is the number of slabs that have a specific defect present and the number of equivalent slabs is the amount of slabs that have the same grade and widths as the defected slabs. The percentage of defected slabs is the ratio of the number of defected slabs to the total number of slabs with equivalent widths and grades expressed as a percentage. From the table it is clear that other inclusions are the most prevalent defect that occurs (28.09%) with depressions second

Table 3.2 Summary of defect rate (before and after grinding) based on a sample of 502 slabs.

	Number of defects	Average defects per slab (N=502)	Number of defected slabs	Number of equivalent slabs	Percent defected slabs
Transversal cracks	4	7.968×10^{-3}	2	71	2.82
Longitudinal cracks	4	7.968×10^{-3}	3	104	2.88
Casting powder entrapment	4	7.968×10^{-3}	4	78	5.13
Other inclusions	328	653.3×10^{-3}	109	388	28.09
Bleeders	9	17.93×10^{-3}	3	151	1.99
Deep oscillation marks	43	85.66×10^{-3}	8	320	2.50
Uneven oscillation marks	26	51.79×10^{-3}	5	243	2.06
Stopmarks	243	484.1×10^{-3}	19	156	12.18
Depressions	247	492.0×10^{-3}	82	335	24.48

(24.48%). Transversal cracks, longitudinal cracks, bleeders, and both types of oscillation marks occur on the least slabs ($< 3\%$). Note that casting powder entrapment has the lowest index of defects (7.968×10^{-3}) but does not have the lowest occurrence on slabs. This means that the defect occurs only on small areas on the surface of a particular slab, but the defect occurs on many slabs.

3.1.3 Auxiliary data

The use of auxiliary data such as lengths and weights of slabs, cast numbers, MPO numbers, front and tail crop lengths *etc.* are also required. This data are obtained from the heat summaries and slab reports provided by the company.

3.1.3.1 Heat summary

The heat summaries correlate the cast numbers to the heat numbers. During each cast, several ladles may be used. Each heat number represents a ladle and naturally a specific steel grade (type). For each cast there is a fixed width. Widths cannot be changed during casting. For each cast there is a front crop and tail crop which are the slabs at the start (front) or end (tail) of the cast which are scrapped. An example of the cast number is N0008434 and the heat number is 418495.

3.1.3.2 Slab report

The slab reports contain information on the actual cast. Each heat number of the specific cast is subdivided into MPO numbers. Each MPO number represents a specific slab. Example of the MPO numbers are 3174953 and 3204950. The first slab in a specific heat is always denoted by xxxxxx1 and is never the front crop. The last slab in a heat is always denoted by xxxxxx0 and is never the tail crop. The slab report contains the actual length and weights of each slab in the specific cast. The slab report also contains the start time and end time of the cast.

3.1.4 Mould variable-defect reconciliation

This section gives a basic overview of the procedure that was followed to extract the relevant data from the mould data using the various components in §3.1.3.

3.1.4.1 Discussion

Since the defect data are given as a function of position (see §3.1.2) and the mould data are time stamped, one is required to find the relationship of position to time. To transform the defect data to time data—so that it can be used together with the time data of the mould variables—would be very difficult because there is no recorded relation between time and position on the slab inspection reports[f]. The easier method would be to re-sample the mould time data to position data.

3.1.4.2 Time-position relationship

The time and position relation is found using the cast number, sampling period[g], casting speed and numerical integration.

Cast number The cast number is found from the mould parameter file[h], and once the start of the cast has been determined from the acceleration of the strand, the relevant heat number is found from subsequent accelerations. This location is the start of the heat.

Sampling period The sampling period is two seconds.

Casting speed The casting speed is used in an integration algorithm to find the corresponding position.

[f] The defect would have to be identified at the meniscus: a very difficult task.
[g] in *seconds*
[h] Also referred to in some cases as the mould variable file.

Numerical integration The relationship between the time of sampling and the position of the slab is achieved through the use of the Galileo transform:

$$x(t) = \int_0^t v(\tau)d\tau, \tag{3.6}$$

where $x(t)$ is the position of the cast as a function of time and $v(t)$ is the casting speed as a function of time. The above equation gives the *hot* position of the strand, while the defect data are cold slab data. The actual cold slab position data—which are needed to compare with the defect data—is found by dividing x by an expansion factor[i], *e.* e was determined by the manufacturers of the caster to be 1.012 for ferritic stainless steels and 1.018 for austenitic stainless steel. This form of the equation is continuous and a discrete (numerical) method of integration *must* be used for our purposes. This is done through the use of a trapezoidal transformation of Eq. 3.6:

$$x_{k+1} = x_k + \frac{1}{2}(t_{k+1} - t_k)v_{k+1} + \sum_{i=0}^{k+1} \epsilon_i, \quad x_0 = 0. \tag{3.7}$$

In Eq.3.7, the position at the x+1-th instance is computed by using the k-th position and adding the trapezoid of the x+1-th instance. The error up to that stage is the sum of all errors made (ϵ). Once again, the cold position, x_{cold} is determined by dividing the hot position (x) by the expansion factor e.

3.1.4.3 Data extraction

The position versus time relation is now available. With this information—and using the heat summary together with the slab reports—one is now in a position to extract the mould data from the relevant mould parameter files. At the end of each heat there is a slowdown in casting speed which clearly defines the boundaries within the file between heats. So, if *e.g.* the data are required for the third slab in the heat (317xxx3), the lengths of the front crop and first two slabs are added to determine the start position of the third slab in the mould parameter file. All mould data from this position to the end of the slab is then extracted from the mould parameter file for further processing.

3.1.4.4 Interpolation

The position data sampling points do not correspond to the defect data sampling points. To ensure that the two sets of data correspond, linear interpolation is performed on the defect

[i] *i.e.* $x_{cold}(t) = \frac{x(t)}{e}$

data at points where position data are available from the mould data, because the mould data are sampled much more frequently than the defect data.

3.1.5 Automation of the procedure

This procedure can be automated if the slab defect data, mould data, slab reports and heat summaries are all incorporated. The implementation of such a system is described in Fig. 3.5. CASTS_MPO.txt contains the cast number vs. MPO number lookup table. The mould variable data are extracted from slabs with MPO numbers given in CASTS_MPO.txt. Starting from the first entry in the CASTS_MPO.txt file, the cast number is determined from the same row as the MPO number in the file. The relevant cast files are then opened. These are the files which contain the relevant mould variable data for the specific cast (*.mld) and the auxiliary file which contains the lengths of each of the slabs in the cast (*.aux). The file which will contain the specific slab's time and position mould variable data are also opened for writing (*.mpf). The next step is to determine the starting and ending lengths of the specific slab in question. This is done by adding the lengths of the slabs up to the beginning of the slab in question and then making this the "start" length. The length of the specific slab in question is then added to this total to give the end length. The time vector in the *.mld file is then integrated until the length obtained is the same as the start length determined earlier. Mould data are then logged to the *.mpf file until the end length is reached. This means that all the data logged in the *.mpf file pertains to that specific slab. Once the end length has been reached, the *.mpf file is closed and the next slab data are created until all slabs in the CASTS_MPO.txt file have been processed. Once this has been done, the position dependent data in the defect files can be interpolated to correspond to the position dependent data in the mould variable file for the specific slab.

3.1.6 General model structure

This section described the data that is involved when trying to train a model to predict defects in the continuous casting process. Many input variables are measured and these have been explained in this section. It has been seen that the treatment of input (mould variable data) involves the utilisation of much information. The extraction of relevant data from the plant data is a tedious task which requires considerable data processing.

Slab inspection reports were used by the operators to log defects that may occur. The specific

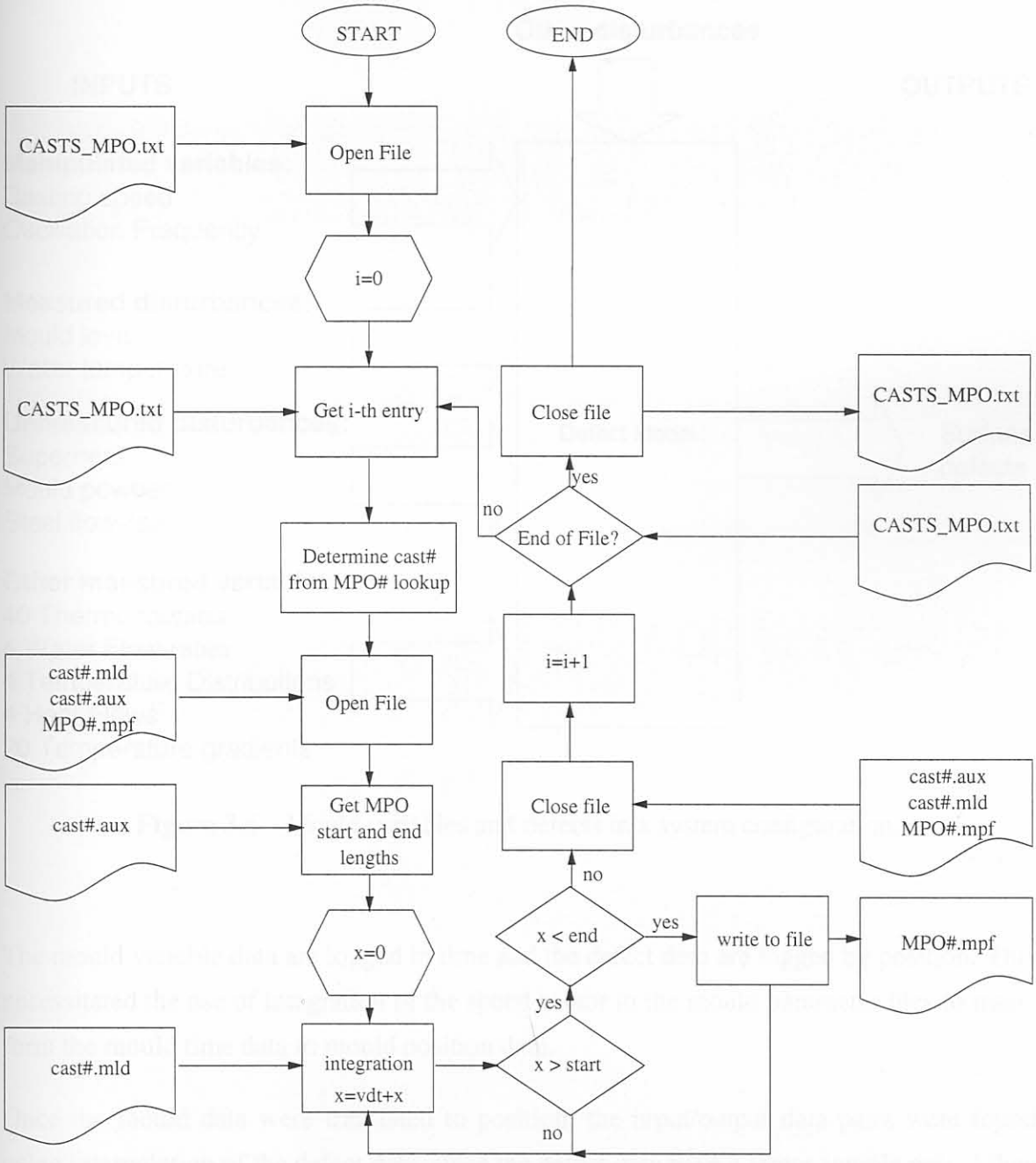

Figure 3.5 Flow chart describing the procedure to extract the mould data from the relevant files.

defect, location, position and severity of the defect was logged on the slab inspection reports. These slab inspection reports were then digitised.

The general input / output model structure is given in Fig. 3.6.

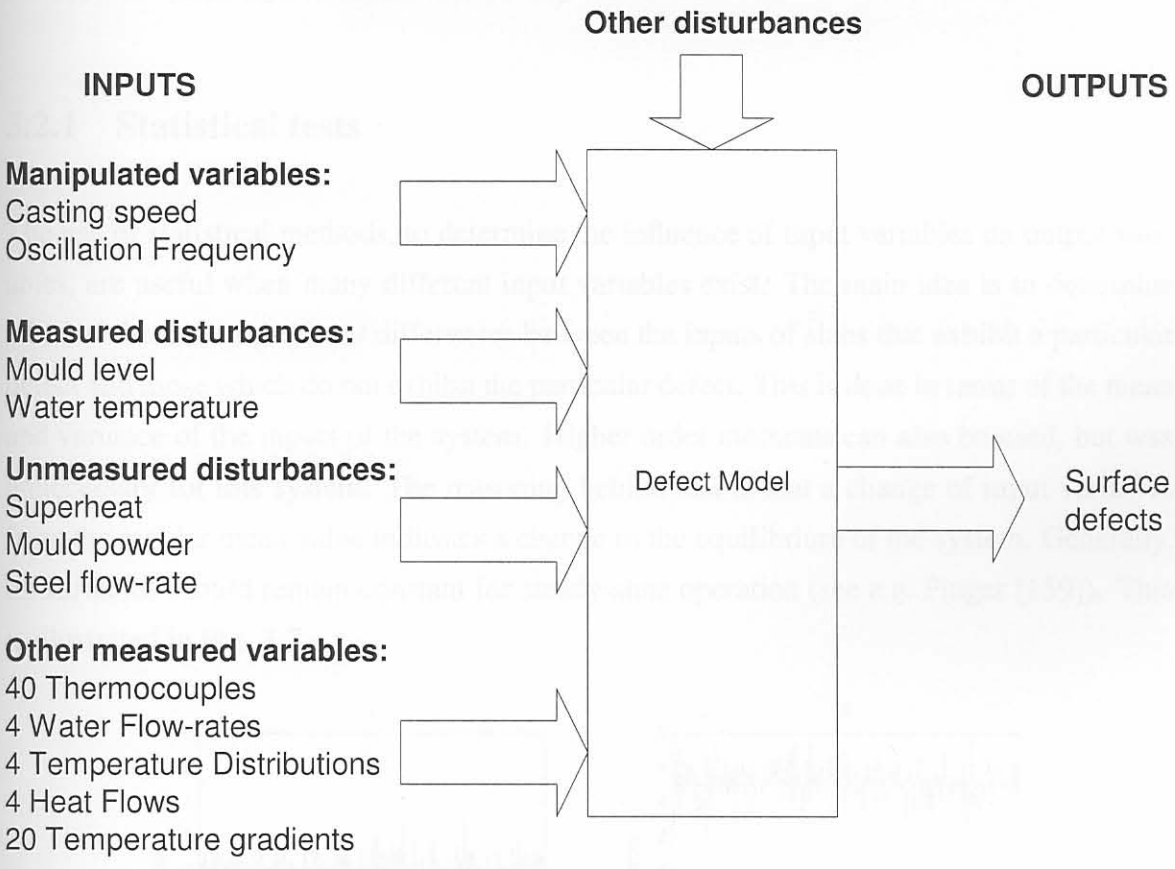

Figure 3.6 Mould variables and defects in a system configuration.

The mould variable data are logged in time and the defect data are logged by position. This necessitated the use of integration of the speed vector in the mould parameter files to transform the mould time data to mould position data.

Once the mould data were translated to position, the input/output data pairs were found using interpolation of the defect data, since the defect data have a larger sample period than the mould data.

With this new data in hand, the variables can be investigated and models can be trained to predict the occurrence of defects.

3.2 Statistical analysis

This section describes the use of statistical analysis to determine which inputs affect the defects and which input variables are closely correlated.

3.2.1 Statistical tests

The use of statistical methods, to determine the influence of input variables on output variables, are useful when many different input variables exist. The main idea is to determine whether there are *significant* differences between the inputs of slabs that exhibit a particular defect and those which do not exhibit the particular defect. This is done in terms of the mean and variance of the inputs of the system. Higher order moments can also be used, but was unnecessary for this system. The reasoning behind this is that a change of input variables from the regular mean value indicates a change in the equilibrium of the system. Generally, all variables should remain constant for steady-state operation (see *e.g.* Pinger [159]). This is illustrated in Fig. 3.7.

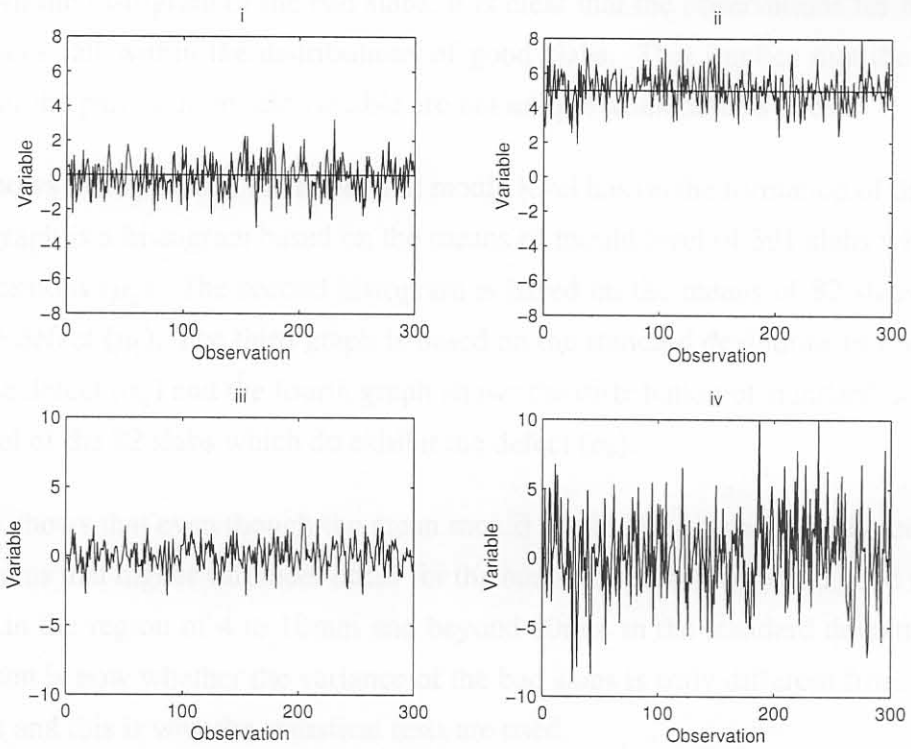

Figure 3.7 Depiction of the effect of different variances and means of a specific variable. i and ii have similar variances but different means while iii and iv have similar means but different variances.

Graph i has a mean value for the variable on the specific slab which is lower than the mean of the variable on a different slab (graph ii). The variances are similar in both cases. Graph iii has a variance lower than that of graph iv, indicating that there was more variation in the variable on the slab in graph iv. The means remain approximately the same for both cases. This reasoning can be extended to the case where both the variance and the mean are different for a variable on specific defected slabs, indicating that there is a significant change in both the location and scatter of the specific variable in question.

By examining the means of a specific input variable of all the slabs which do not have a particular defect contained on the slab (good slabs), and comparing these distributions of means with the distributions of means on slabs which do contain the specific defect (bad slabs), some conclusions can be drawn about the effect of a specific variable on the defect. The same reasoning follows for the variances/standard deviations. This is useful to indicate which variables change when defects occur.

Fig 3.8 shows the concept of means and variances of good slabs versus means and variances of bad slabs for any particular input variable. In this case, many good slabs are used to form the theoretical distribution of a particular variable. Few data exist for the bad slabs (3 in this case). From the histogram of the bad slabs, it is clear that the observations for both means and variances fall within the distributions of good slabs. This implies that the mean and variance for the particular mould variable are not unique when defects occur.

Fig. 3.9 shows histograms of the effect that mould level has on the formation of depressions. The first graph is a histogram based on the means of mould level of 391 slabs which do not have depressions (μ_g). The second histogram is based on the means of 82 slabs which do exhibit the defect (μ_b). The third graph is based on the standard deviations of the 391 slabs without the defect (σ_g) and the fourth graph shows the distribution of standard deviations in mould level of the 82 slabs which do exhibit the defect (σ_b).

The figure shows that even though the mean mould level is the same for both good and bad slabs, it seems that higher variances occur for the bad slabs compared to the good slabs. This is evident in the region of 4 to 10mm and beyond 20mm in the standard deviation graphs. The question is now whether the variance of the bad slabs is truly different from that of the good slabs and this is why the statistical tests are used.

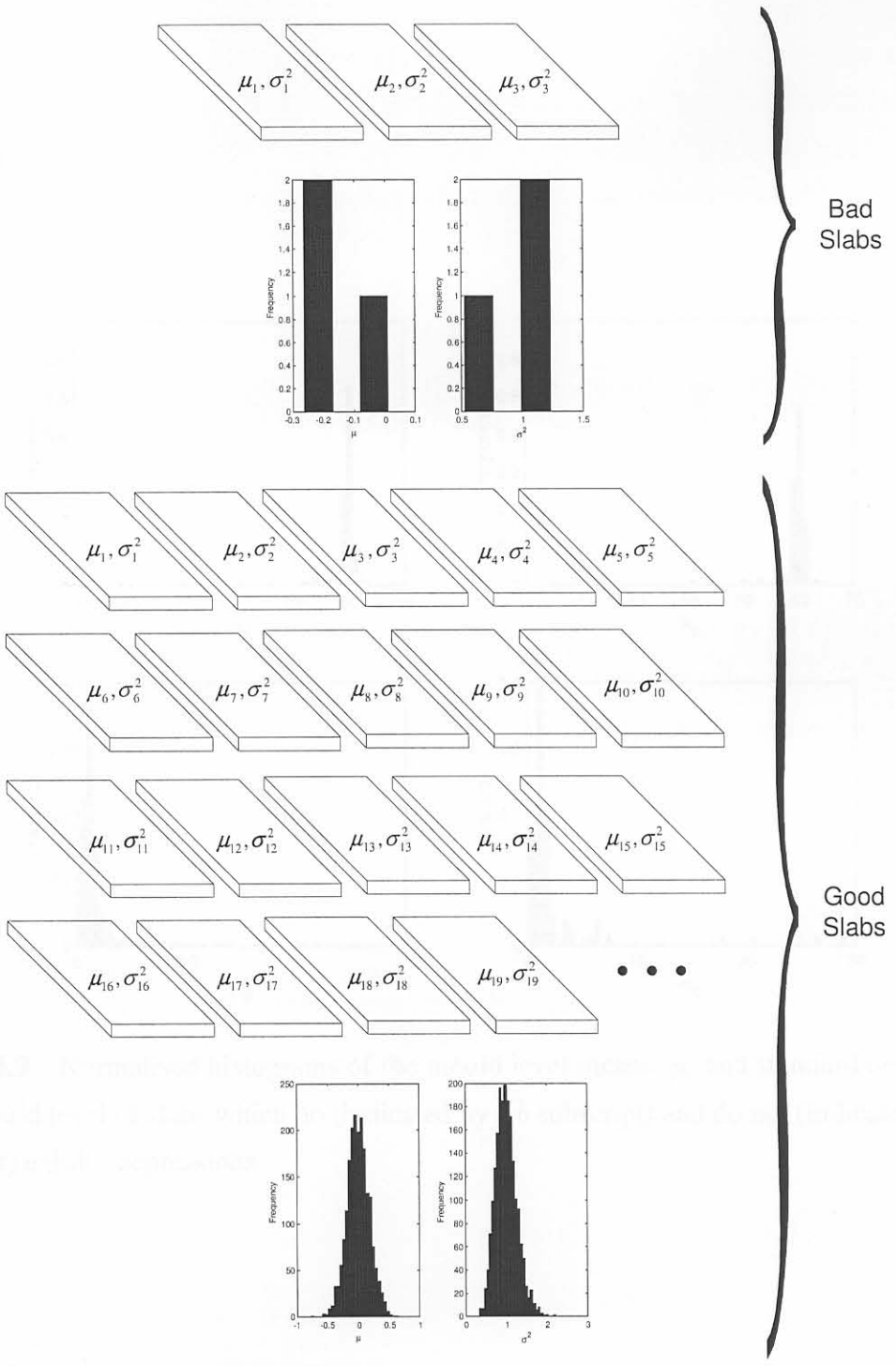

Figure 3.8 Depiction of the distributions of means and variances of bad slabs versus distributions of means and variances of good slabs for a specific input variable.

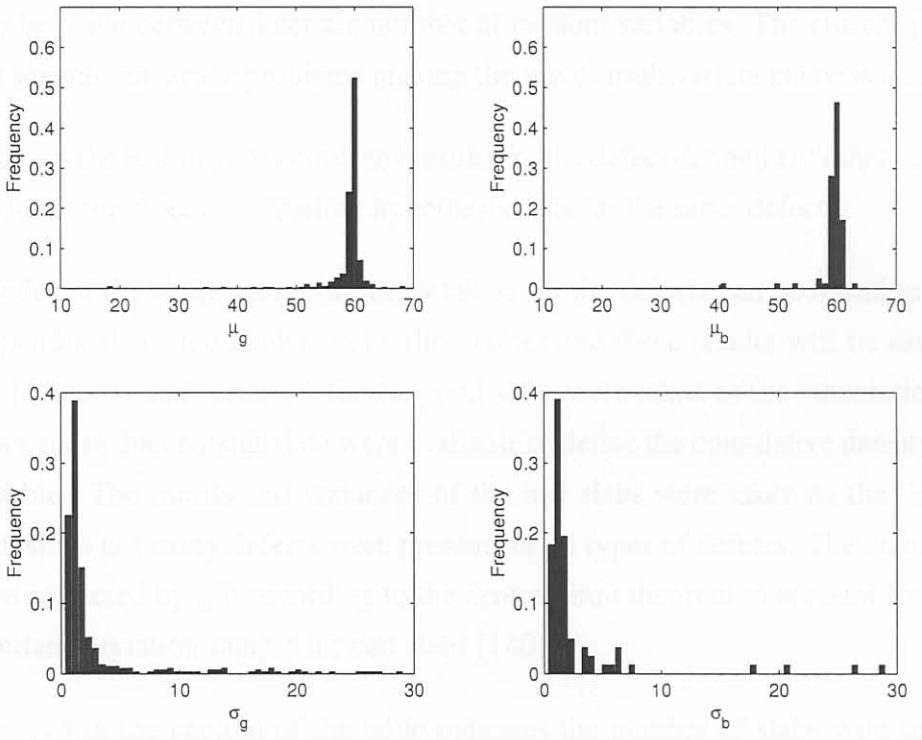

Figure 3.9 Normalised histograms of the mould level means, μ, and standard deviations, σ, of mould level of slabs which do (indicated by a b subscript) and do not (indicated by a g subscript) exhibit depressions.

3.2.1.1 Results

Kolmogorov-Smirnov and Anderson-Darling tests were performed for each defect and the corresponding input variables. These are univariate methods to determine whether a random variable belongs to a given distribution. These methods are preferred (for this investigation) over multivariate methods such as principal component analysis [158] because it is cumbersome to formulate the problem as a multivariate problem, and it appears that not much would be gained as the results of section 3.2.1.2 shows. In a multivariate problem, comparisons are made between a number of random variables. For the current problem, there are two comparisons to be made between a certain number of random variables. The current problem is reduced to several univariate problems making the use of multivariate analysis unnecessary.

Table 3.3 shows the Kolmogorov-Smirnov results for the defect defined as "other inclusions". Table 3.4 shows the Anderson-Darling hypothesis tests for the same defect.

The remainder of the Kolmogorov-Smirnov tables for the defects can be found in appendix A; and appendix B for the Anderson-Darling tables and these results will be discussed in §3.2.1.3. The means and variances for the good slabs were taken as the "theoretical" distribution, since more than enough data were available to define the cumulative density function of the variable. The means and variances of the bad slabs were taken as the "empirical" distribution since not many defects were present for all types of defects. The standard deviations were corrected by $\sqrt{n}$ according to the central limit theorem to account for the small size of standard deviation sample for bad slabs [140].

The $n_{2b} = 114$ in the caption of the table indicates the number of slabs with the specific defect that was used for the test; *i.e.* 114 means and variances were used in two respective Kolmogorov-Smirnov tests and 114 means and variances were used in two respective Anderson-Darling tests (this is a large sample); for each input variable. $n_g = 364$ indicates that 364 good slabs of the same dimensions and steel grades as the bad slabs that do not exhibit the specific defect were used as to generate the theoretical distribution.

$d_c(114) = 0.127$ is the critical value for the test. If the D statistic is less than $d_c(114) = 0.127$, the null hypothesis is accepted and it is concluded that *e.g.* the means are the same for good and bad slabs. If the statistic is rejected (*i.e.* D statistic is higher than the critical value), it means that the conclusion is that *e.g.* the means of good and bad slabs are different and that the input variable is a likely cause of the specific defect.

$1 - \alpha$ is the confidence level for the test, and is usually selected at 95% [140]. $\Delta_{0.95}$ is

Table 3.3 Kolmogorov-Smirnov hypothesis tests for Other Inclusions (defect 2b). n_{2b}=114. n_g =364. $d_c(114)$=0.127. α=0.05. $\Delta_{0.95}$=0.206. $\Delta_{0.5}$=0.122.

Variable	$D_{\mu_{2b}}$	$H_0(\mu_{2b})$	$D_{\sigma^2_{2b}}$	$H_0(\sigma^2_{2b})$	$H_0(\mu_{2b}) \cup H_0(\sigma^2_{2b})$
in1u	0.175	Reject	0.067	Accept	Reject
in1l	0.0977	Accept	0.0697	Accept	Accept
in2u	0.198	Reject	0.127	Accept	Reject
in2l	0.141	Reject	0.14	Reject	Reject
in3u	0.212	Reject	0.153	Reject	Reject
in3l	0.0942	Accept	0.102	Accept	Accept
in4u	0.171	Reject	0.173	Reject	Reject
in4l	0.0769	Accept	0.162	Reject	Reject
in5u	0.0833	Accept	0.207	Reject	Reject
in5l	0.0605	Accept	0.168	Reject	Reject
in6u	0.095	Accept	0.142	Reject	Reject
in6l	0.0967	Accept	0.168	Reject	Reject
in7u	0.215	Reject	0.157	Reject	Reject
in7l	0.143	Reject	0.178	Reject	Reject
in8u	0.145	Reject	0.0473	Accept	Reject
in8l	0.122	Accept	0.0817	Accept	Accept
nl1u	0.261	Reject	0.17	Reject	Reject
nl1l	0.26	Reject	0.0738	Accept	Reject
nl2u	0.31	Reject	0.0743	Accept	Reject
nl2l	0.249	Reject	0.166	Reject	Reject
ou1u	0.199	Reject	0.136	Reject	Reject
ou1l	0.155	Reject	0.0818	Accept	Reject
ou2u	0.129	Reject	0.122	Accept	Reject
ou2l	0.169	Reject	0.0956	Accept	Reject
ou3u	0.228	Reject	0.109	Accept	Reject
ou3l	0.191	Reject	0.149	Reject	Reject
ou4u	0.154	Reject	0.164	Reject	Reject
ou4l	0.221	Reject	0.146	Reject	Reject
ou5u	0.223	Reject	0.133	Reject	Reject
ou5l	0.2	Reject	0.169	Reject	Reject
ou6u	0.36	Reject	0.253	Reject	Reject
ou6l	0.233	Reject	0.214	Reject	Reject
ou7u	0.217	Reject	0.136	Reject	Reject
ou7l	0.204	Reject	0.1	Accept	Reject
ou8u	0.267	Reject	0.126	Accept	Reject
ou8l	0.154	Reject	0.0804	Accept	Reject
nr1u	0.199	Reject	0.119	Accept	Reject
nr1l	0.0899	Accept	0.155	Reject	Reject
nr2u	0.0831	Accept	0.113	Accept	Accept
nr2l	0.133	Reject	0.102	Accept	Reject
Casting Speed	0.193	Reject	0.105	Accept	Reject
Mould Controller Status	0.0605	Accept	0.0736	Accept	Accept
Mould level	0.127	Reject	0.0717	Accept	Reject
Inlet Temperature	0.136	Reject	0.174	Reject	Reject
Flowrate WL	0.0596	Accept	0.0797	Accept	Accept
Flowrate WF	0.117	Accept	0.2	Reject	Reject
Flowrate NL	0.1	Accept	0.0888	Accept	Accept
Flowrate NR	0.0835	Accept	0.0602	Accept	Accept
Delta T WL	0.155	Reject	0.171	Reject	Reject
Delta T WF	0.257	Reject	0.151	Reject	Reject
Delta T NL	0.1	Accept	0.133	Reject	Reject
Delta T NR	0.107	Accept	0.131	Reject	Reject
Oscillation Frequency	0.258	Reject	0.139	Reject	Reject
Drive Current	0.117	Accept	0.111	Accept	Accept
Heat Flux WL	0.117	Accept	0.177	Reject	Reject
Heat Flux WF	0.185	Reject	0.186	Reject	Reject
Heat Flux NL	0.1	Accept	0.128	Reject	Reject
Heat Flux NR	0.107	Accept	0.145	Reject	Reject
in1	0.188	Reject	0.0839	Accept	Reject
in2	0.174	Reject	0.0935	Accept	Reject
in3	0.188	Reject	0.119	Accept	Reject
in4	0.178	Reject	0.13	Reject	Reject
in5	0.181	Reject	0.179	Reject	Reject
in6	0.186	Reject	0.158	Reject	Reject
in7	0.129	Reject	0.119	Accept	Reject
in8	0.0887	Accept	0.0931	Accept	Accept
nl1	0.213	Reject	0.0979	Accept	Reject
nl2	0.211	Reject	0.0491	Accept	Reject
ou1	0.108	Accept	0.0851	Accept	Accept
ou2	0.0891	Accept	0.0861	Accept	Accept
ou3	0.1	Accept	0.0865	Accept	Accept
ou4	0.139	Reject	0.162	Reject	Reject
ou5	0.099	Accept	0.179	Reject	Reject
ou6	0.244	Reject	0.232	Reject	Reject
ou7	0.122	Accept	0.115	Accept	Accept
ou8	0.134	Reject	0.0773	Accept	Reject
nr1	0.265	Reject	0.118	Accept	Reject
nr2	0.127	Accept	0.114	Accept	Accept

Table 3.4 Anderson-Darling hypothesis tests for Other Inclusions (defect 2b). n_{2b}=114. n_g =364. $a_c^2(114)$=2.492. α=0.05.

Variable	$A^2_{\mu_{2b}}$	$H_0(\mu_{2b})$	$A^2_{\sigma^2_{2b}}$	$H_0(\sigma^2_{2b})$	$H_0(\mu_{2b}) \cup H_0(\sigma^2_{2b})$
in1u	4.28	Reject	0.629	Accept	Reject
in1l	1.95	Accept	0.791	Accept	Accept
in2u	∞	Reject	∞	Reject	Reject
in2l	∞	Reject	2.67	Reject	Reject
in3u	9.62	Reject	∞	Reject	Reject
in3l	∞	Reject	∞	Reject	Reject
in4u	∞	Reject	6.33	Reject	Reject
in4l	∞	Reject	5.47	Reject	Reject
in5u	2.34	Accept	7.86	Reject	Reject
in5l	0.652	Accept	6.76	Reject	Reject
in6u	1.67	Accept	4.63	Reject	Reject
in6l	∞	Reject	6.72	Reject	Reject
in7u	7.94	Reject	∞	Reject	Reject
in7l	5.38	Reject	∞	Reject	Reject
in8u	3.9	Reject	0.306	Accept	Reject
in8l	3.6	Reject	0.995	Accept	Reject
nl1u	15.7	Reject	5.06	Reject	Reject
nl1l	15.5	Reject	1.59	Accept	Reject
nl2u	22.8	Reject	1.26	Accept	Reject
nl2l	13.7	Reject	3.94	Reject	Reject
ou1u	5.99	Reject	3.39	Reject	Reject
ou1l	4.82	Reject	1.35	Accept	Reject
ou2u	∞	Reject	2.9	Reject	Reject
ou2l	∞	Reject	1.07	Accept	Reject
ou3u	∞	Reject	1.98	Accept	Reject
ou3l	∞	Reject	3.14	Reject	Reject
ou4u	∞	Reject	6.66	Reject	Reject
ou4l	∞	Reject	6.28	Reject	Reject
ou5u	∞	Reject	2.07	Accept	Reject
ou5l	11.3	Reject	6.9	Reject	Reject
ou6u	32.7	Reject	14	Reject	Reject
ou6l	21.3	Reject	15.6	Reject	Reject
ou7u	∞	Reject	∞	Reject	Reject
ou7l	∞	Reject	∞	Reject	Reject
ou8u	14.5	Reject	2.39	Accept	Reject
ou8l	6.94	Reject	0.757	Accept	Reject
nr1u	8.74	Reject	2.84	Reject	Reject
nr1l	1.8	Accept	∞	Reject	Reject
nr2u	0.772	Accept	∞	Reject	Reject
nr2l	2.32	Accept	∞	Reject	Reject
Casting Speed	∞	Reject	2.09	Accept	Reject
Mould Controller Status	1.62e+003	Reject	90.1	Reject	Reject
Mould level	2.68	Reject	1.09	Accept	Reject
Inlet Temperature	1.8	Accept	3.75	Reject	Reject
Flowrate WL	0.424	Accept	0.988	Accept	Accept
Flowrate WF	2.32	Accept	6.62	Reject	Reject
Flowrate NL	2.03	Accept	1.55	Accept	Accept
Flowrate NR	0.945	Accept	0.406	Accept	Accept
Delta T WL	4.76	Reject	4.65	Reject	Reject
Delta T WF	12.8	Reject	2.93	Reject	Reject
Delta T NL	2.18	Accept	2.77	Reject	Reject
Delta T NR	1.67	Accept	2.27	Accept	Accept
Oscillation Frequency	∞	Reject	19.3	Reject	Reject
Drive Current	1.52	Accept	∞	Reject	Reject
Heat Flux WL	4.82	Reject	6.2	Reject	Reject
Heat Flux WF	5.7	Reject	4.13	Reject	Reject
Heat Flux NL	2.2	Accept	2.79	Reject	Reject
Heat Flux NR	1.66	Accept	2.24	Accept	Accept
in1	∞	Reject	0.69	Accept	Reject
in2	6.44	Reject	1.99	Accept	Reject
in3	∞	Reject	2.06	Accept	Reject
in4	7.21	Reject	∞	Reject	Reject
in5	5.29	Reject	6.72	Reject	Reject
in6	18.8	Reject	5.16	Reject	Reject
in7	3.2	Reject	3.61	Reject	Reject
in8	2.01	Accept	0.855	Accept	Accept
nl1	∞	Reject	1.47	Accept	Reject
nl2	∞	Reject	0.324	Accept	Reject
ou1	1.53	Accept	1.07	Accept	Accept
ou2	2.2	Accept	1.17	Accept	Accept
ou3	3.81	Reject	1.24	Accept	Reject
ou4	9.08	Reject	4.62	Reject	Reject
ou5	5.86	Reject	∞	Reject	Reject
ou6	12.8	Reject	11.7	Reject	Reject
ou7	2.24	Accept	2.72	Reject	Reject
ou8	4.09	Reject	1.12	Accept	Reject
nr1	16.2	Reject	3.23	Reject	Reject
nr2	3.24	Reject	∞	Reject	Reject

the minimum difference between the theoretical and empirical distributions which will be detected with a power of 95%. Similarly, $\Delta_{0.5}$ is the minimum difference between the theoretical and empirical distributions which will be detected with a power of 50%.

$D_{\mu_{2b}}$ is the Kolmogorov-Smirnov test statistic value for bad slabs that exhibit defect 2b ("other inclusions") for a specific input variable. $H_0(D_{\mu_{2b}})$ is the outcome of the test. "Accept" means that the mean of a specific input variable for good and bad slabs is not different. "Reject" means that the means are different.

$D_{\sigma^2_{2b}}$ is the test statistic for the variances of bad slabs, and $H_0(D_{\sigma^2_{2b}})$ is the outcome of the test: "accept" means that the variances of a specific input variable is similar for both good and bad slabs and "reject" means that the variances are not the same.

$H_0(\boldsymbol{\mu}_{2b}) \cup H_0(\boldsymbol{\sigma}^2_{2b})$ is the final result outcome and means that if either the means test or the variances test is rejected, the input quite possibly has an influence on the occurrence of the defect in question. Both tests must be passed before it is decided that the variable has no influence on the defects.

The variables on which tests were performed are in column 1 of tables 3.3 and 3.4.

The Anderson-Darling tests (see table 3.4) have similar hypothesis conclusions as the Kolmogorov-Smirnov tests. The table shows the outcomes for the "other inclusions" defect. $a^2_c(114) = 2.492$ is the critical value for the test with 114 slabs. Note that all mean data are near-normal and all variance data are near χ^2 (skewed normal) so that the critical value of normal distributions of 2.492 reported by Johnson [140] was used for the Anderson-Darling tests, since precise critical values for the distributions are unknown. $A^2_{\mu_{2b}}$ is the test statistic for means and $A^2_{\sigma^2_{2b}}$ is the test statistic for variances. $H_0(\boldsymbol{\mu}_{2b})$ and $H_0(\boldsymbol{\sigma}^2_{2b})$ are the outcomes of the means and variances tests respectively. $H_0(\boldsymbol{\mu}_{2b}) \cup H_0(\boldsymbol{\sigma}^2_{2b})$ is the final outcome of the tests.

3.2.1.2 Interpretation

The Kolmogorov-Smirnov result (table 3.3) shows that most of the thermocouples[j] had an hypothesis rejection on both the means and variances, *i.e.* different from good slabs; implying that the thermocouple temperatures indicate that a (other inclusions) defect is likely to occur. The only outliers in this group are "in1l", "in3l", "in8l" and "nr2u", probably

[j]Thermocouples "ou6l" & "ou6l" are deemed inappropriate because these thermocouples were non-operational for most of the study.

due to bad contact within the mould[k], or simply that the defect never passed close to these thermocouples.

In some instances one of the tests, *e.g.* mean test, is accepted and the other, *e.g.* variance test, not (see "nr1l"). This implies that the scatter of the variable is larger than usual, but it still has a mean similar to that of good slabs. In some instances the variance test was accepted and the mean test not (*e.g.* "in1u"). This means that the scatter is similar to good slab cases but that the mean is different from the good slabs.

Other variables of note that are rejected in the Kolmogorov-Smirnov tests are

- the mould level, with a different mean value from that of good slabs,
- the casting speed, with a mean value different from that of the good slabs,
- water inlet temperature, with a rejection on both the mean and variance,
- wide front face water flow-rate,
- temperature differences,
- all heat fluxes with rejections on the variance tests, and
- most of the longitudinal temperature differences.

The Anderson-Darling tests have similar results for "other inclusions" as the Kolmogorov-Smirnov tests. The test, however, rejects all thermocouple temperatures with the exception of "in1l". The test also rejects variables similar to that of the Kolmogorov-Smirnov test such as casting speed, water inlet temperature, wide front face water flow-rate, heat fluxes and longitudinal temperature differences. In addition, mould level controller status is also rejected. Heat flux on narrow right side is accepted.

The results compare well with published results in the case of mould level, mould oscillation and casting speed (see table 2.1). These three variables were also considered in the published literature to be instrumental in inclusion formation [69]. The literature did however not state that thermocouple temperature or inlet temperature was an influential factor, but the statistical results show otherwise. The test that is probably more accurate is the Kolmogorov-Smirnov test, since it is equipped to deal with such a large number of values from the empirical distribution.

[k] a very common problem

Note that ∞ means that the test statistic was very high, *i.e.* fell completely outside the theoretical distribution.

3.2.1.3 Other defects

The statistical tests for other defects can be found in appendices A & B.

Transversal cracking The Kolmogorov-Smirnov and Anderson-Darling tests have a higher null hypothesis acceptance rate for transversal cracks variables than *e.g.* "other inclusions". This is because less data (only one slab was affected) were available for the tests and the possibility of making a type 1 error was higher (weak conclusions). Four thermocouples, oscillation frequency[1], and some of the longitudinal temperature differences were rejected in the Kolmogorov-Smirnov tests (see table A.1). The Anderson-Darling tests for transversal cracking (see table B.1) rejected seven thermocouples (including the four of the Kolmogorov-Smirnov tests), mould level, casting speed, oscillation frequency, drive current, and many of the longitudinal temperature gradients. From the literature review, transversal cracking is also affected by temperature variation in the mould [71]. This is underlined by the fact that the "in8u" and "in8l" thermocouples were rejected by the Kolmogorov-Smirnov and Anderson-Darling tests respectively. These thermocouples are situated near one of the transversal cracks occurring on the top left side after grinding has taken place. Casting speed and oscillation frequency are also noted from the literature study to be instrumental in the formation of the defect [77], which concurs with the result obtained from the statistical tests. In the defect literature, mould level is not generally noted as an influencing force (contrary to the mould level control literature), but was detected as influential by the statistical tests. Note that the Anderson-Darling test is probably more accurate than the Kolmogorov-Smirnov test because of the low number of samples from the empirical (bad) distribution.

Longitudinal cracking Three slabs contained longitudinal cracks. The Kolmogorov-Smirnov tests (see table A.2) rejected only one thermocouple variable. Other variables that were rejected were the inlet temperature and drive current. The Anderson-Darling tests (table B.2) rejected 6 thermocouple temperatures, mould controller status, drive current and several of

[1]Note that it will be shown later that casting speed and oscillation frequency are linearly dependent. This should have resulted in a rejection for casting speed on the Kolmogorov-Smirnov test. Noting from table A.1 the mean statistic for casting speed (0.971) is extremely close to the critical value (0.975), implying that the weak conclusion could be changed to a rejection of the null hypothesis.

the longitudinal temperature gradients. Mould level is considered based on the literature study to be an influencing factor in the formation of longitudinal cracks. However, the statistical tests show that mould level is not an influencing factor. Saito *et al.* [76] state that mould level has an influence on the formation of longitudinal *corner* cracks. As will be seen later, table 3.8 shows that no longitudinal corner cracks occurred and that is probably why the statistical tests show otherwise. In the Anderson-Darling test mould controller status is rejected, indicating that there is more manual control of mould level during the formation of the defect. Mould oscillation is also excluded as an influencing factor by the statistical tests but not by the literature [87]. This is probably because casting speed and mould oscillation frequency are linearly dependent (as will be seen from cross-correlation tests in §3.2.2) at the plant in question. If casting speed is shown to be an influencing factor, then oscillation frequency should also be an influencing factor. Casting speed is also not rejected by the statistical tests, but is considered based on the literature to be influential in the formation of the defect [88]. In the literature overview (page 21) it is said that casting speed variation or high casting speed is a factor in the formation of the defect. This is however not the case with the three defected slabs in question (graphs of casting speed are not shown).

Casting powder entrapment 7 thermocouple temperatures, wide front face flow-rate and 4 longitudinal thermocouple gradients were rejected for this defect with the Kolmogorov-Smirnov test (table A.3). 16 thermocouple temperatures, casting speed, mould controller status, oscillation frequency, and 12 longitudinal temperature differences were rejected with the Anderson-Darling tests (table B.3). This correlates well with the published results in table 2.1, except for mould level [69].

Bleeders 2 thermocouple temperatures and one thermocouple gradient were rejected by the Kolmogorov-Smirnov tests for the "bleeder" defect. See tables A.5 & B.5. Note that the result for "ou6l" can not be considered because the thermocouple was broken for most of the time period of data gathering. The thermocouple "in8u" is in the vicinity of the occurring defects at the top left location on the slab. No thermocouples were instrumental in the detection of the defects, based on the Anderson-Darling test. This is probably because the sample size is so small, and the Kolmogorov-Smirnov test should therefore be more accurate. The literature overview of table 2.1 showed that temperature was influential in the occurrence of the defect, similar to the result of the statistical tests [99].

Deep oscillation marks For deep oscillation marks, 5 thermocouple temperatures, 2 water flow-rates, 3 temperature differences and all heat fluxes were rejected. 6 longitudinal temperature differences were rejected. The above were all rejected by the Kolmogorov-Smirnov tests (table A.6). 6 thermocouple temperatures, mould controller status, 2 flow-rates, 3 temperature differences, and all the heat fluxes together with some longitudinal temperature differences were rejected by the Anderson-Darling tests (table B.6). The literature shows that mould oscillation [103] and casting speed [91, 160] also have influences, but the statistical tests did not consider this to vary much compared to good slabs.

Uneven oscillation marks These defects saw the rejection of 17 thermocouple temperatures, 3 flow-rates and 10 longitudinal temperature differences (table A.7). The Anderson-Darling test rejected 15 thermocouple temperatures, mould controller status, inlet temperature, 2 flow-rates and 10 longitudinal temperature differences (table B.7). The literature shows that mould oscillation and casting speed also have influences [91, 160], but the statistical tests did not consider this to vary much compared to good slabs.

Stopmarks All thermocouple temperatures were rejected for stopmarks by the Kolmogorov-Smirnov test. Casting speed, mould controller status and mould level were also rejected. All flow rates, heat fluxes and temperature differences were rejected. All longitudinal temperature differences were rejected. Similar results hold for the Anderson-Darling tests (table B.8). Only inlet temperature was not rejected and is thus supposed not to be influential in the formation of the defect. The huge rejection ratio implies that much goes wrong when this defect occurs, which is logical since it usually coincides with an abrupt slow-down of the strand and could probably be predicted by only considering the casting speed.

Depressions 25 thermocouple temperatures, casting speed, inlet temperature, temperature differences, oscillation frequency, heat fluxes and some of the longitudinal temperature differences were rejected for depressions using the Kolmogorov-Smirnov tests (table A.9). Similarly, all thermocouple temperatures except one were rejected using the Anderson-Darling tests (table B.9). Casting speed, mould controller status, inlet temperature, temperature differences, oscillation frequency, and 3 heat fluxes were rejected as well as nearly all the longitudinal temperature differences. Temperatures variations as a cause of depressions agrees with the literature review but all other variables are supposed to be non-influential [110, 111]. The high rejection ratio is probably due to the large sample size. Interestingly enough, mould level was accepted and is thus supposed to be uninfluential.

3.2.1.4 Summarised result

Table 3.5 shows a summary of the statistical results for both the Kolmogorov-Smirnov and Anderson-Darling tests. MCS is the mould controller status, OF the oscillation frequency, and LTD the linear temperature differences.

From the table it is evident that thermocouple temperatures play an important role in the detection or control of the respective defects, since their means and variances are considerably different for bad slabs compared to good slabs. All nine defects continually show that there are differences between good and bad slabs. Casting speed seems to differ from the good slabs only in three cases using the Kolmogorov-Smirnov test and in 5 cases using the Anderson-Darling test. The mould controller status, which describes whether a mould controller was used during operation, is influential only for bleeders using the Kolmogorov-Smirnov test; but is influential in all defects, except transversal cracks, using the Anderson-Darling test. Inlet temperature is influential in three defects, and the flow rates have an influence in 5 defects using the Kolmogorov-Smirnov test and 4 defects using the Anderson-Darling tests. The temperature differences are influential in 4 defects, and the oscillation frequency varies between 4 and 5 defects for the respective tests. Drive current affects three and four defects respectively, and the heat fluxes influence 4 of the defects. The longitudinal temperature differences affect all defects except longitudinal cracks as tested by the Kolmogorov-Smirnov test.

The results indicate that thermocouples are heavily influential in the detection or control of the defects, with some other variables such as casting speed, oscillation frequency, flow rates, temperature differences, drive currents and heat fluxes not far behind.

3.2.2 Correlation

This section describes the use of correlation to determine whether there is linear dependence between variables so that some variables can be dropped from possible modelling strategies.

Tables C.1, C.2, C.3, C.4 and C.5 in appendix C show correlation variables of the time-series inputs split into columns over five tables.

Note that multivariate techniques such as principal component analysis [158] on the correlation table can be used to determine influential variables. These methods were however not considered because enough information is contained in the table itself to make accurate

Table 3.5 Summarised results for Kolmogorov-Smirnov and Anderson-Darling tests. ○ indicates that the variable is a cause of the defect based on the literature survey and ● indicates that the variable is influential based on the goodness-of-fit tests. T is the total number of defects influenced by a variable based on the goodness-of-fit tests.

Variable	Kolmogorov-Smirnov									
	1a	1b	2a	2b	4	5a	5b	6	8	T
Thermocouple	●○	●○	●	●	●○	●○	●○	●	●○	9
Casting Speed	?○	○	○	●○		○	○	●○	●	4
MCS								●		1
Mould Level		○	○	●○				●		2
Inlet Temperature		●		●					●	3
Flow Rate			●	●		●	●	●		5
Delta T				●		●		●	●	4
OF	●○	○	○	●○		○	○	●	●	4
Drive Current	●	●						●		3
Heat Flux				●		●		●	●	4
LTD	●		●	●	●	●	●	●	●	8
	Anderson-Darling									
Thermocouple	●○	●○	●	●	○	●○	●○	●	●○	8
Casting Speed	●○	○	●○	●○		○	○	●○	●	5
MCS		●	●	●	●	●	●	●	●	8
Mould Level	●	○	○	●○				●		3
Inlet Temperature				●			●		●	3
Flow Rate				●		●	●	●		4
Delta T				●		●		●	●	4
OF	●○	○	●○	●○		○	○	●	●	5
Drive Current	●	●		●				●		4
Heat Flux				●		●		●	●	4
LTD	●	●	●	●	●	●	●	●	●	9

judgements on the cause and effect as well as the cross-correlation of the variables. Furthermore, interactive terms are also not considered because it is assumed that the effects are linearly dependant. Sections 3.3 and 3.4 will show that this is an accurate assumption.

The following important observations are made based on the correlation table:

1. The correlation parameter between casting speed (CS) and oscillation frequency (OF) in Table C.5 is one. This indicates that oscillation frequency is linearly dependent on casting speed. This is a common practice in industry [161]. Because of this, oscillation frequency does not provide additional information and can be excluded from the model.

2. Table C.4 shows that the heat fluxes (HWL, HWF, HNL and HNR) are perfectly positively correlated with the temperature differences (DWL, DWF, DNL and DNR respectively). This implies that the heat fluxes can be excluded from the model.

3. The thermocouple temperatures, in turn, have medium ($0.5 < \rho_{XY} \leq 0.75$) to strong ($0.75 < \rho_{XY} \leq 1$) correlations to the temperature differences which indicates that the temperature differences are computed from thermocouple temperatures. This was also validated with plant personnel[m] and thus the temperature differences should also be scrapped from the model.

4. The longitudinal temperature differences also correlate well with the thermocouple temperatures[n]. Therefore they should also be ignored from any model.

5. The drive current (DC) is not related to the mould section of the system and can also therefore be neglected from a model. This is underlined by the fact that correlations with other input variables are weak.

6. The flow rates (FWL, FWF, FNL and FNR) are weakly correlated ($0 \leq \rho_{XY} \leq 0.25$) with all other input variables. This is probably because the flow rates are usually maintained at a maximum with no changes (maximum changes of about 1.5%); implying that they have no effect on the output. The flow rates should then be dropped from the model.

[m]The dependence is not necessarily linear.

[n]These were in fact computed by the author from the thermocouple temperatures with the top row values delayed by the same amount of time as it would take a narrow strip of steel to move from the top row to the bottom row. The correlation with the top row was always strong.

7. The inlet temperature (IT) have a weak to medium correlation with the thermocouple temperatures. It is also very weakly correlated with casting speed. The inlet temperature has a medium correlation to mould level which is probably due to the stochastic nature of mould level.

8. Mould level (ML) is weakly correlated with the thermocouple temperatures. There exists a medium correlation between casting speed and mould level. This could also be due to the stochastic nature of mould level or because there may be some output feedback, *i.e.* as the speed increases, the mould level should drop momentarily. Note however that mould level is controlled at this plant with a slide gate. The effect of mould level may not be linear on other variables, but may have some non-linear effect or a delay may be present. Since it is considered to be an important variable to control, mould level will not be excluded from any model.

9. Mould controller status (MCS) only takes on values of zero or one and can therefore not be included in the linear model.

10. Casting speed has medium to strong correlations with the thermocouple temperatures and should therefore be included in the model as a manipulated variable.

3.2.3 Conclusion

Based on the above results, and the results in §3.2.1, the following conclusions can be made regarding the model structure. Due to the strong variation when defects occur compared to the case when defects do not occur (as indicated by the goodness-of-fit-tests), the thermocouple temperatures are influential (and/or carry much information) in the detection of defects. Note, however, that this does not imply that mould temperature is necessarily a cause in the formation of all the defects. The mould temperature may be influential in the formation of some defects as the literature shows, but the formation of the defects can be detected from temperature readings.

The strong correlation of casting speed with temperature gives an indication that casting speed can be used as a manipulated variable[o] to control temperature. This is also intuitive because a basic energy, mass and momentum balance of the system given by $\frac{\partial H}{\partial t} + \upsilon\frac{\partial H}{\partial z} + \rho\upsilon\frac{\partial \upsilon}{\partial t} = \nabla \cdot K\nabla T$ shows that an increase in casting speed must be balanced by an increase

[o]see Langer and Moll [162], Lally, Biegler, and Henein [163] and Lally, Biegler, and Henein [164] for optimal steady casting speed design to improve quality.

in temperature [35]. Lastly, measured disturbances that have an impact on the mould temperature are inlet temperature and mould level. These are the only variables that remain after the correlation result in table 3.5. These will then be used as measured disturbances, because they should remain constant and can therefore not be controlled. All other variables are left out because they are either non-influential on the defects or they are strongly correlated to the thermocouple temperatures.

It is proposed that the model structure be broken down into two sub-models (compare Fig. 3.6 on p.72). The first sub-model will be called the manipulated variable (MV) to intermediate variable (IV) model and the second sub-model will be called the intermediate variable (IV) to output variable (OV) model. The (only) MV is casting speed and the IVs are the thermocouple temperatures. The OVs are defects. The structure is depicted in Fig. 3.10. The measured disturbances in the MV to IV model are mould level and inlet temperature and

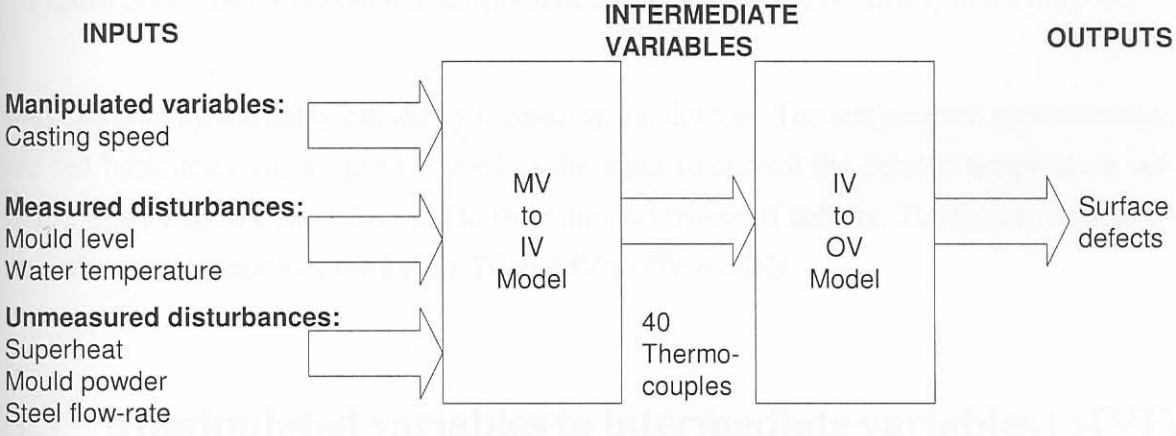

Figure 3.10 Separation of system into two models, manipulated variable to intermediate variable and intermediate variable to output variable.

the unmeasured disturbances are, amongst others, superheat, mould powder addition and flow-rate of steel into the mould.

Inlet (water) temperature was chosen to form part of the MV to IV model because a change in the inlet temperature has a direct effect on the thermocouple temperatures as the correlation showed. However, the variable could also have been made part of the IV to OV model, if desired, but this would be unwise since the variable is influential on the thermocouple temperatures and repetition of information could result. The mould level forms part of the MV to IV model because it is also already a controlled variable. Placing it in as part of the IV to OV model defeats the purpose because the inputs to the IV to OV model must ideally be changeable, and change in the mould level set-point is undesired, though this matter may be explored later.

The usefulness of this separation of the model into two sub-models is that the delay that occurs before the defects are measured is outside the feedback control loop. The IV to OV model can be used to find an optimal set-point for the temperatures and the MV to IV model can be used to design a controller to follow the temperature set-points so that the effect that temperature variation has on the formation of defects is negated. A block diagram of the structure for control is given in Fig.3.11. The temperatures are measured instantaneously,

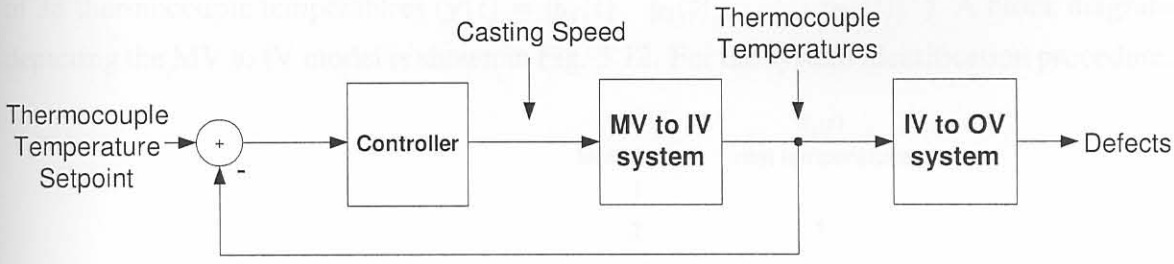

Figure 3.11 Block diagram description of the separation for control systems purposes.

thus eliminating the delay caused by measuring the defects. The temperature measurements are fed back and casting speed is used as the input to control the desired temperature set-point. The IV to MV model is used to infer the occurrence of defects. The next two sections describe the derivation of the MV to IV and IV to OV models.

3.3 Manipulated variables to intermediate variables (MVIV) model

This section describes the derivation of the manipulated to intermediate variables (MV to IV) model using system identification. Specifically, the ARX model structure will be used (see §2.2.4).

Note that in all cases it was verified (but not shown) that the residuals in the models are not auto-correlated (*i.e.* they are Gaussian) and there is no cross correlation between the input and the residuals (*i.e.* no output feedback or delays).

3.3.1 Derivation of the MVIV model

3.3.1.1 MVIV model set-up

The MV to IV model consists of one manipulated variable, casting speed ($u(t)$) and two measured disturbances, mould level ($d_1(t)$) and inlet temperature ($d_2(t)$). The outputs consist of 38 thermocouple temperatures ($\mathbf{y}(t) = [y_1(t) \quad y_2(t) \quad \dots \quad y_{38}(t)]^\top$). A block diagram depicting the MV to IV model is shown in Fig. 3.12. For the system identification procedure,

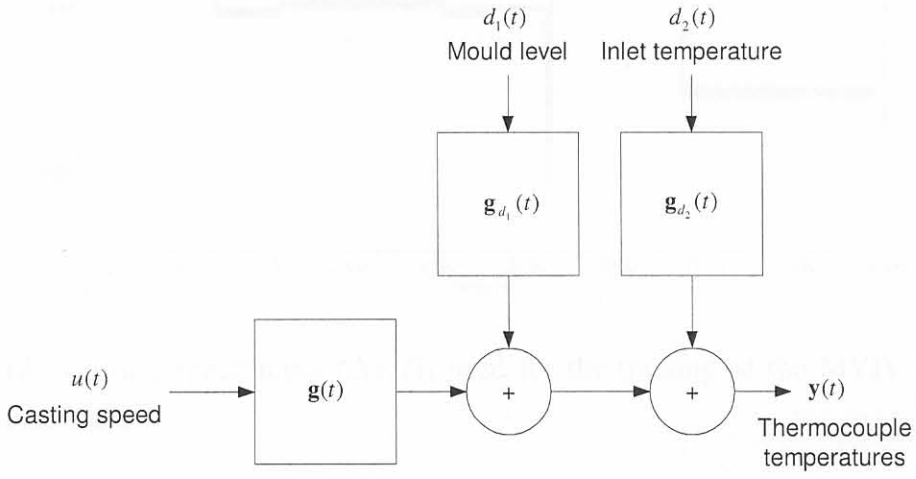

Figure 3.12 Block diagram depiction of the MV to IV model showing, manipulated variable, disturbances and output variables.

casting speed, mould level and inlet temperatures are inputs (*i.e.* $m = 3$ in §2.2.4). The thermocouple temperatures are the outputs (*i.e.* $p = 38$ in §2.2.4). Four models were derived based on the width of the slab that was being cast. These widths are 1060mm, 1280mm to 1290mm, 1320 to 1335mm and 1575mm wide slabs. (No specific variability was noticed when training the models using data which were divided based on the type of steel cast *e.g.* austenitic, ferritic, *etc.*). The normalised inputs used in the training of the 1060mm wide slab models are shown in Figs. 3.13, 3.14 and 3.15. Three important points for the regression procedure have to be mentioned here.

1. The value of the first point of the (time) data used is subtracted from all the data for each input variable so that the regression can be done with data starting from zero. The value of this first data point was then considered to be the offset of the data, and all data then become deviational from this point. This method delivered better results than simply removing the mean of the training data ("zero-order detrend").

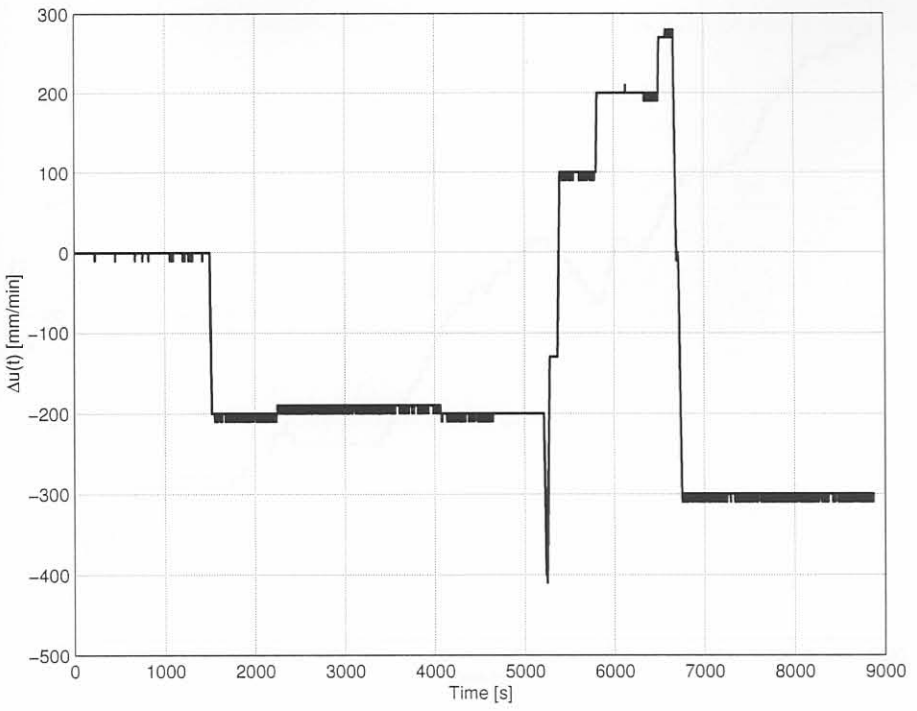

Figure 3.13 Casting speed input ($\Delta u(t)$) used for the training of the MVIV model for 1060mm wide slabs.

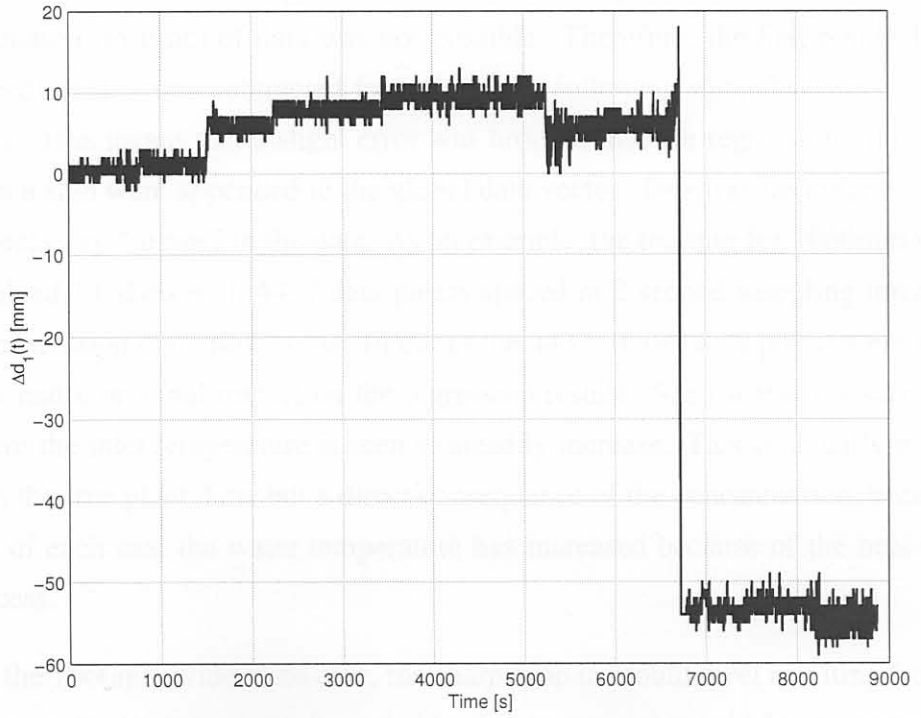

Figure 3.14 Mould level disturbance input ($\Delta d_1(t)$) used for the training of the MVIV model for 1060mm wide slabs.

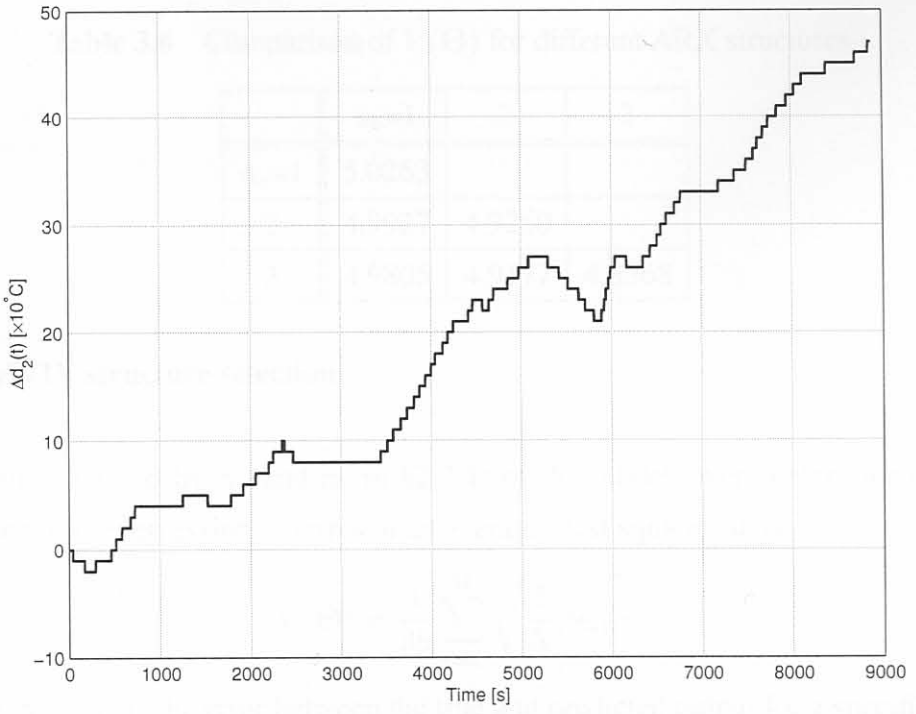

Figure 3.15 Water temperature disturbance input ($\Delta d_2(t)$) used for the training of the MVIV model for 1060mm wide slabs.

2. Since slabs that were inspected did not necessarily follow each other, simple concatenation (in time) of data was not possible. Therefore, the first point of data of a preceding slab was subtracted from data of a following slab. This was done for all slabs. This meant that a slight error was brought into the regression every time data from a slab were appended to the global data vector. This was necessary to eliminate unnecessary "jumps" in the data. As an example, the training for 1060mm wide slabs involved 14 slabs with 4437 data points spaced at 2 second sampling intervals. The concatenation then implies that 14 out of the 4437 (0.3%) data points were erroneous. This had a minimal impact on the regression results. See for interest sake Fig. 3.15 where the inlet temperature is seen to steadily increase. This is actually not the case with the true plant data, but a direct consequence of the concatenation, because at the end of each cast the water temperature has increased because of the heat extraction process.

3. For the 1060mm wide slabs case, the sharp drop in mould level resulting from a sharp decrease in casting speed, is probably due to manual mould level control. This is another reason to include mould level in the model.

Table 3.6 Comparison of $V(\hat{\Theta})$ for different ARX structures.

	n_b=1	2	3
n_a=1	5.0263		
2	4.9927	4.9260	
3	4.9805	4.9177	4.8368

3.3.1.2 MVIV structure selection

The structure (defined by n_a and n_b in §2.2.4) of the models were determined based on performance of the regression in terms of an average least squares fit as

$$V(\hat{\Theta}) = \frac{1}{38}\sum_{i=1}^{38}\sqrt{\frac{1}{N}||\epsilon_i||^2}, \tag{3.8}$$

where $\epsilon_i = \mathbf{y}_i - \hat{\mathbf{y}}_i$ is the error between the true and predicted output for a specific output i, over some time period, $t_0 \leq t \leq t_1$. $||\cdot||$ is the Euclidean norm. N is the number of data points used. The output matrices of Eq. 2.19 are all assumed to be diagonal, since none of the thermocouples are assumed to influence each other. As an example, consider the results of a regression on the 1060mm wide slabs as a function of n_a and n_b; depicted in Table 3.6. The table shows that an increase in regressors (model parameters) does not greatly improve the overall accuracy of the model. For instance, an increment in the number of poles from one to two (*i.e.* n_a increases from one to two while $n_b = 1$) only delivers a 0.7% increase in the overall fit. An increase from $n_a = 1$ and $n_b = 1$ to $n_a = 3$ and $n_b = 3$ only delivers an 3.8% decrease in the error[p]. This is further emphasised when looking at a plot of the model output for one thermocouple, in1u ($\Delta y_1(t)$), with $n_a = 1$ and $n_b = 1$ and $n_a = 3$ and $n_b = 3$ (Fig. 3.16). The figures show that the maximum change is about 2.5°C. Due to this close proximity of the models, the simple first order model ($n_a = 1$ and $n_b = 1$) was used to train the model. Similar results were obtained for the other outputs. Note that no visible delay is detected in the analysis of the residuals.

3.3.1.3 MVIV time domain results

Computer simulation of the model with plant inputs and outputs used to train the MV to IV model delivered good results. Fig. 3.17 shows the output of the model versus the true

[p]For 1280 mm wide slabs, the increase from $n_a = 1$ and $n_b = 1$ to $n_a = 3$ and $n_b = 1$ delivers a 1.2% improvement and for 1575mm wide slabs the increase from $n_a = 1$ and $n_b = 1$ to $n_a = 3$ and $n_b = 3$ delivers a 1.1% improvement. See Appendix D.

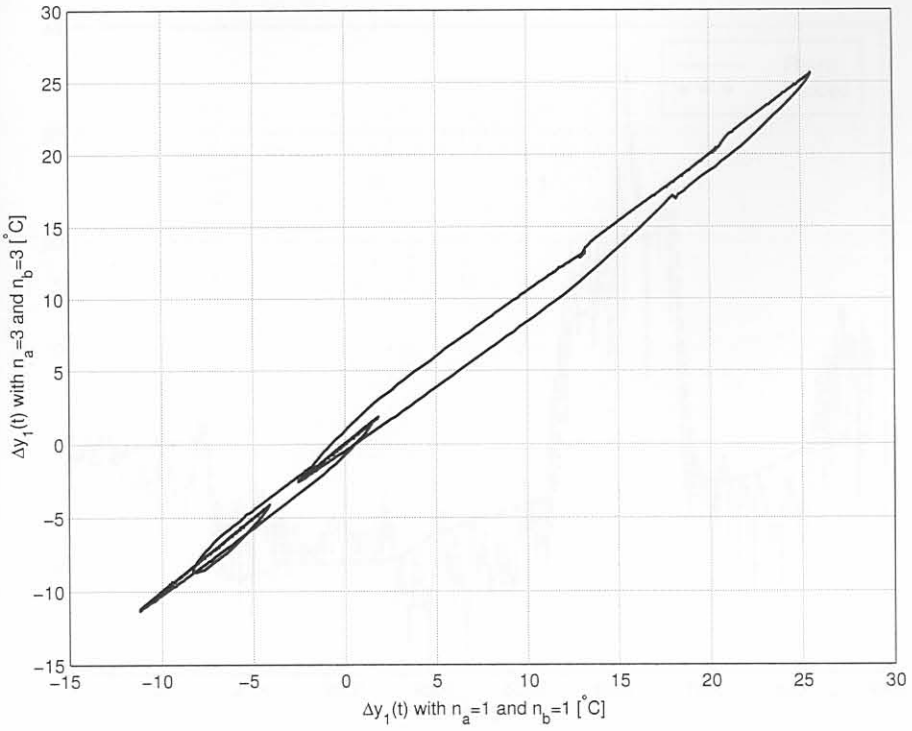

Figure 3.16 Comparison of model outputs for different structures of the MV to IV model for thermocouple in1u ($\Delta y_1(t)$).

plant data for thermocouple in1u (output $\Delta y_1(t)$) for 1060mm wide slabs. Similarly, Fig. 3.18 and Fig. 3.19 show the model and plant outputs for thermocouples nr1u ($\Delta y_{35}(t)$) and nr2u ($\Delta y_{37}(t)$) respectively. Note that similar results were found for 1280mm wide slabs and 1575mm wide slabs. See Appendix D. The noise that is visible can be attributed to measurement noise on the thermocouples; and also unmodelled dynamics because of unmeasured disturbances such as varying flux thickness layers at the mould-strand interface and other unmeasured disturbances such as superheat, steel flow rate *etc.*

3.3.1.4 Validation of the MVIV model

Two-thirds of the data were used to train the MVIV models and one third were used for validation of the MVIV model. Figs. 3.20 and 3.21 show the model outputs for thermocouples in2u and nr1u of the 1280mm wide model based on the *validation data* (not used for model fitting). The inputs (casting speed, mould level and water temperature) can be found in appendix E. The model output follows the true plant data reasonably accurately. The same can be said about the response of the other thermocouples as well as the response of the 1060mm and 1575mm wide slab validation data.

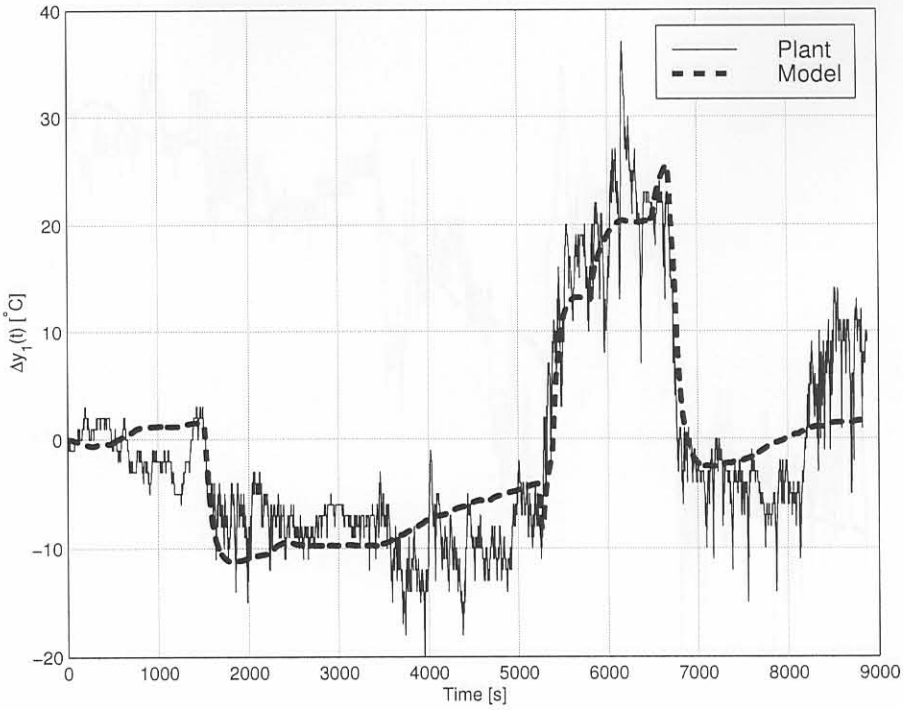

Figure 3.17 Comparison of model output and plant output for thermocouple (output) in1u ($\Delta y_1(t)$) with $n_a = 1$ and $n_b = 1$. The mean square fit is $\sqrt{||\epsilon_1||^2/N} = 4.341$.

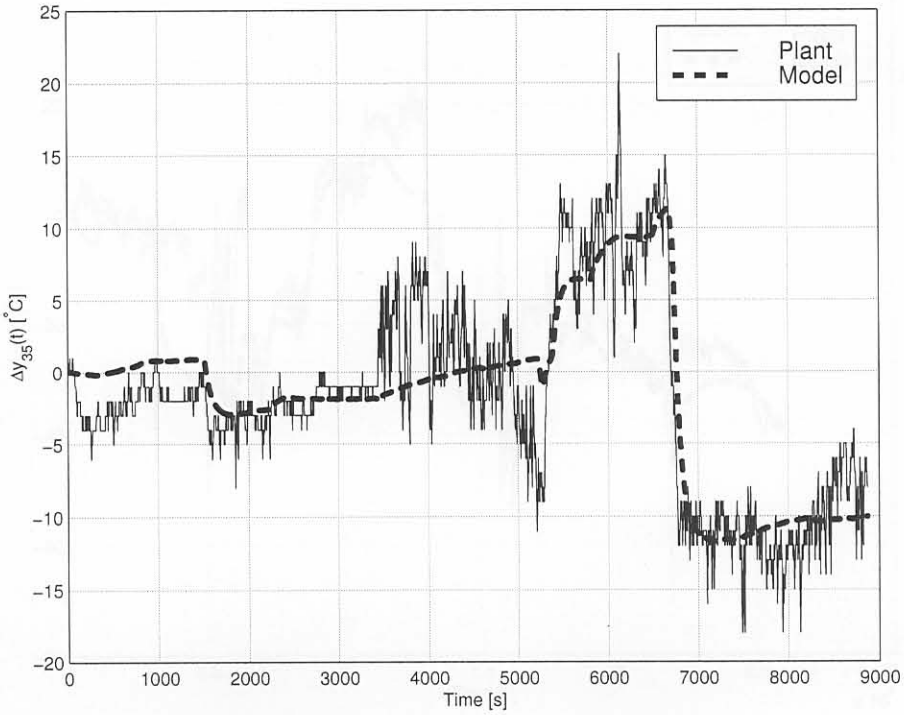

Figure 3.18 Comparison of model output and plant output for thermocouple (output) nr1u ($\Delta y_{35}(t)$) with $n_a = 1$ and $n_b = 1$. $\sqrt{||\epsilon_{35}||^2/N} = 3.131$.

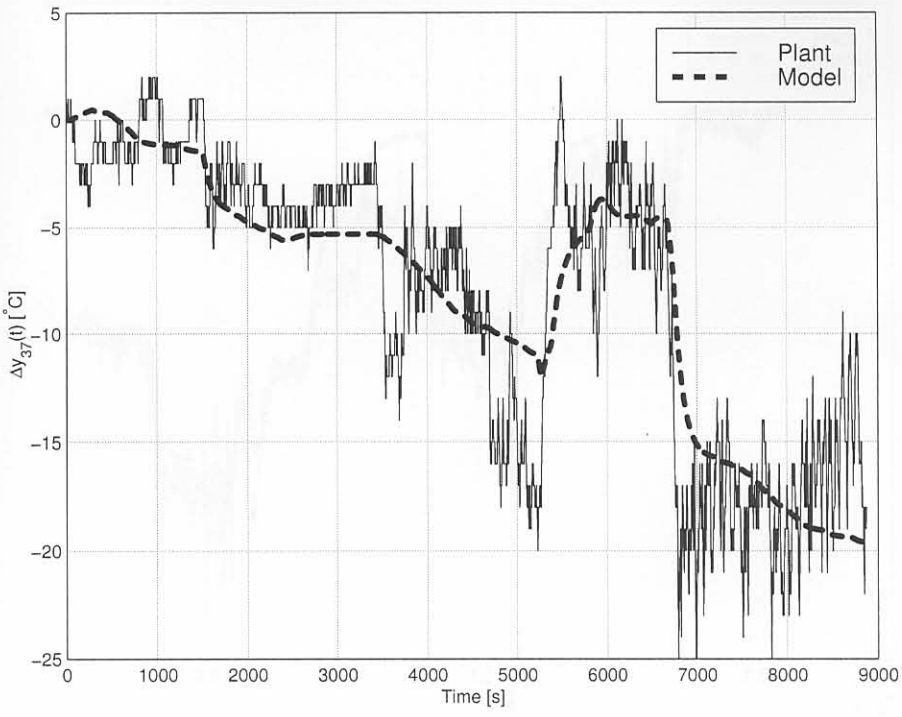

Figure 3.19 Comparison of model output and plant output for thermocouple (output) nr2u ($\Delta y_{37}(t)$) with $n_a = 1$ and $n_b = 1$. $\sqrt{||\epsilon_{37}||^2/N} = 3.235$.

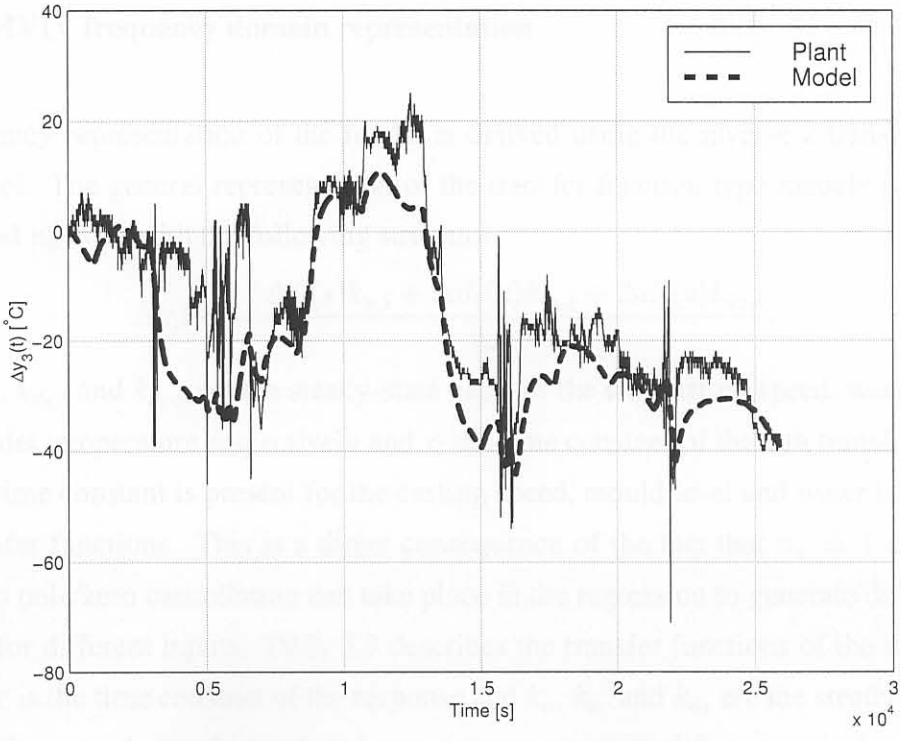

Figure 3.20 Comparison of model output and plant output for thermocouple (output) in2u ($\Delta y_3(t)$) on the *validation data* for 1280mm wide slabs. $\sqrt{||\epsilon_3||^2/N} = 10.411$

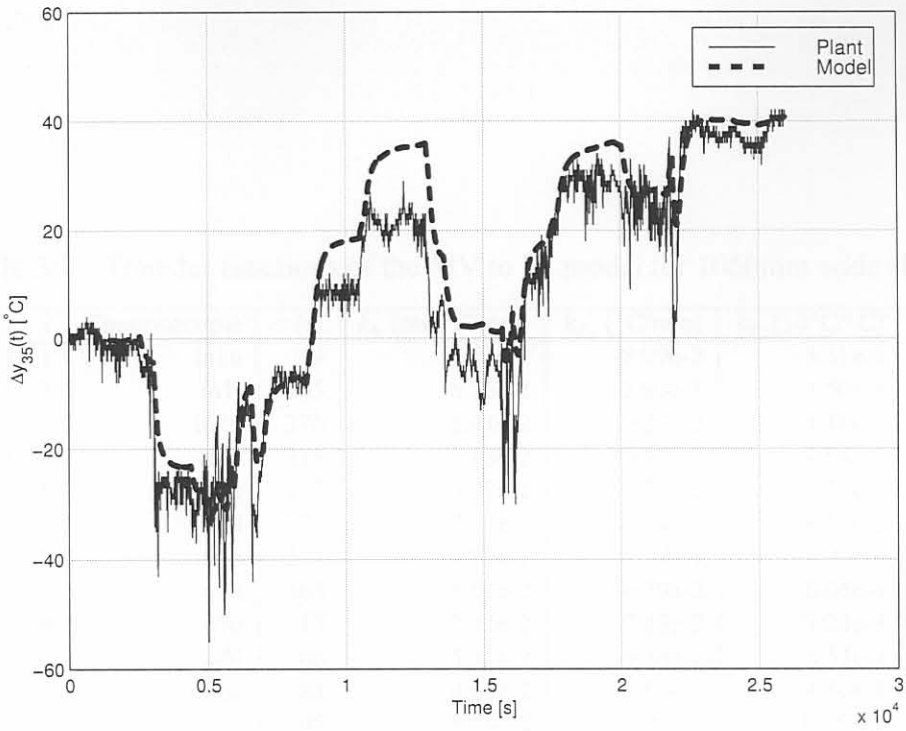

Figure 3.21 Comparison of model output and plant output for thermocouple (output) nr1u ($\Delta y_{35}(t)$) on the *validation data* for 1280mm wide slabs. $\sqrt{||\epsilon_{35}||^2/N} = 7.670$

3.3.1.5 MVIV frequency domain representation

The frequency representation of the model is derived using the inverse z-transform of the ARX model. The general representation of the transfer function type models is first order ($n_a = 1$ and $n_b = 1$) with the following structure.

$$\Delta y_i(s) = \frac{\Delta u(s)k_{u,i} + \Delta d_1(s)k_{d_1,i} + \Delta d_2(s)k_{d_2,i}}{\tau_i s + 1}, \tag{3.9}$$

where $k_{u,i}$, $k_{d_1,i}$ and $k_{d_2,i}$ are the steady-state gains of the i-th casting speed, water temperature and inlet temperature respectively and τ_i the time constant of the i-th transfer function. Only one time constant is present for the casting speed, mould level and water inlet temperature transfer functions. This is a direct consequence of the fact that $n_a = 1$ and $n_b = 1$ because no pole/zero cancellation can take place in the regression to generate different time constants for different inputs. Table 3.7 describes the transfer functions of the model. In the table, τ is the time constant of the response and k_u, k_{d_1} and k_{d_2} are the steady-state gains of the casting speed, mould level and water temperature models respectively. The time-constants vary greatly from values as low as 17 seconds (in5u) to as high as 606 seconds (ou7l). This can be attributed to several factors. Firstly, the contact of the thermocouple to the copper plate may vary from thermocouple to thermocouple, thus making the thermal

Table 3.7 Transfer functions of the MV to IV model for 1060mm wide slabs.

i	Thermocouple	τ [s]	k_u [min°C/mm]	k_{d_1} [°C/mm]	k_{d_2}[10°C/°C]
1	in1u	69	6.07e-2	-8.99e-2	3.31e-1
2	in1l	185	6.75e-2	-2.93e-1	7.50e-1
3	in2u	276	1.44e-2	9.27e-2	-4.16e-1
4	in2l	315	1.88e-2	-9.87e-2	-4.64e-1
5	in3u	117	4.07e-2	1.21e-2	1.58e-1
6	in3l	221	3.22e-2	-1.94e-1	-8.18e-2
7	in4u	235	3.94e-2	1.19e-1	7.96e-1
8	in4l	305	5.51e-2	-6.39e-2	6.05e-1
9	in5u	17	3.11e-2	7.13e-2	1.21e-1
10	in5l	206	5.11e-2	-9.30e-2	5.51e-1
11	in6u	84	4.69e-2	-8.80e-2	4.10e-1
12	in6l	298	8.24e-2	-2.92e-1	1.35e+0
13	in7u	127	4.33e-2	-7.68e-2	2.75e-1
14	in7l	226	6.33e-2	-9.39e-2	9.24e-1
15	in8u	72	3.99e-2	-2.63e-2	1.22e-1
16	in8l	135	4.57e-2	1.41e-1	7.22e-1
17	nl1u	62	1.78e-2	-2.31e-2	1.12e-1
18	nl1l	87	1.34e-2	-1.27e-1	-4.22e-3
19	nl2u	122	1.72e-2	1.90e-1	-3.13e-2
20	nl2l	117	2.44e-2	-4.24e-2	-4.49e-1
21	ou1u	101	6.44e-2	-2.00e-1	-2.48e-2
22	ou1l	165	5.92e-2	5.35e-2	6.43e-1
23	ou2u	137	6.42e-2	-1.40e-1	2.92e-1
24	ou2l	210	6.89e-2	-1.72e-1	5.85e-1
25	ou3u	235	3.49e-2	-1.24e-1	-5.65e-1
26	ou3l	324	6.06e-2	-2.39e-1	-1.74e-1
27	ou4u	241	3.04e-2	3.40e-2	-1.58e-1
28	ou4l	434	2.41e-2	3.17e-2	-3.93e-1
29	ou5u	136	3.82e-2	-2.17e-2	5.15e-1
30	ou5l	247	6.41e-2	-6.37e-2	9.66e-1
31	ou7u	228	7.08e-2	-7.64e-3	1.09e+0
32	ou7l	606	9.65e-2	6.27e-2	2.54e+0
33	ou8u	66	6.82e-2	-2.03e-1	1.70e-1
34	ou8l	169	7.56e-2	-1.70e-1	1.12e+0
35	nr1u	69	2.28e-2	1.77e-1	1.41e-1
36	nr1l	108	2.34e-2	1.16e-1	4.94e-1
37	nr2u	100	1.60e-2	2.02e-2	-2.99e-1
38	nr2l	120	8.71e-3	-2.99e-2	-1.42e-1

resistance different, causing a longer time constant. The effect that an increase in the air gap between the copper and thermocouple has on the thermal resistance (proportional to time constant) is shown in fig. 3.22.

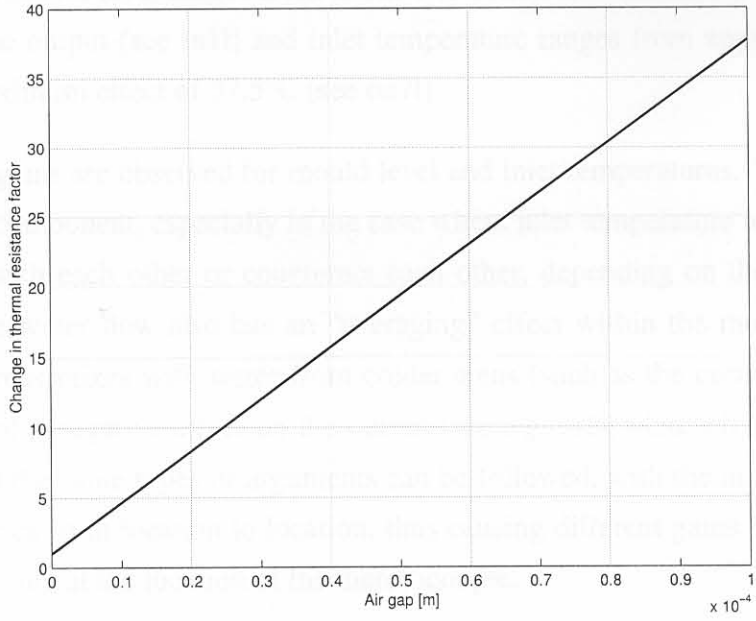

Figure 3.22 Proportional increase in the time constant of the temperature measured by a thermocouple.

The graph was calculated using a convection model describing the proportional change in thermal conductivity of the system when the air gap increases compared to the case when there is no air gap [165]:

$$R_{ch} = \frac{l_{air}/k_{air}}{l_{copper}/k_{copper} + l_{typeK}/k_{typeK}} + 1, \tag{3.10}$$

where l_{air} is the air gap, $l_{copper} = 35$mm is the copper-plate width, $l_{typeK} = 1$mm is the casing width of the thermocouple, and $k_{copper} = 386$W/mK, $k_{air} = 0.027$W/mK, and $k_{typeK} = 65$W/mK are the respective thermal conductivities. An air gap of 90μm caused by a shock to the mould during installation can cause the time constant to increase by a factor of 35 (*e.g.* from 17 to 600 seconds). Good thermocouple installation and maintenance is therefore very important if correct readings are desired. Secondly, the mould plate may vary in thickness from area to area, thus making the thermal resistance different. Thirdly, there may be more mould flux situated in different areas, making the thermal resistance different.

The time constants also increase from the top row to the bottom row, indicating that an increasing shell thickness causes a greater thermal resistance.

Though not immediately clear, the casting speed has the greatest steady-state effect on the outputs. This is because the casting speed can range from 0 to 1000 mm/min. A change of 1000mm/min can have a maximum effect of a 96.5°C change on the ou7l output[q] at steady state. Similarly, mould level ranges from about 0 to 60mm and can have a maximum effect of 17.6°C on the output (see in1l) and inlet temperature ranges from approximately 25 to 40°C with a maximum effect of 37.5°C (see ou7l).

Some negative gains are observed for mould level and inlet temperatures. This may be due to a non-linear component, especially in the case where inlet temperature and casting speed either interact with each other or counteract each other, depending on the temperature of the strand. The water flow also has an "averaging" effect within the mould, since water from warmer areas mixes with water from colder areas (such as the corners), thus having the possibility of a negative effect on the output (see *e.g.* nl1l, nl2u, nl2l, nr2u and nr2l). For mould level the same types of arguments can be followed, with the most feasible being that the flux varies from location to location, thus causing different gains depending on the thickness of the flux at the location of the thermocouple.

Many other (unmeasured) disturbances are also present which can play a role in determining the model parameters. The ARX scheme used is simple to understand and to train and is useful for control system analysis and design. It also proves adequate as a modelling scheme for the MVIV model, in both the frequency and time domains.

See the frequency domain tables in Appendix F for 1280mm and 1575mm wide slabs.

Figs. 3.23, 3.24 and 3.25 depict Bode plots between casting speed, mould level and inlet temperature and the thermocouple temperatures, respectively. Appendix F show the frequency responses for 1280mm and 1575mm wide slabs.

This section presented the MV to IV model derivation using ARX techniques. The resulting model to plant fits are considered very good as shown by the training and validation data, given that there are unmeasured disturbances interacting on the system. Not all data can be shown, due to constraints of space. The MV to IV model can be used to design controllers to follow pre-defined set-points for the thermocouple temperatures.

[q] ou7l has the largest steady state gain

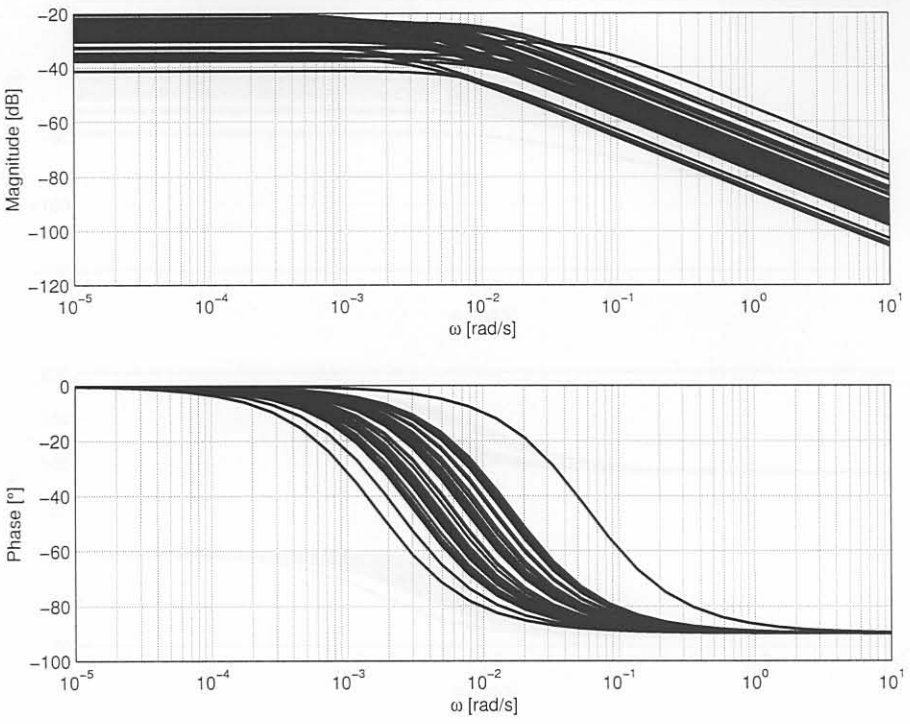

Figure 3.23 Bode plot of the transfer functions between casting speed and the thermocouple temperatures for 1060mm wide slabs.

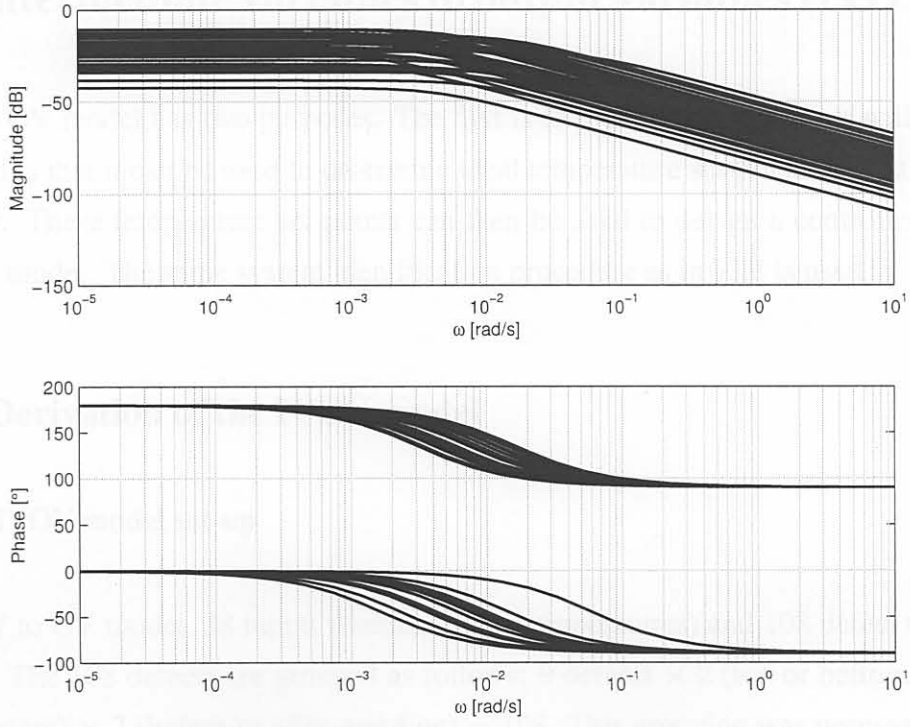

Figure 3.24 Bode plot of the transfer functions between mould level and the thermocouple temperatures for 1060mm wide slabs.

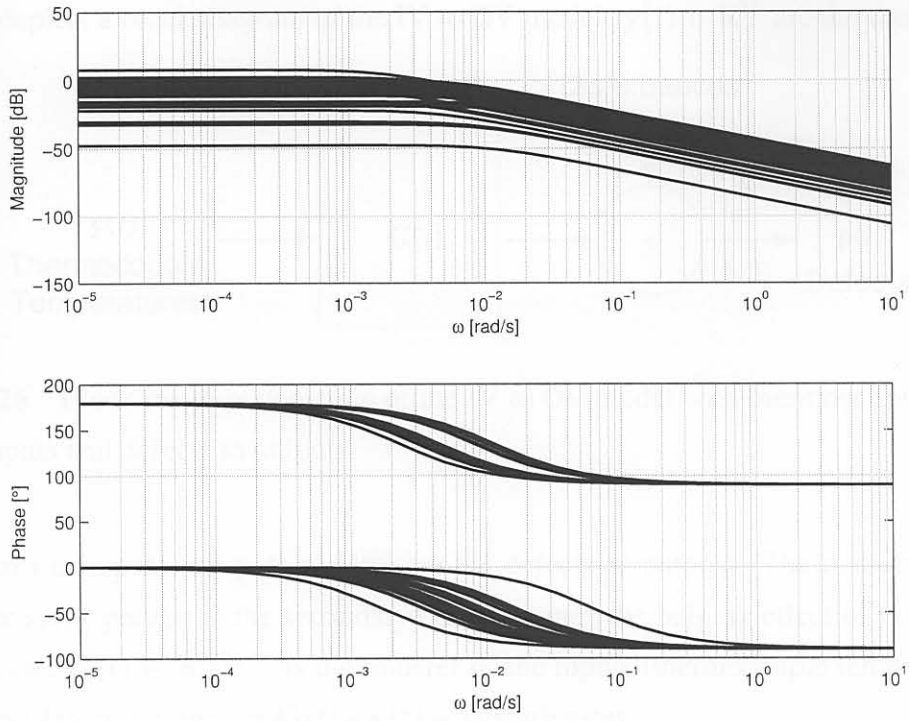

Figure 3.25 Bode plot of the transfer functions between inlet temperature and the thermocouple temperatures for 1060mm wide slabs.

3.4 Intermediate variables to output variables (IVOV) model

The IV to OV model has two purposes. The first is to predict when a defect will occur and the second is that it can be used to determine ideal temperature set-points so that no defects will occur. These temperature set-points can then be used to design a controller using the MV to IV model. The same system identification procedure as in §3.3 is used.

3.4.1 Derivation of the IVOV model

3.4.1.1 IVOV model set-up

For the IV to OV model, 38 inputs (thermocouple temperatures) and 108 defect outputs are available. The 108 defects are grouped as follows: 9 defects $\times$ 2 (top or bottom) $\times$ 3 (left, right or centre) $\times$ 2 (before or after grinding) $= 108$. This grouping was necessary because the defects roughly correspond to the location of the thermocouples. Therefore $m = 38$ and $p = 108$.

Fig. 3.26 depicts a block diagram of the IV to OV model. $\mathbf{y}(t) \in \mathbb{R}^{38}$ are the thermocouple

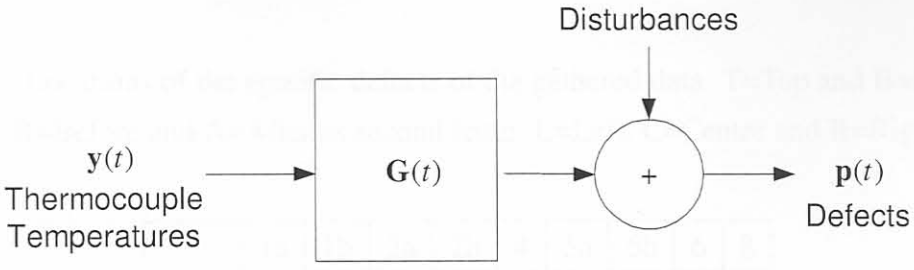

Figure 3.26 Block diagram depiction of the IV to OV model with thermocouple temperatures as inputs and defects as outputs.

temperatures as inputs and $\mathbf{p}(t) \in \mathbb{R}^{108}$ are the defects as outputs. The disturbances may include the spray pattern in the secondary cooling zone[r], the bulging effect of the rollers on the strand *etc.* $\mathbf{G}(t) \in \mathbb{R}^{108\times 38}$ is the transfer of the inputs (thermocouple temperatures) to the outputs (defects) in $\mathbf{p}(t) = \mathbf{G}(t) * \mathbf{y}(t) + \text{Disturbances}$.

Though 108 defects can theoretically be expected, only 70 defects actually occurred during the data gathering period. The defects that did occur are indicated with a • in Table 3.8. Naturally, if defects do not occur, they cannot be detected in the regression and hence do not form part of the model. However, because the structure can later be extended to included defects at all locations, it will be assumed that there are 108 defects present for the model structure definition.

3.4.1.2 IVOV structure selection

The same procedure was followed as with the MVIV model to determine the structure of the model. Table 3.9 shows the mean least squares (as an example) for the longitudinal crack defect (which shows up on the top left portion of the slab only after grinding) with different values for n_a and n_b. A more accurate fit was obtained as the structure size was increased. Based on this result and the fits of the other defects, the optimal choice for the structure was $n_a = 5$ and $n_b = 4$. This model structure contains enough information to detect the defects, and is not too large to handle during training and simulation[s].

Note that no real difference could be detected between the types of steels cast and the widths

[r] see *e.g.* Barozzi, Fontana, and Pragliola [166]

[s] Training was done on a 256MB RAM, 1GHz PentiumIII machine, with typical training times of about 30 minutes.

Table 3.8 Locations of the specific defects of the gathered data. T=Top and B=Bottom as first letter. B=Before and A=After as second letter. L=Left, C=Centre and R=Right as third letter.

	1a	1b	2a	2b	4	5a	5b	6	8
TBL			•	•	•	•	•	•	•
TBC			•	•	•	•	•	•	•
TBR			•	•	•	•	•	•	•
BBL				•		•	•	•	•
BBC				•		•	•	•	•
BBR				•		•	•	•	•
TAL	•			•		•	•	•	•
TAC	•	•		•		•	•	•	•
TAR				•		•	•	•	•
BAL				•		•	•	•	•
BAC			•	•		•	•	•	•
BAR				•		•	•	•	•

Table 3.9 Comparison of $V(\hat{\Theta})$ for different ARX structures for the IVOV model for longitudinal cracks.

	n_b=1	2	3	4	5	6
n_a=1	0.4663					
2	0.4462	0.4583				
3	0.4344	0.4458	0.4314			
4	0.4276	0.4427	0.4285	0.4210		
5	0.4245	0.4418	0.4276	0.4200	0.4166	
6	0.4228	0.4421	0.4275	0.4197	0.4160	0.4143

of the slabs that were cast. Therefore, only one model was derived including all widths and types of steel. The model was, however, derived for each specific defect, to lessen the burden on the processing machine (see footnote s). Data of slabs which have a specific defect and data of slabs with similar characteristics (*i.e.* widths and types) but without defects were included in the training set. This was to ensure that the model also has data where no defects occur to train with.

3.4.1.3 IVOV time domain results

The training procedure of the IVOV model gave satisfactory results on the training data with the structure defined above. Fig. 3.27 shows the model vs. plant output for a transversal crack occurring on the top left location after grinding has taken place. Though the estimate

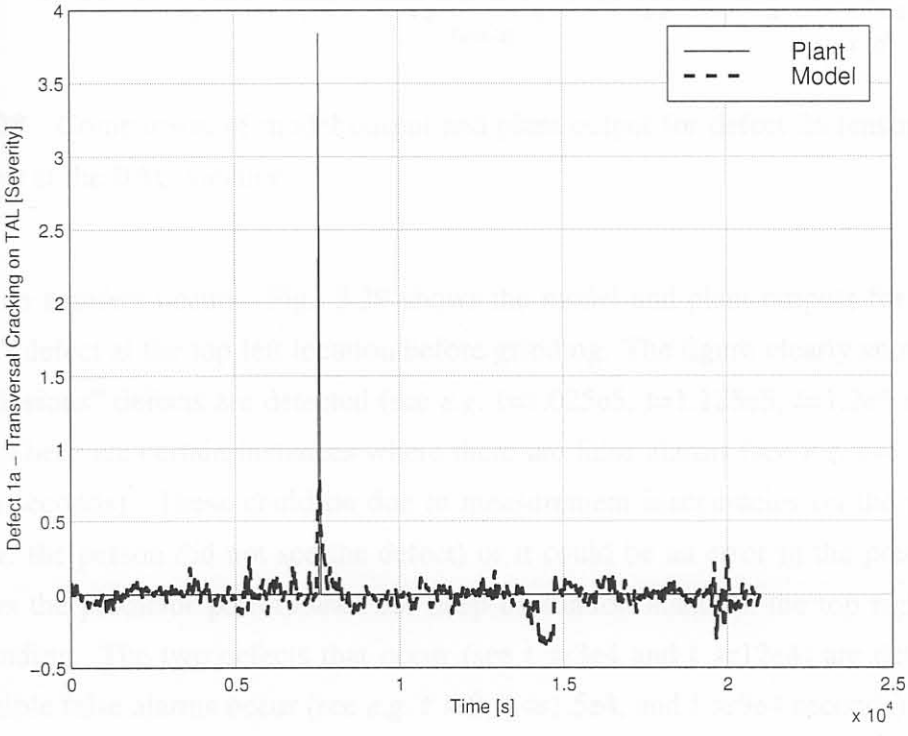

Figure 3.27 Comparison of model output and plant output for defect 1a (transversal crack) at the TAL location.

does not follow the defect output perfectly, a clear increase in the model output is observed when a defect occurs. This non-perfect following is probably due to the fact that the defect measurements are taken by humans and that the severity scale is probably not ordinal. Fig. 3.28 shows the model and plant output for casting powder entrapment at the bottom centre location after grinding. This result is also adequate with a substantial increase in the model

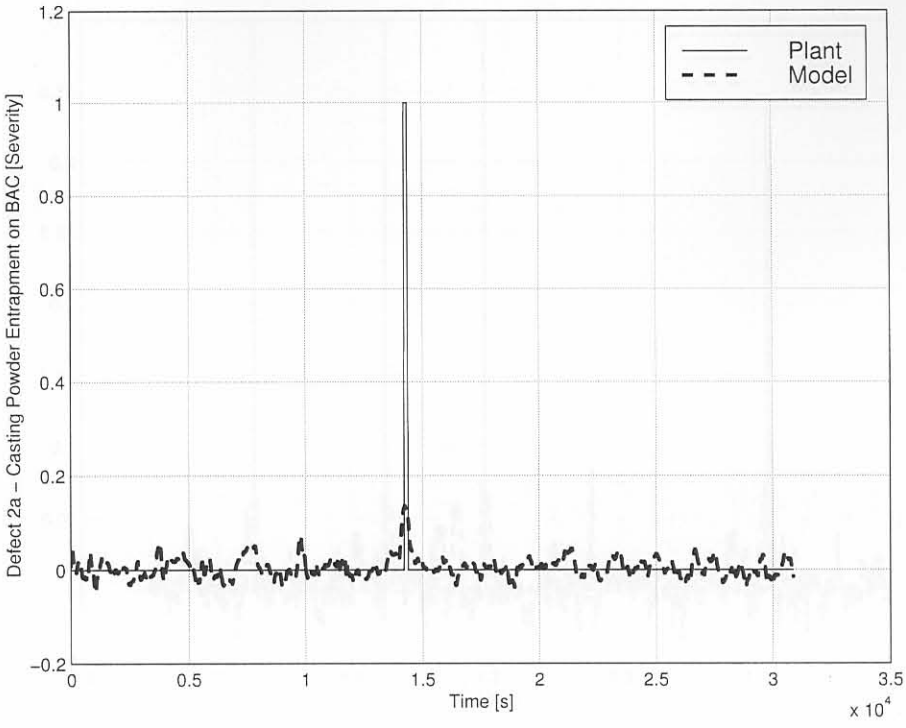

Figure 3.28 Comparison of model output and plant output for defect 2a (casting powder entrapment) at the BAC location.

output when a defect occurs. Fig. 3.29 shows the model and plant outputs for the "other inclusions" defect at the top left location before grinding. The figure clearly shows that the "other inclusions" defects are detected (see *e.g.* t=1.025e5, t=1.125e5, t=1.2e5 and 1.42e5 seconds). There are certain instances where there are false alarms (see *e.g.* t=1.175e5 and t=1.275e5 seconds). These could be due to measurement inaccuracies on the part of the human (*i.e.* the person did not see the defect) or it could be an error in the predictor. Fig 3.30 shows the predictor performance for deep oscillation marks at the top right position before grinding. The two defects that occur (see t ≈3e4 and t ≈12e4) are detected, and some possible false alarms occur (see *e.g.* t ≈0, t ≈1.5e4, and t ≈9e4 seconds). Fig. 3.31 shows the model output for stopmarks at the bottom centre location before grinding. Fig. 3.32 shows the predictor output for depressions at the top left location before grinding has taken place.

The predictor performance using validation data will be discussed in §3.4.5.

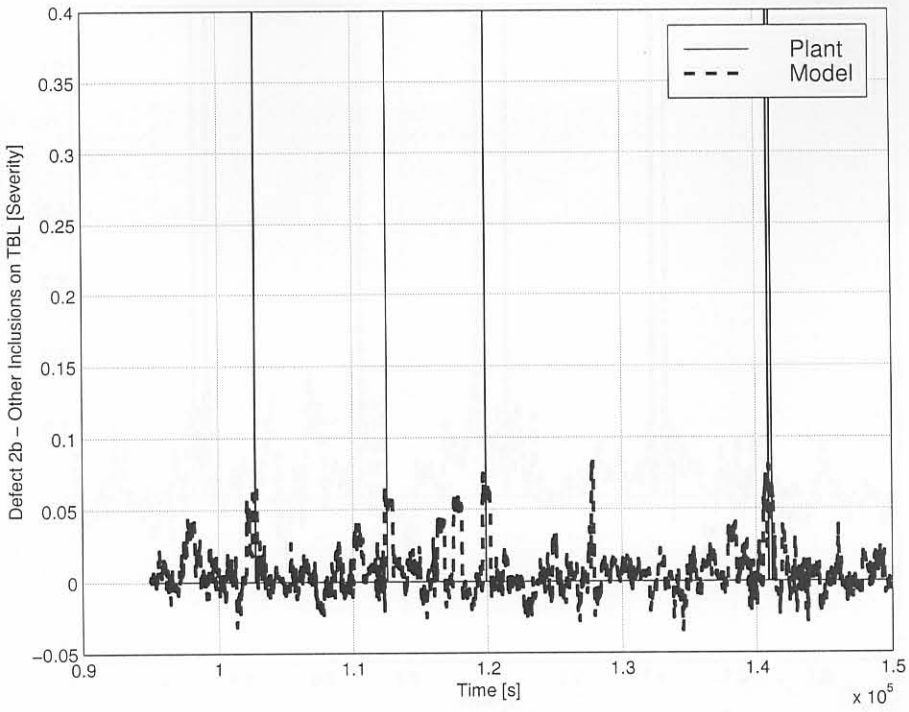

Figure 3.29 Comparison of a portion of the model output and plant output for defect 2b (other inclusions) at the TBL location.

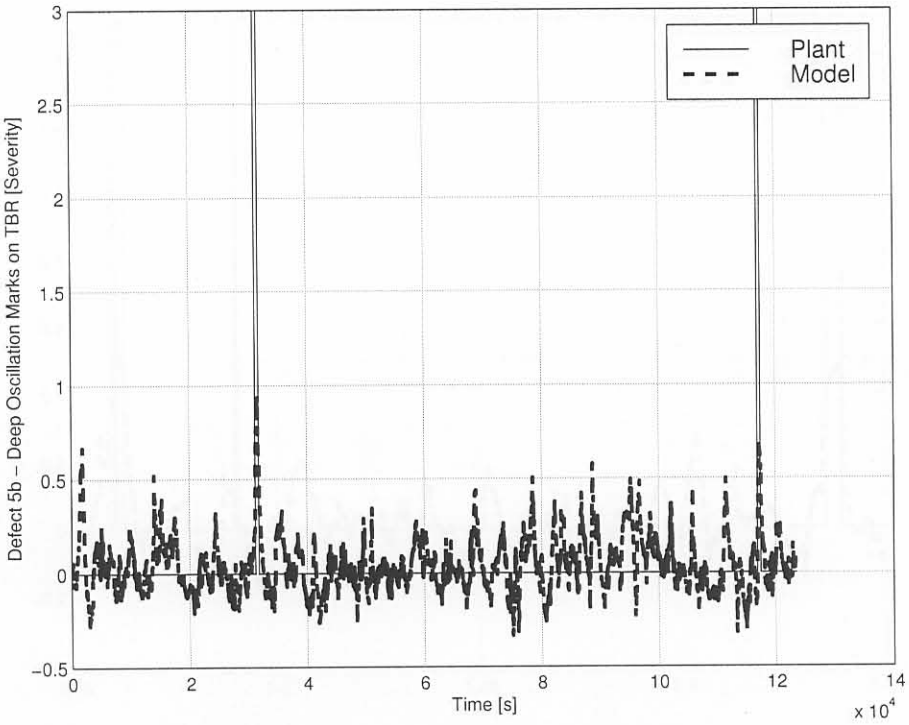

Figure 3.30 Comparison of the model output and plant output for defect 5b (deep oscillation marks) at the TBR location.

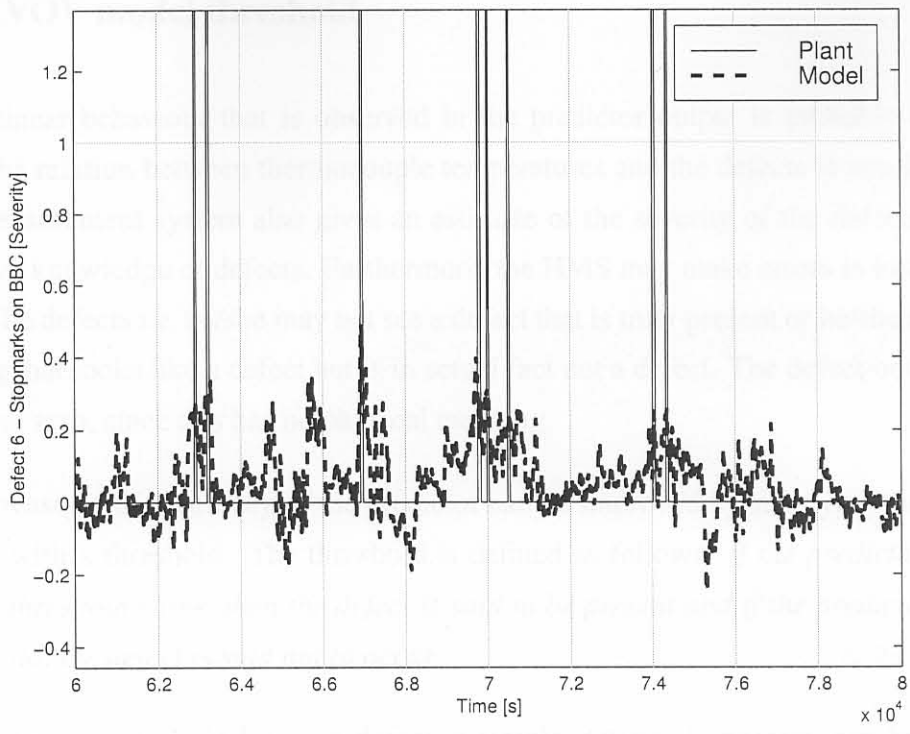

Figure 3.31 Comparison of a portion of the model output and plant output for defect 6 (stopmarks) at the BBC location.

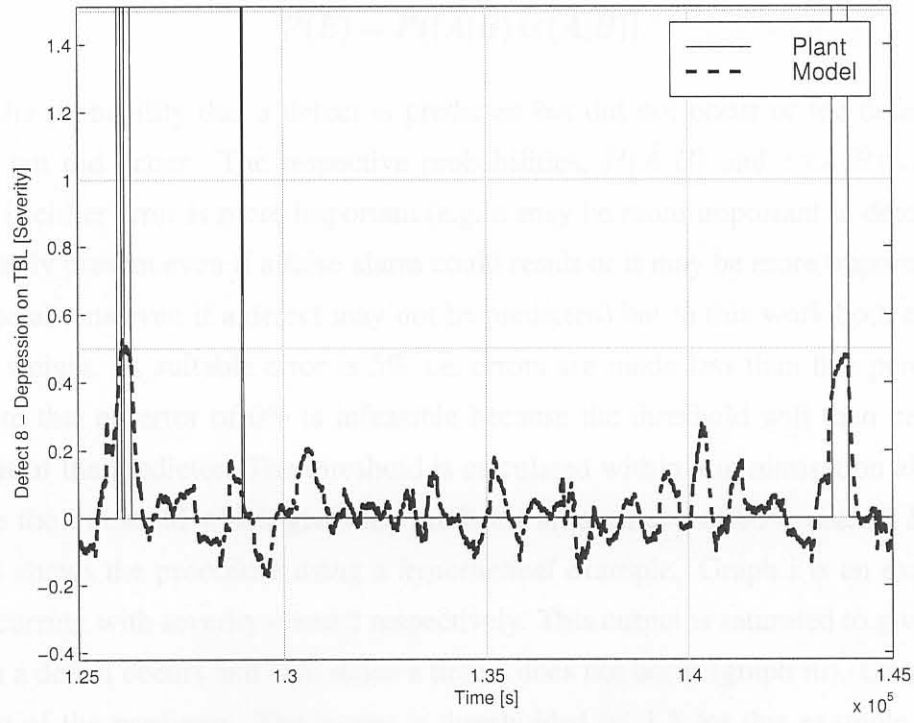

Figure 3.32 Comparison of a portion of the model output and plant output for defect 8 (depression) at the TBL location.

3.4.2 IVOV model threshold

The non-linear behaviour that is observed in the predictor output is probably due to the fact that the relation between thermocouple temperatures and the defects is non-linear. The human measurement system also gives an estimate of the severity of the defects based on his/her own knowledge of defects. Furthermore, the HMS may make errors in his/her observation of the defects *i.e.* he/she may not see a defect that is truly present or he/she may notice something that looks like a defect but is in actual fact not a defect. The defect output cannot be less than zero, since this has no physical meaning.

For these reasons, the accuracy of the predictor can be improved by supplying the detection algorithm with a threshold. The threshold is defined as follows: *if the predictor output is above the threshold value, then the defect is said to be present and if the predictor is below the threshold, the defect is said not to occur.*

To determine the threshold for each defect, a simple statistical approach can be followed. Define A as the event that a defect occurs over time and B as the event that a defect is predicted. Then $\bar{A}$ is the event that a defect does not occur and $\bar{B}$ is the event that a defect was not predicted. Then the probability of a prediction error occurring is given by

$$P(E) = P((\bar{A}|B) \cup (A|\bar{B})). \tag{3.11}$$

$P(E)$ is the probability that a defect is predicted but did not occur or the defect was not predicted but did occur. The respective probabilities, $P(\bar{A}|B)$ and $P(A|\bar{B})$ can also be weighted if either error is more important (*e.g.* it may be more important to detect a defect which is truly present even if a false alarm could result or it may be more important to have fewer false alarms even if a defect may not be predicted) but in this work both errors carry the same weight. A suitable error is 5% *i.e.* errors are made less than five percent of the time. Note that an error of 0% is infeasible because the threshold will then be set above any output of the predictor. The threshold is calculated within a minimisation algorithm to determine the threshold which gives the predictor an accuracy of 95% (*i.e.* $P(E) = 5\%$). Fig. 3.33 shows the procedure using a *hypothetical* example. Graph i is an example of a defect occurring with severity 4 and 2 respectively. This output is saturated to give values of one when a defect occurs and zero when a defect does not occur (graph iii). Graph ii shows the output of the predictor. The output is thresholded (at 1.5 for this example, see graph iv), and set to one to denote a predicted defect and zero to denote no predicted defect. The thresholded output of the predictor is then subtracted from the saturated plant output (graph v) and the absolute value of that difference is then used to predict $P(E)$ (graph vi). The

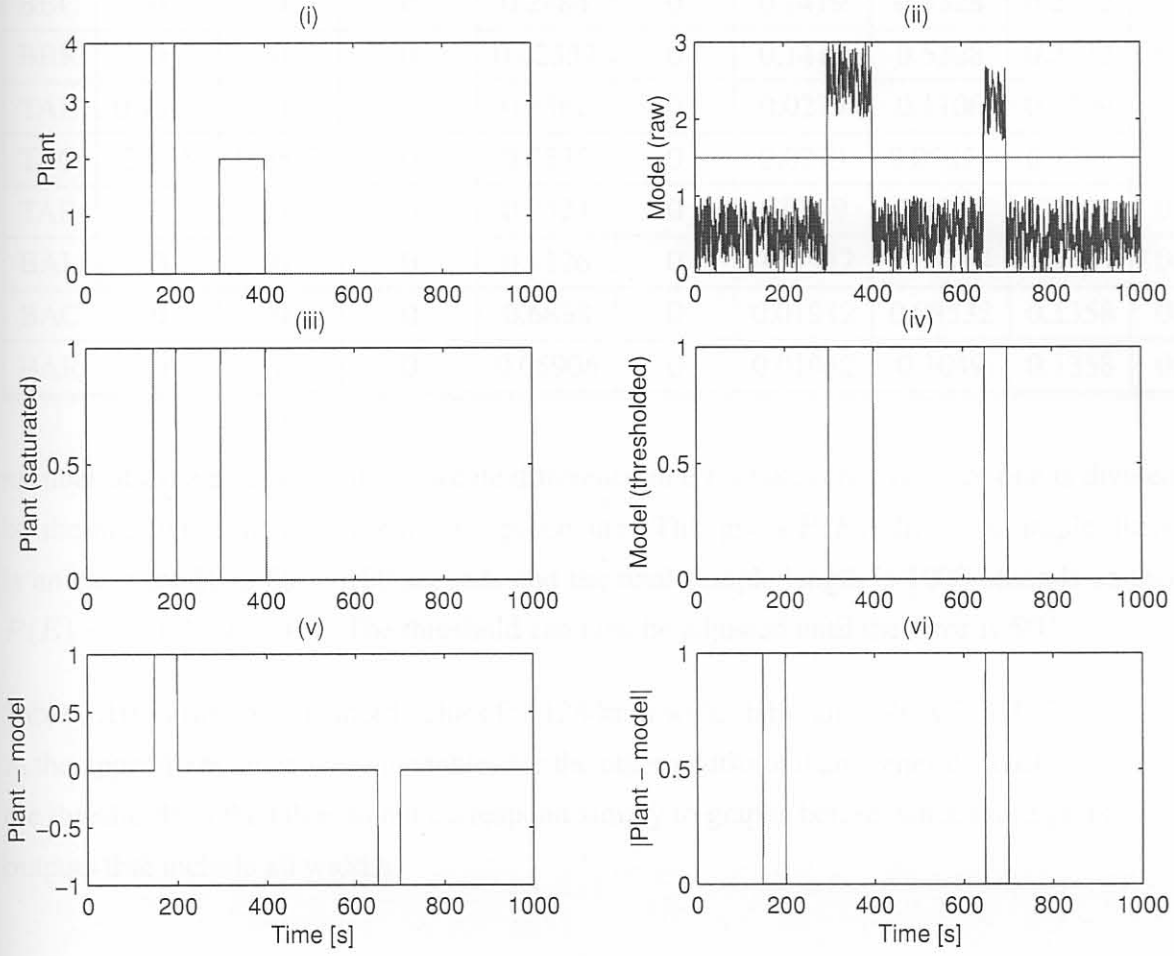

Figure 3.33 Procedure for the calculation of the accuracy of the thresholded predictor output.

Table 3.10 Thresholds for the IVOV predictor for 1280mm wide slabs

	1a	1b	2a	2b	4	5a	5b	6	8
TBL	0	0	0.07379	0.04115	0.4916	0.2216	0.5328	0.3374	0.1682
TBC	0	0	2.662	0.1922	0.1986	0.2187	0.5328	0.3374	0.08673
TBR	0	0	0.03544	0.0253	0.1632	0.1777	0.5328	0.3374	0.1826
BBL	0	0	0	0.06602	0	0.1419	0.5328	0.2732	0.1184
BBC	0	0	0	0.2484	0	0.1419	0.5328	0.2732	0
BBR	0	0	0	0.02357	0	0.1419	0.5328	0.2732	0.1485
TAL	0.7519	0	0	0.2362	0	0.0279	0.1106	0.1799	0.2018
TAC	2.155	0.5597	0	0.7575	0	0.0279	0.09825	0.1799	0.1946
TAR	0	0	0	0.2424	0	0.0279	0.1287	0.1799	0.2001
BAL	0	0	0	0.1126	0	0.01912	0.08764	0.1321	0.1556
BAC	0	0	0	0.6838	0	0.01912	0.08532	0.1358	0.2163
BAR	0	0	0	0.05906	0	0.01912	0.1049	0.1358	0.1455

number of time points that the absolute difference in error takes on a value of one is divided by the number of samples for the test procedure. This gives $P(E)$. In this example, there is an error for $50 + 50 = 100$ seconds and the total sample length is 1000 seconds so that $P(E) = 100/1000 = 0.1$. The threshold can now be adjusted until the error is 5%[t].

Table 3.10 shows the threshold values for 1280mm wide slabs; and tables G.1, G.2, and G.3 in the appendixes show the same tables for the other widths that are generally cast. Note that the thresholds in the table do not correspond simply to graphs before, since those graphs are outputs that include all widths.

3.4.3 IVOV model defected slabs ratios

A comparison of the number of defected slabs that should be sent for direct rolling, and the number of slabs that were predicted to have defects after the threshold has been applied is also informative. Table 3.11 shows the number of slabs that would have been *falsely* sent for grinding based on the output of the predictor for each defect and defect location. N is the number of slabs that were used in the training of the IVOV model. These values are somewhat conservative, since they are linked to a specific defect and location so that

[t]note that in this example it will not be possible to reach 5% since the predictor did not closely predict the defect at 150 seconds

Table 3.11 Number of slabs that would have been sent for processing based on a false alarm from the predictor per defect location using the training data.

	1a	1b	2a	2b	4	5a	5b	6	8
N	55	72	56	412	154	327	244	175	406
TBL	-	-	9	28	2	10	3	27	38
TBC	-	-	0	53	0	7	3	27	61
TBR	-	-	7	50	0	21	3	27	36
BBL	-	-	-	58	-	3	3	38	81
BBC	-	-	-	55	-	3	3	38	22
BBR	-	-	-	50	-	3	3	38	74
TAL	0	-	-	74	-	45	26	48	94
TAC	0	4	-	31	-	45	10	48	58
TAR	-	-	-	76	-	45	24	48	80
BAL	-	-	-	126	-	28	1	59	74
BAC	-	-	0	42	-	28	3	59	67
BAR	-	-	-	171	-	28	3	59	75
AV%	0.0	5.6	7.1	16.5	0.4	6.8	2.9	24.6	15.6

repetition could have occurred because the same slab may have been sent for grinding based on the outcome of the predictor for two or more defects or defect locations. For transversal cracks (1a), the ratio of false alarm slabs to cast slabs (N) is 0% . For longitudinal cracks (1b) it is 5.6% , and for casting powder entrapment it has a mean value of 7.1% [u]. One of the worst performing defects is other inclusions (2a) with a ratio of 16.5% , *i.e.* the conservative estimate of slabs with inclusions that should not have been sent for processing is 16.5% . For bleeders the figure is 0.43% and for deep oscillation marks (5a) it is, on average, 6.8% . For uneven oscillation marks (5b) the ratio is 2.9% , noting that the number of false alarms increases for predictions below surface (after grinding on the top of the slabs). For stopmarks the average value for the ratio is 24.6% and for depressions it is 15.6% .

Table 3.12 shows the ratio of slabs that were predicted to have a specific defect at a specific location to the number of slabs that did have the defect present. Note that these values are conservative because a slab that was not predicted to be defective on one defect and defect location may have been predicted to be defective based on another defect or defect location. Slabs with transversal cracks were identified perfectly, while longitudinal cracks has an accuracy of 33% . Casting powder entrapments were predicted perfectly while other inclusions

[u] AV% denotes the average ratio of falsely predicted slabs to total slabs over all locations.

Table 3.12 Number of slabs that should have been sent for processing based on the predictor where a slab was truly defected using the training data. In $x|y$, x is the number of slabs predicted to have the defect and y is the number of slabs that did have the defect present.

	1a	1b	2a	2b	4	5a	5b	6	8
N	55	72	56	412	154	327	244	175	406
TBL	-	-	1|1	5|6	1|3	2|7	2|2	17|18	5|8
TBC	-	-	1|1	14|28	1|2	3|6	2|2	17|18	4|5
TBR	-	-	1|1	2|4	1|2	3|6	2|2	17|18	4|10
BBL	-	-	-	4|5	-	1|3	2|2	13|15	4|7
BBC	-	-	-	17|25	-	1|3	2|2	13|15	1|2
BBR	-	-	-	2|2	-	1|3	2|2	13|15	5|11
TAL	1|1	-	-	8|42	-	2|2	3|3	14|15	15|30
TAC	1|1	1|3	-	10|72	-	2|2	2|2	14|15	9|32
TAR	-	-	-	9|34	-	2|2	3|3	14|15	16|30
BAL	-	-	-	4|19	-	1|1	1|2	11|12	9|20
BAC	-	-	1|1	8|55	-	1|1	1|2	11|12	12|23
BAR	-	-	-	10|18	-	1|1	1|2	11|12	8|15
AV%	100	33	100	30	43	54	88	92	48

had a success rate of only 30% . Bleeders were predicted only 43% of the time. Deep and uneven oscillation marks were predicted with a success rate of 54 and 88 % respectively on average and stopmarks were predicted with an accuracy of 92% . Depressions were predicted accurately on slabs by 48% .

Some of the "other inclusions" were predicted badly, probably due to a small defect passing between thermocouples (under-sampling of the thermocouples). The reason could also be that the operators were too conservative when making a measurement on other inclusions, thus including insignificant inclusions in the measurement. The inclusion could also have formed after the mould and even outside the casting machine. An example of this is when a slab has to be spot grinded because the slab was placed on a dirty floor, with the sheer weight of the slab making an impression of the dirt (resembling a "cleaned out" inclusion) on its surface. Deep and uneven oscillation marks and stopmarks were predicted in batches of three at the top before, top after, bottom before and bottom after locations. This is because the defects usually affect the whole width of the slab. Depressions were also not predicted accurately because 1575mm wide slabs are also included in the study, and thermocouples are not available near the off-corner of the slabs in this case, a location where the defect is predominant. Overall a conservative average accuracy of about seventy percent over all defects is achieved using the ARX technique as a predictor.

Also note between tables 3.11 and 3.12 that in some instances, such as stopmarks, when the prediction accuracy is high, the false alarm rate is also high. This implies that the method for determining the threshold is of such a nature that the increase in defect prediction accuracy results in an increase in the occurrence of the false alarm. This implies that, if it is desirable to detect when defects occur and some false alarms are allowed, the accuracy of positive defect prediction will also increase. Though more slabs will then have to be inspected before direct rolling or hot charging, more slabs can be direct rolled or hot charged because the slabs do not have to be grinded.

To ensure that the best possible result was obtained, the IVOV model was also trained using casting speed, mould level and inlet temperature as inputs. These results were however not an improvement on the current result. The reasons for not including the casting speed, mould level and inlet temperature in the IVOV model are described in §3.2.

3.4.4 Optimal set-points for IVOV system

With the IVOV model in hand, the next step is to determine which values for the thermocouple temperatures will yield the least amount of defects. These values then become set-points for a defect controller based on the MVIV model. For the smallest number of defects to occur, the best procedure was to assume that the system is at steady-state and then to calculate the values for the thermocouples which will deliver the least amount of defects. In the ARX formulation, the model is of the form[v]

$$\begin{aligned} \mathbf{p}[nT] &+ \mathbf{A}_1\mathbf{p}[(n-1)T] + \cdots + \mathbf{A}_5\mathbf{p}[(n-n_a)T] = \\ \mathbf{B}_0\mathbf{y}[nT] &+ \mathbf{B}_1\mathbf{y}[(n-1)T] + \mathbf{B}_2\mathbf{y}[(n-2)T] + \mathbf{B}_3\mathbf{y}[(n-3)T]. \end{aligned} \tag{3.12}$$

At steady-state, all inputs and all outputs are steady, so that

$$\begin{aligned} \mathbf{p}_{ss} &+ \mathbf{A}_1\mathbf{p}_{ss} + \cdots + \mathbf{A}_5\mathbf{p}_{ss} = \\ \mathbf{B}_0\mathbf{y}_{ss} &+ \mathbf{B}_1\mathbf{y}_{ss} + \mathbf{B}_2\mathbf{y}_{ss} + \mathbf{B}_3\mathbf{y}_{ss}. \end{aligned} \tag{3.13}$$

This implies then that at steady-state,

$$\begin{aligned} (\mathbf{I} &+ \mathbf{A}_1 + \cdots + \mathbf{A}_5)\mathbf{p}_{ss} = \\ (\mathbf{B}_0 &+ \mathbf{B}_1 + \mathbf{B}_2 + \mathbf{B}_3)\mathbf{y}_{ss}, \end{aligned} \tag{3.14}$$

and

$$\mathbf{p}_{ss} = (\mathbf{I} + \mathbf{A}_1 + \cdots + \mathbf{A}_5)^{-1}(\mathbf{B}_0 + \mathbf{B}_1 + \mathbf{B}_2 + \mathbf{B}_3)\mathbf{y}_{ss}, \tag{3.15}$$

To find a non-trivial solution to the above problem (*i.e.* find the values of $\mathbf{y}_{ss}$ s.t. $\mathbf{p}_{ss}$ are at least below the threshold values) one can use a search algorithm together with a least squares error to determine the values for the set-points of the thermocouple temperatures to ensure that no errors occur.

This has been done for the four models involved, and the resulting set-points are shown in Table 3.13 and graphically in Fig. 3.34.

The table and figure show that there is a distinct cooling pattern from the top thermocouple row of the mould to the bottom row. The variation between thermocouples, the non-symmetry (*e.g.* "ou4u", "ou5u", "in4u" and "in5u" are all symmetrically situated but do not have the same values) and the variation for different widths probably has to do with the contact that the thermocouple makes with the copper face. The set-points are based on a subset

[v] $\mathbf{y}$ are the thermocouple inputs (outputs of the MVIV model) and $\mathbf{p}$ are the defects (outputs of the IVOV model). Note that one sample delay has been incorporated into the inputs.

Table 3.13 Optimal temperature set-points, $\mathbf{r}(t)$ for the different MVIV models.

i	Thermocouple	1060mm	1280mm	1320mm	1575mm
1	in1u	104	105	107	104
2	in1l	95	96	100	95
3	in2u	108	107	109	108
4	in2l	95	98	101	95
5	in3u	107	105	109	107
6	in3l	94	93	97	94
7	in4u	106	106	109	106
8	in4l	95	94	92	95
9	in5u	102	105	107	102
10	in5l	94	97	94	94
11	in6u	106	110	109	106
12	in6l	102	103	102	102
13	in7u	108	108	109	108
14	in7l	100	100	99	100
15	in8u	114	105	117	114
16	in8l	106	101	113	106
17	nl1u	83	85	81	83
18	nl1l	80	83	80	80
19	nl2u	86	80	84	86
20	nl2l	75	74	72	75
21	ou1u	105	105	104	105
22	ou1l	92	94	97	92
23	ou2u	107	102	106	107
24	ou2l	99	92	103	99
25	ou3u	104	102	104	104
26	ou3l	94	95	96	94
27	ou4u	106	109	111	106
28	ou4l	90	94	94	90
29	ou5u	98	100	104	98
30	ou5l	93	95	96	93
31	ou7u	105	105	108	105
32	ou7l	97	90	98	97
33	ou8u	106	107	107	106
34	ou8l	96	98	97	96
35	nr1u	97	92	99	97
36	nr1l	90	86	94	90
37	nr2u	95	89	100	95
38	nr2l	86	83	91	86

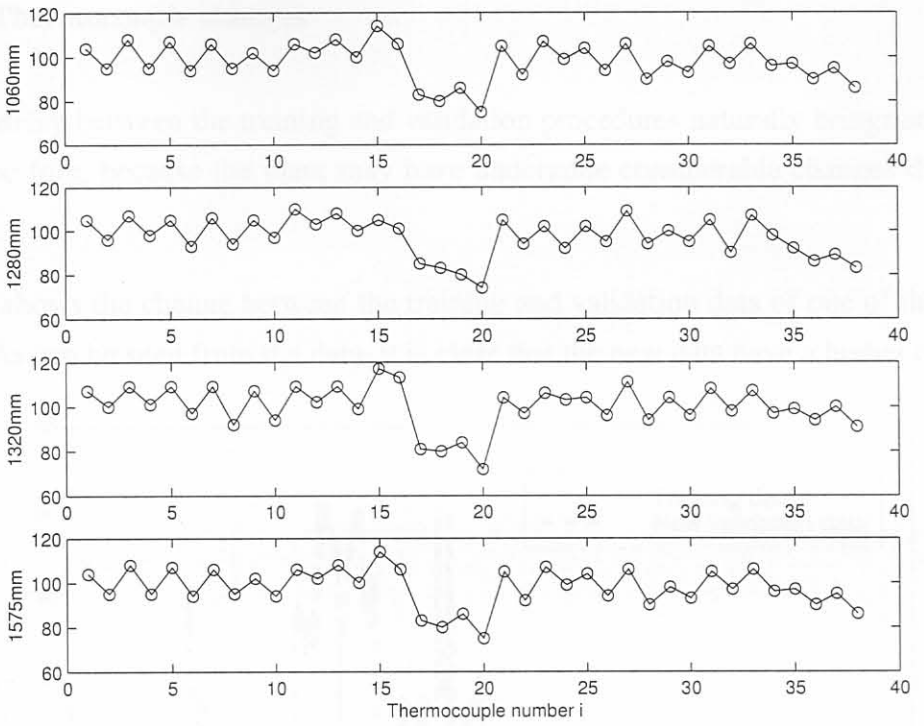

Figure 3.34 Graphical depiction of the optimal thermocouple temperature set-points for different slab widths.

of the occurring defects, and may not include all defects that will be present in the process in the future. However, it is assumed that these set-points will define a scenario which, if followed, can be considered to be the best process set-points for the thermocouple temperatures. Using the above set-points, the MVIV model can be used to derive the optimal casting speed, mould level and inlet water temperature in a similar fashion as was followed using the IVOV model to derive the optimal temperature set-points.

3.4.5 Preliminary validation of the IVOV model

All data gathered over the 6 month period was used to train the IVOV model (approximately 500 slabs), because the occurrence of defects was minimal. This left no more data to validate the IVOV model. To test whether the IVOV model was accurate, new data were gathered over a one-week period (44 slabs)—in the same way as the training data—almost three years after the initial model training procedure.

3.4.5.1 Thermocouple changes

The long delay between the training and validation procedures naturally brings some problems to the fore, because the plant may have undergone considerable changes during that period.

Fig. 3.35 shows the change between the training and validation data of one of the thermocouples. As can be seen from the data, it is clear that the new data have a higher offset than

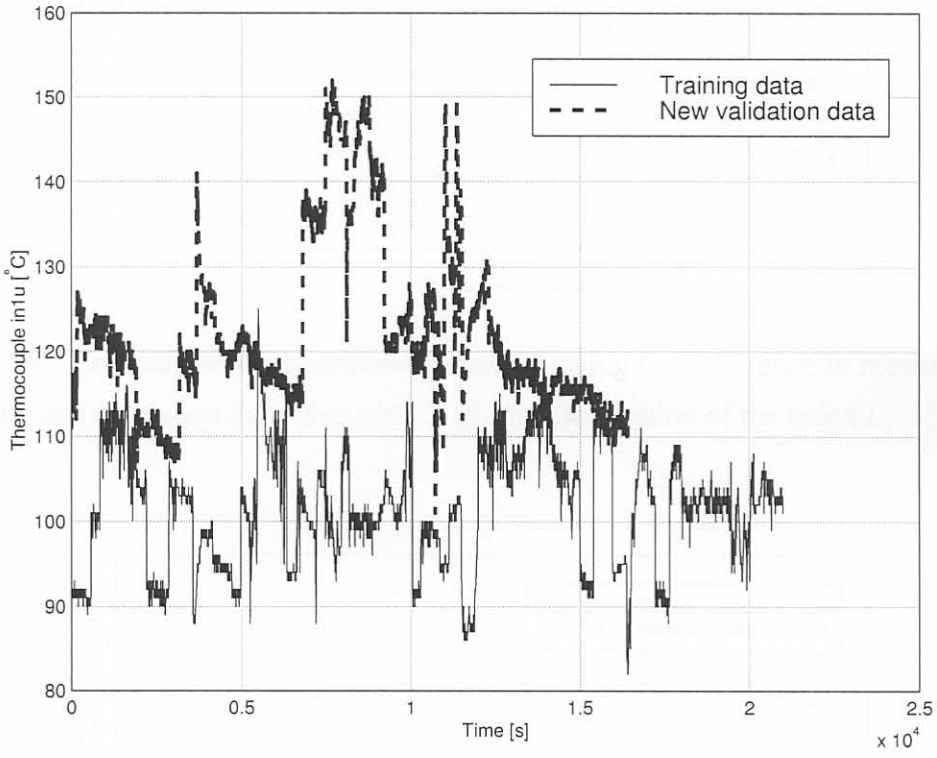

Figure 3.35 Comparison of data for thermocouple in1u showing the difference between the training and validation data.

the old data, and that the variation of the new data is more than that of the old data. This fact is highlighted in Fig. 3.36 and 3.37 which show the means and standard deviations of the various thermocouples for old and new data. On average, the means of the new data are about $15°C$ higher than the old data[w]; and up to $5°C$ difference in variance amplitude between the old and new data is observed(see especially *e.g.* thermocouple 15 which has much less variation in the new data than in the old data).

[w]Thermocouple 36 (nr11) was defective as can be seen from the lower mean and very high standard deviation. To compensate for this, the average of surrounding thermocouples was used to find proper values for the thermocouple.

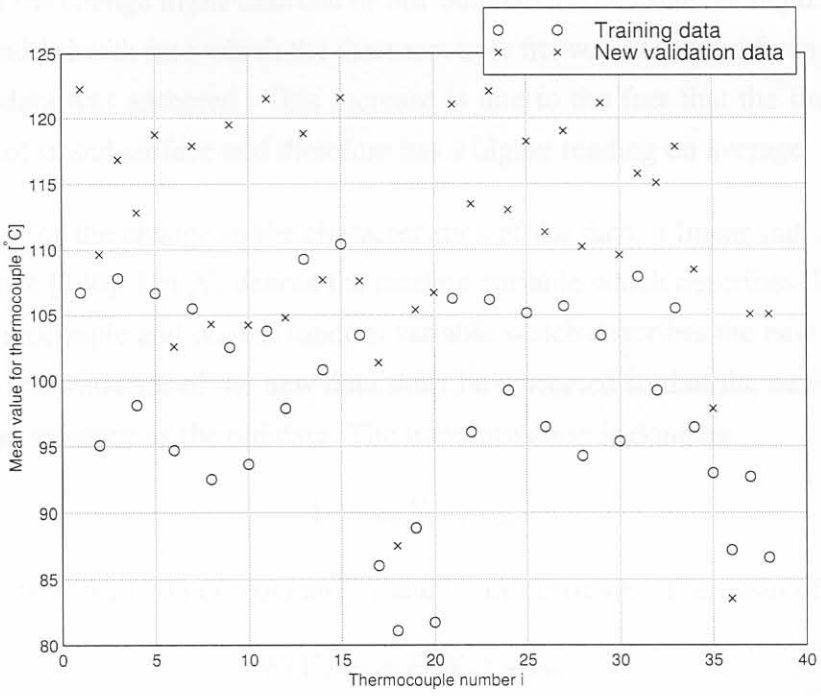

Figure 3.36 Comparison of thermocouple data showing the difference in means between the training and validation data. See table 3.13 for a description of the index i.

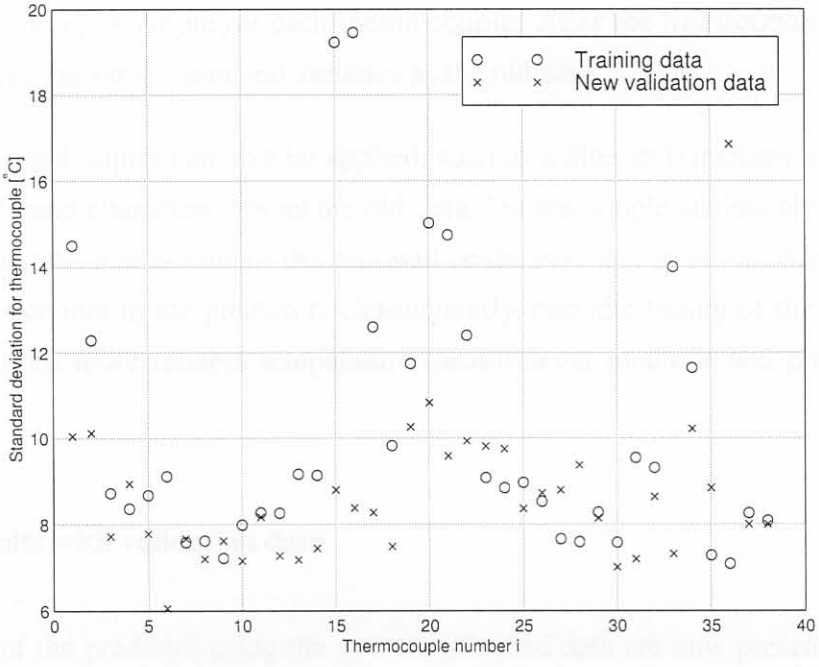

Figure 3.37 Comparison of thermocouple data showing the difference in standard deviations between the training and validation data. See table 3.13 for a description of the index i.

The reason for the change in the data can be attributed to the fact that the depth of the hole in the copper mould sheath into which the thermocouple fits was increased from 3mm to 5mm since the old data was gathered. This increase is due to the fact that the thermocouple is closer to the hot strand surface and therefore has a higher reading on average.

To compensate for the change in the characteristics of the data, a linear statistical transformation was done [140]. Let X_o denote the random variable which describes the old data for a specific thermocouple and X_n the random variable which describes the new data. Assume that the mean and variance of the new data must be corrected so that the new data have the same mean and variance as the old data. The transformation is done by

$$Y = c_1 X_n + c_2, \tag{3.16}$$

where Y is the transformed new data and c_1 and c_2 are constants. The mean of Y is given by

$$E(Y) = c_1 E(X_n) + c_2, \tag{3.17}$$

and the variance is given by

$$V(Y) = c_1^2 V(X_n). \tag{3.18}$$

Since the mean and variance of the new data must be equal to that of the old data, $E(Y) = E(X_o)$ and $V(Y) = V(X_o)$. This produces two equations with two unknowns and the solution of c_1 and c_2 is simple for each thermocouple. After the transformation of the new data, it will have the same mean and variance as the old data.

Note that other techniques can also be applied, such as a filter to transform the new data to have the same band characteristics as the old data, but the simple statistical transformation sufficed. Ultimately, a retraining of the data will be the best way to ensure that new changes are taken into account in the predictor. Consequently, periodic tuning of the predictor will be necessary until more reliable temperature measurement methods and practices can be implemented.

3.4.5.2 Results with validation data

Some results of the predictor using the new transformed data are now presented. Note that no transversal cracks or stopmarks occurred during the period when new data were gathered.

Fig. 3.38 shows the predictor output on the validation data for longitudinal cracking. Note that the threshold was implemented and that a value of 1 on the predictor output implies that a defect occurred and that a value of zero implies that the defect did not occur. 5 defects

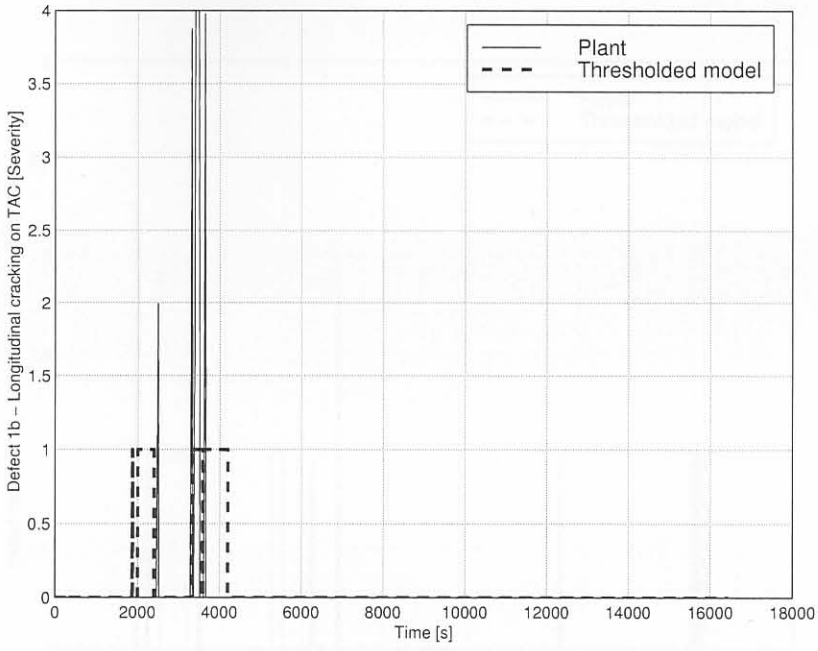

Figure 3.38 Comparison of predictor output and true plant data occurring at TAC position for longitudinal cracks.

occur, at $t \approx 2000$ to $t \approx 4000$ seconds. Note that the defect is predicted at $t \approx 2500$ seconds but the defect actually occurs just after the prediction. This is possibly a consequence of the 0.5 metre distance between defect samples on the slabs. During the period from $t \approx 3200$ to $t \approx 4100$ seconds the predictor indicates that defects occur, but the defect occurs only during a portion of this time. This could imply that the situation was favourable for a defect to occur, but that the defects simply did not occur over the period that the model predicted defects to occur.

Fig. 3.39 shows the occurrence of casting powder entrapment for the new data. Several defects occur, with a long period of defect occurrence from $t \approx 2000$ to $t \approx 3500$ seconds. During this period, defects were predicted, though not precisely at the same time as the defects occurred. The other defects which occurred but which were not predicted could have been deemed to be severe at the time of new data gathering and not at the time of old data gathering[x]. Note that towards the end a defect was predicted but did not occur ($t \approx 16000$ seconds), and may be due to an error in the HMS.

Fig. 3.40 and fig. 3.41 show the predictor outputs for other inclusions at the BBL and BAC locations respectively. Four defects are predicted and one defect actually occurs at the BBL location. Note that there is a slight delay between the defect being predicted and the defect

[x]Inspection of the slabs was performed by the author and some personnel at the steel-making company.

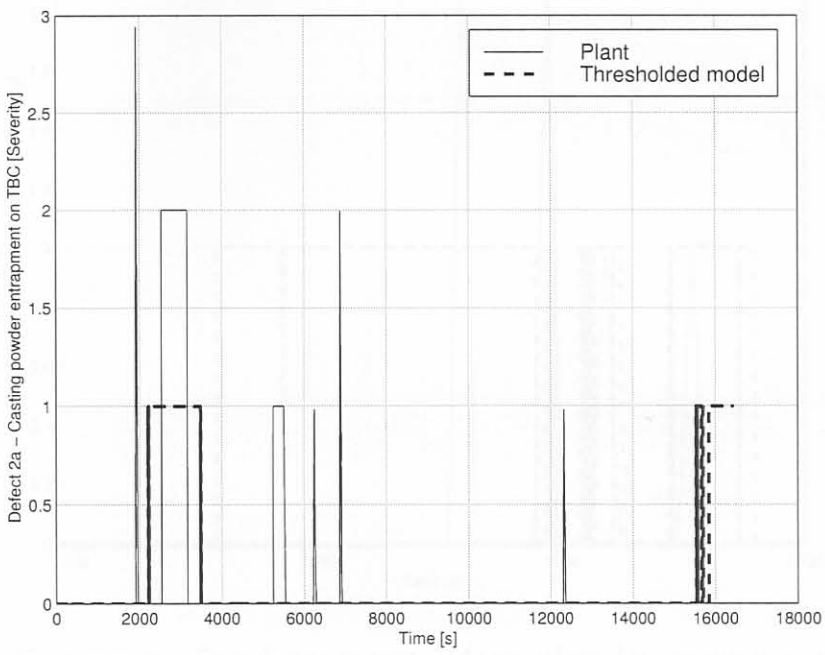

Figure 3.39 Comparison of predictor output and true plant data occurring at TBC position for casting powder entrapment.

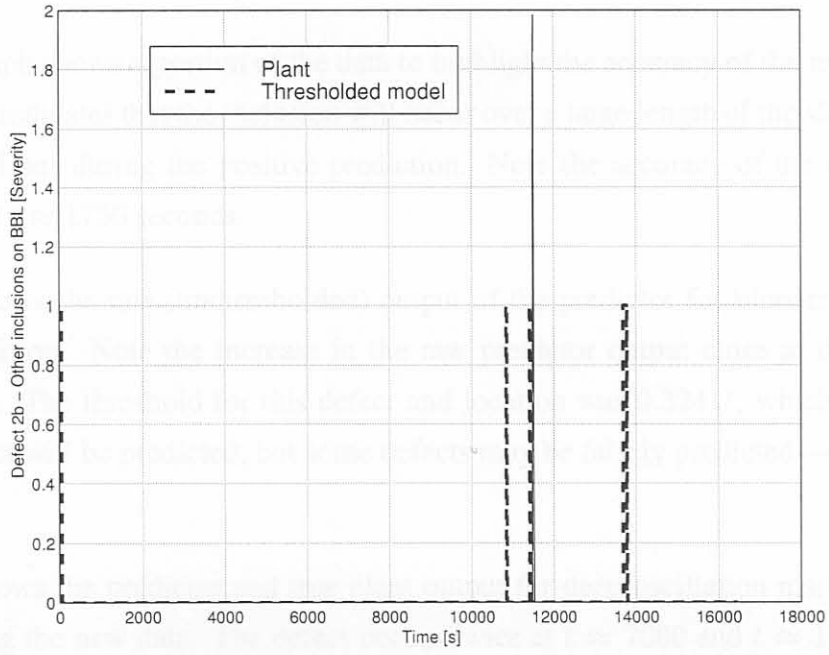

Figure 3.40 Comparison of predictor output and true plant data occurring at BBL position for other inclusions.

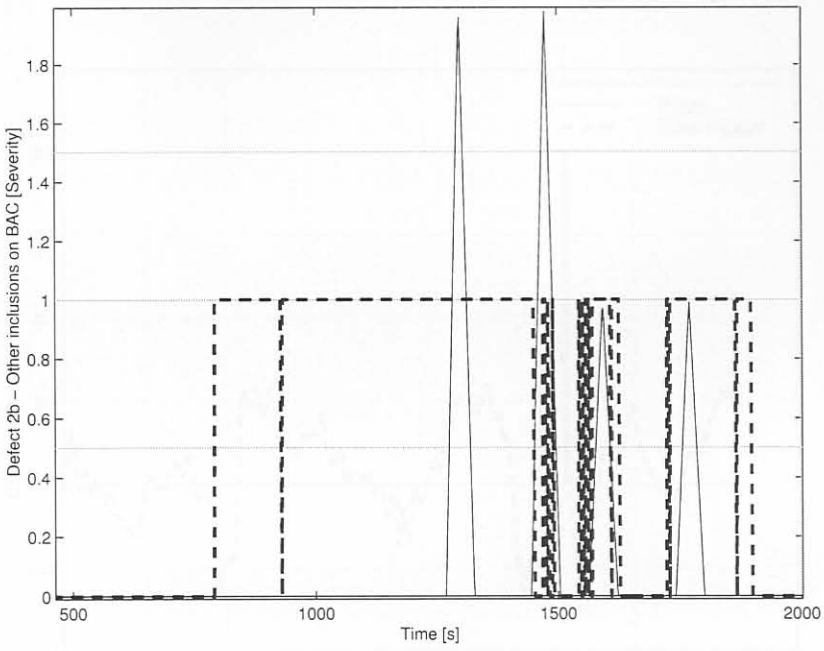

Figure 3.41 Comparison of predictor output and true plant data occurring at BAC position for other inclusions.

occurring at time $t \approx 11500$ seconds. The reason that defects were predicted but were not truly present in the other locations can probably be attributed to the HMS not noticing the defects.

The BAC graph shows a portion of the data to highlight the accuracy of the model. Though the predictor indicates that the inclusion will occur over a large length of the slabs, the defect occurs four times during the positive prediction. Note the accuracy of the model at time $t \approx 1600$ and $t \approx 1750$ seconds.

Fig. 3.42 shows the raw (unthresholded) output of the predictor for bleeders occurring at the TBL position. Note the increase in the raw predictor output close to the occurrence of the defect. The threshold for this defect and location was 0.3241[y], which would imply that the defect will be predicted, but some defects may be falsely predicted—due to the low threshold.

Fig. 3.43 shows the predictor and true plant output for deep oscillation marks at the TBL location using the new data. The defect occurs twice at $t \approx 7000$ and $t \approx 11500$ seconds. Note that a value of 0.5 on the predictor indicates a defect to avoid ambiguity with the plant outputs. The defect at $t \approx 7000$ seconds is predicted and the defect at $t \approx 11500$ is not. This

[y] see table G.1 for the threshold values used for 1060mm wide slabs like the one where this defect occurs.

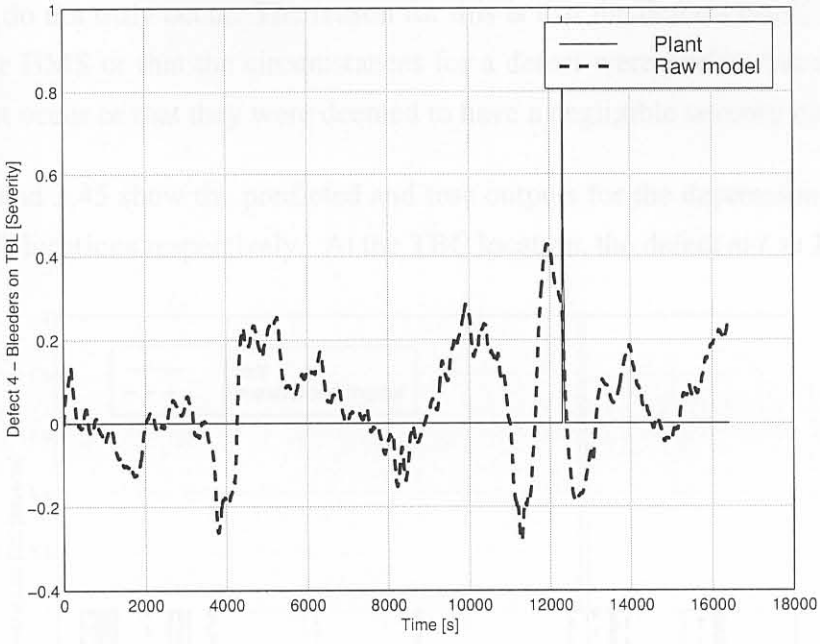

Figure 3.42 Comparison of predictor output and true plant data occurring at TBL position for bleeders.

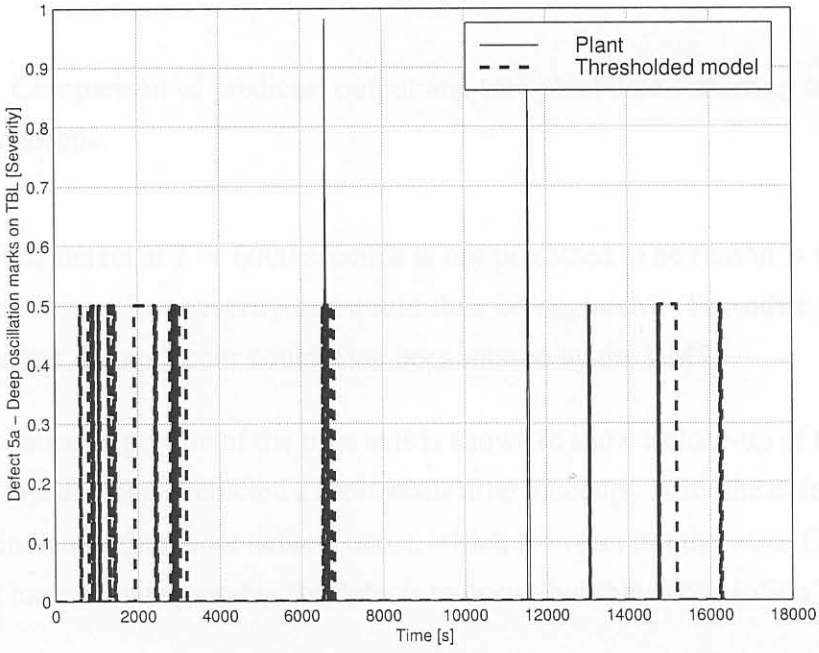

Figure 3.43 Comparison of predictor output and true plant data occurring at TBL position for deep oscillation marks.

could be due to the defect being characterised inaccurately. Furthermore, several defects are predicted but do not truly occur. The reason for this is that the defects could not have been noticed by the HMS or that the circumstances for a defect were perfect but that the defect simply did not occur or that they were deemed to have a negligible severity by the HMS.

Figures 3.44 and 3.45 show the predicted and true outputs for the depression defects at the TBC and BBR locations respectively. At the TBC location, the defect at $t \approx 13000$ seconds

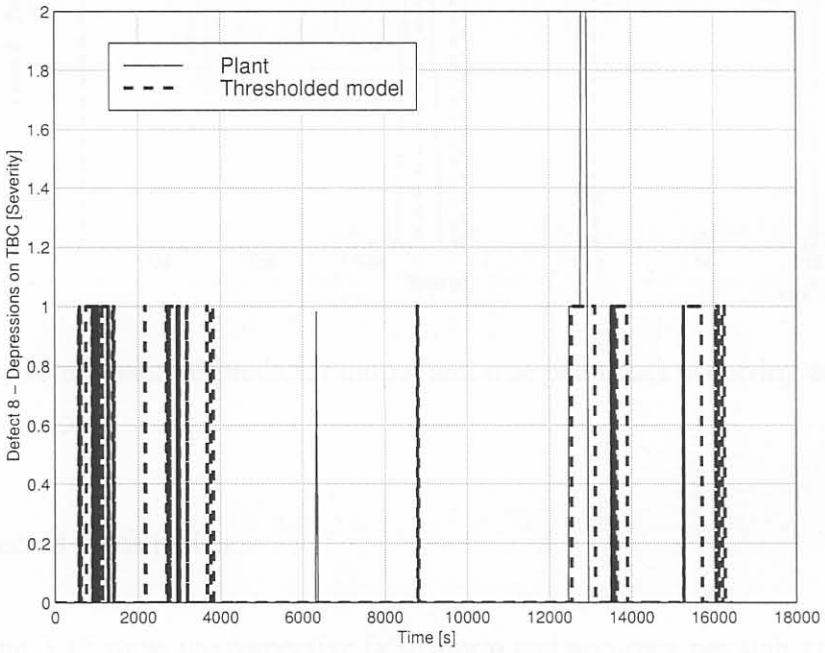

Figure 3.44 Comparison of predictor output and true plant data occurring at the TBC position for depressions.

is predicted. The defect at $t \approx 6000$ seconds is not predicted. The reason is that the defect could have had a very low severity and could thus be neglected. The other defects which were predicted but did not occur could have been missed by the HMS.

At the BBR location, a portion of the time axis is shown to show a close-up of the occurrence of the defect. The defect is predicted a short while after it occurs. After the defect is predicted the predictor indicates that more defects occur, which is in fact not the case. Once again, the situation may have been favourable for defects to occur, but they simply didn't.

Other defect predictions are not shown due to constraint of space, though similar results were obtained.

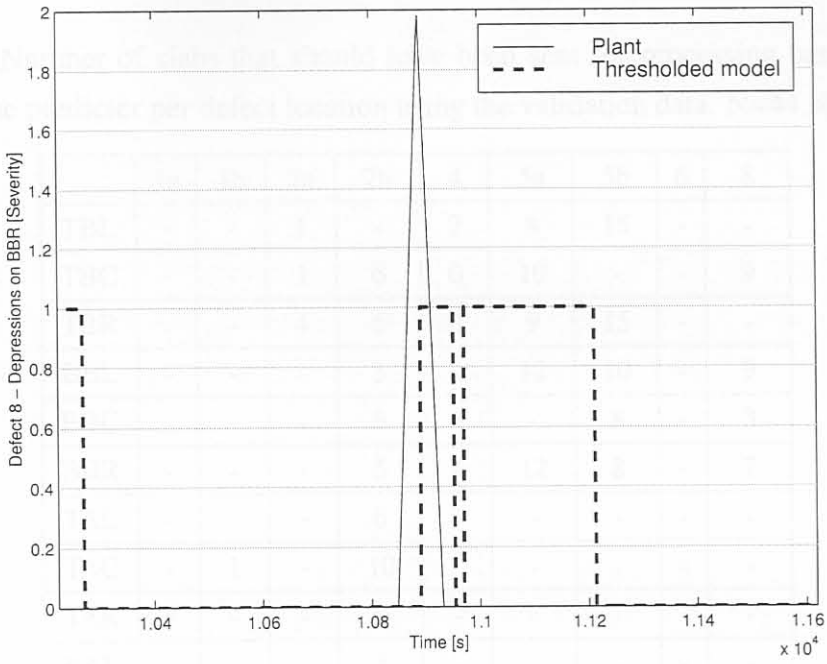

Figure 3.45 Comparison of predictor output and true plant data occurring at the BBR position for depressions.

3.4.5.3 Defected slabs ratios

Tables 3.14 and 3.15 show the respective false alarm and accuracy per slab grinded, respectively, similar to the tables obtained during the training phase (see tables 3.11 and 3.12).

False alarms on one slab was given and the accuracy of defect prediction was 100% for longitudinal cracking. This is impressive since the training data show that the predictor was only 33% accurate. Casting powder entrapment had a decrease in the number of false alarms over that of the training data. The accuracy dropped however considerably from 100% to 30% . This is probably because the defects can pass between two thermocouples. For other inclusions, the number of false alarms in the cases of the training and validation data are comparable at 16% and, through coincidence, the number of accurate defect predictions improved from 30 to 48% in the respective cases. Bleeders had a tenfold increase in the number of false alarms, and a decrease in the amount of accurate predictions. Both types of oscillation marks had an increase in the number of false alarms. Deep oscillation marks improved in accuracy from 54 to 63% and uneven oscillation marks reduced from 88 to 25% . Depressions had the same percentage of false alarms in both cases and an increase in the accuracy of the predictions per slab from 48% to 67% .

The conservative 95% confidence intervals for slabs with defects and positive predictions can

Table 3.14 Number of slabs that should have been sent for processing based on a false alarm from the predictor per defect location using the validation data. N=44 slabs.

	1a	1b	2a	2b	4	5a	5b	6	8
TBL	-	-	1	-	7	8	15	-	-
TBC	-	-	1	6	0	10	-	-	9
TBR	-	-	4	5	0	9	15	-	-
BBL	-	-	-	3	-	12	10	-	9
BBC	-	-	-	8	-	-	8	-	3
BBR	-	-	-	5	-	12	8	-	7
TAL	-	-	-	6	-	-	-	-	-
TAC	-	1	-	10	-	-	-	-	-
TAR	-	-	-	9	-	-	-	-	-
BAL	-	-	-	3	-	-	-	-	-
BAC	-	-	-	17	-	-	-	-	-
BAR	-	-	-	5	-	-	-	-	-
AV%	-	2.3	4.5	16.0	5.3	23.0	25.0	-	15.9

Table 3.15 Number of slabs that should have been sent for processing based on the predictor where a slab was truly defected using the validation data. N=44. In $x|y$, x is the number of slabs predicted to have the defect and y is the number of slabs that did have the defect present.

	1a	1b	2a	2b	4	5a	5b	6	8
TBL	-	-	1|2	-	1|1	1|2	1|1	-	-
TBC	-	-	1|6	1|1	0|2	2|3	-	-	1|2
TBR	-	-	1|2	1|1	0|1	1|2	1|1	-	-
BBL	-	-	-	1|1	-	1|2	0|2	-	1|2
BBC	-	-	-	1|2	-	-	0|1	-	1|1
BBR	-	-	-	0|1	-	5|7	0|3	-	1|1
TAL	-	-	-	1|3	-	-	-	-	-
TAC	-	2|2	-	1|4	-	-	-	-	-
TAR	-	-	-	2|3	-	-	-	-	-
BAL	-	-	-	4|11	-	-	-	-	-
BAC	-	-	-	6|8	-	-	-	-	-
BAR	-	-	-	2|7	-	-	-	-	-
AV%	-	100	30	48	25	63	25	-	67

Table 3.16 Overall conservative 95% confidence intervals on slabs with defects versus slabs that were predicted to have defects.

Defect	Confidence interval
Transversal cracks	$100 < p < 100$
Longitudinal cracks	$17 < p < 100$
Casting powder entrapment	$19 < p < 73$
Other inclusions	$28 < p < 37$
Bleeders	$7 < p < 65$
Deep oscillation marks	$43 < p < 70$
Uneven oscillation marks	$59 < p < 88$
Stopmarks	$88 < p < 96$
Depressions	$41 < p < 55$

be found in table 3.16. These values were calculated using both the training and validation sets where available, because of the few occurrences of defects. Transversal cracks do not have a true confidence interval since the proportion is close to 1. Longitudinal cracks can be up to 100% accurate as was seen with the validation data. Stopmarks seem to fair the best and other inclusions fair the worst.

3.4.5.4 Comparative results

For comparison, the only paper found on the prediction of defects with quantified results is by Hunter *et al.* [18]. Hunter *et al.* [18] use a feed-forward artificial neural network to predict defects from mould variables (including thermocouple temperature measurements). Table 3.17 shows the results of the ARX predictor per defect using the training and validation sets together where available. The calculation of the accuracy is based on predictions per *sample point*. The *sensitivity* is the proportion of correctly predicted sample points to all the sample points where a defect truly occurs. The *specificity* is the proportion of unpredicted defect points to the number of points where defects truly do not occur. The *false alarms* (FA) is the proportion of predicted defect points to the number of points where defects truly do not occur (FA=1-specificity). The *positive predicted value* (PPV) is the number of correct predictions of defects being present to the total number of predictions that the defects are present. The *negative predicted value* (NPV) is the number of correct predictions of defects not being present to the total number of predictions that defects are not present. N is the number of sample points used. Note that this method is conservative if the only consideration is whether

Table 3.17 Accuracy of the ARX predictor using sensitivity.

Defect	Sensitivity	Specificity	FA	PPV	NPV	N
Transversal cracks	73.4	99.5	0.5	51.7	99.8	20998
Longitudinal cracks	63.6	93.5	6.5	16.3	99.2	8212
Casting powder entrapment	8.8	98.6	1.4	4.9	99.3	61768
Other inclusions	24.8	96.6	3.4	13.1	98.4	1171032
Bleeders	14.4	100.0	0.0	98.5	99.6	114027
Deep oscillation marks	42.3	98.7	1.3	12.4	99.7	931428
Uneven oscillation marks	66.3	99.4	0.6	43.0	99.8	740832
Stopmarks	41.3	94.8	5.2	13.0	98.9	509064
Depressions	44.8	96.3	3.7	13.7	99.3	1168272

a slab must be grinded or not.

The result that is given in the paper of Hunter *et al.* [18] is that of the validation set for longitudinal cracking, where a neural network output generates a sensitivity of 61.5% and specificity of 75% . The table shows that the respective values using the ARX methods are 63.6% and 93.5% [z]. This implies that the ARX predictor is marginally more accurate than that published in terms of correct predictions of defects. The specificity however shows that many false alarms occur in the results of the paper, while the ARX predictor has far fewer false alarms (0.5%). An allowed decrease in specificity should also increase the sensitivity. This can be achieved by lowering the threshold. Transversal cracks have the best overall performance, with a sensitivity to predict a crack of 73.4% . Casting powder entrapment fairs the worst with a sensitivity of 8.8% and a PPV of 4.9% . There are however few false alarms (1.4%). Other inclusions have a correct prediction when defects occur over the sample points of nearly 25% . Bleeders have no false alarms, but have low sensitivity. Deep oscillation marks have a sensitivity of 42.3 % and very few false alarms (1.3%). Uneven oscillation marks also have high sensitivity (66.3%) and specificity (99.4%). Stopmarks have a sensitivity of 41.3% and 94.8% specificity so the amount of alarms are low. Depressions have similar sensitivity at 44.8% and specificity of 96.3 %. Overall, the data show that the predictor has few false alarms, but is also not always very accurate. However, comparative results could not be found for other defects.

The predictor of the defects was derived in this section with good results using ARX tech-

[z]Note that the longitudinal values are based on the validation set for comparison. Transversal cracks and stopmarks are based on the training set because none of these defects occurred during the validation phase.

niques together with a threshold. Not all the graphical results could be shown for each of the defects due to space constraint. The IV to OV model can not only be used as a predictor of defects, but in an inversion it can be used to determine the best thermocouple temperature set-points so that no defects occur.

3.5 Conclusion

This chapter presented the methodology and results of a model that can be used for prediction and control of defects in the continuous casting process.

The data gathering procedure of the mould variables (inputs) and the defects (outputs) was described. The inputs are available form the level 2 system of the plant of the industrial partner in real time and the defects are measured by experienced operators several hours after casting of a slab is completed. The procedure to extract the relevant data from the vast amount of data collected from the plant was also described.

Using statistical hypothesis testing and correlation analysis, it was found that the model can be divided into two sub-models. The first model, here called the MV to IV model, describes the dynamic effect of casting speed, as a manipulated variable, and mould level and inlet temperature as two possible disturbances, on the thermocouple temperatures as outputs. The second model is called the IV to OV model and uses the thermocouple temperatures as inputs and the defects as outputs. The IV to OV model is the predictor of the defects. This is convenient as feedback control can now be used because the time delay caused between measurement of the defect and the actual occurrence of the defect is outside the control loop.

The training of the two models was also presented. Both models track the true plant outputs well. System identification techniques in the form of linear auto-regression with exogenous input was found to be a just way to model the process. The IV to OV model could not determine the severity of the defects, but the use of a threshold improved the predictor to the extent that it could tell when and where a defect occurs and which defect was present with relatively high accuracy. Validation data for the IVOV model were not available, due to the comparatively few defects that occurred. Data collected three years later were used to validate the IV to OV model, and the obtained results compare favourably to published results for longitudinal cracking. The MV to IV model was relatively accurate in the presence of noise, even on the validation data.

The IV to OV model can be used in an inverse problem to determine the best temperature set-points for the thermocouples such that no defects occur. These results were shown.

The MV to IV model can now be used to design controllers in a feedback fashion so that the thermocouple temperature set-points can be followed. This is the subject of the next chapter.

Chapter 4

Control

THE split of the continuous casting defect model into a manipulated variable (casting speed) to intermediate variable (temperatures) model (MVIV); and intermediate variable to output variable (defects) model (IVOV) was done to make control of defects possible. Feedback can now be applied using the MVIV model by measuring temperatures (now called "outputs") and applying control by manipulating casting speed (manipulated variable). Regulation of the temperatures at optimal set-points will ensure that defect formation is restricted (see §3.4.4), implying therefore that the defects can be controlled.

The control problem is therefore to control 38 thermocouple temperatures with 1 manipulated variable, casting speed, *i.e.* a SIMO (single-input/multiple-output) problem. If the effect of the manipulated variable on each of the outputs is not the same, the system is not completely output controllable *i.e.* every output can not be driven to a desired output in a finite time [167]. Since the effect of the manipulated variable is not the same on all thermocouples it is impossible, for this system, to achieve perfect control. This is highlighted by the fact that the rank of the output controllability matrix, $[\mathbf{CB} \quad \mathbf{CAB} \quad \mathbf{CA}^2\mathbf{B} \quad \ldots \quad \mathbf{CA}^{38}\mathbf{B}]$ [167], of the MVIV system defined in §3.3.1.5 is 7, 6, 6, and 5 for 1060, 1280, 1320 and 1575mm wide slabs respectively[a]. Since the ranks of the respective models are less than the dimension of the state vector (38), the system is not controllable [167]. The system is, however, stabilisable—because the uncontrollable subspace of the MVIV model is stable[b][169]. The MVIV system is fully state observable *i.e.* the rank of the observability matrix [167] is equal to the dimension of the state vector (38).

[a] These ranks were calculated using the MATLAB Control Systems Toolbox [168].

[b] the whole system is in fact stable.

Because of the controllability limitations of the system a control strategy must be used that makes a trade-off between the quality of control on each of the outputs (intermediate variables). Three such linear controllers will be used to investigate the viability of control of this particular system. Linear control is used because the system can be adequately modelled as a linear time-invariant (LTI) system as shown in chapter 3. The controllers are as follows:

- linear quadratic tracker at steady-state,
- single-output control and
- worst-case control.

The linear quadratic tracker attempts to track the reference inputs as closely as possible on a weighted average basis while maintaining system stability for a LTI system. This has been described by Lewis [170] and an example application for an inverted pendulum (SIMO system) is given in Lewis [148]. The design is usually carried out for steady-state conditions and then used as a sub-optimal tracker for the dynamic case.

The single-output control utilizes the fact that one input should definitely be able to control one output. Therefore, one loop is closed and all other loops are open. The closed-loop output will track the reference input very closely (because that sub-system is controllable), and is only limited by actuator constraints. The disadvantage of this configuration is that only one output is tracked and no true control is applied to the other loops. It is hoped that the overall performance of the system will improve if the right loop is chosen to be closed. No references to this control approach could be found.

The worst-case control utilizes a switching strategy. Controllers are designed for each loop as if each loop is a single-input, single-output (SISO) system. Once an output error is performing at the worst level compared to the error of the other outputs, the controller switches from the active loop to the loop with the worst error, and controls that output. Once the output has improved to a level such that another output has become worse than the current output, the controller switches to that loop and the cycle repeats. Similar strategies can be found in papers by Sun, Ge, and Lee [171], Zhao and Spong [172] and Kordona, Dhurjatia, Fuentesb, and Ogunnaikeb [173]. The strategy is used to prevent any output from straying too far from the reference input. Problems of bump-less transfer [174] and integral windup are prevalent in this control configuration and are addressed in what follows.

The three controllers described above and their performance through simulation will be discussed in this chapter.

4.1 Linear quadratic tracker at steady-state (LQTSS)

This section describes the use of a linear quadratic tracker at steady-state (LQTSS) as a controller for the MV to IV model described in §2.2.5.

4.1.1 Implementation issues

The implementation of such a controller on a real plant is depicted in Fig. 4.1. In this

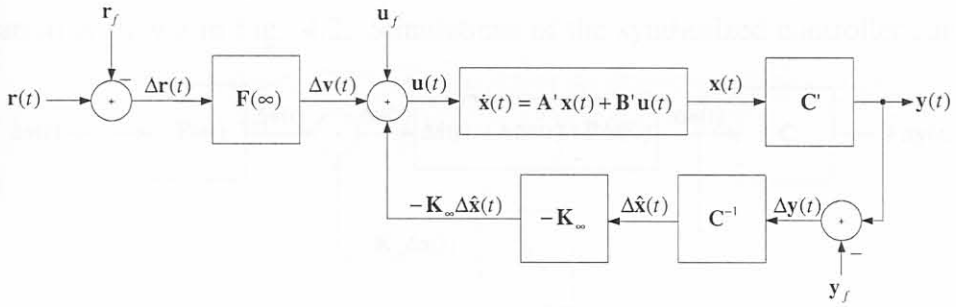

Figure 4.1 Implementation of the LQTSS in practice.

realization, the system $(\mathbf{A}', \mathbf{B}', \mathbf{C}')$ is the actual plant; and $\mathbf{u}(t)$, $\mathbf{x}(t)$ and $\mathbf{y}(t)$ are the true plant inputs, states and outputs respectively. Disturbances are left out at this stage for design purposes.

The "Δ" indicates deviational values of the respective variables and are needed, even in the practical realization since the identified model (and therefore the designed controller) is based on the deviations of parameters from set values.

As an example, if $\mathbf{r}(t)$ denotes the true desired temperature for the system, $\Delta\mathbf{r}(t)$ denotes the deviation of the desired temperature for the system and is calculated by subtracting the offset value from the true value ($\Delta\mathbf{r}(t) = \mathbf{r}(t) - \mathbf{r}_f$).

The deviational estimate of the state of the system ($\Delta\hat{\mathbf{x}}(t)$) is determined by multiplying the measured deviational output, $\Delta\mathbf{y}(t)$, with the inverse of the $\mathbf{C}$ matrix of the identified model since the system has been identified as first order with outputs and states equal.

$\mathbf{F}(\infty) = \mathcal{L}^{-1}\{\mathbf{F}(0)\}$ denotes the time invariant feed-forward gain of the controller and $\mathbf{K}_\infty$ denotes the feedback gain.

A typical sequence of events which might be carried out by a controller is informative to

understand the practical controller structure. The output is measured and the deviational value of the output is determined using the offset value for that output. This value is then multiplied by the C matrix of the *identified* model to give an estimate of the deviational state of the system. The deviational state is then used in the state-feedback realization and multiplied by the feedback gain. The result is added to the feed-forward component. The feed-forward component is determined by multiplying the deviational desired value for the output with the feed-forward gain. The deviational control is then added to the offset value to determine the true control and is then used as the input to the true system.

For simplicity, the control system can be described by the deviational parameters only. This configuration is shown in Fig. 4.2. Simulations of the synthesized controller can be done

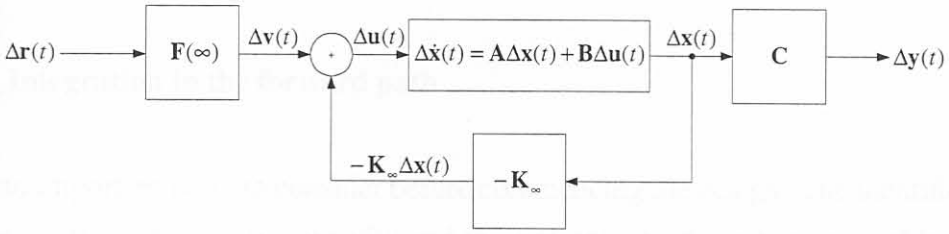

Figure 4.2 Analysis of the deviational LQTSS controller.

using the structure depicted, but care should be taken then when adding and subtracting offsets when the controller is implemented. The inverse of the C′ matrix has been dropped from the figure for the sake of simplicity.

4.1.2 Design overview

Using the design procedure depicted in Fig. 2.22 on page 51, one can now set about to design the LQTSS. Although there are four widths, 1320 and 1280mm wide slabs have very similar models and only the 1280mm wide slabs will be tested. Since there are now three versions of the MVIV models[c], three separate controllers have to be designed.

4.1.2.1 Specifications

The general specification is to design controllers to improve set-point tracking[d] (and thereby reduce the amount of defects) given the optimal set-points, measured disturbances, actua-

[c] 1060mm, 1280 to 1290mm and 1575mm widths

[d] in terms of the SMSMSE in §4.1.2.6.

tor constraints, and the MVIV model. Perfect set-point following is not possible, because the system is not completely output controllable. Mould level and water inlet temperature disturbance rejection should occur in the significant frequency band of the disturbances (see §4.1.4), while a maximum casting speed constraint of 1500mm/min and maximum absolute casting acceleration (slew rate) of 1000 mm/min^2 should not be exceeded.

Note that a controller which forces a decrease in casting speed causes lower throughput of cast product. The quality of cast product is however also important and a trade-off between quality and throughput has to be made. In this work it is assumed that quality is more important and decreases in casting speed are allowed. As will be seen in the remainder, reductions in casting speed are rare for all three types of controllers.

4.1.2.2 Integration in the forward path

There is an important point to consider before commencing the design. The identified model is predominantly first order (*i.e.* type 0); and this presents steady-state error problems in any feedback control scheme [149]. The system is SIMO, that is, it has one input and several outputs. Therefore, an ideal (zero) steady state solution for tracking the reference inputs by the outputs is impossible to achieve. However, the error in this case is the difference between the feed-forward and feedback signals: $\Delta\mathbf{u}(t) = \Delta\mathbf{v}(t) - \mathbf{K}_\infty\Delta\mathbf{x}(t)$; and the designer is in this case interested in having zero steady-state error for this difference. This implies that the *weighted* outputs will track the *weighted* set-points of each of the temperatures by manipulating the input (casting speed).

Since the system is first order, it is necessary to add an integrator in the forward path of the system to ensure that the weighted step reference ($\Delta v(t)$) is followed exactly (type 1). The compensating approach is depicted in Fig. 4.3. In the figure, the state of the original

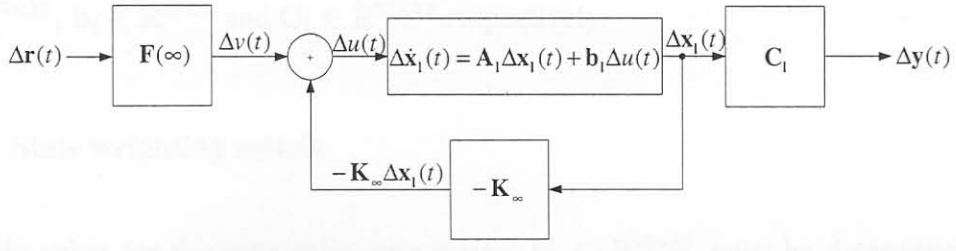

Figure 4.3 Addition of an integrator to the LQTSS.

system represented by the system $(\mathbf{A}, \mathbf{b}, \mathbf{C})$ has been augmented by an integrator of the form

$(a = 0, b = 1, c = 1)$. The compensator plus plant can be represented in state-space by the following system $(\mathbf{A}_1, \mathbf{b}_1, \mathbf{C}_1)$ as

$$\mathbf{A}_1 = \begin{bmatrix} 0 & \emptyset \\ \mathbf{b} & \mathbf{A} \end{bmatrix} \quad \mathbf{b}_1 = \begin{bmatrix} 1 \\ \emptyset \end{bmatrix} \quad \mathbf{C}_1 = \begin{bmatrix} \emptyset & \mathbf{C} \end{bmatrix}, \tag{4.1}$$

and

$$\Delta\dot{\mathbf{x}}_1(t) = \mathbf{A}_1\Delta\mathbf{x}_1(t) + \mathbf{b}_1\Delta u(t) \tag{4.2}$$

$$\Delta\mathbf{y}(t) = \mathbf{C}_1\Delta\mathbf{x}_1(t). \tag{4.3}$$

$\Delta\mathbf{x}_1(t) = [\Delta p(t) \quad \Delta\mathbf{x}^\top(t)]^\top$ is the augmented state of the system, where $p(t)$ is the state of the integrator. $\emptyset$ denotes a vector of zeros. This approach is useful for the design of the LQTSS (see Fig. H.2 on page 245).

The structure depicted in Fig. 4.3 will be used for analysis of the controller for the remainder. However, results of the simulations will enact true plant parameters as well as deviational ones. This was achieved using SIMULINK [175] and the respective analysis schematic models for the system with or without control can be found in Appendix H. The figure does not include the effect of disturbances at this point, as it does not influence the design procedure directly. The effect of disturbances will be investigated in §4.1.3 and §4.1.4.

4.1.2.3 Dimensions

The first step in the design procedure is to determine a model to design the controller from. This has been accomplished previously for all three types of models (see footnote c). With the system $(\mathbf{A}, \mathbf{b}, \mathbf{C})$ available, the next step requires the designer to increase the system from type 0 to type 1 by adding an integrator in the system. This results in a new augmented system $(\mathbf{A}_1, \mathbf{b}_1, \mathbf{C}_1)$. Note that the dimensions of the state, input and output matrices are $\mathbf{A}_1 \in \mathbb{R}^{39\times39}$, $\mathbf{b}_1 \in \mathbb{R}^{39\times1}$ and $\mathbf{C}_1 \in \mathbb{R}^{38\times39}$ respectively.

4.1.2.4 State weighting matrix

A suitable value for the state weighting matrix $\mathbf{H} \in \mathbb{R}^{38\times39}$ must be determined. Since the matrix is multiplied by the state, and since the desired tracking error will be defined as the difference between desired output and true output, the $\mathbf{H}$ matrix can be chosen to equal the output matrix $\mathbf{C}_1$. This ensures that the outputs of the system are worked into the performance index of Eq. 2.49.

4.1.2.5 Error and control weighting

Selection of the weighting matrices $\mathbf{Q}$ and $\mathbf{R}$ is not a trivial procedure. It is known that there is only one manipulated variable (casting speed) and therefore $\mathbf{R} = r \in \mathbb{R}^{1\times 1}$. It is also known that there are 38 outputs (the thermocouple outputs) and thus $\mathbf{Q} \in \mathbb{R}^{38\times 38}$. The design goal is to achieve temperatures that are close to the desired temperatures set-points so that the occurrence of defects is minimised. Therefore it has been decided that it is equally important for the LQTSS to track each of the outputs, and reject disturbances on each of the outputs equally "strongly". This implies that the diagonal matrix $\mathbf{Q}$ will have all elements equal along the main diagonal. This can be expressed mathematically as follows.

$$\mathbf{Q} = q\mathbf{I}_{38}, \tag{4.4}$$

where q is a scalar value indicating the global weight of the tracking error. For constant r values, increasing q improve the performance of the tracker but also increases the required control action. Increasing r with constant q reduces the performance on the tracking error but also reduces the control action. From this, it is interesting to note that the ratio q/r is more useful in determining an optimal value for q, irrespective of the value for r.

Setting about to design a suitable value for q, the designer is not only interested in the improved performance of the system but also the required control action. In this design, the control action is performed by the casting speed, $u(t) = u_1(t)$. Now, the casting speed cannot be too high, with acceptable limits ranging between 600 to 1500 mm/min. Furthermore, the acceleration of the slab can also not be too extreme, with a typical allowable value of $du_1(t)/dt\,|_{max} = 1000\,\text{mm/min}^2$ (slew-rate limitation). The controller design will thus be based of observations of increased performance on the tracking error and constraints imposed on the control action.

With the values for all the weighting matrices known, the designer can proceed to solve the ARE (Eq. 2.50) for $\mathbf{S}_\infty$. With $\mathbf{S}_\infty$ known, the designer can find the feed-forward and state feedback gains from Eqs. 2.51 and 2.48 respectively. Once the gains are known, the controller can be simulated to test the improvement of the system. This was done using SIMULINK (see Figs. H.1 and H.2). If the improvement is unsatisfactory, the ratio q/r can be increased and if the control action is too severe, *i.e.* the casting speed or acceleration is too high, the ratio can be decreased until an optimal point is achieved.

4.1.2.6 q/r ratio

Several different values of the q/r ratio were tested in simulation as depicted in Table 4.1 for 1060mm wide slabs. The SMSMSE[e] value is a mean square error approach to evaluate

Table 4.1 1060mm wide slab errors, maximum acceleration and maximum speeds for the LQTSS implementation at different values of the q/r ratio.

$\frac{q}{r}$	SMSMSE	$\max\lvert du_1/dt\rvert$	$\max(u_1)$
None	5.199	0	955.8
0.001	4.5915	22.48	1075
0.01	4.1619	60.3	1120
0.1	3.8945	135.6	1155
1	3.7586	272.2	1180
10	3.6945	517.8	1196
100	3.6644	957	1206
1000	3.6498	1754	1212
10000	3.6424	2992	1215
115	3.6632	997.9	1206

the overall error between the desired set-points of the temperatures and the temperatures themselves. It is defined for this thesis as $\text{SMSMSE} = \sqrt{\text{MSMSE}}$, where

$$\text{MSMSE} = \frac{1}{38}\sum_{j=1}^{38}\text{MSE}_j. \tag{4.5}$$

$\text{MSE} \in \mathbb{R}^{1\times 38}$ is the mean square error between each of the temperature outputs and their respective set-points[f] defined by

$$\text{MSE}_j = \frac{1}{N}\sum_{i=1}^{N}\left(r_j[i] - y_j[i]\right)^2. \tag{4.6}$$

N is the number of time samples used to calculate the MSE. $r_j[i]$ denotes the i-th sample of the j-th set-point and $y_j[i]$ denotes the i-th sample of the j-th output. $\max|du_1/dt|$ is the maximum acceleration of casting speed which should remain below 1000mm/min^2, and $\max(u_1)$ is the maximum value of the casting speed (typically less than 1500 mm/min).

The first row in Table 4.1 denotes the different evaluation parameters when no control is used *i.e.* open-loop. They were derived by using the optimal casting speed[g] as the input to the system and typical mould level and water temperature as disturbances. For this reason,

[e] Square-root of the Mean Sum of Mean Square Errors

[f] see Eq.2.39

[g] the optimal casting speed is calculated using the optimal thermocouple temperature set-points in an inversion with the MVIV model. For the 1060mm case, this optimal speed is 955mm/min.

the acceleration of the slab remains zero (casting speed is constant). Several q/r ratios were used to design controllers in the form of the $\mathbf{F}(\infty)$ and $\mathbf{K}_\infty$ gains. As can be seen, a controller designed with a q/r ratio of 0.001 improved the overall SMSMSE by approximately 12%. As the ratio is increased, the SMSMSE decreases, implying greater control action in the form of greater acceleration as well as improved set-point tracking. At the point where the ratio is 115, the acceleration of the slab has reached its maximum allowable value of 1000mm/min. This is also graphically depicted in Fig. 4.4. The value of 115 for the ratio is therefore the

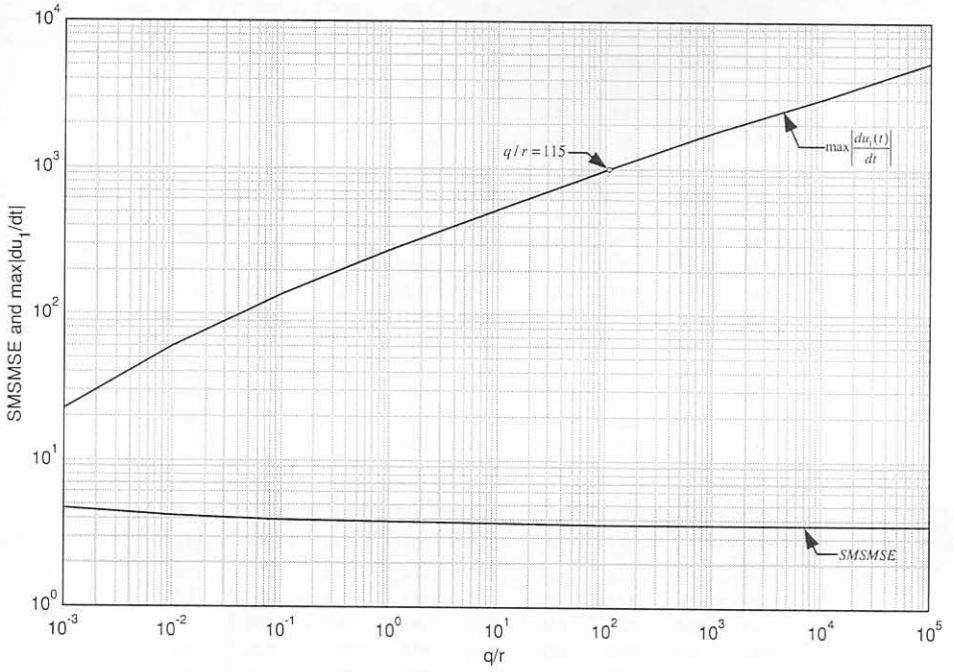

Figure 4.4 SMSMSE and maximum absolute acceleration [mm/min^2] versus q/r ratio for 1060mm slabs.

optimal choice given the model and constraints. At $q/r = 115$, the SMSMSE has improved over the value for no control by approximately 30%.

Inspections of the individual MSE (*i.e.* the effect of the controller on the error of individual set-points) with varying q/r ratios is displayed in Table 4.2. The table shows that some MSEs have been improved dramatically (*e.g.* in5u and in6l) while some have deteriorated (*e.g.* in2u). This is due to the averaging out characteristic of the LQTSS. Overall, an improvement is achieved by looking at the SMSMSE.

Table 4.2 Mean Square Errors for the LQTSS implementation for 1060mm wide slabs at different values of the q/r ratio. $q/r = 115$ has the maximum acceleration of 1000mm/min^2.

$\frac{q}{r}$	in1u	in1l	in2u	in2l	in3u	in3l	in4u	in4l
None	10.7	42.6	10.6	12	2.2	0.569	42.5	21.2
0.001	6.23	27.7	12.8	15	1.38	2.31	33.1	13.1
0.01	3.08	17.3	14.4	17.1	0.969	3.94	26.3	8
0.1	1.78	10.8	15.6	18.7	1.16	5.38	21.7	4.94
1	1.62	7.36	16.4	19.8	1.58	6.46	18.9	3.31
10	1.87	5.53	16.9	20.5	1.97	7.18	17.3	2.45
100	2.16	4.57	17.2	20.9	2.25	7.64	16.4	2
1000	2.38	4.04	17.3	21.1	2.44	7.92	15.9	1.76
10000	2.53	3.75	17.5	21.3	2.56	8.08	15.6	1.62
115	2.17	4.52	17.2	20.9	2.27	7.66	16.3	1.98

$\frac{q}{r}$	in5u	in5l	in6u	in6l	in7u	in7l	in8u	in8l
None	1.63	21.8	15.9	107	6.49	58.6	1.44	43.9
0.001	1.19	14	10.2	76.4	3.64	41.4	1.16	33.1
0.01	0.889	8.55	5.69	56.9	1.67	29.5	1.24	24.4
0.1	0.963	5.21	2.93	44.1	0.741	21.7	1.78	18.5
1	1.2	3.44	1.54	36.6	0.467	17.2	2.44	15.1
10	1.44	2.51	0.893	32.3	0.45	14.7	2.98	13.2
100	1.62	2.03	0.592	29.8	0.5	13.3	3.36	12.1
1000	1.74	1.77	0.447	28.5	0.552	12.5	3.61	11.5
10000	1.82	1.63	0.373	27.7	0.589	12.1	3.76	11.1
115	1.63	2.01	0.58	29.7	0.504	13.2	3.38	12

$\frac{q}{r}$	ou1u	ou1l	ou2u	ou2l	ou3u	ou3l	ou4u	ou4l
None	0.235	32.5	7.21	24.5	21.4	1.79	1.65	6.85
0.001	5.19	21.5	3.9	14.1	29.2	7.54	4.18	9.76
0.01	10.6	13.3	2.14	7.35	35.4	12.3	6.15	11.6
0.1	15.8	8.15	1.99	3.56	40.1	16.5	7.81	13.1
1	20	5.41	2.6	1.78	43.4	19.6	9.01	14
10	22.9	3.99	3.28	1	45.5	21.7	9.81	14.7
100	24.7	3.25	3.82	0.651	46.7	23	10.3	15.1
1000	25.8	2.85	4.18	0.488	47.5	23.8	10.6	15.3
10000	26.5	2.63	4.41	0.409	47.9	24.3	10.8	15.4
115	24.8	3.22	3.84	0.637	46.8	23.1	10.3	15.1

$\frac{q}{r}$	ou5u	ou5l	ou6u	ou6l	ou7u	ou7l	ou8u	ou8l
None	22.3	61	NA	NA	81.2	213	3.01	98
0.001	16	43.4	NA	NA	58.6	164	3.13	71.1
0.01	11	31.3	NA	NA	42.6	140	4.46	51
0.1	7.77	23.4	NA	NA	32.1	123	6.89	37.7
1	5.92	18.8	NA	NA	26	112	9.32	30
10	4.9	16.2	NA	NA	22.5	106	11.2	25.7
100	4.35	14.8	NA	NA	20.6	102	12.5	23.3
1000	4.04	14	NA	NA	19.5	100	13.3	22
10000	3.86	13.5	NA	NA	18.9	98.9	13.8	21.2
115	4.32	14.7	NA	NA	20.5	102	12.6	23.2

$\frac{q}{r}$	nl1u	nl1l	nl2u	nl2l	nr1u	nr1l	nr2u	nr2l
None	1.25	0.0794	0.233	17.7	2.11	21.9	8.12	1.77
0.001	0.749	0.267	0.843	22.7	1.42	17.8	10.4	2.34
0.01	0.37	0.51	1.32	27.1	0.785	14.3	12.4	2.85
0.1	0.173	0.744	1.77	30.6	0.477	11.9	14	3.25
1	0.103	0.926	2.12	33	0.385	10.4	15.1	3.53
10	0.0906	1.05	2.36	34.5	0.382	9.58	15.7	3.7
100	0.0957	1.13	2.51	35.4	0.401	9.1	16.1	3.8
1000	0.104	1.18	2.61	35.9	0.421	8.82	16.4	3.86
10000	0.11	1.21	2.66	36.2	0.434	8.66	16.5	3.9
115	0.0962	1.13	2.52	35.4	0.403	9.08	16.2	3.81

4.1.2.7 Feed-forward and feedback gains

The selected design ratio of 115 resulted in the feed-forward and feedback gain vectors depicted in tables 4.3 and 4.4.

Table 4.3 Feed-forward gain matrix $\mathbf{F}(\infty)$ for 1060mm wide slabs at $q/r = 115$.

in1u	in1l	in2u	in2l	in3u	in3l	in4u	in4l
2.12	2.36	0.505	0.658	1.42	1.12	1.38	1.93
in5u	in5l	in6u	in6l	in7u	in7l	in8u	in8l
1.09	1.78	1.64	2.88	1.51	2.21	1.39	1.6
ou1u	ou1l	ou2u	ou2l	ou3u	ou3l	ou4u	ou4l
2.25	2.07	2.24	2.41	1.22	2.12	1.06	0.842
ou5u	ou5l	ou6u	ou6l	ou7u	ou7l	ou8u	ou8l
1.34	2.24	NA	NA	2.48	3.37	2.38	2.64
nl1u	nl1l	nl2u	nl2l	nr1u	nr1l	nr2u	nr2l
0.621	0.467	0.601	0.851	0.798	0.817	0.56	0.304

Table 4.4 Feedback gain matrix $\mathbf{K}_\infty$ for 1060mm wide slabs at $q/r = 115$. The gain of the integrator state is $k_\infty = 0.230$.

in1u	in1l	in2u	in2l	in3u	in3l	in4u	in4l
2.84	2.07	0.388	0.486	1.5	0.928	1.11	1.44
in5u	in5l	in6u	in6l	in7u	in7l	in8u	in8l
2.79	1.51	2.01	2.16	1.54	1.81	1.83	1.59
ou1u	ou1l	ou2u	ou2l	ou3u	ou3l	ou4u	ou4l
2.54	1.9	2.21	2.02	0.987	1.55	0.851	0.573
ou5u	ou5l	ou6u	ou6l	ou7u	ou7l	ou8u	ou8l
1.32	1.78	NA	NA	2.02	2.14	3.26	2.4
nl1u	nl1l	nl2u	nl2l	nr1u	nr1l	nr2u	nr2l
0.879	0.562	0.622	0.897	1.07	0.892	0.633	0.317

Narrow side gains are on the whole less than wide side gains, specifically for the following two reasons.

- Temperature control is easier to achieve on the narrow sides than the wide sides because the water flow in the copper mould at the narrow sides is approximately 4 times less than at the wide sides. In contrast the wide side is less than 4 times wider than the narrow side. This results in proportionally more water flow in the narrow side which ensures more cooling so that temperature variation is more dramatic when casting speed changes.
- Surface defects on the wide sides were included in the study and not on the narrow sides. This implies that the narrow sides in effect do not affect the design procedure as

much as the wide sides. Care should be taken however that the narrow side-wide side temperature gradient could have an effect on the defects, and can thus not be excluded from the model or the design.

4.1.3 Time-domain results

The following set of figures indicates the effect of the controllers on the system in the time domain. These figures were generated using simulation of the system model with and without controllers. Standard practical disturbances were included to investigate the effectiveness of the controllers. 1060mm wide slabs will be used to discuss the time-domain results and 1280mm wide and 1575mm wide slab results can be found in appendix H.

Fig. 4.5 shows the practical mould level disturbance and Fig. 4.6 shows the practical water temperature disturbance for the controller synthesis for 1060mm wide slabs. The sharp decrease in the mould level at $t \approx 160000$ seconds is probably due to manual mould level control. Fig. 4.7 shows the output of the system when the optimal static control value is

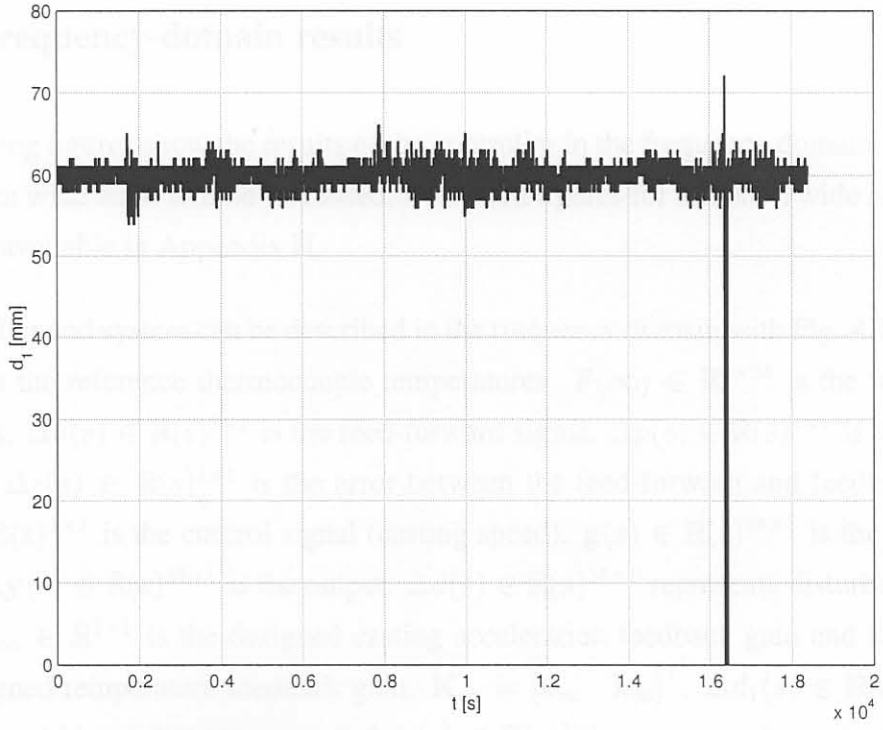

Figure 4.5 Mould level disturbance ($d_1(t)$) used for the simulation of the 1060mm wide slab system.

applied, and Fig. 4.8 shows the outputs when the LQTSS controller is used with 1060mm

wide slabs. The q/r ratio is 115. The figures show that there has been a reduction in the variability of the temperatures. This becomes more evident when looking at the error between the reference output and true output. Figures 4.9 and 4.10 show the errors with and without control. A reduction of about 10°C has been achieved in peak changes of temperature tracking errors when the LQTSS has been used. The set-points are not being followed perfectly, and a reduction in the number of defects of only 18% is achieved. This value was calculated using the IVOV model, and simulating the thermocouple temperatures with, and without the controller implementation. The value is conservative, because it is based on a simulation with the IVOV model predictor. The small reduction in the occurrence of defects is probably due to the fact that good control is difficult to achieve since there are so many outputs which have to be controlled.

Figure 4.11 shows the control signal (casting speed), and Fig. 4.12 the acceleration of the slab for the LQTSS implementation. The speed graph shows that the maximum actuator output constraint (1500mm/min) has not been violated and the acceleration graph shows that the maximum absolute acceleration is less than 1000mm/min^2.

4.1.4 Frequency-domain results

The following figures show the results of the controller in the frequency domain. The figures for 1060mm wide slabs will be discussed, with extra figures for 1280mm wide and 1575mm wide slabs available in Appendix H.

The controller and system can be described in the frequency domain with Fig. 4.13. $\Delta\mathbf{r}(s) \in \mathbb{R}(s)^{38\times1}$ is the reference thermocouple temperatures. $\mathbf{F}(\infty) \in \mathbb{R}^{1\times38}$ is the feed-forward gain matrix. $\Delta v(s) \in \mathbb{R}(s)^{1\times1}$ is the feed-forward signal. $\Delta p(s) \in \mathbb{R}(s)^{1\times1}$ is the feedback signal and $\Delta\epsilon(s) \in \mathbb{R}(s)^{1\times1}$ is the error between the feed-forward and feedback signals. $\Delta u(s) \in \mathbb{R}(s)^{1\times1}$ is the control signal (casting speed). $\mathbf{g}(s) \in \mathbb{R}(s)^{38\times1}$ is the MVIV system, and $\Delta\mathbf{y}(s) \in \mathbb{R}(s)^{38\times1}$ is the output. $\Delta d(s) \in \mathbb{R}(s)^{38\times1}$ represents disturbances on the outputs. $k_\infty \in \mathbb{R}^{1\times1}$ is the designed casting acceleration feedback gain and $\mathbf{k}_\infty \in \mathbb{R}^{38\times1}$ is the designed temperature feedback gain. $\mathbf{K}_\infty = [k_\infty \quad \mathbf{k}_\infty]^\top$. $\Delta d_1(s) \in \mathbb{R}(s)^{1\times1}$ represents the mould level disturbance and $\Delta d_2(s) \in \mathbb{R}(s)^{1\times1}$ represents the water temperature disturbance. $\mathbf{g}_{d_1}(s) \in \mathbb{R}(s)^{38\times1}$ represents the effect or transfer of the mould level on the temperatures and $\mathbf{g}_{d_2}(s) \in \mathbb{R}(s)^{38\times1}$ represents the effect of the water temperature on the temperatures.

The first two figures (Fig. 4.14 and 4.15) show the double-sided spectrum of the two distur-

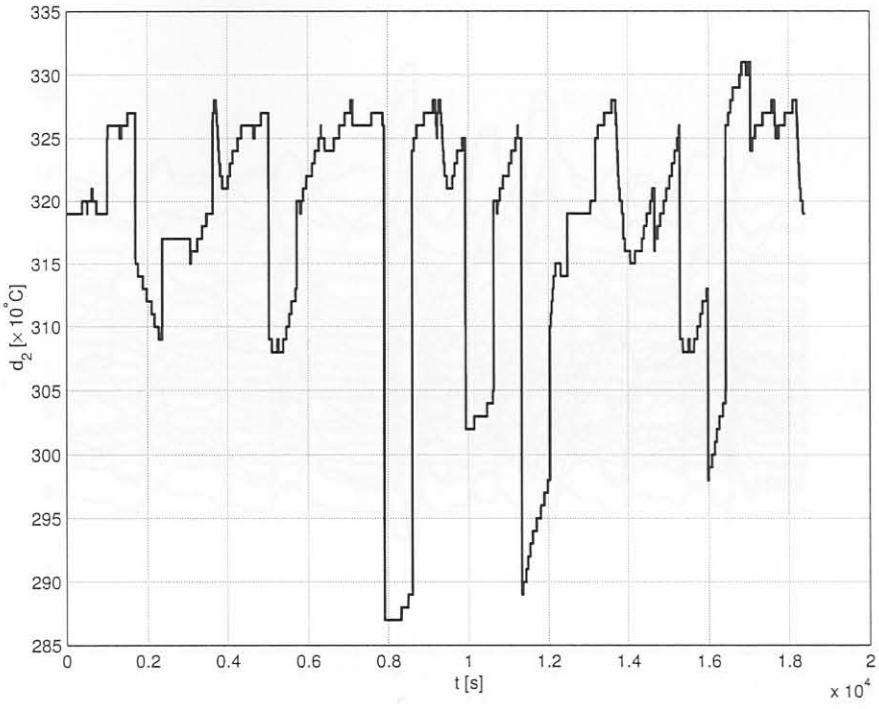

Figure 4.6 Water temperature ($d_2(t)$) disturbance used for the simulation of the 1060mm wide slab system.

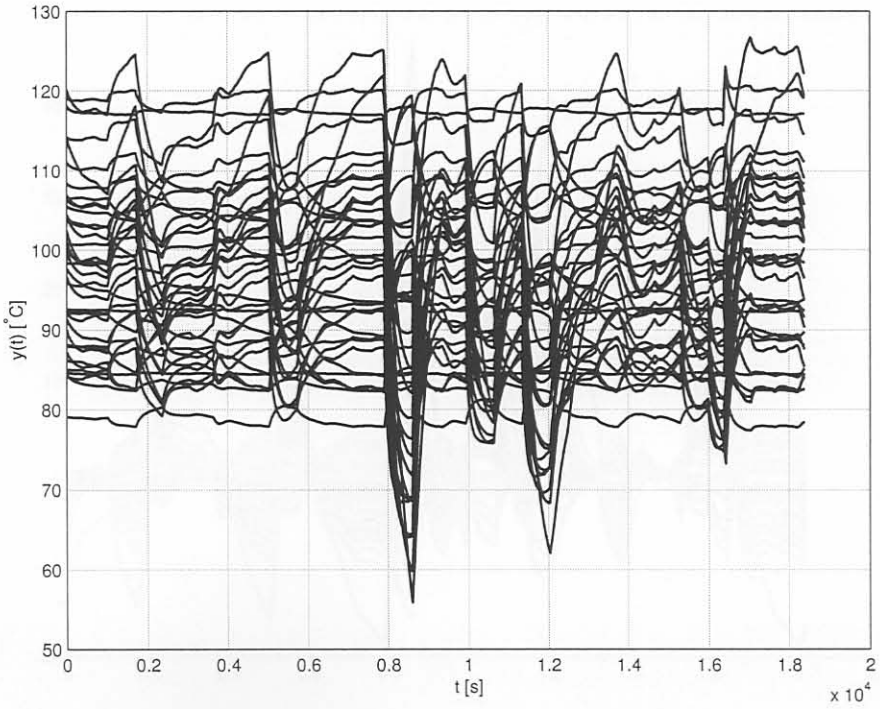

Figure 4.7 Outputs ($\mathbf{y}(t)$) of the system without the LQTSS controller for 1060mm wide slabs.

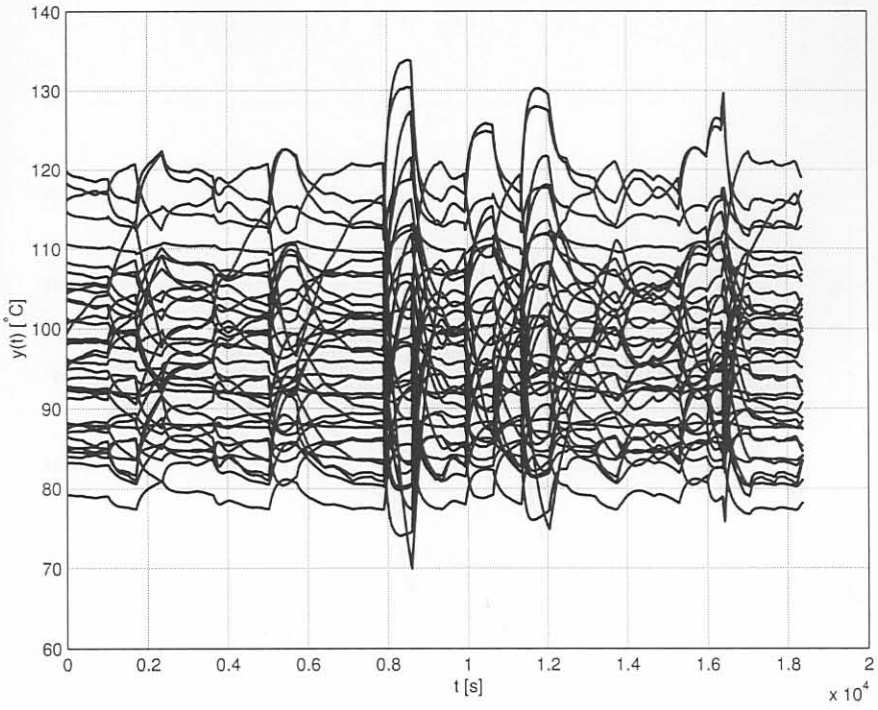

Figure 4.8 Outputs $(\mathbf{y}(t))$ of the system with the LQTSS controller for 1060mm wide slabs.

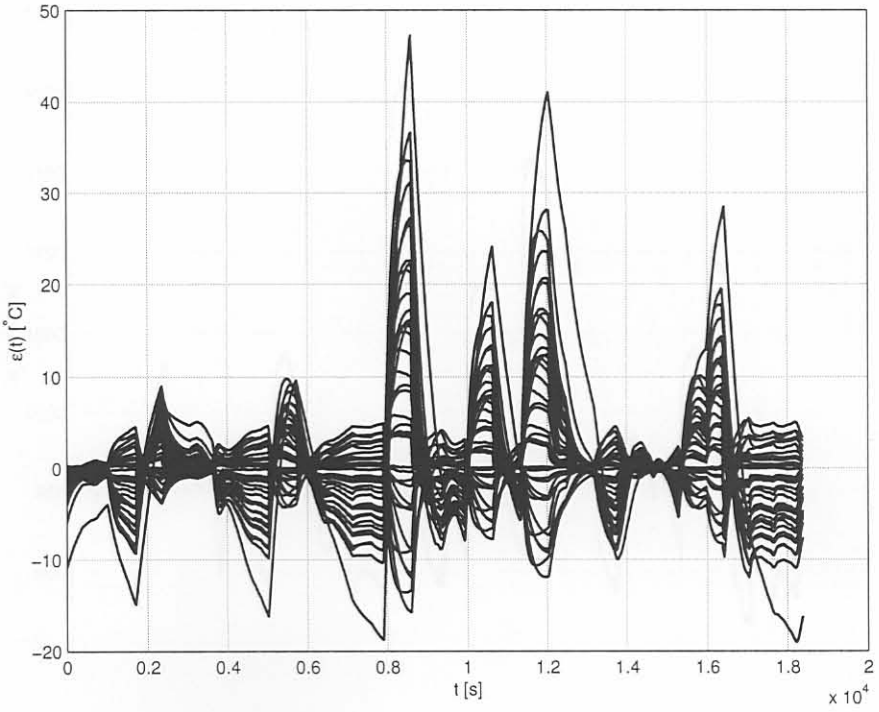

Figure 4.9 Tracking errors of the system without the LQTSS controller for 1060mm wide slabs.

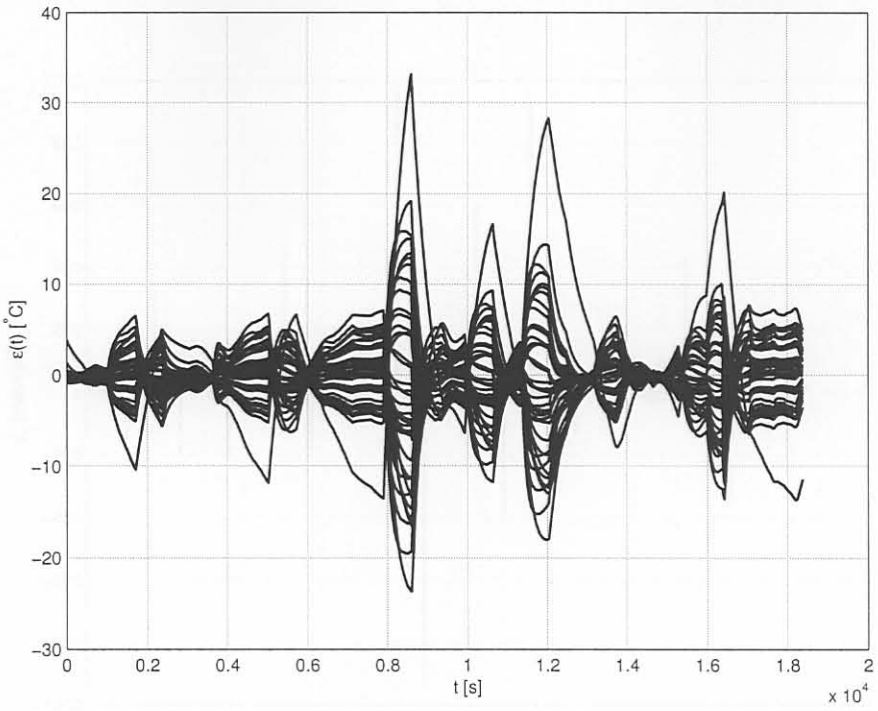

Figure 4.10 Tracking errors of the system with the LQTSS controller for 1060mm wide slabs.

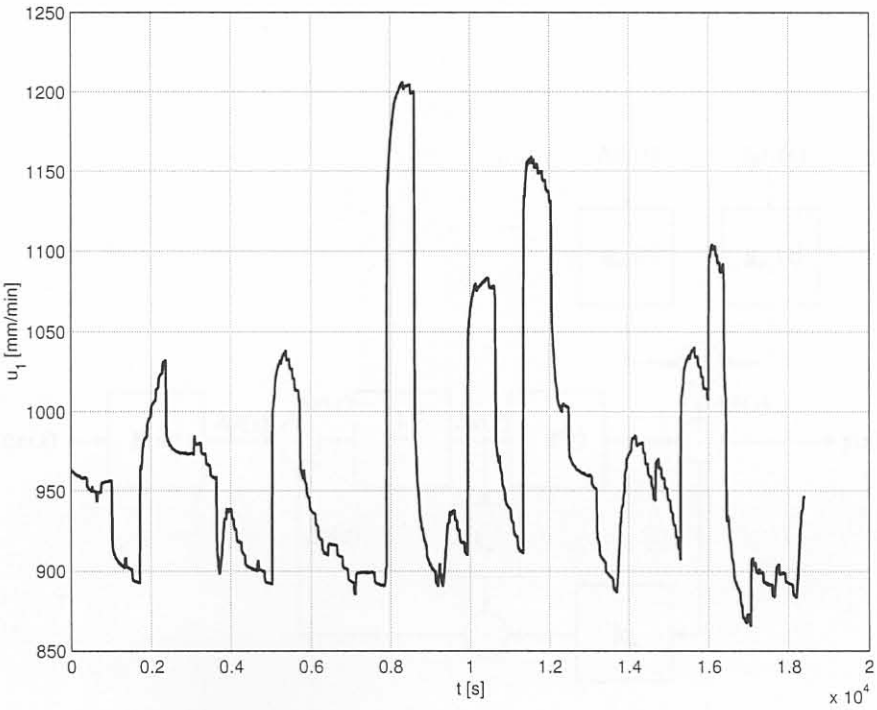

Figure 4.11 Casting speed (casting speed, $u_1(t)$) for the LQTSS controller for 1060mm wide slabs.

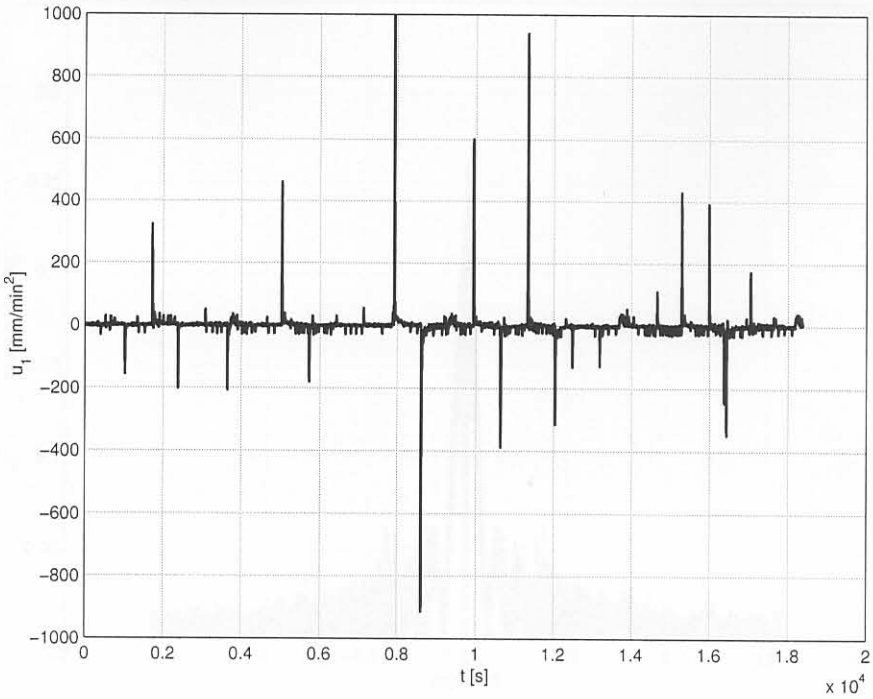

Figure 4.12 Casting acceleration for the LQTSS controller for 1060mm wide slabs.

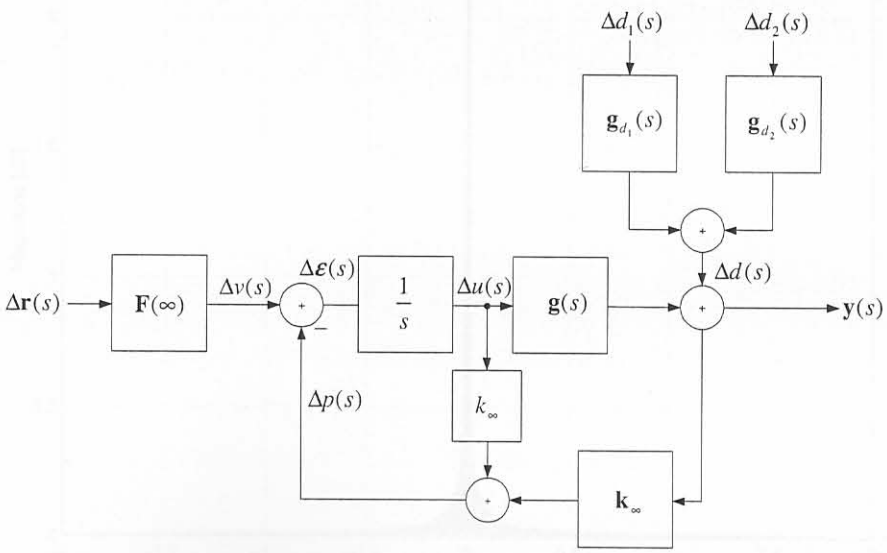

Figure 4.13 Description of the control system in the frequency domain.

bances under investigation, $d_1(j\omega)$ and $d_2(j\omega)$. Fig. 4.16 and Fig. 4.17 show the normalized

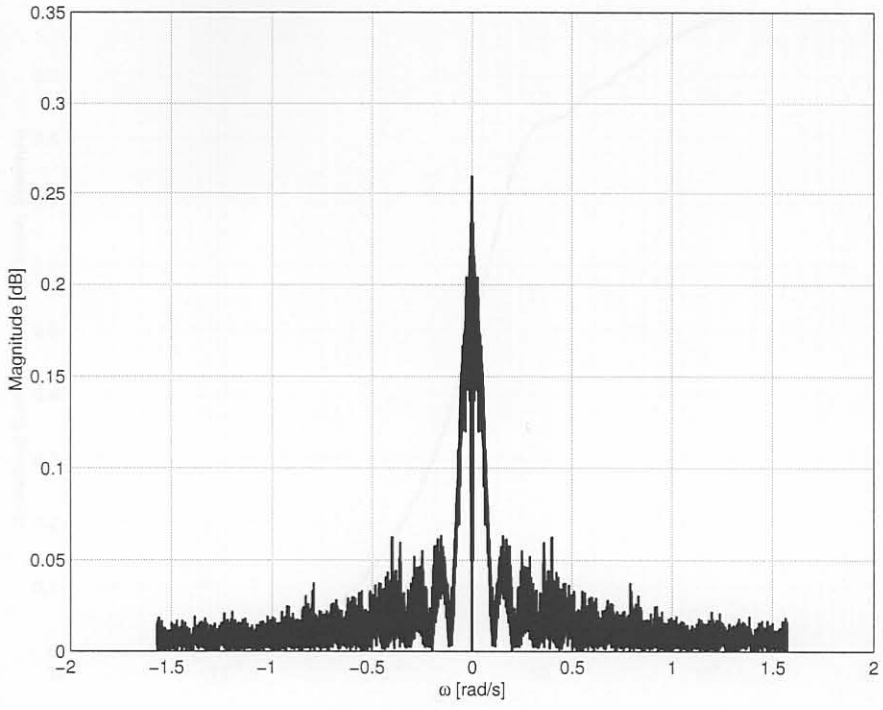

Figure 4.14 Spectrum of mould level disturbance, $d_1(j\omega)$, with average trend removed.

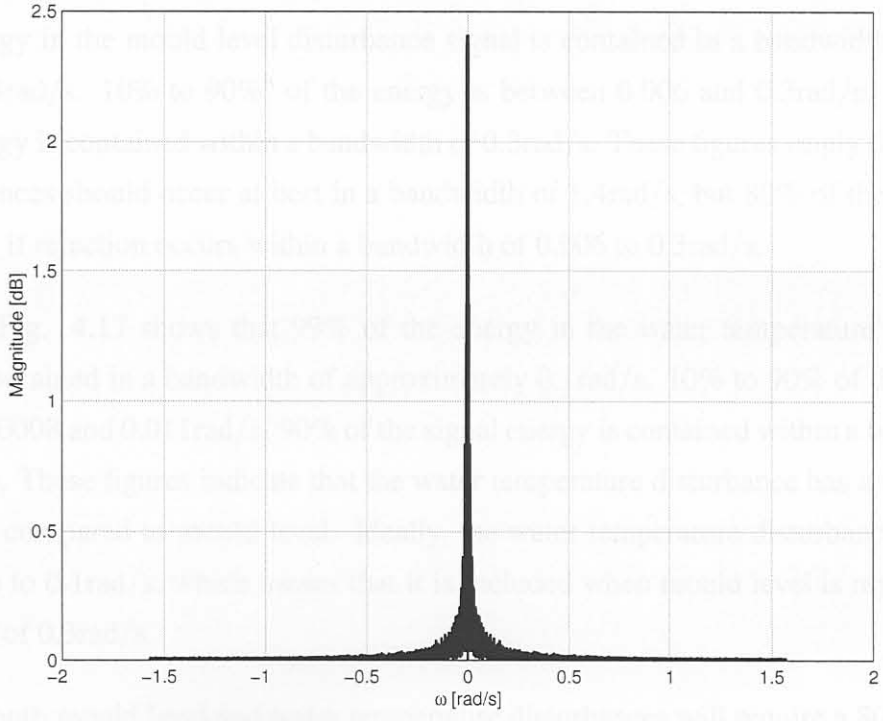

Figure 4.15 Spectrum of water temperature disturbance, $d_2(j\omega)$, with average trend removed.

cumulative energy density spectrum for the two disturbances. Fig. 4.16 shows that 99%

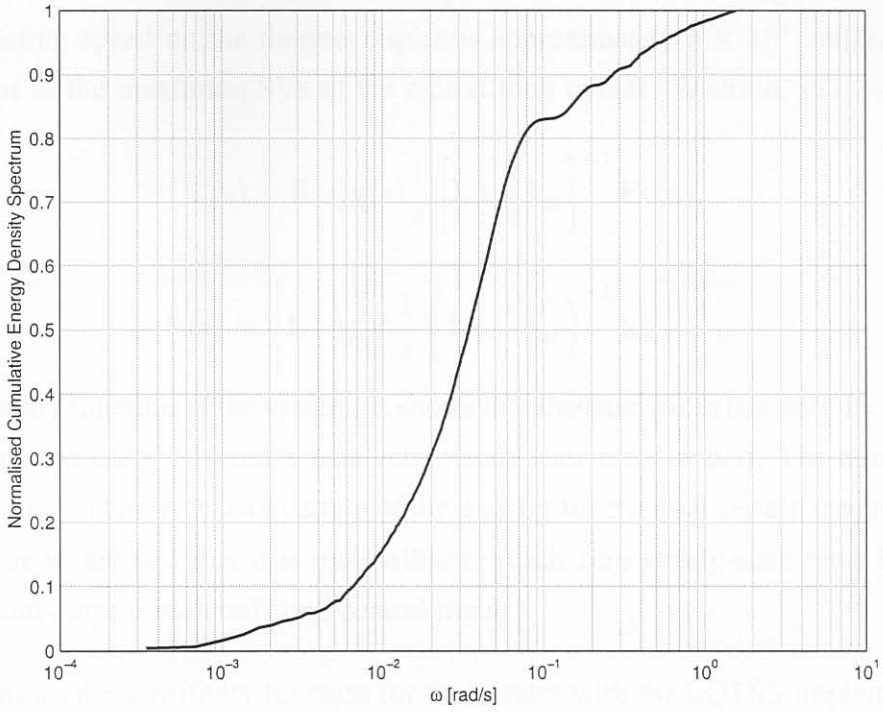

Figure 4.16 Normalized cumulative energy density spectrum for the mould level disturbance

of the energy in the mould level disturbance signal is contained in a bandwidth of approximately 1.4rad/s. 10% to 90%[h] of the energy is between 0.006 and 0.3rad/s. 90% of the signal energy is contained within a bandwidth of 0.3rad/s. These figures imply that rejection of disturbances should occur at best in a bandwidth of 1.4rad/s, but 80% of the energy can be rejected if rejection occurs within a bandwidth of 0.006 to 0.3rad/s.

Similarly, Fig. 4.17 shows that 99% of the energy in the water temperature disturbance signal is contained in a bandwidth of approximately 0.1rad/s. 10% to 90% of the energy is between 0.0008 and 0.011rad/s. 90% of the signal energy is contained within a bandwidth of 0.011rad/s. These figures indicate that the water temperature disturbance has a very narrow bandwidth compared to mould level. Ideally, the water temperature disturbance should be rejected up to 0.1rad/s, which means that it is included when mould level is rejected in the bandwidth of 0.3rad/s.

Rejecting both mould level and water temperature disturbances will require a 80% rejection bandwidth of between 0.0008 and 0.3rad/s.

[h] 80% rejection bandwidth

Fig. 4.18 shows the open-loop SVD plot of the effect of casting speed on the thermocouple temperatures for 1060mm wide slabs. The figure shows that the average bandwidth of the effect of casting speed on the thermocouples is approximately 5×10^{-3}rad/s. Fig. 4.19 shows a plot of the maximum SVs of the closed-loop transfer function, $\mathbf{y}(s) = \mathbf{T}(s)\mathbf{r}(s)$, where

$$\mathbf{T}(s) = \mathbf{S}(s)\mathbf{g}(s)\frac{1}{s}\left[\mathbf{I} + \frac{1}{s}k_\infty\right]^{-1}\mathbf{F}(\infty), \tag{4.7}$$

and

$$\mathbf{S}(s) = \left[\mathbf{I} + \mathbf{g}(s)\frac{1}{s}\left(\mathbf{I} + \frac{1}{s}k_\infty\right)^{-1}\mathbf{k}_\infty\right]^{-1}, \tag{4.8}$$

is the sensitivity function of the system. It shows that the bandwidth has been increased from 5×10^{-3}rad/s to 1.5×10^{-1}rad/s with zero-steady state error *at best*. The minimum SVD can be very low and even at 0 for certain of the transfer functions at certain frequencies. This is mainly due to the fact that it is impossible to reach zero steady-state error between the references and outputs with only one control input.

Fig. 4.20 shows the sensitivity function for the system with the LQTSS implementation. It shows that disturbances acting on the system can be rejected over a range of frequencies up to 1.5×10^{-1}rad/s at best, but could even be amplified at some frequencies in the frequency range. This should be interpreted as an improvement in disturbance rejection on some outputs and a weakening of the disturbance rejection on other.

Figs. 4.21 and 4.22 show the improvement of the addition of control over no control. Even though the sensitivity function showed that there is only disturbance rejection up to approximately 1.5×10^{-1}rad/s, the transfer between the mould level disturbance and the outputs together or without LQTSS control has a -33dB attenuation at 0.3rad/s (the bandwidth of the mould level disturbance) on average. Fig. 4.21 also shows that there is about a 1.5dB improvement in attenuation in the mould level disturbance at low frequencies, decreasing as frequency increases up to about 4×10^{-2}rad/s where the attenuation improvement is marginal.

The water temperature to output temperature transfer function shows that at 0.011rad/s (bandwidth of water temperature disturbance) there is an improvement of about 2.5dB on the attenuation of the disturbance, using the LQTSS. This attenuation improvement increases towards DC. At 8×10^{-4}rad/s there is an improvement in attenuation of about 3dB. At 2×10^{-1}rad/s the attenuation weakens, but is of no concern since this point falls outside the spectrum of the water temperature disturbance.

Fig. 4.23 shows the transfer function defined by $h(s) = p(s)/v(s)$. This is the transfer

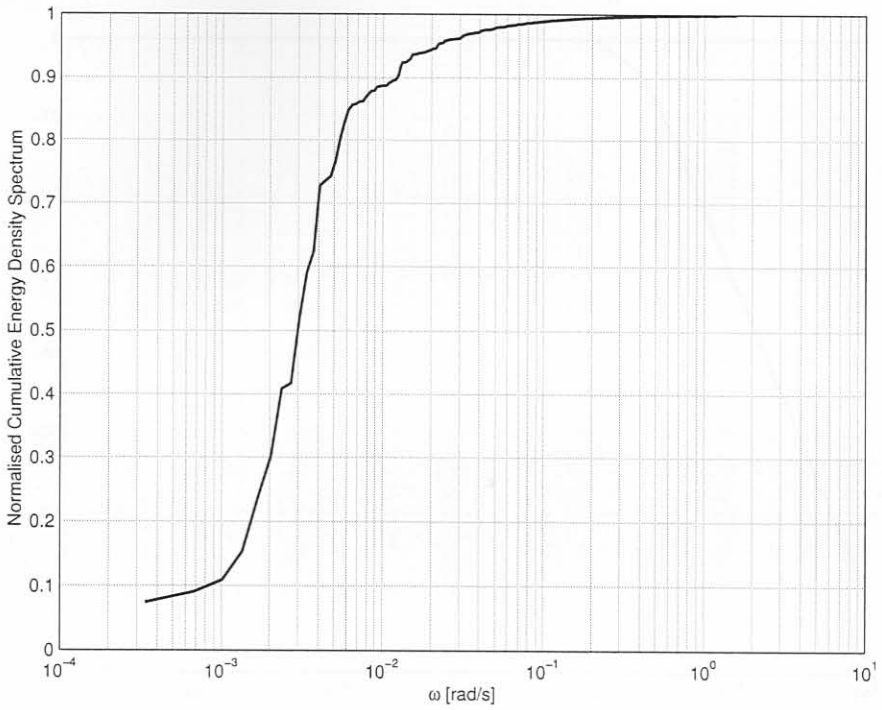

Figure 4.17 Normalized cumulative energy density spectrum for the water temperature disturbance

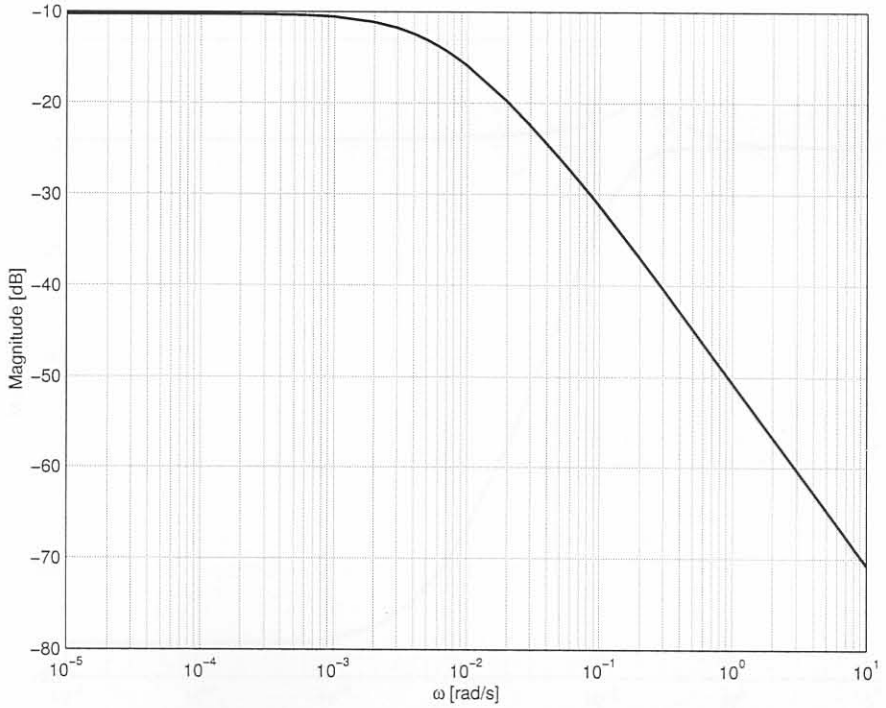

Figure 4.18 Open-loop SVD plot of casting speed to the thermocouple temperatures without control ($\mathbf{g}(s)$).

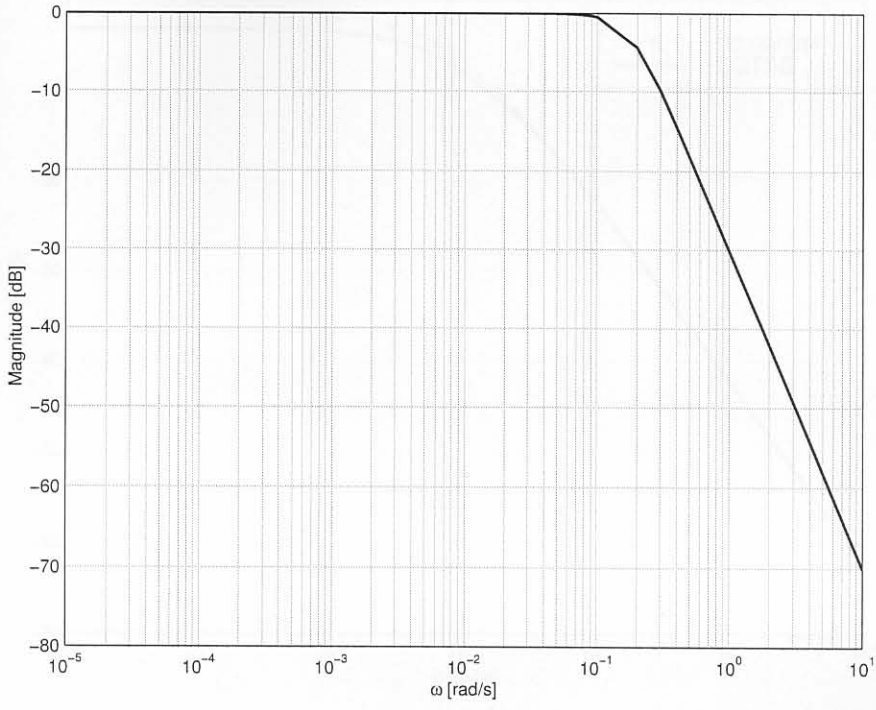

Figure 4.19 Closed-loop maximum SVs plot, $\mathbf{T}(s)$, of the system.

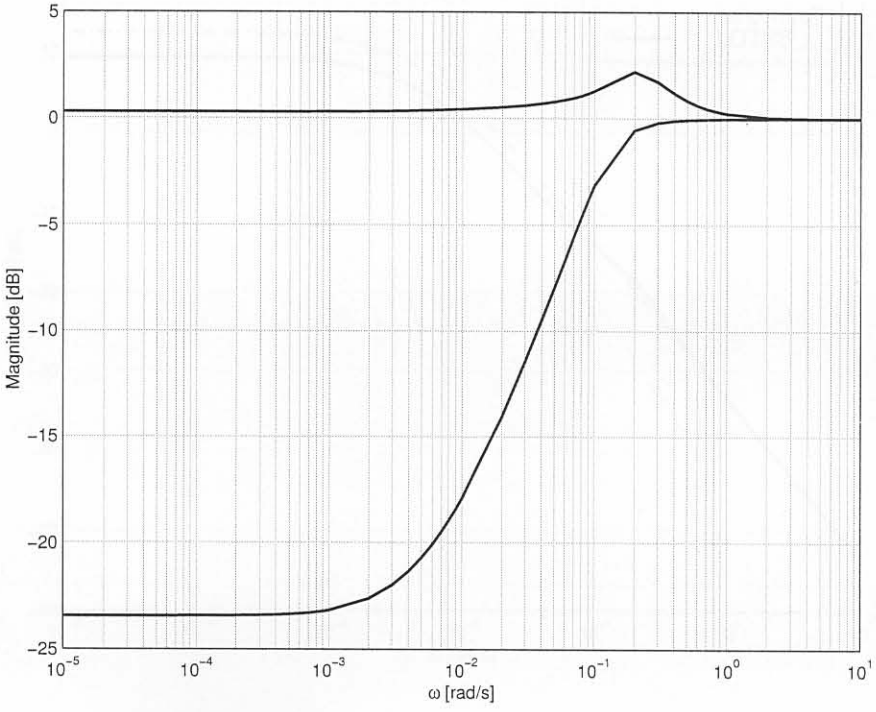

Figure 4.20 Sensitivity function for the system.

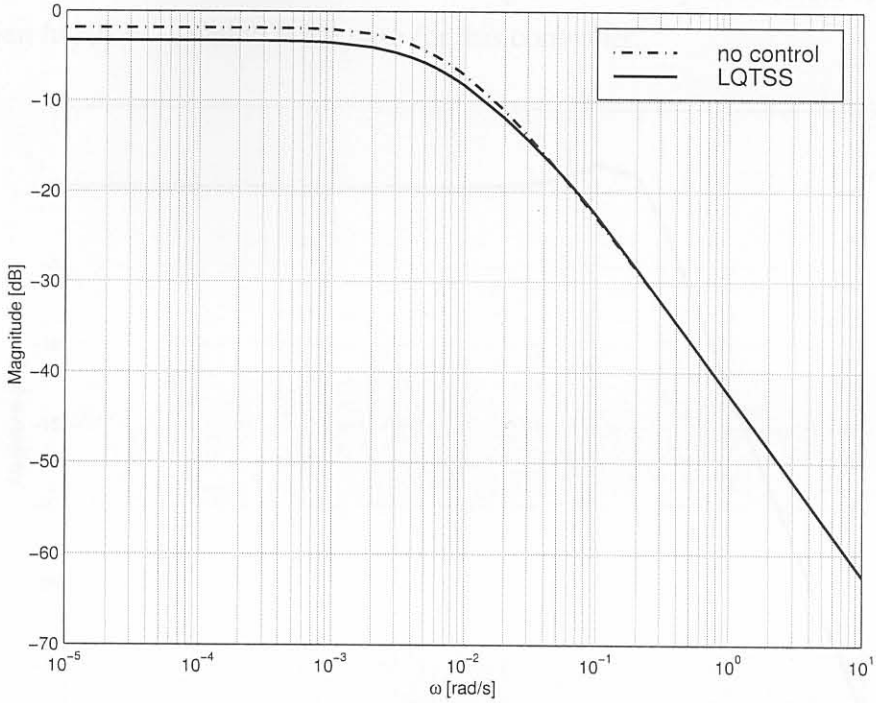

Figure 4.21 Reduction in the effect of mould level disturbance on the output temperatures.

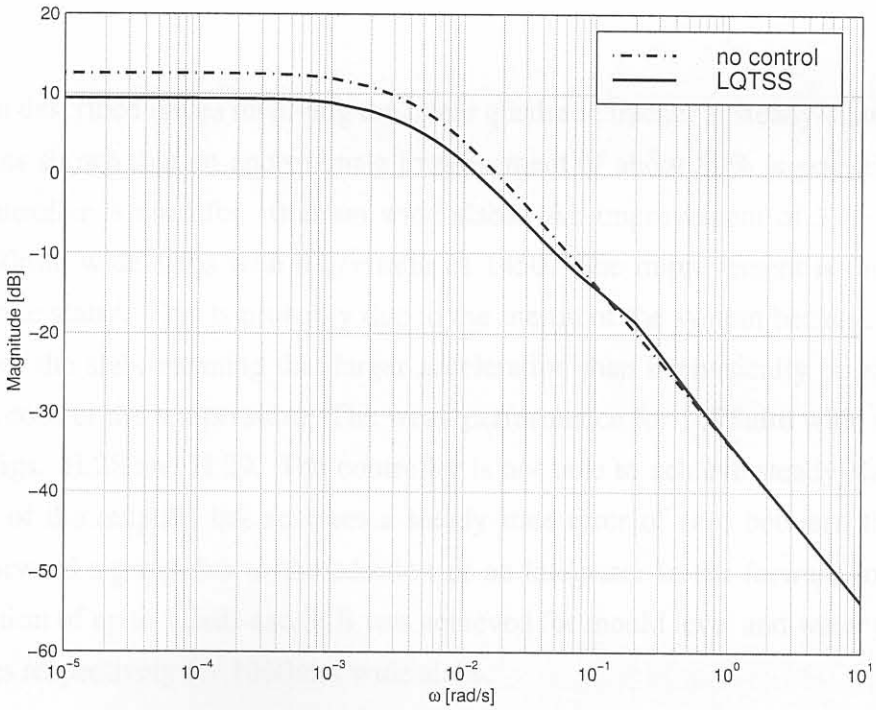

Figure 4.22 Reduction in the effect of water temperature disturbance on the output temperatures.

function between the feed-forward and feedback signals. If steady-state errors for step inputs are zero, then $h(j0) = 1$, which is the case for this controller.

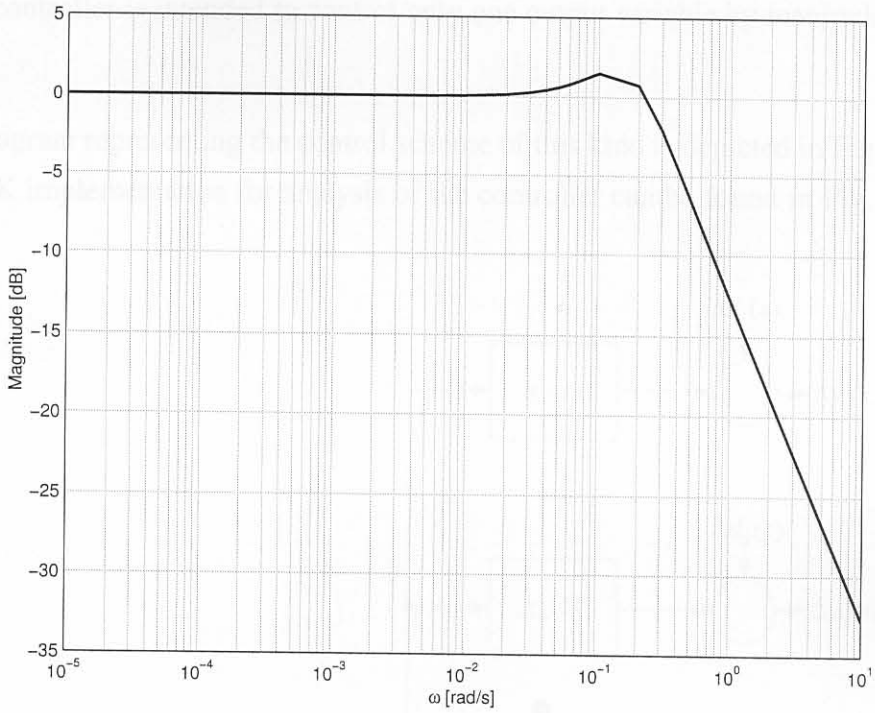

Figure 4.23 Bode plot of the transfer function of $p(s) = h(s)v(s)$.

This section described issues involving the linear quadratic tracker at steady-state implementation. It has shown that an approximate improvement of about 30% is possible when the LQTSS controller is used for 1060mm wide slabs. An improvement of 37% is possible[i] for the 1280mm wide slabs with a q/r ratio of 1450. The improvement is only 0.7% for 1575mm wide slabs[j]. This is probably due to the inertia of the system because of the wide dimension of the slab, meaning that larger acceleration than is physically possible may be required to control the temperature. The weak performance for 1575mm wide slabs is also shown in Figs. H.28 and H.29. The controller is not able to achieve steady-state errors of zero on all of the outputs, but achieves a steady-state error of zero between the feedback and feed-forward signals due to the addition of an integrator in the forward loop. Disturbance rejection of up to 1.5dB and 3dB was achieved for mould level and water temperature disturbances respectively for 1060mm wide slabs.

[i] see Table H.1
[j] see Table H.5

4.2 Single-output control (SOC)

The SOC controller is intended to control only one output variable by manipulating casting speed.

A block diagram representing the control scheme of this kind is depicted in Fig. 4.24, and a SIMULINK implementation for analysis of the controller can be found in Fig. I.1 on page 274.

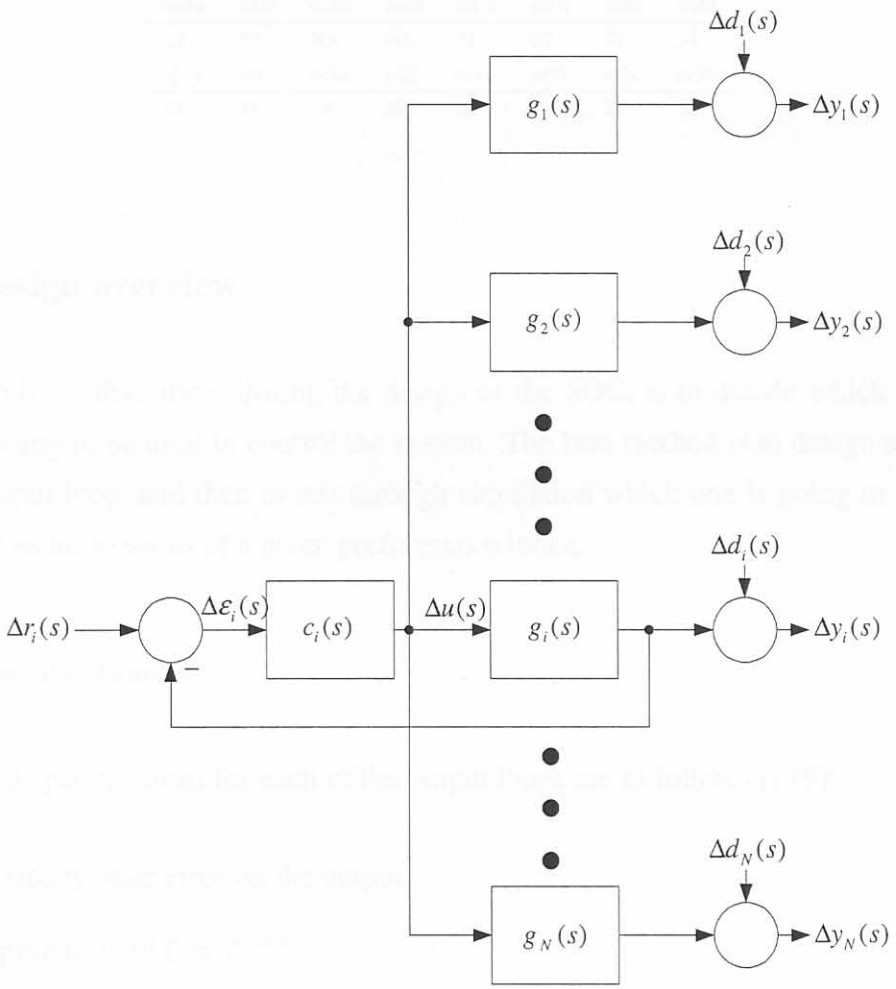

Figure 4.24 Control configuration for the single output control method.

$g_j(s) \in \mathbb{R}(s)^{1\times1}, j = 1, 2, \ldots, N$ denotes the transfer function between casting speed and the j-th thermocouple temperature output ($N = 38$). $\Delta u(s) \in \mathbb{R}(s)^{1\times1}$ is the deviational casting speed, $\Delta y_j(s) \in \mathbb{R}(s)^{1\times1}, j = 1, 2, \ldots, N$ is the j-th deviational thermocouple output and $\Delta d_j(s) \in \mathbb{R}(s)^{1\times1}, j = 1, 2, \ldots, N$ is the j-th deviational disturbance on the j-th output. $\Delta r_i(s) \in \mathbb{R}(s)^{1\times1}$ is the reference set-point for the i-th control loop, and $c_i(s) \in \mathbb{R}(s)^{1\times1}$ is

the controller of the i-th loop. The i-th loop to actual output conversion is given in table 4.5.

Table 4.5 Conversion between loop number, i, and actual output.

in1u	in1l	in2u	in2l	in3u	in3l	in4u	in4l
1	2	3	4	5	6	7	8
in5u	in5l	in6u	in6l	in7u	in7l	in8u	in8l
9	10	11	12	13	14	15	16
ou1u	ou1l	ou2u	ou2l	ou3u	ou3l	ou4u	ou4l
21	22	23	24	25	26	27	28
ou5u	ou5l	ou6u	ou6l	ou7u	ou7l	ou8u	ou8l
29	30	NA	NA	31	32	33	34
nl1u	nl1l	nl2u	nl2l	nr1u	nr1l	nr2u	nr2l
17	18	19	20	35	36	37	38

4.2.1 Design overview

The first problem that arises during the design of the SOC, is to decide which one of the outputs is going to be used to control the system. The best method is to design a controller for each output loop, and then to test through simulation which one is going to deliver the best overall result in terms of a given performance index.

4.2.1.1 Specifications

The standard specifications for each of the output loops are as follows [149]:

1. Zero steady-state error on the output.
2. Damping ratio of $\zeta = 2^{-0.5}$.
3. Maximum bandwidth.
4. Actuator constraints not to be violated.

The design specifications are meant to increase the speed of a loop to a maximum while still maintaining a damping ratio[k] of 0.7071 without breaching the maximum casting speed constraints. The casting speed should remain within about 1500mm/min and the absolute acceleration of the slab (derivative of casting speed) should remain below 1000mm/min^2.

[k]The value chosen for the damping ratio is standard [149], and is the best trade-off between a sluggish response and a large overshoot.

4.2.1.2 PI control

Since the system is of type 0, an integrator must be added in the control loop to increase the system to type 1. This will ensure that the controlled SISO system will have zero steady-state error. A convenient way to design the controllers is to use Evans' root-locus [149], which manipulates a gain in a compensated system. The controller results in a simple PI controller for each i-th loop of the form

$$c_i(s) = k_{i,1} + \frac{k_{i,2}}{s}. \tag{4.9}$$

One zero is placed and one gain is designed to meet the loop specifications [149].

The design process is iterative for each loop, but is simple to carry out, and results in values for $k_{i,1}$ and $k_{i,2}$ for the i-th loop. Eventually, pole-zero plots of the individual loops' closed-loop responses will have a zero to the left of the closed loop poles[1], with the closed loop poles on the $\zeta = 0.7071$ line. This is graphically depicted in Fig. 4.25 for the casting speed to in1u thermocouple system. Following the previous design procedure, the controllers were designed for the 1060mm wide slabs. The results of the values for the proportional and integral gains are given in Tables 4.6 and 4.7.

Table 4.6 1060mm wide slab design values for the proportional gains $k_{i,1}$.

in1u	in1l	in2u	in2l	in3u	in3l	in4u	in4l
226.9	229.9	1874	1510	675.2	1432	447.6	433.9
in5u	in5l	in6u	in6l	in7u	in7l	in8u	in8l
286.5	383.1	290.7	186.4	490.6	249.1	599.1	293.6
ou1u	ou1l	ou2u	ou2l	ou3u	ou3l	ou4u	ou4l
378.3	270	332.7	277.1	607.2	782.2	1351	1601
ou5u	ou5l	ou6u	ou6l	ou7u	ou7l	ou8u	ou8l
419.4	254.8	NA	NA	205.5	201.6	264.8	157.5
nl1u	nl1l	nl2u	nl2l	nr1u	nr1l	nr2u	nr2l
1292	2106	1970	653.9	720.4	620.3	1118	3399

Simulation with each of the respective controllers in the loop delivers the following SMSMSE performance indexes (Table 4.8) for each of the controllers. The table shows that thermocouple output in6u shows the best performance when its controller is used in the loop. Note that this is not better than for the LQTSS 1060mm wide case. Here the MSE was 3.6632, a much better result. This is probably due to the fact that only one loop is used, and all 37 other loops are open. This means that even though near-perfect control can be achieved for one loop, the consequence of not directly controlling all the other loops by leaving them open delivers a worse result than the LQTSS.

[1] the position of the zero is restricted by the actuator constraints

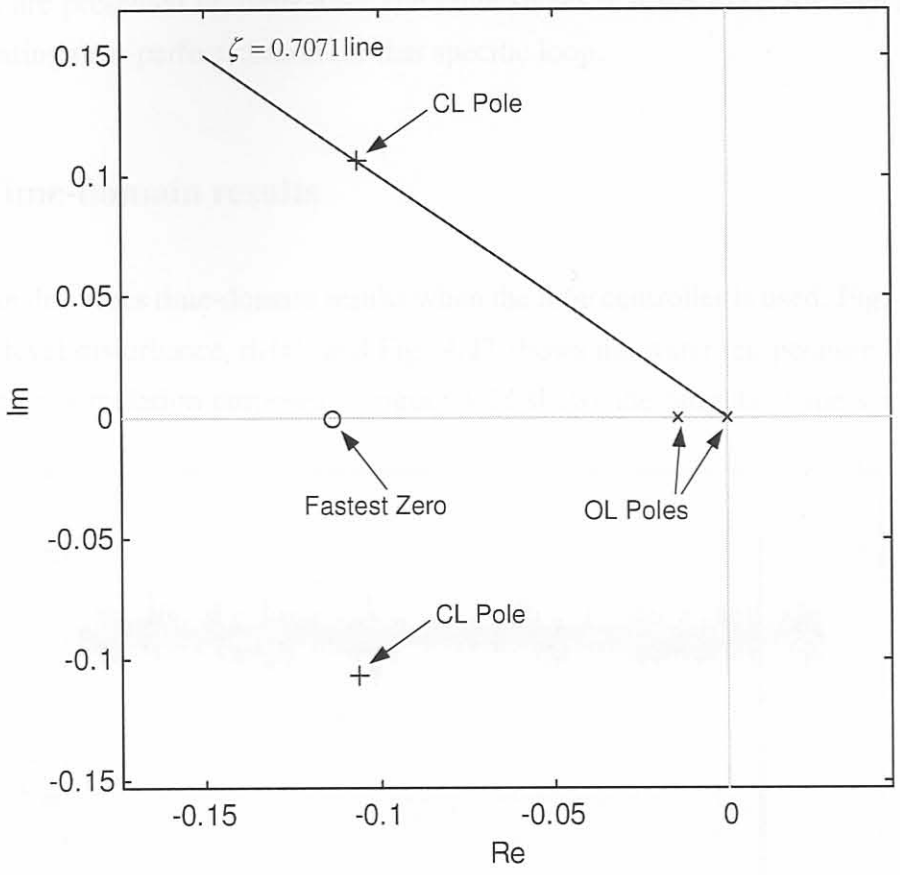

Figure 4.25 Poles and zeros of the open-loop and closed-loop system for 1060mm slabs and the casting speed to in1u thermocouple system. The fastest zero is chosen so that the maximum casting speed constraints are not violated.

Table 4.7 1060mm wide slab design values for the integral gains $k_{i,2}$.

in1u	in1l	in2u	in2l	in3u	in3l	in4u	in4l
25.92	10.9	98.9	73.04	85.17	155.9	18.79	18.49
in5u	in5l	in6u	in6l	in7u	in7l	in8u	in8l
93.75	20.1	27.31	5.463	45.18	9.841	107.4	16.88
ou1u	ou1l	ou2u	ou2l	ou3u	ou3l	ou4u	ou4l
49.71	14.75	28.46	13.95	30.02	59.69	120.6	75.04
ou5u	ou5l	ou6u	ou6l	ou7u	ou7l	ou8u	ou8l
27.84	9.478	NA	NA	7.507	3.582	40.32	6.539
nl1u	nl1l	nl2u	nl2l	nr1u	nr1l	nr2u	nr2l
261.7	366	289.3	50.26	96.14	47.63	111.9	447

Using the thermocouple output in6u loop for control, the MSEs were obtained for each output and are presented in Table 4.9. The table shows that the MSE for in6u is virtually zero, indicating near-perfect control for that specific loop.

4.2.2 Time-domain results

This section describes time-domain results when the in6u controller is used. Fig. 4.26 shows the mould level disturbance, $d_1(t)$, and Fig. 4.27 shows the water temperature disturbance, $d_2(t)$, used for simulation purposes. Figure 4.28 shows the outputs of the system for the

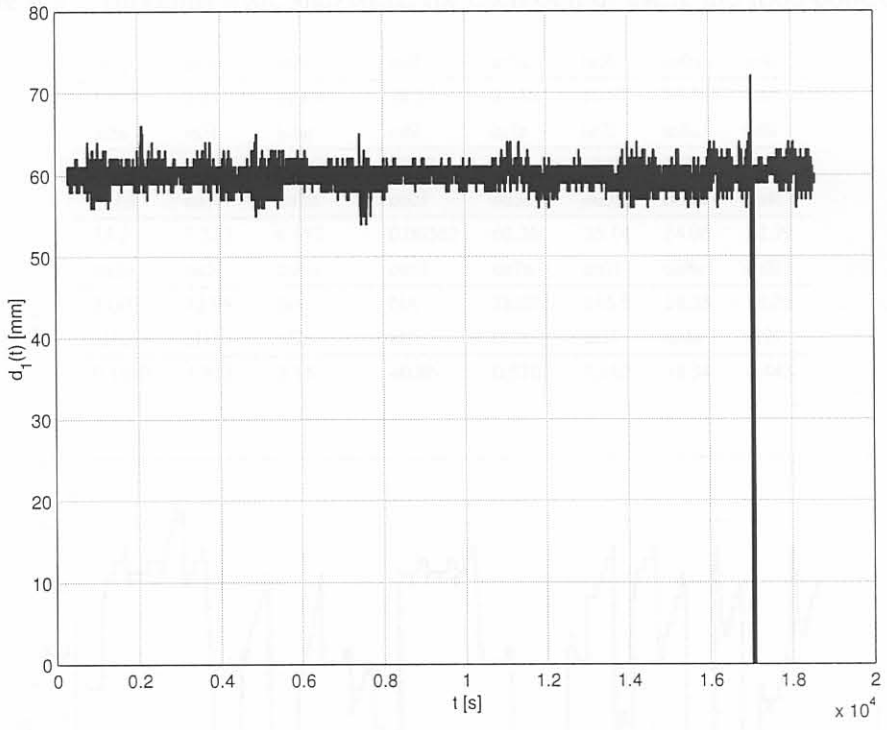

Figure 4.26 Mould level disturbance for the simulation with SOC for 1060mm wide slabs.

SOC control. As can be seen, one of the outputs remains near constant at the temperature set-point, while other temperatures vary. This output is thermocouple in6u. Fig. 4.29 shows the errors between the reference output temperatures and the achieved output temperatures. The result is very similar to that of the LQTSS case, but the peak responses are higher than in the LQTSS case. The casting speed (control signal) and the acceleration of the slab is shown in Figs. 4.30 and 4.31 The acceleration constraint is breached only in two cases at time $t = 3000$ and $t = 11000$ seconds approximately. The control approximately follows the inverse of the water temperature, because this disturbance has the greatest effect on the output temperature (compared to the mould level disturbance).

Table 4.8 1060mm wide slab SMSMSE for each controller in the loop.

in1u	in1l	in2u	in2l	in3u	in3l	in4u	in4l
4.362	4.121	17.6	15.83	4.678	6.684	6.448	4.109
in5u	in5l	**in6u**	in6l	in7u	in7l	in8u	in8l
4.69	4.088	**4.027**	5.184	4.224	4.713	4.881	5.049
ou1u	ou1l	ou2u	ou2l	ou3u	ou3l	ou4u	ou4l
5.913	4.103	4.539	4.036	12.16	6.784	7.627	12.19
ou5u	ou5l	ou6u	ou6l	ou7u	ou7l	ou8u	ou8l
4.468	4.837	NA	NA	4.924	8.875	5.042	4.761
nl1u	nl1l	nl2u	nl2l	nr1u	nr1l	nr2u	nr2l
4.225	5.968	6.447	13.1	4.326	6.791	13.17	12.22

Table 4.9 1060mm wide slab MSE for each output using the in6u controller.

in1u	in1l	in2u	in2l	in3u	in3l	in4u	in4l
3.989	2.21	22.05	28.33	3.635	10.87	16.54	1.15
in5u	in5l	in6u	in6l	in7u	in7l	in8u	in8l
2.601	0.9246	0.002515	28.82	1.01	11.07	5.093	9.854
ou1u	ou1l	ou2u	ou2l	ou3u	ou3l	ou4u	ou4l
33.2	1.532	6.657	0.06362	60.36	35.14	14.06	22.39
ou5u	ou5l	ou6u	ou6l	ou7u	ou7l	ou8u	ou8l
3.007	12.99	NA	NA	18.07	146.9	18.35	18.26
nl1u	nl1l	nl2u	nl2l	nr1u	nr1l	nr2u	nr2l
0.1863	1.513	3.15	40.86	0.5765	8.162	18.34	4.443

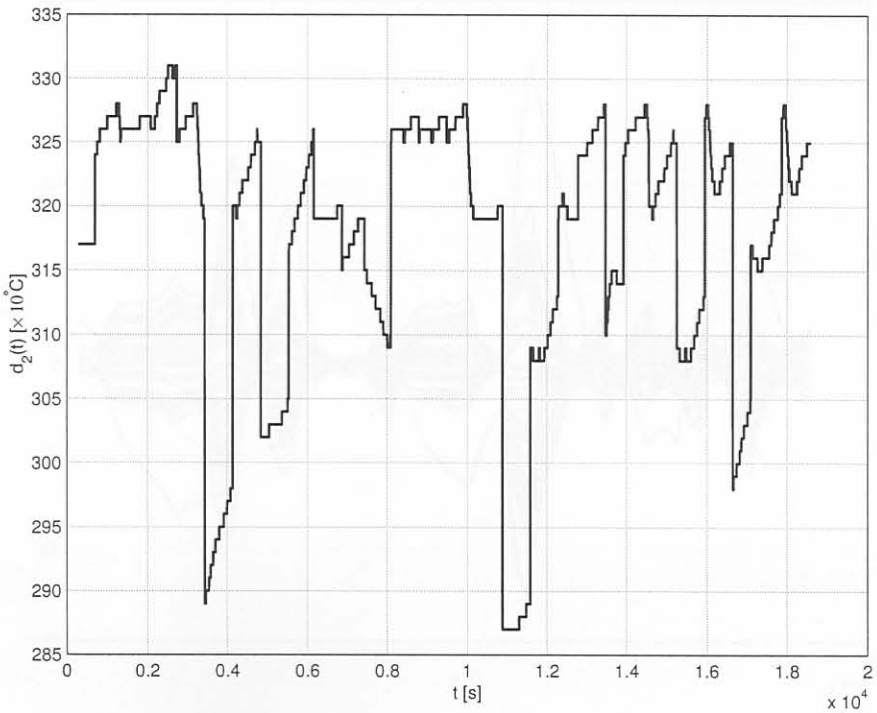

Figure 4.27 Water temperature disturbance for the simulation with SOC for 1060mm wide slabs.

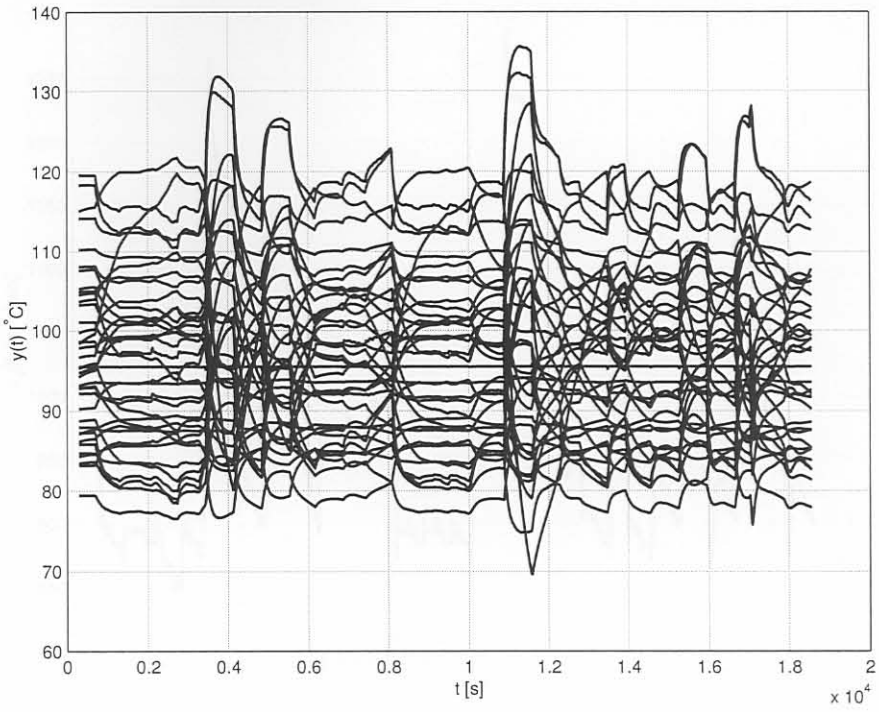

Figure 4.28 Thermocouple temperature outputs for 1060mm wide slabs when thermocouple in6u is used in a feedback configuration.

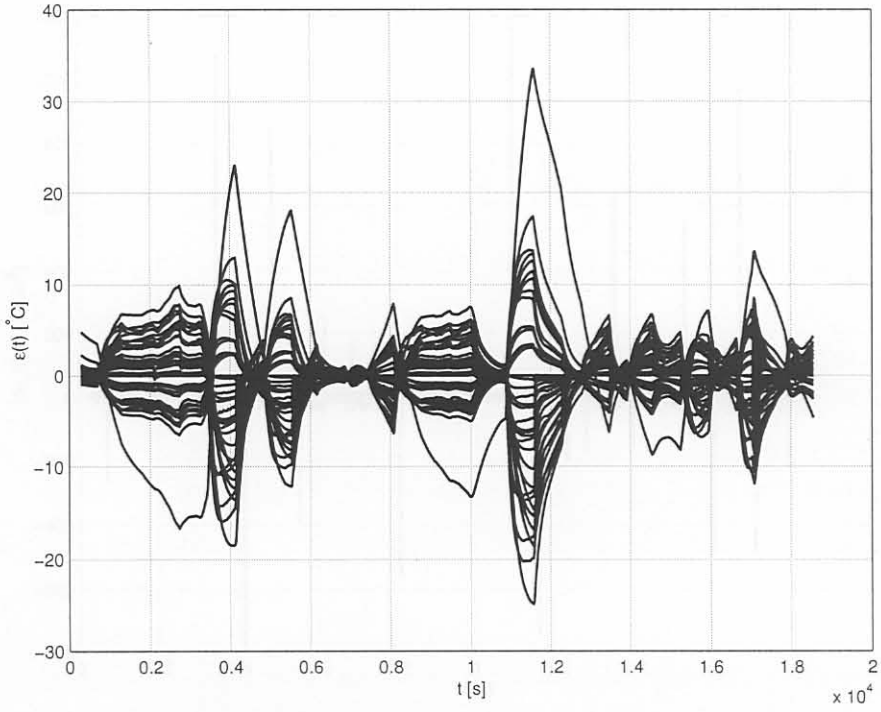

Figure 4.29 Thermocouple temperature errors for 1060mm wide slabs when thermocouple in6u is used in a feedback configuration.

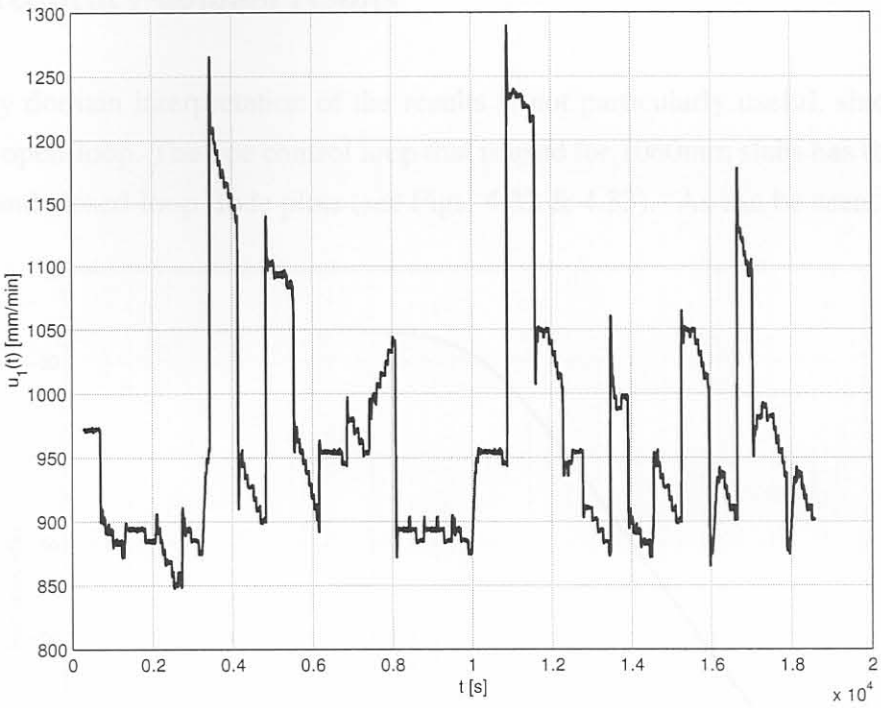

Figure 4.30 Control signal for 1060mm wide slabs when thermocouple in6u is used in a feedback configuration.

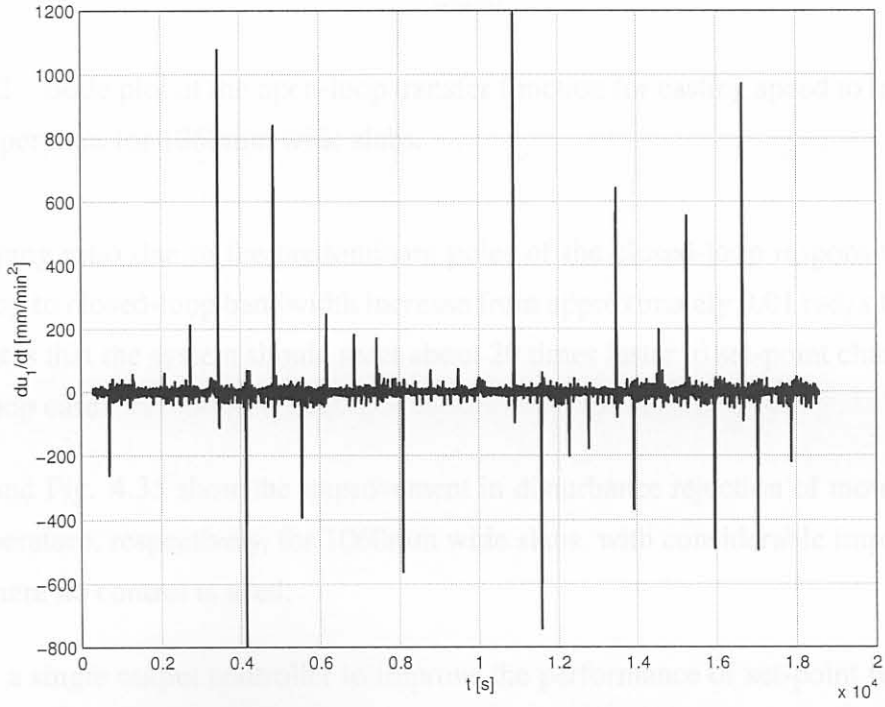

Figure 4.31 Slab acceleration for 1060mm wide slabs when thermocouple in6u is used in a feedback configuration.

4.2.3 Frequency-domain results

A frequency domain interpretation of the results is not particularly useful, since 37 of the outputs are open-loop. The one control loop that is used for 1060mm slabs has the following open-loop and closed-loop Bode plots (see Figs. 4.32 & 4.33). As can be seen, the approx-

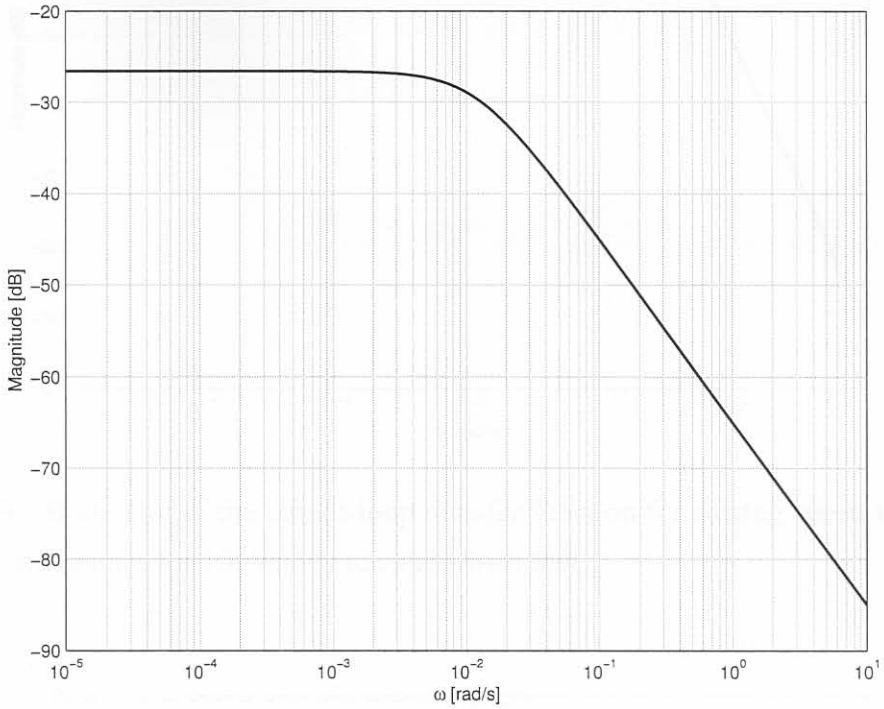

Figure 4.32 Bode plot of the open-loop transfer function for casting speed to in6u thermocouple temperature for 1060mm wide slabs.

imate damping ratio due to the predominant poles of the closed-loop response is 0.7 with an open-loop to closed-loop bandwidth increase from approximately 0.01 rad/s to 0.2 rad/s. This indicates that the system should react about 20 times faster to set-point changes than in the open-loop case.

Fig. 4.34 and Fig. 4.35 show the improvement in disturbance rejection of mould level and water temperature, respectively, for 1060mm wide slabs, with considerable improvement to the case where no control is used.

The use of a single output controller to improve the performance of set-point following for output disturbances was described. For 1060mm slabs, the improvement is approximately 23% over the case where no control is used. For 1280 and 1575mm slabs, the improvements are 39% and -2% respectively. The control has deteriorated when SOC is used on the 1575mm wide slabs and 1280mm wide slabs, compared with the LQTSS case. More results

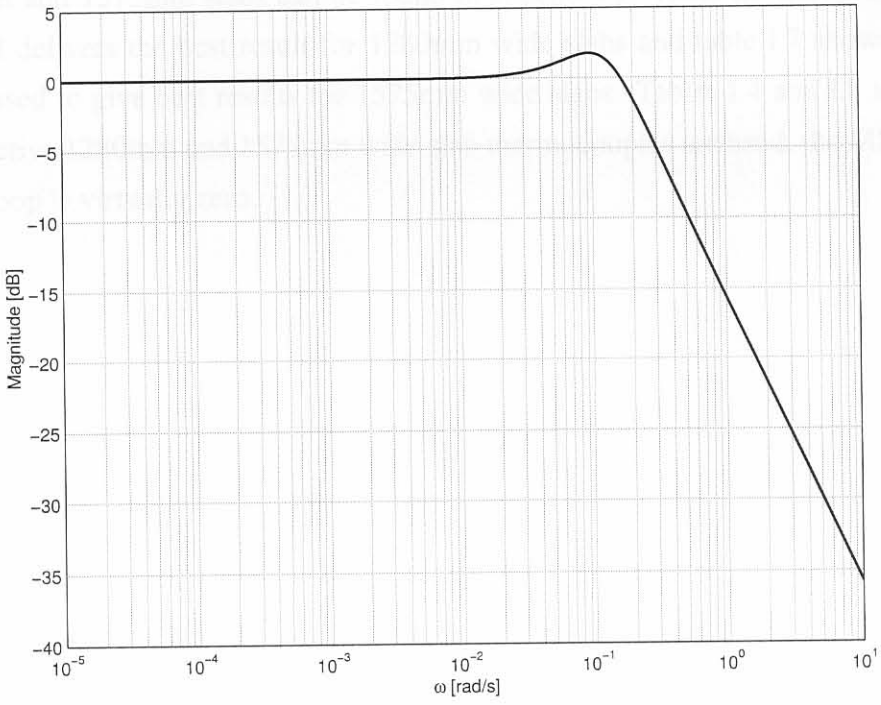

Figure 4.33 Bode plot of the closed-loop transfer function for casting speed to in6u thermocouple temperature for 1060mm wide slabs with SOC.

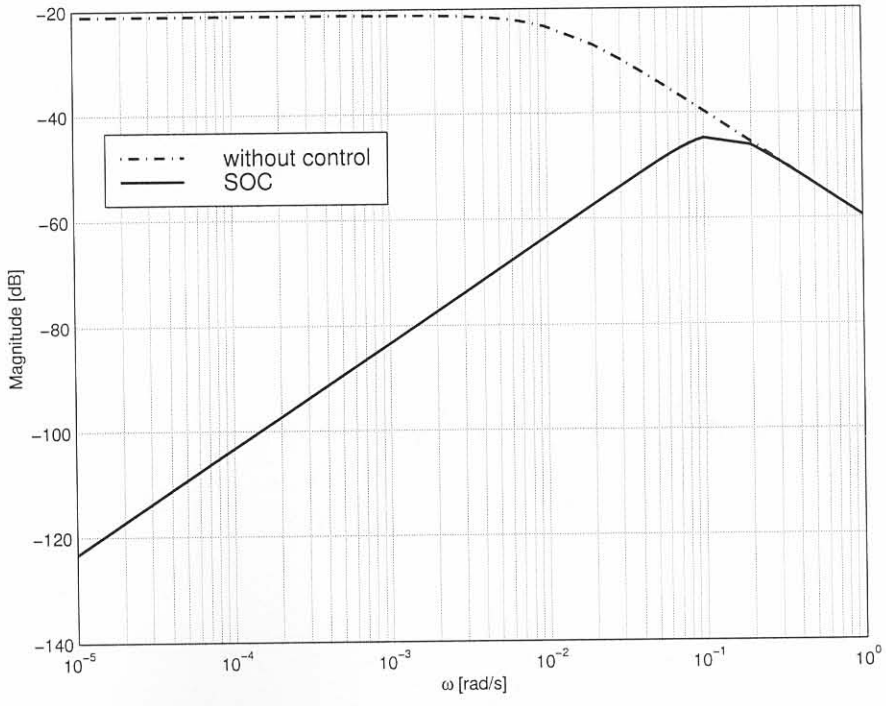

Figure 4.34 Bode plot of the rejection of the mould level disturbance for casting speed to in6u thermocouple temperature for 1060mm wide slabs using SOC.

for 1280mm and 1575mm slabs can be found in appendix I. Table I.3 shows that thermocouple ou2l delivers the best result for 1280mm wide slabs and table I.7 shows that ou5u should be used to give best results for 1575mm wide slabs. Tables I.4 and I.8 show that if these respective 1280mm and 1575mm wide slab thermocouples are used, the MSEs for that particular loop is virtually zero.

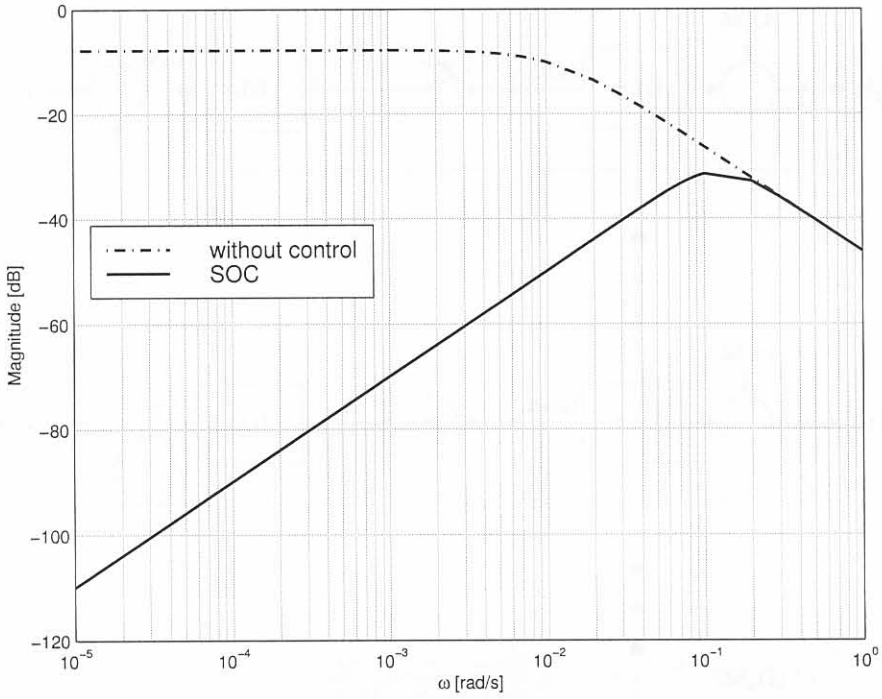

Figure 4.35 Bode plot of the rejection of water temperature disturbance for casting speed to in6u thermocouple temperature for 1060mm wide slabs using SOC.

4.3 Worst-case control (WCC)

This section describes the use of a worst-case control configuration. The basic idea is to utilize the SOC controllers, but to switch to the loop with the largest error. Fig. 4.36 shows the basic control configuration.

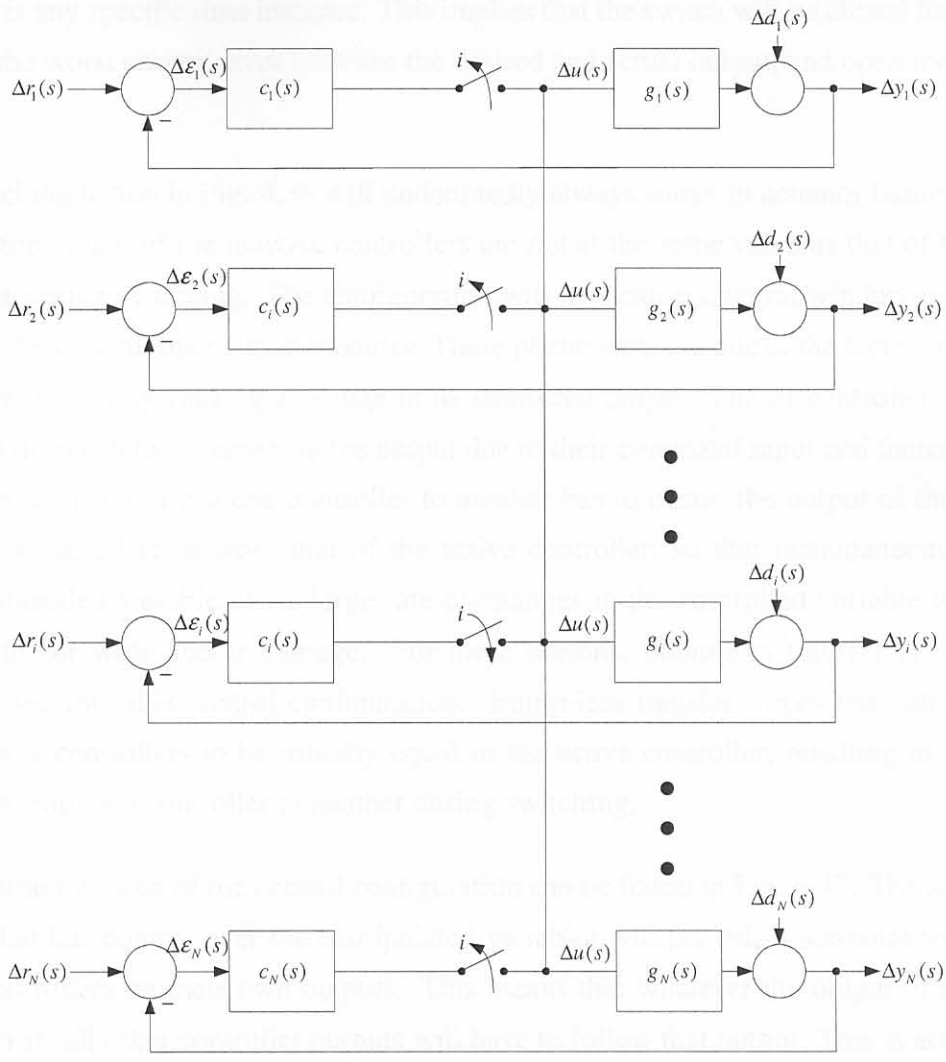

Figure 4.36 Control configuration for the worst case control method.

All variables and specifications are the same as in the SOC (§4.2).

4.3.1 Design overview

The switches between the controller output and manipulated variables are activated whenever the i-th output is performing the worst. During switching, the selected controller becomes

active and the remaining 37 controllers become inactive. This means that the casting speed is adjusted by the i-th controller whose loop output is the worst[m]. Mathematically, this can be written as follows and is known here as the switching criterion:

$$i = j|\max|\epsilon_j(t = t_1)|, \tag{4.10}$$

where t_1 is any specific time instance. This implies that the switch will be closed for the loop that has the worst current error between the desired and actual output, and open for all other loops.

The switching action in Fig. 4.36 will undoubtedly always cause an actuator bump to occur, because the output of the inactive controllers are not at the same value as that of the active controller during switching. The configuration will also cause integral windup, because all PI controllers are running simultaneously. These phenomena are due to the fact that only one controller is actively causing a change in its measured output. The PI controllers on 37 of the loops do not detect changes in the output due to their command input and therefore wind up. When a change from one controller to another has to occur, the output of the inactive controllers are different from that of the active controller, so that instantaneous changes in the controlled variable cause large rate-of-changes in the controlled variable which can cause actuator wear and/or damage. For these reasons, bump-less transfer [174] is also incorporated into this control configuration. Bump-less transfer forces the outputs of all the inactive controllers to be initially equal to the active controller, resulting in a smooth transition from one controller to another during switching.

The modified version of the control configuration can be found in Fig. 4.37. The active controller (that has control over the manipulated variable) will provide a set-point to all other active controllers on their own outputs. This means that whatever the output of the active controller is, all other controller outputs will have to follow that output. This is achieved by forming a feedback loop in parallel with the normal feedback loop of the controller $c_j(s)$. This new error signal $\gamma_j(s)$ is an input for the normal systems described in Fig. 4.36. Simultaneously, the WCC output feedback and set-points are disturbances for the bump-less transfer element (the controllers $c_j(s)$ look like plants to the bump-less transfer elements). Integral wind-up will also be eliminated because the purpose of the inactive systems is to follow the error between their output and the output of the active controller. Note that the active controller will not be adversely affected through the bump-less transfer because the bump-less transfer summation node subtracts the same signal from itself, thus providing an input disturbance of zero to the active controller.

[m] *i.e.* it has the largest absolute error between set-point and output

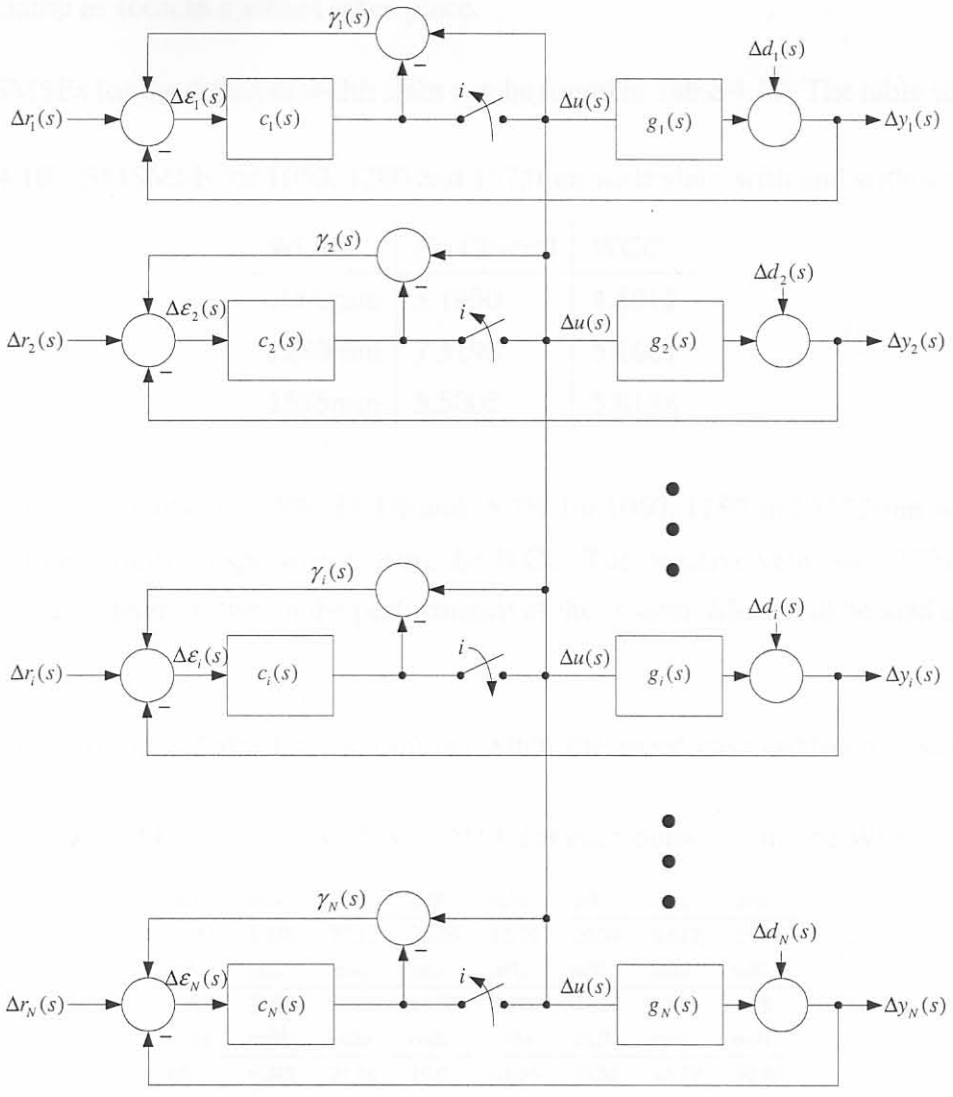

Figure 4.37 Control configuration for the worst case control method with bump-less transfer.

No extra dynamics have been added to the bump-less transfer system in order to keep the design simple. The loops increase in speed due to the $c_j(s)$ controllers. Because of the large response times of the system together with the actuator constraint, the inactive loops will adequately follow the active loop. Some dynamics can be added (see [174]).

Switches should not be placed in the WCC feedback path, because this will result in an actuator bump as soon as a switch takes place.

The SMSMSEs for the different width slabs can be found in Table 4.10. The table shows that

Table 4.10 SMSMSE for 1060, 1280 and 1575mm wide slabs with and without WCC.

Width	No Control	WCC
1060mm	5.1990	4.5012
1280mm	7.5198	5.1681
1575mm	5.5005	5.8138

there are improvements of 13.4%, 31.3% and -5.7% for 1060, 1280 and 1575mm wide slabs compared to no control respectively, using the WCC. The negative value for 1575mm wide slabs indicates a deterioration in the performance of the system. More will be said about this later (§4.4).

Table 4.11 shows the MSEs for each output when the worst-case control is used. These

Table 4.11 1060mm wide slab MSE for each output using the WCC.

in1u	in1l	in2u	in2l	in3u	in3l	in4u	in4l
21.37	5.488	27.12	35.86	12.79	20.39	8.627	2.928
in5u	in5l	in6u	in6l	in7u	in7l	in8u	in8l
8.364	3.087	5.428	11.63	8.376	4.823	15.1	4.78
ou1u	ou1l	ou2u	ou2l	ou3u	ou3l	ou4u	ou4l
68.57	4.345	27.56	10.9	81.65	66.52	23.79	30.94
ou5u	ou5l	ou6u	ou6l	ou7u	ou7l	ou8u	ou8l
1.796	5.351	NA	NA	7.603	85.99	49.74	8.629
nl1u	nl1l	nl2u	nl2l	nr1u	nr1l	nr2u	nr2l
1.496	3.067	5.818	52.93	2.659	4.88	23.63	5.882

figures show that the MSE ranges from very good values (*e.g.* 1.796 for ou5u) to very bad values (*e.g.* 68.57 for ou1u). This can probably be attributed to the fact that some outputs are above their reference values and some are below. This causes the control to decrease or increase depending on which loop is active, one above or one below the reference, with a net-effect of doing nothing to improve the overall response of the system.

4.3.2 Time-domain results

The following figures pertain to the 1060mm wide slabs. Results of 1280mm and 1575mm wide slabs can be found in appendix J.

Fig. 4.38 shows the mould level disturbance, $d_1(t)$, and Fig. 4.39 shows the water temperature disturbance, $d_2(t)$, used for simulation purposes. Fig. 4.40 shows the outputs when

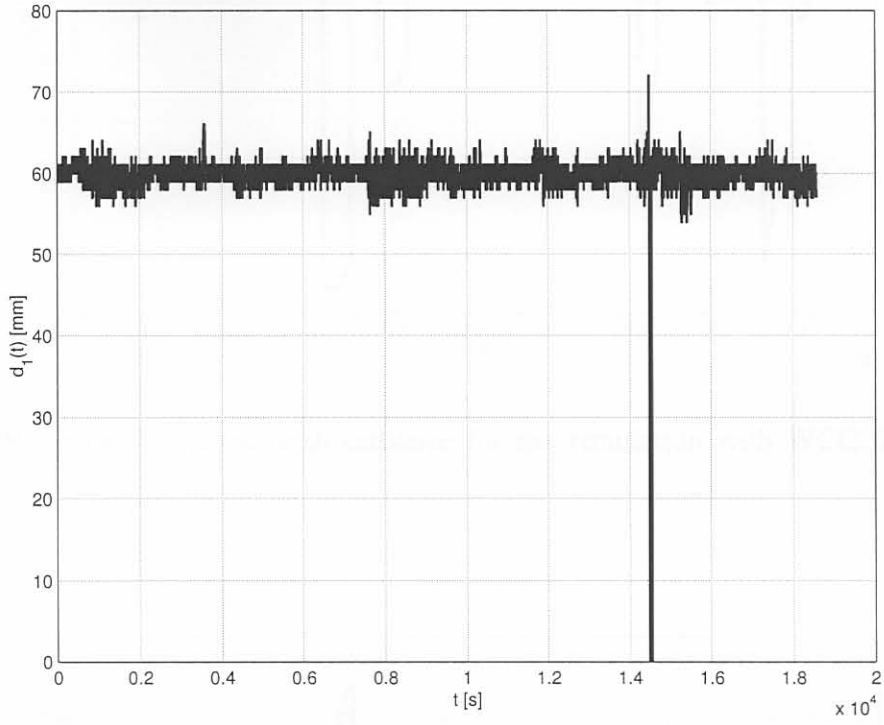

Figure 4.38 Mould level disturbance for the simulation with WCC for 1060mm wide slabs.

the worst-case control is used and Fig. 4.41 shows the tracking error on the output. These figures show a similar response to the LQTSS case for the specific disturbances, but peak values for temperature deviations are higher than in the LQTSS case.

Fig. 4.42 shows the control signal and Fig. 4.43 shows the acceleration of the slab. Fig. 4.44 shows the output of the switching criterion (*i.e.* which loop is active). These figures show that the casting speed remains below 1500mm/min, with the acceleration constraint being violated only twice, at approximately $t = 7000$s. Switching occurs mainly between loops 25 and 32 (*i.e.* thermocouples 25 and 32, see table 3.7 for a description of the indexes, i, for the thermocouples). These loops switch between each other because as one becomes active and tries to drive its negative output error to zero by increasing casting speed, the other loop's temperature also increases. The new controller then decreases the casting speed to drive

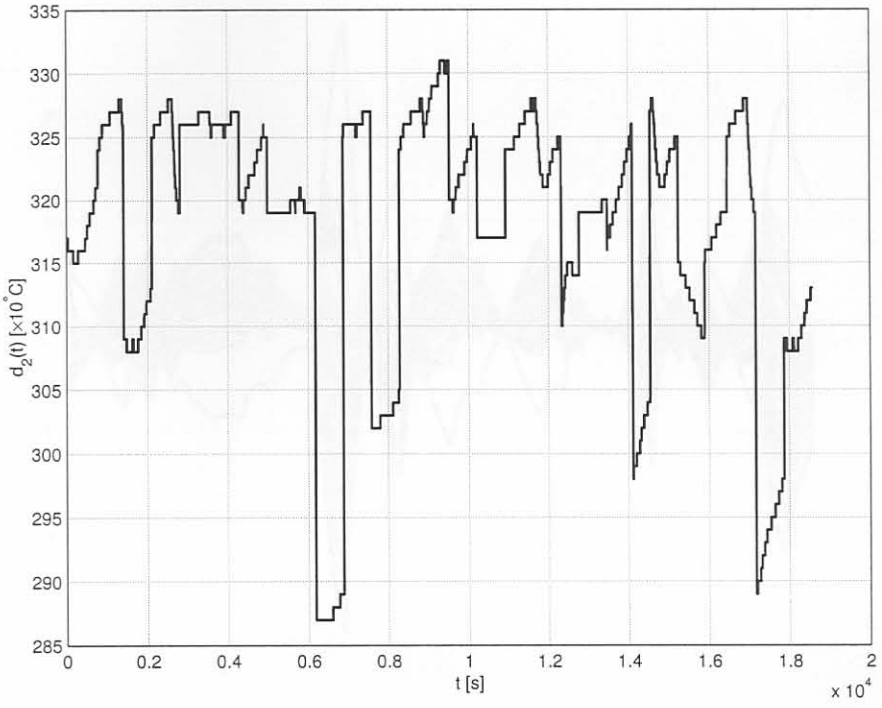

Figure 4.39 Water temperature disturbance for the simulation with WCC for 1060mm wide slabs.

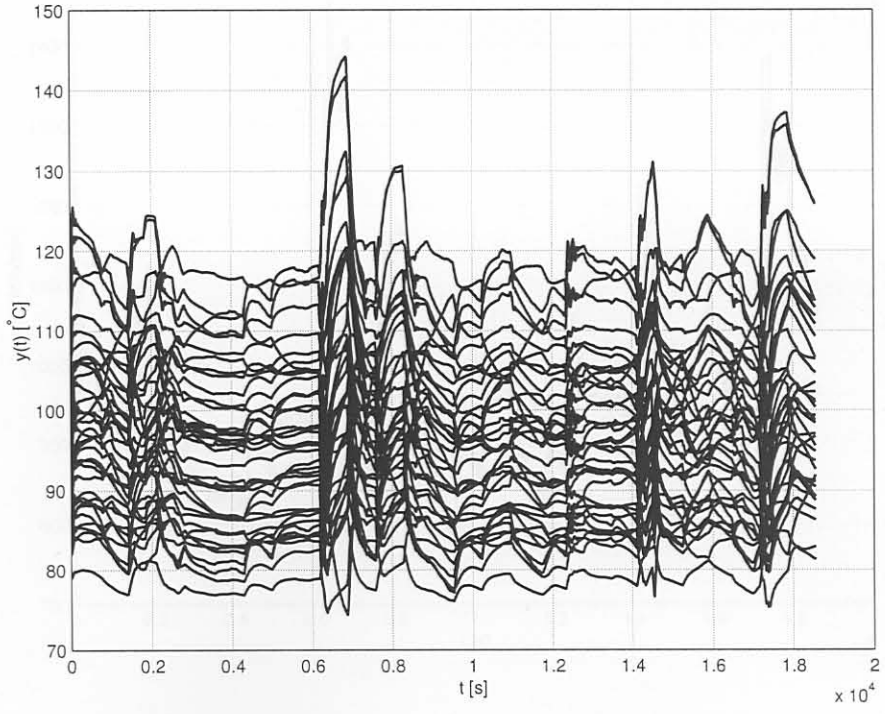

Figure 4.40 Outputs for 1060mm wide slabs and the worst-case control configuration.

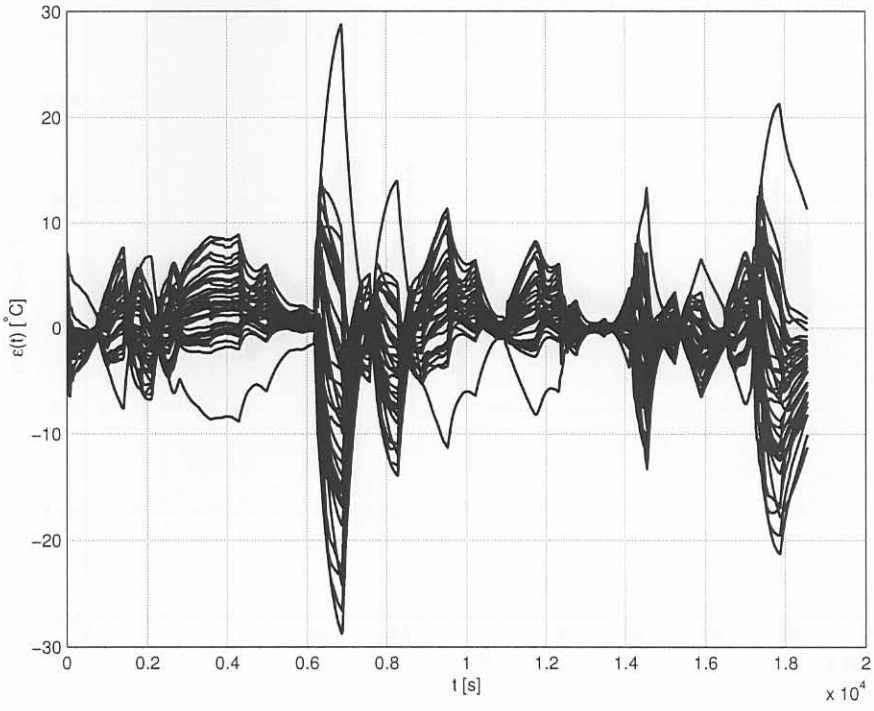

Figure 4.41 Errors for 1060mm wide slabs and the worst-case control configuration.

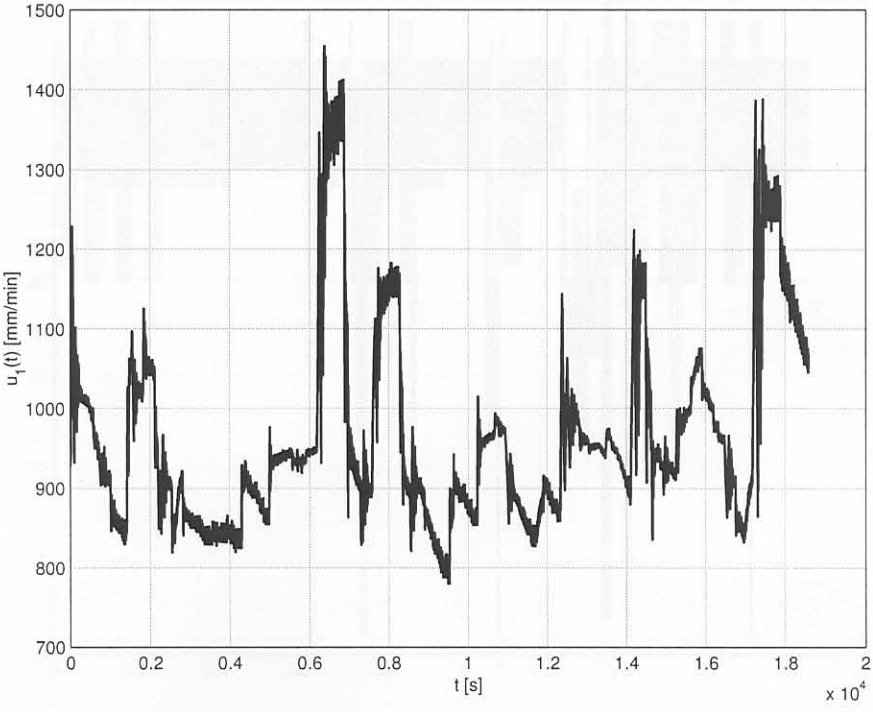

Figure 4.42 Control signal for 1060mm wide slabs and the worst-case control configuration.

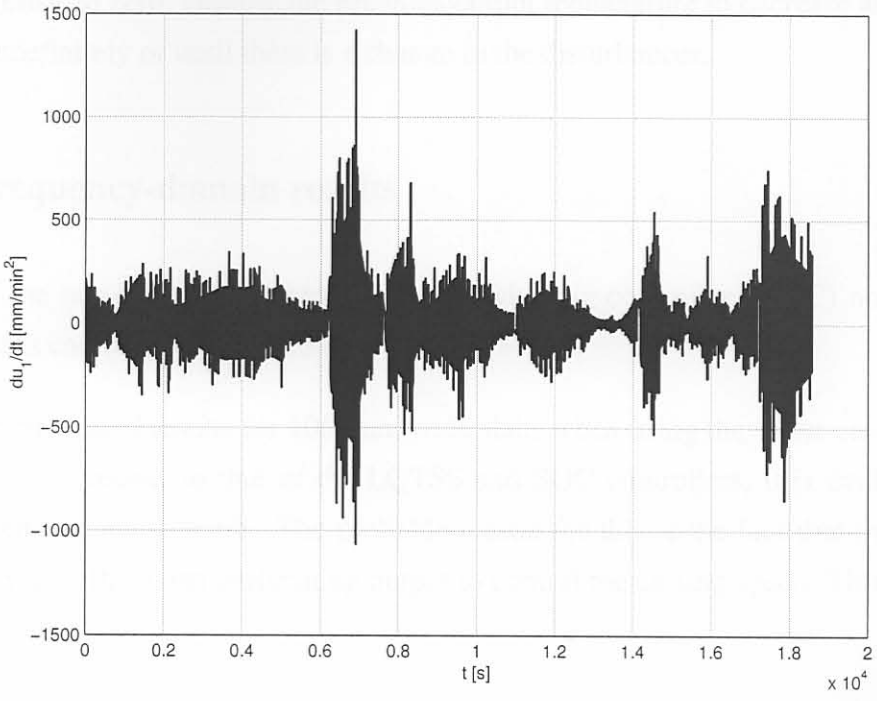

Figure 4.43 Acceleration of the slab 1060mm wide slabs and the worst-case control configuration.

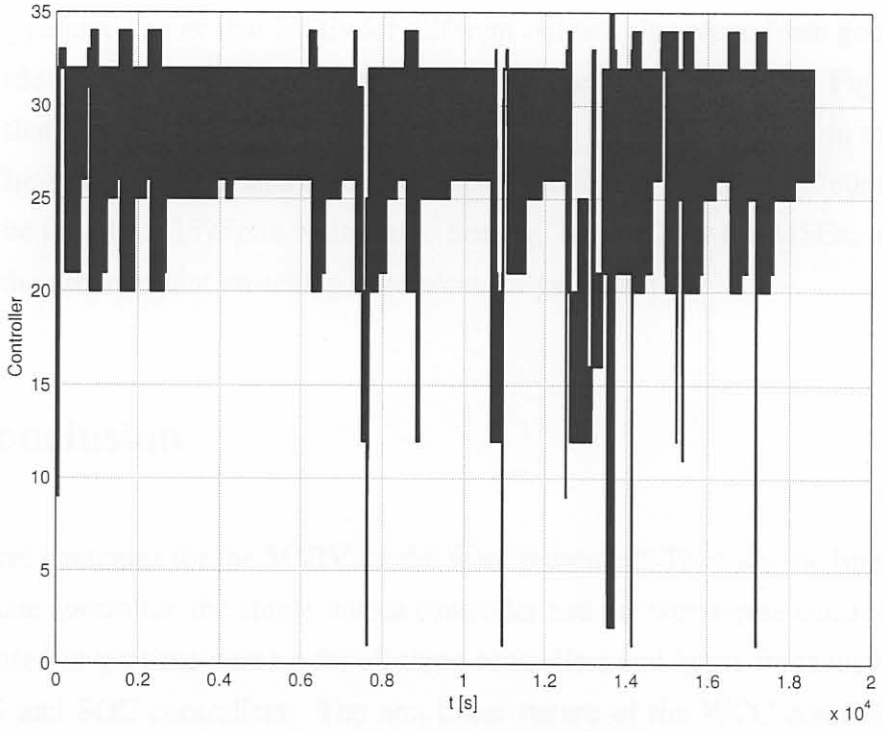

Figure 4.44 Output of the switching criterion of 1060mm wide slabs and the worst-case control configuration.

its positive error to zero, causing the previous output temperature to decrease and the cycle continues indefinitely or until there is a change in the disturbances.

4.3.3 Frequency-domain results

Because of the non-linear characteristic of the switching controller (WCC) no frequency-domain results can be given.

This section presented results for 1060mm wide slabs when using the worst-case controller. Comparing these results to that of the LQTSS and SOC controllers, it is evident that the WCC delivers the worst result. The probable reason for this is the fact that the controller continuously uses the worst performing output to control the casting speed. This means two things:

1. The active loop does not necessarily ensure the best control for all other loops.
2. The active loop is incapable to correct its output fast enough before it becomes inactive and switches to another loop.

Results in appendix J show that MSEs for different outputs also range from good to bad for 1280mm wide slabs (*e.g.* the in5u and nl2l loops in Table J.1 on page 287). Fig. J.6 on page 290 shows that alternation between control loops 8 and 19 is predominant in the switching criterion. The SMSMSE is in this case also worse than for LQTSS or SOC control. Similar results can be found for 1575mm wide slabs. See *e.g.* Table J.2 for the MSEs; and Fig. J.11 shows that the predominant switching is between loops 19 and 28.

4.4 Conclusion

Three control strategies for the MVIV model were presented. They are the linear quadratic at steady-state controller, the single output controller and the worst-case controller. Results were presented in the time-domain for all three controllers and in the frequency domain for the LQTSS and SOC controllers. The non-linear nature of the WCC controller does not permit a frequency-domain analysis of the controller.

Results in terms of the SMSMSE for each of the controllers with specific slab widths is presented in table 4.12. The table shows that the overall best controller is the LQTSS, with

improvements of 29.5%, 40.0% and 0.7% over the uncontrolled case for 1060, 1280 and 1575mm wide slabs respectively. The closest rival is the SOC controller with improvements of 22.5%, 38.9% and -2.2% for 1060, 1280 and 1575mm wide slabs respectively. This means that the LQTSS controller is 7%, 1.1% and 2.9% better than the SOC controller for the respective widths. The worst controller is the WCC with improvements of 13.4%, 31.3% and -5.7% for the respective widths.

The following conclusions can be drawn from table 4.12.

- Disturbances have a larger effect on the 1280mm wide slabs than 1060mm and 1575mm slabs. The SMSMSE for 1280mm wide slabs is much larger than that of 1060mm and 1575mm wide slabs in the uncontrolled case. This means that the operating conditions for 1280mm are further from the ideal than for the other two widths. The controllers can compensate for this incorrect operating condition of 1280mm wide slabs more effectively and thus the improvement is more dramatic.
- Traditionally, wider slabs have more surface defect problems than narrower slabs. This is evident from the few defects that occur on 1060mm wide slabs compared to 1280mm and 1575mm wide slabs. This means that narrower slabs are less sensitive to temperature changes.
- Less data were available for narrower slabs than for wider slabs, implying that defects occurred less frequently.
- There happened to be less defects on 1575mm slabs than on 1280mm wide slabs. This means that compensation is more dramatic for 1280mm wide slabs than for 1575mm wide slabs.
- Mould temperatures for wider slabs are more insensitive to casting speed changes. This is especially the case for 1575mm slabs where deterioration of the tracking per-

Table 4.12 Comparison of SMSMSE and improvements for each width and control method.

Width [mm]	No Control	LQTSS		SOC		WCC	
	SMSMSE	SMSMSE	Imp.	SMSMSE	Imp.	SMSMSE	Imp.
1060	5.1990	3.6632	29.5%	4.027	22.5%	4.5012	13.4%
1280	7.5198	4.5139	40.0%	4.597	38.9%	5.1681	31.3%
1575	5.5005	5.4614	0.7%	5.622	-2.2%	5.8138	-5.7%

formance has occurred for SOC and WCC. Limitations on casting speed and casting acceleration prohibits compensation for disturbances for the 1575mm slabs.

Chapter 5

Conclusion

THIS chapter presents a summary of the work, some conclusions, and recommendations for future work. A brief assessment of the work will be given, highlighting the main contributions. Future research that can follow from this work is considered.

5.1 Summary

Chapter 1 presented an introduction to the thesis. Some background on the process was given with a brief explanation of the continuous casting process and its merits over traditional ingot casting. The motivation for the research work was given, noting that direct rolling and hot charging are technologies that most steel-making companies strive for. These technologies can only be implemented once post-casting defect treatment in the form of grinding can be eliminated. The use of a predictor to determine when defects will occur is advantageous since slabs that do not have defects can be directly rolled or hot charged. Controlling the occurrence of defects can lead to all slabs being directly rolled or hot charged. The thesis focused on the application of the methods on a continuous casting plant in South Africa.

Chapter 2 gave an overview of the process and an account of the most useful literature for the thesis. The defects that were studied in this thesis were perused so that a thorough understanding of the variables which are instrumental in defect formation was obtained. Goodness-of-fit tests known as the Kolmogorov-Smirnov and Anderson-Darling tests were explained. These tests determine whether an empirical statistical distribution forms part of a given theoretical distribution. Correlation analysis was also explained and is used to test

cross-correlation between inputs. Time-series modelling in the form of ARX was explained, and is the modelling scheme used in this thesis. A linear quadratic tracker operating at steady-state was chosen as an adequate method for controlling the SIMO plant. The theory behind the LQTSS was given.

Chapter 3 dealt with modelling aspects. The data that was available from the level 2 system of the plant was described. The data was divided into three sections, namely mould data, defect data and auxiliary data. The mould data was used as inputs to the model and the defect data was used as the outputs. Defect data was gathered by the human measurement system. Each operator of the HMS marked a slab inspection report to indicate the position, type, severity and location of a specific defect when it occurred. This data was digitised and used to generate the output data. The auxiliary data aids in the extraction of data form the plant databases. The relation between position and time was reconciled by integrating the casting speed with respect to time. This was necessary because defect data has a position dimension and mould data has a time dimension. The statistical goodness-of-fit tests exploit the stationarity of the process to determine which mould variables significantly differ between slabs with- and slabs without defects. When the good and bad slabs were statistically different for a specific input variable based on mean and standard deviation, that variable was considered to be influential in the occurrence of a defect or could aid in the detection of a defect. These results were used in conjunction with correlation values between inputs to make sure that information in inputs are not repeated *i.e.* inputs are not cross-correlated. The result was that casting speed, mould level, inlet temperature and the thermocouple temperatures were influential in– or could detect– the occurrence of defects. Casting speed, thermocouple temperature and mould level were correlated with the thermocouple temperatures. Casting speed acted as a manipulated variable and mould level and inlet temperature acted as measured disturbances.

The fact that the temperatures were mostly rejected in the goodness-of-fit tests when defects occur implies that the model could be reduced to two models. The first is a MV to IV model and relates the effect of casting speed, mould level and inlet temperature to the thermocouple temperatures. The second is the IV to OV model and relates the thermocouple temperatures to the defects. This implies that the thermocouple temperatures can be used to detect the defects, and not that the thermocouple temperatures necessarily cause the defects. The models were trained using plant data. Both the MVIV and IVOV models gave good results in mimicking the plant data and this was emphasized by the testing with validation data. Comparison to published predictors could only be made for the longitudinal cracking defect, as results for other defects could not be found. For longitudinal cracks, sensitivity and

specificity are 2.1% and 18.5% respectively better than the published result of the artificial neural network of Hunter *et al.* [18]. A threshold was applied to the IVOV model to reduce the number of false alarms while still detecting the defects accurately. The IVOV model was then used to determine optimal set-points for the thermocouple temperatures such that no defects occur. This was done using an inversion of the IVOV model.

Chapter 4 presented control techniques to maintain the thermocouple temperature at the desired thermocouple temperature set-points. These methods were not implemented in practice but three controllers were implemented in simulation. The LQTSS controller was ideal to handle the SIMO system, since it has an averaging effect on the outputs and thereby reduces the average tracking error. The second controller was the single output controller which used one output for control. This output was selected after designing SISO control loops for each output and selecting the one which gave the best overall performance for the system. The third controller used bump-less transfer to control that output which is performing the worst at a specific point in time by switching to that loop in a bump-less fashion. This controller is known as the worst case controller. The LQTSS gave the best improvement in overall set-point tracking over all slab widths, with the SOC controller coming in second best. The WCC controller had the worst response.

5.2 Assessment of study

It was found that the model describing the effect of mould variables on the formation of surface defects can be broken down into two separate cascaded models. The first sub-model describes the effect of casting speed, mould level and water inlet temperature on the thermocouple temperatures (MVIV). The second sub-model describes the effect of thermocouple temperatures on the formation of defects (IVOV). The IVOV model is used as a predictor of defects and this implies that thermocouple temperatures can be used to infer the formation of defects. The MVIV model is used to control the formation of defects which result from mould temperature variation. The model separation is a significant contribution because it allows feedback control to be used. The delay between the formation and measurement of defects is moved outside the loop by using the (defect inferring) thermocouple temperatures as the output variables.

The ARX modelling technique was shown to be a valid approach for the MVIV and IVOV models. The ARX technique is simple and can be used for analysis and design using standard control system techniques. This is a significant reduction in modelling complexity over

techniques such as artificial neural networks and expert systems; and allows first principles to be worked into the model. The MVIV model output is influenced by disturbances, but follows the thermocouple temperatures well. The IVOV model is a good predictor of defects. The uncertainty in the accuracy of the HMS is overshadowed by good validation results for the IVOV model. Threshold values on the outputs of the IVOV model are used to indicate whether a specific defect will occur at a particular position and location. The MVIV and IVOV models were trained and validated on different sets of data to show the robustness of the models.

The IVOV model was also used to determine ideal thermocouple temperature distributions in the mould. Since the thermocouple temperatures infer defects, (constant) thermocouple temperatures must exist in a sub-space where no defects occur due to mould temperature variation. The calculation of these temperatures was done by determining the thermocouple temperatures that will not cause any defects.

The fourth contribution is that control can be used to reduce the variation in thermocouple temperatures. Three controllers were compared to illustrate the effectiveness of control. Though improvements of temperature variations over the uncontrolled case can be as high as 30%, the reduction of actual defects is difficult to estimate because the controllers could not be tested on a real plant.

The research publications that originate from this work have been given in §1.5.

The work deals with the application of the techniques on practical data. Therefore the models in this thesis cannot be presumed to work on any plant, but rather that the techniques can be applied by process engineers to determine models for their plant. Similarly, the optimal thermocouple temperatures that were found using the IVOV model also only account for the plant in question. They are optimal for this scenario only. The methods prove to work well, even when *e.g.* the IVOV model was only validated on data obtained three years after model training. Naturally, as is the case with any model, further tuning of the model will result in even better results.

Though many defects did arise, not all locations on the slabs necessarily had all the defects. This implies that the predictor cannot detect defects when the defects actually occur at locations where the predictor was not trained to look for defects. This can be overcome by training with more data.

5.3 Recommendations for future work

An improvement for this system is to eliminate the noise of the defect measurement system (HMS) used. Three people were used to gather defect data. Between them, inconsistent measurements already add a measure of noise to the system. One operator may have given a severity of 4 to a defect and thought it was casting powder entrapment while another person would have given a severity of 3 and said that the defect was some other inclusion. Another problem is that defects may have gone unnoticed, or may even have been disregarded. This leads to false results and is probably why some defects are predicted but not actually seen. The improvement would be remarkable if some unbiased measurement system such as a laser profilometer or electronic imaging system could have been used to measure the surface profile. Such systems are usually costly, and are in essence not used after casting but after rolling, because end-product is assumed to be more important than intermediate stages of the process. The use of electronic measurement of surface profile also means that data can be gathered for more slabs, thus having more data to work with. This could also improve the model response and the predictor accuracy. If an electronic measurement system is not available, studies can be undertaken to determine the accuracy of the HMS.

Several problems exist with the measurement of temperature in the mould, which fall outside the practical reach of the author. The thermocouples are usually fed from the backing plate, through the water chamber into the copper sheath. A small hole (3mm to 5mm in diameter) is drilled in the copper sheath and the thermocouple point is meant to intrude into that hole. The first problem is that the thermocouple does not necessarily enter into the hole. This causes no contact of copper and the thermocouple point so that a very high thermal resistance (air) is present. The second problem is that some thermocouples do enter the hole but are deformed (possibly from too much pressure during insertion) so that contact of the sides of some thermocouples are made to the side of the hole that was drilled. This results in a higher thermal conductance than other thermocouples. The third problem is that the rigorous motion of the mould can cause the thermocouple to get dislodged or break contact with the copper so that the thermal resistance is increased. Usually a high conductivity paste is used to decrease the thermal resistance between the copper and thermocouple point. This paste can also get dislodged so that the thermal resistance is increased. These problems can possibly be solved by using a spring-loaded system for each thermocouple, so that the thermocouple always makes contact with the copper.

The result of inadequate measurements is that the model is not necessarily an exact reflection of the plant, and that the control results are not as good as they could be. The IVOV

model does however predict the defects, because the variability of the measurement system is worked into the IVOV model due to the large amount of data that was used. The control systems do improve the tracking of the thermocouple set-points, though the MVIV model includes the dynamic effect of the thermocouples.

An increase in the number of thermocouples would also improve the accuracy of the predictor and controller. When few thermocouples are used, not all areas of the slabs are measured (see *e.g.* Fig. 2.2 and Fig. 3.2), implying that the mould is essentially under-sampled. Another problem is the spacing between thermocouples. Some defects which are localised such as casting powder entrapment, other inclusions and bleeders may move between two thermocouples, thus causing the predictor to "miss" the defects and not signal an alarm. Mahapatra *et al.* [160] report using 114 thermocouples arranged in as many as 17 rows along the length of the mould compared to the industrial partner who uses only 40 spaced in two rows 15 cm apart. (Hunter *et al.* [18] use 39 thermocouples in each wide face). Defects which form lower in the mould will probably not be detected.

Based on this work, the control of the temperature in the mould seems to be a fundamental problem. Note that the models derived in this thesis have two functions: firstly, to predict when defects will occur based on thermocouple measurements and secondly, to design controllers to control the thermocouple temperatures. Controlling the temperature will not necessarily ensure that a defect will be removed. This is especially true in the case of inclusions. An increase in the temperature of the surface may cause the inclusion to entrain back into the liquid pool, after which it may propagate back to the meniscus. The main problem with temperature control is the number of manipulated variables that are available. Usually only casting speed is a manipulated variable. In this thesis, 38 temperatures had to be controlled using only one manipulated variable which is fundamentally an uncontrollable system. Even when lumping the thermocouples into single values such as bottom and top rows, reducing the 38 intermediate variables to 19 and reducing thermocouple pairs with similar responses into groups of say, 3 to 4, leaves 5 intermediate variables. This still then remains a fundamentally uncontrollable system, because one manipulated variable is available and 5 intermediate variables have to be controlled.

A solution to the above problem is to redesign the mould so that water flow in the mould itself can be controlled in several chambers between the backing plate and copper face. The approach is similar to zone water flow-rate control in the secondary cooling zone [35]. Currently water is circulated at the maximum constant flow-rate possible. The addition of the water flow- rate control together with casting speed as manipulated variables allows differ-

ent sections of the mould to be cooled individually and as a whole, thus making temperature control more feasible. Care should be taken in this approach to ensure that the flow-rates for each chamber are adequate to extract enough heat so that solidification of the liquid pool can take place.

With the above comments taken into consideration, direct rolling and hot charging are technologies that will probably take a while before they can be fully implemented in a real continuous casting plant, without any post-casting inspection or treatment.

References

[1] H.F. Schrewe. *Continuous Casting of Steel—Fundamental Principles and Practices.* Verlag Stahleisen, Düsseldorf, english edition, 1987. Translated by Paul Knighton.

[2] H.-F. Marten. New approaches in plant technology to increase quality and productivity. *Metallurgical Plant and Technology*, 9(5):39–55, 1986.

[3] H. Wiesinger, G. Holleis, K. Schwaha, and F. Hirschmanner. Design of CC machines for hot charging and direct rolling. In T.B. Harabuchi and R.D. Pehlke, editors, *Continuous casting*, volume Four, Design and Operations, pages 227–255. The Iron and Steel Society, Warrendale, 1988.

[4] G. Holleis, H. Bumberger, T. Fastner, F. Hirschmanner, and K. Schwaha. Prerequisites for production of continuously cast semis for direct rolling and hot charging. In *Continuous Casting '85*, pages 46.1–46.7, London, 1985.

[5] F. Hollander and S.P.A. Zuurbier. Accurate temperature control of the reheating process at mixed cold and hot charging. In *Scanheating: Proceedings of the International Conference on Process Control and Energy Savings in Reheating Furnaces, June 12-14, Luleå, Sweden*, pages 6.1–6.36, 1985.

[6] J.A. Doherty. Linking continuous casting and rolling. In T.B. Harabuchi and R.D. Pehlke, editors, *Continuous casting*, volume Four, Design and Operations, pages 209–211. The Iron and Steel Society, Warrendale, 1988.

[7] V.V. Orobtsev, R.O. Perel'man, and A.D. Belyanskii. Problems with organizing the hot-charging of continuous-cast slabs. *Metallurg*, 32(11-12):37–38, November 1988. Translation.

[8] D. Kothe, F.-P. Pleschiutschnigg, and F. Boehl. Slab and strip casting technology. *Steel Times International*, 14(2):36,38, March 1990.

[9] N.L. Samways. LTV Steel's new direct hot charge complex and continuous anneal line at Cleveland. *Iron and Steel Engineer*, 71(9):CI–111–CI–122, 1994.

[10] N. Moritama, O. Tsubakihara, M. Okimori, E. Ikezaki, and K. Isogami. Techniques for producing defect-free slabs at high enough temperatures for direct rolling. *Iron and Steelmaker*, 14(8):22–28, August 1987.

[11] K.H. Klein, G. Paul, and V. Koster. Substantial energy-saving measures at continuous casting facility in West Germany. *Industrial Heating*, 53(11):24–29, November 1986.

[12] H. Preißl, J. Weiß, Norbert Hübner, J. Spiess, and F. Milani. Process optimization for maximum availability in continuous casting. *Metallurgical Plant and Technology International*, 17(5):52–58, 1994.

[13] T. Fastner, H. Preißl, N. Hübner, H.-P. Narzt, J. Vlcek, and W. Marschal. Automatisierte Qualitätssteuerung beim Stranggießen von Brammen für den Heißeinsatz. *Stahl und Eisen*, 114(11):57–62, 1994.

[14] G. Steinbauer and W. Siefer. Informationstechniken zur Gußfehlerdiagnose und ihre Einfügung in die EDV-gestützte Betriebskontrole. *Giessereiforschung*, 40(3):81–94, 1988.

[15] R.C. Creese, M. Jaraiedi, and S. Waibogha. A quality control system for casting defects. In *40th Annual Quality Control Proceedings, 19–21 May, Anaheim, USA*, pages 89–95. American Society for Quality Control, 1986.

[16] N.L. Samways. Continuous casting at Sparrows Point: A success story. *Iron and Steel Engineer*, 64(10):17–25, October 1987.

[17] K. Hatanaka, T. Tanaka, and H. Kominami. Breakout forecasting system based on multiple neural networks for continuous casting in steel production. *Fujitsu Scientific and Technical Journal*, 29(3):265–270, September 1993.

[18] N.S. Hunter, A.S. Normanton, D. Scoones, A. Spaccarotella, M. Milone, F. Vicino, J.Y. Lamant, H. Morand, and P. Do Thong. The influence of mould metallurgy on surface defects in peritectic carbon and austenitic stainless steels. *La Revue de Métallurgie-CIT*, 96(4):473–482, April 1999.

[19] K. Matsuzuka, N. Fujita, T. Yabuta, and H. Itoh. Advanced direct rolling operation realized by a schedule-free rolling technology at Yawata Works. *La Revue de Métallurgie-CIT*, 86(5):413–422, May 1989.

[20] I.K. Craig, F.R. Camisani-Calzolari, and P.C. Pistorius. A contemplative stance on the automation of continuous casting in steel processing. *Control Engineering Practice*, 9(9):1013–1020, 2001. Suggested from [28].

[21] F.R. Camisani-Calzolari, I.K. Craig, and P.C. Pistorius. Quality prediction in the continuous casting of stainless steel slabs using time-series methods. *ISIJ International*, 2003. Submitted.

[22] F.R. Camisani-Calzolari, I.K. Craig, and P.C. Pistorius. Mould temperature control in continuous casting for the reduction of surface defects. *ISIJ International*, 2003. Submitted.

[23] F.R. Camisani-Calzolari, I.K. Craig, and P.C. Pistorius. Quality prediction in continuous casting of stainless steel slabs. *Journal of the South African Institute of Mining and Metallurgy*, 2003. Submitted, suggested from [29].

[24] F.R. Camisani-Calzolari, I.K. Craig, and P.C. Pistorius. A proposed control system/CAQC methodology and prediction system for the improvement of surface defects in the continuous casting of slabs. In *Preprints of the IFAC Workshop on Future Trends in Automation in Mineral and Metal Processing, Finland, 22–24 August*, pages 402–406, 2000.

[25] F.R. Camisani-Calzolari, I.K. Craig, and P.C. Pistorius. A prediction system based on system identification techniques for the eradication of surface defects in the continuous casting of slabs. In *Proceedings of the 3rd International Conference on Control Theory and Applications, Pretoria, South Africa, 12–14 December*, pages 162–166. IEEE, 2001.

[26] F.R. Camisani-Calzolari, I.K. Craig, and P.C. Pistorius. Control structure for the reduction of defects in continuous casting. In *Proceedings of the 15th IFAC World Congress, Barcelona, Spain, 21-26 July*, volume O, pages 149–154, 2002.

[27] F.R. Camisani-Calzolari, I.K. Craig, and P.C. Pistorius. Defect and mould variable prediction in continuous casting. In *31st International Symposium on Computer Applications in the Minerals Industries (APCOM 2003), Cape Town, South Africa, 14-16 May*, 2003. Accepted.

[28] I.K. Craig, F.R. Camisani-Calzolari, and P.C. Pistorius. A contemplative stance on the automation of continuous casting in steel processing. In *Preprints of the IFAC Workshop on Future Trends in Automation in Mineral and Metal Processing, Finland, 22–24 August*, pages 80–85, 2000.

[29] F.R. Camisani-Calzolari, I.K. Craig, and P.C. Pistorius. Quality prediction in continuous casting of stainless steel slabs. In *Colloquium on the state of the art of automation and control in the minerals and metals processing industries, Johannesburg, South Africa, 18 March*, pages 1–17. SAIMM, 2003. Paper 1, Session 2.

[30] F.R. Camisani-Calzolari, I.K. Craig, and P.C. Pistorius. An overview of surface defects in continuous casting. In *IFAC Workshop on New Technologies for Automation of Metallurgical Industry, Shanghai, China, 11-13 October*, 2003. Accepted.

[31] G.E.P. Box, G.M. Jenkins, and G.C. Reinsel. *Time series analysis–forecasting and control*. Prentice Hall, Englewood Cliffs, 1994.

[32] R.L. Hill and J.H. Wilson. Reliable liquid steel flow control contributes to productivity, cast slab quality and machine availablity at US Steel Gary Works. In *Continuous Casting '85*, pages 52.1–52.7, London, 1985.

[33] G. Harry. *Mold Powders for Continuous Casting and Bottom Pour Teeming*. Iron and Steel Society, Warrendale, 1987.

[34] J.M. Burgess, H.M. Guzman, and Y.P. Singh. Mold oscillator mechanisms for continuous casters, synthesis and computerized design. In *Proceedings of the 1989 ASME International Computers in Engineering Conference and Exposition, 3 August–30 July, Anaheim, USA*, volume 1, pages 257–264, 1989.

[35] F.R. Camisani-Calzolari. Modelling and control of the secondary cooling zone in continuous casting. Master's thesis, University of Pretoria, 1998.

[36] K. Brückner. New technologies and facilities for continuous casting and rolling of steel. *Metallurgical Plant and Technology*, 11(6):34–44, 1988.

[37] J.-P. Birat, M. Larrecq, J.-Y. Lamant, and J. Pétégnief. The continuous casting mold: a basic tool for surface quality and strand productivity. In *Steelmaking Conference Proceedings, Warrendale, USA*, pages 39–50, 1991.

[38] R. De Keyser. Predictive mould level control in a continuous steel casting line. In *Proceedings of the 13th IFAC Triennial World Congress, 30 June–5 July, San Francisco, USA*, pages 487–492, 1996.

[39] R.M.C. De Keyser. Improved mould level control in a continuous steel casting line. In *Proceedings of the Conference of Automation in Mining, Metallurgy and Minerals Processing, 25-31 August, Sun City, South Africa*, pages 127–132. IFAC, 1995.

[40] M. Inkinen, P. Lautala, and E. Saarelainen. Fuzzy-guided mould level control in continuous steel casting. In *Proceedings of the Conference of Automation in Mining, Metallurgy and Minerals Processing, 25-31 August, Sun City, South Africa*, pages 133–138. IFAC, 1995.

[41] F. Kong and R. De Keyser. Identification and control of the mould level in a continuous casting machine. In *Proceedings of the Second IEEE Conference on Control Applications, 13-16 September*, pages 53–58, 1993.

[42] S.F. Graebe, G.C. Goodwin, and G. Elsley. Control design and implementation in continuous steel casting. *IEEE Control Systems Magazine*, pages 64–71, August 1995.

[43] M.S. Jenkins, B.G. Thomas, W.C. Chen, and R.B. Mahapatra. Investigation of strand surface defects using mold instrumentation and modelling. In *Steelmaking Conference Proceedings, Warrendale, USA*, pages 337–345, 1994.

[44] P. Nilles and C. Marique. Secondary steelmaking, a must for meeting steel consumers' demands. *Metallurgical Plant and Technology*, 12(5):72–88, 1989.

[45] P.-O. Mellberg. Automatic metal level and slag transfer control in continuous casting. In *Continuous Casting '85*, pages 55.1–55.6, London, 1985.

[46] T. Hesketh, D.J. Clements, and R. Williams. Adaptive mould level control for continuous casting slabs. *Automatica*, 29(4):851–864, 1993.

[47] M. Hattori, S. Nagata, A. Inaba, S. Ishitobi, T. Yamamoto, T. Okada, and M. Zeze. Development of technology to eliminate centerline segregation in continuously cast slabs. *Iron and Steelmaker*, 16(6):34–39, June 1989.

[48] P. Andrzejewski, K.-U. Köhler, and W. Pluschkell. Model investigations on the fluid flow in continuous casting moulds of wide dimensions. *Steel Research*, 63(6):242–246, 1992.

[49] T.J. Manayathara, T-C Tsao, J. Bentsman, and D. Ross. Rejection of unknown periodic load disturbances in continuous steel casting process using learning repetitive control approach. *IEEE Transactions on Control Systems Technology*, 4(3):259–265, May 1996.

[50] J.K. Brimacombe and I.V. Samarasekera. Fundamental analysis of the continuous casting process for quality improvements. In *Indo-U.S. Workshop on Materials Processing*, pages 179–222, 1988.

[51] M. Gagné and E. Thibault. Behaviour of inclusions during rolling of continuously cast billets. *CIM Bulletin*, 91(1021):98–103, June 1998.

[52] Y. Nuri, K. Umezawa, F. Nomura, and M. Nishida. Idenitifcation of Alumina-clusters and exogeneous inclusions from mold powder in CC slabs. *Transactions ISIJ*, 26(11): 955–962, 1986.

[53] J.K. Brimacombe and K. Sorimachi. Crack formation in the continuous casting of steel. *Metallurgical Transactions B*, 8:489–505, 1977.

[54] J.K. Brimacombe, E.B. Hawbolt, and F. Weinberg. Formation of off-corner internal cracks in continuously-cast billets. *Canadian Metallurgical Quarterly*, 19:215–227, 1980.

[55] J.K. Brimacombe, F. Weinberg, and E.B. Hawbolt. Formation of longitudinal, midface cracks in continuously-cast slabs. *Metallurgical Transactions B*, 10:279–292, 1979.

[56] M. El-Bealy. On the mechanism of halfwaycracks and macro-segregation in continuously cast steel slabs— (i). halfway cracks. *Scandinavian Journal of Metallurgy*, 24 (3):63–80, 1995.

[57] J.K. Brimacombe. Design of continuous casting machines based on a heat-flow analysis: State-of-the-art review. *Canadian Metallurgical Quarterly*, 15(2):163–175, 1976.

[58] M. El-Bealy. On the mechanism of halfwaycracks and macro-segregation in continuously cast steel slabs— (ii). macrosegregation. *Scandinavian Journal of Metallurgy*, 24(3):106–120, 1995.

[59] R.L. Newton, F.J. Leese, G. Maw, T. McHugh, J. Morris, G.K. Knotman, D. Vincent, and J.M. Young. *Definitions and Causes of Continuous Casting Defects*. The Iron and Steel Institute, Percy Lund, Humphreys and Co, London, 1967. Prepared by the Nomenclature of Continuous Casting Defects Group of the Steelmaking Division, British Iron and Steel Research Association.

[60] B. Mintz, S. Yue, and J.J. Jones. Hot ductility of steels and its relationship to the problem of transverse cracking during continuous casting. *International Materials Reviews*, 36(5):187–217, 1991.

[61] T.J.H. Billany, A.S. Normanton, K.C. Mills, and P. Grieveson. Surface cracking in continuously cast products. *Ironmaking and Steelmaking*, 18(6):403–410, 1991.

[62] K. Yasumoto, Y. Maehara, T. Nagamichi, and H. Tomono. Effect of thermo-mechanical history on surface cracking of As-cast low carbon low alloy steel slabs. *ISIJ International*, 29(11):933–939, 1989.

[63] A. Diener, A. Drastik, B. Redenz, and K. Wagner. Investigation of straightening process in circular-arc type slab caster and resulting stresses and strains in strand. In *Continuous Casting '85*, pages 69.1–69.6, London, 1985.

[64] K. Harste and K.-H. Tacke. Slab caster design criteria for high quality steel. In *Ironmaking conference proceedings, April, Chicago, USA*, pages 743–752, 1997.

[65] E.S. Szekeres. Overview of mold oscillation in continuous casting. *Iron and Steel Engineer*, 73(7):29–37, July 1996.

[66] E. Takeuchi and J.K. Brimacombe. Effect of oscillation mark formation on the surface quality of continuously cast steel slabs. *Metallurgical Transactions B*, 16B(3):605–625, September 1985.

[67] M.M. Wolf. Mold oscillation guidelines. In *Steelmaking Conference Proceedings, Washington, USA*, pages 51–71, 1991.

[68] J.L. Muller. Détection des défauts de surface sur les demi-produits chauds par courants de Foucault. *Revue de Métallurgie-CIT*, 84(6):483–486, June 1987.

[69] H. Hiebler. *Gmelin-Durrer, Metallurgy of Iron*, volume 11a, Practice of Steelmaking 5: Continuous casting. Springer-Verlag, Berlin, 1992.

[70] R.J. Gray, A. Perkins, and B. Walker. Quality of continuously cast slabs. In *Solidification and Casting of Metals, Proceedings of an International Conference on Solidification, 18-21 July*, pages 300–305. The Metals Society, 1977.

[71] W.H. Emling. Breakout prevention. *Iron and Steelmaker*, 21(7):47–48, July 1994.

[72] B. Mintz. The influence of composition on the hot ductility of steels and to the problem of transverse cracking. *ISIJ International*, 39(9):833–855, 1999.

[73] M.H. Burden, G.D. Funnell, A.G. Whitaker, and J.M. Young. Origins of defects in continuously cast blooms produced on a curved mould machine. In *Solidification and Casting of Metals, Proceedings of an International Conference on Solidification, 18-21 July*, pages 279–286. The Metals Society, 1977.

[74] K.D. Unger, W. Biesterfeld, F. Berentzen, and R. Thielmann. Metallurgical problems encountered in stainless steel continuous casting. In *Continuous Casting '85*, pages 61.1–61.7, London, 1985.

[75] S.D. Razumov, V.V. Zabil'skii, V.I. Umanets, V.I. Lebedev, and V.A. Obukhov. Influence of chemical composition of steel on quality of continuously cast billet. *Steel in the USSR*, 16(5):225–228, May 1986.

[76] T. Saito, M. Kimura, H. Ueta, T. Kimura, K. Takemoto, and T. Mine. Prevention of surface crack formation in continuous cast slab. *Kobelco Technology Review*, (11): 54–57, June 1991.

[77] J. Leclerc and W. Pollak. Continuous cast slab defects related to final product quality and associated operating precautions. In *Continuous casting of steel. Proceedings of an international conference*, pages 125–134. The Metals Society, 1977.

[78] N.S. Hunter, J.D. Madill, D.J. Scoones, P.N. Hewitt, and D. Stewart. Progress in mould thermal monitoring. *Steel Technology International*, pages 171–174, 1996.

[79] D.E. Humphreys, J.D. Madill, V. Ludlow, D. Stewart, S.G. Thornton, and A.S. Normanton. Application of mould thermal monitoring in the study of slab surface quality for heavy plate grades at Scunthorpe works, British Steel. In *1st European Conference on Continuous Casting, September, Florence, Italy*, pages 1.529–1.540, September 1991.

[80] K. Nakajima, S. Hiraki, M. Kawamoto, and T. Kanazawa. Influence of mold heat flux on longitudinal surface cracks during high-speed continuous casting of steel slab. *The Sumitomo Search*, (55):32–39, May 1994.

[81] S.L. Kang, I. J. Lee, S.D. Shin, S.M. Yang, H.B. Lee, J. Choi, and I.R. Lee. Optimization of casting conditions by the measurement of mold wall temperature at Pohang Works. In *77th Steelmaking Conference Proceedings, Warrendale*, volume 77, pages 347–356, 1994.

[82] K.-H. Kim, T.-J. Yeo, K.H. Oh, and D.N. Lee. Effect of carbon and sulfur in continuously cast strand on longitudinal surface cracks. *ISIJ International*, 36(3):284–289, 1996.

[83] B.P. Moiseev, V.S. Esaulov, V.A. Nikolaev, V.V. Emel'yanov, and N.I. Gubin. Nature of longitudinal surface cracks in continuously cast slabs. *Steel in the USSR*, 16(12): 590–593, December 1986.

[84] R.A. Heard and A. McLean. Quality of hcc products. In R.A. Heard and A. McLean, editors, *Continuous casting*, volume Five, Horizontal Continuous Casting, chapter 3, pages 87–95. The Iron and Steel Society, 1988.

[85] T.W. Clyne and G.J. Davies. Comparison between experimental data and theoretical predictions relating to dependence of solidification cracking on composition. In *Solidification and Casting of Metals, Proceedings of an International Conference on Solidification, 18-21 July*, pages 275–278. The Metals Society, 1977.

[86] Ya.N. Malinochka, L.A. Moiseeva, T.V. Esaulova, V.S. Esaulov, and Yu.S. Shmelev. Some defects in continuously cast slabs and improving steel quality. *Steel in the USSR*, 17(10):448–451, October 1987.

[87] M. Kawamoto, Y. Tsukaguchi, N. Nishida, T. Kanazawa, and S. Hiraki. Improvement of the initial stage of solidification by using mild cooling mold powder. *ISIJ International*, 37(2):134–139, 1997.

[88] W.R. Irving and A. Perkins. Basic parameters affecting the quality of continuously cast slabs. In *Continuous casting of steel. Proceedings of an international conference, Biarritz, France 31 May–2 June*, pages 107–115. The Metals Society, 1977.

[89] N.A. McPherson and S.L. McIntosh. Mold powder related defects in some continuously cast steel products. *Iron and Steelmaker*, 14(6):19–25, June 1987.

[90] A.W. Cramb and I. Jimbo. Interfacial considerations in continuous casting. *Iron and Steelmaker*, 16(6):43–55, June 1989.

[91] R.B. Mahapatra, J.K. Brimacombe, and I.V. Smarasekera. Mold behaviour and its influence on quality in the continuous casting of steel slabs: Part 2. mold heat transfer, mold flux behavior, formation of oscillation marks, longitudinal off-corner depressions, and subsurface cracks. *Metallurgical Transactions B*, 22B(6):875–888, December 1991.

[92] K.C. Mills, P. Grieveson, A. Olusanya, and S. Bagha. Effect of casting powder on heat transfer in continuous casting. In *Continuous Casting '85*, pages 57.1–57.7, London, 1985.

[93] K.C. Mills. The performance of casting powders and their effect on surface quality. In *Steelmaking Conference Proceedings, Washington, USA*, pages 121–129, 1991.

[94] R.W. Soares, M.V.A. Fonseca, R. Neuman, V.J. Menezes, A.O. Lavinas, and J. Dweck. An application of differential thermal analysis to determine the change

in thermal properties of mold powders used in continuous casting of steel slabs. *Thermochimica Acta*, 318(1-2):131–136, 1998.

[95] J. Savage and W.H. Pritchard. The problem of rupture of the billet in the continuous casting of steel. *Journal of the Iron and Steel Institute*, 178:269–277, November 1954.

[96] K.E. Blazek and I.G. Saucedo. Characterization of the formation, propagation, and recovery of sticker/hanger type breakouts. *ISIJ International*, 30(6):435–443, 1990.

[97] K.C. Mills, T.J.H. Billany, A.S. Normanton, B. Walker, and P. Grieveson. Causes of sticker breakout during continuous casting. *Ironmaking and Steelmaking*, 18(4): 253–265, 1991.

[98] K.E. Blazek and I.G. Saucedo. Recovery of sticker-type breakouts. *Iron and Steelmaker*, pages 28–36, November 1989.

[99] S. Kumar, B.N. Walker, I.V. Samarasekera, and J.K. Brimacombe. Chaos at the meniscus - the genesis of defects in continuously cast steel billets. In *13th PTD Conference Proceedings, Nashville, USA*, pages 119–141, 1995.

[100] M. Bobadilla, J.M. Jolivet, J.Y. Lamant, and M. Larrecq. Continuous casting of steel: a close connection between solidification studies and industrial process development. *Materials Science and Engineering A*, A173(1-2):275–285, 1993.

[101] J.L. Brendzy, I.A. Bakshi, I.V. Samarasekera, and J.K. Brimacombe. Mould–strand interaction in continuous casting of steel billets part II lubrication and oscillation mark formation. *Ironmaking and Steelmaking*, 20(1):63–75, 1993.

[102] M. Suzuki, H. Mizukami, T. Kitagawa, K. Kawakami, S. Uchida, and Y. Komatsu. Development of a new mold oscillation mode for high speed continuous casting of steel slabs. *ISIJ International*, 31(3):254–261, 1991.

[103] B. Lindorfer, H. Hödl, and K. Mörwald. Technological packages for high performance slab casting. *MPT International*, 22(1):66–68, 1998.

[104] R.B. Mahapatra, J.K. Brimacombe, and I.V. Samarasekera. The influence of mould design and operation on oscillation-mark formation, heat transfer and quality in the continuous casting of steel slabs. *La metallurgia italiana*, 83(12):1105–1112, 1991.

[105] M.J. Hague and D. Parlington. Diagnostic aids for quality improvement and maintenance in continuous casters. *Iron and Steel Engineer*, 65(5):36–42, May 1988.

[106] AEC. Glossary of terms. Web site, 2003. Aluminium Extruders Council, http://www.aec.org/resources/cyber_gloss7.html, last visited on 30 January 2003.

[107] S. Chandra, J.K. Brimacombe, and I.V. Samarasekera. Mould-strand interaction in continuous casting of steel billets. part 3 mould heat transfer and taper. *Ironmaking and Steelmaking*, 20(2):104–112, 1993.

[108] A. Spaccarotella, R. Moretti, G. Di Schino, and G. Provantini. Influence of mould oscillation and powder lubrication on surface quality of austenitic stainless steel slabs at Terni Works. In *Continuous Casting '85*, pages 42.1–42.11, London, 1985.

[109] M.M. Wolf. Mold length in slab casting – a review. *Iron and Steelmaker*, 23(2):47–51, February 1996.

[110] M. Wolf. Strand surface quality of austenitic stainless steels: Part 1 macroscopic shell growth and ferrite distribution. *Ironmaking and Steelmaking*, 13(5):248–257, 1986.

[111] M. Wolf. Strand surface quality of austenitic stainless steels: Part 2 microscopic solidification structure. *Ironmaking and Steelmaking*, 13(5):258–262, 1986.

[112] M.R. Ozgu. Continuous caster instrumentation: state-of-the-art review. *Canadian Metallurgical Quarterly*, 35(3):199–223, 1996.

[113] M.I. Chipalo, M.D. Gilchrist, and R.A. Smith. A finite element technique for the investigation of the shape development of planar cracks with initially irregular profiles. *International Journal of Mechanical Sciences*, 32(3):243–251, 1990.

[114] M.D. Gilchrist and R.A. Smith. Finite element modelling of fatigue crack shapes. *Fatigue and Fracture of Engineering Materials & Structures*, 14(6):617–626, 1991.

[115] H. Kametani. Fractal analysis of the surface cracks on continuously cast steel slabs. *Metallurgical and Materials Transactions B*, 29B(6):1261–1267, December 1998.

[116] M. De Santis and A. Ferretti. Thermo-fluid-dynamics modelling of the solidification process and behaviour of non-metallic inclusions in the continuous casting slabs. *ISIJ International*, 36(6):673–680, 1996.

[117] D. Bouris and G. Bergeles. Investigation of inclusion re-entainment from the steel-slag interface. *Metallurgical and Materials Transactions B*, 29B(3):641–649, 1998.

[118] I. Sawada, E. Takeuchi, H. Tanaka, K. Okazawa, and K. Shigematsu. Development and application of simulator for analyzing molten steel flow and inclusion behavior in continuous casters. Technical Report 67, Nippon Steel, October 1995. pp.7–12.

[119] W. Yamada, S. Fukumoto, H. Tanaka, T. Matsumiya, and M. Wajima. Development and application of computer simulation techniques for analyzing composition, particle size distribution, and amount of nonmetallic inclusions in steel. Technical Report 67, Nippon Steel, October 1995. pp. 21–28.

[120] R.M. McDavid and B.G. Thomas. Flow and thermal behavior of the top surface flux/powder layers in continuous casting molds. *Metallurgical and Materials Transactions B*, 27B(4):672–685, August 1996.

[121] C. Bailey, P. Chow, M. Cross, Y. Fryer, and K. Pericleous. Multiphysics modelling of the metals casting process. *Proceedings of the Royal Society of London. Series A, Mathematical and Physical Sciences*, 452:459–486, 1996.

[122] B.R. Henriksen, E.K. Jensen, and D. Mortensen. Interpretation of measured temperatures and the bleed out phenomenon of billet casting applying the mathematical model alsim. In *Light Metals 1999*, pages 721–727. The Minerals, Metals and Materials Society, 1999.

[123] J.R. King, A.A. Lacey, C.P. Please, P. Willmott, and A. Zoryk. The formation of oscillation marks on continuously cast steel. *Mathematical Engineering in Industry*, 4(2):91–106, 1993.

[124] H. Sha, R. Diedrichs, and K. Schwerdtfeger. Dynamic behavior of a liquid/liquid interface at an oscillating wall. *Metallurgical and Materials Transactions B*, 27B(2): 305–314, April 1996.

[125] B.G. Thomas, A. Moitra, and H. Zhu. Coupled thermo-mechanical model of solidifying steel shell applied to depression defects in continuous-cast slabs. In M. Cross and J. Campbell, editors, *Modelling of Casting, Welding and Advanced Solidification Processes VII, September, London*, pages 241–248, 1995.

[126] B.G. Thomas, A. Moitra, and R. McDavid. Simulation of longitudinal off-corner depressions in continuously cast steel slabs. *Iron and Steelmaker*, pages 57–70, April 1996.

[127] B.G. Thomas, D. Lui, and B. Ho. Effect of transverse depressions and oscillation marks on heat transfer in the continuous casting mold. In *Proceedings of a Symposium on the Application of Sensors and Modeling to Materials Processing, 9–13 February, Orlando, USA*, pages 117–142, 1997.

[128] P. Gugliermina, Y. Codur, and J.M. Cardouat. Tapping good steel on time. *Ironmaking and Steelmaking*, 14(2):79–83, 1987.

[129] W. R. Irving. On line quality control for continuously cast semis. *Ironmaking and Steelmaking*, 17(3):197–202, 1990.

[130] M.W. Short, B. Barber, A.S. Normanton, B. Patrick, and R.A. York. Temperature prediction and control during continuous casting. In *Ironmaking Conference Proceedings, 13–16 April, Chicago, USA*, pages 655–659, 1997.

[131] S.E. Royzman. Coefficient of friction between strand and mould during continuous casting: mathematical model. *Ironmaking and Steelmaking*, 24(6):484–488, 1997.

[132] R.J. O'Malley. Observations of various steady state and dynamic thermal behaviors in a continuous casting mold. In *Steelmaking Conference Proceedings, 26-29 March, Pittsburgh, USA*, pages 13–32, 1999.

[133] T. Matsumiya, T. Ohashi, and Y. Abe. Mathematical analysis on thermal and unbending deformation of continuously cast slabs. In *Modeling and Control of Casting and Welding Processes, 12-17 January, Santa Barbara, USA*, pages 523–538. AIME, 1986.

[134] B.Q. Li and Y. Ruan. Integrated finite element model for transient fluid flow and thermal stresses during continuous casting. *Journal of Thermal Stresses*, 18:359–381, 1995.

[135] J.Y. Lamant, M. Larrecq, J.P. Birat, J.L. Hensgen, J.D. Weber, and J.C. Dhuyvetter. Study of slab bulging in continuous caster. In *Continuous Casting '85*, pages 37.1–37.8, London, 1985.

[136] K. Harste, M. Deisinger, I. Steinert, and K. Tacke. Thermische und mechanische Modelle zum Stranggießen. *Stahl und Eisen*, 115(4):111–118, 1995.

[137] S.K. Das and A. Sarkar. Computational modelling of thermal transport phenomena in continuous casting process based on non-orthogonal control volume approach. *Communications in Numerical Methods in Engineering*, 12(10):657–671, 1996.

[138] D.A. Breslin, A. Hetherington, and P.N. Walker. Continuous casting excellence by design. *Metallurgical Plant and Technology International*, 22(3):68–77, 1999.

[139] R.B. D'Agostino and M.A. Stephens. *Goodness-Of-Fit Techniques*. Marcel-Dekker, New York, 1986.

[140] R.A. Johnson. *Miller and Freund's Probability and Statistics for Engineers*. Prentice Hall, Englewood Cliffs, 1994.

[141] F.J. Massey Jr. The Kolmogorov-Smirnov test for goodness of fit. *Journal of the American Statistical Association*, 46(253–256):68–78, 1951.

[142] T.W. Anderson and D.A. Darling. Asymptotic theory of certain "goodness-of-fit" criteria based on stochastic processes. *The Annals of Mathematical Statistics*, 23: 193–212, 1952.

[143] H. Peters, N. Link, and T. Heckenthaler. Application of data mining techniques to find correlation between quality data and process variables. In *Preprints of the 10th IFAC Symposium on Automation in Mining, Mineral and Metal Processing (MMM2001), 4-6 September, Tokyo, Japan*, pages 141–146, 2001.

[144] D.C. Montgomery, G.C. Runger, and N.F. Hubele. *Engineering Statistics*. John Wiley & Sons, New York, 2nd edition, 2001.

[145] J. Ikäheimonen, K. Leiviskä, J. Russka, and J. Matkala. Nozzle clogging prediction in continuous casting of steel. In *Preprints of the 15th IFAC World Congress, Barcelona, Spain, 21-26 July*, 2002. Paper T-Th-E12 02.

[146] L. Ljung. *System Identification—Theory for the User*. Prentice Hall, Englewood Cliffs, 1987.

[147] L. Ljung. *System Identification Toolbox for use with MATLAB®*. The MathWorks Inc, Natick, 1995.

[148] F.L. Lewis. Optimal control. In W.S. Levine, editor, *The Control Handbook*, chapter 48, pages 759–778. CRC Press, IEEE Press, Boca Raton, 1996.

[149] N. S. Nise. *Control Systems Engineering*. John Wiley & Sons, New York, 3rd edition, 2000.

[150] K. Fisher and R.M. Mesic. Design and development of Dofasco's quality information database. *Iron and Steel Engineer*, 66(10):22–28, October 1989.

[151] M. Mayos, J.M. Turon, P. Alexandre, J.L. Salon, M. Depeyris, and J.C. Rios. Non destructive on-line inspection of the whole surface of continuously cast slabs. *La Revue de Métallurgie-CIT*, 90(6):824–828, June 1993.

[152] T.J. Knox. Measurement and analysis – a basis for steel quality and customer confidence. *Ironmaking and Steelmaking*, 18(3):196–200, 1991.

[153] D. Foster. Surface inspection of continuously cast slabs. *Metals and Materials*, 7(5): 291–298, May 1991.

[154] R. Brockhoff, F. Hücking, E. Wagener, and W. Reichelt. In-line quality determination of continuously cast material. In *Continuous Casting '85*, pages 60.1–60.10, London, 1985.

[155] D.E. Seborg, T.F. Edgar, and D.A. Mellichamp. *Process dynamics and control*. Wiley Series in Chemical Engineering. John WIley & Sons, New York, 1989.

[156] R.S. Bogartz. *An introduction to the analysis of variance*. Praeger, Westport, 1994.

[157] G. Keppel. *Design and Analysis—A researcher's handbook*. Prentice Hall, Englewood Cliffs, 3rd edition, 1991.

[158] R. Christensen. *Analysis of Variance, Design and Regression—Applied Statistical Methods*. Chapman & Hall, London, 1996.

[159] H. Pinger. Computer aided quality control in an integrated steelworks. *Steel Times*, 217(10):559,563, October 1989.

[160] R.B. Mahapatra, J.K. Brimacombe, I.V. Samarasekera, N. Walker, E.A. Paterson, and J.D. Young. Mold behaviour and its influence on quality in the continuous casting of steel slabs: Part 1. industrial trials, mold temperature measurements, and mathematical modeling. *Metallurgical Transactions B*, 22B(6):861–873, December 1991.

[161] J.R. Boyle, J.A. Penrice, and T. Reynolds. Machine design for maximising quality, throughput and availability. In *Continuous Casting '85*, pages 62.1–62.10, London, 1985.

[162] M. Langer and H. Moll. Process automation and modelling for consistent quality. *Steel Times International*, 14(2):40 & 42, March 1990.

[163] B. Lally, L.T. Biegler, and H. Henein. Optimization and continuous casting: Part i. problem formulation and solution strategy. *Metallurgical Transactions B*, 22B(5): 641–648, 1991.

[164] B. Lally, L.T. Biegler, and H. Henein. Optimization and continuous casting: Part ii. application to industrial casters. *Metallurgical Transactions B*, 22B(5):649–659, 1991.

[165] A.F. Mills. *Heat Transfer*. Irwin, International Student Edition edition, 1992.

[166] S. Barozzi, P. Fontana, and P. Pragliola. Computer control and optimization of secondary cooling during continuous casting. *Iron and Steel Engineer*, 63(11):21–25, November 1986.

[167] K. Furuta, A. Sano, and D. Atherton. *State Variable Methods in Automatic Control*. John Wiley & Sons, Chichester, 1988.

[168] A. Grace, A.J. Laub, J.N. Little, and C.M. Thompson. *Control System Toolbox for use with MATLAB®*. The MathWorks Inc, Natick, 1992.

[169] G.C. Goodwin, S.F. Graebe, and M.E. Salgado. *Control System Design*. Prentice Hall, Upper Saddle River, 2001.

[170] F.L. Lewis. *Optimal Control*. Wiley, New York, 1986.

[171] Z. Sun, S.S. Ge, and T.H. Lee. Controllability and reachability criteria for switched linear systems. *Automatica*, 38(5):775–786, 2002.

[172] J. Zhao and M.W. Spong. Hybrid control for global stabilization of the cart-pendulum system. *Automatica*, 37(12):1941–1951, 2001.

[173] A. Kordona, P. S. Dhurjatia, Y. O. Fuentesb, and B. A. Ogunnaikeb. An intelligent parallel control system structure for plants with multiple operating regimes. *Journal of Process Control*, 9(5):453–460, October 1999.

[174] R.H. Middleton, S.F. Graebe, A. Ahlén, and J.S. Shamma. Design methods. In W.S. Levine, editor, *The Control Handbook*, chapter 20, pages 377–396. CRC Press, IEEE Press, Boca Raton, 1996. See §20.2.

[175] Mathworks. *Simulink®—Dynamic System Simulation Software—User's guide*. The Mathworks Inc, Natick, 1992.

Appendix A

Kolmogorov-Smirnov tables

Table A.1 Kolmogorov-Smirnov hypothesis tests for Transversal Cracks (defect 1a). n_{1a}=1. n_g =70. $d_c(1)$=0.975. α=0.05. $\Delta_{0.95}$=2.2. $\Delta_{0.5}$=1.3.

Variable	$D_{\mu_{1a}}$	$H_0(\mu_{1a})$	$D_{\sigma^2_{1a}}$	$H_0(\sigma^2_{1a})$	$H_0(\mu_{1a}) \cup H_0(\sigma^2_{1a})$
in1u	0.614	Accept	0.886	Accept	Accept
in1l	0.8	Accept	0.843	Accept	Accept
in2u	0.6	Accept	0.929	Accept	Accept
in2l	0.971	Accept	0.9	Accept	Accept
in3u	0.557	Accept	0.914	Accept	Accept
in3l	0.914	Accept	0.929	Accept	Accept
in4u	0.529	Accept	0.886	Accept	Accept
in4l	0.529	Accept	0.943	Accept	Accept
in5u	0.543	Accept	0.929	Accept	Accept
in5l	0.814	Accept	0.914	Accept	Accept
in6u	0.743	Accept	0.8	Accept	Accept
in6l	0.8	Accept	0.914	Accept	Accept
in7u	0.571	Accept	0.886	Accept	Accept
in7l	0.814	Accept	0.9	Accept	Accept
in8u	0.9	Accept	0.914	Accept	Accept
in8l	0.986	Reject	0.943	Accept	Reject
nl1u	0.629	Accept	0.871	Accept	Accept
nl1l	0.714	Accept	0.843	Accept	Accept
nl2u	0.543	Accept	0.914	Accept	Accept
nl2l	0.614	Accept	0.914	Accept	Accept
ou1u	0.843	Accept	0.929	Accept	Accept
ou1l	0.529	Accept	0.943	Accept	Accept
ou2u	0.786	Accept	0.8	Accept	Accept
ou2l	0.886	Accept	0.9	Accept	Accept
ou3u	0.743	Accept	0.857	Accept	Accept
ou3l	0.871	Accept	0.929	Accept	Accept
ou4u	0.8	Accept	0.857	Accept	Accept
ou4l	0.743	Accept	0.886	Accept	Accept
ou5u	0.6	Accept	0.9	Accept	Accept
ou5l	0.743	Accept	0.971	Accept	Accept
ou6u	0.6	Accept	0.9	Accept	Accept
ou6l	0.8	Accept	0.943	Accept	Accept
ou7u	0.757	Accept	0.729	Accept	Accept
ou7l	0.829	Accept	0.9	Accept	Accept
ou8u	0.871	Accept	0.843	Accept	Accept
ou8l	0.6	Accept	0.914	Accept	Accept
nr1u	0.971	Accept	0.914	Accept	Accept
nr1l	1	Reject	0.729	Accept	Reject
nr2u	0.986	Reject	0.886	Accept	Reject
nr2l	0.986	Reject	0.814	Accept	Reject
Casting Speed	0.971	Accept	0.943	Accept	Accept
Mould Controller Status	0.943	Accept	0.943	Accept	Accept
Mould level	0.971	Accept	0.971	Accept	Accept
Inlet Temperature	0.886	Accept	0.586	Accept	Accept
Flowrate WL	0.743	Accept	0.5	Accept	Accept
Flowrate WF	0.886	Accept	0.7	Accept	Accept
Flowrate NL	0.543	Accept	0.671	Accept	Accept
Flowrate NR	0.843	Accept	0.8	Accept	Accept
Delta T WL	0.829	Accept	0.929	Accept	Accept
Delta T WF	0.829	Accept	0.929	Accept	Accept
Delta T NL	0.957	Accept	0.914	Accept	Accept
Delta T NR	0.886	Accept	0.886	Accept	Accept
Oscillation Frequency	0.986	Reject	0.943	Accept	Reject
Drive Current	0.771	Accept	0.986	Reject	Reject
Heat Flux WL	0.829	Accept	0.929	Accept	Accept
Heat Flux WF	0.829	Accept	0.914	Accept	Accept
Heat Flux NL	0.957	Accept	0.914	Accept	Accept
Heat Flux NR	0.886	Accept	0.886	Accept	Accept
in1	0.986	Reject	0.957	Accept	Reject
in2	0.986	Reject	0.971	Accept	Reject
in3	1	Reject	0.957	Accept	Reject
in4	0.7	Accept	0.971	Accept	Accept
in5	0.871	Accept	0.943	Accept	Accept
in6	1	Reject	0.957	Accept	Reject
in7	0.971	Accept	0.957	Accept	Accept
in8	1	Reject	0.943	Accept	Reject
nl1	0.586	Accept	0.571	Accept	Accept
nl2	0.543	Accept	0.757	Accept	Accept
ou1	0.957	Accept	0.857	Accept	Accept
ou2	1	Reject	0.9	Accept	Reject
ou3	1	Reject	0.914	Accept	Reject
ou4	1	Reject	0.929	Accept	Reject
ou5	0.886	Accept	0.957	Accept	Accept
ou6	0.5	Accept	0.957	Accept	Accept
ou7	1	Reject	0.943	Accept	Reject
ou8	0.971	Accept	0.814	Accept	Accept
nr1	0.8	Accept	0.814	Accept	Accept
nr2	0.614	Accept	0.614	Accept	Accept

Table A.2 Kolmogorov-Smirnov hypothesis tests for Longitudinal Cracks (defect 1b). n_{1b}=3. n_g =114. $d_c(3)$=0.708. α=0.05. $\Delta_{0.95}$=1.27. $\Delta_{0.5}$=0.751.

Variable	$D_{\mu_{1b}}$	$H_0(\mu_{1b})$	$D_{\sigma^2_{1b}}$	$H_0(\sigma^2_{1b})$	$H_0(\mu_{1b}) \cup H_0(\sigma^2_{1b})$
in1u	0.439	Accept	0.421	Accept	Accept
in1l	0.368	Accept	0.333	Accept	Accept
in2u	0.491	Accept	0.36	Accept	Accept
in2l	0.404	Accept	0.351	Accept	Accept
in3u	0.482	Accept	0.64	Accept	Accept
in3l	0.535	Accept	0.412	Accept	Accept
in4u	0.456	Accept	0.623	Accept	Accept
in4l	0.535	Accept	0.395	Accept	Accept
in5u	0.325	Accept	0.518	Accept	Accept
in5l	0.474	Accept	0.368	Accept	Accept
in6u	0.535	Accept	0.395	Accept	Accept
in6l	0.395	Accept	0.412	Accept	Accept
in7u	0.368	Accept	0.307	Accept	Accept
in7l	0.351	Accept	0.307	Accept	Accept
in8u	0.36	Accept	0.535	Accept	Accept
in8l	0.342	Accept	0.281	Accept	Accept
nl1u	0.316	Accept	0.368	Accept	Accept
nl1l	0.474	Accept	0.491	Accept	Accept
nl2u	0.298	Accept	0.544	Accept	Accept
nl2l	0.43	Accept	0.588	Accept	Accept
ou1u	0.456	Accept	0.447	Accept	Accept
ou1l	0.254	Accept	0.439	Accept	Accept
ou2u	0.605	Accept	0.421	Accept	Accept
ou2l	0.316	Accept	0.272	Accept	Accept
ou3u	0.518	Accept	0.57	Accept	Accept
ou3l	0.579	Accept	0.474	Accept	Accept
ou4u	0.57	Accept	0.316	Accept	Accept
ou4l	0.509	Accept	0.368	Accept	Accept
ou5u	0.377	Accept	0.254	Accept	Accept
ou5l	0.43	Accept	0.307	Accept	Accept
ou6u	0.544	Accept	0.544	Accept	Accept
ou6l	0.737	Reject	0.456	Accept	Reject
ou7u	0.526	Accept	0.482	Accept	Accept
ou7l	0.351	Accept	0.325	Accept	Accept
ou8u	0.553	Accept	0.5	Accept	Accept
ou8l	0.351	Accept	0.377	Accept	Accept
nr1u	0.57	Accept	0.342	Accept	Accept
nr1l	0.658	Accept	0.272	Accept	Accept
nr2u	0.658	Accept	0.412	Accept	Accept
nr2l	0.649	Accept	0.421	Accept	Accept
Casting Speed	0.509	Accept	0.412	Accept	Accept
Mould Controller Status	0.193	Accept	0.193	Accept	Accept
Mould level	0.43	Accept	0.368	Accept	Accept
Inlet Temperature	0.579	Accept	0.711	Reject	Reject
Flowrate WL	0.316	Accept	0.535	Accept	Accept
Flowrate WF	0.447	Accept	0.482	Accept	Accept
Flowrate NL	0.298	Accept	0.307	Accept	Accept
Flowrate NR	0.36	Accept	0.491	Accept	Accept
Delta T WL	0.289	Accept	0.632	Accept	Accept
Delta T WF	0.404	Accept	0.307	Accept	Accept
Delta T NL	0.5	Accept	0.447	Accept	Accept
Delta T NR	0.5	Accept	0.439	Accept	Accept
Oscillation Frequency	0.509	Accept	0.421	Accept	Accept
Drive Current	0.816	Reject	0.509	Accept	Reject
Heat Flux WL	0.447	Accept	0.623	Accept	Accept
Heat Flux WF	0.632	Accept	0.307	Accept	Accept
Heat Flux NL	0.5	Accept	0.447	Accept	Accept
Heat Flux NR	0.5	Accept	0.439	Accept	Accept
in1	0.386	Accept	0.518	Accept	Accept
in2	0.333	Accept	0.456	Accept	Accept
in3	0.333	Accept	0.614	Accept	Accept
in4	0.509	Accept	0.518	Accept	Accept
in5	0.5	Accept	0.465	Accept	Accept
in6	0.658	Accept	0.447	Accept	Accept
in7	0.509	Accept	0.412	Accept	Accept
in8	0.333	Accept	0.395	Accept	Accept
nl1	0.447	Accept	0.36	Accept	Accept
nl2	0.43	Accept	0.298	Accept	Accept
ou1	0.482	Accept	0.43	Accept	Accept
ou2	0.333	Accept	0.228	Accept	Accept
ou3	0.658	Accept	0.412	Accept	Accept
ou4	0.658	Accept	0.5	Accept	Accept
ou5	0.588	Accept	0.333	Accept	Accept
ou6	0.421	Accept	0.491	Accept	Accept
ou7	0.553	Accept	0.386	Accept	Accept
ou8	0.439	Accept	0.474	Accept	Accept
nr1	0.439	Accept	0.298	Accept	Accept
nr2	0.316	Accept	0.447	Accept	Accept

Table A.3 Kolmogorov-Smirnov hypothesis tests for Casting Powder Entrapment (defect 2a). n_{2a}=4. n_g =83. $d_c(4)$=0.624. α=0.05. $\Delta_{0.95}$=1.1. $\Delta_{0.5}$=0.65.

Variable	$D_{\mu_{2a}}$	$H_0(\mu_{2a})$	$D_{\sigma^2_{2a}}$	$H_0(\sigma^2_{2a})$	$H_0(\mu_{2a}) \cup H_0(\sigma^2_{2a})$
in1u	0.654	Reject	0.34	Accept	Reject
in1l	0.446	Accept	0.485	Accept	Accept
in2u	0.605	Accept	0.482	Accept	Accept
in2l	0.325	Accept	0.398	Accept	Accept
in3u	0.617	Accept	0.47	Accept	Accept
in3l	0.184	Accept	0.651	Reject	Reject
in4u	0.509	Accept	0.639	Reject	Reject
in4l	0.53	Accept	0.602	Accept	Accept
in5u	0.367	Accept	0.566	Accept	Accept
in5l	0.352	Accept	0.795	Reject	Reject
in6u	0.494	Accept	0.325	Accept	Accept
in6l	0.304	Accept	0.497	Accept	Accept
in7u	0.437	Accept	0.542	Accept	Accept
in7l	0.202	Accept	0.473	Accept	Accept
in8u	0.533	Accept	0.509	Accept	Accept
in8l	0.59	Accept	0.614	Accept	Accept
nl1u	0.352	Accept	0.373	Accept	Accept
nl1l	0.283	Accept	0.425	Accept	Accept
nl2u	0.449	Accept	0.34	Accept	Accept
nl2l	0.38	Accept	0.364	Accept	Accept
ou1u	0.617	Accept	0.506	Accept	Accept
ou1l	0.446	Accept	0.38	Accept	Accept
ou2u	0.476	Accept	0.482	Accept	Accept
ou2l	0.313	Accept	0.38	Accept	Accept
ou3u	0.259	Accept	0.506	Accept	Accept
ou3l	0.464	Accept	0.518	Accept	Accept
ou4u	0.316	Accept	0.41	Accept	Accept
ou4l	0.521	Accept	0.47	Accept	Accept
ou5u	0.25	Accept	0.627	Reject	Reject
ou5l	0.497	Accept	0.687	Reject	Reject
ou6u	0.34	Accept	0.47	Accept	Accept
ou6l	0.367	Accept	0.377	Accept	Accept
ou7u	0.533	Accept	0.304	Accept	Accept
ou7l	0.307	Accept	0.377	Accept	Accept
ou8u	0.521	Accept	0.422	Accept	Accept
ou8l	0.337	Accept	0.627	Reject	Reject
nr1u	0.485	Accept	0.434	Accept	Accept
nr1l	0.386	Accept	0.434	Accept	Accept
nr2u	0.428	Accept	0.542	Accept	Accept
nr2l	0.446	Accept	0.506	Accept	Accept
Casting Speed	0.488	Accept	0.413	Accept	Accept
Mould Controller Status	0.425	Accept	0.449	Accept	Accept
Mould level	0.494	Accept	0.328	Accept	Accept
Inlet Temperature	0.578	Accept	0.518	Accept	Accept
Flowrate WL	0.47	Accept	0.223	Accept	Accept
Flowrate WF	0.518	Accept	0.651	Reject	Reject
Flowrate NL	0.53	Accept	0.373	Accept	Accept
Flowrate NR	0.301	Accept	0.494	Accept	Accept
Delta T WL	0.476	Accept	0.28	Accept	Accept
Delta T WF	0.464	Accept	0.328	Accept	Accept
Delta T NL	0.452	Accept	0.506	Accept	Accept
Delta T NR	0.47	Accept	0.373	Accept	Accept
Oscillation Frequency	0.488	Accept	0.413	Accept	Accept
Drive Current	0.307	Accept	0.428	Accept	Accept
Heat Flux WL	0.476	Accept	0.292	Accept	Accept
Heat Flux WF	0.464	Accept	0.34	Accept	Accept
Heat Flux NL	0.452	Accept	0.506	Accept	Accept
Heat Flux NR	0.47	Accept	0.386	Accept	Accept
in1	0.392	Accept	0.521	Accept	Accept
in2	0.367	Accept	0.361	Accept	Accept
in3	0.214	Accept	0.605	Accept	Accept
in4	0.473	Accept	0.663	Reject	Reject
in5	0.53	Accept	0.663	Reject	Reject
in6	0.578	Accept	0.605	Accept	Accept
in7	0.506	Accept	0.642	Reject	Reject
in8	0.437	Accept	0.566	Accept	Accept
nl1	0.449	Accept	0.289	Accept	Accept
nl2	0.494	Accept	0.566	Accept	Accept
ou1	0.545	Accept	0.518	Accept	Accept
ou2	0.292	Accept	0.545	Accept	Accept
ou3	0.533	Accept	0.506	Accept	Accept
ou4	0.569	Accept	0.482	Accept	Accept
ou5	0.59	Accept	0.614	Accept	Accept
ou6	0.557	Accept	0.654	Reject	Reject
ou7	0.389	Accept	0.437	Accept	Accept
ou8	0.404	Accept	0.617	Accept	Accept
nr1	0.373	Accept	0.244	Accept	Accept
nr2	0.566	Accept	0.53	Accept	Accept

Table A.4 Kolmogorov-Smirnov hypothesis tests for Other Inclusions (defect 2b). n_{2b}=114. n_g =364. $d_c(114)$=0.127. α=0.05. $\Delta_{0.95}$=0.206. $\Delta_{0.5}$=0.122.

Variable	$D_{\mu_{2b}}$	$H_0(\mu_{2b})$	$D_{\sigma^2_{2b}}$	$H_0(\sigma^2_{2b})$	$H_0(\mu_{2b}) \cup H_0(\sigma^2_{2b})$
in1u	0.175	Reject	0.067	Accept	Reject
in1l	0.0977	Accept	0.0697	Accept	Accept
in2u	0.198	Reject	0.127	Accept	Reject
in2l	0.141	Reject	0.14	Reject	Reject
in3u	0.212	Reject	0.153	Reject	Reject
in3l	0.0942	Accept	0.102	Accept	Accept
in4u	0.171	Reject	0.173	Reject	Reject
in4l	0.0769	Accept	0.162	Reject	Reject
in5u	0.0833	Accept	0.207	Reject	Reject
in5l	0.0605	Accept	0.168	Reject	Reject
in6u	0.095	Accept	0.142	Reject	Reject
in6l	0.0967	Accept	0.168	Reject	Reject
in7u	0.215	Reject	0.157	Reject	Reject
in7l	0.143	Reject	0.178	Reject	Reject
in8u	0.145	Reject	0.0473	Accept	Reject
in8l	0.122	Accept	0.0817	Accept	Accept
nl1u	0.261	Reject	0.17	Reject	Reject
nl1l	0.26	Reject	0.0738	Accept	Reject
nl2u	0.31	Reject	0.0743	Accept	Reject
nl2l	0.249	Reject	0.166	Reject	Reject
ou1u	0.199	Reject	0.136	Reject	Reject
ou1l	0.155	Reject	0.0818	Accept	Reject
ou2u	0.129	Reject	0.122	Accept	Reject
ou2l	0.169	Reject	0.0956	Accept	Reject
ou3u	0.228	Reject	0.109	Accept	Reject
ou3l	0.191	Reject	0.149	Reject	Reject
ou4u	0.154	Reject	0.164	Reject	Reject
ou4l	0.221	Reject	0.146	Reject	Reject
ou5u	0.223	Reject	0.133	Reject	Reject
ou5l	0.2	Reject	0.169	Reject	Reject
ou6u	0.36	Reject	0.253	Reject	Reject
ou6l	0.233	Reject	0.214	Reject	Reject
ou7u	0.217	Reject	0.136	Reject	Reject
ou7l	0.204	Reject	0.1	Accept	Reject
ou8u	0.267	Reject	0.126	Accept	Reject
ou8l	0.154	Reject	0.0804	Accept	Reject
nr1u	0.199	Reject	0.119	Accept	Reject
nr1l	0.0899	Accept	0.155	Reject	Reject
nr2u	0.0831	Accept	0.113	Accept	Accept
nr2l	0.133	Reject	0.102	Accept	Reject
Casting Speed	0.193	Reject	0.105	Accept	Reject
Mould Controller Status	0.0605	Accept	0.0736	Accept	Accept
Mould level	0.126	Accept	0.0717	Accept	Accept
Inlet Temperature	0.136	Reject	0.174	Reject	Reject
Flowrate WL	0.0596	Accept	0.0797	Accept	Accept
Flowrate WF	0.117	Accept	0.2	Reject	Reject
Flowrate NL	0.1	Accept	0.0888	Accept	Accept
Flowrate NR	0.0835	Accept	0.0602	Accept	Accept
Delta T WL	0.155	Reject	0.171	Reject	Reject
Delta T WF	0.257	Reject	0.151	Reject	Reject
Delta T NL	0.1	Accept	0.133	Reject	Reject
Delta T NR	0.107	Accept	0.131	Reject	Reject
Oscillation Frequency	0.258	Reject	0.139	Reject	Reject
Drive Current	0.117	Accept	0.111	Accept	Accept
Heat Flux WL	0.117	Accept	0.177	Reject	Reject
Heat Flux WF	0.185	Reject	0.186	Reject	Reject
Heat Flux NL	0.1	Accept	0.128	Reject	Reject
Heat Flux NR	0.107	Accept	0.145	Reject	Reject
in1	0.188	Reject	0.0839	Accept	Reject
in2	0.174	Reject	0.0935	Accept	Reject
in3	0.188	Reject	0.119	Accept	Reject
in4	0.178	Reject	0.13	Reject	Reject
in5	0.181	Reject	0.179	Reject	Reject
in6	0.186	Reject	0.158	Reject	Reject
in7	0.129	Reject	0.119	Accept	Reject
in8	0.0887	Accept	0.0931	Accept	Accept
nl1	0.213	Reject	0.0979	Accept	Reject
nl2	0.211	Reject	0.0491	Accept	Reject
ou1	0.108	Accept	0.0851	Accept	Accept
ou2	0.0891	Accept	0.0861	Accept	Accept
ou3	0.1	Accept	0.0865	Accept	Accept
ou4	0.139	Reject	0.162	Reject	Reject
ou5	0.099	Accept	0.179	Reject	Reject
ou6	0.244	Reject	0.232	Reject	Reject
ou7	0.122	Accept	0.115	Accept	Accept
ou8	0.134	Reject	0.0773	Accept	Reject
nr1	0.265	Reject	0.118	Accept	Reject
nr2	0.127	Accept	0.114	Accept	Accept

Table A.5 Kolmogorov-Smirnov hypothesis tests for Bleeders (defect 4). n_4=3. n_g =175. $d_c(3)$=0.708. α=0.05. $\Delta_{0.95}$=1.27. $\Delta_{0.5}$=0.751.

Variable	D_{μ_4}	$H_0(\mu_4)$	$D_{\sigma_4^2}$	$H_0(\sigma_4^2)$	$H_0(\mu_4) \cup H_0(\sigma_4^2)$
in1u	0.389	Accept	0.234	Accept	Accept
in1l	0.455	Accept	0.309	Accept	Accept
in2u	0.434	Accept	0.469	Accept	Accept
in2l	0.309	Accept	0.417	Accept	Accept
in3u	0.314	Accept	0.463	Accept	Accept
in3l	0.455	Accept	0.587	Accept	Accept
in4u	0.305	Accept	0.429	Accept	Accept
in4l	0.421	Accept	0.472	Accept	Accept
in5u	0.341	Accept	0.297	Accept	Accept
in5l	0.261	Accept	0.371	Accept	Accept
in6u	0.406	Accept	0.48	Accept	Accept
in6l	0.571	Accept	0.446	Accept	Accept
in7u	0.371	Accept	0.354	Accept	Accept
in7l	0.411	Accept	0.509	Accept	Accept
in8u	0.276	Accept	0.377	Accept	Accept
in8l	0.261	Accept	0.709	Reject	Reject
nl1u	0.663	Accept	0.68	Accept	Accept
nl1l	0.491	Accept	0.467	Accept	Accept
nl2u	0.646	Accept	0.31	Accept	Accept
nl2l	0.6	Accept	0.354	Accept	Accept
ou1u	0.314	Accept	0.457	Accept	Accept
ou1l	0.307	Accept	0.255	Accept	Accept
ou2u	0.286	Accept	0.45	Accept	Accept
ou2l	0.387	Accept	0.547	Accept	Accept
ou3u	0.377	Accept	0.36	Accept	Accept
ou3l	0.37	Accept	0.543	Accept	Accept
ou4u	0.394	Accept	0.314	Accept	Accept
ou4l	0.455	Accept	0.335	Accept	Accept
ou5u	0.432	Accept	0.404	Accept	Accept
ou5l	0.423	Accept	0.461	Accept	Accept
ou6u	0.434	Accept	0.623	Accept	Accept
ou6l	0.503	Accept	0.817	Reject	Reject
ou7u	0.383	Accept	0.297	Accept	Accept
ou7l	0.337	Accept	0.341	Accept	Accept
ou8u	0.291	Accept	0.358	Accept	Accept
ou8l	0.33	Accept	0.415	Accept	Accept
nr1u	0.295	Accept	0.552	Accept	Accept
nr1l	0.444	Accept	0.524	Accept	Accept
nr2u	0.404	Accept	0.337	Accept	Accept
nr2l	0.421	Accept	0.423	Accept	Accept
Casting Speed	0.484	Accept	0.472	Accept	Accept
Mould Controller Status	0.185	Accept	0.185	Accept	Accept
Mould level	0.37	Accept	0.434	Accept	Accept
Inlet Temperature	0.337	Accept	0.316	Accept	Accept
Flowrate WL	0.32	Accept	0.592	Accept	Accept
Flowrate WF	0.514	Accept	0.293	Accept	Accept
Flowrate NL	0.48	Accept	0.282	Accept	Accept
Flowrate NR	0.429	Accept	0.322	Accept	Accept
Delta T WL	0.451	Accept	0.461	Accept	Accept
Delta T WF	0.509	Accept	0.421	Accept	Accept
Delta T NL	0.577	Accept	0.375	Accept	Accept
Delta T NR	0.354	Accept	0.455	Accept	Accept
Oscillation Frequency	0.467	Accept	0.253	Accept	Accept
Drive Current	0.358	Accept	0.455	Accept	Accept
Heat Flux WL	0.518	Accept	0.472	Accept	Accept
Heat Flux WF	0.537	Accept	0.421	Accept	Accept
Heat Flux NL	0.577	Accept	0.381	Accept	Accept
Heat Flux NR	0.354	Accept	0.455	Accept	Accept
in1	0.274	Accept	0.253	Accept	Accept
in2	0.571	Accept	0.417	Accept	Accept
in3	0.326	Accept	0.52	Accept	Accept
in4	0.316	Accept	0.509	Accept	Accept
in5	0.318	Accept	0.4	Accept	Accept
in6	0.457	Accept	0.474	Accept	Accept
in7	0.267	Accept	0.606	Accept	Accept
in8	0.366	Accept	0.514	Accept	Accept
nl1	0.394	Accept	0.467	Accept	Accept
nl2	0.589	Accept	0.501	Accept	Accept
ou1	0.577	Accept	0.324	Accept	Accept
ou2	0.358	Accept	0.552	Accept	Accept
ou3	0.248	Accept	0.484	Accept	Accept
ou4	0.299	Accept	0.375	Accept	Accept
ou5	0.41	Accept	0.512	Accept	Accept
ou6	0.52	Accept	0.874	Reject	Reject
ou7	0.337	Accept	0.312	Accept	Accept
ou8	0.364	Accept	0.352	Accept	Accept
nr1	0.484	Accept	0.444	Accept	Accept
nr2	0.56	Accept	0.27	Accept	Accept

Table A.6 Kolmogorov-Smirnov hypothesis tests for Deep Oscillation Marks (defect 5a). n_{5a}=8. n_g =354. $d_c(8)$=0.457. α=0.05. $\Delta_{0.95}$=0.778. $\Delta_{0.5}$=0.46.

Variable	$D_{\mu_{5a}}$	$H_0(\mu_{5a})$	$D_{\sigma^2_{5a}}$	$H_0(\sigma^2_{5a})$	$H_0(\mu_{5a}) \cup H_0(\sigma^2_{5a})$
in1u	0.216	Accept	0.473	Reject	Reject
in1l	0.215	Accept	0.516	Reject	Reject
in2u	0.303	Accept	0.276	Accept	Accept
in2l	0.383	Accept	0.263	Accept	Accept
in3u	0.186	Accept	0.35	Accept	Accept
in3l	0.22	Accept	0.325	Accept	Accept
in4u	0.316	Accept	0.296	Accept	Accept
in4l	0.233	Accept	0.404	Accept	Accept
in5u	0.331	Accept	0.361	Accept	Accept
in5l	0.332	Accept	0.331	Accept	Accept
in6u	0.28	Accept	0.322	Accept	Accept
in6l	0.402	Accept	0.338	Accept	Accept
in7u	0.316	Accept	0.31	Accept	Accept
in7l	0.264	Accept	0.33	Accept	Accept
in8u	0.308	Accept	0.248	Accept	Accept
in8l	0.358	Accept	0.342	Accept	Accept
nl1u	0.343	Accept	0.417	Accept	Accept
nl1l	0.38	Accept	0.369	Accept	Accept
nl2u	0.352	Accept	0.263	Accept	Accept
nl2l	0.319	Accept	0.525	Reject	Reject
ou1u	0.275	Accept	0.227	Accept	Accept
ou1l	0.22	Accept	0.206	Accept	Accept
ou2u	0.164	Accept	0.333	Accept	Accept
ou2l	0.2	Accept	0.354	Accept	Accept
ou3u	0.24	Accept	0.397	Accept	Accept
ou3l	0.313	Accept	0.481	Reject	Reject
ou4u	0.328	Accept	0.454	Accept	Accept
ou4l	0.284	Accept	0.317	Accept	Accept
ou5u	0.364	Accept	0.348	Accept	Accept
ou5l	0.477	Reject	0.333	Accept	Reject
ou6u	0.376	Accept	0.337	Accept	Accept
ou6l	0.373	Accept	0.35	Accept	Accept
ou7u	0.285	Accept	0.371	Accept	Accept
ou7l	0.243	Accept	0.358	Accept	Accept
ou8u	0.379	Accept	0.309	Accept	Accept
ou8l	0.328	Accept	0.307	Accept	Accept
nr1u	0.447	Accept	0.254	Accept	Accept
nr1l	0.347	Accept	0.294	Accept	Accept
nr2u	0.285	Accept	0.248	Accept	Accept
nr2l	0.364	Accept	0.281	Accept	Accept
Casting Speed	0.271	Accept	0.282	Accept	Accept
Mould Controller Status	0.169	Accept	0.174	Accept	Accept
Mould level	0.291	Accept	0.262	Accept	Accept
Inlet Temperature	0.174	Accept	0.22	Accept	Accept
Flowrate WL	0.173	Accept	0.369	Accept	Accept
Flowrate WF	0.226	Accept	0.227	Accept	Accept
Flowrate NL	0.521	Reject	0.189	Accept	Reject
Flowrate NR	0.465	Reject	0.297	Accept	Reject
Delta T WL	0.353	Accept	0.398	Accept	Accept
Delta T WF	0.463	Reject	0.324	Accept	Reject
Delta T NL	0.458	Reject	0.296	Accept	Reject
Delta T NR	0.47	Reject	0.348	Accept	Reject
Oscillation Frequency	0.274	Accept	0.28	Accept	Accept
Drive Current	0.203	Accept	0.395	Accept	Accept
Heat Flux WL	0.593	Reject	0.437	Accept	Reject
Heat Flux WF	0.647	Reject	0.336	Accept	Reject
Heat Flux NL	0.458	Reject	0.296	Accept	Reject
Heat Flux NR	0.472	Reject	0.34	Accept	Reject
in1	0.363	Accept	0.598	Reject	Reject
in2	0.357	Accept	0.323	Accept	Accept
in3	0.314	Accept	0.29	Accept	Accept
in4	0.257	Accept	0.328	Accept	Accept
in5	0.185	Accept	0.355	Accept	Accept
in6	0.234	Accept	0.352	Accept	Accept
in7	0.323	Accept	0.35	Accept	Accept
in8	0.196	Accept	0.463	Reject	Reject
nl1	0.4	Accept	0.607	Reject	Reject
nl2	0.345	Accept	0.341	Accept	Accept
ou1	0.285	Accept	0.242	Accept	Accept
ou2	0.172	Accept	0.402	Accept	Accept
ou3	0.315	Accept	0.441	Accept	Accept
ou4	0.383	Accept	0.35	Accept	Accept
ou5	0.214	Accept	0.32	Accept	Accept
ou6	0.342	Accept	0.351	Accept	Accept
ou7	0.291	Accept	0.401	Accept	Accept
ou8	0.176	Accept	0.48	Reject	Reject
nr1	0.47	Reject	0.297	Accept	Reject
nr2	0.508	Reject	0.282	Accept	Reject

Table A.7 Kolmogorov-Smirnov hypothesis tests for Uneven Oscillation Marks (defect 5b). n_{5b}=5. n_g =256. $d_c(5)$=0.565. α=0.05. $\Delta_{0.95}$=0.984. $\Delta_{0.5}$=0.581.

Variable	$D_{\mu_{5b}}$	$H_0(\mu_{5b})$	$D_{\sigma^2_{5b}}$	$H_0(\sigma^2_{5b})$	$H_0(\mu_{5b}) \cup H_0(\sigma^2_{5b})$
in1u	0.515	Accept	0.363	Accept	Accept
in1l	0.387	Accept	0.374	Accept	Accept
in2u	0.409	Accept	0.543	Accept	Accept
in2l	0.327	Accept	0.523	Accept	Accept
in3u	0.5	Accept	0.664	Reject	Reject
in3l	0.312	Accept	0.527	Accept	Accept
in4u	0.527	Accept	0.574	Reject	Reject
in4l	0.402	Accept	0.295	Accept	Accept
in5u	0.676	Reject	0.633	Reject	Reject
in5l	0.281	Accept	0.527	Accept	Accept
in6u	0.48	Accept	0.598	Reject	Reject
in6l	0.633	Reject	0.496	Accept	Reject
in7u	0.586	Reject	0.574	Reject	Reject
in7l	0.336	Accept	0.265	Accept	Accept
in8u	0.637	Reject	0.633	Reject	Reject
in8l	0.562	Accept	0.299	Accept	Accept
nl1u	0.594	Reject	0.538	Accept	Reject
nl1l	0.53	Accept	0.53	Accept	Accept
nl2u	0.535	Accept	0.379	Accept	Accept
nl2l	0.551	Accept	0.491	Accept	Accept
ou1u	0.551	Accept	0.547	Accept	Accept
ou1l	0.641	Reject	0.359	Accept	Reject
ou2u	0.527	Accept	0.562	Accept	Accept
ou2l	0.336	Accept	0.48	Accept	Accept
ou3u	0.578	Reject	0.559	Accept	Reject
ou3l	0.309	Accept	0.582	Reject	Reject
ou4u	0.641	Reject	0.539	Accept	Reject
ou4l	0.383	Accept	0.531	Accept	Accept
ou5u	0.613	Reject	0.5	Accept	Reject
ou5l	0.273	Accept	0.668	Reject	Reject
ou6u	0.441	Accept	0.621	Reject	Reject
ou6l	0.379	Accept	0.668	Reject	Reject
ou7u	0.48	Accept	0.578	Reject	Reject
ou7l	0.359	Accept	0.391	Accept	Accept
ou8u	0.445	Accept	0.355	Accept	Accept
ou8l	0.453	Accept	0.373	Accept	Accept
nr1u	0.402	Accept	0.39	Accept	Accept
nr1l	0.523	Accept	0.287	Accept	Accept
nr2u	0.484	Accept	0.476	Accept	Accept
nr2l	0.437	Accept	0.398	Accept	Accept
Casting Speed	0.378	Accept	0.363	Accept	Accept
Mould Controller Status	0.267	Accept	0.275	Accept	Accept
Mould level	0.334	Accept	0.221	Accept	Accept
Inlet Temperature	0.324	Accept	0.445	Accept	Accept
Flowrate WL	0.225	Accept	0.625	Reject	Reject
Flowrate WF	0.707	Reject	0.707	Reject	Reject
Flowrate NL	0.57	Reject	0.252	Accept	Reject
Flowrate NR	0.234	Accept	0.297	Accept	Accept
Delta T WL	0.262	Accept	0.512	Accept	Accept
Delta T WF	0.316	Accept	0.323	Accept	Accept
Delta T NL	0.457	Accept	0.48	Accept	Accept
Delta T NR	0.461	Accept	0.421	Accept	Accept
Oscillation Frequency	0.456	Accept	0.316	Accept	Accept
Drive Current	0.449	Accept	0.308	Accept	Accept
Heat Flux WL	0.409	Accept	0.523	Accept	Accept
Heat Flux WF	0.409	Accept	0.323	Accept	Accept
Heat Flux NL	0.453	Accept	0.48	Accept	Accept
Heat Flux NR	0.461	Accept	0.417	Accept	Accept
in1	0.461	Accept	0.299	Accept	Accept
in2	0.433	Accept	0.539	Accept	Accept
in3	0.519	Accept	0.512	Accept	Accept
in4	0.59	Reject	0.339	Accept	Reject
in5	0.71	Reject	0.472	Accept	Reject
in6	0.773	Reject	0.609	Reject	Reject
in7	0.512	Accept	0.613	Reject	Reject
in8	0.562	Accept	0.52	Accept	Accept
nl1	0.367	Accept	0.628	Reject	Reject
nl2	0.508	Accept	0.555	Accept	Accept
ou1	0.457	Accept	0.406	Accept	Accept
ou2	0.609	Reject	0.449	Accept	Reject
ou3	0.574	Reject	0.41	Accept	Reject
ou4	0.539	Accept	0.476	Accept	Accept
ou5	0.809	Reject	0.456	Accept	Reject
ou6	0.66	Reject	0.52	Accept	Reject
ou7	0.27	Accept	0.434	Accept	Accept
ou8	0.304	Accept	0.288	Accept	Accept
nr1	0.581	Reject	0.296	Accept	Reject
nr2	0.284	Accept	0.507	Accept	Accept

Table A.8 Kolmogorov-Smirnov hypothesis tests for Stopmarks (defect 6). n_6=19. n_g =170. $d_c(19)$=0.301. α=0.05. $\Delta_{0.95}$=0.505. $\Delta_{0.5}$=0.298.

Variable	D_{μ_6}	$H_0(\mu_6)$	$D_{\sigma_6^2}$	$H_0(\sigma_6^2)$	$H_0(\mu_6) \cup H_0(\sigma_6^2)$
in1u	0.29	Accept	0.742	Reject	Reject
in1l	0.396	Reject	0.695	Reject	Reject
in2u	0.426	Reject	0.748	Reject	Reject
in2l	0.514	Reject	0.672	Reject	Reject
in3u	0.349	Reject	0.742	Reject	Reject
in3l	0.408	Reject	0.707	Reject	Reject
in4u	0.337	Reject	0.742	Reject	Reject
in4l	0.244	Accept	0.724	Reject	Reject
in5u	0.385	Reject	0.725	Reject	Reject
in5l	0.35	Reject	0.718	Reject	Reject
in6u	0.396	Reject	0.737	Reject	Reject
in6l	0.602	Reject	0.642	Reject	Reject
in7u	0.426	Reject	0.73	Reject	Reject
in7l	0.508	Reject	0.654	Reject	Reject
in8u	0.349	Reject	0.701	Reject	Reject
in8l	0.531	Reject	0.583	Reject	Reject
nl1u	0.567	Reject	0.719	Reject	Reject
nl1l	0.52	Reject	0.777	Reject	Reject
nl2u	0.348	Reject	0.707	Reject	Reject
nl2l	0.331	Reject	0.625	Reject	Reject
ou1u	0.308	Reject	0.765	Reject	Reject
ou1l	0.325	Reject	0.677	Reject	Reject
ou2u	0.291	Accept	0.73	Reject	Reject
ou2l	0.56	Reject	0.683	Reject	Reject
ou3u	0.402	Reject	0.724	Reject	Reject
ou3l	0.495	Reject	0.684	Reject	Reject
ou4u	0.567	Reject	0.742	Reject	Reject
ou4l	0.467	Reject	0.771	Reject	Reject
ou5u	0.361	Reject	0.73	Reject	Reject
ou5l	0.455	Reject	0.695	Reject	Reject
ou6u	0.313	Reject	0.66	Reject	Reject
ou6l	0.313	Reject	0.678	Reject	Reject
ou7u	0.508	Reject	0.742	Reject	Reject
ou7l	0.554	Reject	0.689	Reject	Reject
ou8u	0.502	Reject	0.777	Reject	Reject
ou8l	0.537	Reject	0.718	Reject	Reject
nr1u	0.554	Reject	0.719	Reject	Reject
nr1l	0.292	Accept	0.678	Reject	Reject
nr2u	0.368	Reject	0.737	Reject	Reject
nr2l	0.361	Reject	0.731	Reject	Reject
Casting Speed	0.748	Reject	0.748	Reject	Reject
Mould Controller Status	0.666	Reject	0.666	Reject	Reject
Mould level	0.631	Reject	0.408	Reject	Reject
Inlet Temperature	0.18	Accept	0.207	Accept	Accept
Flowrate WL	0.167	Accept	0.438	Reject	Reject
Flowrate WF	0.325	Reject	0.572	Reject	Reject
Flowrate NL	0.215	Accept	0.326	Reject	Reject
Flowrate NR	0.227	Accept	0.672	Reject	Reject
Delta T WL	0.683	Reject	0.707	Reject	Reject
Delta T WF	0.724	Reject	0.701	Reject	Reject
Delta T NL	0.747	Reject	0.689	Reject	Reject
Delta T NR	0.695	Reject	0.725	Reject	Reject
Oscillation Frequency	0.748	Reject	0.766	Reject	Reject
Drive Current	0.259	Accept	0.407	Reject	Reject
Heat Flux WL	0.671	Reject	0.713	Reject	Reject
Heat Flux WF	0.666	Reject	0.707	Reject	Reject
Heat Flux NL	0.747	Reject	0.689	Reject	Reject
Heat Flux NR	0.695	Reject	0.725	Reject	Reject
in1	0.489	Reject	0.76	Reject	Reject
in2	0.342	Reject	0.789	Reject	Reject
in3	0.224	Accept	0.783	Reject	Reject
in4	0.28	Accept	0.76	Reject	Reject
in5	0.186	Accept	0.759	Reject	Reject
in6	0.413	Reject	0.725	Reject	Reject
in7	0.233	Accept	0.771	Reject	Reject
in8	0.472	Reject	0.719	Reject	Reject
nl1	0.566	Reject	0.642	Reject	Reject
nl2	0.46	Reject	0.384	Reject	Reject
ou1	0.206	Accept	0.724	Reject	Reject
ou2	0.413	Reject	0.783	Reject	Reject
ou3	0.115	Accept	0.76	Reject	Reject
ou4	0.151	Accept	0.777	Reject	Reject
ou5	0.154	Accept	0.742	Reject	Reject
ou6	0.365	Reject	0.701	Reject	Reject
ou7	0.224	Accept	0.772	Reject	Reject
ou8	0.202	Accept	0.718	Reject	Reject
nr1	0.542	Reject	0.343	Reject	Reject
nr2	0.265	Accept	0.713	Reject	Reject

Table A.9 Kolmogorov-Smirnov hypothesis tests for Depressions (defect 8). n_8=82. n_g =391. $d_c(82)$=0.15. α=0.05. $\Delta_{0.95}$=0.243. $\Delta_{0.5}$=0.144.

Variable	D_{μ_8}	$H_0(\mu_8)$	$D_{\sigma_8^2}$	$H_0(\sigma_8^2)$	$H_0(\mu_8) \cup H_0(\sigma_8^2)$
in1u	0.171	Reject	0.0953	Accept	Reject
in1l	0.109	Accept	0.0691	Accept	Accept
in2u	0.165	Reject	0.089	Accept	Reject
in2l	0.118	Accept	0.107	Accept	Accept
in3u	0.194	Reject	0.0994	Accept	Reject
in3l	0.121	Accept	0.132	Accept	Accept
in4u	0.159	Reject	0.151	Reject	Reject
in4l	0.0873	Accept	0.107	Accept	Accept
in5u	0.0679	Accept	0.15	Accept	Accept
in5l	0.0871	Accept	0.183	Reject	Reject
in6u	0.0719	Accept	0.118	Accept	Accept
in6l	0.108	Accept	0.151	Reject	Reject
in7u	0.185	Reject	0.143	Accept	Reject
in7l	0.148	Accept	0.189	Reject	Reject
in8u	0.154	Reject	0.056	Accept	Reject
in8l	0.177	Reject	0.0876	Accept	Reject
nl1u	0.176	Reject	0.169	Reject	Reject
nl1l	0.164	Reject	0.066	Accept	Reject
nl2u	0.23	Reject	0.0641	Accept	Reject
nl2l	0.2	Reject	0.148	Accept	Reject
ou1u	0.142	Accept	0.123	Accept	Accept
ou1l	0.1	Accept	0.068	Accept	Accept
ou2u	0.14	Accept	0.118	Accept	Accept
ou2l	0.134	Accept	0.133	Accept	Accept
ou3u	0.21	Reject	0.146	Accept	Reject
ou3l	0.242	Reject	0.183	Reject	Reject
ou4u	0.09	Accept	0.126	Accept	Accept
ou4l	0.166	Reject	0.151	Reject	Reject
ou5u	0.141	Accept	0.123	Accept	Accept
ou5l	0.168	Reject	0.182	Reject	Reject
ou6u	0.264	Reject	0.217	Reject	Reject
ou6l	0.247	Reject	0.215	Reject	Reject
ou7u	0.222	Reject	0.0898	Accept	Reject
ou7l	0.168	Reject	0.19	Reject	Reject
ou8u	0.231	Reject	0.182	Reject	Reject
ou8l	0.134	Accept	0.127	Accept	Accept
nr1u	0.161	Reject	0.0855	Accept	Reject
nr1l	0.133	Accept	0.0743	Accept	Accept
nr2u	0.119	Accept	0.0827	Accept	Accept
nr2l	0.151	Reject	0.152	Reject	Reject
Casting Speed	0.196	Reject	0.0735	Accept	Reject
Mould Controller Status	0.0575	Accept	0.0496	Accept	Accept
Mould level	0.0934	Accept	0.0794	Accept	Accept
Inlet Temperature	0.129	Accept	0.187	Reject	Reject
Flowrate WL	0.0876	Accept	0.0943	Accept	Accept
Flowrate WF	0.12	Accept	0.0625	Accept	Accept
Flowrate NL	0.124	Accept	0.14	Accept	Accept
Flowrate NR	0.0891	Accept	0.131	Accept	Accept
Delta T WL	0.228	Reject	0.115	Accept	Reject
Delta T WF	0.274	Reject	0.155	Reject	Reject
Delta T NL	0.152	Reject	0.12	Accept	Reject
Delta T NR	0.162	Reject	0.114	Accept	Reject
Oscillation Frequency	0.2	Reject	0.171	Reject	Reject
Drive Current	0.145	Accept	0.0964	Accept	Accept
Heat Flux WL	0.158	Reject	0.178	Reject	Reject
Heat Flux WF	0.185	Reject	0.166	Reject	Reject
Heat Flux NL	0.152	Reject	0.117	Accept	Reject
Heat Flux NR	0.162	Reject	0.113	Accept	Reject
in1	0.268	Reject	0.0887	Accept	Reject
in2	0.26	Reject	0.0968	Accept	Reject
in3	0.19	Reject	0.122	Accept	Reject
in4	0.116	Accept	0.127	Accept	Accept
in5	0.203	Reject	0.183	Reject	Reject
in6	0.194	Reject	0.179	Reject	Reject
in7	0.105	Accept	0.148	Accept	Accept
in8	0.174	Reject	0.046	Accept	Reject
nl1	0.206	Reject	0.108	Accept	Reject
nl2	0.191	Reject	0.0967	Accept	Reject
ou1	0.185	Reject	0.0969	Accept	Reject
ou2	0.145	Accept	0.151	Reject	Reject
ou3	0.117	Accept	0.15	Accept	Accept
ou4	0.116	Accept	0.148	Accept	Accept
ou5	0.0968	Accept	0.148	Accept	Accept
ou6	0.175	Reject	0.211	Reject	Reject
ou7	0.0882	Accept	0.169	Reject	Reject
ou8	0.24	Reject	0.139	Accept	Reject
nr1	0.24	Reject	0.118	Accept	Reject
nr2	0.136	Accept	0.118	Accept	Accept

Appendix B

Anderson-Darling tables

Table B.1 Anderson-Darling hypothesis tests for Transversal Cracks (defect 1a). n_{1a}=1. n_g =70. $a_c^2(1)$=2.492. α=0.05.

Variable	$A^2_{\mu_{1a}}$	$H_0(\mu_{1a})$	$A^2_{\sigma^2_{1a}}$	$H_0(\sigma^2_{1a})$	$H_0(\mu_{1a}) \cup H_0(\sigma^2_{1a})$
in1u	0.44	Accept	1.29	Accept	Accept
in1l	0.833	Accept	1.02	Accept	Accept
in2u	0.427	Accept	1.71	Accept	Accept
in2l	2.58	Reject	1.41	Accept	Reject
in3u	0.399	Accept	1.55	Accept	Accept
in3l	1.55	Accept	1.71	Accept	Accept
in4u	0.39	Accept	1.29	Accept	Accept
in4l	0.39	Accept	1.92	Accept	Accept
in5u	0.394	Accept	1.71	Accept	Accept
in5l	0.889	Accept	1.55	Accept	Accept
in6u	0.655	Accept	0.833	Accept	Accept
in6l	0.833	Accept	1.55	Accept	Accept
in7u	0.407	Accept	1.29	Accept	Accept
in7l	0.889	Accept	1.41	Accept	Accept
in8u	1.41	Accept	1.55	Accept	Accept
in8l	3.26	Reject	1.92	Accept	Reject
nl1u	0.455	Accept	1.19	Accept	Accept
nl1l	0.589	Accept	1.02	Accept	Accept
nl2u	0.394	Accept	1.55	Accept	Accept
nl2l	0.44	Accept	1.55	Accept	Accept
ou1u	1.02	Accept	1.71	Accept	Accept
ou1l	0.39	Accept	1.92	Accept	Accept
ou2u	0.782	Accept	0.833	Accept	Accept
ou2l	1.29	Accept	1.41	Accept	Accept
ou3u	0.655	Accept	1.1	Accept	Accept
ou3l	1.19	Accept	1.71	Accept	Accept
ou4u	0.833	Accept	1.1	Accept	Accept
ou4l	0.655	Accept	1.29	Accept	Accept
ou5u	0.427	Accept	1.41	Accept	Accept
ou5l	0.655	Accept	2.58	Reject	Reject
ou6u	0.427	Accept	1.41	Accept	Accept
ou6l	0.833	Accept	1.92	Accept	Accept
ou7u	0.693	Accept	0.621	Accept	Accept
ou7l	0.952	Accept	1.41	Accept	Accept
ou8u	1.19	Accept	1.02	Accept	Accept
ou8l	0.427	Accept	1.55	Accept	Accept
nr1u	2.58	Reject	1.55	Accept	Reject
nr1l	∞	Reject	0.621	Accept	Reject
nr2u	3.26	Reject	1.29	Accept	Reject
nr2l	3.26	Reject	0.889	Accept	Reject
Casting Speed	2.58	Reject	1.92	Accept	Reject
Mould Controller Status	1.92	Accept	1.92	Accept	Accept
Mould level	2.58	Reject	2.58	Reject	Reject
Inlet Temperature	1.29	Accept	0.416	Accept	Accept
Flowrate WL	0.655	Accept	0.386	Accept	Accept
Flowrate WF	1.29	Accept	0.561	Accept	Accept
Flowrate NL	0.394	Accept	0.511	Accept	Accept
Flowrate NR	1.02	Accept	0.833	Accept	Accept
Delta T WL	0.952	Accept	1.71	Accept	Accept
Delta T WF	0.952	Accept	1.71	Accept	Accept
Delta T NL	2.19	Accept	1.55	Accept	Accept
Delta T NR	1.29	Accept	1.29	Accept	Accept
Oscillation Frequency	3.26	Reject	1.92	Accept	Reject
Drive Current	0.735	Accept	3.26	Reject	Reject
Heat Flux WL	0.952	Accept	1.71	Accept	Accept
Heat Flux WF	0.952	Accept	1.55	Accept	Accept
Heat Flux NL	2.19	Accept	1.55	Accept	Accept
Heat Flux NR	1.29	Accept	1.29	Accept	Accept
in1	3.26	Reject	2.19	Accept	Reject
in2	3.26	Reject	2.58	Reject	Reject
in3	26.6	Reject	2.19	Accept	Reject
in4	0.561	Accept	2.58	Reject	Reject
in5	1.19	Accept	1.92	Accept	Accept
in6	26.6	Reject	2.19	Accept	Reject
in7	2.58	Reject	2.19	Accept	Reject
in8	26.6	Reject	1.92	Accept	Reject
nl1	0.416	Accept	0.407	Accept	Accept
nl2	0.394	Accept	0.693	Accept	Accept
ou1	2.19	Accept	1.1	Accept	Accept
ou2	26.6	Reject	1.41	Accept	Reject
ou3	26.6	Reject	1.55	Accept	Reject
ou4	26.6	Reject	1.71	Accept	Reject
ou5	1.29	Accept	2.19	Accept	Accept
ou6	0.386	Accept	2.19	Accept	Accept
ou7	26.6	Reject	1.92	Accept	Reject
ou8	2.58	Reject	0.889	Accept	Reject
nr1	0.833	Accept	0.889	Accept	Accept
nr2	0.44	Accept	0.44	Accept	Accept

Table B.2 Anderson-Darling hypothesis tests for Longitudinal Cracks (defect 1b). n_{1b}=3. n_g =114. $a_c^2(3)$=2.492. α=0.05.

Variable	$A^2_{\mu_{1b}}$	$H_0(\mu_{1b})$	$A^2_{\sigma^2_{1b}}$	$H_0(\sigma^2_{1b})$	$H_0(\mu_{1b}) \cup H_0(\sigma^2_{1b})$
in1u	0.818	Accept	0.556	Accept	Accept
in1l	∞	Reject	0.419	Accept	Reject
in2u	0.858	Accept	0.423	Accept	Accept
in2l	0.537	Accept	0.534	Accept	Accept
in3u	1.14	Accept	1.36	Accept	Accept
in3l	1.08	Accept	0.704	Accept	Accept
in4u	0.66	Accept	1.28	Accept	Accept
in4l	0.865	Accept	0.52	Accept	Accept
in5u	0.357	Accept	0.813	Accept	Accept
in5l	0.989	Accept	0.581	Accept	Accept
in6u	1.46	Accept	0.644	Accept	Accept
in6l	0.582	Accept	0.505	Accept	Accept
in7u	0.474	Accept	0.31	Accept	Accept
in7l	0.347	Accept	0.426	Accept	Accept
in8u	∞	Reject	0.93	Accept	Reject
in8l	∞	Reject	0.273	Accept	Reject
nl1u	0.718	Accept	0.559	Accept	Accept
nl1l	1.1	Accept	0.883	Accept	Accept
nl2u	0.456	Accept	0.829	Accept	Accept
nl2l	1	Accept	1.06	Accept	Accept
ou1u	0.875	Accept	0.642	Accept	Accept
ou1l	0.302	Accept	0.542	Accept	Accept
ou2u	1.94	Accept	0.672	Accept	Accept
ou2l	0.731	Accept	0.258	Accept	Accept
ou3u	1.35	Accept	1.05	Accept	Accept
ou3l	1.12	Accept	0.796	Accept	Accept
ou4u	1.78	Accept	0.379	Accept	Accept
ou4l	0.725	Accept	0.436	Accept	Accept
ou5u	0.441	Accept	0.258	Accept	Accept
ou5l	0.642	Accept	0.302	Accept	Accept
ou6u	0.872	Accept	0.89	Accept	Accept
ou6l	1.89	Accept	0.7	Accept	Accept
ou7u	1.01	Accept	0.965	Accept	Accept
ou7l	0.57	Accept	0.416	Accept	Accept
ou8u	1.57	Accept	0.951	Accept	Accept
ou8l	0.525	Accept	0.409	Accept	Accept
nr1u	1.39	Accept	0.404	Accept	Accept
nr1l	∞	Reject	0.266	Accept	Reject
nr2u	∞	Reject	0.502	Accept	Reject
nr2l	∞	Reject	0.671	Accept	Reject
Casting Speed	1.25	Accept	0.75	Accept	Accept
Mould Controller Status	4.25	Reject	1.49	Accept	Reject
Mould level	0.695	Accept	0.492	Accept	Accept
Inlet Temperature	1.49	Accept	1.84	Accept	Accept
Flowrate WL	0.411	Accept	1.01	Accept	Accept
Flowrate WF	0.953	Accept	0.91	Accept	Accept
Flowrate NL	0.353	Accept	0.356	Accept	Accept
Flowrate NR	0.385	Accept	0.884	Accept	Accept
Delta T WL	0.343	Accept	1.43	Accept	Accept
Delta T WF	0.627	Accept	0.381	Accept	Accept
Delta T NL	1.24	Accept	0.848	Accept	Accept
Delta T NR	1.11	Accept	0.678	Accept	Accept
Oscillation Frequency	1.06	Accept	0.627	Accept	Accept
Drive Current	3.63	Reject	1.33	Accept	Reject
Heat Flux WL	0.813	Accept	1.41	Accept	Accept
Heat Flux WF	1.57	Accept	0.389	Accept	Accept
Heat Flux NL	1.24	Accept	0.928	Accept	Accept
Heat Flux NR	1.11	Accept	0.73	Accept	Accept
in1	0.901	Accept	0.731	Accept	Accept
in2	8.57	Reject	0.658	Accept	Reject
in3	8.63	Reject	1.1	Accept	Reject
in4	1.34	Accept	0.904	Accept	Accept
in5	1.08	Accept	0.684	Accept	Accept
in6	11.9	Reject	0.8	Accept	Reject
in7	9.37	Reject	0.496	Accept	Reject
in8	8.68	Reject	0.484	Accept	Reject
nl1	∞	Reject	0.514	Accept	Reject
nl2	0.997	Accept	0.332	Accept	Accept
ou1	9.08	Reject	0.546	Accept	Reject
ou2	8.59	Reject	0.229	Accept	Reject
ou3	11.9	Reject	0.501	Accept	Reject
ou4	4.24	Reject	0.711	Accept	Reject
ou5	1.82	Accept	0.391	Accept	Accept
ou6	0.626	Accept	0.722	Accept	Accept
ou7	9.41	Reject	0.436	Accept	Reject
ou8	8.83	Reject	0.758	Accept	Reject
nr1	0.949	Accept	0.299	Accept	Accept
nr2	0.315	Accept	0.738	Accept	Accept

Table B.3 Anderson-Darling hypothesis tests for Casting Powder Entrapment (defect 2a). n_{2a}=4. n_g =83. $a_c^2(4)$=2.492. α=0.05.

Variable	$A^2_{\mu_{2a}}$	$H_0(\mu_{2a})$	$A^2_{\sigma^2_{2a}}$	$H_0(\sigma^2_{2a})$	$H_0(\mu_{2a}) \cup H_0(\sigma^2_{2a})$
in1u	2.87	Reject	0.65	Accept	Reject
in1l	0.879	Accept	1.01	Accept	Accept
in2u	3.14	Reject	0.808	Accept	Reject
in2l	0.601	Accept	0.869	Accept	Accept
in3u	1.87	Accept	0.848	Accept	Accept
in3l	0.181	Accept	2.6	Reject	Reject
in4u	0.945	Accept	1.95	Accept	Accept
in4l	1.32	Accept	2.3	Accept	Accept
in5u	0.822	Accept	1.68	Accept	Accept
in5l	0.663	Accept	4.13	Reject	Reject
in6u	1.52	Accept	0.593	Accept	Accept
in6l	0.584	Accept	7.93	Reject	Reject
in7u	1.53	Accept	1.27	Accept	Accept
in7l	0.37	Accept	2.39	Accept	Accept
in8u	∞	Reject	0.99	Accept	Reject
in8l	∞	Reject	1.73	Accept	Reject
nl1u	0.801	Accept	0.515	Accept	Accept
nl1l	0.308	Accept	1.03	Accept	Accept
nl2u	1.03	Accept	0.518	Accept	Accept
nl2l	1.1	Accept	0.568	Accept	Accept
ou1u	3.35	Reject	0.91	Accept	Reject
ou1l	1.77	Accept	0.873	Accept	Accept
ou2u	2.34	Accept	1	Accept	Accept
ou2l	∞	Reject	0.993	Accept	Reject
ou3u	0.405	Accept	1.52	Accept	Accept
ou3l	7.67	Reject	0.969	Accept	Reject
ou4u	0.581	Accept	1.12	Accept	Accept
ou4l	7.21	Reject	1.74	Accept	Reject
ou5u	∞	Reject	1.86	Accept	Reject
ou5l	7.82	Reject	2.42	Accept	Reject
ou6u	0.539	Accept	1.03	Accept	Accept
ou6l	0.625	Accept	0.873	Accept	Accept
ou7u	8.46	Reject	0.437	Accept	Reject
ou7l	0.589	Accept	0.744	Accept	Accept
ou8u	2.06	Accept	0.924	Accept	Accept
ou8l	0.714	Accept	1.86	Accept	Accept
nr1u	∞	Reject	1.06	Accept	Reject
nr1l	∞	Reject	1.28	Accept	Reject
nr2u	1.56	Accept	1.17	Accept	Accept
nr2l	1.63	Accept	1.26	Accept	Accept
Casting Speed	8.55	Reject	0.879	Accept	Reject
Mould Controller Status	6.8	Reject	2.09	Accept	Reject
Mould level	1.32	Accept	0.564	Accept	Accept
Inlet Temperature	1.61	Accept	1.38	Accept	Accept
Flowrate WL	1	Accept	0.34	Accept	Accept
Flowrate WF	1.28	Accept	1.77	Accept	Accept
Flowrate NL	1.38	Accept	0.845	Accept	Accept
Flowrate NR	0.495	Accept	1.54	Accept	Accept
Delta T WL	2.07	Accept	0.316	Accept	Accept
Delta T WF	1.56	Accept	0.407	Accept	Accept
Delta T NL	1.73	Accept	1.12	Accept	Accept
Delta T NR	2.2	Accept	0.806	Accept	Accept
Oscillation Frequency	8.55	Reject	1.44	Accept	Reject
Drive Current	0.43	Accept	1.44	Accept	Accept
Heat Flux WL	2.07	Accept	0.327	Accept	Accept
Heat Flux WF	1.55	Accept	0.483	Accept	Accept
Heat Flux NL	1.73	Accept	1.12	Accept	Accept
Heat Flux NR	2.2	Accept	0.826	Accept	Accept
in1	∞	Reject	1.51	Accept	Reject
in2	0.649	Accept	1.19	Accept	Accept
in3	0.315	Accept	8.39	Reject	Reject
in4	1.58	Accept	9.05	Reject	Reject
in5	1.97	Accept	9.98	Reject	Reject
in6	2.08	Accept	9.6	Reject	Reject
in7	2.23	Accept	3.32	Reject	Reject
in8	1.52	Accept	1.67	Accept	Accept
nl1	1.05	Accept	0.361	Accept	Accept
nl2	0.874	Accept	1.35	Accept	Accept
ou1	1.87	Accept	1.28	Accept	Accept
ou2	6.44	Reject	2.06	Accept	Reject
ou3	7.95	Reject	1.54	Accept	Reject
ou4	8.12	Reject	1.09	Accept	Reject
ou5	7.72	Reject	2.61	Reject	Reject
ou6	7.47	Reject	2.88	Reject	Reject
ou7	0.948	Accept	1.71	Accept	Accept
ou8	1.01	Accept	3.03	Reject	Reject
nr1	0.833	Accept	0.337	Accept	Accept
nr2	1.2	Accept	1.42	Accept	Accept

Table B.4 Anderson-Darling hypothesis tests for Other Inclusions (defect 2b). n_{2b}=114. n_g =364. $a_c^2(114)$=2.492. α=0.05.

Variable	$A^2_{\mu_{2b}}$	$H_0(\mu_{2b})$	$A^2_{\sigma^2_{2b}}$	$H_0(\sigma^2_{2b})$	$H_0(\mu_{2b}) \cup H_0(\sigma^2_{2b})$
in1u	4.28	Reject	0.629	Accept	Reject
in1l	1.95	Accept	0.791	Accept	Accept
in2u	∞	Reject	∞	Reject	Reject
in2l	∞	Reject	2.67	Reject	Reject
in3u	9.62	Reject	∞	Reject	Reject
in3l	∞	Reject	∞	Reject	Reject
in4u	∞	Reject	6.33	Reject	Reject
in4l	∞	Reject	5.47	Reject	Reject
in5u	2.34	Accept	7.86	Reject	Reject
in5l	0.652	Accept	6.76	Reject	Reject
in6u	1.67	Accept	4.63	Reject	Reject
in6l	∞	Reject	6.72	Reject	Reject
in7u	7.94	Reject	∞	Reject	Reject
in7l	5.38	Reject	∞	Reject	Reject
in8u	3.9	Reject	0.306	Accept	Reject
in8l	3.6	Reject	0.995	Accept	Reject
nl1u	15.7	Reject	5.06	Reject	Reject
nl1l	15.5	Reject	1.59	Accept	Reject
nl2u	22.8	Reject	1.26	Accept	Reject
nl2l	13.7	Reject	3.94	Reject	Reject
ou1u	5.99	Reject	3.39	Reject	Reject
ou1l	4.82	Reject	1.35	Accept	Reject
ou2u	∞	Reject	2.9	Reject	Reject
ou2l	∞	Reject	1.07	Accept	Reject
ou3u	∞	Reject	1.98	Accept	Reject
ou3l	∞	Reject	3.14	Reject	Reject
ou4u	∞	Reject	6.66	Reject	Reject
ou4l	∞	Reject	6.28	Reject	Reject
ou5u	∞	Reject	2.07	Accept	Reject
ou5l	11.3	Reject	6.9	Reject	Reject
ou6u	32.7	Reject	14	Reject	Reject
ou6l	21.3	Reject	15.6	Reject	Reject
ou7u	∞	Reject	∞	Reject	Reject
ou7l	∞	Reject	∞	Reject	Reject
ou8u	14.5	Reject	2.39	Accept	Reject
ou8l	6.94	Reject	0.757	Accept	Reject
nr1u	8.74	Reject	2.84	Reject	Reject
nr1l	1.8	Accept	∞	Reject	Reject
nr2u	0.772	Accept	∞	Reject	Reject
nr2l	2.32	Accept	∞	Reject	Reject
Casting Speed	∞	Reject	2.09	Accept	Reject
Mould Controller Status	1.62e+003	Reject	90.1	Reject	Reject
Mould level	2.68	Reject	1.09	Accept	Reject
Inlet Temperature	1.8	Accept	3.75	Reject	Reject
Flowrate WL	0.424	Accept	0.988	Accept	Accept
Flowrate WF	2.32	Accept	6.62	Reject	Reject
Flowrate NL	2.03	Accept	1.55	Accept	Accept
Flowrate NR	0.945	Accept	0.406	Accept	Accept
Delta T WL	4.76	Reject	4.65	Reject	Reject
Delta T WF	12.8	Reject	2.93	Reject	Reject
Delta T NL	2.18	Accept	2.77	Reject	Reject
Delta T NR	1.67	Accept	2.27	Accept	Accept
Oscillation Frequency	∞	Reject	19.3	Reject	Reject
Drive Current	1.52	Accept	∞	Reject	Reject
Heat Flux WL	4.82	Reject	6.2	Reject	Reject
Heat Flux WF	5.7	Reject	4.13	Reject	Reject
Heat Flux NL	2.2	Accept	2.79	Reject	Reject
Heat Flux NR	1.66	Accept	2.24	Accept	Accept
in1	∞	Reject	0.69	Accept	Reject
in2	6.44	Reject	1.99	Accept	Reject
in3	∞	Reject	2.06	Accept	Reject
in4	7.21	Reject	∞	Reject	Reject
in5	5.29	Reject	6.72	Reject	Reject
in6	18.8	Reject	5.16	Reject	Reject
in7	3.2	Reject	3.61	Reject	Reject
in8	2.01	Accept	0.855	Accept	Accept
nl1	∞	Reject	1.47	Accept	Reject
nl2	∞	Reject	0.324	Accept	Reject
ou1	1.53	Accept	1.07	Accept	Accept
ou2	2.2	Accept	1.17	Accept	Accept
ou3	3.81	Reject	1.24	Accept	Reject
ou4	9.08	Reject	4.62	Reject	Reject
ou5	5.86	Reject	∞	Reject	Reject
ou6	12.8	Reject	11.7	Reject	Reject
ou7	2.24	Accept	2.72	Reject	Reject
ou8	4.09	Reject	1.12	Accept	Reject
nr1	16.2	Reject	3.23	Reject	Reject
nr2	3.24	Reject	∞	Reject	Reject

Table B.5 Anderson-Darling hypothesis tests for Bleeders (defect 4). n_4=3. n_g =175. $a_c^2(3)$=2.492. α=0.05.

Variable	$A^2_{\mu_4}$	$H_0(\mu_4)$	$A^2_{\sigma_4^2}$	$H_0(\sigma_4^2)$	$H_0(\mu_4) \cup H_0(\sigma_4^2)$
in1u	0.635	Accept	0.249	Accept	Accept
in1l	0.613	Accept	0.425	Accept	Accept
in2u	0.558	Accept	0.865	Accept	Accept
in2l	0.318	Accept	0.574	Accept	Accept
in3u	0.396	Accept	0.99	Accept	Accept
in3l	0.797	Accept	1.79	Accept	Accept
in4u	0.626	Accept	0.518	Accept	Accept
in4l	0.687	Accept	1.05	Accept	Accept
in5u	0.583	Accept	0.301	Accept	Accept
in5l	0.268	Accept	0.454	Accept	Accept
in6u	0.862	Accept	0.626	Accept	Accept
in6l	1.07	Accept	0.625	Accept	Accept
in7u	0.396	Accept	0.547	Accept	Accept
in7l	0.533	Accept	0.756	Accept	Accept
in8u	0.429	Accept	0.615	Accept	Accept
in8l	0.295	Accept	1.78	Accept	Accept
nl1u	1.52	Accept	1.59	Accept	Accept
nl1l	1.25	Accept	0.779	Accept	Accept
nl2u	1.74	Accept	0.694	Accept	Accept
nl2l	2.1	Accept	0.748	Accept	Accept
ou1u	0.353	Accept	0.84	Accept	Accept
ou1l	0.279	Accept	0.312	Accept	Accept
ou2u	0.324	Accept	0.648	Accept	Accept
ou2l	0.442	Accept	1.09	Accept	Accept
ou3u	0.51	Accept	0.506	Accept	Accept
ou3l	0.492	Accept	1.17	Accept	Accept
ou4u	1.08	Accept	0.343	Accept	Accept
ou4l	0.842	Accept	0.397	Accept	Accept
ou5u	0.618	Accept	0.75	Accept	Accept
ou5l	0.606	Accept	1.51	Accept	Accept
ou6u	0.697	Accept	1.26	Accept	Accept
ou6l	0.912	Accept	2.92	Reject	Reject
ou7u	0.468	Accept	0.314	Accept	Accept
ou7l	0.336	Accept	0.487	Accept	Accept
ou8u	0.304	Accept	0.524	Accept	Accept
ou8l	0.427	Accept	0.51	Accept	Accept
nr1u	0.584	Accept	1.46	Accept	Accept
nr1l	0.64	Accept	1.16	Accept	Accept
nr2u	0.618	Accept	0.461	Accept	Accept
nr2l	0.582	Accept	0.56	Accept	Accept
Casting Speed	1.24	Accept	0.861	Accept	Accept
Mould Controller Status	4.81	Reject	1.92	Accept	Reject
Mould level	0.49	Accept	0.677	Accept	Accept
Inlet Temperature	0.353	Accept	0.768	Accept	Accept
Flowrate WL	0.411	Accept	1.65	Accept	Accept
Flowrate WF	0.727	Accept	0.507	Accept	Accept
Flowrate NL	0.746	Accept	0.373	Accept	Accept
Flowrate NR	0.671	Accept	0.821	Accept	Accept
Delta T WL	0.794	Accept	0.785	Accept	Accept
Delta T WF	1.07	Accept	0.539	Accept	Accept
Delta T NL	1.38	Accept	0.395	Accept	Accept
Delta T NR	0.78	Accept	0.662	Accept	Accept
Oscillation Frequency	1.75	Accept	0.613	Accept	Accept
Drive Current	0.436	Accept	0.726	Accept	Accept
Heat Flux WL	1.05	Accept	0.719	Accept	Accept
Heat Flux WF	1.39	Accept	0.521	Accept	Accept
Heat Flux NL	1.38	Accept	0.394	Accept	Accept
Heat Flux NR	0.78	Accept	0.671	Accept	Accept
in1	0.265	Accept	0.316	Accept	Accept
in2	1.16	Accept	0.599	Accept	Accept
in3	0.401	Accept	1.5	Accept	Accept
in4	0.891	Accept	1.21	Accept	Accept
in5	0.289	Accept	0.496	Accept	Accept
in6	0.704	Accept	0.621	Accept	Accept
in7	0.269	Accept	1.23	Accept	Accept
in8	1.12	Accept	1.18	Accept	Accept
nl1	0.434	Accept	0.916	Accept	Accept
nl2	1.13	Accept	0.875	Accept	Accept
ou1	0.981	Accept	0.413	Accept	Accept
ou2	0.432	Accept	1.14	Accept	Accept
ou3	0.279	Accept	0.832	Accept	Accept
ou4	0.647	Accept	0.466	Accept	Accept
ou5	0.514	Accept	1.26	Accept	Accept
ou6	0.933	Accept	3.68	Reject	Reject
ou7	0.375	Accept	0.393	Accept	Accept
ou8	0.502	Accept	0.409	Accept	Accept
nr1	0.835	Accept	0.817	Accept	Accept
nr2	1.03	Accept	0.448	Accept	Accept

Table B.6 Anderson-Darling hypothesis tests for Deep Oscillation Marks (defect 5a). n_{5a}=8. n_g =354. $a_c^2(8)$=2.492. α=0.05.

Variable	$A^2_{\mu_{5a}}$	$H_0(\mu_{5a})$	$A^2_{\sigma^2_{5a}}$	$H_0(\sigma^2_{5a})$	$H_0(\mu_{5a}) \cup H_0(\sigma^2_{5a})$
in1u	0.692	Accept	2.87	Reject	Reject
in1l	0.43	Accept	4.12	Reject	Reject
in2u	0.853	Accept	1.3	Accept	Accept
in2l	1.67	Accept	0.972	Accept	Accept
in3u	0.282	Accept	2.14	Accept	Accept
in3l	0.43	Accept	1.49	Accept	Accept
in4u	0.874	Accept	1.48	Accept	Accept
in4l	0.44	Accept	1.8	Accept	Accept
in5u	0.935	Accept	1.78	Accept	Accept
in5l	0.682	Accept	1.82	Accept	Accept
in6u	0.97	Accept	1.62	Accept	Accept
in6l	1.39	Accept	1.96	Accept	Accept
in7u	1.04	Accept	1.29	Accept	Accept
in7l	0.479	Accept	2.3	Accept	Accept
in8u	1.15	Accept	0.771	Accept	Accept
in8l	1.31	Accept	1.49	Accept	Accept
nl1u	1.71	Accept	2.09	Accept	Accept
nl1l	1.13	Accept	2.08	Accept	Accept
nl2u	0.796	Accept	0.772	Accept	Accept
nl2l	1.05	Accept	2.64	Reject	Reject
ou1u	0.814	Accept	0.6	Accept	Accept
ou1l	0.683	Accept	0.468	Accept	Accept
ou2u	0.328	Accept	1.25	Accept	Accept
ou2l	0.428	Accept	2.15	Accept	Accept
ou3u	0.764	Accept	1.72	Accept	Accept
ou3l	0.806	Accept	2.26	Accept	Accept
ou4u	1.27	Accept	2.51	Reject	Reject
ou4l	0.791	Accept	2.06	Accept	Accept
ou5u	1.37	Accept	1.36	Accept	Accept
ou5l	1.8	Accept	1.25	Accept	Accept
ou6u	1.62	Accept	1.98	Accept	Accept
ou6l	1.38	Accept	4.57	Reject	Reject
ou7u	0.713	Accept	2.06	Accept	Accept
ou7l	0.694	Accept	1.87	Accept	Accept
ou8u	1.42	Accept	1.24	Accept	Accept
ou8l	1.3	Accept	1.22	Accept	Accept
nr1u	2.18	Accept	0.609	Accept	Accept
nr1l	2.19	Accept	0.983	Accept	Accept
nr2u	1.74	Accept	0.531	Accept	Accept
nr2l	2.8	Reject	0.764	Accept	Reject
Casting Speed	0.921	Accept	0.973	Accept	Accept
Mould Controller Status	13.1	Reject	5.7	Reject	Reject
Mould level	0.908	Accept	0.998	Accept	Accept
Inlet Temperature	0.376	Accept	0.431	Accept	Accept
Flowrate WL	0.311	Accept	1.78	Accept	Accept
Flowrate WF	1.37	Accept	0.993	Accept	Accept
Flowrate NL	4.11	Reject	0.37	Accept	Reject
Flowrate NR	2.75	Reject	0.939	Accept	Reject
Delta T WL	2.16	Accept	1.88	Accept	Accept
Delta T WF	3.64	Reject	1.48	Accept	Reject
Delta T NL	3.83	Reject	1.26	Accept	Reject
Delta T NR	3.49	Reject	1.27	Accept	Reject
Oscillation Frequency	1.02	Accept	2.16	Accept	Accept
Drive Current	0.72	Accept	1.35	Accept	Accept
Heat Flux WL	4.13	Reject	2.07	Accept	Reject
Heat Flux WF	5.32	Reject	1.43	Accept	Reject
Heat Flux NL	3.83	Reject	1.09	Accept	Reject
Heat Flux NR	3.5	Reject	1.23	Accept	Reject
in1	1.23	Accept	4.31	Reject	Reject
in2	1.34	Accept	1.98	Accept	Accept
in3	0.889	Accept	4.15	Reject	Reject
in4	1.13	Accept	2.01	Accept	Accept
in5	0.409	Accept	2.98	Reject	Reject
in6	0.61	Accept	3.09	Reject	Reject
in7	1.08	Accept	2.43	Accept	Accept
in8	0.407	Accept	2.17	Accept	Accept
nl1	1.96	Accept	4.81	Reject	Reject
nl2	1.9	Accept	0.925	Accept	Accept
ou1	0.651	Accept	0.759	Accept	Accept
ou2	0.404	Accept	2.39	Accept	Accept
ou3	0.835	Accept	2.31	Accept	Accept
ou4	1.97	Accept	1.49	Accept	Accept
ou5	0.446	Accept	1.06	Accept	Accept
ou6	1.13	Accept	2.23	Accept	Accept
ou7	0.772	Accept	5.7	Reject	Reject
ou8	0.57	Accept	3.26	Reject	Reject
nr1	3.17	Reject	0.849	Accept	Reject
nr2	3.57	Reject	1.2	Accept	Reject

Table B.7 Anderson-Darling hypothesis tests for Uneven Oscillation Marks (defect 5b). n_{5b}=5. n_g =256. $a_c^2(5)$=2.492. α=0.05.

Variable	$A^2_{\mu_{5b}}$	$H_0(\mu_{5b})$	$A^2_{\sigma^2_{5b}}$	$H_0(\sigma^2_{5b})$	$H_0(\mu_{5b}) \cup H_0(\sigma^2_{5b})$
in1u	1.99	Accept	1.01	Accept	Accept
in1l	1.12	Accept	1.08	Accept	Accept
in2u	1.84	Accept	2.29	Accept	Accept
in2l	0.886	Accept	1.7	Accept	Accept
in3u	1.84	Accept	2.45	Accept	Accept
in3l	0.467	Accept	1.48	Accept	Accept
in4u	2.23	Accept	1.83	Accept	Accept
in4l	0.9	Accept	0.675	Accept	Accept
in5u	3.2	Reject	2.15	Accept	Reject
in5l	0.482	Accept	1.45	Accept	Accept
in6u	1.85	Accept	2.38	Accept	Accept
in6l	3.34	Reject	1.29	Accept	Reject
in7u	2.38	Accept	2.44	Accept	Accept
in7l	5.72	Reject	0.828	Accept	Reject
in8u	2.14	Accept	2.57	Reject	Reject
in8l	1.55	Accept	0.649	Accept	Accept
nl1u	2.89	Reject	2.12	Accept	Reject
nl1l	3.91	Reject	1.97	Accept	Reject
nl2u	2.08	Accept	1.4	Accept	Accept
nl2l	3.04	Reject	2.04	Accept	Reject
ou1u	2.23	Accept	6.4	Reject	Reject
ou1l	2.51	Reject	1.03	Accept	Reject
ou2u	2.62	Reject	2.3	Accept	Reject
ou2l	0.575	Accept	1.41	Accept	Accept
ou3u	2.36	Accept	2.64	Reject	Reject
ou3l	0.547	Accept	2.37	Accept	Accept
ou4u	3.95	Reject	1.6	Accept	Reject
ou4l	0.697	Accept	1.71	Accept	Accept
ou5u	3.16	Reject	2.08	Accept	Reject
ou5l	0.519	Accept	2.43	Accept	Accept
ou6u	1.23	Accept	3.24	Reject	Reject
ou6l	0.827	Accept	2.74	Reject	Reject
ou7u	1.15	Accept	1.73	Accept	Accept
ou7l	0.781	Accept	0.746	Accept	Accept
ou8u	1.29	Accept	1.09	Accept	Accept
ou8l	1.45	Accept	1.63	Accept	Accept
nr1u	0.902	Accept	0.819	Accept	Accept
nr1l	2.25	Accept	0.664	Accept	Accept
nr2u	1.16	Accept	1.37	Accept	Accept
nr2l	0.913	Accept	0.819	Accept	Accept
Casting Speed	0.848	Accept	1.11	Accept	Accept
Mould Controller Status	7.13	Reject	3.3	Reject	Reject
Mould level	0.63	Accept	0.487	Accept	Accept
Inlet Temperature	0.532	Accept	6.88	Reject	Reject
Flowrate WL	0.497	Accept	2.03	Accept	Accept
Flowrate WF	3.89	Reject	2.76	Reject	Reject
Flowrate NL	3.2	Reject	0.406	Accept	Reject
Flowrate NR	0.343	Accept	0.501	Accept	Accept
Delta T WL	0.345	Accept	1.32	Accept	Accept
Delta T WF	0.497	Accept	0.553	Accept	Accept
Delta T NL	1.61	Accept	1.63	Accept	Accept
Delta T NR	1.27	Accept	1.26	Accept	Accept
Oscillation Frequency	1.49	Accept	1.1	Accept	Accept
Drive Current	1.49	Accept	0.707	Accept	Accept
Heat Flux WL	0.786	Accept	1.34	Accept	Accept
Heat Flux WF	0.897	Accept	0.502	Accept	Accept
Heat Flux NL	1.6	Accept	1.59	Accept	Accept
Heat Flux NR	1.27	Accept	1.23	Accept	Accept
in1	1.38	Accept	0.76	Accept	Accept
in2	1.38	Accept	1.55	Accept	Accept
in3	1.66	Accept	1.47	Accept	Accept
in4	2.58	Reject	0.813	Accept	Reject
in5	6.17	Reject	1.72	Accept	Reject
in6	∞	Reject	2.01	Accept	Reject
in7	1.31	Accept	2.2	Accept	Accept
in8	1.92	Accept	1.88	Accept	Accept
nl1	0.872	Accept	3.46	Reject	Reject
nl2	1.77	Accept	3.68	Reject	Reject
ou1	1.42	Accept	0.92	Accept	Accept
ou2	3.27	Reject	1.37	Accept	Reject
ou3	4.25	Reject	0.805	Accept	Reject
ou4	3.21	Reject	1.57	Accept	Reject
ou5	5.29	Reject	1.51	Accept	Reject
ou6	2.51	Reject	7.54	Reject	Reject
ou7	0.388	Accept	0.918	Accept	Accept
ou8	0.572	Accept	0.709	Accept	Accept
nr1	1.97	Accept	0.779	Accept	Accept
nr2	0.45	Accept	1.46	Accept	Accept

Table B.8 Anderson-Darling hypothesis tests for Stopmarks (defect 6). n_6=19. n_g =170. $a_c^2(19)$=2.492. α=0.05.

Variable	$A^2_{\mu_6}$	$H_0(\mu_6)$	$A^2_{\sigma_6^2}$	$H_0(\sigma_6^2)$	$H_0(\mu_6) \cup H_0(\sigma_6^2)$
in1u	2.12	Accept	32.3	Reject	Reject
in1l	5.03	Reject	21.6	Reject	Reject
in2u	5.3	Reject	38.5	Reject	Reject
in2l	9.97	Reject	27	Reject	Reject
in3u	4.34	Reject	32.5	Reject	Reject
in3l	4.73	Reject	35.6	Reject	Reject
in4u	5.16	Reject	31.9	Reject	Reject
in4l	1.46	Accept	44	Reject	Reject
in5u	4.39	Reject	30.6	Reject	Reject
in5l	2.8	Reject	52.7	Reject	Reject
in6u	6.64	Reject	28	Reject	Reject
in6l	∞	Reject	18.8	Reject	Reject
in7u	8.35	Reject	31.1	Reject	Reject
in7l	10.6	Reject	30.5	Reject	Reject
in8u	6.72	Reject	25.8	Reject	Reject
in8l	13.5	Reject	17.6	Reject	Reject
nl1u	∞	Reject	29.8	Reject	Reject
nl1l	∞	Reject	39	Reject	Reject
nl2u	2.59	Reject	27.2	Reject	Reject
nl2l	3.73	Reject	25	Reject	Reject
ou1u	2.02	Accept	29.2	Reject	Reject
ou1l	2.58	Reject	20.8	Reject	Reject
ou2u	3.41	Reject	32.2	Reject	Reject
ou2l	15	Reject	19.5	Reject	Reject
ou3u	∞	Reject	26.9	Reject	Reject
ou3l	9.93	Reject	24.2	Reject	Reject
ou4u	13.7	Reject	29.1	Reject	Reject
ou4l	8.08	Reject	30.9	Reject	Reject
ou5u	6.05	Reject	26.5	Reject	Reject
ou5l	9.73	Reject	23.5	Reject	Reject
ou6u	3.33	Reject	20.1	Reject	Reject
ou6l	2.88	Reject	19.6	Reject	Reject
ou7u	10.4	Reject	29.9	Reject	Reject
ou7l	10.7	Reject	20.2	Reject	Reject
ou8u	12.1	Reject	30.1	Reject	Reject
ou8l	15.5	Reject	18.8	Reject	Reject
nr1u	13.5	Reject	22.3	Reject	Reject
nr1l	4.25	Reject	21.9	Reject	Reject
nr2u	5.29	Reject	31.6	Reject	Reject
nr2l	4.47	Reject	33.4	Reject	Reject
Casting Speed	25.6	Reject	29.9	Reject	Reject
Mould Controller Status	14.9	Reject	22	Reject	Reject
Mould level	16.5	Reject	5.74	Reject	Reject
Inlet Temperature	1.39	Accept	0.716	Accept	Accept
Flowrate WL	1.02	Accept	6.13	Reject	Reject
Flowrate WF	1.85	Accept	8.02	Reject	Reject
Flowrate NL	1.08	Accept	2.49	Accept	Accept
Flowrate NR	1.24	Accept	19.2	Reject	Reject
Delta T WL	24.6	Reject	21.4	Reject	Reject
Delta T WF	30.1	Reject	23.4	Reject	Reject
Delta T NL	26.3	Reject	17.3	Reject	Reject
Delta T NR	22.5	Reject	23.8	Reject	Reject
Oscillation Frequency	25.8	Reject	38.1	Reject	Reject
Drive Current	1.35	Accept	6.94	Reject	Reject
Heat Flux WL	24.1	Reject	22	Reject	Reject
Heat Flux WF	29.1	Reject	23.4	Reject	Reject
Heat Flux NL	26.3	Reject	17.1	Reject	Reject
Heat Flux NR	22.5	Reject	23.6	Reject	Reject
in1	4.76	Reject	26.2	Reject	Reject
in2	2.92	Reject	33	Reject	Reject
in3	1.44	Accept	37.3	Reject	Reject
in4	3.23	Reject	49	Reject	Reject
in5	0.798	Accept	30.1	Reject	Reject
in6	5.83	Reject	28.5	Reject	Reject
in7	1.02	Accept	29.3	Reject	Reject
in8	7.72	Reject	26.7	Reject	Reject
nl1	11.9	Reject	19.6	Reject	Reject
nl2	8.43	Reject	7.42	Reject	Reject
ou1	0.802	Accept	41.8	Reject	Reject
ou2	5.67	Reject	31.2	Reject	Reject
ou3	0.334	Accept	28	Reject	Reject
ou4	0.795	Accept	52	Reject	Reject
ou5	0.562	Accept	28.7	Reject	Reject
ou6	1.89	Accept	37.4	Reject	Reject
ou7	1.08	Accept	33.3	Reject	Reject
ou8	0.793	Accept	28.6	Reject	Reject
nr1	10.5	Reject	4.57	Reject	Reject
nr2	1.9	Accept	20.4	Reject	Reject

Table B.9 Anderson-Darling hypothesis tests for Depressions (defect 8). n_8=82. n_g =391. $a_c^2(82)$=2.492. α=0.05.

Variable	$A^2_{\mu_8}$	$H_0(\mu_8)$	$A^2_{\sigma^2_8}$	$H_0(\sigma^2_8)$	$H_0(\mu_8) \cup H_0(\sigma^2_8)$
in1u	4.4	Reject	1.09	Accept	Reject
in1l	1.27	Accept	0.518	Accept	Accept
in2u	∞	Reject	∞	Reject	Reject
in2l	∞	Reject	1.59	Accept	Reject
in3u	4.29	Reject	∞	Reject	Reject
in3l	∞	Reject	∞	Reject	Reject
in4u	∞	Reject	2.49	Reject	Reject
in4l	∞	Reject	1.74	Accept	Reject
in5u	0.676	Accept	3.49	Reject	Reject
in5l	0.65	Accept	4.61	Reject	Reject
in6u	∞	Reject	1.63	Accept	Reject
in6l	∞	Reject	3.08	Reject	Reject
in7u	4.28	Reject	1.68	Accept	Reject
in7l	4.1	Reject	3.55	Reject	Reject
in8u	4.19	Reject	0.201	Accept	Reject
in8l	5.57	Reject	0.746	Accept	Reject
nl1u	4.94	Reject	2.81	Reject	Reject
nl1l	4.88	Reject	0.534	Accept	Reject
nl2u	6.59	Reject	0.286	Accept	Reject
nl2l	5.1	Reject	2.02	Accept	Reject
ou1u	∞	Reject	0.719	Accept	Reject
ou1l	∞	Reject	0.256	Accept	Reject
ou2u	∞	Reject	2.06	Accept	Reject
ou2l	2.58	Reject	1.33	Accept	Reject
ou3u	∞	Reject	1.76	Accept	Reject
ou3l	∞	Reject	3.45	Reject	Reject
ou4u	∞	Reject	2.23	Accept	Reject
ou4l	∞	Reject	2.65	Reject	Reject
ou5u	∞	Reject	1.18	Accept	Reject
ou5l	5.12	Reject	4.98	Reject	Reject
ou6u	15.6	Reject	8.01	Reject	Reject
ou6l	16.4	Reject	9.2	Reject	Reject
ou7u	∞	Reject	∞	Reject	Reject
ou7l	∞	Reject	3.11	Reject	Reject
ou8u	5.9	Reject	3.57	Reject	Reject
ou8l	2.81	Reject	1.27	Accept	Reject
nr1u	3.49	Reject	0.495	Accept	Reject
nr1l	2.12	Accept	∞	Reject	Reject
nr2u	2.09	Accept	∞	Reject	Reject
nr2l	3.22	Reject	∞	Reject	Reject
Casting Speed	7.26	Reject	0.972	Accept	Reject
Mould Controller Status	204	Reject	61.9	Reject	Reject
Mould level	1.33	Accept	0.641	Accept	Accept
Inlet Temperature	2.46	Accept	3.64	Reject	Reject
Flowrate WL	0.765	Accept	0.696	Accept	Accept
Flowrate WF	1.49	Accept	0.408	Accept	Accept
Flowrate NL	1.08	Accept	1.3	Accept	Accept
Flowrate NR	0.984	Accept	1.56	Accept	Accept
Delta T WL	7.83	Reject	1.35	Accept	Reject
Delta T WF	8.58	Reject	3.11	Reject	Reject
Delta T NL	2.1	Accept	1.36	Accept	Accept
Delta T NR	2.82	Reject	1.22	Accept	Reject
Oscillation Frequency	8.98	Reject	14.6	Reject	Reject
Drive Current	1.97	Accept	0.757	Accept	Accept
Heat Flux WL	2.92	Reject	3.1	Reject	Reject
Heat Flux WF	4.15	Reject	4.07	Reject	Reject
Heat Flux NL	2.22	Accept	1.26	Accept	Accept
Heat Flux NR	3.02	Reject	1.16	Accept	Reject
in1	9.29	Reject	0.75	Accept	Reject
in2	5.82	Reject	∞	Reject	Reject
in3	∞	Reject	1.86	Accept	Reject
in4	2.38	Accept	1.98	Accept	Accept
in5	4.73	Reject	4.7	Reject	Reject
in6	6.38	Reject	4.72	Reject	Reject
in7	2.07	Accept	2.53	Reject	Reject
in8	5.57	Reject	0.258	Accept	Reject
nl1	∞	Reject	1.52	Accept	Reject
nl2	4.08	Reject	1.01	Accept	Reject
ou1	3.23	Reject	0.926	Accept	Reject
ou2	2.2	Accept	3.2	Reject	Reject
ou3	2.93	Reject	4.01	Reject	Reject
ou4	2.98	Reject	2.94	Reject	Reject
ou5	3.92	Reject	3.26	Reject	Reject
ou6	4.86	Reject	8.39	Reject	Reject
ou7	0.822	Accept	3.28	Reject	Reject
ou8	7.2	Reject	2.14	Accept	Reject
nr1	8.72	Reject	2.02	Accept	Reject
nr2	2.56	Reject	∞	Reject	Reject

Appendix C

Correlation

Table C.1 Correlation of input variables.

	in1u	in1l	in2u	in2l	in3u	in3l	in4u	in4l	in5u	in5l	in6u	in6l	in7u	in7l	in8u	in8l
in1u	1	0.89	0.9	0.69	0.9	0.54	0.68	0.18	0.76	0.29	0.85	0.57	0.9	0.77	0.82	0.72
in1l	0.89	1	0.79	0.74	0.8	0.63	0.66	0.27	0.77	0.4	0.81	0.62	0.79	0.79	0.81	0.86
in2u	0.9	0.79	1	0.82	0.86	0.38	0.75	0.26	0.75	0.31	0.88	0.57	0.96	0.85	0.76	0.7
in2l	0.69	0.74	0.82	1	0.6	0.38	0.65	0.37	0.67	0.38	0.8	0.65	0.83	0.93	0.66	0.74
in3u	0.9	0.8	0.86	0.6	1	0.52	0.75	0.29	0.75	0.38	0.78	0.54	0.83	0.69	0.7	0.62
in3l	0.54	0.63	0.38	0.38	0.52	1	0.12	0.51	0.46	0.59	0.41	0.67	0.44	0.42	0.6	0.48
in4u	0.68	0.66	0.75	0.65	0.75	0.12	1	0.3	0.74	0.36	0.78	0.44	0.73	0.68	0.5	0.58
in4l	0.18	0.27	0.26	0.37	0.29	0.51	0.3	1	0.44	0.91	0.32	0.65	0.32	0.37	0.32	0.27
in5u	0.76	0.77	0.75	0.67	0.75	0.46	0.74	0.44	1	0.53	0.78	0.62	0.76	0.71	0.8	0.75
in5l	0.29	0.4	0.31	0.38	0.38	0.59	0.36	0.91	0.53	1	0.42	0.73	0.37	0.39	0.45	0.4
in6u	0.85	0.81	0.88	0.8	0.78	0.41	0.78	0.32	0.78	0.42	1	0.56	0.91	0.77	0.79	0.78
in6l	0.57	0.62	0.57	0.65	0.54	0.67	0.44	0.65	0.62	0.73	0.56	1	0.62	0.7	0.68	0.5
in7u	0.9	0.79	0.96	0.83	0.83	0.44	0.73	0.32	0.76	0.37	0.91	0.62	1	0.85	0.79	0.7
in7l	0.77	0.79	0.85	0.93	0.69	0.42	0.68	0.37	0.71	0.39	0.77	0.7	0.85	1	0.7	0.77
in8u	0.82	0.81	0.76	0.66	0.7	0.6	0.5	0.32	0.8	0.45	0.79	0.68	0.79	0.7	1	0.78
in8l	0.72	0.86	0.7	0.74	0.62	0.48	0.58	0.27	0.75	0.4	0.78	0.5	0.7	0.77	0.78	1
nl1u	0.86	0.75	0.87	0.73	0.8	0.37	0.73	0.23	0.69	0.27	0.81	0.53	0.87	0.78	0.71	0.61
nl1l	0.85	0.72	0.88	0.7	0.82	0.34	0.71	0.23	0.7	0.27	0.82	0.51	0.87	0.75	0.74	0.59
nl2u	0.86	0.72	0.82	0.61	0.78	0.34	0.6	0.18	0.65	0.21	0.77	0.45	0.82	0.71	0.79	0.61
nl2l	0.81	0.68	0.81	0.63	0.76	0.28	0.63	0.19	0.64	0.19	0.75	0.44	0.8	0.72	0.73	0.58
ou1u	0.93	0.85	0.88	0.72	0.82	0.5	0.65	0.13	0.73	0.26	0.86	0.55	0.87	0.75	0.83	0.72
ou1l	0.8	0.86	0.76	0.76	0.72	0.51	0.63	0.18	0.73	0.32	0.75	0.63	0.73	0.8	0.77	0.81
ou2u	0.9	0.85	0.91	0.76	0.88	0.47	0.78	0.37	0.81	0.43	0.92	0.56	0.93	0.8	0.8	0.77
ou2l	0.69	0.72	0.74	0.65	0.71	0.37	0.63	0.46	0.68	0.49	0.65	0.54	0.69	0.79	0.66	0.73
ou3u	0.84	0.82	0.87	0.79	0.84	0.5	0.76	0.4	0.8	0.42	0.87	0.59	0.9	0.82	0.74	0.74
ou3l	0.72	0.72	0.74	0.67	0.79	0.5	0.68	0.51	0.69	0.51	0.63	0.69	0.71	0.82	0.6	0.61
ou4u	0.72	0.74	0.71	0.54	0.74	0.27	0.81	0.25	0.7	0.39	0.82	0.32	0.69	0.58	0.57	0.71
ou4l	0.12	0.19	0.12	-0.02	0.26	0.29	0.25	0.69	0.29	0.76	0.19	0.37	0.1	0.09	0.24	0.18
ou5u	0.61	0.61	0.63	0.5	0.65	0.17	0.81	0.24	0.54	0.36	0.73	0.3	0.62	0.51	0.36	0.54
ou5l	0.14	0.21	0.31	0.31	0.33	0.07	0.55	0.63	0.41	0.64	0.24	0.48	0.26	0.39	0.13	0.23
ou6u	0.86	0.8	0.87	0.82	0.8	0.36	0.78	0.15	0.73	0.21	0.85	0.51	0.89	0.83	0.66	0.71
ou6l	0.79	0.76	0.8	0.75	0.8	0.41	0.76	0.35	0.72	0.39	0.72	0.61	0.78	0.86	0.58	0.67
ou7u	0.9	0.8	0.92	0.67	0.86	0.48	0.66	0.3	0.77	0.41	0.85	0.55	0.91	0.75	0.82	0.72
ou7l	0.78	0.8	0.82	0.72	0.75	0.38	0.69	0.4	0.73	0.47	0.76	0.59	0.78	0.84	0.75	0.79
ou8u	0.94	0.81	0.89	0.67	0.85	0.46	0.65	0.15	0.73	0.25	0.81	0.52	0.87	0.76	0.79	0.68
ou8l	0.91	0.87	0.8	0.63	0.84	0.56	0.61	0.18	0.7	0.31	0.73	0.6	0.76	0.75	0.77	0.7
nr1u	0.92	0.79	0.87	0.66	0.85	0.43	0.66	0.22	0.71	0.28	0.81	0.54	0.87	0.76	0.8	0.65
nr1l	0.89	0.77	0.86	0.69	0.84	0.41	0.67	0.23	0.68	0.26	0.8	0.55	0.86	0.78	0.76	0.64
nr2u	0.9	0.86	0.87	0.75	0.82	0.46	0.72	0.26	0.79	0.37	0.85	0.58	0.88	0.81	0.81	0.79
nr2l	0.86	0.8	0.88	0.77	0.77	0.37	0.71	0.22	0.71	0.28	0.86	0.52	0.9	0.8	0.75	0.73
CS	0.74	0.67	0.69	0.53	0.69	0.41	0.52	0.24	0.68	0.29	0.64	0.46	0.68	0.66	0.72	0.63
MCS	0.18	0.19	0.16	0.31	0.07	0.23	-0.07	0.09	0.24	0.03	0.1	0.23	0.16	0.35	0.33	0.28
ML	0.15	0.18	0.15	0.3	0.06	0.25	-0.08	0.09	0.19	0.05	0.08	0.22	0.12	0.34	0.3	0.28
IT	0.23	0.39	0.18	0.21	0.21	0.22	0.35	0.21	0.35	0.36	0.37	0.31	0.2	0.16	0.26	0.37
FWL	-0.01	0	0	0	-0.02	-0.01	-0.01	-0.01	0	0	0	-0.01	-0.01	0	-0.01	0.01
FWF	-0.02	-0.02	-0.01	0	-0.02	-0.01	-0.02	0	-0.01	0	-0.01	-0.01	-0.01	-0.01	-0.01	0
FNL	-0.01	-0.02	-0.01	-0.01	-0.02	0	-0.02	-0.01	-0.01	-0.02	-0.01	-0.01	-0.01	-0.01	-0.01	0
FNR	-0.01	-0.01	0	0.01	-0.02	0	-0.01	0	0	-0.01	0	0	0	0.01	0	0.01
DWL	0.67	0.78	0.66	0.65	0.63	0.38	0.62	0.23	0.79	0.39	0.69	0.51	0.63	0.69	0.71	0.84
DWF	0.57	0.69	0.54	0.54	0.55	0.33	0.56	0.21	0.77	0.37	0.57	0.47	0.52	0.58	0.64	0.76
DNL	0.81	0.84	0.73	0.59	0.74	0.39	0.59	0.07	0.78	0.22	0.69	0.44	0.68	0.68	0.79	0.81
DNR	0.8	0.82	0.76	0.65	0.72	0.3	0.65	0.06	0.78	0.19	0.73	0.44	0.7	0.74	0.79	0.83
OF	0.75	0.68	0.7	0.54	0.7	0.41	0.53	0.24	0.69	0.3	0.65	0.47	0.68	0.68	0.72	0.64
DC	0.01	0.04	0	0	0.01	0.1	-0.02	0.08	0.03	0.11	0.05	0.04	0.03	-0.03	0.04	0.05
HWL	0.66	0.77	0.65	0.64	0.62	0.37	0.6	0.22	0.78	0.38	0.68	0.5	0.62	0.68	0.71	0.84
HWF	0.57	0.68	0.54	0.53	0.54	0.32	0.55	0.19	0.76	0.36	0.56	0.46	0.52	0.58	0.64	0.76
HNL	0.81	0.83	0.72	0.59	0.74	0.39	0.59	0.07	0.78	0.22	0.69	0.44	0.68	0.68	0.79	0.81
HNR	0.8	0.82	0.76	0.65	0.72	0.3	0.65	0.06	0.78	0.19	0.73	0.44	0.7	0.74	0.79	0.83
in1	-0.85	-0.52	-0.78	-0.45	-0.76	-0.28	-0.52	-0.03	-0.53	-0.08	-0.65	-0.35	-0.78	-0.53	-0.62	-0.36
in2	-0.69	-0.45	-0.7	-0.18	-0.75	-0.17	-0.49	0.02	-0.45	-0.07	-0.53	-0.17	-0.62	-0.32	-0.5	-0.28
in3	-0.66	-0.48	-0.73	-0.42	-0.79	0.11	-0.79	0.03	-0.55	-0.02	-0.62	-0.15	-0.65	-0.5	-0.39	-0.38
in4	-0.58	-0.5	-0.61	-0.44	-0.59	0.18	-0.83	0.28	-0.48	0.17	-0.6	-0.06	-0.55	-0.47	-0.31	-0.43
in5	-0.56	-0.48	-0.53	-0.39	-0.48	0.04	-0.47	0.37	-0.61	0.35	-0.47	0	-0.49	-0.42	-0.45	-0.45
in6	-0.48	-0.39	-0.52	-0.34	-0.43	0.13	-0.52	0.2	-0.36	0.17	-0.67	0.25	-0.5	-0.27	-0.31	-0.45
in7	-0.66	-0.44	-0.66	-0.34	-0.63	-0.26	-0.47	-0.11	-0.47	-0.17	-0.67	-0.24	-0.74	-0.28	-0.55	-0.3
in8	-0.25	-0.03	-0.19	0.03	-0.21	-0.25	0.06	-0.12	-0.18	-0.14	-0.12	-0.34	-0.24	0	-0.45	0.21
nl1	0.23	0.1	0.27	0.09	0.26	-0.01	0.14	0.07	0.2	0.06	0.24	0.07	0.24	0.13	0.29	0.09
nl2	-0.44	-0.38	-0.34	-0.16	-0.35	-0.33	-0.14	-0.04	-0.27	-0.15	-0.33	-0.21	-0.34	-0.22	-0.45	-0.34
ou1	-0.63	-0.39	-0.61	-0.29	-0.54	-0.22	-0.34	0	-0.36	-0.04	-0.57	-0.16	-0.63	-0.29	-0.5	-0.23
ou2	-0.66	-0.54	-0.63	-0.5	-0.61	-0.34	-0.54	-0.07	-0.53	-0.14	-0.75	-0.28	-0.71	-0.39	-0.54	-0.42
ou3	-0.58	-0.55	-0.6	-0.55	-0.51	-0.26	-0.5	-0.1	-0.55	-0.14	-0.73	-0.21	-0.69	-0.44	-0.56	-0.53
ou4	-0.63	-0.59	-0.61	-0.55	-0.54	-0.04	-0.61	0.29	-0.47	0.21	-0.67	-0.03	-0.61	-0.51	-0.38	-0.57
ou5	-0.35	-0.28	-0.2	-0.08	-0.19	-0.06	-0.1	0.45	-0.02	0.37	-0.35	0.24	-0.24	-0.01	-0.16	-0.21
ou6	-0.58	-0.52	-0.59	-0.56	-0.45	-0.15	-0.48	0.15	-0.43	0.08	-0.64	-0.18	-0.65	-0.45	-0.47	-0.46
ou7	-0.52	-0.32	-0.5	-0.2	-0.49	-0.32	-0.22	0.01	-0.35	-0.09	-0.46	-0.17	-0.54	-0.18	-0.41	-0.19
ou8	-0.59	-0.36	-0.65	-0.44	-0.51	-0.09	-0.43	-0.02	-0.46	-0.04	-0.59	-0.15	-0.67	-0.44	-0.49	-0.34
nr1	-0.6	-0.48	-0.5	-0.28	-0.49	-0.3	-0.35	-0.11	-0.5	-0.22	-0.49	-0.3	-0.52	-0.37	-0.57	-0.42
nr2	-0.24	-0.29	-0.1	-0.05	-0.26	-0.33	-0.15	-0.17	-0.34	-0.3	-0.1	-0.26	-0.09	-0.15	-0.29	-0.28

Table C.2 Correlation of input variables.

	nl1u	nl1l	nl2u	nl2l	ou1u	ou1l	ou2u	ou2l	ou3u	ou3l	ou4u	ou4l	ou5u	ou5l	ou6u	ou6l
in1u	0.86	0.85	0.86	0.81	0.93	0.8	0.9	0.69	0.84	0.72	0.72	0.12	0.61	0.14	0.86	0.79
in1l	0.75	0.72	0.72	0.68	0.85	0.86	0.85	0.72	0.82	0.72	0.74	0.19	0.61	0.21	0.8	0.76
in2u	0.87	0.88	0.82	0.81	0.88	0.76	0.91	0.74	0.87	0.74	0.71	0.12	0.63	0.31	0.87	0.8
in2l	0.73	0.7	0.61	0.63	0.72	0.76	0.76	0.65	0.79	0.67	0.54	-0.02	0.5	0.31	0.82	0.75
in3u	0.8	0.82	0.78	0.76	0.82	0.72	0.88	0.71	0.84	0.79	0.74	0.26	0.65	0.33	0.8	0.8
in3l	0.37	0.34	0.34	0.28	0.5	0.51	0.47	0.37	0.5	0.5	0.27	0.29	0.17	0.07	0.36	0.41
in4u	0.73	0.71	0.6	0.63	0.65	0.63	0.78	0.63	0.76	0.68	0.81	0.25	0.81	0.55	0.78	0.76
in4l	0.23	0.23	0.18	0.19	0.13	0.18	0.37	0.46	0.4	0.51	0.25	0.69	0.24	0.63	0.15	0.35
in5u	0.69	0.7	0.65	0.64	0.73	0.73	0.81	0.68	0.8	0.69	0.7	0.29	0.54	0.41	0.73	0.72
in5l	0.27	0.27	0.21	0.19	0.26	0.32	0.43	0.49	0.42	0.51	0.39	0.76	0.36	0.64	0.21	0.39
in6u	0.81	0.82	0.77	0.75	0.86	0.75	0.92	0.65	0.87	0.63	0.82	0.19	0.73	0.24	0.85	0.72
in6l	0.53	0.51	0.45	0.44	0.55	0.63	0.56	0.54	0.59	0.69	0.32	0.37	0.3	0.48	0.51	0.61
in7u	0.87	0.87	0.82	0.8	0.87	0.73	0.93	0.69	0.9	0.71	0.69	0.1	0.62	0.26	0.89	0.78
in7l	0.78	0.75	0.71	0.72	0.75	0.8	0.8	0.79	0.82	0.82	0.58	0.09	0.51	0.39	0.83	0.86
in8u	0.71	0.74	0.79	0.73	0.83	0.77	0.8	0.66	0.74	0.6	0.57	0.24	0.36	0.13	0.66	0.58
in8l	0.61	0.59	0.61	0.58	0.72	0.81	0.77	0.73	0.74	0.61	0.71	0.18	0.54	0.23	0.71	0.67
nl1u	1	0.95	0.87	0.88	0.84	0.74	0.85	0.67	0.82	0.73	0.66	0.1	0.6	0.25	0.83	0.79
nl1l	0.95	1	0.9	0.92	0.83	0.7	0.86	0.68	0.81	0.71	0.66	0.14	0.57	0.21	0.79	0.75
nl2u	0.87	0.9	1	0.96	0.82	0.7	0.83	0.72	0.77	0.69	0.63	0.18	0.48	0.13	0.72	0.7
nl2l	0.88	0.92	0.96	1	0.78	0.68	0.81	0.7	0.76	0.7	0.6	0.13	0.48	0.18	0.73	0.71
ou1u	0.84	0.83	0.82	0.78	1	0.87	0.86	0.59	0.79	0.62	0.71	0.07	0.59	0.11	0.84	0.72
ou1l	0.74	0.7	0.7	0.68	0.87	1	0.75	0.65	0.72	0.69	0.64	0.08	0.51	0.26	0.78	0.77
ou2u	0.85	0.86	0.83	0.81	0.86	0.75	1	0.79	0.94	0.75	0.81	0.23	0.67	0.28	0.84	0.78
ou2l	0.67	0.68	0.72	0.7	0.59	0.65	0.79	1	0.73	0.85	0.63	0.46	0.48	0.5	0.59	0.76
ou3u	0.82	0.81	0.77	0.76	0.79	0.72	0.94	0.73	1	0.79	0.74	0.15	0.62	0.3	0.86	0.8
ou3l	0.73	0.71	0.69	0.7	0.62	0.69	0.75	0.85	0.79	1	0.58	0.37	0.51	0.57	0.68	0.89
ou4u	0.66	0.66	0.63	0.6	0.71	0.64	0.81	0.63	0.74	0.58	1	0.39	0.88	0.34	0.71	0.68
ou4l	0.1	0.14	0.18	0.13	0.07	0.08	0.23	0.46	0.15	0.37	0.39	1	0.31	0.62	-0.1	0.18
ou5u	0.6	0.57	0.48	0.48	0.59	0.51	0.67	0.48	0.62	0.51	0.88	0.31	1	0.44	0.69	0.65
ou5l	0.25	0.21	0.13	0.18	0.11	0.26	0.28	0.5	0.3	0.57	0.34	0.62	0.44	1	0.22	0.5
ou6u	0.83	0.79	0.72	0.73	0.84	0.78	0.84	0.59	0.86	0.68	0.71	-0.1	0.69	0.22	1	0.83
ou6l	0.79	0.75	0.7	0.71	0.72	0.77	0.78	0.76	0.8	0.89	0.68	0.18	0.65	0.5	0.83	1
ou7u	0.8	0.82	0.82	0.78	0.87	0.71	0.91	0.74	0.83	0.7	0.75	0.27	0.61	0.28	0.79	0.76
ou7l	0.76	0.77	0.8	0.77	0.72	0.75	0.84	0.94	0.78	0.84	0.71	0.41	0.55	0.46	0.68	0.8
ou8u	0.84	0.85	0.86	0.83	0.91	0.78	0.86	0.68	0.77	0.69	0.68	0.1	0.57	0.16	0.82	0.79
ou8l	0.79	0.78	0.81	0.77	0.84	0.83	0.79	0.71	0.73	0.76	0.65	0.18	0.53	0.19	0.75	0.8
nr1u	0.89	0.89	0.91	0.9	0.87	0.76	0.87	0.72	0.8	0.73	0.67	0.16	0.55	0.2	0.8	0.79
nr1l	0.89	0.89	0.91	0.91	0.84	0.76	0.85	0.72	0.81	0.75	0.64	0.13	0.55	0.22	0.81	0.8
nr2u	0.87	0.84	0.82	0.8	0.87	0.81	0.88	0.73	0.83	0.71	0.73	0.16	0.63	0.3	0.86	0.81
nr2l	0.89	0.86	0.83	0.83	0.85	0.77	0.87	0.68	0.84	0.67	0.71	0.09	0.63	0.24	0.86	0.77
CS	0.73	0.72	0.77	0.76	0.72	0.69	0.69	0.68	0.62	0.67	0.53	0.2	0.4	0.29	0.64	0.73
MCS	0.21	0.2	0.26	0.27	0.22	0.32	0.12	0.24	0.11	0.26	-0.14	-0.15	-0.25	0	0.15	0.29
ML	0.17	0.15	0.2	0.2	0.22	0.31	0.09	0.25	0.07	0.24	-0.11	-0.09	-0.22	0.03	0.12	0.27
IT	0.12	0.09	0.06	0.04	0.22	0.32	0.29	0.16	0.3	0.15	0.44	0.24	0.41	0.19	0.22	0.13
FWL	0	0	0	0	0.01	0.01	0	0	-0.01	-0.01	0.01	0	0.01	-0.01	0	0
FWF	-0.01	-0.02	-0.02	-0.02	-0.02	-0.01	-0.02	-0.02	-0.02	-0.01	-0.02	-0.01	-0.02	0	-0.02	-0.02
FNL	-0.01	-0.02	-0.02	-0.02	-0.02	-0.02	-0.01	-0.02	-0.02	-0.02	-0.01	-0.02	-0.01	-0.01	-0.02	-0.01
FNR	0	0	0	0	0	0.01	0	0	0	0	-0.01	-0.02	-0.01	-0.01	0	0.01
DWL	0.57	0.54	0.52	0.52	0.66	0.77	0.69	0.67	0.65	0.57	0.64	0.17	0.5	0.37	0.67	0.65
DWF	0.47	0.44	0.41	0.42	0.56	0.7	0.58	0.59	0.55	0.51	0.53	0.15	0.41	0.4	0.58	0.57
DNL	0.69	0.7	0.72	0.69	0.75	0.78	0.75	0.72	0.69	0.64	0.65	0.12	0.44	0.16	0.69	0.69
DNR	0.73	0.75	0.77	0.76	0.77	0.82	0.78	0.76	0.72	0.66	0.68	0.1	0.48	0.21	0.72	0.72
OF	0.73	0.73	0.77	0.77	0.73	0.7	0.7	0.69	0.63	0.68	0.55	0.21	0.41	0.3	0.65	0.74
DC	-0.03	-0.02	-0.04	-0.04	0.01	-0.01	0.03	-0.02	0.03	-0.04	0.05	0.07	0.06	-0.01	0	-0.05
HWL	0.56	0.53	0.52	0.52	0.66	0.77	0.68	0.67	0.64	0.57	0.62	0.16	0.48	0.36	0.66	0.64
HWF	0.46	0.43	0.41	0.42	0.56	0.7	0.57	0.58	0.54	0.51	0.52	0.15	0.39	0.39	0.57	0.57
HNL	0.69	0.69	0.72	0.69	0.75	0.78	0.75	0.72	0.69	0.64	0.65	0.12	0.44	0.16	0.69	0.69
HNR	0.73	0.75	0.77	0.76	0.77	0.82	0.77	0.76	0.72	0.66	0.68	0.1	0.48	0.2	0.72	0.72
in1	-0.75	-0.78	-0.78	-0.75	-0.76	-0.52	-0.71	-0.47	-0.63	-0.52	-0.5	0	-0.45	-0.03	-0.69	-0.6
in2	-0.59	-0.65	-0.67	-0.62	-0.62	-0.36	-0.62	-0.47	-0.51	-0.44	-0.55	-0.23	-0.47	-0.14	-0.49	-0.45
in3	-0.67	-0.71	-0.66	-0.68	-0.59	-0.47	-0.68	-0.56	-0.63	-0.56	-0.67	-0.09	-0.64	-0.34	-0.67	-0.64
in4	-0.6	-0.58	-0.5	-0.52	-0.57	-0.53	-0.57	-0.36	-0.53	-0.38	-0.67	0.15	-0.67	-0.18	-0.7	-0.56
in5	-0.51	-0.51	-0.52	-0.52	-0.56	-0.51	-0.49	-0.29	-0.49	-0.29	-0.41	0.39	-0.26	0.15	-0.6	-0.43
in6	-0.47	-0.49	-0.49	-0.48	-0.5	-0.31	-0.57	-0.27	-0.49	-0.11	-0.67	0.12	-0.58	0.15	-0.53	-0.29
in7	-0.59	-0.62	-0.59	-0.55	-0.64	-0.32	-0.67	-0.26	-0.61	-0.25	-0.53	-0.07	-0.49	0.02	-0.57	-0.33
in8	-0.24	-0.33	-0.35	-0.32	-0.27	-0.04	-0.14	0.01	-0.11	-0.06	0.12	-0.12	0.21	0.13	-0.01	0.05
nl1	0.12	0.42	0.33	0.37	0.21	0.08	0.27	0.23	0.21	0.15	0.18	0.17	0.05	-0.05	0.09	0.1
nl2	-0.3	-0.27	-0.49	-0.22	-0.42	-0.29	-0.38	-0.32	-0.3	-0.24	-0.33	-0.19	-0.16	0.11	-0.23	-0.2
ou1	-0.56	-0.6	-0.59	-0.53	-0.68	-0.23	-0.58	-0.21	-0.48	-0.19	-0.44	-0.01	-0.4	0.16	-0.5	-0.29
ou2	-0.61	-0.62	-0.52	-0.5	-0.7	-0.47	-0.72	-0.14	-0.68	-0.25	-0.59	0.14	-0.53	0.12	-0.69	-0.4
ou3	-0.54	-0.54	-0.5	-0.48	-0.6	-0.42	-0.7	-0.28	-0.76	-0.2	-0.58	0.14	-0.45	0.12	-0.66	-0.32
ou4	-0.58	-0.55	-0.49	-0.49	-0.65	-0.57	-0.62	-0.27	-0.62	-0.29	-0.69	0.4	-0.63	0.14	-0.79	-0.53
ou5	-0.23	-0.24	-0.26	-0.21	-0.37	-0.16	-0.26	0.12	-0.2	0.17	-0.37	0.38	-0.37	0.67	-0.34	-0.02
ou6	-0.54	-0.51	-0.44	-0.44	-0.62	-0.47	-0.56	-0.14	-0.58	-0.14	-0.45	0.39	-0.45	0.19	-0.77	-0.29
ou7	-0.38	-0.4	-0.36	-0.32	-0.54	-0.24	-0.45	-0.03	-0.39	-0.09	-0.34	0.09	-0.32	0.12	-0.47	-0.24
ou8	-0.56	-0.59	-0.56	-0.56	-0.62	-0.36	-0.59	-0.34	-0.5	-0.27	-0.43	0.08	-0.38	-0.03	-0.58	-0.44
nr1	-0.49	-0.5	-0.54	-0.47	-0.57	-0.42	-0.54	-0.42	-0.45	-0.35	-0.45	-0.18	-0.31	-0.04	-0.42	-0.41
nr2	-0.08	-0.06	-0.09	-0.03	-0.19	-0.26	-0.16	-0.24	-0.12	-0.23	-0.17	-0.23	-0.11	-0.2	-0.12	-0.23

Table C.3 Correlation of input variables.

	ou7u	ou7l	ou8u	ou8l	nr1u	nr1l	nr2u	nr2l	CS	MCS	ML	IT	FWL	FWF	FNL	FNR
in1u	0.9	0.78	0.94	0.91	0.92	0.89	0.9	0.86	0.74	0.18	0.15	0.23	-0.01	-0.02	-0.01	-0.01
in1l	0.8	0.8	0.81	0.87	0.79	0.77	0.86	0.8	0.67	0.19	0.18	0.39	0	-0.02	-0.02	-0.01
in2u	0.92	0.82	0.89	0.8	0.87	0.86	0.87	0.88	0.69	0.16	0.15	0.18	0	-0.01	-0.01	0
in2l	0.67	0.72	0.67	0.63	0.66	0.69	0.75	0.77	0.53	0.31	0.3	0.21	0	0	-0.01	0.01
in3u	0.86	0.75	0.85	0.84	0.85	0.84	0.82	0.77	0.69	0.07	0.06	0.21	-0.02	-0.02	-0.02	-0.02
in3l	0.48	0.38	0.46	0.56	0.43	0.41	0.46	0.37	0.41	0.23	0.25	0.22	-0.01	-0.01	0	0
in4u	0.66	0.69	0.65	0.61	0.66	0.67	0.72	0.71	0.52	-0.07	-0.08	0.35	-0.01	-0.02	-0.02	-0.01
in4l	0.3	0.4	0.15	0.18	0.22	0.23	0.26	0.22	0.24	0.09	0.09	0.21	-0.01	0	-0.01	0
in5u	0.77	0.73	0.73	0.7	0.71	0.68	0.79	0.71	0.68	0.24	0.19	0.35	0	-0.01	-0.01	0
in5l	0.41	0.47	0.25	0.31	0.28	0.26	0.37	0.28	0.29	0.03	0.05	0.36	0	0	-0.02	-0.01
in6u	0.85	0.76	0.81	0.73	0.81	0.8	0.85	0.86	0.64	0.1	0.08	0.37	0	-0.01	-0.01	0
in6l	0.55	0.59	0.52	0.6	0.54	0.55	0.58	0.52	0.46	0.23	0.22	0.31	-0.01	-0.01	-0.01	0
in7u	0.91	0.78	0.87	0.76	0.87	0.86	0.88	0.9	0.68	0.16	0.12	0.2	-0.01	-0.01	-0.01	0
in7l	0.75	0.84	0.76	0.75	0.76	0.78	0.81	0.8	0.66	0.35	0.34	0.16	0	-0.01	-0.01	0.01
in8u	0.82	0.75	0.79	0.77	0.8	0.76	0.81	0.75	0.72	0.33	0.3	0.26	-0.01	-0.01	-0.01	0
in8l	0.72	0.79	0.68	0.7	0.65	0.64	0.79	0.73	0.63	0.28	0.28	0.37	0.01	0	0	0.01
nl1u	0.8	0.76	0.84	0.79	0.89	0.89	0.87	0.89	0.73	0.21	0.17	0.12	0	-0.01	-0.01	0
nl1l	0.82	0.77	0.85	0.78	0.89	0.89	0.84	0.86	0.72	0.2	0.15	0.09	0	-0.02	-0.02	0
nl2u	0.82	0.8	0.86	0.81	0.91	0.91	0.82	0.83	0.77	0.26	0.2	0.06	0	-0.02	-0.02	0
nl2l	0.78	0.77	0.83	0.77	0.9	0.91	0.8	0.83	0.76	0.27	0.2	0.04	0	-0.02	-0.02	0
ou1u	0.87	0.72	0.91	0.84	0.87	0.84	0.87	0.85	0.72	0.22	0.22	0.22	0.01	-0.02	-0.02	0
ou1l	0.71	0.75	0.78	0.83	0.76	0.76	0.81	0.77	0.69	0.32	0.31	0.32	0.01	-0.01	-0.02	0.01
ou2u	0.91	0.84	0.86	0.79	0.87	0.85	0.88	0.87	0.69	0.12	0.09	0.29	0	-0.02	-0.01	0
ou2l	0.74	0.94	0.68	0.71	0.72	0.72	0.73	0.68	0.68	0.24	0.25	0.16	0	-0.02	-0.02	0
ou3u	0.83	0.78	0.77	0.73	0.8	0.81	0.83	0.84	0.62	0.11	0.07	0.3	-0.01	-0.02	-0.02	0
ou3l	0.7	0.84	0.69	0.76	0.73	0.75	0.71	0.67	0.67	0.26	0.24	0.15	-0.01	-0.01	-0.02	0
ou4u	0.75	0.71	0.68	0.65	0.67	0.64	0.73	0.71	0.53	-0.14	-0.11	0.44	0.01	-0.02	-0.01	-0.01
ou4l	0.27	0.41	0.1	0.18	0.16	0.13	0.16	0.09	0.2	-0.15	-0.09	0.24	0	-0.01	-0.02	-0.02
ou5u	0.61	0.55	0.57	0.53	0.55	0.55	0.63	0.63	0.4	-0.25	-0.22	0.41	0.01	-0.02	-0.01	-0.01
ou5l	0.28	0.46	0.16	0.19	0.2	0.22	0.3	0.24	0.29	0	0.03	0.19	-0.01	0	-0.01	-0.01
ou6u	0.79	0.68	0.82	0.75	0.8	0.81	0.86	0.86	0.64	0.15	0.12	0.22	0	-0.02	-0.02	0
ou6l	0.76	0.8	0.79	0.8	0.79	0.8	0.81	0.77	0.73	0.29	0.27	0.13	0	-0.02	-0.01	0.01
ou7u	1	0.82	0.91	0.81	0.87	0.84	0.88	0.85	0.76	0.17	0.15	0.18	0	-0.02	-0.01	0
ou7l	0.82	1	0.77	0.8	0.8	0.79	0.81	0.77	0.71	0.22	0.22	0.25	0	-0.01	-0.02	0
ou8u	0.91	0.77	1	0.91	0.92	0.89	0.87	0.84	0.8	0.29	0.26	0.11	0	-0.02	-0.01	-0.01
ou8l	0.81	0.8	0.91	1	0.86	0.85	0.82	0.76	0.75	0.24	0.22	0.25	0	-0.01	-0.02	-0.01
nr1u	0.87	0.8	0.92	0.86	1	0.97	0.9	0.89	0.83	0.29	0.24	0.1	0	-0.01	-0.02	0.01
nr1l	0.84	0.79	0.89	0.85	0.97	1	0.88	0.89	0.81	0.29	0.23	0.1	-0.01	-0.02	-0.02	0.01
nr2u	0.88	0.81	0.87	0.82	0.9	0.88	1	0.94	0.8	0.27	0.23	0.22	0	-0.02	-0.03	0
nr2l	0.85	0.77	0.84	0.76	0.89	0.89	0.94	1	0.74	0.2	0.15	0.2	-0.01	-0.02	-0.02	0.01
CS	0.76	0.71	0.8	0.75	0.83	0.81	0.8	0.74	1	0.58	0.54	-0.09	-0.01	-0.02	-0.01	0
MCS	0.17	0.22	0.29	0.24	0.29	0.29	0.27	0.2	0.58	1	0.89	-0.45	0.01	0	0	0.02
ML	0.15	0.22	0.26	0.22	0.24	0.23	0.23	0.15	0.54	0.89	1	-0.49	0.02	0	0.02	0.02
IT	0.18	0.25	0.11	0.25	0.1	0.1	0.22	0.2	-0.09	-0.45	-0.49	1	0	0	-0.01	0
FWL	0	0	0	0	0	-0.01	0	-0.01	-0.01	0.01	0.02	0	1	-0.29	-0.11	-0.06
FWF	-0.02	-0.01	-0.02	-0.01	-0.01	-0.02	-0.02	-0.02	-0.02	0	0	0	-0.29	1	0.06	0.28
FNL	-0.01	-0.02	-0.01	-0.02	-0.02	-0.02	-0.03	-0.02	-0.01	0	0.02	-0.01	-0.11	0.06	1	0.23
FNR	0	0	-0.01	-0.01	0.01	0.01	0	0.01	0	0.02	0.02	0	-0.06	0.28	0.23	1
DWL	0.68	0.72	0.65	0.66	0.62	0.6	0.76	0.69	0.66	0.27	0.22	0.44	0	0	-0.01	0.01
DWF	0.58	0.61	0.55	0.57	0.52	0.5	0.68	0.58	0.61	0.29	0.23	0.41	0.01	-0.01	-0.01	0
DNL	0.75	0.78	0.79	0.83	0.76	0.73	0.8	0.73	0.74	0.29	0.24	0.28	0	-0.01	0	0
DNR	0.75	0.83	0.79	0.81	0.78	0.76	0.82	0.77	0.74	0.3	0.26	0.28	0.01	-0.01	0	0.01
OF	0.77	0.72	0.81	0.76	0.84	0.82	0.81	0.75	1	0.57	0.54	-0.09	0	-0.02	-0.01	0
DC	0.03	-0.02	-0.02	-0.02	-0.02	-0.02	0.02	0.02	-0.04	-0.07	-0.07	0.1	0.03	-0.02	0.01	0.01
HWL	0.68	0.71	0.65	0.66	0.62	0.6	0.76	0.68	0.67	0.3	0.25	0.42	0.06	-0.02	-0.02	0.01
HWF	0.57	0.61	0.55	0.57	0.52	0.5	0.67	0.57	0.62	0.31	0.26	0.39	-0.01	0.05	-0.01	0.02
HNL	0.75	0.78	0.79	0.83	0.76	0.73	0.8	0.73	0.74	0.29	0.24	0.28	-0.01	-0.01	0.04	0.01
HNR	0.75	0.83	0.79	0.81	0.78	0.76	0.82	0.77	0.74	0.3	0.26	0.28	0	0	0.01	0.04
in1	-0.77	-0.54	-0.84	-0.7	-0.81	-0.78	-0.7	-0.69	-0.62	-0.12	-0.07	0.03	0.01	0.01	0	0.01
in2	-0.76	-0.52	-0.71	-0.6	-0.68	-0.63	-0.57	-0.56	-0.53	0.11	0.12	-0.05	0.01	0.02	0.02	0.02
in3	-0.66	-0.61	-0.67	-0.57	-0.68	-0.69	-0.63	-0.64	-0.52	0.08	0.11	-0.08	0.02	0.02	0.02	0.02
in4	-0.49	-0.46	-0.57	-0.51	-0.54	-0.54	-0.57	-0.59	-0.38	0.12	0.13	-0.23	0	0.02	0.01	0.01
in5	-0.47	-0.37	-0.57	-0.49	-0.52	-0.5	-0.52	-0.52	-0.47	-0.23	-0.17	-0.06	0	0.02	0	-0.01
in6	-0.5	-0.35	-0.48	-0.32	-0.46	-0.44	-0.47	-0.53	-0.33	0.1	0.1	-0.15	0	0.01	0	0
in7	-0.71	-0.35	-0.62	-0.44	-0.62	-0.58	-0.58	-0.61	-0.39	0.17	0.22	-0.16	0.03	0.01	0	0.01
in8	-0.24	-0.04	-0.27	-0.19	-0.31	-0.27	-0.14	-0.13	-0.22	-0.12	-0.08	0.13	0.03	0.01	0.02	0.02
nl1	0.29	0.25	0.27	0.21	0.26	0.26	0.13	0.16	0.18	0.01	-0.02	-0.07	0.01	-0.02	-0.04	-0.02
nl2	-0.42	-0.36	-0.41	-0.43	-0.38	-0.32	-0.34	-0.29	-0.29	-0.04	-0.08	-0.08	0.01	0	0.01	0.01
ou1	-0.65	-0.31	-0.64	-0.44	-0.6	-0.54	-0.51	-0.54	-0.4	0.04	0.03	0.04	0.01	0.02	0	0
ou2	-0.62	-0.29	-0.61	-0.47	-0.58	-0.56	-0.59	-0.62	-0.35	0.09	0.13	-0.29	0.01	0.02	-0.01	0
ou3	-0.58	-0.36	-0.5	-0.35	-0.51	-0.49	-0.57	-0.62	-0.29	0.1	0.14	-0.32	0	0.02	0.01	0
ou4	-0.53	-0.39	-0.6	-0.51	-0.54	-0.54	-0.6	-0.64	-0.37	0.02	0.04	-0.25	-0.01	0.01	0	-0.01
ou5	-0.21	0.02	-0.31	-0.24	-0.25	-0.22	-0.22	-0.27	-0.03	0.21	0.21	-0.14	-0.02	0.01	0	0
ou6	-0.5	-0.25	-0.51	-0.38	-0.48	-0.48	-0.56	-0.61	-0.28	0.08	0.11	-0.23	0	0.01	0.02	0.01
ou7	-0.64	-0.08	-0.54	-0.32	-0.44	-0.39	-0.44	-0.43	-0.36	0.01	0.03	0.02	0	0.02	0	0.01
ou8	-0.67	-0.38	-0.72	-0.35	-0.62	-0.56	-0.58	-0.6	-0.55	-0.23	-0.21	0.18	-0.01	0.01	-0.01	0
nr1	-0.6	-0.47	-0.63	-0.52	-0.66	-0.45	-0.57	-0.49	-0.55	-0.17	-0.19	-0.05	-0.02	0	0.02	0.01
nr2	-0.22	-0.22	-0.23	-0.29	-0.17	-0.1	-0.32	0.02	-0.31	-0.22	-0.27	-0.08	-0.02	0	0.02	0.01

Table C.4 Correlation of input variables.

	DWL	DWF	DNL	DNR	OF	DC	HWL	HWF	HNL	HNR	in1	in2	in3	in4	in5	in6
in1u	0.67	0.57	0.81	0.8	0.75	0.01	0.66	0.57	0.81	0.8	-0.85	-0.69	-0.66	-0.58	-0.56	-0.48
in1l	0.78	0.69	0.84	0.82	0.68	0.04	0.77	0.68	0.83	0.82	-0.52	-0.45	-0.48	-0.5	-0.48	-0.39
in2u	0.66	0.54	0.73	0.76	0.7	0	0.65	0.54	0.72	0.76	-0.78	-0.7	-0.73	-0.61	-0.53	-0.52
in2l	0.65	0.54	0.59	0.65	0.54	0	0.64	0.53	0.59	0.65	-0.45	-0.18	-0.42	-0.44	-0.39	-0.34
in3u	0.63	0.55	0.74	0.72	0.7	0.01	0.62	0.54	0.74	0.72	-0.76	-0.75	-0.79	-0.59	-0.48	-0.43
in3l	0.38	0.33	0.39	0.3	0.41	0.1	0.37	0.32	0.39	0.3	-0.28	-0.17	0.11	0.18	0.04	0.13
in4u	0.62	0.56	0.59	0.65	0.53	-0.02	0.6	0.55	0.59	0.65	-0.52	-0.49	-0.79	-0.83	-0.47	-0.52
in4l	0.23	0.21	0.07	0.06	0.24	0.08	0.22	0.19	0.07	0.06	-0.03	0.02	0.03	0.28	0.37	0.2
in5u	0.79	0.77	0.78	0.78	0.69	0.03	0.78	0.76	0.78	0.78	-0.53	-0.45	-0.55	-0.48	-0.61	-0.36
in5l	0.39	0.37	0.22	0.19	0.3	0.11	0.38	0.36	0.22	0.19	-0.08	-0.07	-0.02	0.17	0.35	0.17
in6u	0.69	0.57	0.69	0.73	0.65	0.05	0.68	0.56	0.69	0.73	-0.65	-0.53	-0.62	-0.6	-0.47	-0.67
in6l	0.51	0.47	0.44	0.44	0.47	0.04	0.5	0.46	0.44	0.44	-0.35	-0.17	-0.15	-0.06	0	0.25
in7u	0.63	0.52	0.68	0.7	0.68	0.03	0.62	0.52	0.68	0.7	-0.78	-0.62	-0.65	-0.55	-0.49	-0.5
in7l	0.69	0.58	0.68	0.74	0.68	-0.03	0.68	0.58	0.68	0.74	-0.53	-0.32	-0.5	-0.47	-0.42	-0.27
in8u	0.71	0.64	0.79	0.79	0.72	0.04	0.71	0.64	0.79	0.79	-0.62	-0.5	-0.39	-0.31	-0.45	-0.31
in8l	0.84	0.76	0.81	0.83	0.64	0.05	0.84	0.76	0.81	0.83	-0.36	-0.28	-0.38	-0.43	-0.45	-0.45
nl1u	0.57	0.47	0.69	0.73	0.73	-0.03	0.56	0.46	0.69	0.73	-0.75	-0.59	-0.67	-0.6	-0.51	-0.47
nl1l	0.54	0.44	0.7	0.75	0.73	-0.02	0.53	0.43	0.69	0.75	-0.78	-0.65	-0.71	-0.58	-0.51	-0.49
nl2u	0.52	0.41	0.72	0.77	0.77	-0.04	0.52	0.41	0.72	0.77	-0.78	-0.67	-0.66	-0.5	-0.52	-0.49
nl2l	0.52	0.42	0.69	0.76	0.77	-0.04	0.52	0.42	0.69	0.76	-0.75	-0.62	-0.68	-0.52	-0.52	-0.48
ou1u	0.66	0.56	0.75	0.77	0.73	0.01	0.66	0.56	0.75	0.77	-0.76	-0.62	-0.59	-0.57	-0.56	-0.5
ou1l	0.77	0.7	0.78	0.82	0.7	-0.01	0.77	0.7	0.78	0.82	-0.52	-0.36	-0.47	-0.53	-0.51	-0.31
ou2u	0.69	0.58	0.75	0.78	0.7	0.03	0.68	0.57	0.75	0.77	-0.71	-0.62	-0.68	-0.57	-0.49	-0.57
ou2l	0.67	0.59	0.72	0.76	0.69	-0.02	0.67	0.58	0.72	0.76	-0.47	-0.47	-0.56	-0.36	-0.29	-0.27
ou3u	0.65	0.55	0.69	0.72	0.63	0.03	0.64	0.54	0.69	0.72	-0.63	-0.51	-0.63	-0.53	-0.49	-0.49
ou3l	0.57	0.51	0.64	0.66	0.68	-0.04	0.57	0.51	0.64	0.66	-0.52	-0.44	-0.56	-0.38	-0.29	-0.11
ou4u	0.64	0.53	0.65	0.68	0.55	0.05	0.62	0.52	0.65	0.68	-0.5	-0.55	-0.67	-0.67	-0.41	-0.67
ou4l	0.17	0.15	0.12	0.1	0.21	0.07	0.16	0.15	0.12	0.1	0	-0.23	-0.09	0.15	0.39	0.12
ou5u	0.5	0.41	0.44	0.48	0.41	0.06	0.48	0.39	0.44	0.48	-0.45	-0.47	-0.64	-0.67	-0.26	-0.58
ou5l	0.37	0.4	0.16	0.21	0.3	-0.01	0.36	0.39	0.16	0.2	-0.03	-0.14	-0.34	-0.18	0.15	0.15
ou6u	0.67	0.58	0.69	0.72	0.65	0	0.66	0.57	0.69	0.72	-0.69	-0.49	-0.67	-0.7	-0.6	-0.53
ou6l	0.65	0.57	0.69	0.72	0.74	-0.05	0.64	0.57	0.69	0.72	-0.6	-0.45	-0.64	-0.56	-0.43	-0.29
ou7u	0.68	0.58	0.75	0.75	0.77	0.03	0.68	0.57	0.75	0.75	-0.77	-0.76	-0.66	-0.49	-0.47	-0.5
ou7l	0.72	0.61	0.78	0.83	0.72	-0.02	0.71	0.61	0.78	0.83	-0.54	-0.52	-0.61	-0.46	-0.37	-0.35
ou8u	0.65	0.55	0.79	0.79	0.81	-0.02	0.65	0.55	0.79	0.79	-0.84	-0.71	-0.67	-0.57	-0.57	-0.48
ou8l	0.66	0.57	0.83	0.81	0.76	-0.02	0.66	0.57	0.83	0.81	-0.7	-0.6	-0.57	-0.51	-0.49	-0.32
nr1u	0.62	0.52	0.76	0.78	0.84	-0.02	0.62	0.52	0.76	0.78	-0.81	-0.68	-0.68	-0.54	-0.52	-0.46
nr1l	0.6	0.5	0.73	0.76	0.82	-0.02	0.6	0.5	0.73	0.76	-0.78	-0.63	-0.69	-0.54	-0.5	-0.44
nr2u	0.76	0.68	0.8	0.82	0.81	0.02	0.76	0.67	0.8	0.82	-0.7	-0.57	-0.63	-0.57	-0.52	-0.47
nr2l	0.69	0.58	0.73	0.77	0.75	0.02	0.68	0.57	0.73	0.77	-0.69	-0.56	-0.64	-0.59	-0.52	-0.53
CS	0.66	0.61	0.74	0.74	1	-0.04	0.67	0.62	0.74	0.74	-0.62	-0.53	-0.52	-0.38	-0.47	-0.33
MCS	0.27	0.29	0.29	0.3	0.57	-0.07	0.3	0.31	0.29	0.3	-0.12	0.11	0.08	0.12	-0.23	0.1
ML	0.22	0.23	0.24	0.26	0.54	-0.07	0.25	0.26	0.24	0.26	-0.07	0.12	0.11	0.13	-0.17	0.1
IT	0.44	0.41	0.28	0.28	-0.09	0.1	0.42	0.39	0.28	0.28	0.03	-0.05	-0.08	-0.23	-0.06	-0.15
FWL	0	0.01	0	0.01	0	0.03	0.06	-0.01	-0.01	0	0.01	0.01	0.02	0	0	0
FWF	0	-0.01	-0.01	-0.01	-0.02	-0.02	-0.02	0.05	-0.01	0	0.01	0.02	0.02	0.02	0.02	0.01
FNL	-0.01	-0.01	0	0	-0.01	0.01	-0.02	-0.01	0.04	0.01	0	0.02	0.02	0.01	0	0
FNR	0.01	0	0	0.01	0	0.01	0.01	0.02	0.01	0.04	0.01	0.02	0.02	0.01	-0.01	0
DWL	1	0.96	0.87	0.86	0.67	0.04	1	0.96	0.87	0.86	-0.36	-0.33	-0.46	-0.48	-0.5	-0.35
DWF	0.96	1	0.83	0.8	0.62	0.03	0.96	1	0.83	0.8	-0.28	-0.27	-0.41	-0.45	-0.5	-0.24
DNL	0.87	0.83	1	0.96	0.74	-0.02	0.88	0.83	1	0.96	-0.56	-0.52	-0.58	-0.56	-0.66	-0.41
DNR	0.86	0.8	0.96	1	0.75	-0.03	0.86	0.8	0.96	1	-0.56	-0.49	-0.63	-0.62	-0.68	-0.46
OF	0.67	0.62	0.74	0.75	1	-0.04	0.67	0.63	0.74	0.75	-0.63	-0.53	-0.52	-0.39	-0.48	-0.33
DC	0.04	0.03	-0.02	-0.03	-0.04	1	0.03	0.02	-0.02	-0.03	0.03	0	0.05	0.07	0.07	-0.03
HWL	1	0.96	0.88	0.86	0.67	0.03	1	0.96	0.87	0.86	-0.36	-0.33	-0.45	-0.47	-0.51	-0.35
HWF	0.96	1	0.83	0.8	0.63	0.02	0.96	1	0.83	0.8	-0.28	-0.27	-0.4	-0.44	-0.5	-0.24
HNL	0.87	0.83	1	0.96	0.74	-0.02	0.87	0.83	1	0.96	-0.56	-0.52	-0.58	-0.56	-0.66	-0.41
HNR	0.86	0.8	0.96	1	0.75	-0.03	0.86	0.8	0.96	1	-0.55	-0.49	-0.63	-0.62	-0.68	-0.46
in1	-0.36	-0.28	-0.56	-0.56	-0.63	0.03	-0.36	-0.28	-0.56	-0.55	1	0.79	0.68	0.51	0.51	0.44
in2	-0.33	-0.27	-0.52	-0.49	-0.53	0	-0.33	-0.27	-0.52	-0.49	0.79	1	0.74	0.5	0.43	0.47
in3	-0.46	-0.41	-0.58	-0.63	-0.52	0.05	-0.45	-0.4	-0.58	-0.63	0.68	0.74	1	0.81	0.59	0.59
in4	-0.48	-0.45	-0.56	-0.62	-0.39	0.07	-0.47	-0.44	-0.56	-0.62	0.51	0.5	0.81	1	0.69	0.65
in5	-0.5	-0.5	-0.66	-0.68	-0.48	0.07	-0.51	-0.5	-0.66	-0.68	0.51	0.43	0.59	0.69	1	0.55
in6	-0.35	-0.24	-0.41	-0.46	-0.33	-0.03	-0.35	-0.24	-0.41	-0.46	0.44	0.47	0.59	0.65	0.55	1
in7	-0.29	-0.21	-0.37	-0.34	-0.39	-0.09	-0.27	-0.2	-0.37	-0.34	0.74	0.73	0.54	0.41	0.36	0.56
in8	0.1	0.09	-0.08	-0.04	-0.22	0.01	0.1	0.09	-0.08	-0.04	0.45	0.38	0.07	-0.13	0.07	-0.16
nl1	0.06	0.03	0.22	0.25	0.19	0.01	0.07	0.03	0.22	0.25	-0.32	-0.36	-0.31	-0.1	-0.16	-0.21
nl2	-0.19	-0.12	-0.36	-0.3	-0.29	-0.01	-0.19	-0.12	-0.36	-0.3	0.38	0.39	0.18	0.12	0.16	0.2
ou1	-0.16	-0.07	-0.32	-0.31	-0.4	-0.04	-0.16	-0.07	-0.32	-0.31	0.73	0.69	0.47	0.34	0.36	0.52
ou2	-0.34	-0.26	-0.39	-0.39	-0.34	-0.08	-0.33	-0.25	-0.39	-0.39	0.61	0.47	0.46	0.5	0.45	0.62
ou3	-0.43	-0.34	-0.43	-0.45	-0.29	-0.09	-0.42	-0.33	-0.43	-0.45	0.45	0.36	0.41	0.45	0.47	0.66
ou4	-0.5	-0.41	-0.55	-0.6	-0.38	0	-0.49	-0.4	-0.55	-0.6	0.5	0.37	0.59	0.79	0.71	0.75
ou5	-0.02	0.08	-0.19	-0.18	-0.03	-0.06	-0.02	0.08	-0.19	-0.18	0.34	0.25	0.18	0.37	0.37	0.63
ou6	-0.41	-0.34	-0.4	-0.43	-0.28	-0.05	-0.4	-0.33	-0.4	-0.43	0.5	0.32	0.42	0.57	0.55	0.59
ou7	-0.22	-0.19	-0.26	-0.19	-0.36	-0.08	-0.22	-0.18	-0.26	-0.19	0.61	0.62	0.34	0.23	0.31	0.39
ou8	-0.34	-0.27	-0.39	-0.42	-0.55	0	-0.35	-0.27	-0.39	-0.42	0.7	0.59	0.53	0.42	0.47	0.55
nr1	-0.4	-0.35	-0.51	-0.49	-0.55	0.01	-0.4	-0.35	-0.5	-0.49	0.57	0.51	0.35	0.28	0.34	0.3
nr2	-0.33	-0.38	-0.32	-0.27	-0.31	-0.02	-0.33	-0.38	-0.32	-0.27	0.12	0.11	0.06	0.05	0.1	-0.11

Table C.5 Correlation of input variables.

	in7	in8	nl1	nl2	ou1	ou2	ou3	ou4	ou5	ou6	ou7	ou8	nr1	nr2
in1u	**-0.66**	-0.25	0.23	*-0.44*	**-0.63**	**-0.66**	**-0.58**	**-0.63**	*-0.35*	**-0.58**	**-0.52**	**-0.59**	**-0.6**	-0.24
in1l	*-0.44*	-0.03	0.1	*-0.38*	*-0.39*	**-0.54**	**-0.55**	**-0.59**	*-0.28*	**-0.52**	*-0.32*	*-0.36*	*-0.48*	*-0.29*
in2u	**-0.66**	-0.19	*0.27*	*-0.34*	**-0.61**	**-0.63**	**-0.6**	**-0.61**	-0.2	**-0.59**	*-0.5*	**-0.65**	*-0.5*	-0.1
in2l	*-0.34*	0.03	0.09	-0.16	*-0.29*	*-0.5*	**-0.55**	**-0.55**	-0.08	**-0.56**	-0.2	*-0.44*	*-0.28*	-0.05
in3u	**-0.63**	-0.21	*0.26*	*-0.35*	**-0.54**	**-0.61**	**-0.51**	**-0.54**	-0.19	*-0.45*	*-0.49*	**-0.51**	*-0.49*	*-0.26*
in3l	*-0.26*	-0.25	-0.01	*-0.33*	-0.22	*-0.34*	*-0.26*	-0.04	-0.06	-0.15	*-0.32*	-0.09	*-0.3*	*-0.33*
in4u	*-0.47*	0.06	0.14	-0.14	*-0.34*	**-0.54**	*-0.5*	**-0.61**	-0.1	*-0.48*	-0.22	*-0.43*	*-0.35*	-0.15
in4l	-0.11	-0.12	0.07	-0.04	0	-0.07	-0.1	*0.29*	*0.45*	0.15	0.01	-0.02	-0.11	-0.17
in5u	*-0.47*	-0.18	0.2	*-0.27*	*-0.36*	**-0.53**	**-0.55**	*-0.47*	-0.02	*-0.43*	*-0.35*	*-0.46*	*-0.5*	*-0.34*
in5l	-0.17	-0.14	0.06	-0.15	-0.04	-0.14	-0.14	0.21	*0.37*	0.08	-0.09	-0.04	-0.22	*-0.3*
in6u	**-0.67**	-0.12	0.24	*-0.33*	**-0.57**	**-0.75**	**-0.73**	**-0.67**	*-0.35*	**-0.64**	*-0.46*	**-0.59**	*-0.49*	-0.1
in6l	-0.24	*-0.34*	0.07	-0.21	-0.16	*-0.28*	-0.21	-0.03	0.24	-0.18	-0.17	-0.15	*-0.3*	*-0.26*
in7u	**-0.74**	-0.24	0.24	*-0.34*	**-0.63**	**-0.71**	**-0.69**	**-0.61**	-0.24	**-0.65**	**-0.54**	**-0.67**	**-0.52**	-0.09
in7l	*-0.28*	0	0.13	-0.22	*-0.29*	*-0.39*	*-0.44*	**-0.51**	-0.01	*-0.45*	-0.18	*-0.44*	*-0.37*	-0.15
in8u	**-0.55**	*-0.45*	*0.29*	*-0.45*	*-0.5*	**-0.54**	**-0.56**	*-0.38*	-0.16	*-0.47*	*-0.41*	*-0.49*	**-0.57**	*-0.29*
in8l	*-0.3*	0.21	0.09	*-0.34*	-0.23	*-0.42*	**-0.53**	**-0.57**	-0.21	*-0.46*	-0.19	*-0.34*	*-0.42*	*-0.28*
nl1u	**-0.59**	-0.24	0.12	*-0.3*	**-0.56**	**-0.61**	**-0.54**	**-0.58**	-0.23	**-0.54**	*-0.38*	**-0.56**	*-0.49*	-0.08
nl1l	**-0.62**	*-0.33*	*0.42*	*-0.27*	**-0.6**	**-0.62**	**-0.54**	**-0.55**	-0.24	**-0.51**	*-0.4*	**-0.59**	*-0.5*	-0.06
nl2u	**-0.59**	*-0.35*	*0.33*	*-0.49*	**-0.59**	**-0.52**	*-0.5*	*-0.49*	*-0.26*	*-0.44*	*-0.36*	**-0.56**	**-0.54**	-0.09
nl2l	**-0.55**	*-0.32*	*0.37*	-0.22	**-0.53**	*-0.5*	*-0.48*	*-0.49*	-0.21	*-0.44*	*-0.32*	**-0.56**	*-0.47*	-0.03
ou1u	**-0.64**	*-0.27*	0.21	*-0.42*	**-0.68**	**-0.7**	**-0.6**	**-0.65**	*-0.37*	**-0.62**	**-0.54**	**-0.62**	**-0.57**	-0.19
ou1l	*-0.32*	-0.04	0.08	*-0.29*	-0.23	*-0.47*	*-0.42*	**-0.57**	-0.16	*-0.47*	-0.24	*-0.36*	*-0.42*	*-0.26*
ou2u	**-0.67**	-0.14	*0.27*	*-0.38*	**-0.58**	**-0.72**	**-0.7**	**-0.62**	*-0.26*	**-0.56**	*-0.45*	**-0.59**	**-0.54**	-0.16
ou2l	*-0.26*	0.01	0.23	*-0.32*	-0.21	-0.14	*-0.28*	*-0.27*	0.12	-0.14	-0.03	*-0.34*	*-0.42*	-0.24
ou3u	**-0.61**	-0.11	0.21	*-0.3*	*-0.48*	**-0.68**	*-0.76*	**-0.62**	-0.2	**-0.58**	*-0.39*	*-0.5*	*-0.45*	-0.12
ou3l	-0.25	-0.06	0.15	-0.24	-0.19	-0.25	-0.2	*-0.29*	0.17	-0.14	-0.09	*-0.27*	*-0.35*	-0.23
ou4u	**-0.53**	0.12	0.18	*-0.33*	*-0.44*	**-0.59**	**-0.58**	**-0.69**	*-0.37*	*-0.45*	*-0.34*	*-0.43*	*-0.45*	-0.17
ou4l	-0.07	-0.12	0.17	-0.19	-0.01	0.14	0.14	*0.4*	*0.38*	*0.39*	0.09	0.08	-0.18	-0.23
ou5u	*-0.49*	0.21	0.05	-0.16	*-0.4*	**-0.53**	*-0.45*	**-0.63**	*-0.37*	*-0.45*	*-0.32*	*-0.38*	*-0.31*	-0.11
ou5l	0.02	0.13	-0.05	0.11	0.16	0.12	0.12	0.14	**0.67**	0.19	0.12	-0.03	-0.04	-0.2
ou6u	**-0.57**	-0.01	0.09	-0.23	*-0.5*	**-0.69**	**-0.66**	*-0.79*	*-0.34*	*-0.77*	*-0.47*	**-0.58**	*-0.42*	-0.12
ou6l	*-0.33*	0.05	0.1	-0.2	*-0.29*	*-0.4*	*-0.32*	**-0.53**	-0.02	*-0.29*	-0.24	*-0.44*	*-0.41*	-0.23
ou7u	**-0.71**	-0.24	*0.29*	*-0.42*	**-0.65**	**-0.62**	**-0.58**	**-0.53**	-0.21	*-0.5*	**-0.64**	**-0.67**	**-0.6**	-0.22
ou7l	*-0.35*	-0.04	0.25	*-0.36*	*-0.31*	*-0.29*	*-0.36*	*-0.39*	0.02	-0.25	-0.08	*-0.38*	*-0.47*	-0.22
ou8u	**-0.62**	*-0.27*	*0.27*	*-0.41*	**-0.64**	**-0.61**	*-0.5*	**-0.6**	*-0.31*	**-0.51**	**-0.54**	**-0.72**	**-0.63**	-0.23
ou8l	*-0.44*	-0.19	0.21	*-0.43*	*-0.44*	*-0.47*	*-0.35*	**-0.51**	-0.24	*-0.38*	*-0.32*	*-0.35*	**-0.52**	*-0.29*
nr1u	**-0.62**	*-0.31*	*0.26*	*-0.38*	**-0.6**	**-0.58**	**-0.51**	**-0.54**	-0.25	*-0.48*	*-0.44*	**-0.62**	**-0.66**	-0.17
nr1l	**-0.58**	*-0.27*	*0.26*	*-0.32*	**-0.54**	**-0.56**	*-0.49*	**-0.54**	-0.22	*-0.48*	*-0.39*	**-0.56**	*-0.45*	-0.1
nr2u	**-0.58**	-0.14	0.13	*-0.34*	**-0.51**	**-0.59**	**-0.57**	**-0.6**	-0.22	**-0.56**	*-0.44*	**-0.58**	**-0.57**	*-0.32*
nr2l	**-0.61**	-0.13	0.16	*-0.29*	**-0.54**	**-0.62**	**-0.62**	**-0.64**	*-0.27*	**-0.61**	*-0.43*	**-0.6**	*-0.49*	0.02
CS	*-0.39*	-0.22	0.18	*-0.29*	*-0.4*	*-0.35*	*-0.29*	*-0.37*	-0.03	*-0.28*	*-0.36*	**-0.55**	**-0.55**	*-0.31*
MCS	0.17	-0.12	0.01	-0.04	0.04	0.09	0.1	0.02	0.21	0.08	0.01	-0.23	-0.17	-0.22
ML	0.22	-0.08	-0.02	-0.08	0.03	0.13	0.14	0.04	0.21	0.11	0.03	-0.21	-0.19	*-0.27*
IT	-0.16	0.13	-0.07	-0.08	0.04	*-0.29*	*-0.32*	-0.25	-0.14	-0.23	0.02	0.18	-0.05	-0.08
FWL	0.03	0.03	0.01	0.01	0.01	0.01	0	-0.01	-0.02	0	0	-0.01	-0.02	-0.02
FWF	0.01	0.01	-0.02	0	0.02	0.02	0.02	0.01	0.01	0.01	0.02	0.01	0	0
FNL	0	0.02	-0.04	0.01	0	-0.01	0.01	0	0	0.02	0	-0.01	0.02	0.02
FNR	0.01	0.02	-0.02	0.01	0	0	0	-0.01	0	0.01	0.01	0	0.01	0.01
DWL	*-0.29*	0.1	0.06	-0.19	-0.16	*-0.34*	*-0.43*	*-0.5*	-0.02	*-0.41*	-0.22	*-0.34*	*-0.4*	*-0.33*
DWF	-0.21	0.09	0.03	-0.12	-0.07	*-0.26*	*-0.34*	*-0.41*	0.08	*-0.34*	-0.19	*-0.27*	*-0.35*	*-0.38*
DNL	*-0.37*	-0.08	0.22	*-0.36*	*-0.32*	*-0.39*	*-0.43*	**-0.55**	-0.19	*-0.4*	*-0.26*	*-0.39*	**-0.51**	*-0.32*
DNR	*-0.34*	-0.04	0.25	*-0.3*	*-0.31*	*-0.39*	*-0.45*	**-0.6**	-0.18	*-0.43*	-0.19	*-0.42*	*-0.49*	*-0.27*
OF	*-0.39*	-0.22	0.19	*-0.29*	*-0.4*	*-0.34*	*-0.29*	*-0.38*	-0.03	*-0.28*	*-0.36*	**-0.55**	**-0.55**	*-0.31*
DC	-0.09	0.01	0.01	-0.01	-0.04	-0.08	-0.09	0	-0.06	-0.05	-0.08	0	0.01	-0.02
HWL	*-0.27*	0.1	0.07	-0.19	-0.16	*-0.33*	*-0.42*	*-0.49*	-0.02	*-0.4*	-0.22	*-0.35*	*-0.4*	*-0.33*
HWF	-0.2	0.09	0.03	-0.12	-0.07	-0.25	*-0.33*	*-0.4*	0.08	*-0.33*	-0.18	*-0.27*	*-0.35*	*-0.38*
HNL	*-0.37*	-0.08	0.22	*-0.36*	*-0.32*	*-0.39*	*-0.43*	**-0.55**	-0.19	*-0.4*	*-0.26*	*-0.39*	*-0.5*	*-0.32*
HNR	*-0.34*	-0.04	0.25	*-0.3*	*-0.31*	*-0.39*	*-0.45*	**-0.6**	-0.18	*-0.43*	-0.19	*-0.42*	*-0.49*	*-0.27*
in1	**0.74**	*0.45*	*-0.32*	*0.38*	**0.73**	**0.61**	*0.45*	*0.5*	*0.34*	*0.5*	**0.61**	**0.7**	**0.57**	0.12
in2	**0.73**	*0.38*	*-0.36*	*0.39*	**0.69**	*0.47*	*0.36*	*0.37*	0.25	*0.32*	**0.62**	**0.59**	**0.51**	0.11
in3	**0.54**	0.07	*-0.31*	0.18	*0.47*	*0.46*	*0.41*	**0.59**	0.18	*0.42*	*0.34*	**0.53**	*0.35*	0.06
in4	*0.41*	-0.13	-0.1	0.12	*0.34*	*0.5*	*0.45*	*0.79*	*0.37*	**0.57**	0.23	*0.42*	*0.28*	0.05
in5	*0.36*	0.07	-0.16	0.16	*0.36*	*0.45*	*0.47*	**0.71**	*0.37*	**0.55**	*0.31*	*0.47*	*0.34*	0.1
in6	**0.56**	-0.16	-0.21	0.2	**0.52**	**0.62**	**0.66**	**0.75**	**0.63**	**0.59**	*0.39*	**0.55**	*0.3*	-0.11
in7	*1*	*0.43*	*-0.27*	*0.34*	*0.79*	*0.79*	**0.7**	*0.47*	*0.42*	**0.61**	*0.77*	**0.65**	*0.47*	-0.02
in8	*0.43*	*1*	*-0.33*	0.23	*0.46*	0.24	0.11	-0.22	-0.04	0.08	*0.37*	*0.28*	*0.29*	0.04
nl1	*-0.27*	*-0.33*	*1*	0	*-0.3*	-0.18	-0.16	-0.04	-0.09	-0.04	-0.16	-0.25	-0.14	0.06
nl2	*0.34*	0.23	0	*1*	*0.39*	0.25	0.23	0.17	0.25	0.18	0.24	0.19	*0.41*	0.2
ou1	*0.79*	*0.46*	*-0.3*	*0.39*	*1*	**0.69**	**0.57**	*0.44*	*0.49*	**0.53**	**0.71**	**0.69**	*0.5*	0
ou2	*0.79*	0.24	-0.18	0.25	**0.69**	*1*	*0.82*	**0.69**	**0.56**	**0.73**	**0.68**	**0.57**	*0.38*	-0.01
ou3	**0.7**	0.11	-0.16	0.23	**0.57**	*0.82*	*1*	**0.69**	*0.5*	*0.77*	**0.53**	**0.51**	*0.34*	-0.06
ou4	*0.47*	-0.22	-0.04	0.17	*0.44*	**0.69**	**0.69**	*1*	**0.66**	**0.75**	*0.41*	*0.49*	*0.31*	-0.01
ou5	*0.42*	-0.04	-0.09	0.25	*0.49*	**0.56**	*0.5*	**0.66**	*1*	**0.56**	*0.39*	*0.29*	0.21	-0.12
ou6	**0.61**	0.08	-0.04	0.18	**0.53**	**0.73**	*0.77*	**0.75**	**0.56**	*1*	**0.54**	**0.51**	0.25	-0.06
ou7	*0.77*	*0.37*	-0.16	0.24	**0.71**	**0.68**	**0.53**	*0.41*	*0.39*	**0.54**	*1*	**0.65**	*0.41*	0.09
ou8	**0.65**	*0.28*	-0.25	0.19	**0.69**	**0.57**	**0.51**	*0.49*	*0.29*	**0.51**	**0.65**	*1*	**0.53**	0.03
nr1	*0.47*	*0.29*	-0.14	*0.41*	*0.5*	*0.38*	*0.34*	*0.31*	0.21	0.25	*0.41*	**0.53**	*1*	*0.32*
nr2	-0.02	0.04	0.06	0.2	0	-0.01	-0.06	-0.01	-0.12	-0.06	0.09	0.03	*0.32*	*1*

Appendix D

MVIV model time response

D.1 1280mm wide slabs

Table D.1 Comparison of $V(\hat{\Theta})$ for different ARX structures for 1280mm wide slabs.

	n_b=1	2	3
n_a=1	12.8579		
2	12.7289	12.7664	
3	12.7073	12.7422	12.7469

D.2 1575mm wide slabs

Table D.2 Comparison of $V(\hat{\Theta})$ for different ARX structures for 1575mm wide slabs.

	n_b=1	2	3
n_a=1	7.9015		
2	7.9207	7.9174	
3	7.8327	7.8285	7.8163

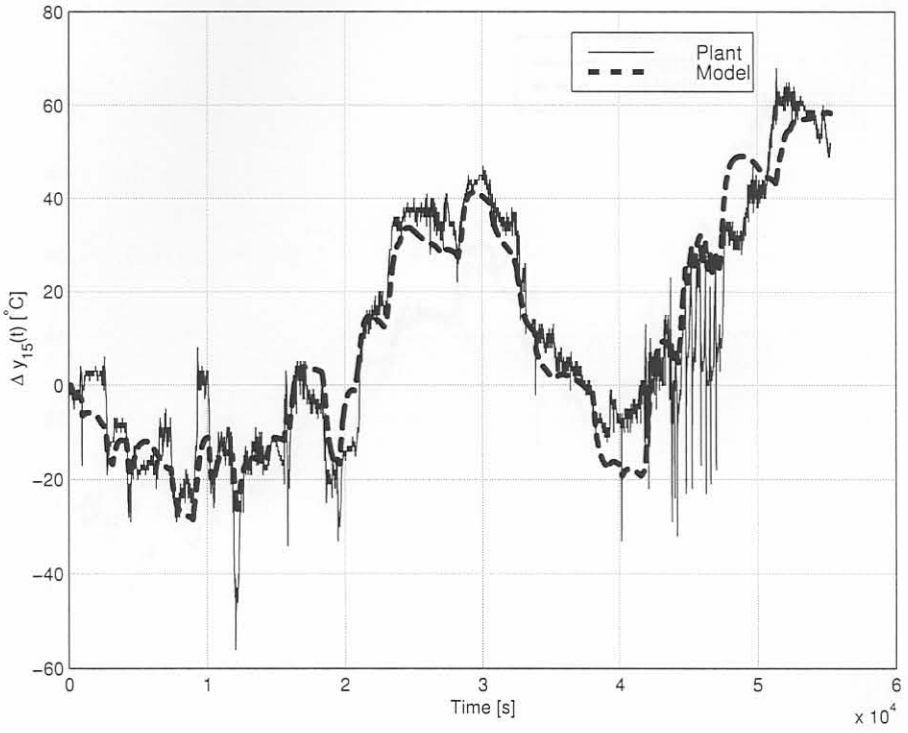

Figure D.1 Comparison of model output and plant output for thermocouple (output) in8u ($\Delta y_{15}(t)$) with $n_a = 1$ and $n_b = 1$ and 1280mm wide slabs.

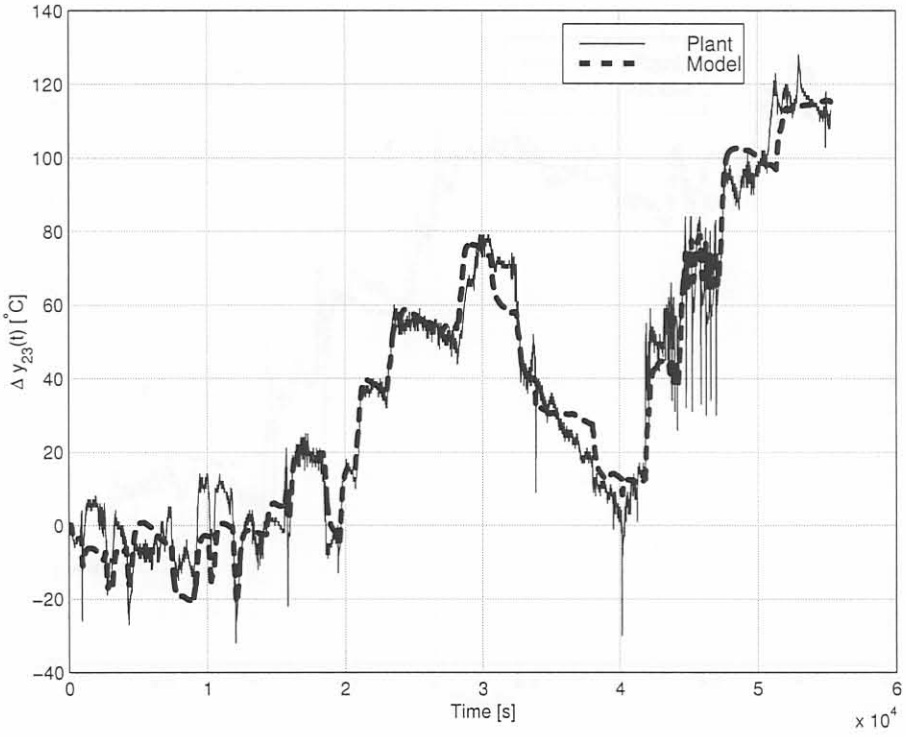

Figure D.2 Comparison of model output and plant output for thermocouple (output) ou2u ($\Delta y_{23}(t)$) with $n_a = 1$ and $n_b = 1$ and 1280mm wide slabs.

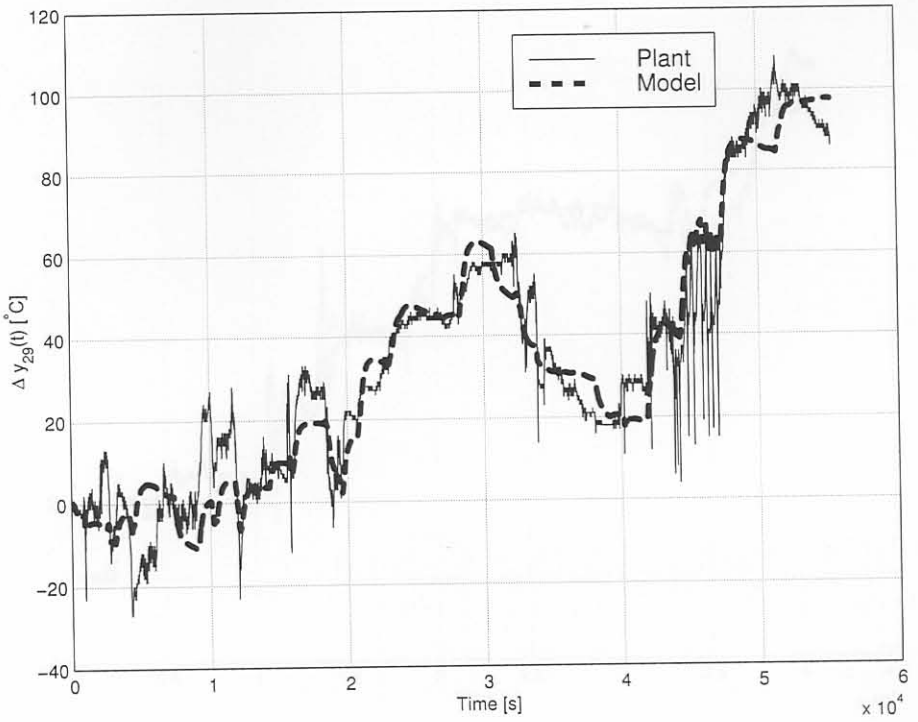

Figure D.3 Comparison of model output and plant output for thermocouple (output) ou5u ($\Delta y_{29}(t)$) with $n_a = 1$ and $n_b = 1$ and 1280mm wide slabs.

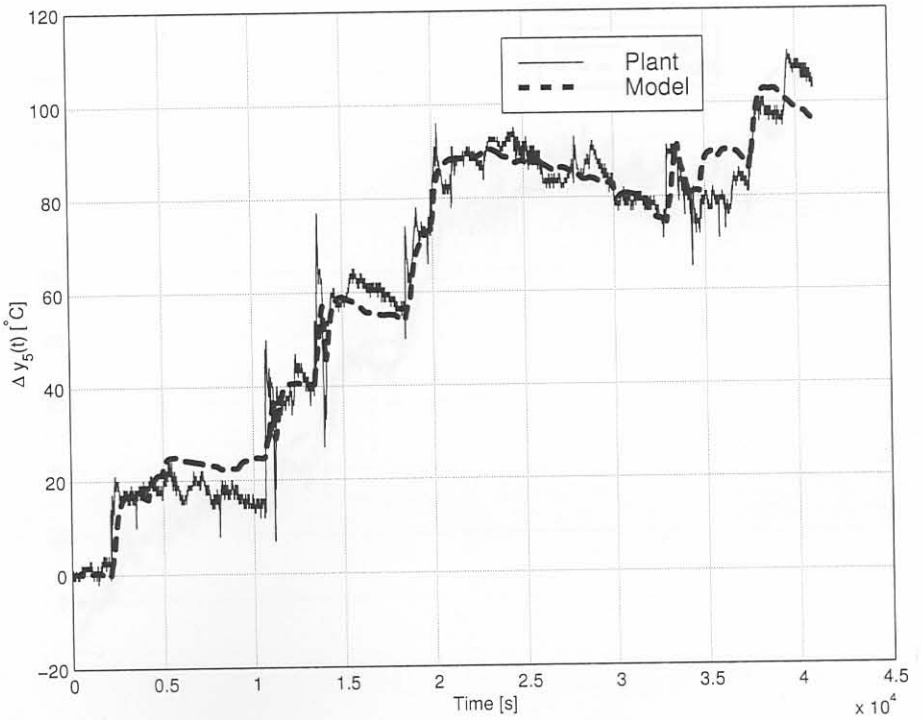

Figure D.4 Comparison of model output and plant output for thermocouple (output) in3u ($\Delta y_5(t)$) with $n_a = 1$ and $n_b = 1$ and 1575mm wide slabs.

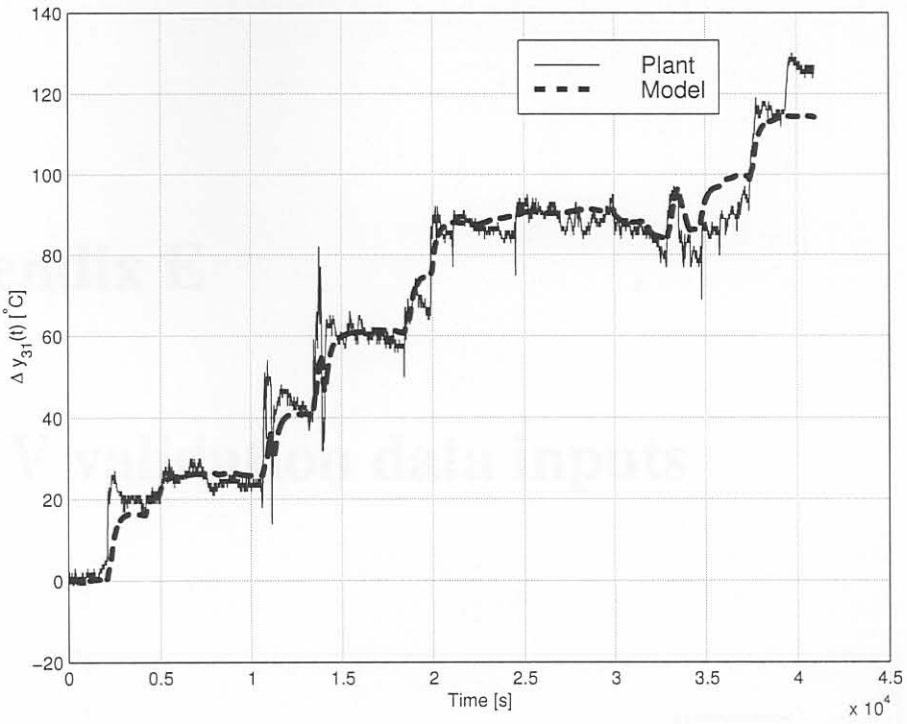

Figure D.5 Comparison of model output and plant output for thermocouple (output) ou7u ($\Delta y_{31}(t)$) with $n_a = 1$ and $n_b = 1$ and 1575mm wide slabs.

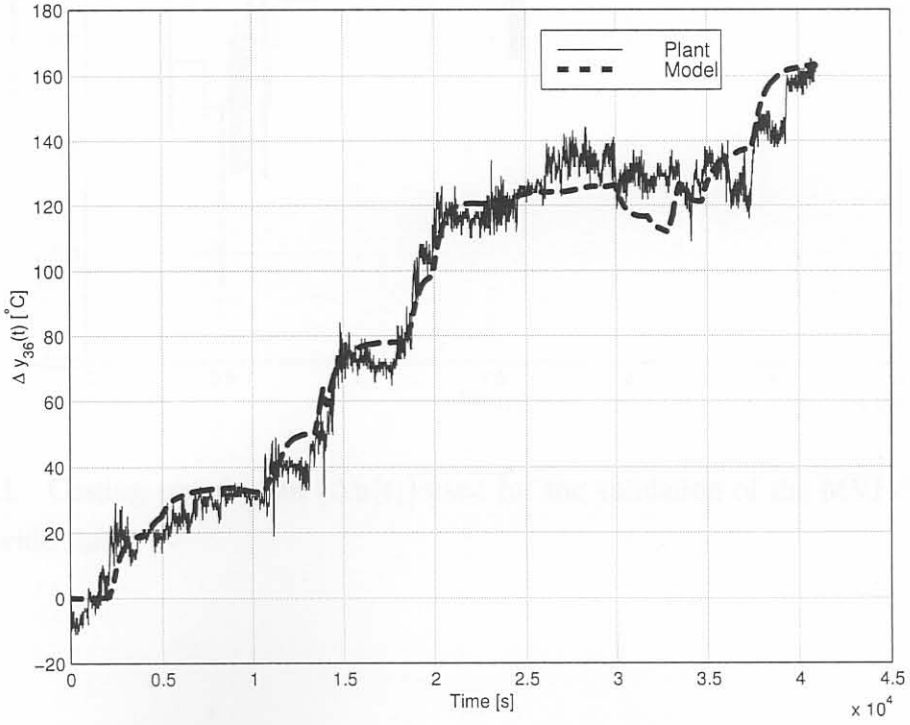

Figure D.6 Comparison of model output and plant output for thermocouple (output) nr11 ($\Delta y_{36}(t)$) with $n_a = 1$ and $n_b = 1$ and 1575mm wide slabs.

Appendix E

MVIV validation data inputs

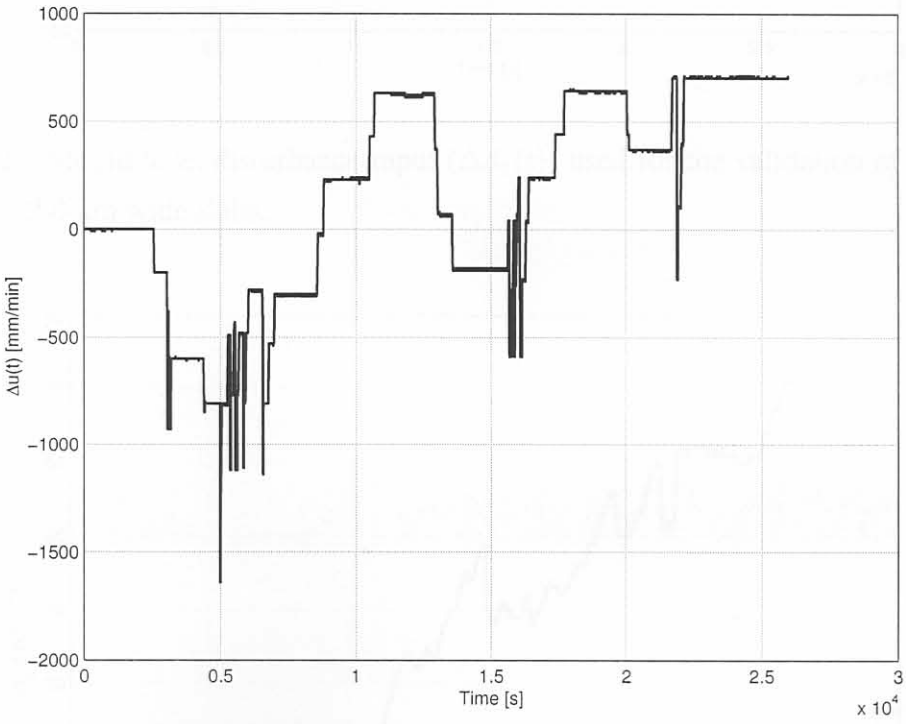

Figure E.1 Casting speed input ($\Delta u(t)$) used for the validation of the MVIV model for 1280mm wide slabs.

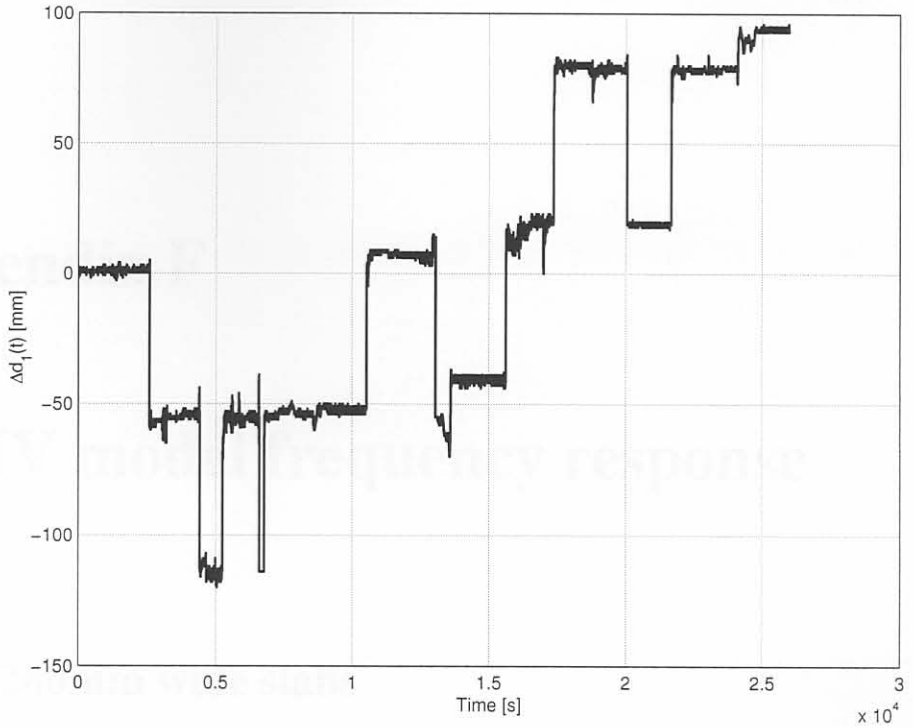

Figure E.2 Mould level disturbance input ($\Delta d_1(t)$) used for the validation of the MVIV model for 1280mm wide slabs.

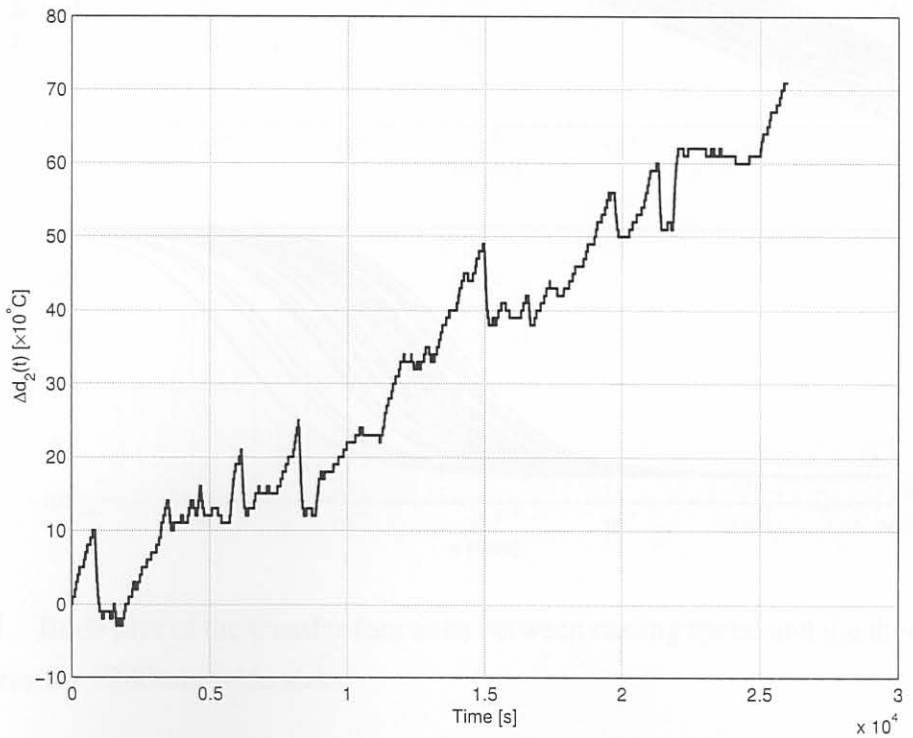

Figure E.3 Water temperature disturbance input ($\Delta d_2(t)$) used for the validation of the MVIV model for 1280mm wide slabs.

Appendix F

MVIV model frequency response

F.1 1280mm wide slabs

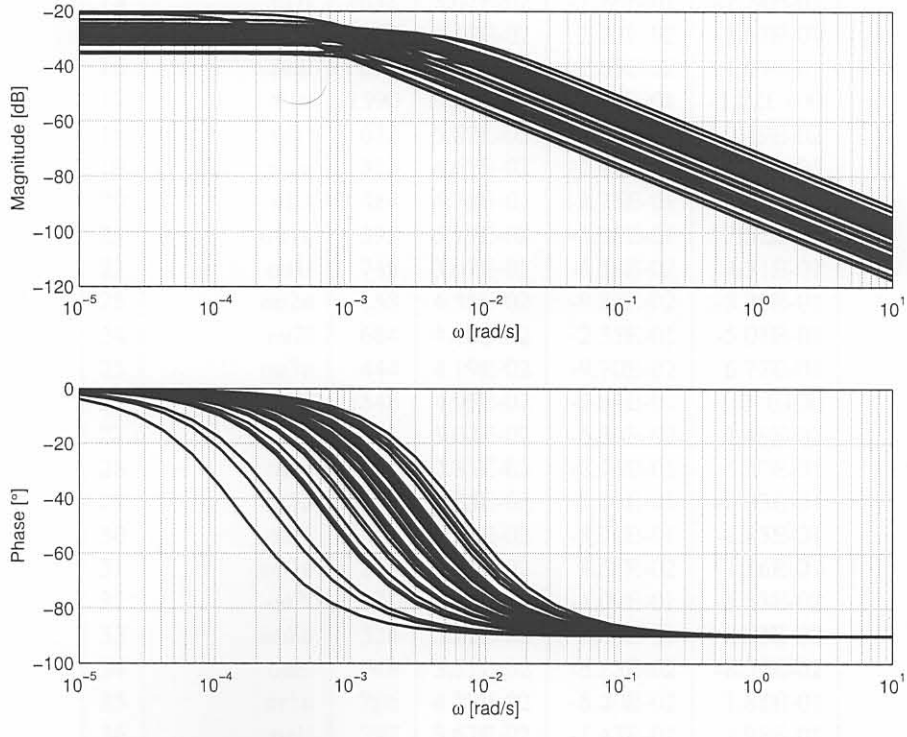

Figure F.1 Bode plot of the transfer functions between casting speed and the thermocouple temperatures for 1280mm wide slabs.

Table F.1 Transfer functions of the MV to IV model for 1280mm wide slabs.

i	Thermocouple	τ	k_u	k_{d_1}	k_{d_2}
1	in1u	180	3.33E-02	3.25E-02	-2.88E-01
2	in1l	512	2.47E-02	-2.55E-02	-2.48E-01
3	in2u	324	5.21E-02	-2.05E-01	-8.31E-01
4	in2l	1265	4.67E-02	-3.03E-01	-9.70E-01
5	in3u	348	3.11E-02	-1.97E-03	-5.43E-01
6	in3l	3721	6.06E-02	-9.04E-01	-1.17E+00
7	in4u	420	4.03E-02	-2.01E-01	-4.04E-01
8	in4l	6598	8.93E-02	-1.67E+00	-1.92E+00
9	in5u	197	1.81E-02	-5.74E-02	-1.57E-01
10	in5l	2991	4.81E-02	-6.79E-01	-1.06E+00
11	in6u	447	4.11E-02	-2.15E-01	-6.33E-01
12	in6l	1484	4.23E-02	-4.70E-01	-7.67E-01
13	in7u	302	3.32E-02	-4.18E-02	-4.69E-01
14	in7l	638	3.07E-02	-1.76E-01	-7.74E-01
15	in8u	279	3.10E-02	2.22E-02	-3.67E-01
16	in8l	672	1.70E-02	7.05E-02	1.69E-01
17	nl1u	1590	9.26E-02	-5.07E-01	-1.22E+00
18	nl1l	672	5.82E-02	-1.38E-01	-9.49E-02
19	nl2u	313	4.67E-02	-2.30E-02	4.53E-01
20	nl2l	484	4.78E-02	-1.75E-01	1.97E-01
21	ou1u	395	5.19E-02	-1.08E-01	-7.52E-01
22	ou1l	745	3.67E-02	-6.54E-02	-4.51E-01
23	ou2u	153	4.35E-02	-9.33E-02	-3.28E-01
24	ou2l	684	4.18E-02	-2.35E-01	-5.01E-01
25	ou3u	444	4.19E-02	-9.70E-02	-6.77E-01
26	ou3l	1548	4.95E-02	-2.64E-01	-1.01E+00
27	ou4u	321	3.07E-02	-6.30E-02	-1.49E-01
28	ou4l	981	2.81E-02	-2.76E-01	-5.37E-01
29	ou5u	286	3.35E-02	-1.06E-01	-2.03E-01
30	ou5l	1563	3.38E-02	-3.76E-01	-4.85E-01
31	ou7u	226	3.65E-02	4.58E-02	-1.26E-01
32	ou7l	611	3.65E-02	-1.09E-01	-3.53E-02
33	ou8u	324	3.28E-02	2.00E-01	-8.93E-02
34	ou8l	748	3.51E-02	-6.25E-02	-8.55E-02
35	nr1u	206	4.79E-02	-6.20E-02	1.88E-01
36	nr1l	297	3.67E-02	-1.43E-01	2.98E-01
37	nr2u	904	6.97E-02	-4.15E-01	-7.08E-01
38	nr2l	435	5.08E-02	-2.52E-01	-2.15E-01

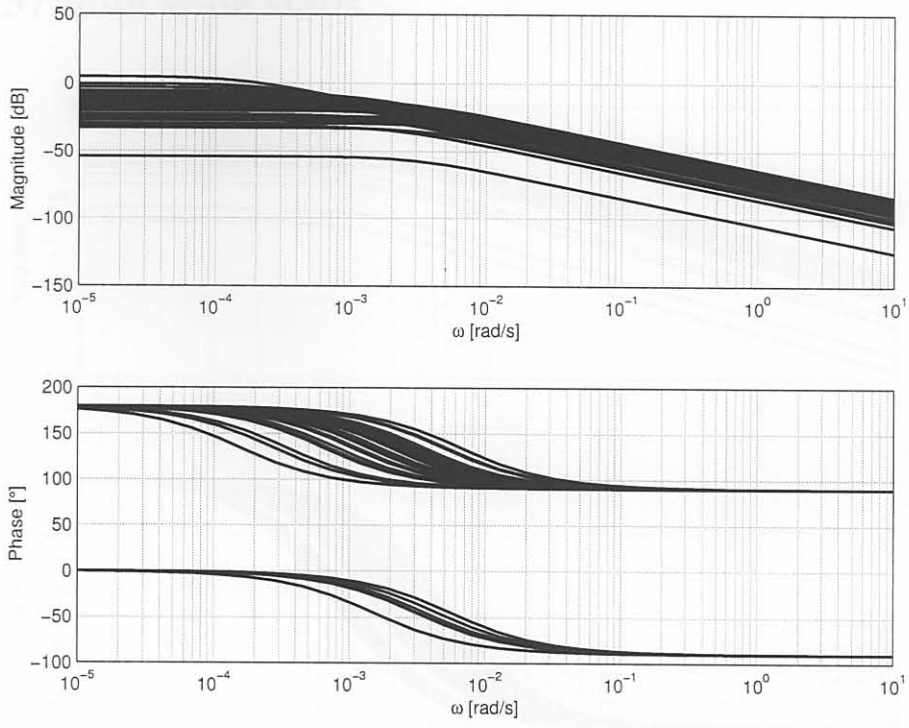

Figure F.2 Bode plot of the transfer functions between mould level and the thermocouple temperatures for 1280mm wide slabs.

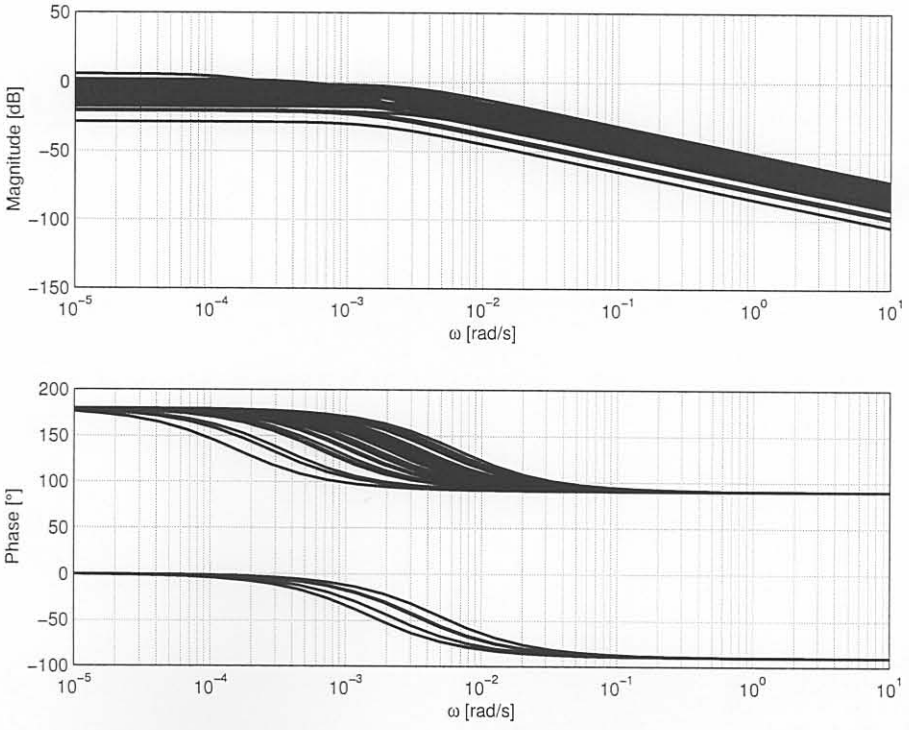

Figure F.3 Bode plot of the transfer functions between inlet temperature and the thermocouple temperatures for 1280mm wide slabs.

F.2 1575mm wide slabs

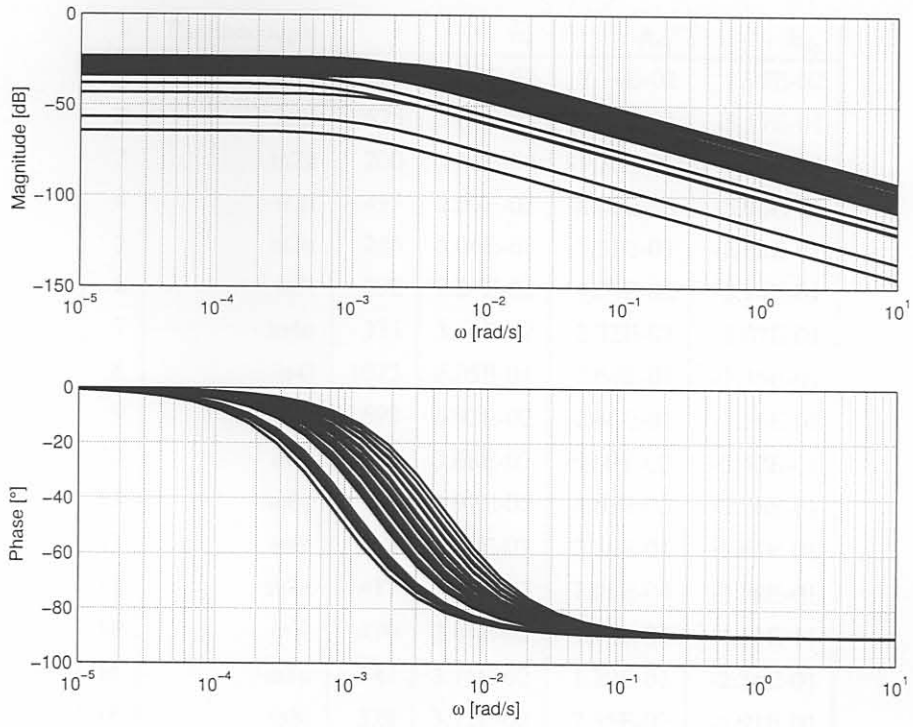

Figure F.4 Bode plot of the transfer functions between casting speed and the thermocouple temperatures for 1575mm wide slabs.

Table F.2 Transfer functions of the MV to IV model for 1575mm wide slabs.

i	Thermocouple	τ	k_u	k_{d_1}	k_{d_2}
1	in1u	221	3.55E-02	7.74E-02	1.95E-02
2	in1l	675	3.64E-02	1.77E-01	-5.57E-01
3	in2u	200	4.64E-02	-1.26E-01	7.54E-02
4	in2l	497	2.59E-02	-8.03E-03	-5.96E-01
5	in3u	245	5.06E-02	-1.31E-01	-2.62E-01
6	in3l	292	3.24E-02	4.04E-02	-5.14E-01
7	in4u	333	3.64E-02	2.32E-02	-1.07E-01
8	in4l	1073	6.05E-04	2.64E-01	-1.35E-01
9	in5u	598	6.92E-02	-2.88E-01	-7.56E-01
10	in5l	539	3.68E-02	-9.09E-02	-5.47E-01
11	in6u	389	3.92E-02	-4.63E-03	-2.26E-01
12	in6l	668	6.74E-03	2.36E-01	-1.61E-01
13	in7u	417	4.95E-02	7.06E-04	-3.78E-01
14	in7l	470	2.44E-02	1.44E-01	-4.13E-01
15	in8u	347	3.75E-02	1.20E-01	-2.56E-01
16	in8l	329	3.72E-02	7.35E-02	-5.91E-01
17	nl1u	285	2.00E-02	-1.31E-01	3.77E-01
18	nl1l	613	3.34E-02	-2.60E-01	4.70E-01
19	nl2u	463	6.03E-02	-3.59E-01	2.71E-01
20	nl2l	385	3.15E-02	-1.78E-01	2.17E-01
21	ou1u	379	2.30E-02	2.10E-01	-4.92E-02
22	ou1l	1316	2.10E-02	2.64E-01	-2.89E-01
23	ou2u	290	4.68E-02	-2.60E-02	-4.14E-01
24	ou2l	1145	5.56E-02	-5.22E-02	-1.02E+00
25	ou3u	380	3.66E-02	5.19E-02	-9.08E-03
26	ou3l	686	2.88E-02	1.86E-01	-3.27E-01
27	ou4u	348	3.55E-02	4.75E-02	2.92E-02
28	ou4l	945	1.44E-03	3.13E-01	-1.35E-01
29	ou5u	498	4.99E-02	-1.11E-01	-3.98E-01
30	ou5l	1305	1.24E-02	1.25E-01	-2.34E-02
31	ou7u	256	4.38E-02	-1.23E-01	7.27E-02
32	ou7l	647	4.37E-02	-1.31E-01	-5.69E-01
33	ou8u	406	3.59E-02	4.96E-02	-9.96E-02
34	ou8l	532	4.26E-02	5.63E-02	-8.63E-01
35	nr1u	619	3.81E-02	1.16E-02	6.97E-01
36	nr1l	459	4.91E-02	-3.13E-02	1.78E-01
37	nr2u	675	2.65E-02	7.52E-02	1.23E+00
38	nr2l	1013	4.19E-02	-7.61E-02	1.25E+00

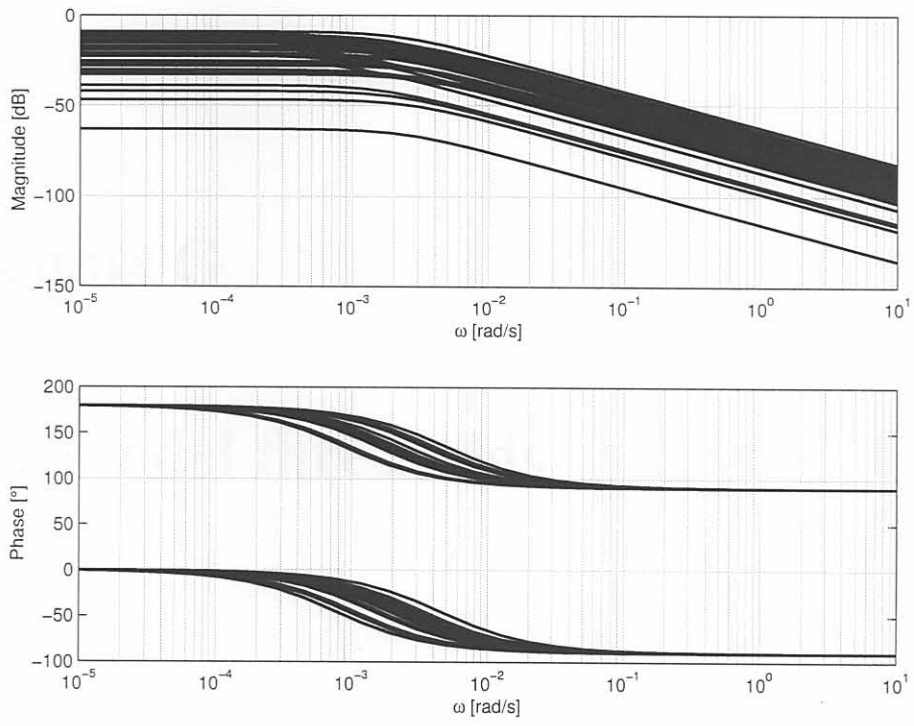

Figure F.5 Bode plot of the transfer functions between mould level and the thermocouple temperatures for 1575mm wide slabs.

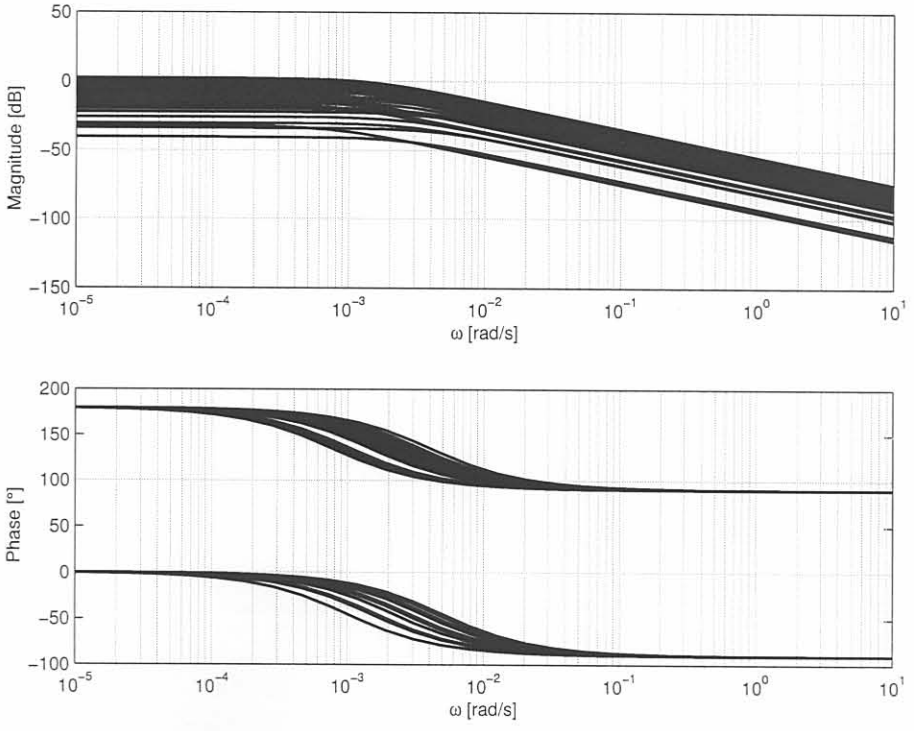

Figure F.6 Bode plot of the transfer functions between inlet temperature and the thermocouple temperatures for 1575mm wide slabs.

Appendix G

IVOV model thresholds

Table G.1 Thresholds for the IVOV predictor for 1060mm wide slabs

	1a	1b	2a	2b	4	5a	5b	6	8
TBL	0	0	0	0	0.3241	0.3249	0	0	0.3204
TBC	0	0	0	0.2131	0	0.2223	0	0	0.1249
TBR	0	0	0	0	0	0.2174	0	0	0.2553
BBL	0	0	0	0.06797	0	0.2734	0	0	0.2433
BBC	0	0	0	0.1323	0	0.2734	0	0	0.04449
BBR	0	0	0	0	0	0.2734	0	0	0.2383
TAL	0	0	0	0.3255	0	0	0	0	0.1257
TAC	0	0	0	0.8919	0	0	0	0	0.4165
TAR	0	0	0	0.2991	0	0	0	0	0.1628
BAL	0	0	0	0.06184	0	0	0	0	0.1337
BAC	0	0	0.09355	0.9357	0	0	0	0	0.317
BAR	0	0	0	0.0474	0	0	0	0	0.1357

Table G.2 Thresholds for the IVOV predictor for 1320mm wide slabs

	1a	1b	2a	2b	4	5a	5b	6	8
TBL	0	0	0	0.03973	0.5165	0.2003	0	0.4401	0.1701
TBC	0	0	0	0.1984	0	0.1933	0	0.4401	0.0766
TBR	0	0	0	0.02151	0	0.1852	0	0.4401	0.1539
BBL	0	0	0	0.05918	0	0	0	0.2846	0.07791
BBC	0	0	0	0.2291	0	0	0	0.2846	0.025
BBR	0	0	0	0.01764	0	0	0	0.2846	0.1551
TAL	0	0	0	0.2232	0	0	0.09609	0.1803	0.1555
TAC	0	0.5323	0	0.6739	0	0	0	0.1803	0.1997
TAR	0	0	0	0.2567	0	0	0.1095	0.1803	0.141
BAL	0	0	0	0.1073	0	0	0	0.1203	0.09857
BAC	0	0	0	0.5426	0	0	0	0.1213	0.1414
BAR	0	0	0	0.0547	0	0	0	0.1213	0.1138

Table G.3 Thresholds for the IVOV predictor for 1575mm wide slabs

	1a	1b	2a	2b	4	5a	5b	6	8
TBL	0	0	0	0	0	0	0	0.1996	0
TBC	0	0	0	0.1067	0	0	0	0.1996	0
TBR	0	0	0	0	0	0	0	0.1996	0
BBL	0	0	0	0	0	0	0	0.1597	0.09185
BBC	0	0	0	0.1127	0	0	0	0.1597	0
BBR	0	0	0	0	0	0	0	0.1597	0.08158
TAL	0	0	0	0.1385	0	0	0	0.06923	0.09947
TAC	0	0	0	0.3336	0	0	0	0.06923	0.1165
TAR	0	0	0	0.149	0	0	0	0.06923	0.1191
BAL	0	0	0	0.04642	0	0	0	0.06108	0.07018
BAC	0	0	0	0.2952	0	0	0	0.05896	0.1117
BAR	0	0	0	0.03535	0	0	0	0.05896	0.08297

Appendix H

LQTSS

H.1 SIMULINK implementation

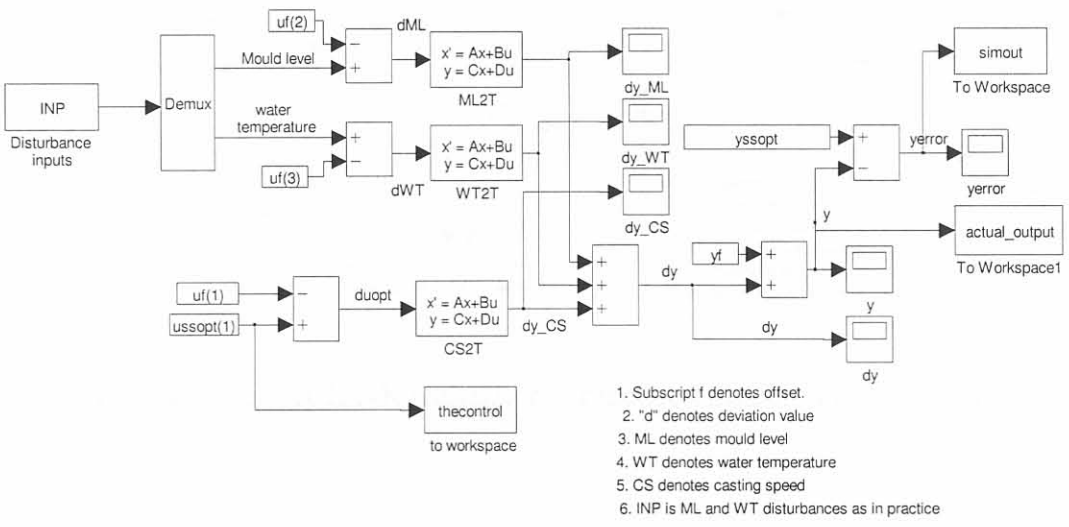

Figure H.1 SIMULINK realization for the MVIV model.

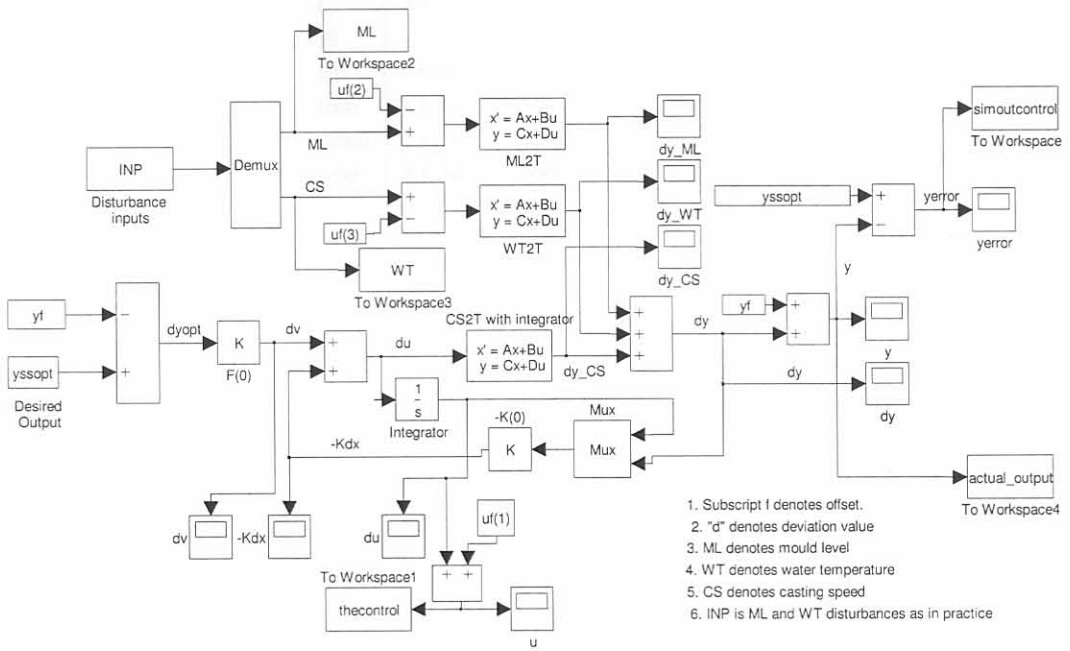

Figure H.2 SIMULINK realization for the LQTSS controller synthesis.

H.2 1280mm wide slabs results

H.2.1 Tabled results

Table H.1 1280mm wide slab errors, maximum accellaration and maximum speeds for the LQTSS implementation at different values of the q/r ratio.

$\frac{q}{r}$	SMSMSE	$\max\lvert du_1/dt \rvert$	$\max(u_1)$
None	7.1598	0	724.1
0.001	4.727	10.81	927.1
0.01	4.6325	34.64	936.8
0.1	4.5739	75.67	948.4
1	4.5427	142.3	958
10	4.5268	271.5	962.1
100	4.5186	501.4	966
1000	4.5143	918	968.5
10000	4.5122	1620	969.7
1450	4.5139	1000	968.8

Table H.2 Mean Square Errors for the LQTSS implementation for 1280mm wide slabs at different values of the q/r ratio. $q/r = 1450$ has the maximum accellaration of 1000mm/min^2.

$\frac{q}{r}$	in1u	in1l	in2u	in2l	in3u	in3l	in4u	in4l
None	6	5.06	70.8	92.9	22.2	204	22	550
0.001	10.8	3.27	8.92	8.78	3.73	31.5	5.17	135
0.01	9.37	2.69	6.71	9.36	2.91	34.8	3.78	146
0.1	8.38	2.31	5.13	9.86	2.34	37.2	2.85	153
1	7.81	2.09	4.29	10.2	2.05	38.8	2.32	158
10	7.5	1.97	3.88	10.5	1.9	39.8	2.04	162
100	7.33	1.9	3.68	10.7	1.82	40.4	1.88	163
1000	7.24	1.86	3.58	10.8	1.78	40.7	1.8	165
10000	7.2	1.84	3.52	10.8	1.76	40.9	1.76	165
1450	7.23	1.85	3.57	10.8	1.78	40.8	1.79	165

$\frac{q}{r}$	in5u	in5l	in6u	in6l	in7u	in7l	in8u	in8l
None	3.06	149	44.5	80.9	18.7	56.1	9.72	3.3
0.001	1.92	28.1	4.19	8.35	4.09	10.5	5.88	19.4
0.01	1.53	30.4	3.17	9.05	3.01	10.6	4.8	18.7
0.1	1.24	32.2	2.5	9.61	2.25	10.7	4.06	18.3
1	1.07	33.4	2.15	10	1.84	10.9	3.64	18
10	0.984	34.1	1.98	10.3	1.62	11	3.41	17.9
100	0.937	34.5	1.9	10.4	1.51	11	3.29	17.8
1000	0.911	34.8	1.86	10.5	1.45	11.1	3.23	17.7
10000	0.898	34.9	1.84	10.6	1.42	11.1	3.19	17.7
1450	0.908	34.8	1.86	10.6	1.45	11.1	3.22	17.7

$\frac{q}{r}$	ou1u	ou1l	ou2u	ou2l	ou3u	ou3l	ou4u	ou4l
None	50.1	17.1	12.4	31.4	40	93.2	2.82	36.7
0.001	7.68	3.89	14.7	2.96	4.55	6.59	10.2	4.3
0.01	5.48	2.94	12.3	1.98	3.35	7.17	9.11	4.48
0.1	4	2.34	10.5	1.37	2.55	7.66	8.35	4.64
1	3.2	2	9.5	1.03	2.14	8.04	7.9	4.77
10	2.79	1.81	8.94	0.86	1.93	8.3	7.64	4.86
100	2.57	1.71	8.64	0.767	1.82	8.46	7.49	4.92
1000	2.46	1.65	8.48	0.717	1.77	8.56	7.41	4.95
10000	2.4	1.62	8.4	0.691	1.74	8.61	7.37	4.97
1450	2.44	1.64	8.46	0.712	1.76	8.57	7.4	4.96

$\frac{q}{r}$	ou5u	ou5l	ou6u	ou6l	ou7u	ou7l	ou8u	ou8l
None	5.93	38.2	NA	NA	0.89	1.17	1.64	1.33
0.001	9.04	2.03	NA	NA	24.2	21.8	32.2	18.8
0.01	7.75	2.18	NA	NA	22.5	20.1	30.6	17.2
0.1	6.87	2.33	NA	NA	21.3	18.9	29.5	16.1
1	6.35	2.45	NA	NA	20.6	18.2	28.9	15.5
10	6.06	2.53	NA	NA	20.2	17.8	28.5	15.1
100	5.9	2.59	NA	NA	20	17.5	28.3	14.9
1000	5.81	2.62	NA	NA	19.9	17.4	28.2	14.8
10000	5.77	2.64	NA	NA	19.8	17.3	28.1	14.7
1450	5.8	2.63	NA	NA	19.9	17.4	28.2	14.8

$\frac{q}{r}$	nl1u	nl1l	nl2u	nl2l	nr1u	nr1l	nr2u	nr2l
None	168	3.12	14.6	1.45	2.06	4.31	70.5	12.3
0.001	6.31	54.1	116	62.5	72.6	52.9	9.86	22.2
0.01	3.88	49.7	112	59.1	69.5	50.9	7.05	19.4
0.1	2.57	46.8	110	56.8	67.5	49.6	5.31	17.6
1	1.91	45	108	55.4	66.3	48.7	4.34	16.5
10	1.58	44	107	54.5	65.6	48.2	3.8	15.8
100	1.42	43.3	107	54	65.1	47.9	3.5	15.5
1000	1.33	43	107	53.8	64.9	47.7	3.34	15.3
10000	1.29	42.8	106	53.6	64.8	47.7	3.25	15.2
1450	1.32	42.9	107	53.7	64.8	47.7	3.32	15.2

Table H.3 Feedback gain matrix $\mathbf{K}_\infty$ for 1280mm wide slabs at $q/r = 1450$.

The gain of the integrator state is $k_\infty = 0.221$.

in1u	in1l	in2u	in2l	in3u	in3l	in4u	in4l
8.04	3.47	9.06	4.8	5.22	4.99	6.17	6.86
in5u	in5l	in6u	in6l	in7u	in7l	in8u	in8l
4.15	4.1	6.13	4.17	5.98	3.94	5.83	2.14
ou1u	ou1l	ou2u	ou2l	ou3u	ou3l	ou4u	ou4l
8.18	4.45	11.6	5.23	6.27	4.82	5.37	3.11
ou5u	ou5l	ou6u	ou6l	ou7u	ou7l	ou8u	ou8l
6.21	3.29	NA	NA	7.7	4.77	5.69	4.25
nl1u	nl1l	nl2u	nl2l	nr1u	nr1l	nr2u	nr2l
8.96	7.34	8.27	6.88	10.7	6.66	7.91	7.67

Table H.4 Feedforward gain matrix $\mathbf{F}$ for 1280mm wide slabs at $q/r = 1450$.

in1u	in1l	in2u	in2l	in3u	in3l	in4u	in4l
4.52	3.35	7.08	6.34	4.22	8.23	5.47	12.1
in5u	in5l	in6u	in6l	in7u	in7l	in8u	in8l
2.46	6.54	5.58	5.75	4.5	4.16	4.21	2.3
ou1u	ou1l	ou2u	ou2l	ou3u	ou3l	ou4u	ou4l
7.04	4.98	5.91	5.67	5.7	6.72	4.17	3.82
ou5u	ou5l	ou6u	ou6l	ou7u	ou7l	ou8u	ou8l
4.54	4.59	NA	NA	4.96	4.95	4.45	4.76
nl1u	nl1l	nl2u	nl2l	nr1u	nr1l	nr2u	nr2l
12.6	7.91	6.35	6.5	6.51	4.98	9.46	6.9

H.2.2 Time-domain results

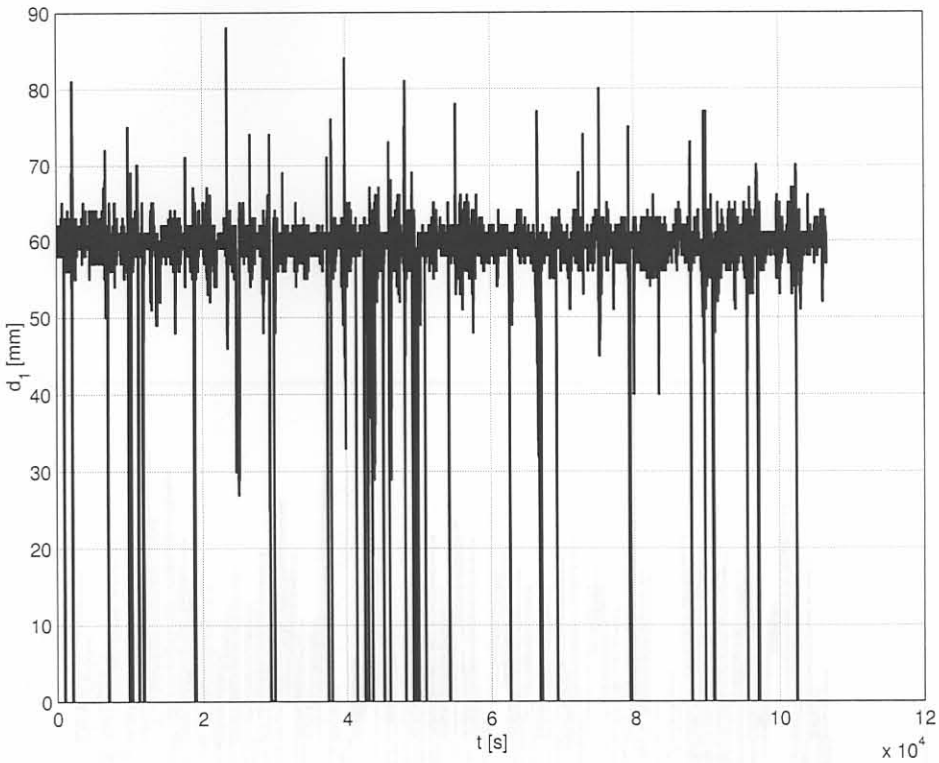

Figure H.3 Mould level disturbance ($d_1(t)$) used for the simulation of the 1280mm wide slab system.

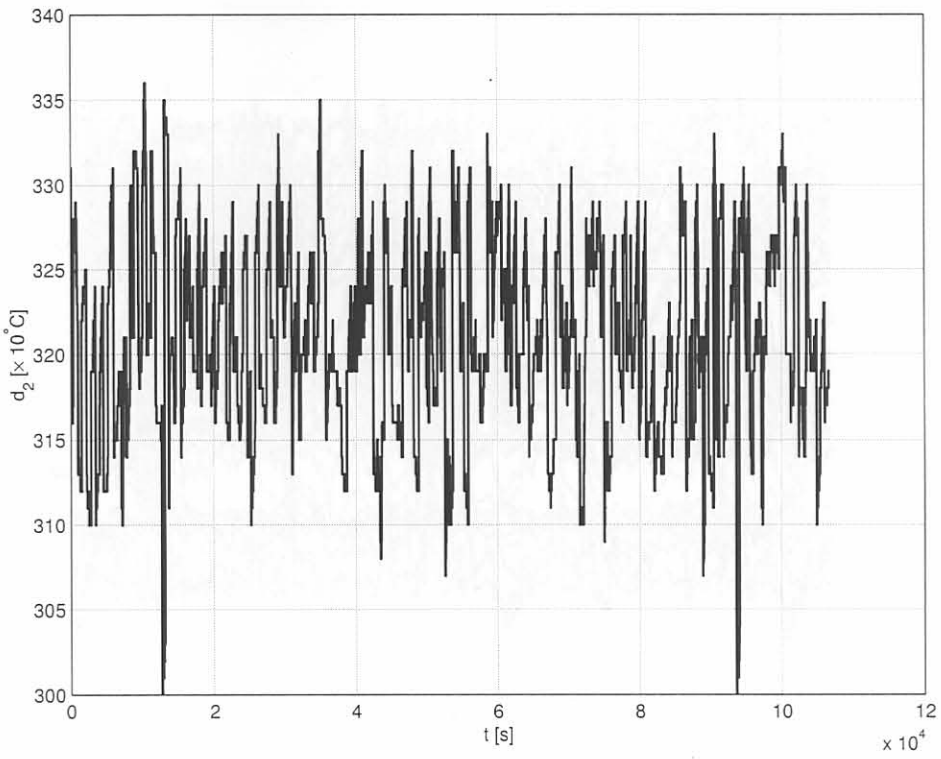

Figure H.4 Water temperature ($d_2(t)$) disturbance used for the simulation of the 1280mm wide slab system.

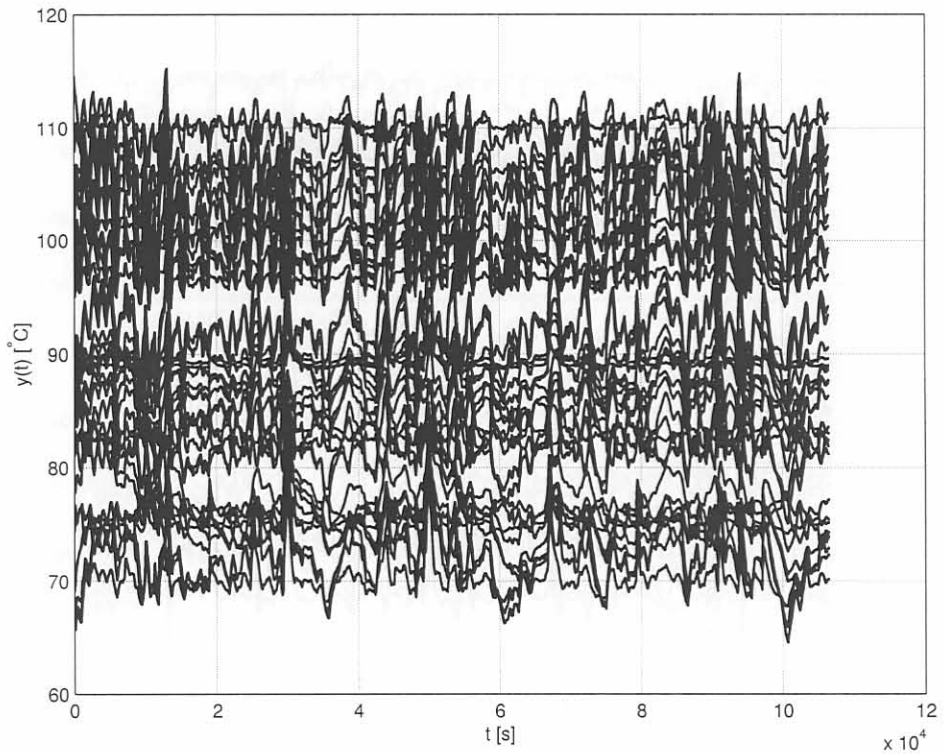

Figure H.5 Outputs ($\mathbf{y}(t)$) of the system without the LQTSS controller for 1280mm wide slabs.

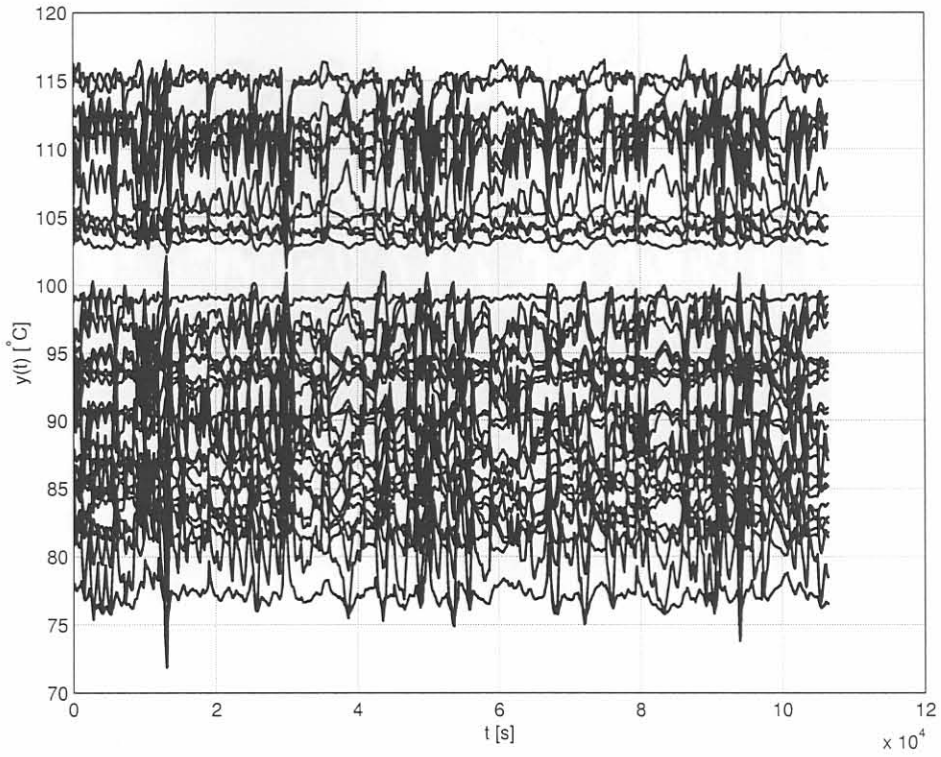

Figure H.6 Outputs ($\mathbf{y}(t)$) of the system with the LQTSS controller for 1280mm wide slabs.

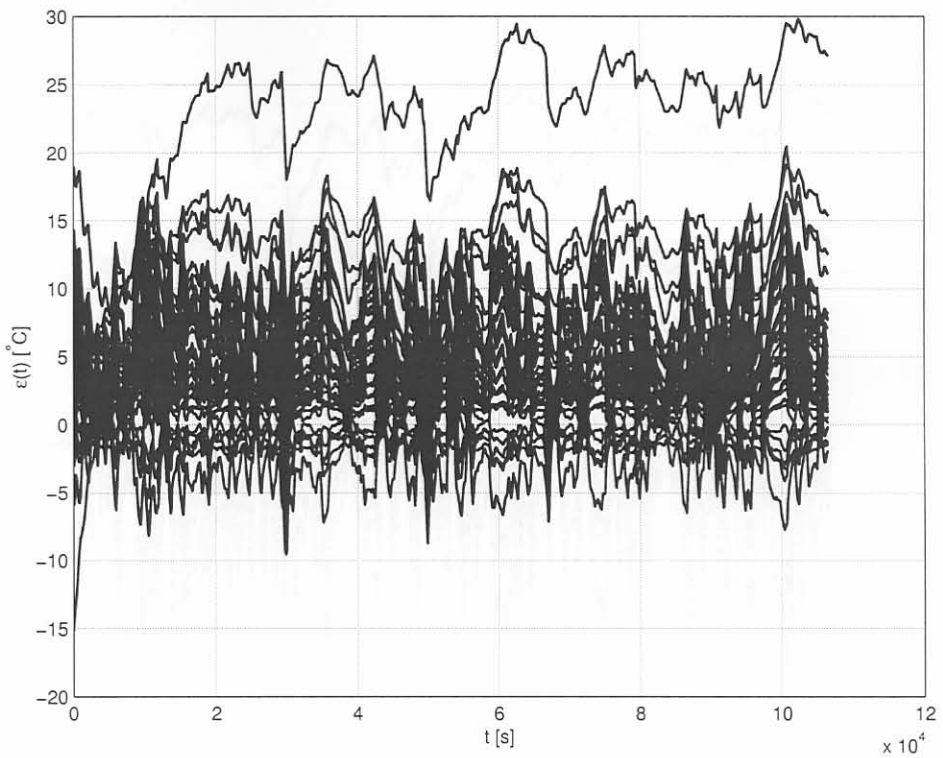

Figure H.7 Tracking errors of the system without the LQTSS controller for 1280mm wide slabs.

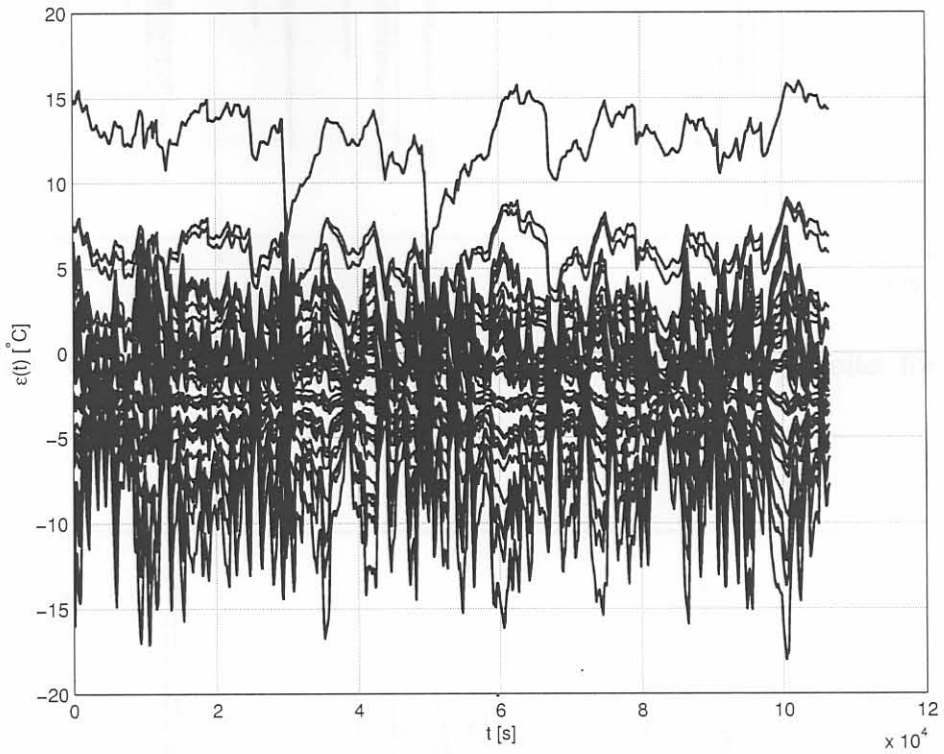

Figure H.8 Tracking errors of the system with the LQTSS controller for 1280mm wide slabs.

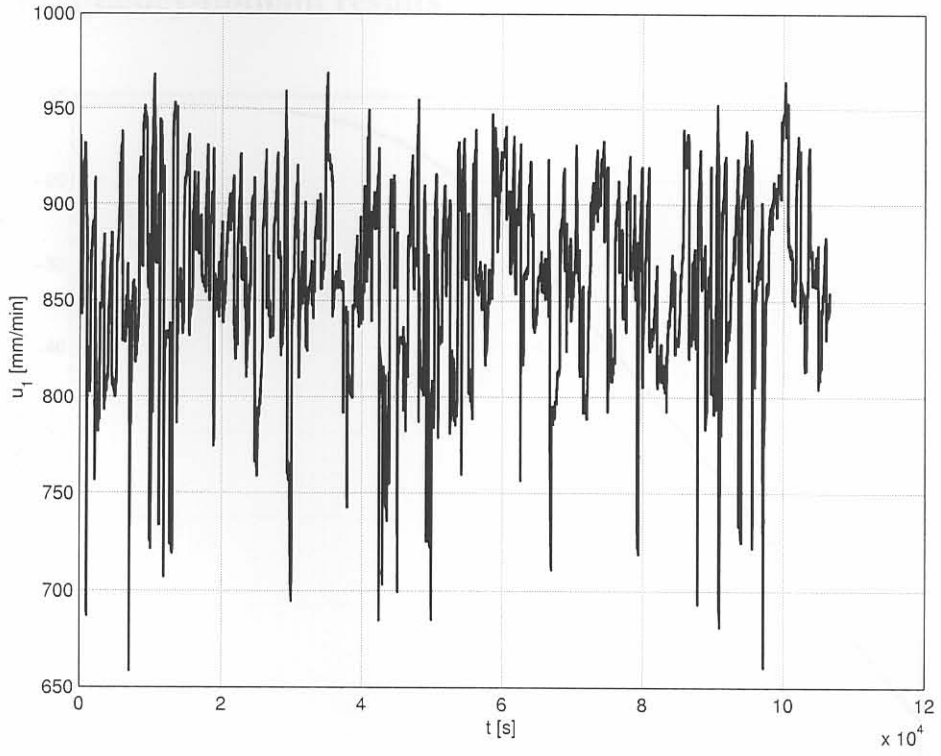

Figure H.9 Casting speed (casting speed, $u_1(t)$) for the LQTSS controller for 1280mm wide slabs.

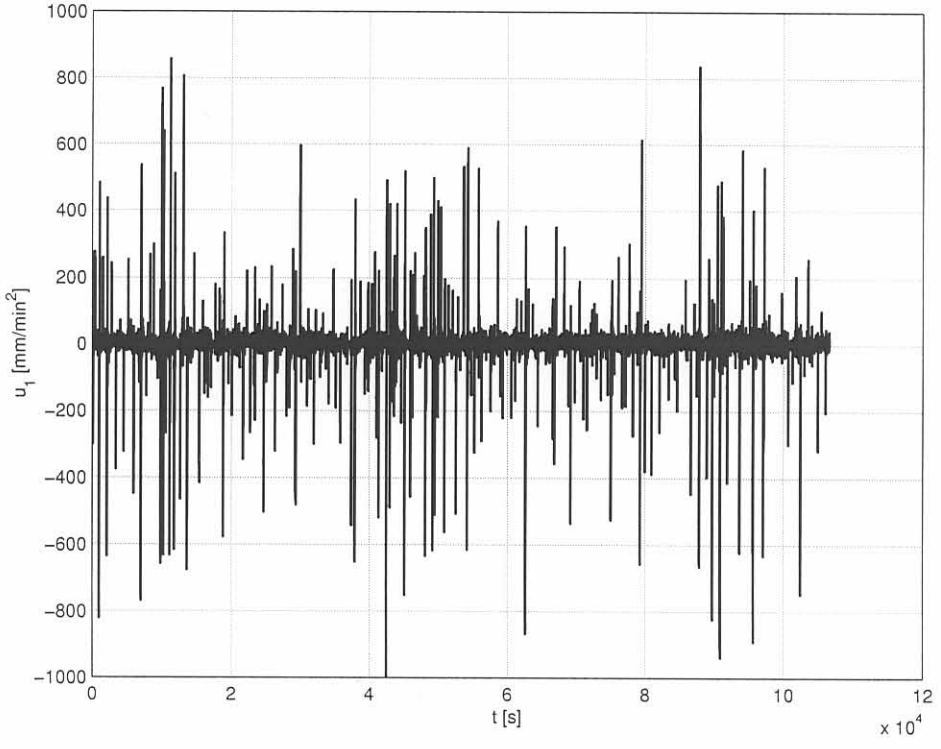

Figure H.10 Casting accellaration for the LQTSS controller for 1280mm wide slabs.

H.2.3 Frequency-domain results

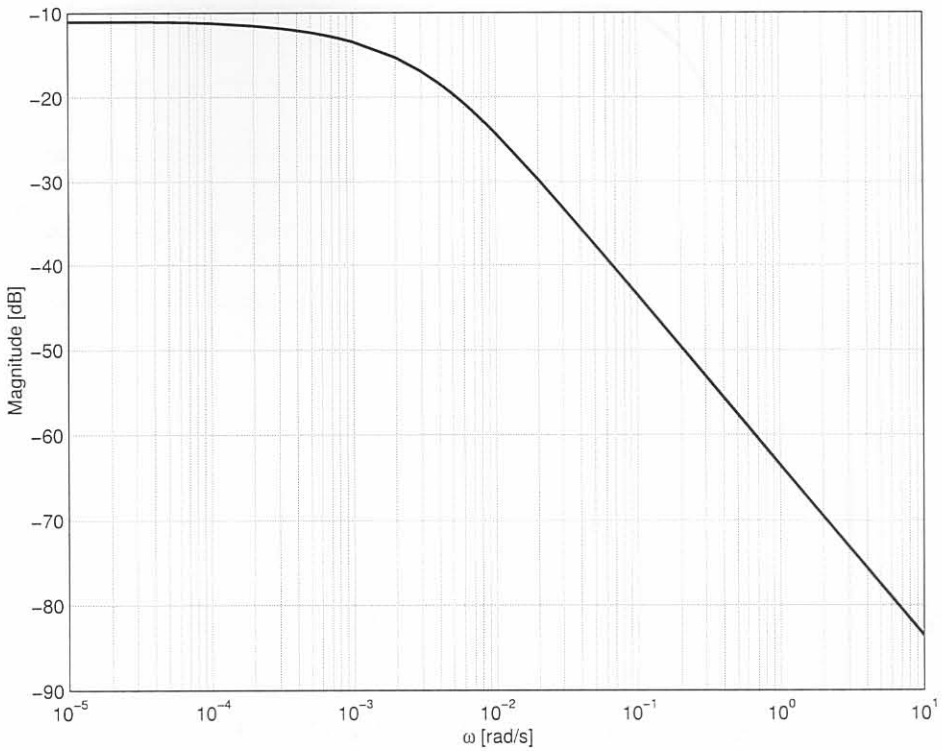

Figure H.11 Open-loop SVD plot of casting speed to the thermocouple temperatures without control ($\mathbf{g}(s)$).

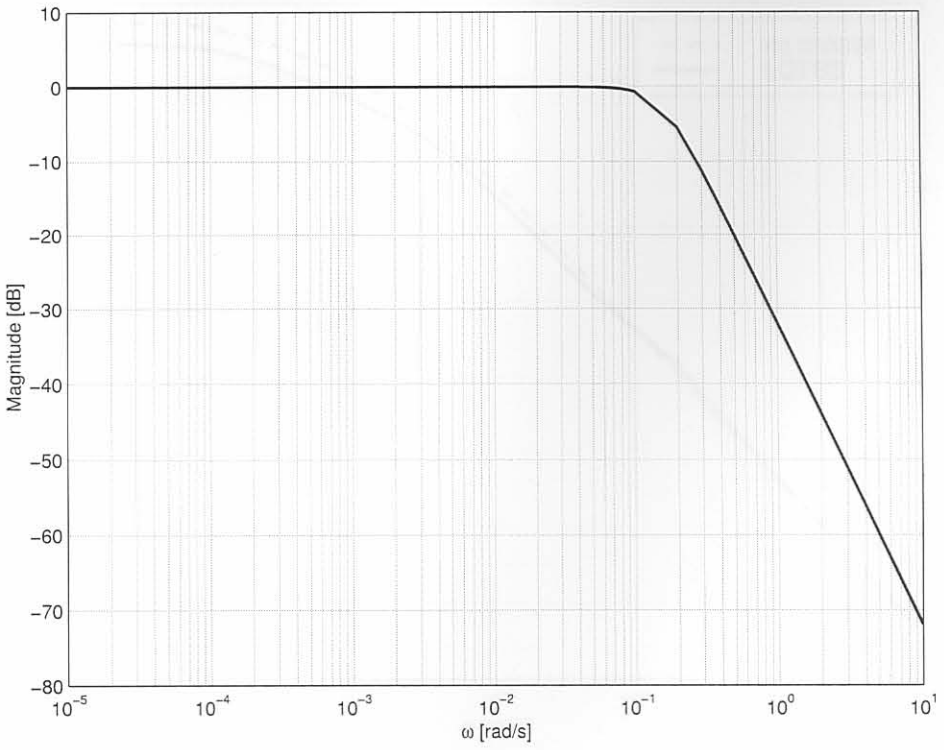

Figure H.12 Closed-loop SVD plot, $\mathbf{T}(s)$, of the system.

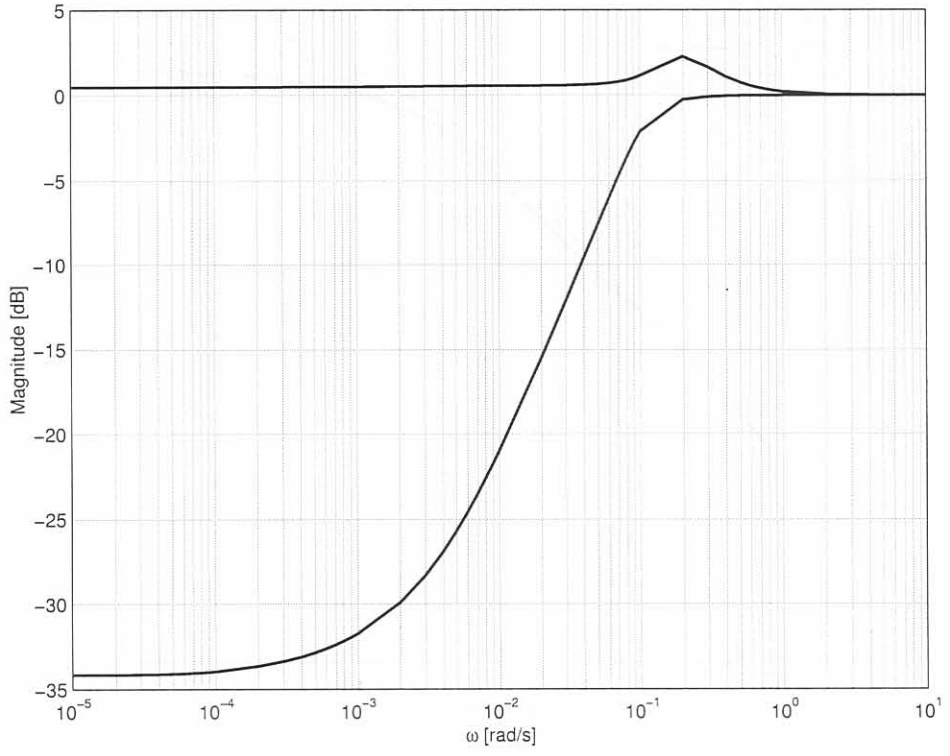

Figure H.13 Sensitivity function for the system.

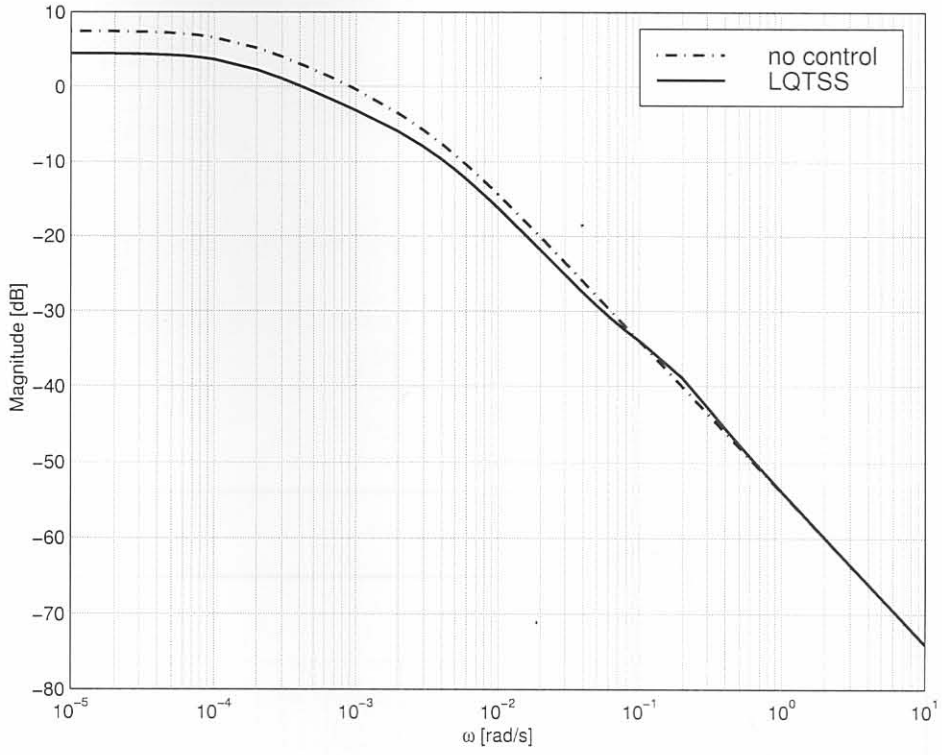

Figure H.14 Reduction in the effect of mould level disturbance on the output temperatures.

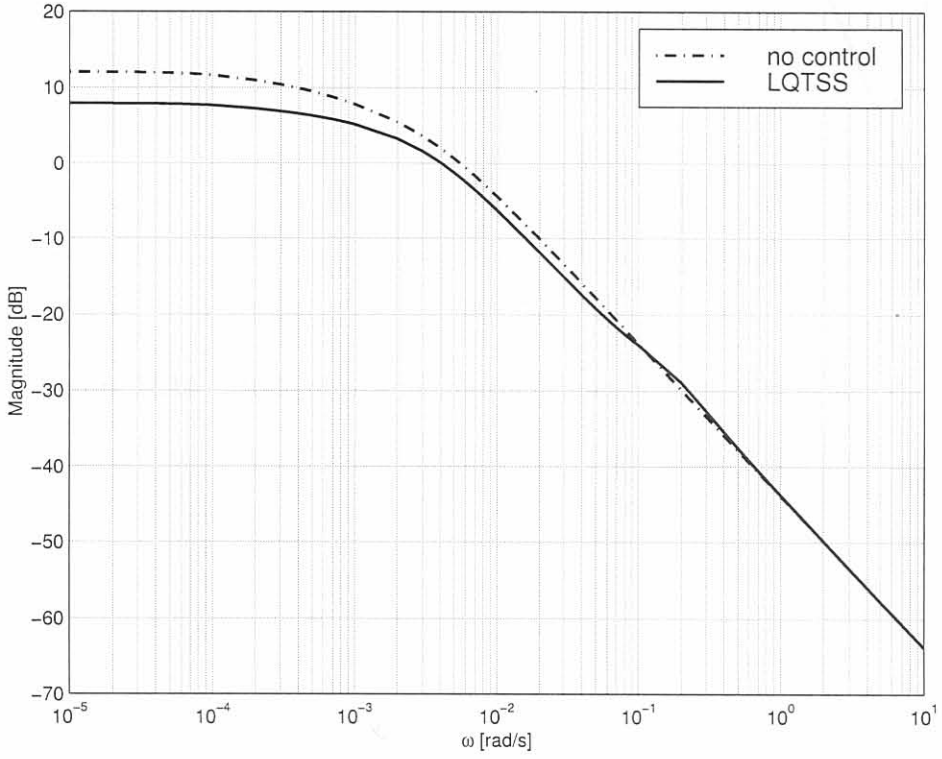

Figure H.15 Reduction in the effect of water temperature disturbance on the output temperatures.

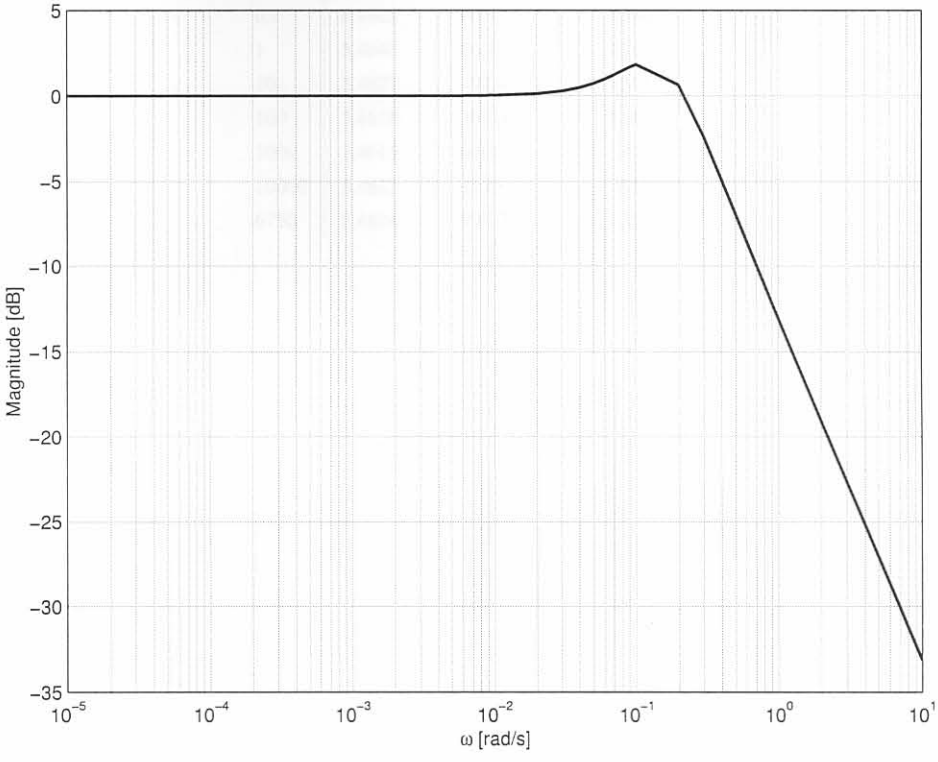

Figure H.16 Bode plot of the transfer function of $p(s) = h(s)v(s)$.

H.3 1575mm wide slabs results

H.3.1 Tabled results

Table H.5 1575mm wide slab errors, maximum accellaration and maximum speeds for the LQTSS implementation at different values of the q/r ratio.

$\frac{q}{r}$	SMSMSE	$\max\|du_1/dt\|$	$\max(u_1)$
None	5.5005	0	1255
0.001	5.5002	7.123	1304
0.01	5.4817	15.96	1311
0.1	5.4702	40.38	1330
1	5.4648	86.87	1339
10	5.4627	192.4	1345
100	5.4618	359.3	1349
1000	5.4615	640.9	1351
10000	5.4613	1115	1353
6750	5.4614	999.7	1353

Table H.6 Mean Square Errors for the LQTSS implementation for 1575mm wide slabs for different values of the q/r ratio. $q/r = 6750$ has the maximum accellaration of 1000 mm/min^2.

$\frac{q}{r}$	in1u	in1l	in2u	in2l	in3u	in3l	in4u	in4l
None	2.94	61.4	12	20.1	5.15	25.8	1.78	48.6
0.001	3.59	63.8	11.2	20.1	3.97	25.9	2.01	49.9
0.01	3.55	61.9	12.4	19.1	3.51	24.3	1.7	49.8
0.1	3.56	60.6	13.4	18.3	3.16	23.1	1.49	49.8
1	3.58	59.7	14.1	17.8	3.01	22.3	1.37	49.8
10	3.6	59.2	14.6	17.5	2.97	21.9	1.31	49.8
100	3.61	58.9	14.8	17.4	2.96	21.6	1.28	49.8
1000	3.61	58.7	15	17.3	2.96	21.5	1.26	49.8
10000	3.62	58.7	15	17.2	2.96	21.4	1.25	49.8
6750	3.62	58.7	15	17.3	2.96	21.4	1.25	49.8

$\frac{q}{r}$	in5u	in5l	in6u	in6l	in7u	in7l	in8u	in8l
None	17.7	8.21	3.07	42.6	9.2	38.7	21.2	39.5
0.001	13.6	7.57	3.07	43.5	9.26	39.6	22.1	39.9
0.01	12.6	6.63	2.49	43.3	7.98	38.6	21	37.8
0.1	11.8	5.93	2.07	43.1	7.03	37.8	20.1	36.2
1	11.5	5.51	1.82	43	6.47	37.3	19.6	35.2
10	11.3	5.28	1.69	42.9	6.16	37	19.3	34.6
100	11.2	5.15	1.62	42.9	5.99	36.8	19.1	34.3
1000	11.2	5.08	1.58	42.8	5.89	36.7	19	34.1
10000	11.1	5.04	1.56	42.8	5.84	36.7	19	34
6750	11.1	5.04	1.57	42.8	5.85	36.7	19	34

$\frac{q}{r}$	ou1u	ou1l	ou2u	ou2l	ou3u	ou3l	ou4u	ou4l
None	27.4	62.1	9.73	36.7	1.63	41.7	0.918	65.8
0.001	28.5	65.9	9.4	37.3	2.11	43.6	1.36	67.3
0.01	28	64.9	7.92	35	1.99	42.5	1.39	67.3
0.1	27.6	64.3	6.75	33.3	1.94	41.7	1.44	67.2
1	27.3	63.9	6.06	32.3	1.92	41.2	1.49	67.2
10	27.2	63.6	5.68	31.7	1.91	40.9	1.52	67.2
100	27.1	63.5	5.48	31.3	1.91	40.7	1.54	67.2
1000	27	63.4	5.37	31.1	1.91	40.6	1.55	67.2
10000	27	63.4	5.32	31	1.91	40.6	1.56	67.2
6750	27	63.4	5.32	31	1.91	40.6	1.56	67.2

$\frac{q}{r}$	ou5u	ou5l	ou6u	ou6l	ou7u	ou7l	ou8u	ou8l
None	4.08	9.33	NA	NA	11.4	6.67	3.38	59.1
0.001	2.97	10.1	NA	NA	10.7	5.55	3.81	60
0.01	2.29	9.89	NA	NA	11.7	4.7	3.45	57.4
0.1	1.8	9.76	NA	NA	12.5	4.09	3.19	55.4
1	1.53	9.67	NA	NA	13.1	3.74	3.05	54.2
10	1.39	9.62	NA	NA	13.5	3.55	2.96	53.5
100	1.33	9.59	NA	NA	13.7	3.44	2.92	53.1
1000	1.29	9.57	NA	NA	13.8	3.38	2.9	52.8
10000	1.27	9.56	NA	NA	13.9	3.35	2.88	52.7
6750	1.27	9.56	NA	NA	13.9	3.35	2.88	52.7

$\frac{q}{r}$	nl1u	nl1l	nl2u	nl2l	nr1u	nr1l	nr2u	nr2l
None	33.9	84.8	104	31.7	25.5	4.25	60.4	107
0.001	33.6	83.2	100	30.8	25.3	4.06	60.4	105
0.01	34.5	85.1	104	32	26.9	5.01	62.1	108
0.1	35.4	86.6	106	32.9	28.2	5.79	63.5	110
1	35.9	87.6	108	33.5	29.1	6.31	64.3	111
10	36.2	88.1	109	33.9	29.5	6.63	64.8	112
100	36.4	88.5	110	34.1	29.8	6.82	65.1	113
1000	36.5	88.7	111	34.2	30	6.92	65.3	113
10000	36.5	88.8	111	34.3	30.1	6.98	65.4	113
6750	36.5	88.8	111	34.3	30.1	6.98	65.4	113

Table H.7 Feedback gain matrix $\mathbf{K}_\infty$ for 1575mm wide slabs at $q/r = 6750$.

The gain of the integrator state is $k_\infty = 0.316$.

in1u	in1l	in2u	in2l	in3u	in3l	in4u	in4l
17	10.2	23.6	8.22	22.8	13.3	13.9	0.146
in5u	in5l	in6u	in6l	in7u	in7l	in8u	in8l
20.4	11.3	13.9	1.9	17	7.93	14.1	14.3
ou1u	ou1l	ou2u	ou2l	ou3u	ou3l	ou4u	ou4l
8.25	4.86	19.2	13.3	13.1	8.05	13.3	0.362
ou5u	ou5l	ou6u	ou6l	ou7u	ou7l	ou8u	ou8l
15.8	2.87	NA	NA	19.3	12.5	12.5	13.1
nl1u	nl1l	nl2u	nl2l	nr1u	nr1l	nr2u	nr2l
8.29	9.74	19.7	11.2	11.1	16.1	7.47	10.3

Table H.8 Feedforward gain matrix $\mathbf{F}$ for 1575mm wide slabs at $q/r = 6750$.

in1u	in1l	in2u	in2l	in3u	in3l	in4u	in4l
12.4	12.7	16.2	9.02	17.6	11.3	12.7	0.211
in5u	in5l	in6u	in6l	in7u	in7l	in8u	in8l
24.1	12.8	13.7	2.35	17.2	8.51	13.1	13
ou1u	ou1l	ou2u	ou2l	ou3u	ou3l	ou4u	ou4l
8.02	7.32	16.3	19.4	12.7	10	12.4	0.5
ou5u	ou5l	ou6u	ou6l	ou7u	ou7l	ou8u	ou8l
17.4	4.33	NA	NA	15.2	15.2	12.5	14.8
nl1u	nl1l	nl2u	nl2l	nr1u	nr1l	nr2u	nr2l
6.96	11.6	21	11	13.3	17.1	9.25	14.6

H.3.2 Time-domain results

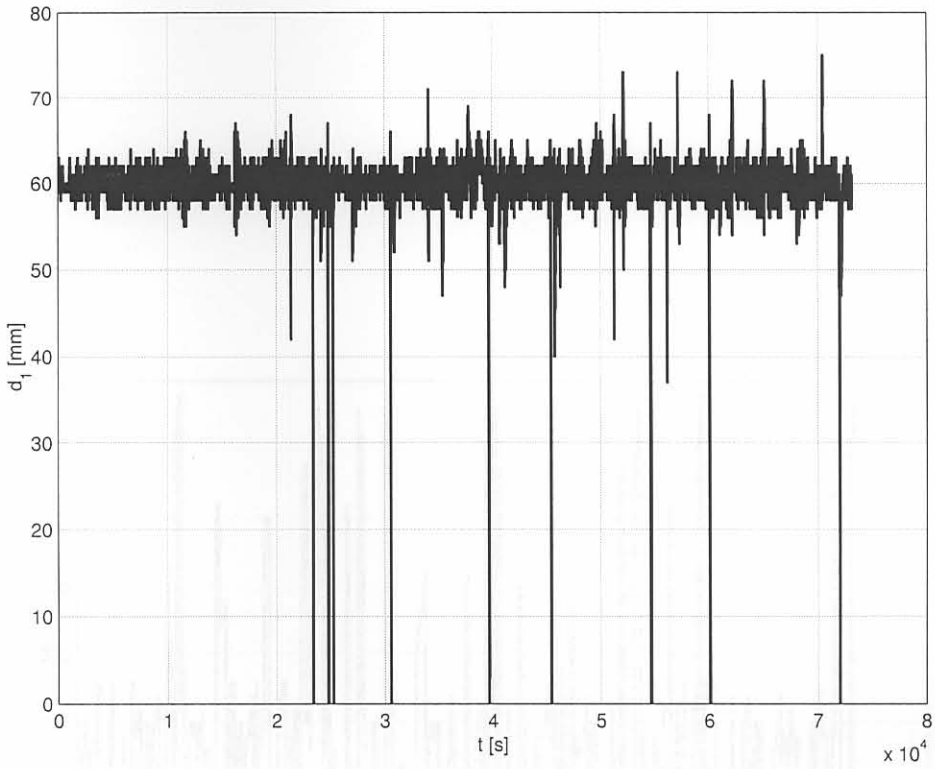

Figure H.17 Mould level disturbance ($d_1(t)$) used for the simulation of the 1575mm wide slab system.

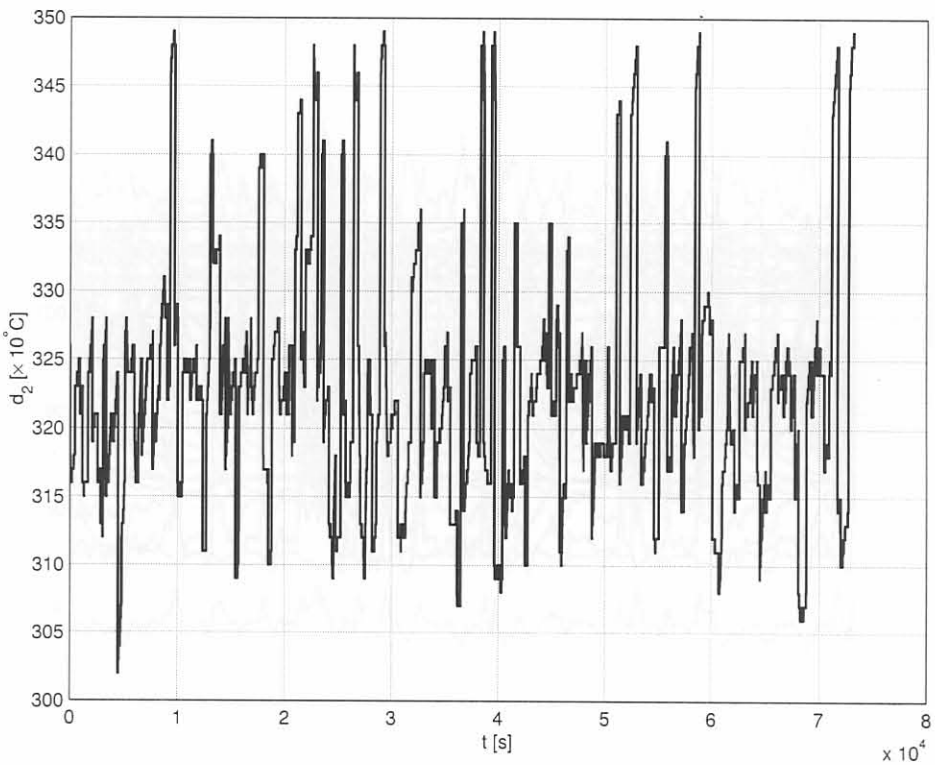

Figure H.18 Water temperature ($d_2(t)$) disturbance used for the simulation of the 1575mm wide slab system.

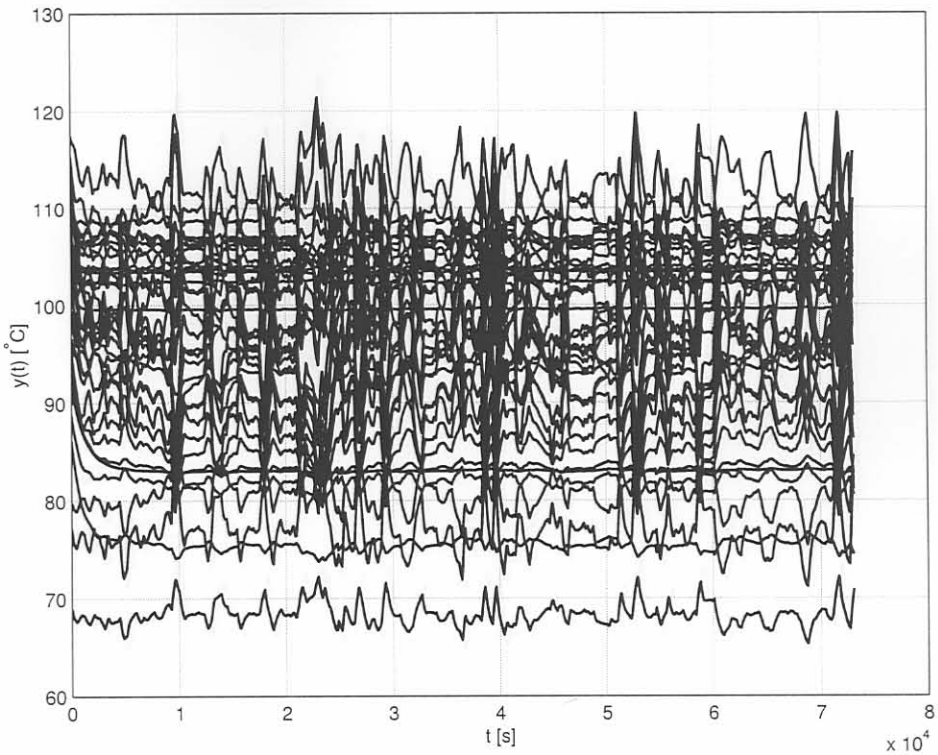

Figure H.19 Outputs $(\mathbf{y}(t))$ of the system without the LQTSS controller for 1575mm wide slabs.

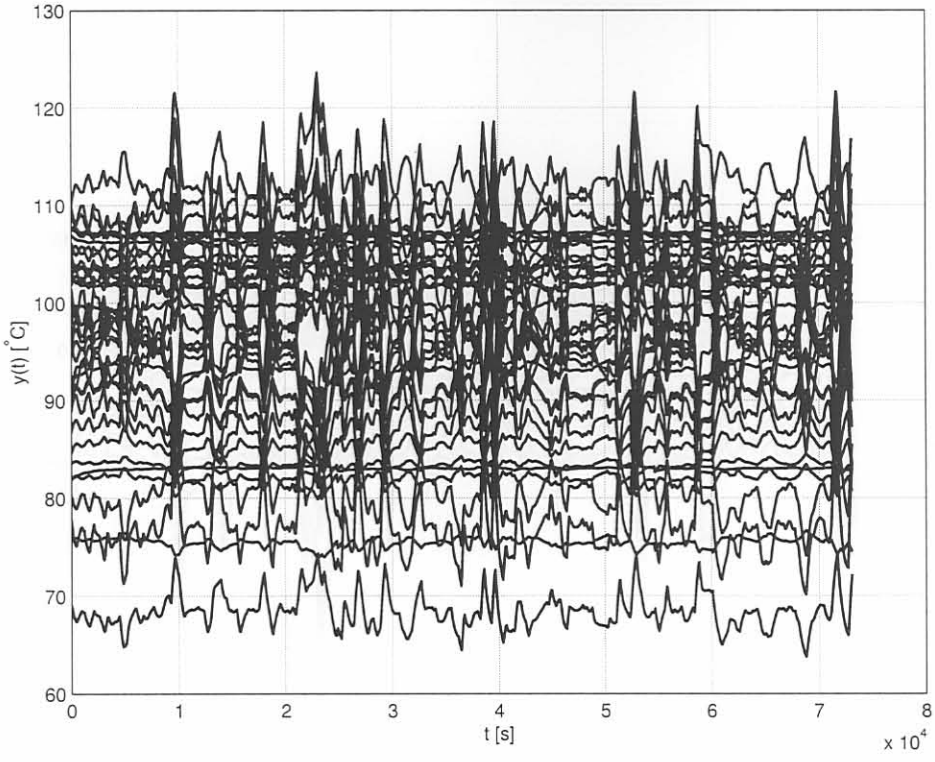

Figure H.20 Outputs $(\mathbf{y}(t))$ of the system with the LQTSS controller for 1575mm wide slabs.

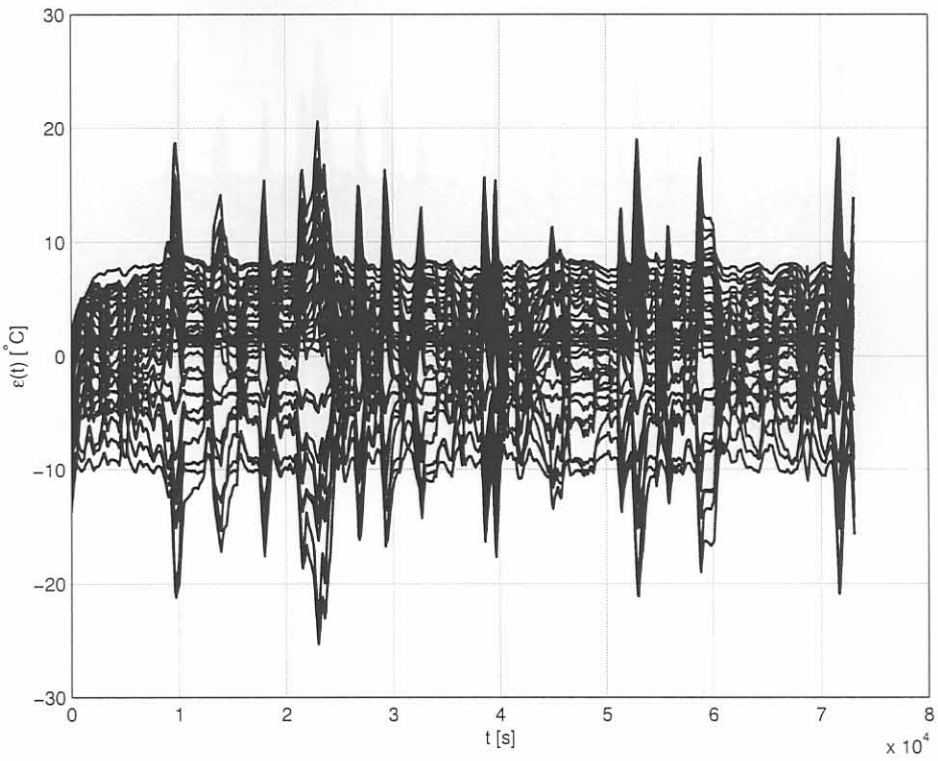

Figure H.21 Tracking errors of the system without the LQTSS controller for 1575mm wide slabs.

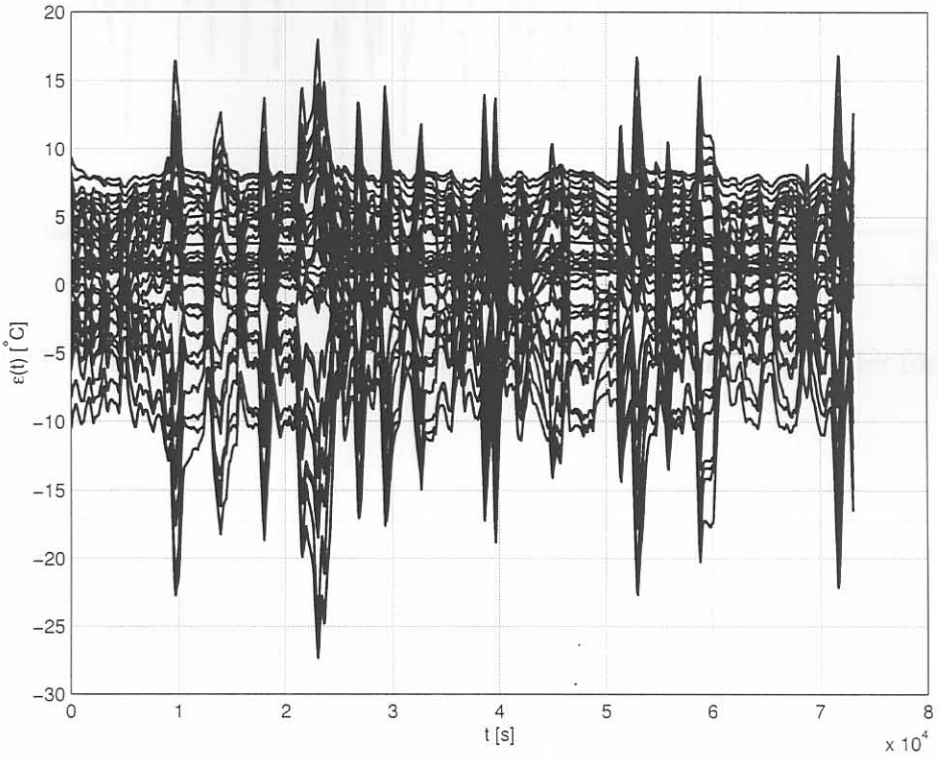

Figure H.22 Tracking errors of the system with the LQTSS controller for 1575mm wide slabs.

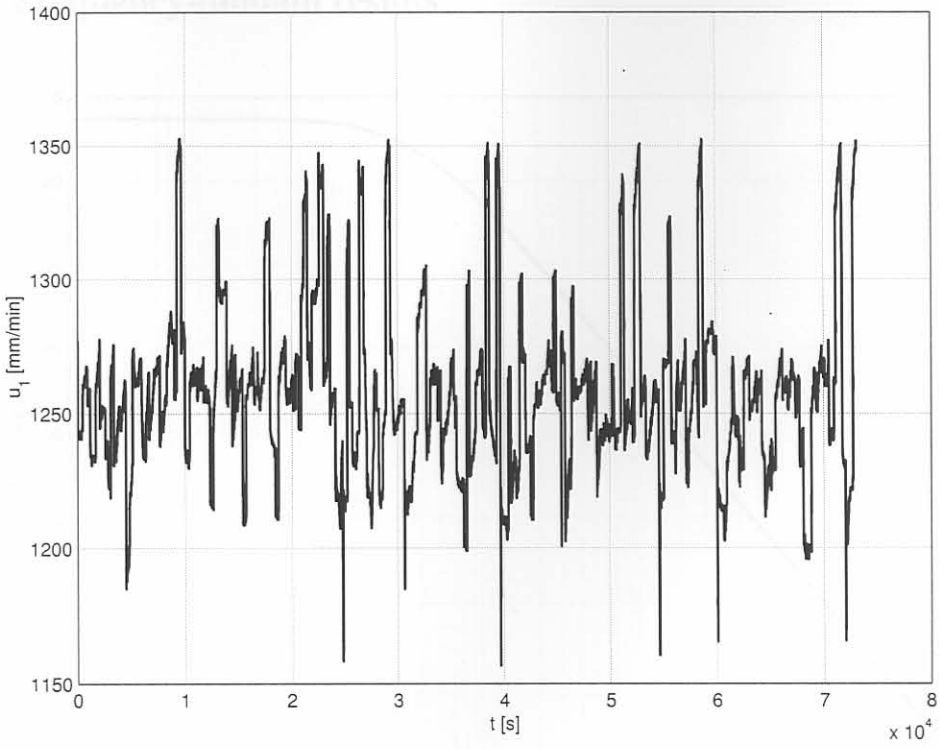

Figure H.23 Casting speed (casting speed, $u_1(t)$) for the LQTSS controller for 1575mm wide slabs.

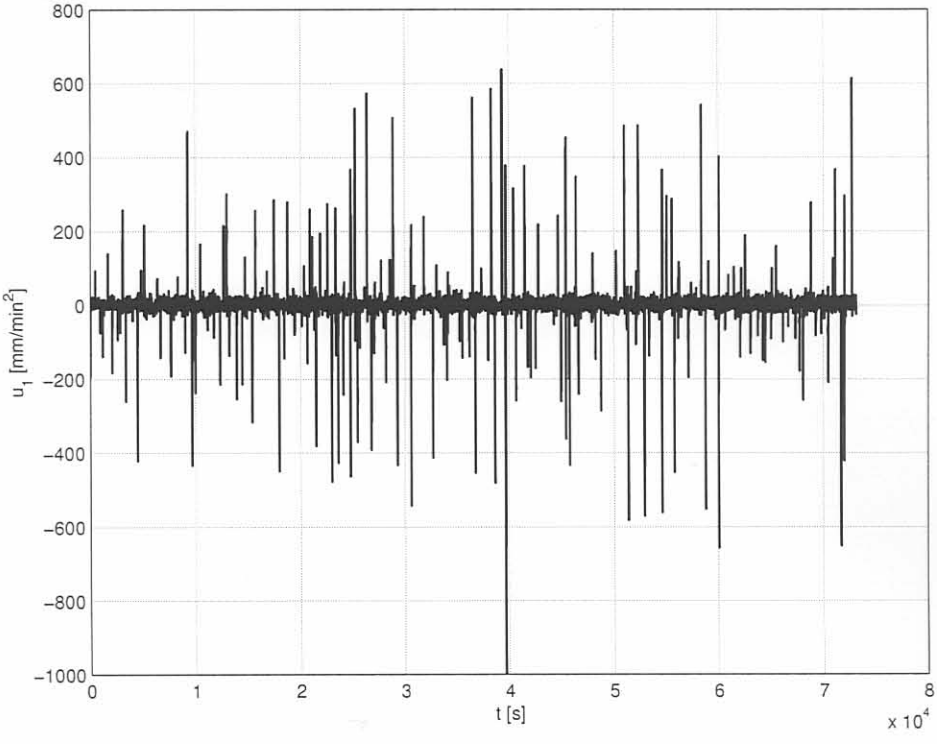

Figure H.24 Casting accellaration for the LQTSS controller for 1575mm wide slabs.

H.3.3 Frequency-domain results

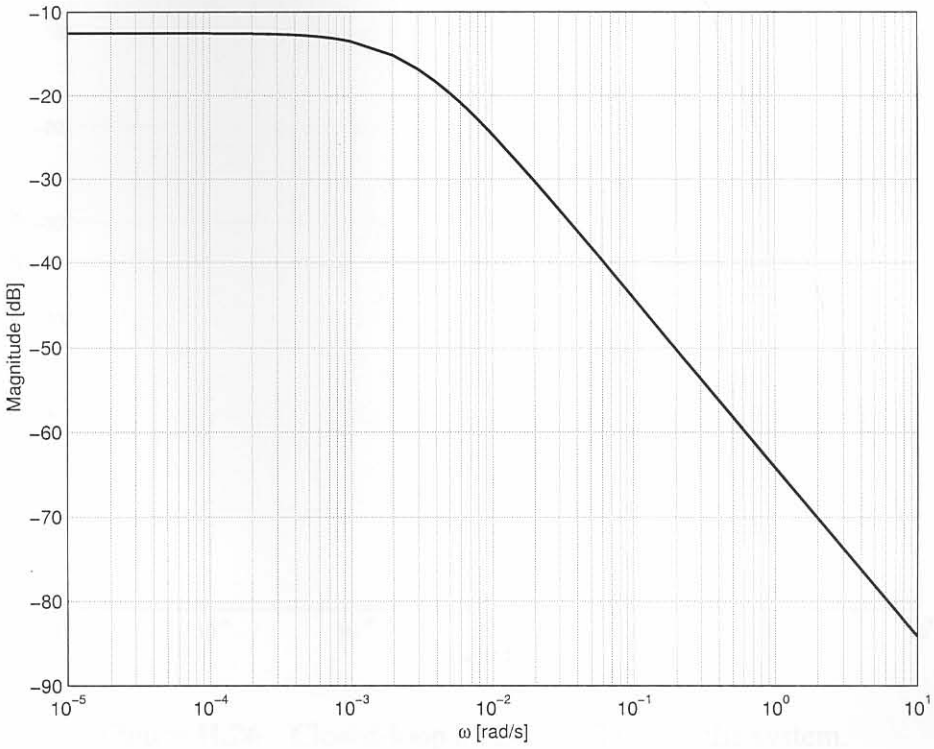

Figure H.25 Open-loop SVD plot of casting speed to the thermocouple temperatures without control ($\mathbf{g}(s)$).

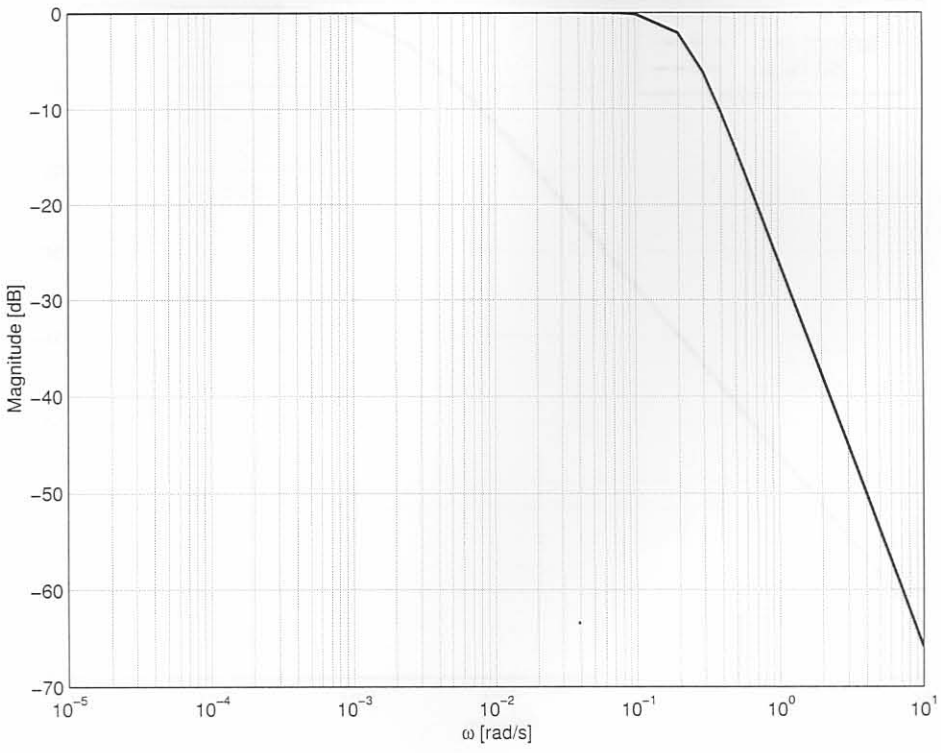

Figure H.26 Closed-loop SVD plot, $\mathbf{T}(s)$, of the system.

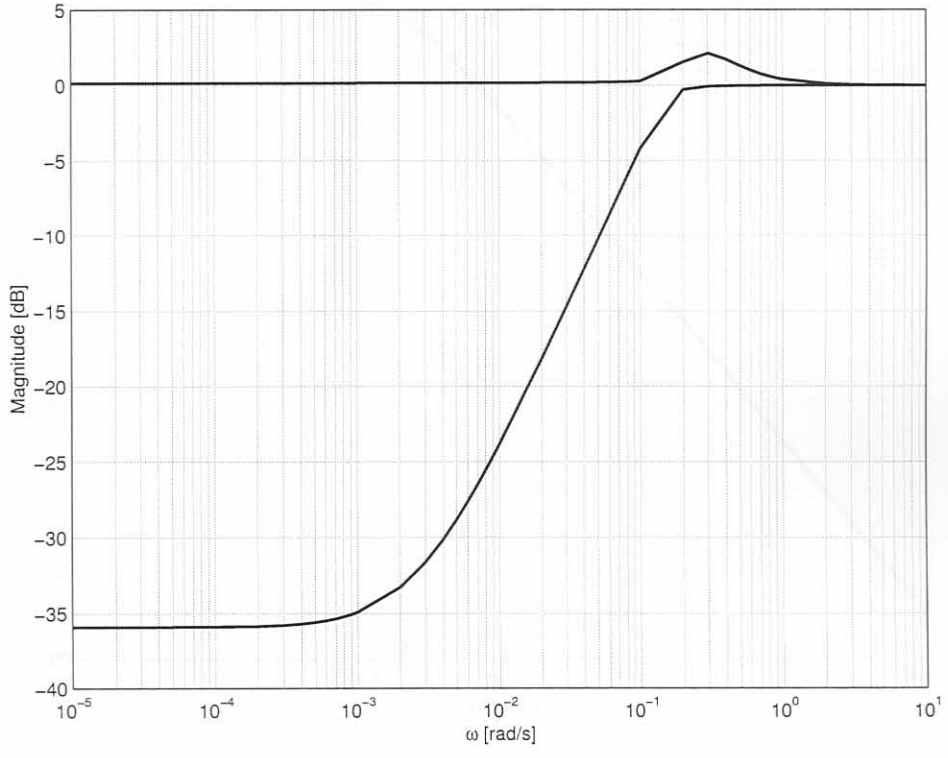

Figure H.27 Sensitivity function for the system.

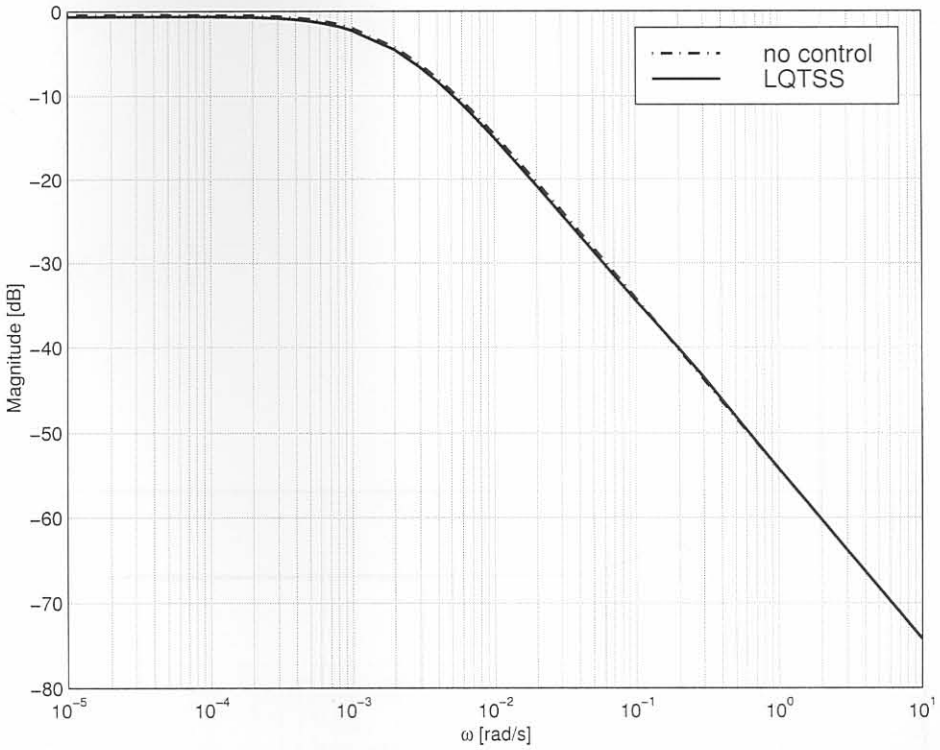

Figure H.28 Reduction in the effect of mould level disturbance on the output temperatures.

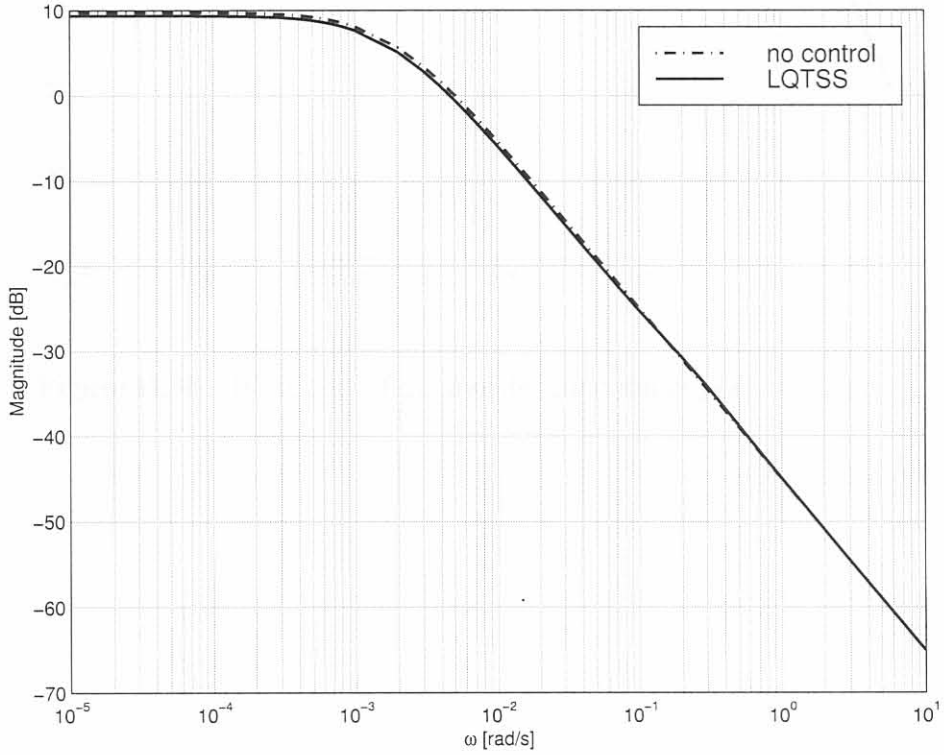

Figure H.29 Reduction in the effect of water temperature disturbance on the output temperatures.

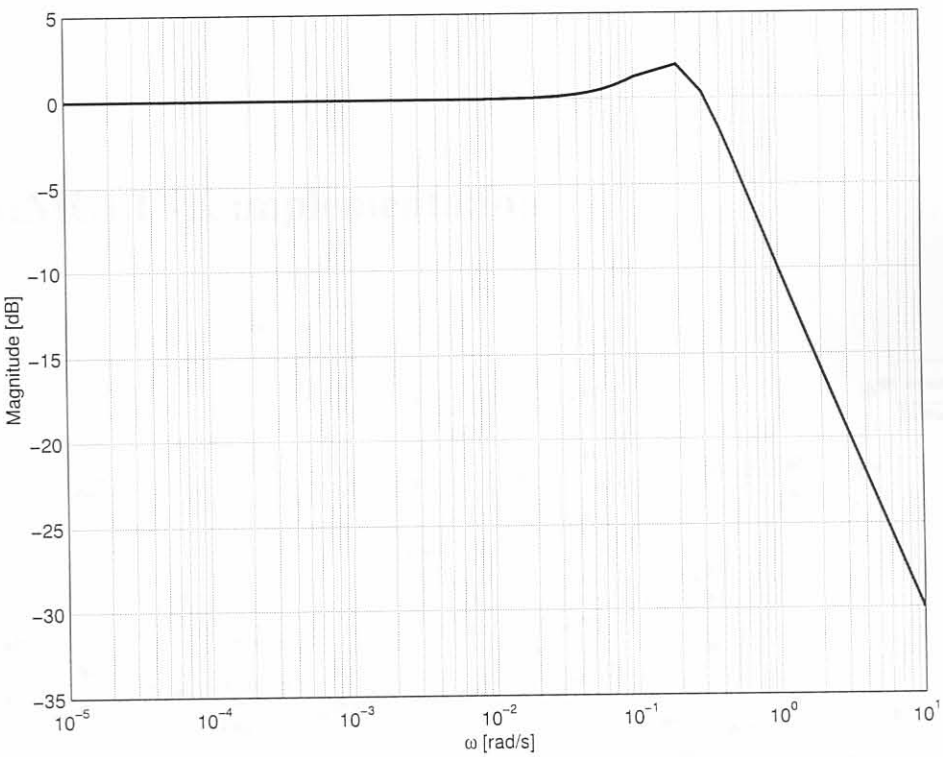

Figure H.30 Bode plot of the transfer function of $p(s) = h(s)v(s)$.

Appendix I

SOC

I.1 SIMULINK implementation

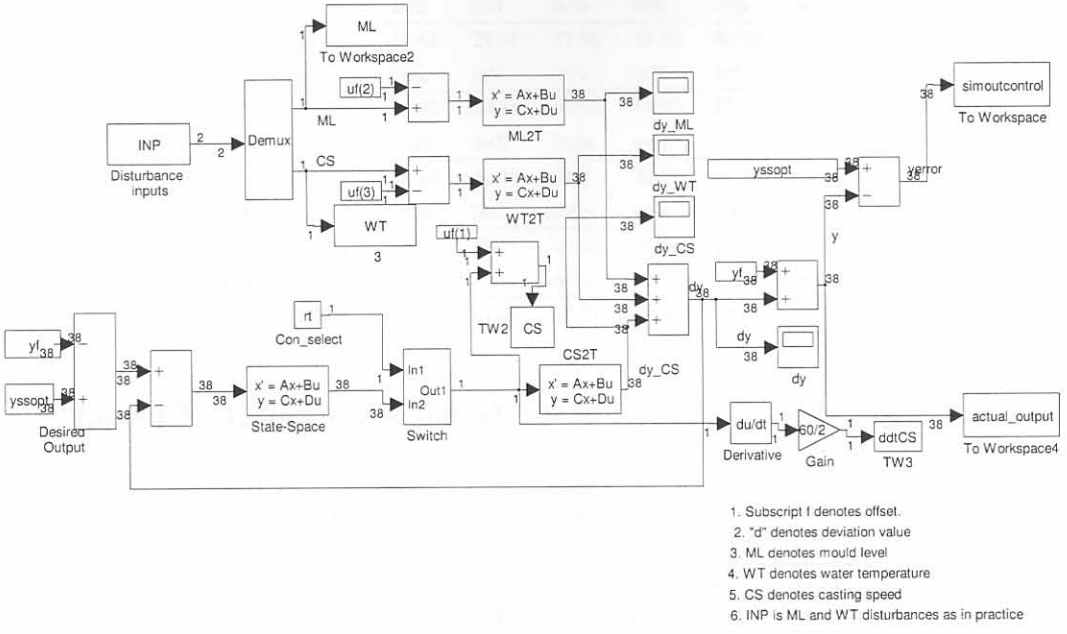

Figure I.1 SIMULINK realization for the SOC controller synthesis.

I.2 1280mm wide slabs results

I.2.1 Tabled results

Table I.1 1280mm wide slab design values for the proportional gains $k_{i,1}$.

in1u	in1l	in2u	in2l	in3u	in3l	in4u	in4l
604	1810	474.3	1110	1100	1323	900	1052
in5u	in5l	in6u	in6l	in7u	in7l	in8u	in8l
1800	1566	835.6	1398	993.5	1286	941.9	2234
ou1u	ou1l	ou2u	ou2l	ou3u	ou3l	ou4u	ou4l
585.6	1344	389.7	1159	827.4	1168	899.8	2046
ou5u	ou5l	ou6u	ou6l	ou7u	ou7l	ou8u	ou8l
793.9	107.6	NA	NA	517.2	898.9	663.4	1066
nl1u	nl1l	nl2u	nl2l	nr1u	nr1l	nr2u	nr2l
551.2	464.9	342	480.5	293.6	520.6	610	520.5

Table I.2 1280mm wide slab design values for the integral gains $k_{i,2}$.

in1u	in1l	in2u	in2l	in3u	in3l	in4u	in4l
37.25	82.45	19.61	23.62	57.36	14.62	40.99	7.655
in5u	in5l	in6u	in6l	in7u	in7l	in8u	in8l
158.8	20.26	34.03	28.85	57.63	41.83	52.76	66.33
ou1u	ou1l	ou2u	ou2l	ou3u	ou3l	ou4u	ou4l
24.03	46.29	24.18	42.76	34.2	22.58	41.59	62.11
ou5u	ou5l	ou6u	ou6l	ou7u	ou7l	ou8u	ou8l
39.72	0.2084	NA	NA	23.95	25.61	24.33	28.09
nl1u	nl1l	nl2u	nl2l	nr1u	nr1l	nr2u	nr2l
9.197	10.08	9.873	12.43	11.51	18.52	15.03	17.07

Table I.3 1280mm wide slab SMSMSE for each controller in the loop.

in1u	in1l	in2u	in2l	in3u	in3l	in4u	in4l
5.404	4.902	4.8	6.061	4.781	7.75	4.611	10.27
in5u	in5l	in6u	in6l	in7u	in7l	in8u	in8l
4.842	8.315	4.836	6.332	4.63	7.138	4.897	11.73
ou1u	ou1l	ou2u	**ou2l**	ou3u	ou3l	ou4u	ou4l
4.625	4.654	5.122	**4.597**	4.728	5.764	5.667	6.291
ou5u	ou5l	ou6u	ou6l	ou7u	ou7l	ou8u	ou8l
5.243	5.505	NA	NA	6.663	6.475	8.052	6.337
nl1u	nl1l	nl2u	nl2l	nr1u	nr1l	nr2u	nr2l
4.668	6.424	10.37	7.812	8.258	9.03	4.601	5.357

Table I.4 1280mm wide slab MSE for each output using the ou2l controller.

in1u	in1l	in2u	in2l	in3u	in3l	in4u	in4l
7.168	1.439	2.123	13.01	1.291	49.41	0.7046	191.3
in5u	in5l	in6u	in6l	in7u	in7l	in8u	in8l
0.7297	41.19	1.281	12.87	0.8113	12.04	2.732	17.51
ou1u	ou1l	ou2u	ou2l	ou3u	ou3l	ou4u	ou4l
1.06	0.9161	8.004	0.001855	1.068	10.79	6.871	5.764
ou5u	ou5l	ou6u	ou6l	ou7u	ou7l	ou8u	ou8l
5.139	3.402	NA	NA	20.02	15.98	28.15	13.42
nl1u	nl1l	nl2u	nl2l	nr1u	nr1l	nr2u	nr2l
0.7659	39.29	107.5	51.53	66.2	47.57	0.9056	12.98

I.2.2 Time-domain results

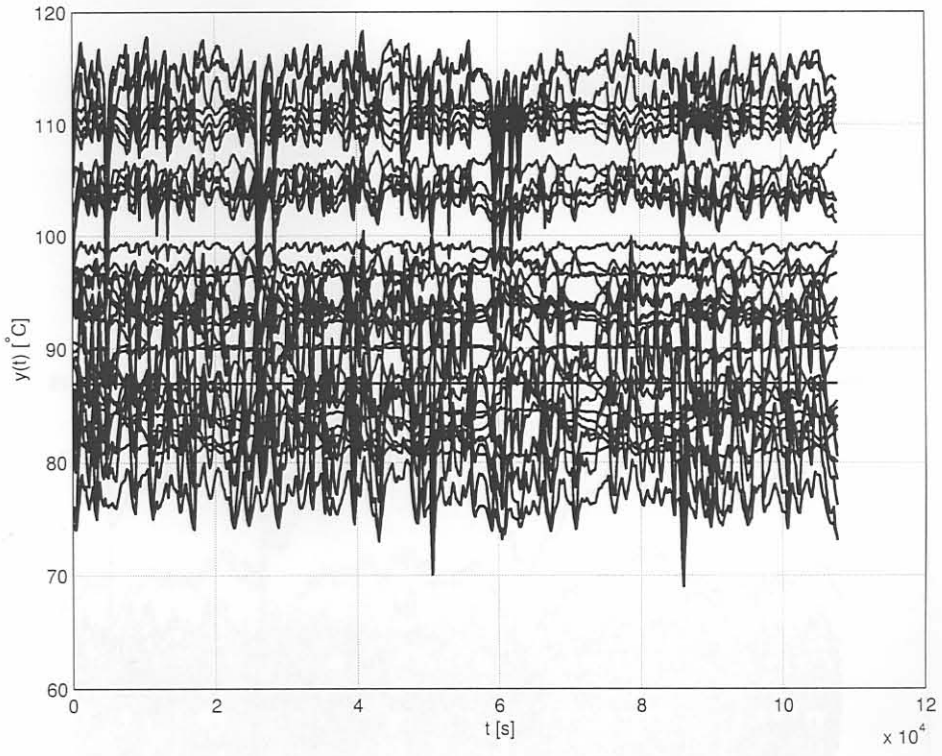

Figure I.2 Thermocouple temperature outputs for 1280mm wide slabs when thermocouple ou2l is used in a feedback configuration.

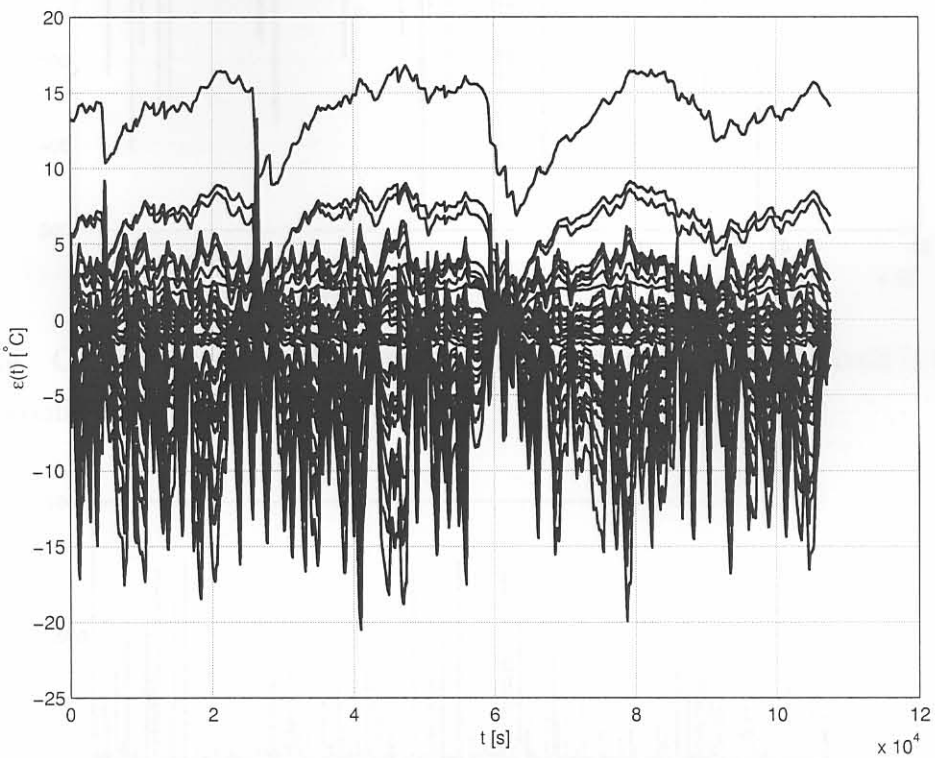

Figure I.3 Thermocouple temperature errors for 1280mm wide slabs when thermocouple ou21 is used in a feedback configuration.

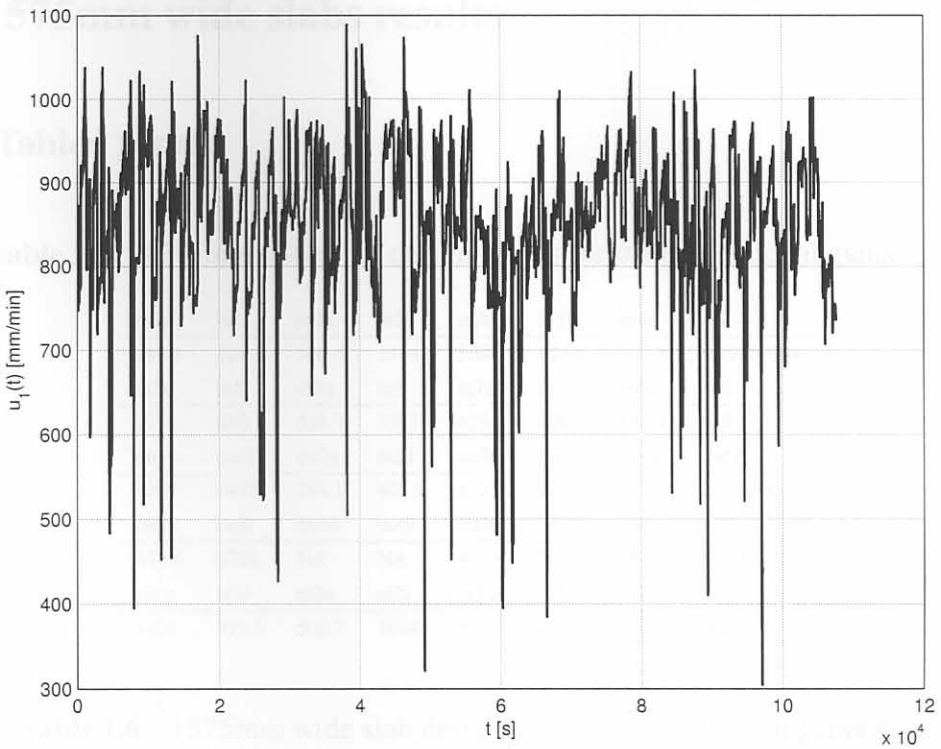

Figure I.4 Control signal for 1280mm wide slabs when thermocouple ou2l is used in a feedback configuration.

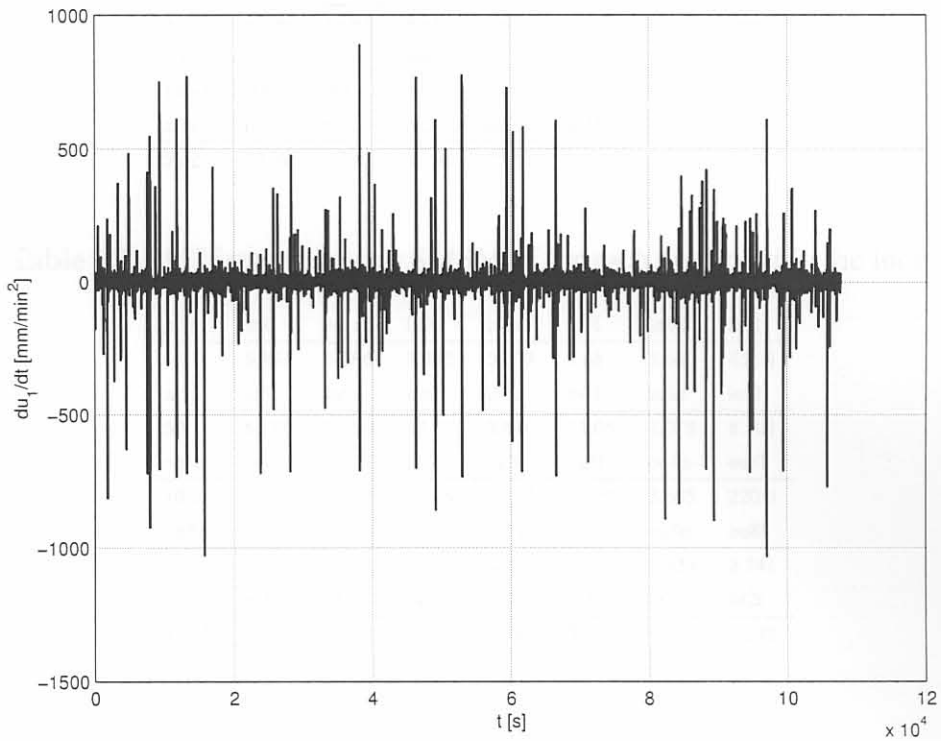

Figure I.5 Slab accellaration for 1280mm wide slabs when thermocouple ou2l is used in a feedback configuration.

I.3 1575mm wide slabs results

I.3.1 Tabled results

Table I.5 1575mm wide slab design values for the proportional gains $k_{i,1}$.

in1u	in1l	in2u	in2l	in3u	in3l	in4u	in4l
485.1	728.3	386.4	1196	360	627.6	607.5	8.594e+004
in5u	in5l	in6u	in6l	in7u	in7l	in8u	in8l
375	830	598.7	5593	429.8	1069	530.4	528.1
ou1u	ou1l	ou2u	ou2l	ou3u	ou3l	ou4u	ou4l
1003	1975	394.1	603.9	632.5	1014	637.2	3.086e+004
ou5u	ou5l	ou6u	ou6l	ou7u	ou7l	ou8u	ou8l
514.6	4706	NA	NA	483.6	729.5	667.6	556.1
nl1u	nl1l	nl2u	nl2l	nr1u	nr1l	nr2u	nr2l
1238	976.3	500.7	1084	876.6	495.4	1019	802.9

Table I.6 1575mm wide slab design values for the integral gains $k_{i,2}$.

in1u	in1l	in2u	in2l	in3u	in3l	in4u	in4l
21.15	15.39	19.3	39.76	14.86	24.05	22.01	2163
in5u	in5l	in6u	in6l	in7u	in7l	in8u	in8l
8.776	25.1	19.64	166.4	12.02	31.98	16.79	17.39
ou1u	ou1l	ou2u	ou2l	ou3u	ou3l	ou4u	ou4l
33.26	32.69	13.91	9.388	20.96	23.07	22.58	756.5
ou5u	ou5l	ou6u	ou6l	ou7u	ou7l	ou8u	ou8l
14.31	109.1	NA	NA	21.94	19.12	21.4	13.43
nl1u	nl1l	nl2u	nl2l	nr1u	nr1l	nr2u	nr2l
58.2	27.59	17.43	50.92	25.11	14.24	21.96	14.14

Table I.7 1575mm wide slab SMSMSE for each controller in the loop.

in1u	in1l	in2u	in2l	in3u	in3l	in4u	in4l
5.871	9.941	6.386	8.455	5.699	7.68	5.66	453.4
in5u	in5l	in6u	in6l	in7u	in7l	in8u	in8l
5.9	6.118	5.669	37.78	5.846	11.05	7.078	8.108
ou1u	ou1l	ou2u	ou2l	ou3u	ou3l	ou4u	ou4l
10.23	16.01	5.822	7.288	5.722	10.21	5.695	220.9
ou5u	ou5l	ou6u	ou6l	ou7u	ou7l	ou8u	ou8l
5.622	11.34	NA	NA	6.43	5.887	5.823	8.741
nl1u	nl1l	nl2u	nl2l	nr1u	nr1l	nr2u	nr2l
12.71	12.37	8.734	9.054	8.284	5.954	14.52	12.49

Table I.8 1575mm wide slab MSE for each output using the ou5u controller.

in1u	in1l	in2u	in2l	in3u	in3l	in4u	in4l
7.774	60.98	20.7	16.56	2.993	20.08	3.049	50.05
in5u	in5l	in6u	in6l	in7u	in7l	in8u	in8l
4.656	3.397	2.28	43.45	6.3	37.46	20.71	32.92
ou1u	ou1l	ou2u	ou2l	ou3u	ou3l	ou4u	ou4l
29.06	65.92	4.463	32.95	4.705	42.56	4.637	67.52
ou5u	ou5l	ou6u	ou6l	ou7u	ou7l	ou8u	ou8l
0.02098	10.22	NA	NA	17.94	1.404	4.795	52.45
nl1u	nl1l	nl2u	nl2l	nr1u	nr1l	nr2u	nr2l
39.54	90.94	113.7	36.32	37.48	12.09	75.99	122.9

I.3.2 Time-domain results

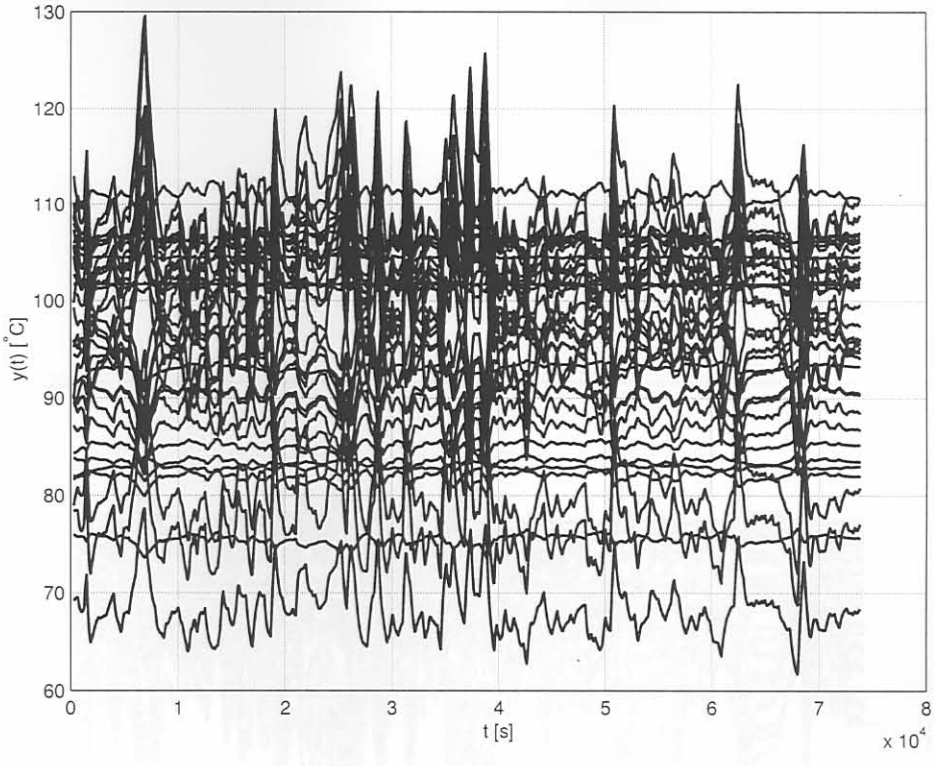

Figure I.6 Thermocouple temperature outputs for 1575mm wide slabs when thermocouple ou5u is used in a feedback configuration.

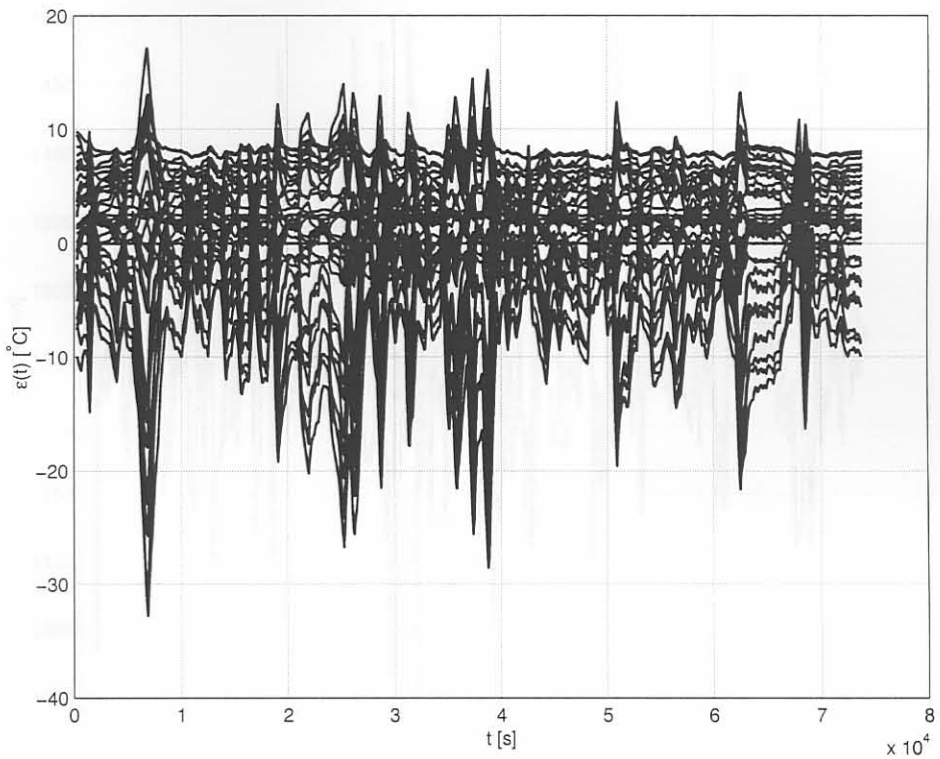

Figure I.7 Thermocouple temperature errors for 1575mm wide slabs when thermocouple ou5u is used in a feedback configuration.

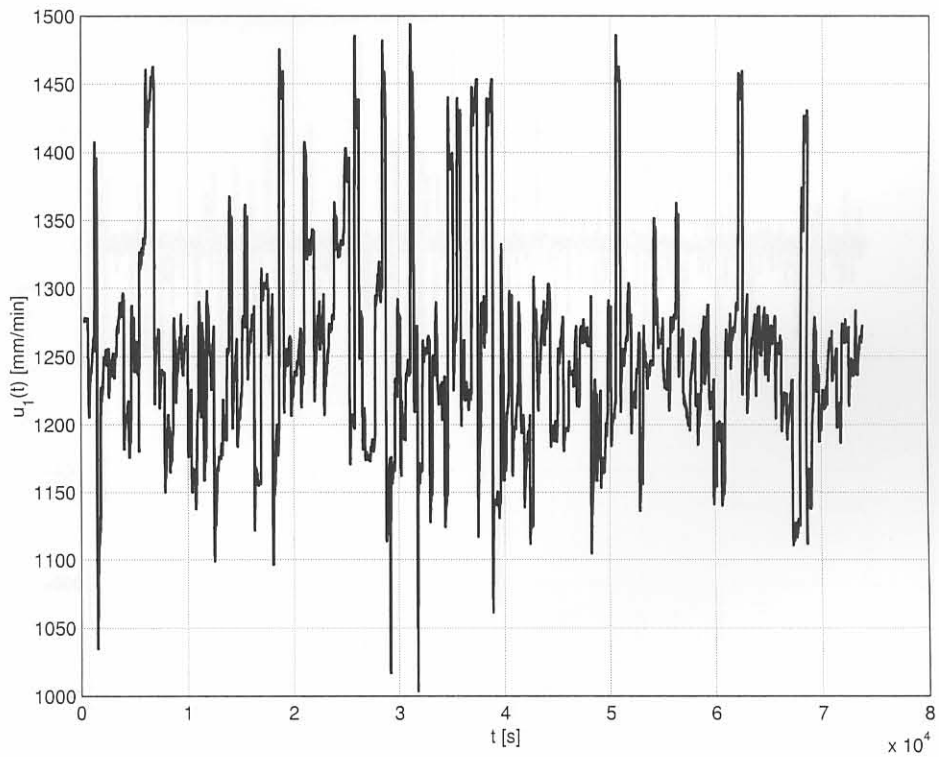

Figure I.8 Control signal for 1575mm wide slabs when thermocouple ou5u is used in a feedback configuration.

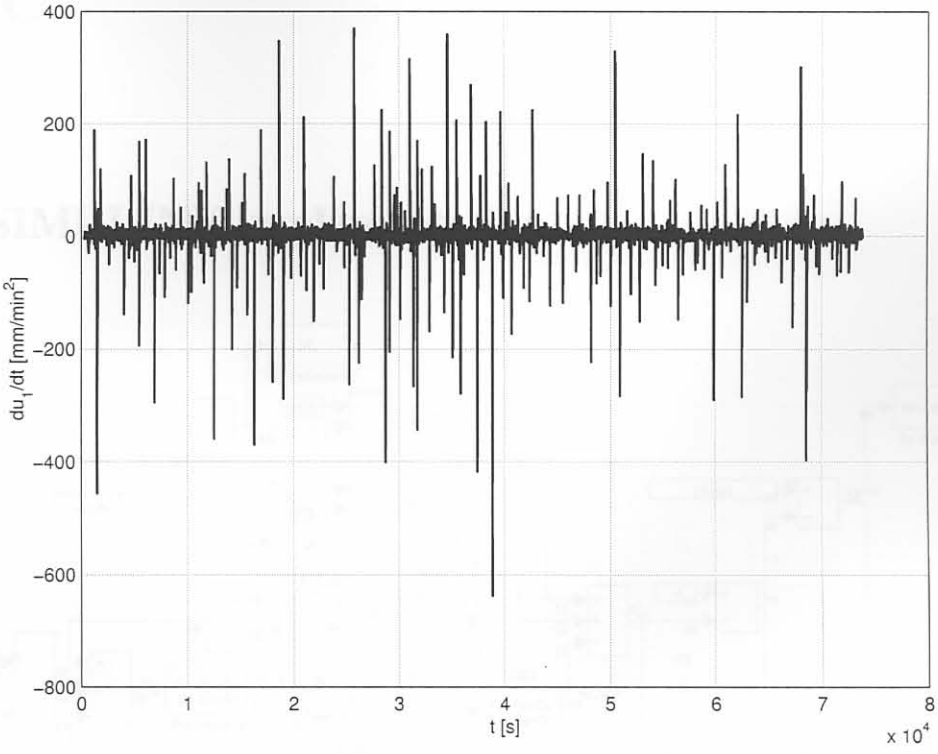

Figure I.9 Slab accellaration for 1575mm wide slabs when thermocouple ou5u is used in a feedback configuration.

Appendix J

WCC

J.1 SIMULINK implementation

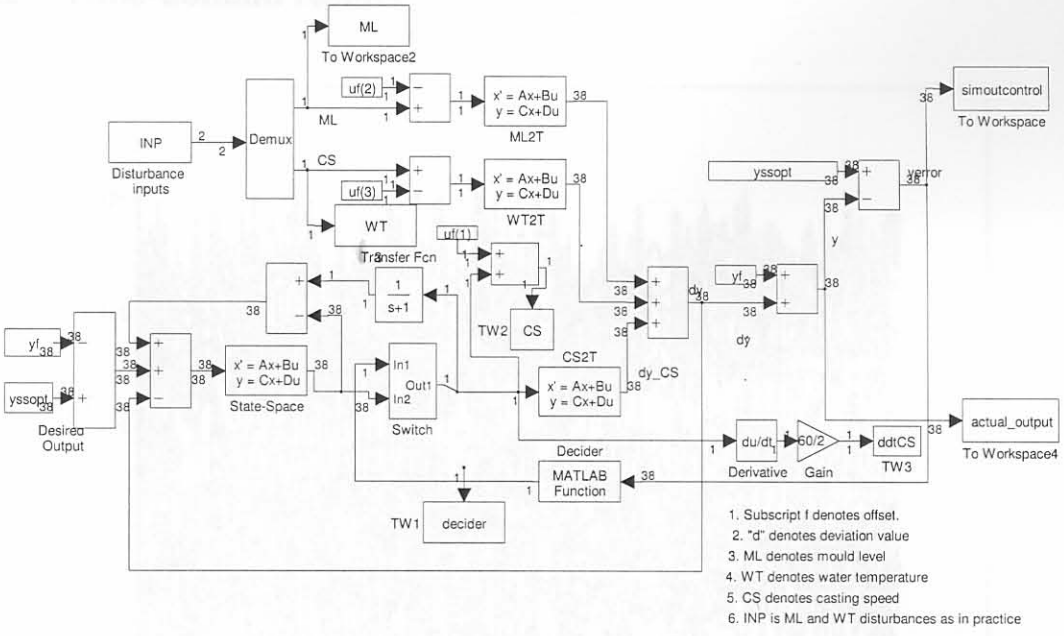

Figure J.1 SIMULINK realization for the WCC controller synthesis. Note that a fast unity gain filter with a time constant of 1 second has been added to break the algebraic loop in SIMULINK.

J.2 1280mm wide slab results

J.2.1 Tabled results

Table J.1 1280mm wide slab MSE for each output using WCC.

in1u	in1l	in2u	in2l	in3u	in3l	in4u	in4l
17.33	5.375	18.75	10.06	8.153	29.1	9.471	127.9
in5u	in5l	in6u	in6l	in7u	in7l	in8u	in8l
3.277	26.52	8.622	8.381	8.975	12.33	10.79	21.35
ou1u	ou1l	ou2u	ou2l	ou3u	ou3l	ou4u	ou4l
17.48	7.38	23.67	6.235	10.46	7.834	13.82	4.713
ou5u	ou5l	ou6u	ou6l	ou7u	ou7l	ou8u	ou8l
13.01	2.207	NA	NA	31.37	26.06	39.27	22.88
nl1u	nl1l	nl2u	nl2l	nr1u	nr1l	nr2u	nr2l
14.88	65.34	126	70.13	82.1	57.04	17.64	28.98

J.2.2 Time-domain results

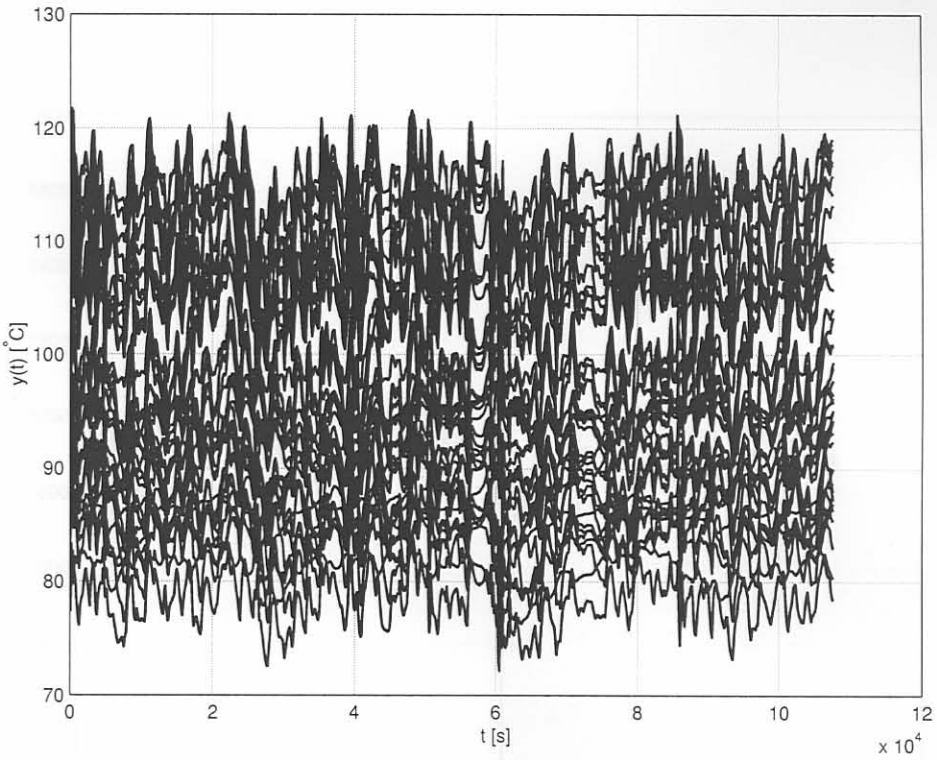

Figure J.2 Outputs for 1280mm wide slabs and the worst-case control configuration.

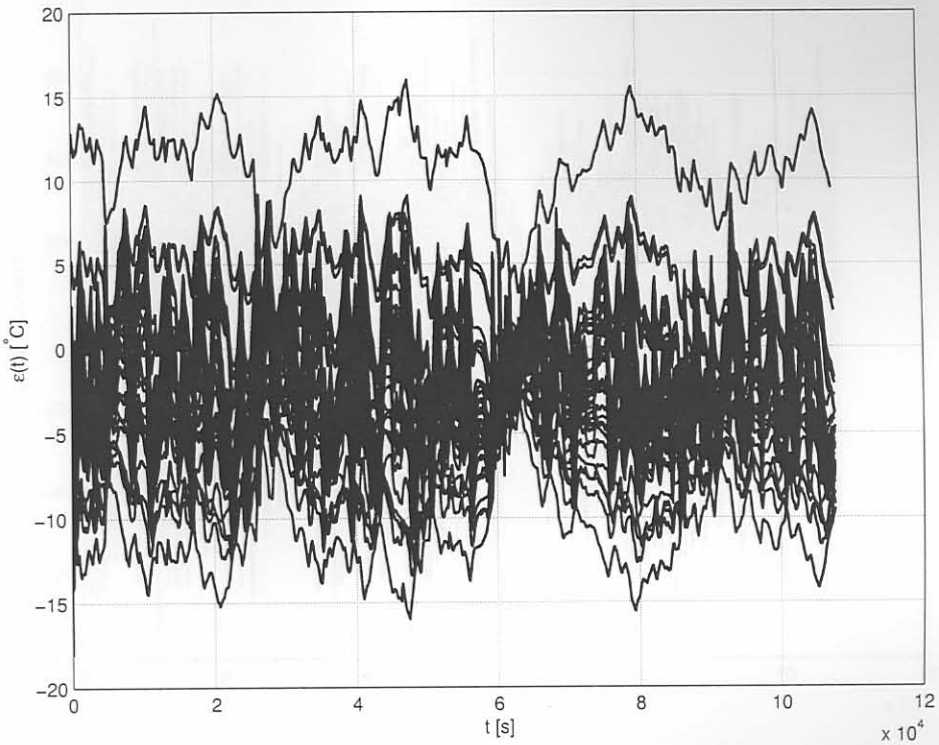

Figure J.3 Errors for 1280mm wide slabs and the worst-case control configuration.

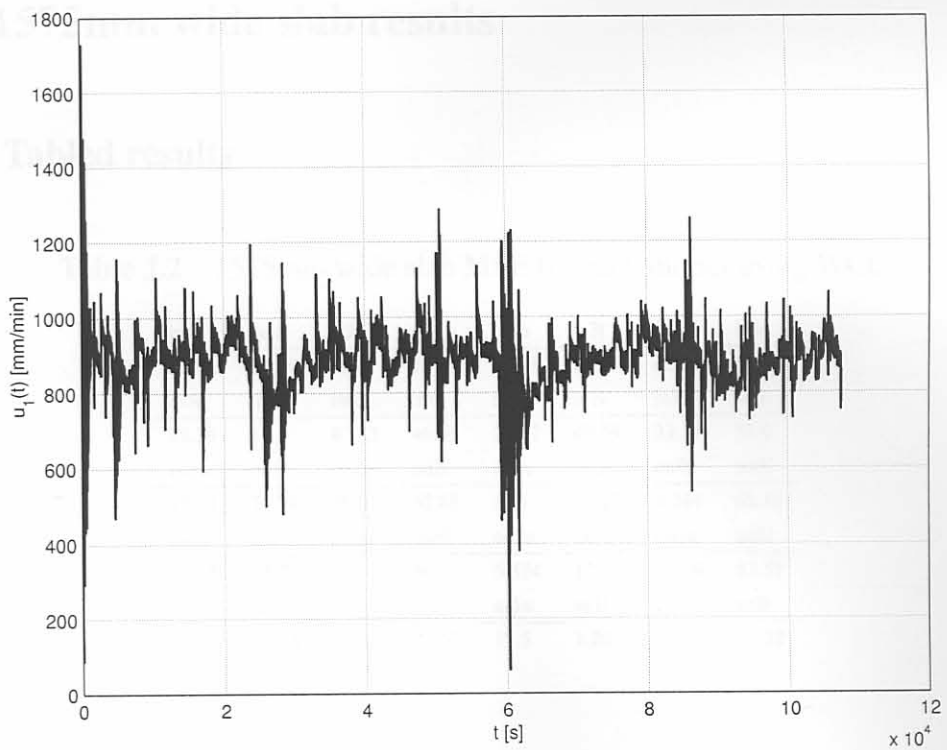

Figure J.4 Control signal for 1280mm wide slabs and the worst-case control configuration.

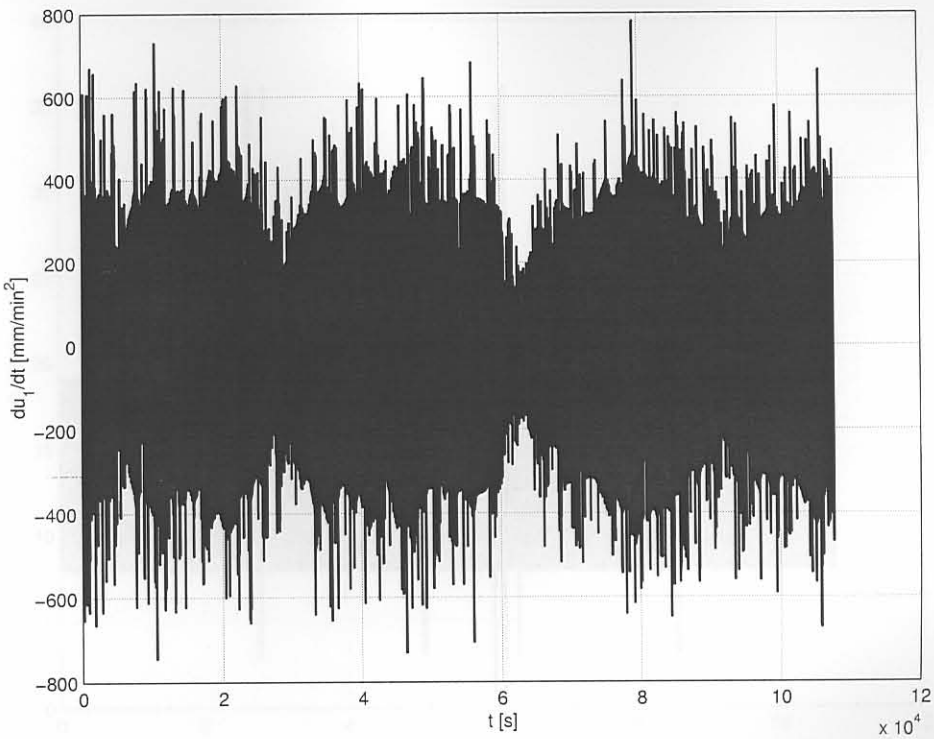

Figure J.5 Accellaration of the slab 1280mm wide slabs and the worst-case control configuration.

J.3 1575mm wide slab results

J.3.1 Tabled results

Table J.2 1575mm wide slab MSE for each output using WCC.

in1u	in1l	in2u	in2l	in3u	in3l	in4u	in4l
8.082	82.56	6.169	28.59	5.896	37.21	6.304	50.29
in5u	in5l	in6u	in6l	in7u	in7l	in8u	in8l
19.39	14.8	8.723	46.05	20.82	49.59	33.57	55.9
ou1u	ou1l	ou2u	ou2l	ou3u	ou3l	ou4u	ou4l
35.13	75.71	20.03	62.85	5.91	55.22	4.244	68.16
ou5u	ou5l	ou6u	ou6l	ou7u	ou7l	ou8u	ou8l
8.365	12.2	NA	NA	5.574	12.37	8.909	83.52
nl1u	nl1l	nl2u	nl2l	nr1u	nr1l	nr2u	nr2l
28.27	68.63	72.33	22.67	17.5	1.09	54.44	87.32

J.3.2 Time-domain results

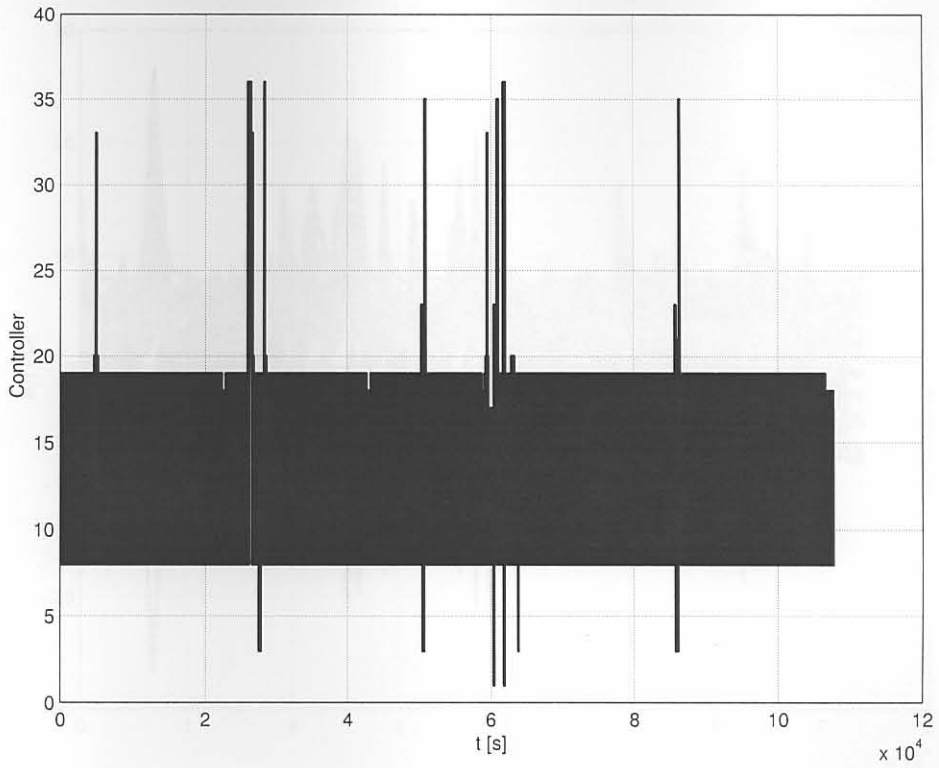

Figure J.6 Output of the switching criterion of 1280mm wide slabs and the worst-case control configuration.

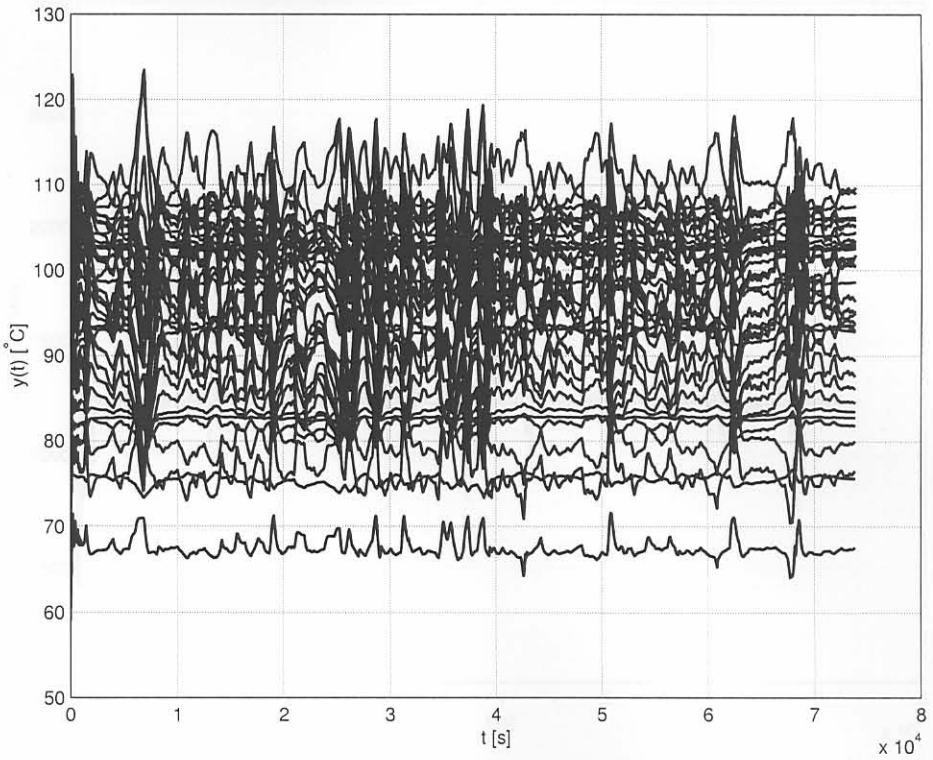

Figure J.7 Outputs for 1575mm wide slabs and the worst-case control configuration.

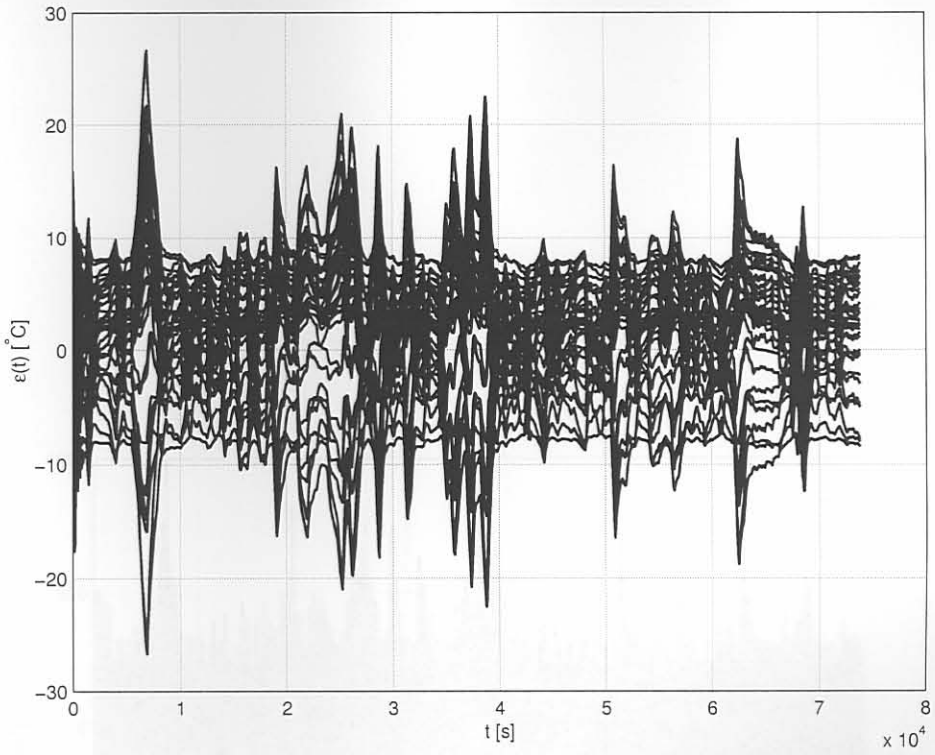

Figure J.8 Errors for 1575mm wide slabs and the worst-case control configuration.

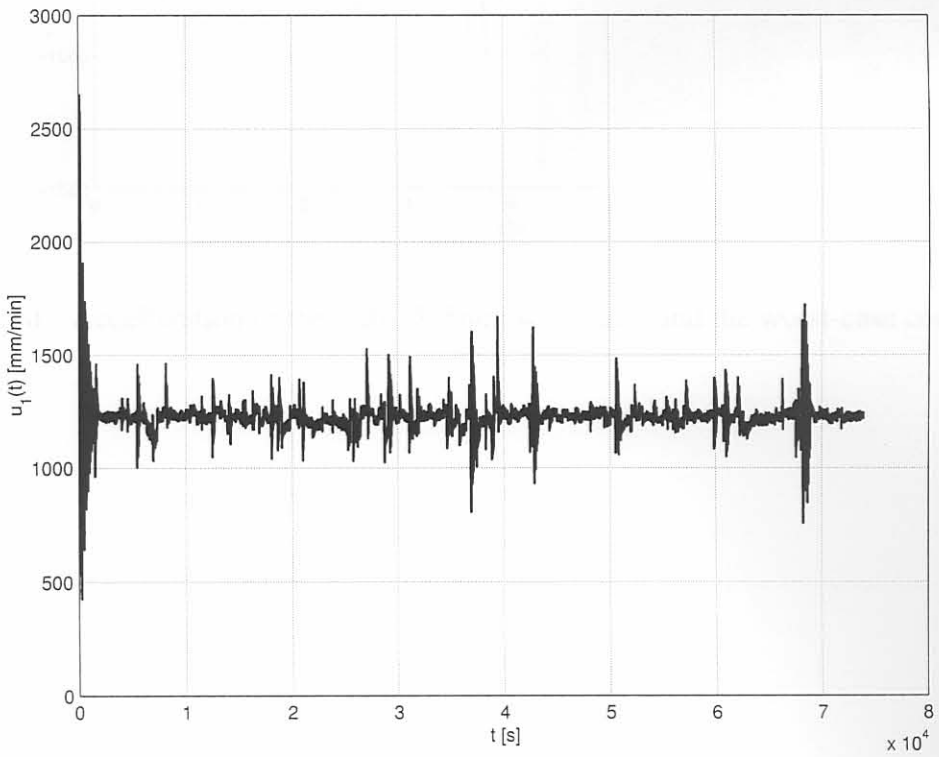

Figure J.9 Control signal for 1575mm wide slabs and the worst-case control configuration.

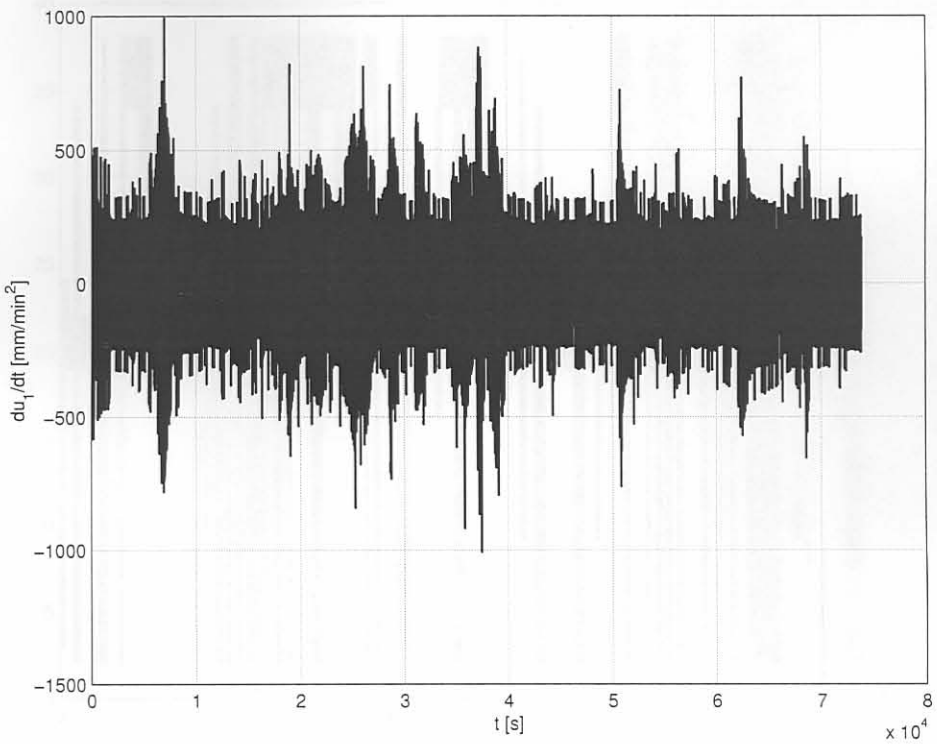

Figure J.10 Accellaration of the slab 1575mm wide slabs and the worst-case control configuration.

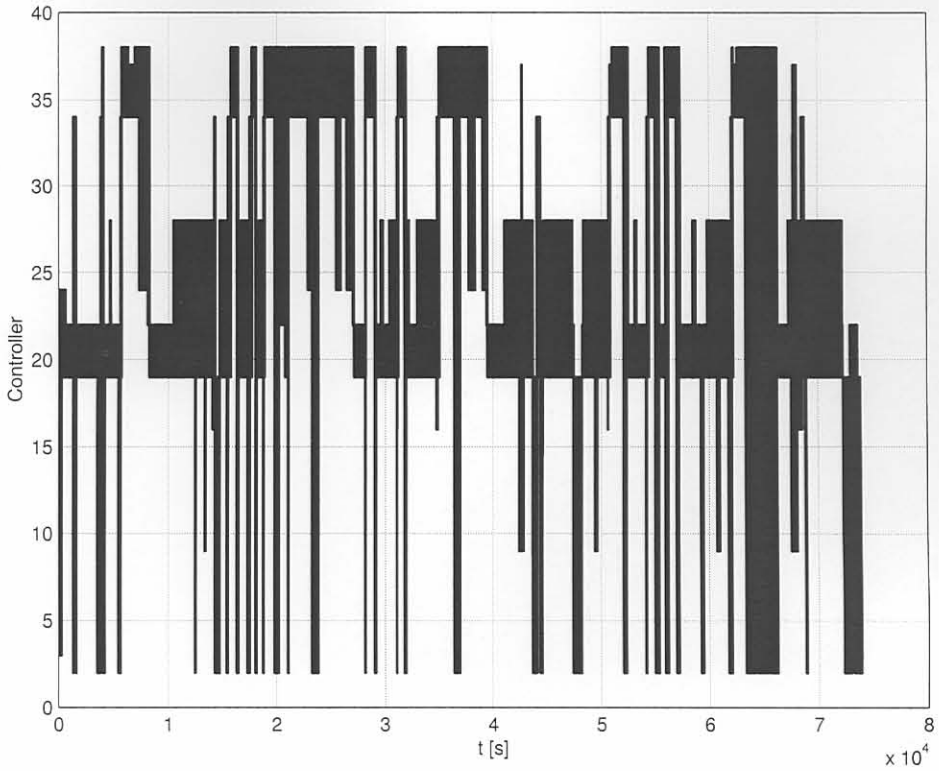

Figure J.11 Output of the switching criterion of 1575mm wide slabs and the worst-case control configuration.